Public Works
Canada

Travaux publics
Canada

Architectural and
Engineering Services

Services d'architecture
et de génie

Canada

89-02031/

Public Works Canada
Architectural and Engineering Services
Technology

AES/SAG 1-2:88-5v1

ICE FORCES
ON MARINE STRUCTURES
Volume 1 - CALCULATIONS

May 1987

Preparation Agency:
C.M.E.L. Enterprises Ltd.

Sponsoring Agency:
Panel for Energy Research
and Development (PERD)
Marine Product Line, Headquarters
Project Manager: M.S. Cheung

The contents of this document represent the views of the authors and are not necessarily the views or policies of the Department of Public Works.

The Minister of Public Works makes no representation or warranty, express or implied, with respect to this publication or the programs or information described in this publication, their quality, merchantability, or fitness for any particular purpose, or their adequacy to produce any particular result. In no event shall the Minister or Her Majesty the Queen in right of Canada, Her employees, servants or agents be legally liable to any person or persons for any damage, whether direct, indirect or consequential, resulting from the use of said publication or the programs or the information contained herein.

Published by Architectural and Engineering Services
Public Works Canada

© Minister of Supply and Services Canada 1988

Cat. No. W62-11/88-5-1E

ISBN 0-662-16284-6

Public Works Canada Travaux publics Canada

DOCUMENT DATA

1. Document Title

ICE FORCES ON MARINE STRUCTURES
Volume 1 - CALCULATIONS

2. Control Number

AES/SAG 1-2:88-5v1

3. Date

May 1987

4. Author(s)

T.B. Morrison, R.W. Marcellus, N.F.B. Allyn, J. Tseng

5. Consultant's Ref. No.

6. Project Manager

M.S. Cheung

7. Discipline Series No.

8. Preparation Agency and Address

CMEL Enterprises Ltd.
P.O. Box 220
Spencerville, Ontario
KOE 1X0

9. Document Type

Technical Report

10. No. of Pages

132

11. Sponsoring Agency and Address

Panel for Energy Research and Development (PERD)
and Public Works Canada, Marine Product Line
Sir Charles Tupper Bldg., Riverside Drive
OTTAWA, Ontario K1A 0M2

12. PWC File No.

6200-31

13. PWC Project No.

601061

14. Supplementary Notes

15. SSC Publication No.

W62-11/88-5-1E

16. ISBN

0-662-16284-6

17. Abstract

This is Volume 1 of a two-volume report describing methods for calculating ice forces on various marine structures. It is intended for use as a guideline for engineers engaged in designing and building large structures in ice-covered waters. It provides detailed procedures and equations for predicting ice loads under various conditions and scenarios.

Guidelines are provided for calculating ice forces on four generic types of marine structures: vertical-sided structures, sloping structures, floating structures, and aritifical islands. For each type, and general approach to the work is described followed by an example.

All the methods described in the report use analytic or numerical models based on estimated mechanical properties of ice. A detailed discussion and state-of-the-art review of methodologies in current use is provided in the companion volume entitled Ice Forces on Marine Structures Volume 2: Discussion.

18. Distribution Statement

Copies are available from:
Documentation Centre
Public Works Canada
Sir Charles Tupper Bldg., Riverside Dr.
Ottawa, Ontario K1A 0M2

19. Keywords

Ice forces; marine caissons; ice/structure interactions

20. Documentation Centre Catalogue No.

MA 100

21. Price

No charge

DPW 2398 (86/09)

Travaux publics Canada Public Works Canada

FICHE SIGNALÉTIQUE DE DOCUMENT

1. Titre du document

ICE FORCES ON MARINE STRUCTURES
(FORCES EXERCÉES PAR LES GLACES SUR LES OUVRAGES MARITIMES)
Volume 1 - CALCULATIONS

2. Numéro de contrôle

AES/SAG 1-2:88-5v1

3. Date

mai 1987

4. Auteur (s)

T.B. Morrison, R.W. Marcellus, N.F.B. Allyn, J. Tseng

5. No de réf. du conseil

6. Chargé de projet

M.S. Cheung

7. No de la collection technique

8. Nom et adresse de l'organisme rédacteur

CMEL Enterprises Ltd.
B.P. 220
Spencerville, Ontario
KOE 1X0

9. Type de document

Rapport technique

10. Nombre de page

132

11. Nom et adresse de l'organisme promoteur

Comité de la recherche et du développement énergétiques et Travaux publics Canada,
Travaux maritimes, Immeuble Sir-Charles-Tupper,
Promenade Riverside, OTTAWA (Ontario) K1A OM2

12. No de dossier de TPC

6200-31

13. No de projet de TPC

601061

14. Notes

15. No de publication de ASC

W62-11/88-5-1E

16. ISBN

0-662-16284-6

17. Résumé

Volume 1 du rapport en deux volumes décrivant les méthodes de calcul des forces exercées par les glaces sur les ouvrages maritimes. Il est destiné à l'usage des ingénieurs chargés de la conception et de la construction de grands ouvrages dans les eaux couverts de glaces. Le volume renferme des méthodes détaillées et des équations permettant de prévoir les charges de glace selon des conditions ou des déroulements de nature variée.

Les directives sont données pour le calcul des forces exercées par les glaces sur quatre types génériques d'ouvrages maritimes : ouvrages à parois verticales, ouvrages inclinés, ouvrages flottant et îles artificielles. Pour chaque type, une approche générale est précisée, suivie d'un exemple. Toutes les méthodes décrites dans le rapport font appel à des modèles analytiques ou numériques fondés sur les propriétés mécaniques estimées de la glace. Le second volume, intitulé Ice Forces on Marine Structures Volume 2: Discussion, présente un exposé détaillé et une revue de l'état actuel des connaissances en ce qui a trait à la méthodologie présentement employée.

18. Diffusion

Exemplaires disponibles du:
Centre de documentation
Travaux publics Canada
Imm. Sir-Charles-Tupper, Prom. Riverside
OTTAWA, Ontario K1A OM2

19. Mots clés

Forces exercées par les glaces; caissons; interactions glaces/ouvrages

20. No de catalogue du centre de documentation

MA 100

21. Prix

Sans frais

MTP 2398 (86/09)

PREFACE

This report is one of several reports on research work in the field of marine engineering, indentified and managed by the Marine Product Line and Technology Resources groups of Public Works Canada, with funds provided by the Interdepartmental Panel on Energy Research and Development (PERD).

PERD was established in 1974 to coordinate research on energy by the Federal Government with objectives to provide, in conjunction with efforts in the private sector and the provinces, the technical basis for:

- maintaining oil self-sufficiency over the short term, in view of dwindling conventional supplies;

- developing a diversified energy economy, less dependent on oil and gas in the mid-term; and

- making Canadians less reliant on non-renewable energy sources in the long term.

The research work undertaken by Public Works Canada in Marine Engineering with funds from PERD has been directed particularly toward the following two main topics:

1. Ice/Structure Interaction
2. Construction and Towing of Reinforced Concrete Caissons in the Arctic.

This report is being published with a view to enhancing the technology in the field of Marine Engineering and contributing toward the objectives of PERD.

TABLE OF CONTENTS

PREFACE i

LIST OF FIGURES iii

LIST OF TABLES vii

1. INTRODUCTION 1-1

2. CALCULATION PROCEDURES FOR CALCULATING ICE LOADS ON VERTICAL SIDED STRUCTURES 2-1

2.1 The General Ice Load Types 2-1
2.2 Particulars of Ice Load Calculations 2-2
2.2.1 The Brittle Ice Failure Pressure 2-2
2.2.2 Calculation of Ice Load Based on Empirical Data 2-2
2.2.3 Other Modes of Ice Failure 2-5
2.2.4 Probabilistic Calculations 2-5
2.3 Example Calculations 2-7
2.3.1 Brittle Failure of First-Year and Multi-Year Ice Sheets Interacting with Wide Structures 2-7
2.3.2 Brittle Failure of a Multi-Year Ridge with an Offshore Structure 2-8
2.3.3 Brittle Failure of a First-Year Ridge Interacting with an Offshore Structure 2-15
2.3.4 The Failure of Ice by Buckling 2-19
2.3.4.1 Buckling of a Single Ice Sheet 2-19
2.3.4.2 Buckling of a Collection of Floes 2-19
2.3.5 Ductile Failure of an Ice Sheet Surrounding a Structure 2-26
2.4 The Korzhavin Methodology of Calculating Ice Loads on Narrow Structures 2-28
2.4.1 The Indentation Factor: I 2-28
2.4.2 The Contact Factor: C 2-30
2.4.3 The Shape Factor: M 2-31
2.4.4 Ductile Failure of an Ice Sheet Against a Narrow Structure 2-32
2.4.5 Brittle Failure of an Ice Sheet Against a Semi-Circular Structure 2-35
2.5 Suggested Calculation Procedures - Sea Ice 2-37

TABLE OF CONTENTS (cont'd)

3. CALCULATION PROCEDURES FOR CALCULATING ICE LOADS ON SLOPING STRUCTURES 3-1

3.1 General 3-1
3.2 Ice/Structure Load Scenario Calculations 3-4
3.2.1 The Adhesion Force 3-4
3.2.2 Ice Sheet/Sloping Structure Interaction 3-6
3.2.2.1 Croasdale's Theory 3-6
3.2.2.2 Ralston's Theory 3-11
3.2.3 Interaction of a Consolidated Ridge with a Sloping Structure 3-15
3.2.4 Interaction of an Unconsolidated Ridge with a Sloping Structure 3-18

4. CALCULATION PROCEDURES FOR CALCULATING ICE LOADS ON FLOATING STRUCTURES 4-1

4.1 General 4-1
4.1.1 Introduction 4-1
4.1.2 Types of Floating Structures 4-2
4.1.3 Ice Types 4-8
4.1.4 The Ice/Floating Structure Interaction 4-9
4.2 Ice Force Calculation Considerations 4-11
4.2.1 Interaction Geometry and Ice Properties 4-11
4.2.2 Description of the Floating Structure Properties 4-14
4.2.3 Description of Other Environmental Conditions 4-22
4.3 The Interaction of a Bergy Bit with an Arctic Class IV Vessel 4-23
4.3.1 Vessel 4-23
4.3.2 Ice 4-26
4.3.3 Other Environmental Data 4-28
4.3.4 Sample Analysis 4-28

5. CALCULATION PROCEDURES FOR CALCULATING ICE LOADS ON ARTIFICIAL ISLANDS 5-1

5.1 General 5-1
5.1.1 Types of Artifical Islands 5-1
5.1.2 Geographic Considerations 5-6
5.1.3 Ice Types and Features to be Considered 5-7
5.1.4 Types of Ice Interactions with Artifical Islands 5-8
5.2 Example Calculation 5-12
5.2.1 Structure 5-12
5.2.2 Location 5-12
5.2.3 Ice Types and Features 5-12
5.2.4 Ice/Artifical Island Interaction 5-14
5.2.5 Summer Floe/Berm Interaction 5-16

REFERENCES

LIST OF FIGURES

2.1 Empirical Peak Ice Failure Pressure Aspect Ratio Relationships, Showing Recently Released Ice Load Measurements for Comparison 2-3

2.2 Failure Pressure as a Function of Area 2-4

2.3 Ice Failing at the Gulf Molikpaq Structure 2-6

2.4 Profile and Plan Views of the Multi-Year Ridge Used in the Scenario 2-9

2.5 Detail of Forces Acting of the Structure and the Ridge at the Moment of Breakout 2-10

2.6 Force-Time Histories for the Interaction Showing Limit Stress Load, Breakout Ridge Load and Brittle Failure Load Subsequent to Ridge Breakout 2-11

2.7 Croasdale (1980) Shear Failure Analysis of an Unconsolidated Ridge 2-16

2.8 Prodanovic (1981) Shearing and Bearing Capacity Type Failure Modes for Ridges 2-16

2.9 Cross-Section of First-Year Ridge Used by Prodanovic 2-18

2.10 Dimensionless Loads for Crushing and Shearing Failure Modes for a First-Year Ridge 2-18

2.11 Comparison of Experimental and Theoretical Buckling Loads 2-20

2.12 Illustration of Instability Conditions for Floes in Close Pack Conditions 2-22

2.13 Illustration of Broken Ice Instability 2-25

2.14 Comparisons of Measured and Calculated Stress at First Crack for Different Ice Types 2-27

2.15 Indentation Factor for Columnar and Granular Ice 2-29

LIST OF FIGURES (cont'd)

3.1 Types of Sloping Structures 3-3

3.2 Values of the Two Coefficients C_1 and C_2 as a Function of Slope Angle 3-9

3.3 Coefficients to Determine Ice Forces on Conical Structures 3-12

3.4 Croasdale (1980) Shear Failure Analysis of an Unconsolidated Ridge 3-19

4.1 Illustration of a Catenary Moored Drillship 4-3

4.2 The Gulf Conical Drilling Unit, Kulluk, in Close Pack Ice 4-3

4.3 Illustration of a Semisubmersible with Inverted Collars 4-4

4.4 Illustration of a Semisubmersible with Inclined Columns 4-4

4.5 Illustration of a Storage Tanker with an Articulated Mooring 4-5

4.6 Illustration of a Shuttle Tanker with an Articulated Mooring 4-6

4.7 Illustration of a Tension Leg Platform with Additional Catanery Mooring 4-7

4.8 Illustration of a Buoyant Articulated Loading Tower 4-7

4.9 Interaction Geometries for Semisubmersibles and SPM (Single Point Mooring) Systems 4-12

4.10 Body Plan of a 200,000 DWT Tanker 4-24

4.11 Configuration of Vessel and Mooring System Used in the Analysis 4-24

4.12 Schematic of Ice Features Used in the Analysis 4-27

4.13 Ice/Vessel Contact Pressure 4-30

4.14 Ice/Vessel Contact Force 4-30

4.15 Ice/Vessel Contact Depth 4-31

LIST OF FIGURES (cont'd)

4.16 Ice/Vessel Contact Width 4-31

4.17 Global Translational Mooring Forces 4-32

4.18 Global Rotational Mooring Forces 4-32

4.19 Mooring Line Forces 4-33

4.20 Translations of the Vessel 4-33

4.21 Rotations of the Vessel 4-34

5.1 Schematic of a Sacrificial Beach Artificial Island 5-2

5.2 Schematic of a Slope Protected Artificial Island 5-3

5.3 Schematic of a Caisson Retained Artificial Island 5-5

5.4 Illustrations of Ride-Up and Passive Failure 5-9

5.5 Illustrations of Several Failure Mechanisms 5-10

5.6 Schematic of the Artificial Island Used in the Analysis 5-13

5.7 Forces Acting on the Ice Floe 5-17

LIST OF TABLES

2.1 Values for the Contact Factor, C, from Korzhavin (1971) 2-30

2.2 Values of the Shape Coefficient, from Soviet Construction Standards and Rules, Moscow, 1983 2-31

3.1 Example Parameters Used in the Ralston Methodology Analysis 3-13

3.2 Results of Analysis Based on the Ralston Methodology 3-14

3.3 Example Parameters Used in the Ralston Consolidated Ridge Analysis 3-17

4.1 Sizes of Selected Elements Based on the Canadian Arctic Shipping Pollution Prevention Regulations (CASPPR) Based on the Proposed Framing Layout 4-21

4.2 Vessel Midbody Criteria for an Arctic Water Pollution Prevention Act Class 4 Vessel 4-25

5.1 Output from Ice Floe/Artificial Island Analysis 5-18

1.0 Introduction

In this volume of the study specific procedures for calculating ice forces on four generic types of marine structures are presented. Extensive background material and discussions are presented in the companion report of this study entitled "Ice Forces on Marine Structures, Volume II"

The four generic types of structures are, in order of presentation:

1. Vertical Sided Structures,
2. Sloping Structures,
3. Floating Structures, and
4. Artificial Islands.

In each of the four cases a general outline of the approach (or approaches if applicable) used to calculate ice forces on each type of structure is presented first. This is followed by an example for one structure of the generic type.

The case of a vertical sided structure is examined first. Both sloping planes and conical structures are used as examples of sloping structures. An Arctic Class Vessel is used as an example of a floating structure. Finally, a medium water depth slope protected design artificial island is used as an example for the lattermost generic type of structure.

Often ice laod determination is aided by the use of computer programs to perform the calculations. In this fashion optimization of the structure's characteristics, and risk analysis procedures can be more readily implemented into the design process. Parenthetically, there are nearly as many computer programs as there are researchers, and to document them all would prove prohibitive. Instead, the physical principals used to determine ice loads have been stressed.

In summary, one should be aware that these calculation procedures should not be used indiscriminately for detailed structure design. They are used here to point out the complexities of the problems and to illustrate what factors should be included in any design scenario.

2.0 Calculation Procedures for Calculating Ice Loads on Vertical Sided Structures

2.1 The General Ice Load Types

The general methodology of estimating ice loads on vertical sided structures is to multiply the area of interaction by an estimated failure pressure.

There are three categories of ice loads:

Limit-Stress:	A limit-stress load is the product of the structure width, ice thickness and ice failure pressure. The limit-stress load is defined as that load due to an ice feature fully enveloping the structure. If the ice feature geometry at the leading edge is not vertical (e.g. a ridge is present at the edge) the limit-stress load is not reached until the uniform maximum thickness of the ridge is failing along the whole ice/structure interface. A limit-stress load is the maximum load any given ice feature is capable of exerting on a structure.
Limit-Energy:	A limit-energy load is less than the limit-stress load. The ice feature does not fully envelop the structure. The limit-energy load is defined as the product of the chord diameter of the interaction surface (not necessarily the width of the structure), the average thickness of ice interacting with the structure, and the assumed ice failure pressure. If the structure is eventually fully enveloped by the ice feature the limit-energy load is usually equal to the limit-stress load. If the structure does not become fully enveloped by the ice feature the limit-energy load is equal to that load exerted on the structure just before the ice feature's forward motion ceases.

Limit-Environmental: When an ice feature is initially at rest against a structure and no ice failure occurs, the load on the structure is limited to the sum of the wind and current drag force vectors and the force vectors exerted on the ice feature by adjacent ice features (if present).

2.2 Particulars of Ice Load Calculations

2.2.1 The Brittle Ice Failure Pressure

The most difficult problem in the determination of ice loads on structures is the determination of the ice failure pressure. The method most in favour currently is to use empirical ice failure pressure data obtained at the large scale to estimate ice failure pressures. Large scale empirical data and a relationship between chord diameter and average ice thickness is shown in Figure 2.1. An area of interaction-ice failure pressure relationship which can also be used is illustrated in Figure 2.2. In essence the ice failure pressure for any given situation is assumed to equal the ice failure pressure observed in the past for similar ice properties and geometries of interaction.

2.2.2 Calculation of Ice Load Based on Empirical Data

The ice load exerted on a structure, in the ice brittle failure mode, can be estimated by multiplying the ice failure pressure obtained from Figure 2.1 or Figure 2.2 by the chord width of the interaction and the average ice thickness in contact with the structure.

The line in Figure 2.1 is the estimated failure pressure for cold multi-year ice, as would impact a structure during winter. For summer interactions the strength would be expected to be less, however the use of the cold temperature failure pressure estimate would be conservative.

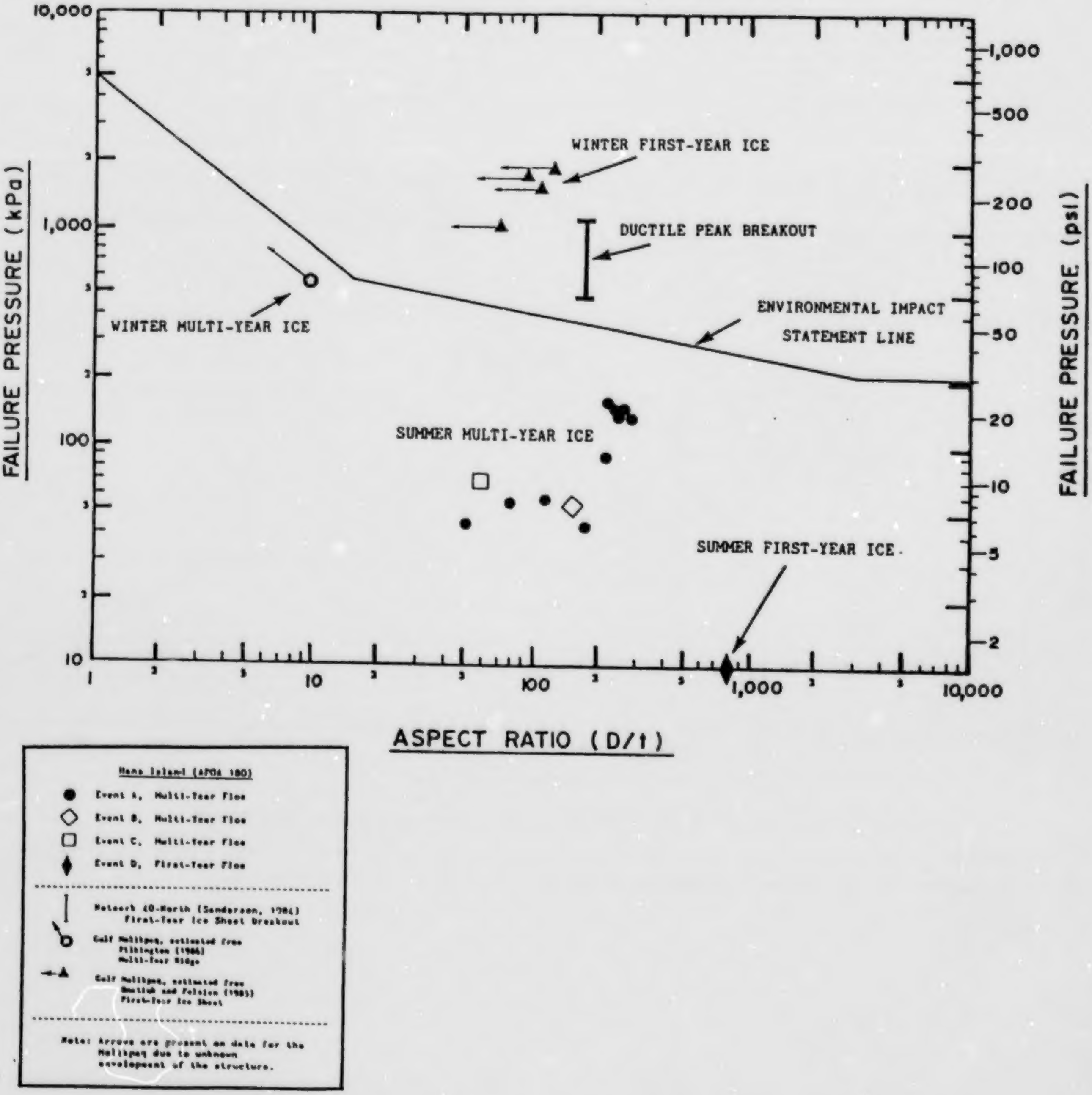

Figure 2.1 Empirical Peak Ice Failure Pressure Aspect Ratio Relationships, Showing Recently Released Ice Load Measurements for Comparison.

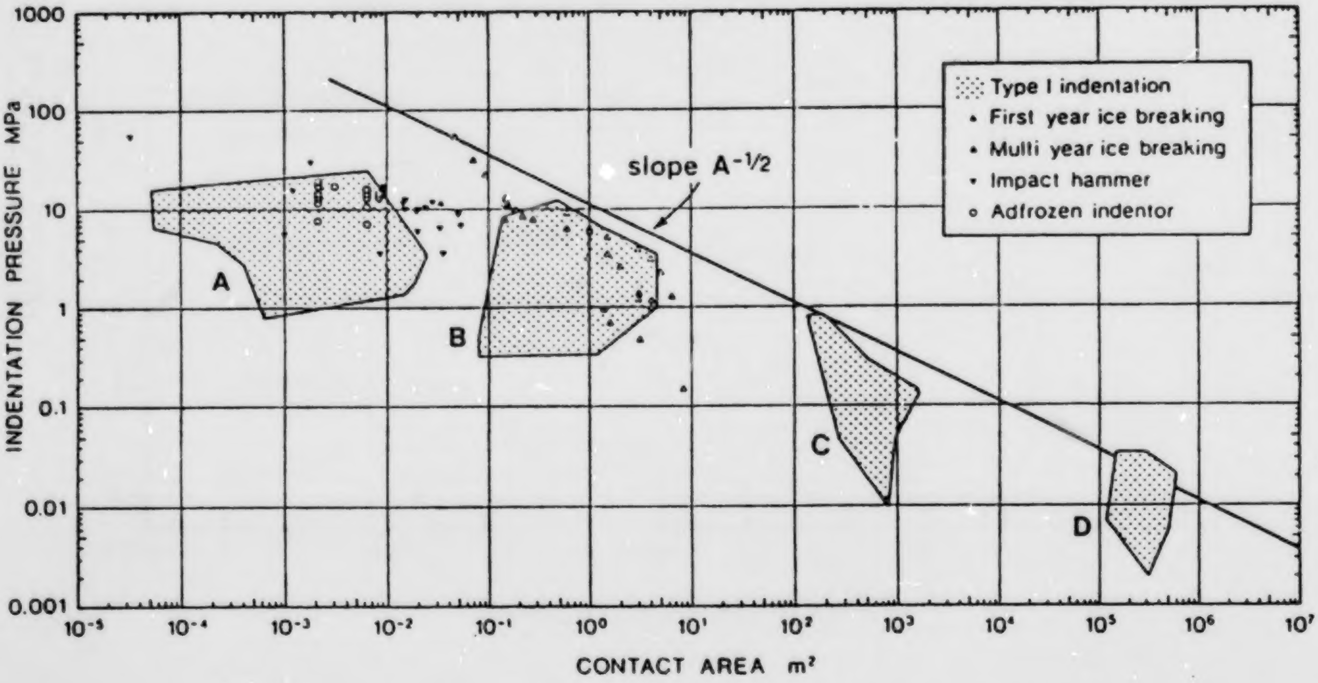

General trend of pressure-area curve, with data groups.

A: *Laboratory tests*

B: *Medium-scale in situ tests, lighthouses and bridge piers*

C: *Full-scale Arctic islands and structures*

D: *Meso-scale models.*

Figure 2.2 Failure Pressure as a Function of Area (Sanderson, 1986).

For multi-year ridges the calculation of failure pressure is assumed to be given by the same line as for multi-year ice, i.e. Figures 2.1 and 2.2.

2.2.3 Other Modes of Ice Failure

Large scale shearing or flexure of the ice feature may be a more probable failure mode than crushing at the ice/structure interface. It may also be possible for a ridge to shear out of a floe and stop moving, leaving the floe to move past the ridge and the structure. Large scale cracking of a floe may also occur. Figure 2.3 shows the interaction of thick multi-year ice with Gulf's Molikpaq structure in the Beaufort Sea.

2.2.4 Probabilistic Calculations

For ice thicker than one metre or so, many of the interactions between floes and structures will be of the limit-energy type. While the determination of the limit-stress load is relatively simple, the probabilistic aspects of the estimation of return-period ice loads is more complicated due to the many factors which must be taken into account. Computer models of the energy dissipated as a function of penetration during ice/structure interactions are particularly suited to probabilistic analyses. In this fashion the parameters of ice features which generate the largest ice loads can be determined. The return period loads can also be determined.

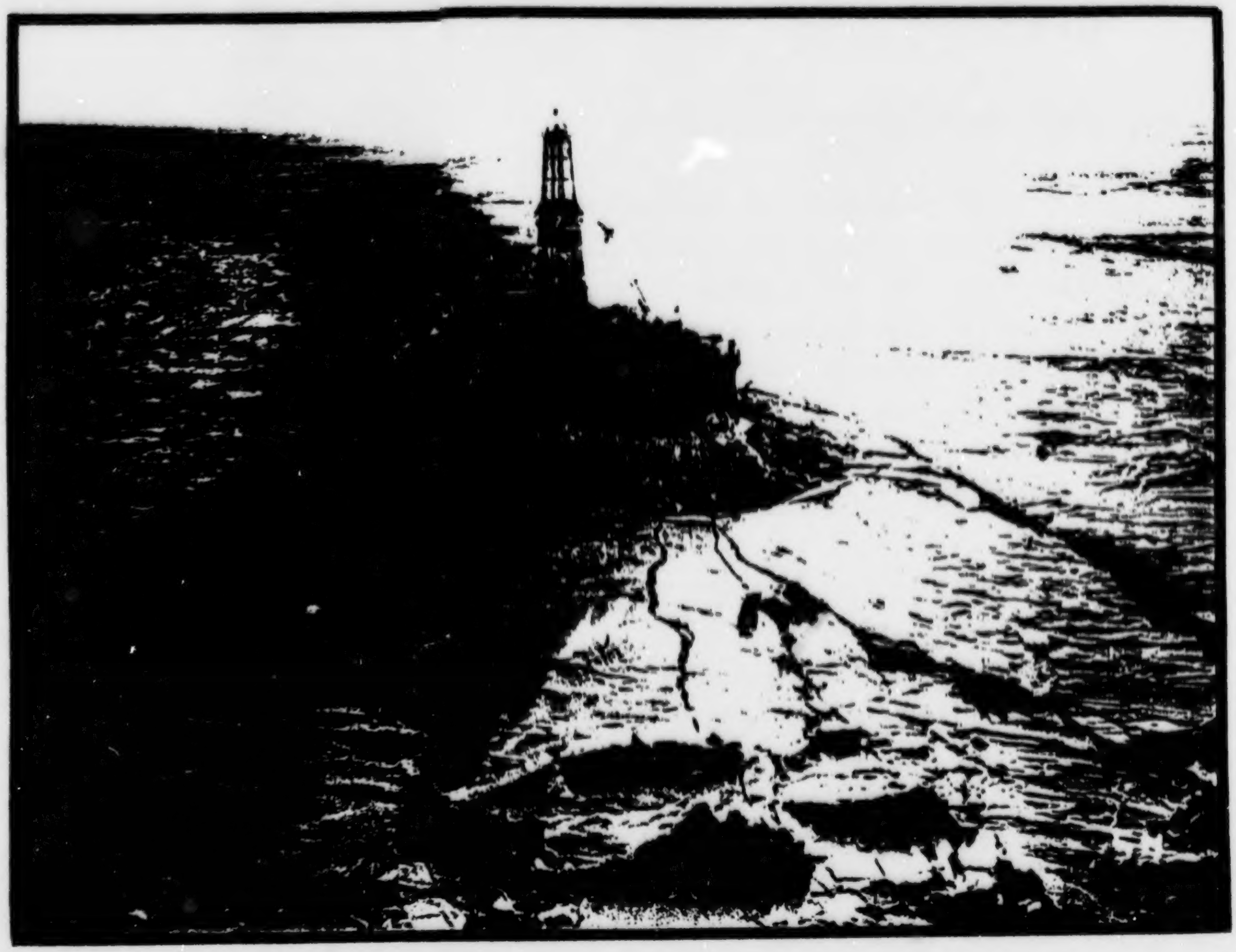

Figure 2.3 Ice Failing at the Gulf Molikpaq Structure (photo Courtesy Gulf Canada).

2.3 Example Calculations

In the remaining sections of this chapter the following scenario calculations are presented.

1: Brittle failure of first-year and multi-year ice sheets interacting with wide structures,

2: Brittle failure of a multi-year ridge interacting with a wide structure,

3: Brittle failure of a first-year ridge interacting with a wide structure,

4: Buckling failure of first-year ice sheets and small first-year floes interacting with a wide structure, and

5: Ductile failure of an ice sheet surrounding a structure.

2.3.1 Brittle Failure of First-Year and Multi-Year Ice Sheets Interacting with Wide Structures

The interaction of an ice sheet or floe with an offshore structure is the most typical type of interaction. When edge geometry characteristics are not of concern (or the edge of the floe has been crushed) an ice failure pressure can be estimated based on the ice type.

For first-year sea ice sheets and floes impacting at speeds such that the ice fails in a brittle manner, an ice failure pressure of 1.75 MPa (250 psi) has been measured in the Beaufort Sea.

For multi-year floes the empirical data based on Figures 2.1 and 2.2 can be used to estimate the failure pressure.

The load on the structure is the product of the chord width, the average ice thickness at the ice/structure interface, and the peak ice failure pressure.

2.3.2 Brittle Failure of a Multi-Year Ridge Interacting with an Offshore Structure

A multi-year ridge is composed of solid ice throughout its entire thickness.

It is tacitly assumed in this study that a multi-year ridge will generally satisfy the failure pressure relationships illustrated in Figures 2.1 and 2.2.

Due to the large area of interaction, which occurs rapidly when a multi-year ridge is interacting with a structure, the load exerted on a structure can be expected to reach large values quickly. It is therefore more likely for an ice floe with a ridge at the leading edge to dissipate all of its energy before full envelopment of the structure occurs. A particular example has been chosen to illustrate the energy dissipation during an interaction, and to also show how other effects may come into play, which serve to reduce the load exerted on the structure.

Multi-Year Ridge Interaction With a Wide Structure

This example was chosen not to represent typical conditions, per se, but rather to illustrate some of the variety of interactions which can occur. The following example shows that many factors can affect the interaction scenario, and in particular shows that shearing on a large scale, with transfer of failure from the ridge/structure interface to the ridge/floe interface can significantly reduce the load.

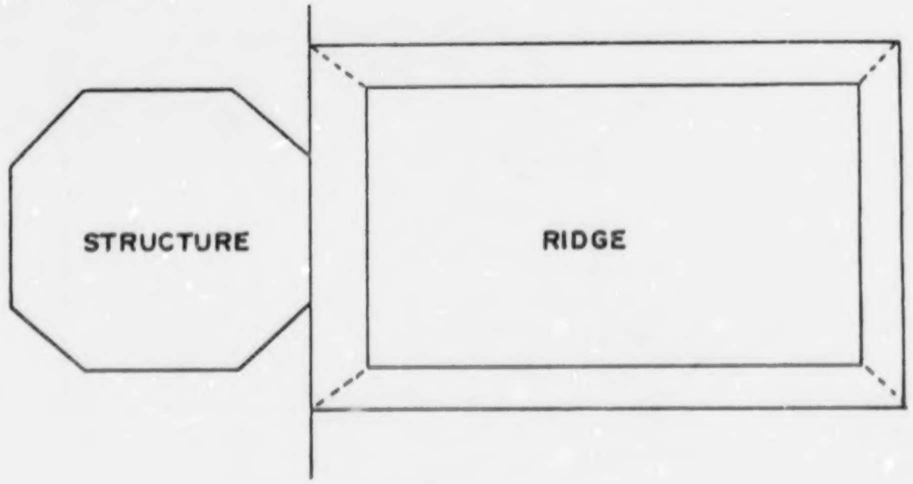
STRUCTURE
RIDGE

PLAN VIEW

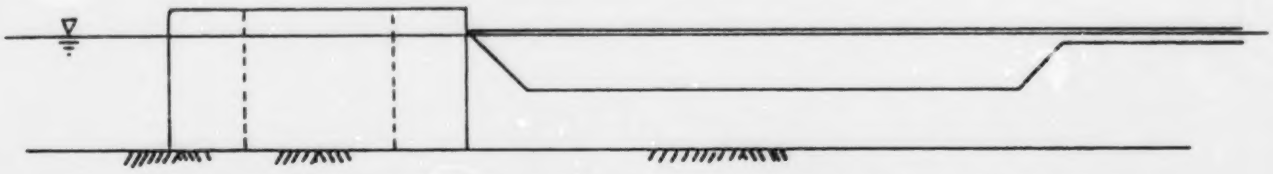

PROFILE VIEW

Figure 2.4 Profile and Plan Views of the Multi-Year Ridge Used in the Scenario.

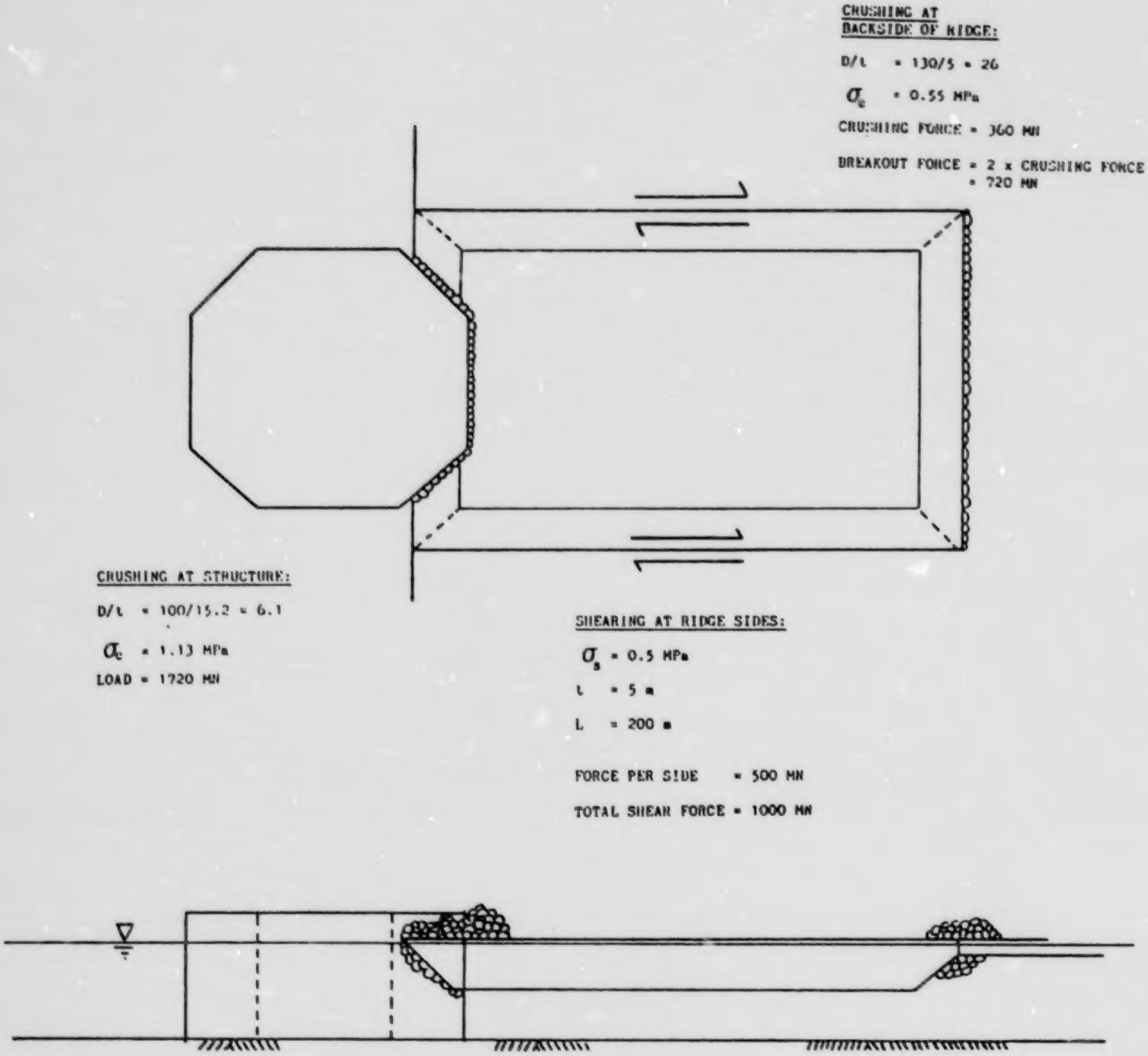
CRUSHING AT BACKSIDE OF RIDGE:
D/t = 130/5 = 26
σ_c = 0.55 MPa
CRUSHING FORCE = 360 MN
BREAKOUT FORCE = 2 x CRUSHING FORCE = 720 MN
CRUSHING AT STRUCTURE:
D/t = 100/15.2 = 6.1
σ_c = 1.13 MPa
LOAD = 1720 MN
SHEARING AT RIDGE SIDES:
σ_s = 0.5 MPa
t = 5 m
L = 200 m
FORCE PER SIDE = 500 MN
TOTAL SHEAR FORCE = 1000 MN

Figure 2.5 Detail of Forces Acting on the Structure and the Ridge at the Moment of Breakout.

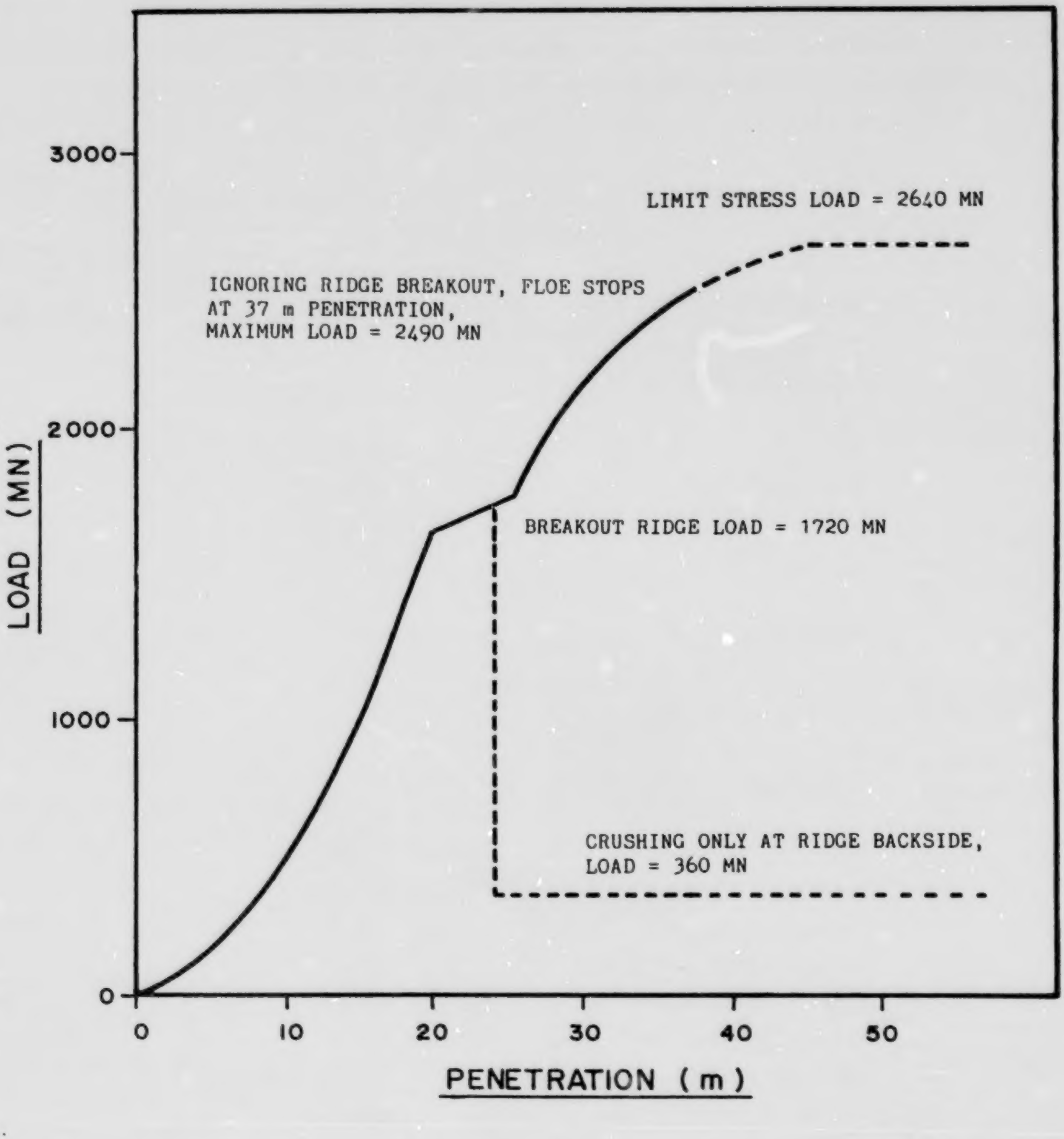

Figure 2.6 Force-Time Histories for the Interaction Showing Limit Stress Load, Breakout Ridge Load and Brittle Failure Load Subsequent to Ridge Breakout.

Example Calculation

The end-on ridge situation refers to the situation illustrated in Figure 2.4. The structure is impacted by a nearly square multi-year ridge or hummock field.

The conditions at breakout of the ridge are shown in Figure 2.5, and Figure 2.6 is a plot of the load versus penetration for both scenarios.

The parameters in this example calculation are:

Environmental:

Water depth:	35 m
Wind speed:	12.5 m/s
Current speed:	0.50 m/s

Structure:

Octagonal in shape, width:	100 m

Ice Floe:

Shape:	circular
Diameter:	10 km
Average thickness:	5 m
Maximum ridge thickness:	20 m
Ridge dimensions at top:	130 m x 200 m
Ridge dimensions at bottom:	100 m x 165 m
Angle at ridge leading edge:	45° to horizontal
Initial floe velocity:	0.50 m/s

The Interaction Scenario

The object of the analysis is to determine the load the ice feature described above exerts on the vertically sided structure. If the crushing load at the ridge/structure interface is great enough it is possible for the ice to shear along the edges of the ridge, and for crushing to be initiated in the thin ice at the backside of the ridge. The ridge thus stops moving towards the structure and becomes separate from the floe. The floe shears past the ridge and structure, and the load exerted on the structure is equal to that of crushing at the backside of the ridge.

If the possibility of the ridge breaking out of the floe is not included in the analysis (and the floe is given more energy) the ultimate load on the structure is caused by full envelopment of the ridge at about 45 m penetration (i.e. the front of the ridge has traveled 45 metres). The load at full envelopment, of the limit stress variety, is 2.64 GN, based on the empirical ice failure pressure relationship illustrated in Figure 2.1.

The ridge breakout scenario is responsible for a reduction in the load which the structure must bear. The "breakout" load is calculated by determining the force necessary to shear the ridge out of the floe and to initiate crushing at the backside of the ridge.

In the example above the crushing load at the backside of the ridge is calculated as 360 MN (D/t ratio of 130/5=26, for an estimated large scale empirical ice failure pressure of 0.55 MPa). To initiate crushing, a "breakout factor" of 2.0 is used. This means that to initiate crushing an estimated load of 720 MN is necessary.

The shearing force is calculated by multiplying the area of ice sheared by an assumed shear strength of the ice (0.5 MPa). The area is calculated as 5 m thickness x 200 m length = 1000 m^2. The force per side is calculated as 500 MN; that for both sides is 1000 MN.

Therefore, when the load caused by crushing at the ridge/structure interface is greater than the estimated breakout load (1000 MN + 2.0 x 360 MN) of 1720 MN, breakout should occur, the sides of the ridge will shear, the crushing at the structure/ridge interface will stop, and crushing at a load of 360 MN will continue at the backside of the ridge.

As part of the design process examples such as that reviewed here are included in the analysis of ice loading conditions. The lack of ice loading examples of complex interactions such as ridge breakout highlights one of the major problems of the design engineer: Empirical observations, to date, are only capable of indirectly supporting important design scenarios. Further documented observations of multi-year ridges interacting with structures are desirable.

2.3.3 Brittle Failure of a First-Year Ridge Interacting with an Offshore Structure

The Croasdale Ridge Shear Model

Based on a simple shear failure Croasdale (1980) proposed the following formula for the load on a structure during the interaction with a first-year (unconsolidated) ridge. The assumed failure mode is shown in Figure 2.7.

$$L = \frac{2 B t^2}{3} (\rho_w - \rho_i) g \tan (\phi)$$

where:

B = the width of the ridge,
t = the keel draft of the ridge,
g = 9.81 m/s^2,
ρ_i = density of ice,
ρ_w = density of water, and
ϕ = the internal angle of friction of the ridge.

In the above equation the influence of the sail is ignored.

The load L is that load exerted on the structure as a "plug" of the ridge is sheared from the remaining portions. The load is therefore independent of the width of the structure.

It is possible to include the presence of a consolidated layer in Croasdale's model by assuming the ice at the ice/structure interface crushes at 1.75 MPa for ice of the same state as first-year Beaufort Sea ice.

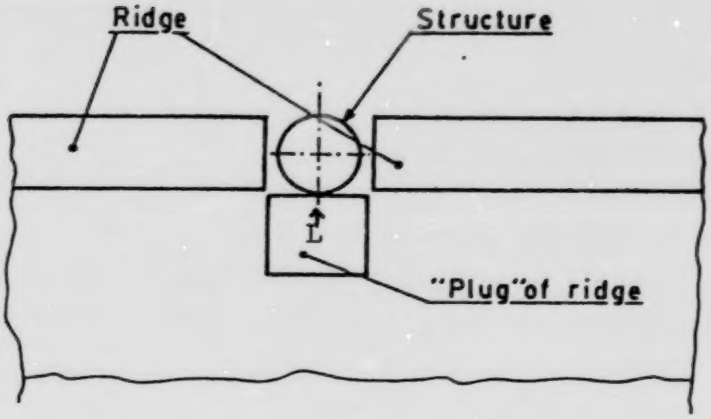
Ridge
Structure
L
"Plug"of ridge

Figure 2.7 Croasdale (1980) Shear Failure Analysis of an Unconsolidated Ridge.

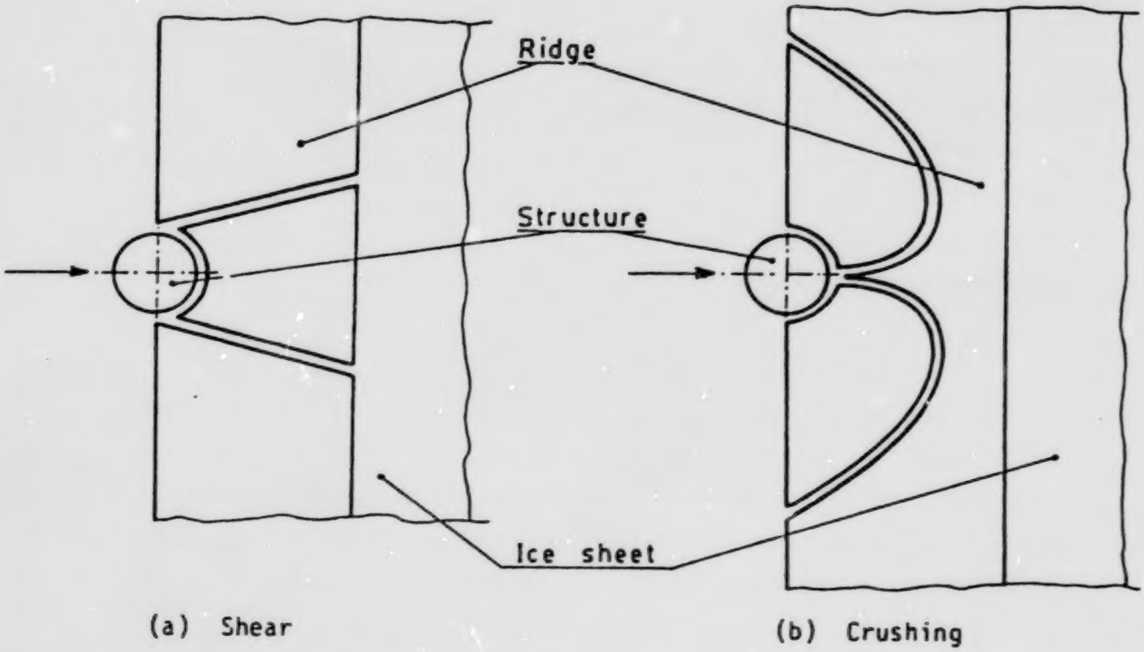
Ridge
Structure
Ice sheet

(a) Shear

(b) Crushing

Figure 2.8 Prodanovic (1981) Shearing and Bearing Capacity Type Failure Modes for Ridges.

The Prodanovic Bearing Capacity Model

In this model Prodanovic (1981) included the capability for a consolidated layer to be present at the upper portions of the ridge. The consolidated layer and blocky portions of the ridge are assumed to fail separately, and the total load equal to their sum.

A Prandtl indentor (or velocity field) was modeled by Prodanovic. Aside for the usual assumptions of isotropy and homogeneity in the blocky portion of the ridge it's strength was assumed to increase directly with confinement.

In Figure 2.8 failure modes of the ridge used by Prodanovic (1980) are shown. A profile of the ridge is shown in Figure 2.9, and a dimensionless load analysis diagram is shown in Figure 2.10. In Figure 2.10 P is the load, C is the cohesion of the blocks, D is the diameter of the structure and K is the ratio of keel depth below the ice sheet to sail height above the ice sheet (in Figure 2.10 K = 5 S, or five times the sail height above the ice sheet). Recall that the first-year ice sheet failure is calculated by assuming a failure pressure of 1.75 MPa for ice of the same state as first-year Beaufort Sea ice.

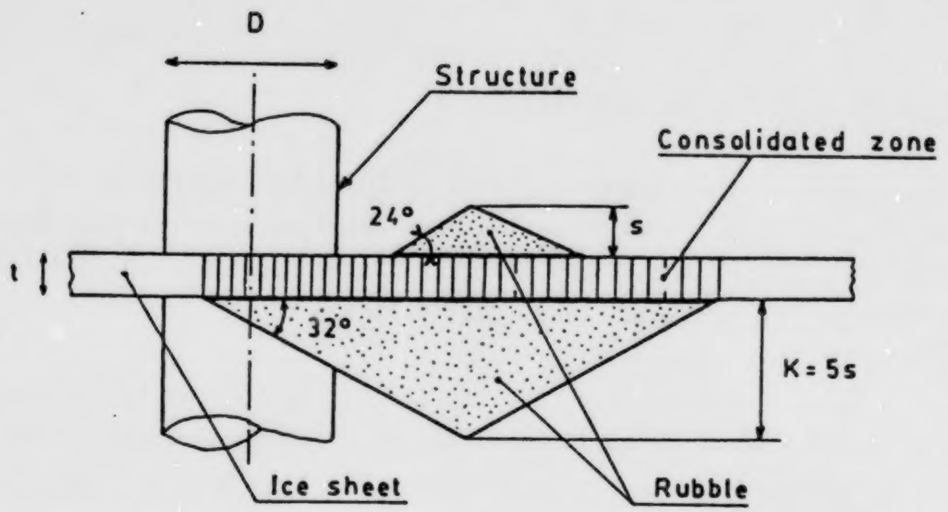
D
Structure
Consolidated zone
24°
s
t
32°
K = 5s
Ice sheet
Rubble

Figure 2.9 Cross-Section of First-Year Ridge Used by Prodanovic.

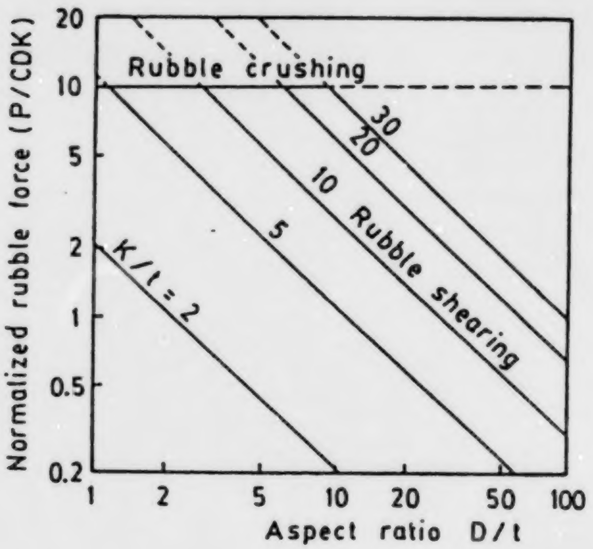

Figure 2.10 Dimensionless Loads for Crushing and Shearing Failure Modes for a First-Year Ridge, (from Prodanovic, 1981).

2.3.4 The Failure of Ice by Buckling

There are three distinct types of buckling failure of ice appropriate for structure design considerations. An ice sheet can fail by large scale buckling, be it by elastic criteria such as at a high strain rate, or by creep. As well, small floes in close pack conditions can buckle, and load floating vessels such as drillships, or semisubmersibles.

In this section of the report buckling by creep will not be examined. The reader is referred to Sjolind (1984, 1985) for a viscoelastic buckling analysis of beams and plates resting on elastic foundations.

2.3.4.1 Buckling of a Single Ice Sheet

Figure 2.11, from Sodhi (1986), prepared for the Third IAHR State-of-the-Art Report on Ice Loading on Offshore Structures, is a dimensionless plot of theory and experimental results on buckling ice loads on structures. The hinged and frictionless conditions are end conditions for the ice.

The calculations are based on beams on elastic foundations. End conditions are either hinged, or frictional; the two types of end conditions cover all cases.

2.3.4.2 Buckling of a Collection of Floes

Hetenyi (1946) examined the elastic stability of straight bars. His calculations can be used to calculate the instability load caused by out-of-plane buckling of floes in close pack conditions.

The instability stress for floes calculated here is most often used in analyzing loads on the legs of semisubmersibles or other floating structures such as a drillship, where the structure can not withstand large global loads.

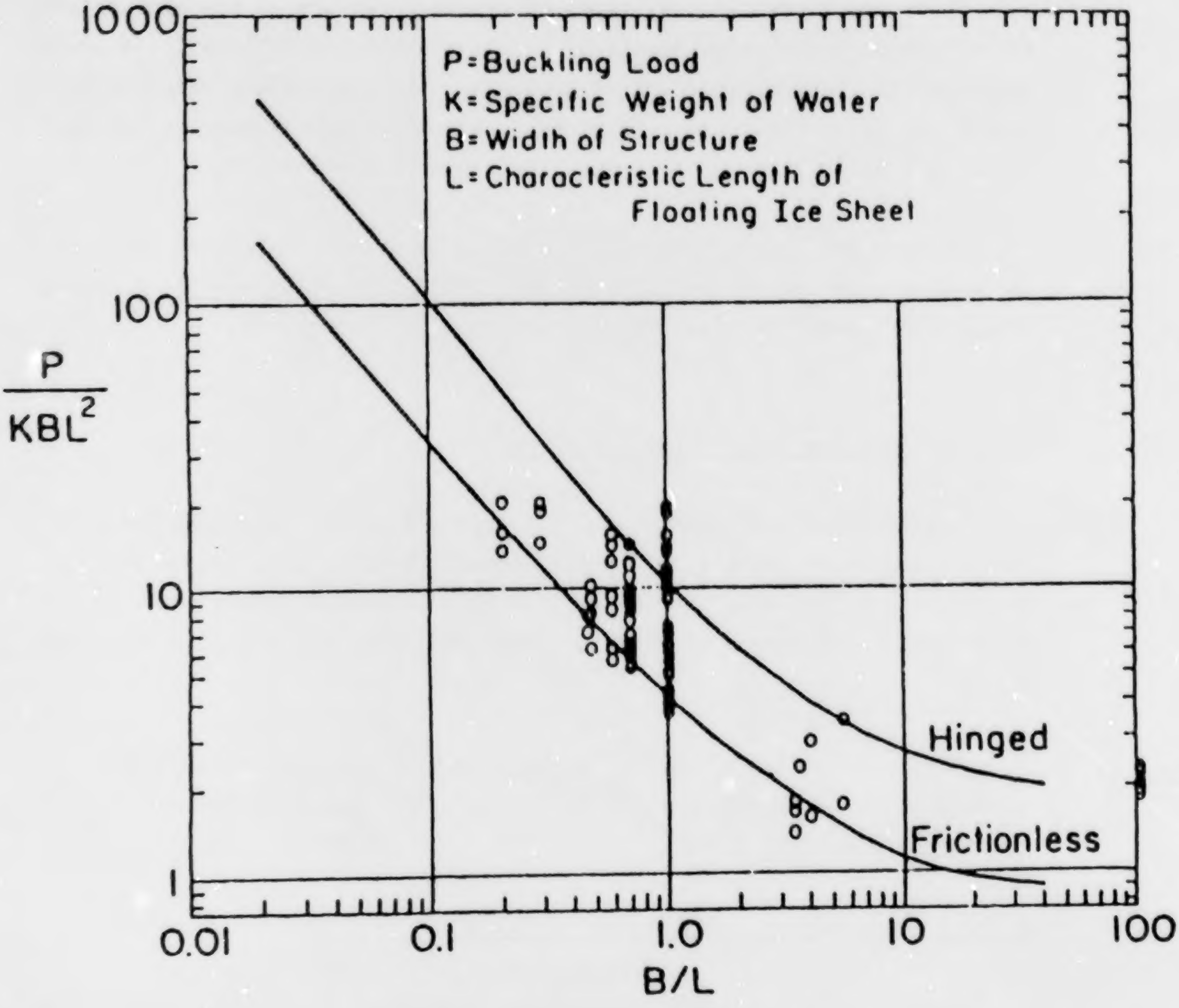

Figure 2.11 Comparison of Experimental and Theoretical Buckling Loads. Heavy Lines: Theoretical Results from Sodhi (1979); Circles: Experimental Results (Sodhi et al., 1983).

A plot of the conditions for elastic instability in bars resting on an elastic foundation is shown in dimensionless form in Figure 2.12.

As the full theory is given in Hetenyi (1946), only a summary will be reviewed here. The bars can deflect in one of two ways; the ends of the bars can both move in the same direction as the floes buckle, or they can move in opposite directions. The former situation is referred to as symmetrical buckling, and the latter, antisymmetrical buckling. New variables X and Y are defined as follows:

$X = f_{ins} / f_e$
= ratio of instability load to Euler load, and

where:

f_{ins} = instability load, and
f_e = l^2/pi^2 E I, the Euler load for a hinged-end bar of length l and flexural rigidity EI.

$Y = [k\ l^4 / E\ I]^{\frac{1}{2}}$

where:

k = foundation modulus,
l = length of bar,
E = Young's Modulus, and
I = Moment of Inertia per unit width, $t^3/12$.

The quotient f_{ins}/f_e is to be determined (the ratio of instability load to Euler buckling load). Thus, Y must be determined first. For an accurate determination of the load, and a determination of which way the floes will buckle the graph in Figure 2.12 should be referred to. It should be noted that an approximate estimate of the load can be obtained by dividing Y by 10. The straight dotted line in the figure has a slope of π^2, which is close to 10 (i.e. the slope of the instability curve

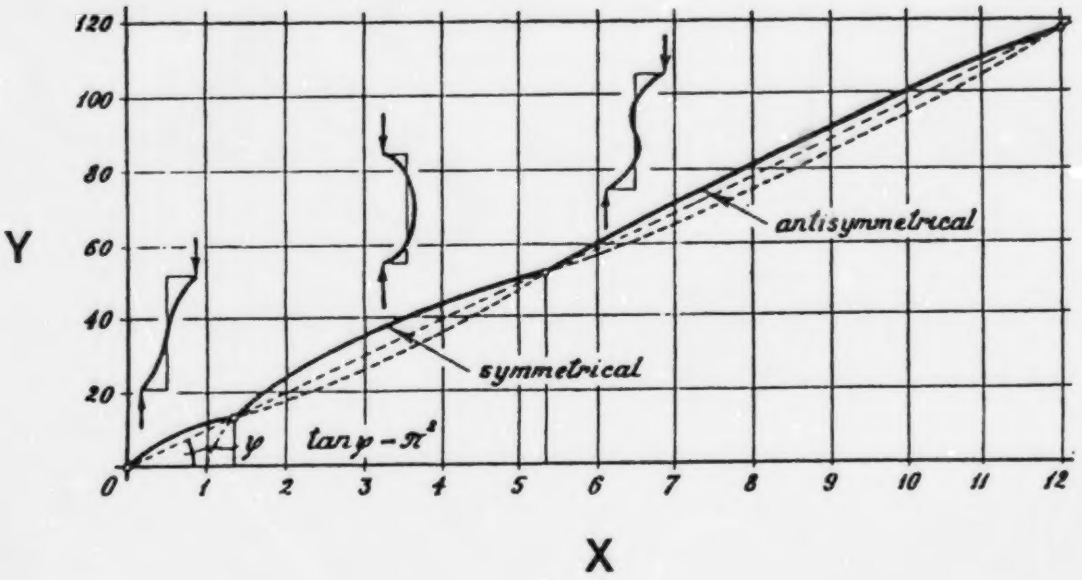

Figure 2.12 Illustration of Instability Conditions for Floes in Close Pack Conditions (Hetenyi, 1946).

approximates the critical conditions for buckling of a semi-infinite beam. Where more accuracy is necessary, the thick continuous line is to be used in the calculations.

Note that most realistic conditions such as that illustrated below yield Y values very close to zero. In cases such as these it is more appropriate to divide Y by 10 to estimate X.

Example Calculation of Floes Buckling

Consider floes about 2 metres square, with a thickness of 30 cm. The instability load is determined to be about 80 kN per metre width. For a semi-submersible leg of width about 10 metres the critical load would be 800 kN; for a drillship with a length of about 100 m, the critical load would be 8 MN.

Close Pack Ice Conditions: Calculation of Out-of-Plane Instability Load Conditions Based on Buckling

floe shape, $l \times l$ = 2 m x 2 m

thickness, t = 0.3 m

Young's Modulus, E = 7000 MPa

foundation modulus, k = $(1025 \text{ kg m}^{-3})\,(9.81 \text{ m s}^{-2})$
= $10{,}055 \text{ N m}^{-3}$
= 0.01 MN/m^3

Moment of Inertia per unit width, I, = $t^3/12$

Euler Buckling:

$$f_e = l^2 / pi^2 \; E \; I = 40 \text{ MN/m}$$

$$Y = [k \; l^4 / E \; I]^{\frac{1}{2}} = 0.02$$

Calculation of Instability Load:

$$f_{ins} = Y \; f_e / \; 10 = 0.08 \text{ MN/m width}$$
$$= \; 80 \text{ kN/m}$$

The 2 m by 2 m by 30 cm thick ice floes have an instability force to buckling of 80 kN/m width. If wind or current stresses in the pack ice are such that a stress of 80 kN/m are realized, the small floes will buckle and the load on the structure will be reduced. The situation is illustrated in Figure 2.13.

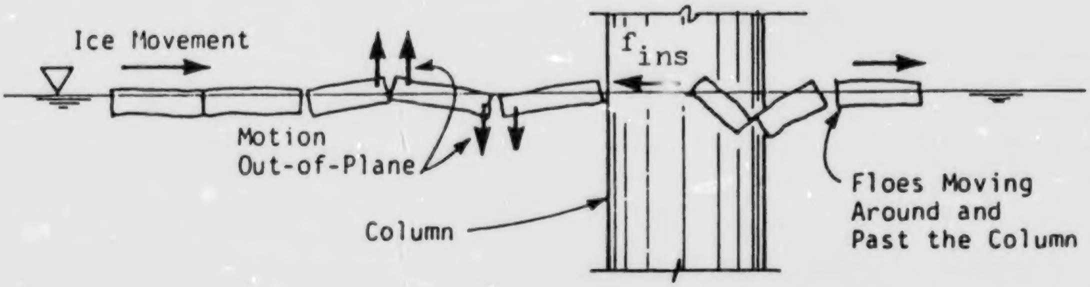
Ice Movement
f_{ins}
Motion
Out-of-Plane
Column
Floes Moving
Around and
Past the Column

Figure 2.13 Illustration of Broken Ice Instability

2.3.5 Ductile Failure of an Ice Sheet Surrounding a Structure

It is possible to estimate the stress at which first cracks will form in an ice ice sample based on Sinha's theory of the critical delayed elastic strain (reviewed in Sections 3.3 and 5.2.3.8 of Volume II). Sinha's theory has been applied to failure of ice at the transition from ductile to brittle failure and, in particular, to estimate the landfast ice "breakout" failure stress.

At breakout the sheet fails at the structure and the ice sheet begins to move. Based on estimates of wind speeds and durations Sanderson and Child (1986) proposed that it was reasonable that measured breakout stresses were equal to or less than about 1 MPa. After the formation of the first crack they proposed that ultimate failure of the ice would occur shortly thereafter.

In Figure 2.14 some data presented by Sinha (1985) and two estimates of the stress at first crack are illustrated.

Figure 2.14 can be used to estimate the strength of ice if the stress rate is known. Based on some simple calculations Sanderson and Child (1986) proposed that breakout failure pressures in the Canadian Beaufort Sea should be on the order of 1 MPa.

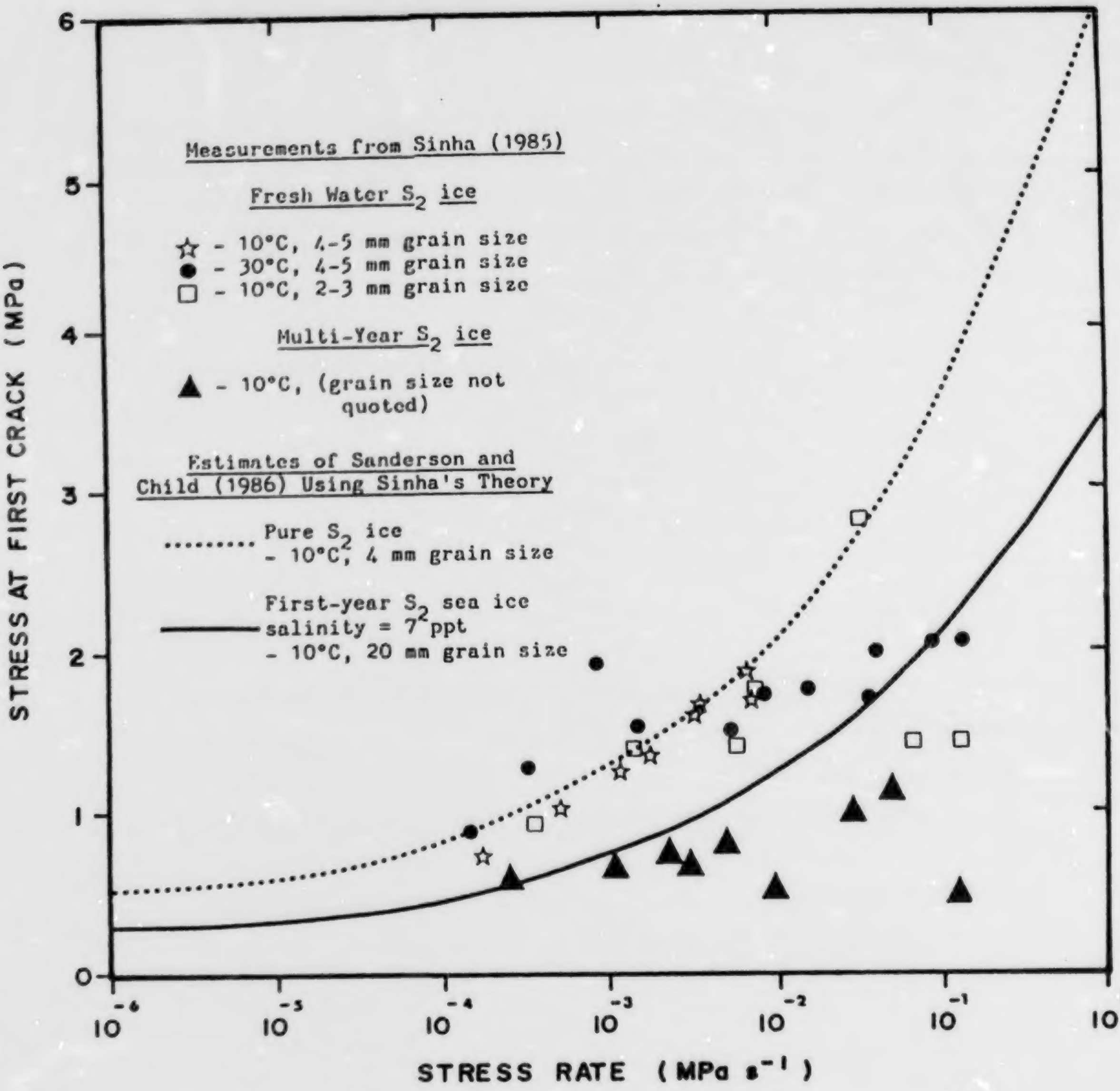

Figure 2.14 Comparisons of Measured and Calculated Stress at First Crack for Different Ice Types.

2.4 The Korzhavin Methodology of Calculating Ice Loads on Narrow Structures

In the laboratory the unconfined horizontal compressive strength of ice is usually measured. The Korzhavin Methodology relates laboratory measurements to failure pressures of ice on structures in the field. The reader is warned that there is a wide variety of interpretation of the Korzhavin Methodology in the literature.

The factors incorporated into the Korzhavin Methodology are:

- Indentation or confinement influence on the ice failure pressure,
- Contact at the ice/structure interface influence, and
- Shape of the interaction surface influence.

A velocity or strain rate term is also included in the methodology.

Two different representations of the Korzhavin Methodology are discussed below.

In both cases the user determines appropriate values for the indentation factor, I, the shape factor, M, and the contact factor, C. The ice failure pressure for the given situation is then calculated, and finally, the load on the structure is estimated.

2.4.1 The Indentation Factor: I

Timco (1984) presented the graph of the indentation factor, I, shown in Figure 2.15. The indentation factor is different for columnar and granular ice due to the different amounts of anisotropy.

For columnar ice I is equal to 3 for large aspect ratio's. For granular ice I is equal to approximately 1.

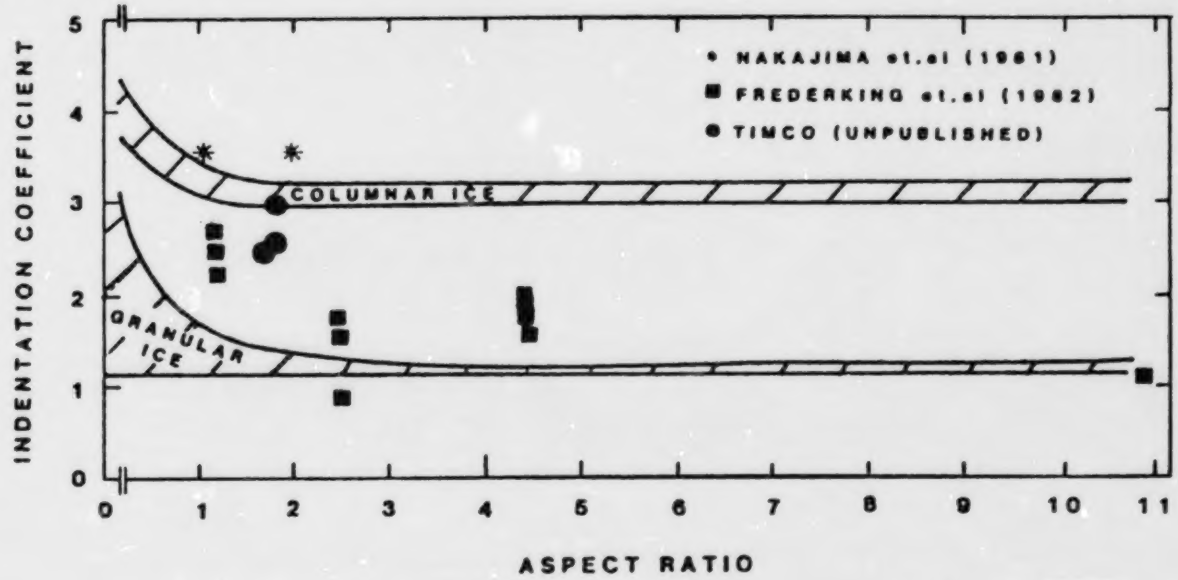

Figure 2.15 Indentation Factor for Columnar and Granular Ice (Timco, 1984)

2.4.2 The Contact Factor: C

The contact factor, C, is used to take into account the fact that the ice sheet will not be in contact with the structure over the whole width of the structure. The value of C is equal to 1.0 for perfect contact between the ice and the structure, and is of lessor magnitude for imperfect contact.

Korzhavin gave values of C dependent on the velocity of the ice as shown in Table 2.1.

Table 2.1

Values of the Contact Factor, C, From Korzhavin (1971)

Width of Support (interaction width) (m)	Velocity of Floe Movement (m/s)		
	0.5	1.0	2.0
3 - 5	0.70	0.60	0.50
6 - 8	0.60	0.50	0.40

For "frozen-in" conditions, or low strain rate interactions the contact factor is set equal to 1.0. For higher speeds of interaction the contact factor is less than 1.0 to account for a lack of perfect contact between the ice and the structure.

The Shape Factor: M

The shape factor M takes into account the difference between a "flat wall" structure and structures of other shapes. In Table 2.2 values of the shape coefficient from SNiP 2.06.04-82, the Soviet Construction Standards and Rules, Moscow, 1983, are shown.

Table 2.2

Values of the Shape Coefficient, From Soviet Construction Standards and Rules, Moscow, 1983.

Coefficient	Polyhedron (semi-circle)	Rectangle i.e. flat	Triangle with open angle in the horizontal plane (degrees)					
			45	60	75	90	120	150
M_1	0.90	1.00	0.54	0.59	0.64	0.69	0.77	1.00

2.4.4 Ductile Failure of an Ice Sheet Against a Narrow Structure

Consider a structure which will be exposed to both ice sheet ductile failure loads and impacts from moving floes. Timco (1986) has presented such an example, modeling the interaction of ice with a leg of a semisubmersible.

The objective of the analysis is to calculate the maximum ice load exerted on a semi-circular structure when the ice is failing in a ductile manner. The ice is assumed to be columnar, 0.5 metres thick. The structure has a width of 2 metres. The ice is moving, very slowly, at a rate of 0.5 m/hr.

Korzhavin Equation for Ductile Failure

In the ductile mode Timco used the following form of the Korzhavin equation:

$$L = C\,M\,I\,D\,t\,\sigma_u$$

where:

C = contact factor,

M = shape factor,

I = indentation factor,

D = chord width of interaction surface,

t = average ice thickness in contact with the structure, and

σ_u = uniaxial unconfined compressive strength of ice at the strain rate of interest.

Contact Factor

The ice fails in a ductile manner at lower strain rates (See Figure 3.1 in Volume II). The contact factor is set equal to 1.0, i.e. the ice and structure are in perfect contact.

Shape Factor

The shape coefficient is set equal to 0.9 at full envelopment.

Indentation Factor

At an aspect ratio of 4 (D = 2 m, t = 0.5 m) the indentation factor is estimated to be equal to 3. The columnar ice is more anisotropic than granular ice; the anisotropy of columnar ice gives the ice a greater indentation strength than granular ice. In Figure 2.15 values of the indentation factor from Timco (1984) are shown.

Strain Rate and Uniaxial Unconfined Compressive Strength of Ice

The strain rate appropriate for use is not exactly known, however Ralston's suggested estimate of V/2D is widely used. The unconfined uniaxial compressive strength of the ice is determined by the strain rate calculated using Ralston's formula.

Many relationships have been derived to estimate the strength of ice based on the strain rate of the interaction. Here the relationship measured by Sinha (1986), obtained for first-year ice at Mould Bay, will be used.

$$\sigma = 70.6\ \dot{\epsilon}^{0.335}$$

where:

σ = failure stress (MPa), and
$\dot{\epsilon}$ = strain rate (s^{-1}).

The above relationship is to be used below the transition from ductile to brittle failure, i.e. at strain rates below about $2 \times 10^{-3}\ x^{-1}$.

At strain rates above the brittle/ductile transition the strength can be assumed to remain at the maximum, or it can be assumed to decrease slightly.

For this example the strain rate is equal to:

$$V/2D = (0.5\ m/hr\ /\ 2\ m)\ /\ (3600\ s/hr) = 7 \times 10^{-5}\ s^{-1}.$$

Based on Sinha's relationship the unconfined uniaxial compressive strength of the columnar ice is equal to:

$$\sigma_u = 70.6\ (\ 7 \times 10^{-5}\ s^{-1}\ )^{0.335} = 2.86\ MPa$$

The Estimated Maximum Ice Load on the Structure

The estimated ice load on the structure at full envelopment is:

$$L = C\ M\ I\ D\ t\ \sigma_u$$

$$= 1.0 \times 0.90 \times 3.0 \times 2 \times 0.5 \times 2.86\ MN$$
$$= 7.7\ MN$$

2.4.5 Brittle Failure of an Ice Sheet Against a Semi-Circular Structure

Three of the values used in the Korzhavin Methodology are different when brittle failure is addressed.

Contact Factor

The contact factor is not equal to 1 but is less. The reduction in the contact factor accounts for the lack of perfect contact and non-simultaneous failure of ice at the ice/structure surface.

Indentation Factor

A common indentation factor used for columnar brittle ice failure is that proposed by Afanasev et al. (1973).

$I = [\ 5\ (D/t) + 1\ ]^{\frac{1}{2}}$ for $1 < D/t < 6$, and

$I = 4 - 1.55\ (D/t)$ for $D/t < 1$.

The contact factor is included in the determination of I in this case.

Ice Strength

The other factor which changes is the strength of the ice. In the case of brittle failure a predetermined or estimated strain rate is not used, but rather a representative maximum ice strength is used. Typically the strength is on the order of a few MPa, usually greater than 2 but less than 4.

Summary of Use of the Korzhavin Methodology

The Korzhavin Methodology acquired wide usage in the industry before large scale empirical data were available. These days empirical data are available to indicate what typical ice failure pressures are. In particular the data summarized and presented by Sanderson (1986) (shown in Figure 2.2 includes failure pressures measured by many researchers. Perhaps in the future it will be possible to use an empirical relationship, such as Sanderson's, to estimate ice loads on narrow structures as is done for wide structures. Having that ability would reduce much uncertainty in the estimated ice load due to the selection of the appropriate ice strength to include in a Korzhavin type analysis is a difficult task.

The Korzhavin Methodology is not used in global load estimation for large structures due to other effects which come into play on the large scale but are not observed on the small scale.

The Road and Transportation Association of Canada review of ice effects on bridges (Neill, 1981) examines in detail the problems of estimating ice loads on bridge piers. Where it is desired to estimate ice loads on narrow structures the RTAC report should as well be reviewed.

Ice/structure dynamics have not been examined herein. The Korzhavin procedure outlined above determines maximum ice loads, i.e. loads at full envelopment.

2.5 Suggested Calculation Procedures - Sea Ice

Multi-Year Ice Floes and Ridges Global Load

Wide Structures Only

- Determine chord width and average thickness of interaction surface to estimate the D/t ratio. Based on the value of D/t, estimate the failure pressure based on the large scale empirical estimates such as that shown in Figure 2.1. The product of the failure pressure, chord width and average thickness is equal to the load on the structure. The pressure-area relationship shown in Figure 2.2 can also be used as an estimate.

First-Year Ice Sheets Global Loads

Wide Structures

- Determine the product of chord width and ice thickness and multiply by 1.75 MPa (250 psi) to determine the first-year ice sheet load for ice of the same state as first-year Beaufort Sea ice.

First-Year Ridges

- Use the Croasdale shearing model, or the Prodanovic bearing capacity model to determine the load due to the unconsolidated portions of the ridge. Add to those values the product of chord width, thickness and assumed failure pressure of 1.75 MPa, for ice of the same state as first-year Beaufort Sea ice.

Narrow Structures

- Use of a Korzhavin-type methodology is recommended for consolidated ice failing against narrow structures. If empirical data are available for the same ice type and state, those data should be used as a guide.

Local Loads

- See Section 5.7 in Volume II.

3.0 Calculation Procedures for Calculating Ice Loads on Sloping Structures

3.1 General

A sloping structure is designed to fail ice by initiating a bending failure. There are at present many analytical models of the interaction of an ice sheet with a sloping structure, be it cone shaped (Ralston, 1977, 1979a, 1979b; Danys and Bercha, 1976; Edwards and Croasdale, 1976) or in the form of an inclined plane (Frederking and Timco, 1985; Frederking, 1979; Croasdale, 1980). Models of the interaction of an unconsolidated ridge with a sloping structure are not prevalent in the public literature due to the sloping structure having little advantage over a vertical sided structure (i.e. the loads are nearly the same). Unfortunately, the state-of-the-art of consolidated ridge/sloping structure interactions is such that the user is forced to use either simple analytical procedures or complicated computer models. There is little "middle ground" where the user can perform his or her own calculations for comparison purposes to the same extent as for ice sheet/sloping structure interactions or for consolidated ridge/vertical sided structure interactions.

Much of the theory of offshore sloping structures was developed during the 1970's when it appeared as if they could be more economical than vertical walled (or near vertical walled) structures such as the Gulf/Dome Tarsiut Caisson's, the Dome Petroleum SSDC, and the ESSO Caisson retained Island. Large scale verification of the analytical procedures is limited to large scale model tests. Smaller scale variation is limited to ice basin tests using both real and synthetic ice.

Sloping structures can break ice in one of two modes and are referred to as "upward-breaking" or "downward-breaking" depending on whether the ice is forced up out of the water or down into the water.

In general with respect to predicting ice loads, sloping structures can be categorized as being of the following types:

- conical structures with a relatively narrow superstructure,
- sloping structures with a wide superstructure, and
- downward-breaking sloping structures.

The three types are illustrated schematically in Figure 3.1.

Relevant sloping structure parameters for ice load calculations can be listed as:

- slope angle,
- ice to structure friction,
- water depth (limitation of thickness of ice feature),
- structure width,
- superstructure geometry, and
- whether the structure is upward or downward-breaking.

The main difference in the way ice forces are generated on the different types of sloping structures relates to the differences in clearing loads.

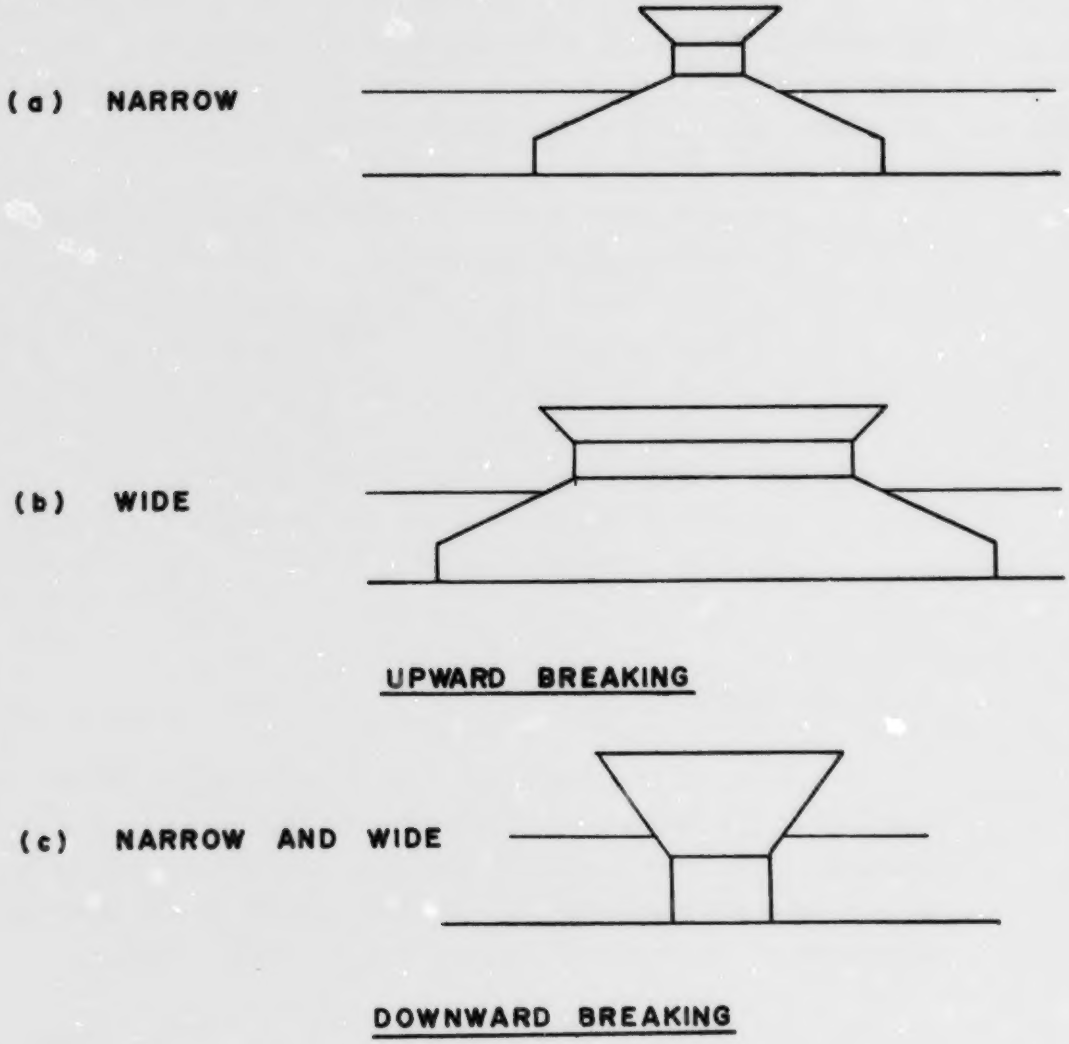
(a) NARROW
(b) WIDE
UPWARD BREAKING
(c) NARROW AND WIDE
DOWNWARD BREAKING

Figure 3.1 Types of Sloping Structures

3.2 Ice/Structure Load Scenario Calculations

An engineer must take into account several effects when calculating the ice loads exerted on sloping structures. The load on a sloping structure can depend on several geometrical properties of the structure. Some of the dependencies are:

- adhesion force depends on the slope angle, width and friction properties of the structure,

- ride-up force (or clearing load) depends on the slope angle, friction properties, width and freeboard of the structure,

- ice breaking force depends on the slope angle and friction properties, and whether the ice fails simultaneously across the width as it breaks.

3.2.1 The Adhesion Force

In calm conditions the ice is capable of adhering to the side of the structure. The bond has a large effect on the force the ice is capable of exerting on the structure. For instance, for thin ice sheets buckling may be more probable than breaking the adhesion bond due to the critical dependence of the buckling force on the ice sheet thickness.

The horizontal force necessary to break the adfreeze bond completely around a conical structure can be calculated as:

$$F_H \text{ necessary to break Adfreeze} = \frac{\pi\ t\ q\ D}{\sin(\alpha)\ \cos(\alpha)}$$

where:

t = the ice sheet thickness,

q = the adfreeze bond strength,

D = the waterline diameter of the structure, and

α = the slope angle of the structure.

Unfortunately, the adhesion strength of ice is less well documented than many of the other parameters. In Section 3.4.5 of Volume II the summary of adhesion strength by Cammaert et al., (1986) is presented. The research reviewed by them was performed on test piles, not sloping structures. There is a wide difference in strength between the results of different researchers. The strength has been shown to depend on ice salinity, stress rate, temperature and pile diameter. The reader should be warned that it may not be appropriate to use values such as these for designing a sloping structure. Croasdale (1980) used an adhesion strength of 700 kPa in his calculations.

Using Croasdale's value for the adhesion bond strength of 700 kPa it can be estimated that for a structure 100 m wide, bonded to a 2 m thick ice sheet, with a slope angle of 60° the adhesion bond strength is 1 GN. A structure of the same characteristics but with a 45° angle would have a bond strength of 880 MN. It is obvious that these forces are very large, and that for this reason perhaps sloping structures should only be constructed in regions where the probability of ice adhering to the structure is small, or alternatively where special measures are taken to ensure against adhesion such as low friction coatings or surface heating. Care should be taken not to ignore the possibility of ice failing at a lessor load such as crushing.

3.2.2 Ice Sheet/Sloping Structure Interactions

A properly designed sloping structure will break ice with minimum effort. The force necessary to break ice is directly proportional to the flexural strength of the ice. In order to optimize the structure careful account must be taken of the slope and friction characteristics.

In this section two methodologies will be reviewed. The first is that due to Croasdale (1980) where the motion of ice up an inclined plane is examined, and account is taken of the width of the structure. The second is that due to Ralston (1977, 1979a,b) where the interaction of sheet ice and a conical structure was modeled.

While the Croasdale theory is the simpler of the two methodologies and its results can only be considered as approximate compared to Ralston's theory, it is useful to review Croasdale's work due to it being much more transparent and easier to understand than that of Ralston.

3.2.2.1 Croasdale's Theory

The structure Croasdale (1980) examined was an inclined plane. The calculation was specifically for an inclined plane. Three-dimensional effects are accounted for by multiplying the two-dimensional ice breaking force component by a function of the characteristic length of the ice feature.

Two coefficients are first determined. The coefficients, labeled C_1 and C_2, depend on the characteristic length of the ice feature, the slope angle and the ice/structure friction coefficient.

$$C_1 = 0.68 \quad \frac{\sin(\alpha) + \mu\cos(\alpha)}{\cos(\alpha) - \mu\sin(\alpha)}$$

$$C_2 = \frac{[\sin(\alpha) + \mu\cos(\alpha)]^2}{\cos(\alpha) - \mu\ \sin(\alpha)} + \frac{\sin(\alpha) + \mu\cos(\alpha)}{\tan(\alpha)}$$

In the first coefficient the multiplier 0.68 is derived based on the following formula for the characteristic length:

$$l = [4\ E\ I\ /\ k]^{\frac{1}{4}}$$

If the following formula is used to calculate the characteristic length a multiplier of 0.962 is derived.

$$l = [E\ I\ /\ k]^{\frac{1}{4}}$$

where:

E = Young's Modulus, (7 GPa in the calculations),
I = the moment of inertia, $t^3/12$,
k = the foundation modulus, in this case the unit weight of water ($9.81\ m\ s^{-2} \times 1025\ kg\ m^{-3}$), and
t = ice sheet thickness.

The researcher should be aware of the two values for l. What is important to realize is that some "characteristic length" is used as a normalizing parameter. The characteristic length formula used to derive the value of 0.68 for C_1 is that used by Hetenyi (1946) and other researchers.

The horizontal force per unit width an ice sheet exerts on a structure is calculated as:

$$H/b = C_1 \ \sigma_f \ [\ \rho_w \ g \ t^5/E\ ]^{1/4} + C_2 \ Z \ \rho_i \ g$$

where b is the width of the structure, Z is the ride-up height (or freeboard for brevity), and ρ_i is the density of ice.

Values of the two coefficients as functions of the slope angle and friction coefficient are shown in Figure 3.2. Croasdale (1980) used values of the coefficients for angles between 20 and 70 degrees.

An Example

As an example consider a 50 m wide conical shaped structure sloped at a 30° angle, being impacted by an ice sheet 0.5 m thick. The freeboard of the structure is 10 m.

The following values are determined:

$C_1 = 0.60$
$C_2 = 1.76$

Horizontal Component of Breaking Force = 306 kN
Horizontal Component of Ride-Up Force = 4.0 MN
Total Load = 4.3 MN

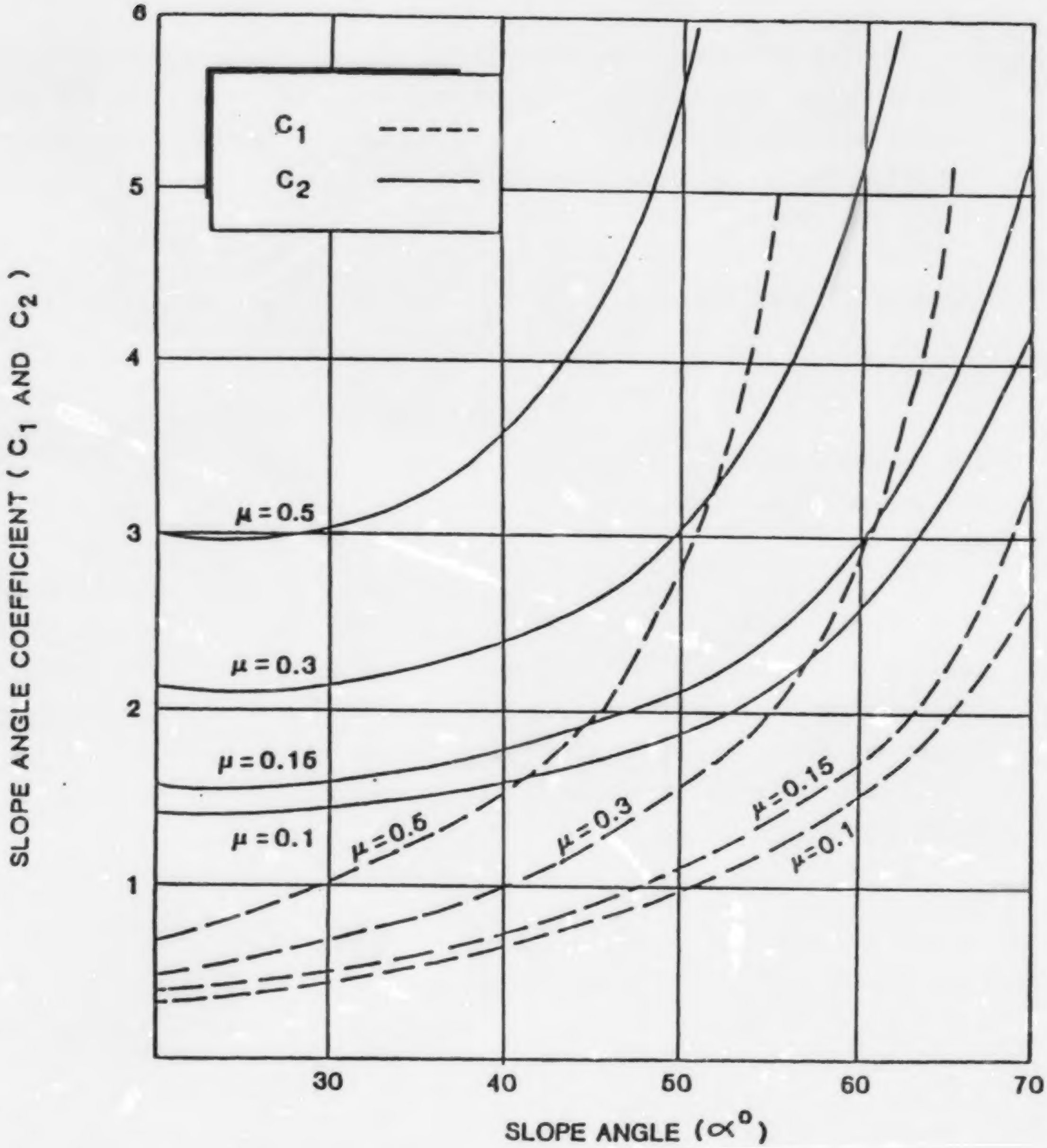

Figure 3.2 Values of the Two Coefficients C_1 and C_2 as a Function of Slope Angle

In this simple case the ice breaking force is small compared to the ride-up force. The calculation outlined above does not account for three-dimensional characteristics of the interaction. Croasdale suggested modifying the ice breaking force by a function of the characteristic length of the ice sheet:

$$\text{factor} = 1 + \frac{1}{4}\pi^2 \, l \, / \, b$$

where:

l = the characteristic length, and
b = the structure width.

For the structure examined above the characteristic length is about 15 m, so the factor would be 1.74 (i.e. the ice breaking component of the load is multiplied by 1.74). For such a thin ice sheet the characteristic length is small. For thicker ice sheets the characteristic length is much larger and therefore may be larger than the structure diameter. In the latter case the modification to the ice breaking component of the load becomes more significant.

3.2.2.2 Ralston's Theory

Ralston (1977, 1979) used an elastic/plastic analysis of the interaction of sheet ice with conical structures to determine the ice loads.

It is possible to computerize Ralston's results and determine loads based on input to a computer program, however, Ralston reduced the mathematical unpleasantries into graphical form for rapid calculation.

In Figure 3.3 the graphs from Ralston's work are presented. The six dimensionless coefficients are multiplied by ice characteristics to determine the load.

Consider the same example as that previously, the structure and ice parameters are reviewed in Table 3.1.

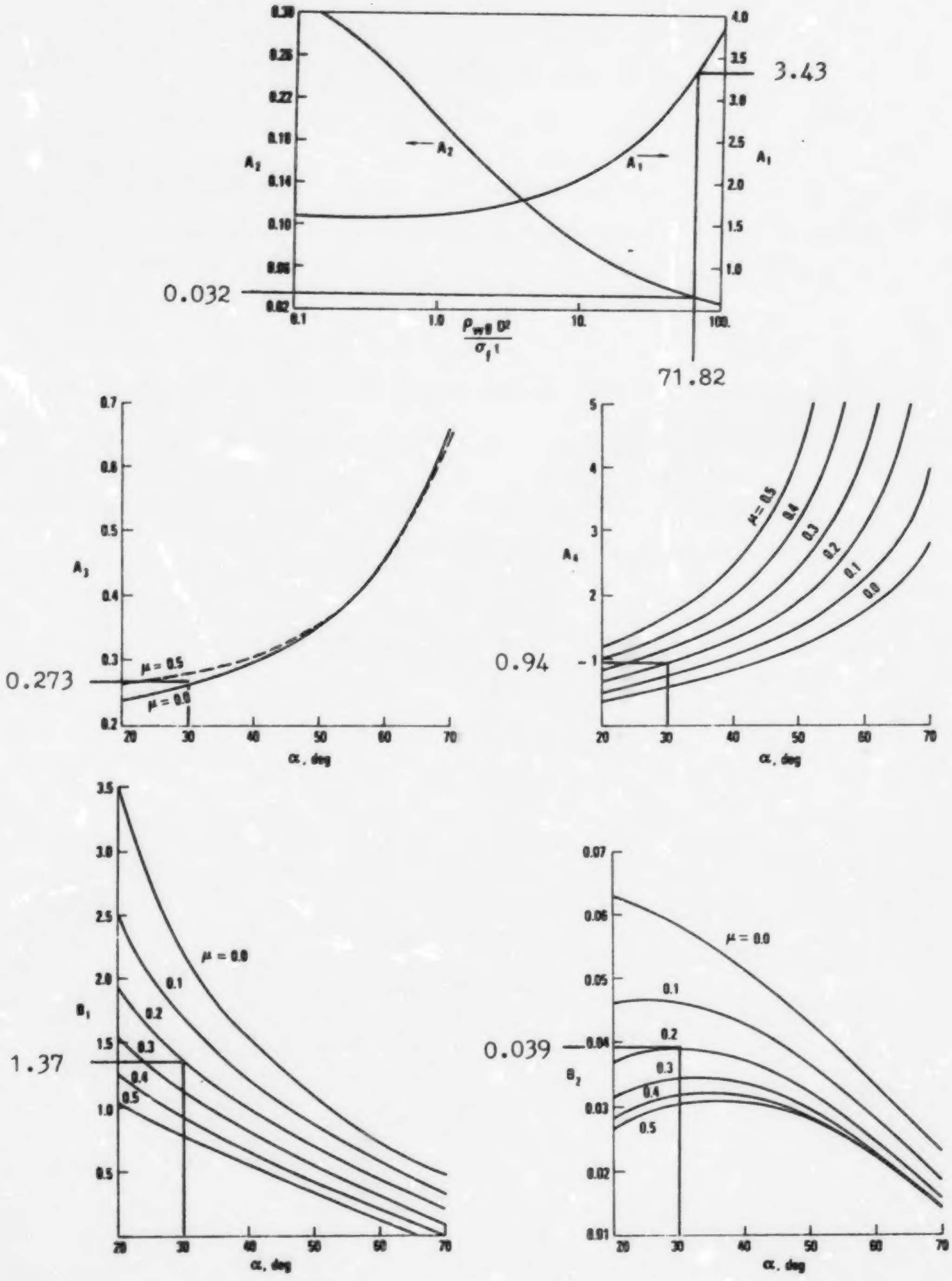

Figure 3.3 Coefficients to Determine Ice Forces on Conical Structures (Ralston, 1977).

Table 3.1

Example Parameters Used in the Ralston Methodology Analysis

Structure Parameters

Width:	50 m
Slope:	30°
Friction:	0.2
Freeboard:	10 m

Ice Parameters

Thickness:	0.5 m
σ_f:	700 kPa
E:	7.0 GPa
Density:	920 kg m^{-3} (actually, Ralston sets the density of ice to 90% the water density, so for a density of water of 1025 kg m^{-3} a value of 922.5 kg m^{-3} would be used).

$$\rho_w \; g \; D^2 \; / \; \sigma_f \; t \; = 71.82$$

The output and loads are shown in Table 3.2; Figure 3.3 shows how the coefficients were derived using Ralston's figures.

Table 3.2

Results of Analysis Based on the Ralston Methodology

Structure Top Diameter	15.4 m
Horizontal Force	3.86 MN
Vertical Force	5.71 MN

Horizontal Force Components:

Ice Sheet Breaking Force	0.94 MN
Ice Sheet Ride-up Force	2.92 MN

Values of Coefficients:

X-Axis for A_1 and A_2	71.82
A_1	3.431
A_2	0.032
A_3	0.273
A_4	0.939
B_1	1.367
B_2	0.039

3.2.3 Interaction of a Consolidated Ridge with a Sloping Structure

Ralston (1977) provided formulae and graphs to determine the vertical load on a conical structure needed to crack a consolidated ridge based on purely elastic failure. Two cracking conditions must be accounted for:

1 - initial cracking at the centre of the ridge, and

2 - hinge cracking away from the centre of the ridge.

The vertical loads for the two cracking conditions are:

$$R_{V,\ \mathrm{initial}} = 4\ I\ \sigma_f\ /\ y_t\ l$$

$$R_{V,\ \mathrm{hinge}} = 6.20\ I\ \sigma_f\ /\ y^{b}\,{}^{l}$$

where:

I = the moment of inertia of the ridge,
σ_f = the flexural strength of the ice,
$y_{t,b}$ = the distances from the neutral axis to the top and bottom of the ridge respectively, and
l = the characteristic length of the ridge $[\ 4\ E\ I\ /\ k\ ]^{\frac{1}{4}}$
where: E is the Young's Modulus and k is the foundation modulus (here taken to be the unit weight of water, 10055 Nm^{-3}.

The horizontal forces on the structure can be calculated using the ratio:

$$H = V \frac{\sin(\alpha) + \mu \cos(\alpha)}{\cos(\alpha) - \mu \sin(\alpha)}$$

The loads necessary to break a ridge are substantially higher than ice sheet loads. In Table 3.3 an example of the loads that a consolidated ridge may exert on a structure using Ralston's methodology are presented.

It should be realized that the ice feature must have, at the beginning of the interaction, sufficient energy to overcome dissipation of energy before the ridge cracks. To determine the amount of energy necessary use is made of incremental (i.e. computer program) analyses, or where simple analytical models are being used, integration of the energy dissipation equation is performed.

Table 3.3

Example Parameters Used in the Ralston Consolidated Ridge Analysis

---

Structure Parameters

Width: 50 m
Slope: 30°
Friction: 0.2
Freeboard: 10 m

Ridge Parameters

Thickness: 15.2 m
Width: 30.5 m
σ_f: 689 kPa (100 psi)
E: 7.0 GPa
Density: 920 kg m^{-3}

Characteristic Length: 160 m

Initial Crack Load: 20.5 MN (vertical)
Hinge Crack Load: 31.6 MN (vertical)

Initial Crack Load: 28.7 MN (horizontal)
Hinge Crack Load: 44.2 MN (horizontal)

3.2.4 Interaction of an Unconsolidated Ridge with a Sloping Structure

A sloping structure offers little advantage over a vertical sided structure for dissipating the load from an unconsolidated ridge. The reason for this is that the unconsolidated ridge is not capable of acting as a unit, and can conform to the shape of the structure.

Croasdale's formula (Croasdale, 1980) for shearing an unconsolidated ridge can be used to estimate the load.

$$L = \frac{2\,B\,t^2}{3} \left(\rho_w - \rho_i \right) g \tan(\phi)$$

where:

B = the width of the ridge,

t = the keel draft of the ridge,

g = 9.81 m s^{-2},

$\rho_{i,w}$ = densities of ice and water, 920 and 1025 kg m^{-3},

ϕ = internal angle of friction of the ridge, 45° is a reasonable assumption.

The load is independent of the width of the structure due to the assumed shearing motion removing a "plug" from the ridge, as shown in Figure 3.4.

If a consolidated layer is present in the ridge the user has two options. The consolidated layer can be assumed to fail according to the Croasdale Methodology, or the Ralston Methodology reviewed above.

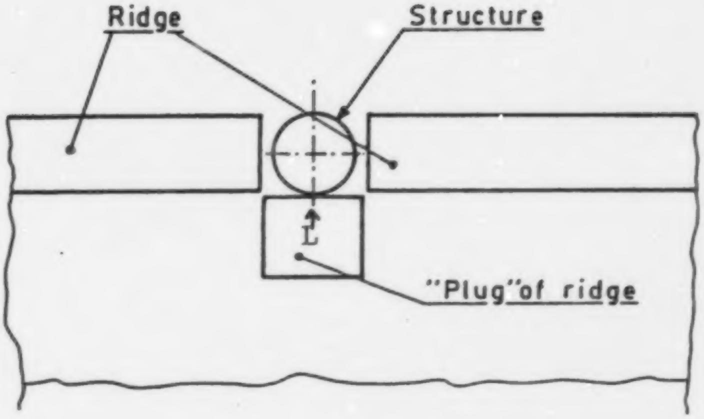
Ridge
Structure
L
"Plug" of ridge

Figure 3.4 Croasdale (1980) Shear Failure Analysis of an Unconsolidated Ridge.

4.0 Calculation Procedures for Calculating Ice Loads on Floating Structures

4.1 General

4.1.1 Introduction

The advantages of floating structures in environments where ice encroachment is minimal, are as follows:

- the cost effectiveness of the floating structure scenario,
- rapid field development due to shorter construction time by modifying structures,
- minimal demobilization costs caused by removal of the system after field development and subsequent abandonment.

The design of an ice resisting floating structure is governed by three considerations:

- the design ice conditions,
- the geometry of the structure, and
- the force limit that the ice is capable of generating or that the structure is capable of resisting.

In this section the types of floating structures, the geographic locations and their ice conditions, and the necessary data for analyzing the ice/floating structure interaction are described. A sample analysis is provided for a collision between an Arctic Class vessel and a bergy bit using the computer software developed in AOGA (Alaska Oil and Gas Association) Project 340.

4.1.2 Types of Floating Structures

In the 1970's successful operations were conducted from Dome Petroleum operated drillships in the Beaufort Sea. In 1983, a conical drilling unit operated by Gulf, the Kulluk, started operations in the Beaufort. The Kulluk is ice strengthened to the Arctic Class IV classification of the Canadian Arctic Shipping Pollution Prevention Rules. The Kulluk is designed for drilling on location in continuous ice of 1.2 metre thickness. With the help of ice management by icebreakers, the vessels are able to operate in harsher ice conditions.

The semisubmersibles drilling on the Grand Banks have not been ice strengthened and as such the rigs move off location whenever pack ice drifts south into the drilling acreage such as occurred a few years ago in the spring when a large section of pack ice drifted towards the region. Current technology, however, shows that these floating structures can perform in harsh combined wind, current, wave and ice conditions.

Several recent studies have investigated the use of floating structures in subarctic areas such as the Grand Banks and the Navarin Basin. Potential ice resisting configurations of floating systems include:

- catenary moored drillships,
- conical drilling unit,
- semisubmersibles with inverted conical collars,
- semisubmersibles with inclined columns,
- storage tankers with articulated moorings,
- shuttle tankers with articulated moorings,
- tension leg platforms with additional catenary mooring, and
- buoyant articulated loading towers.

These different systems are shown in Figures 4.1 to 4.8.

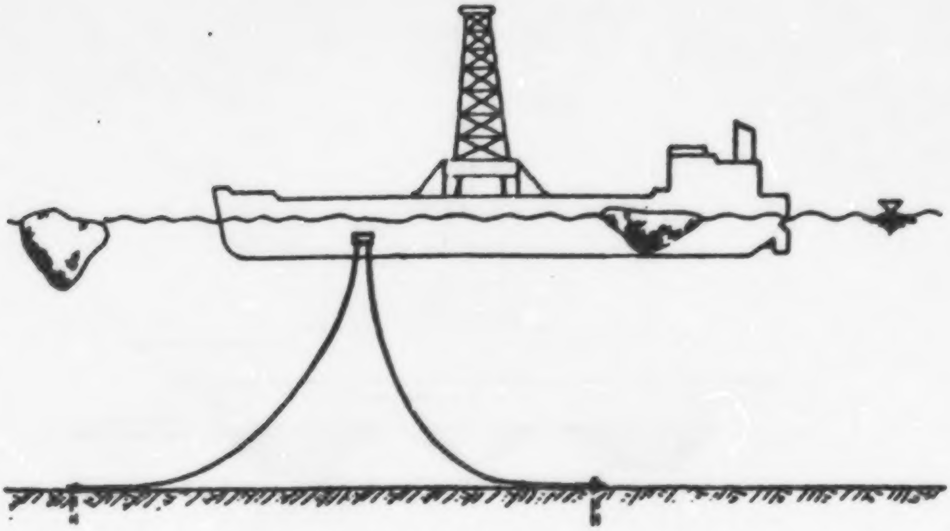

Figure 4.1 Illustration of a Catenary Moored Drillship.

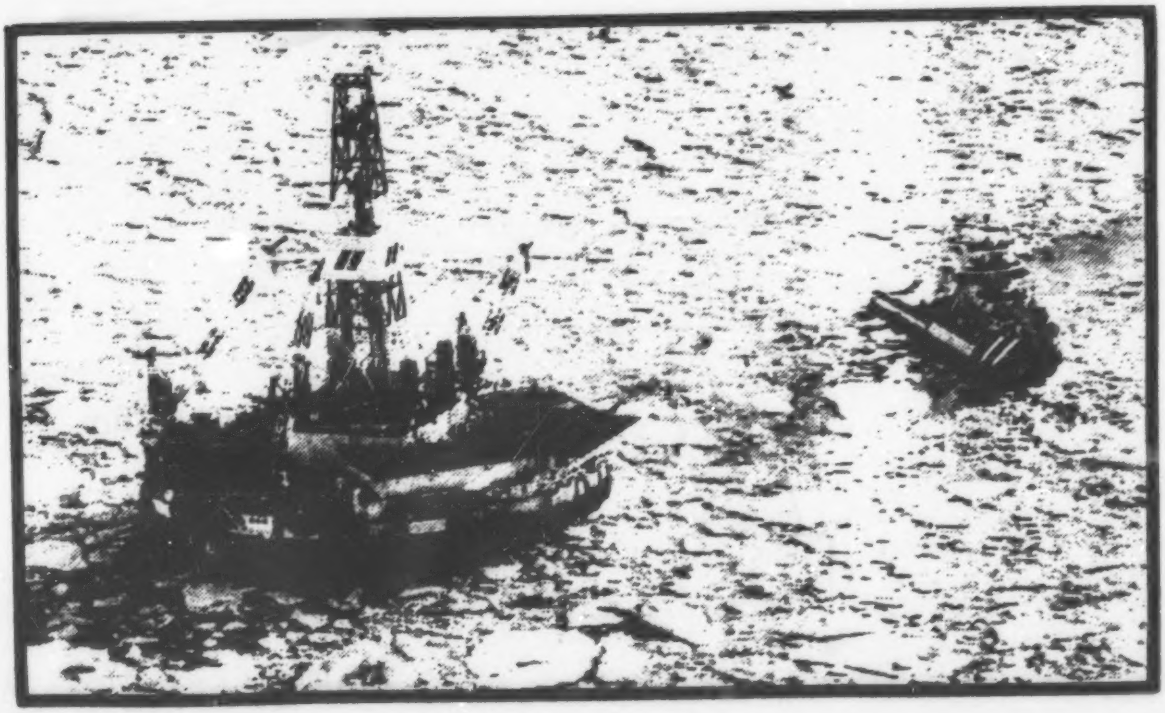

Figure 4.2 The Gulf Conical Drilling Unit, Kulluk, in Close Pack Ice.

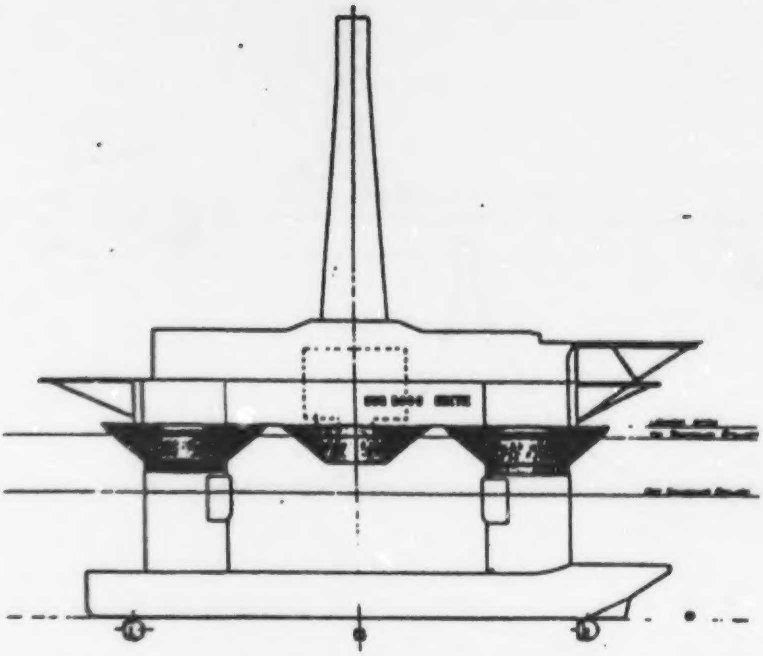

Figure 4.3 Illustration of a Semisubmersible with Inverted Collars.

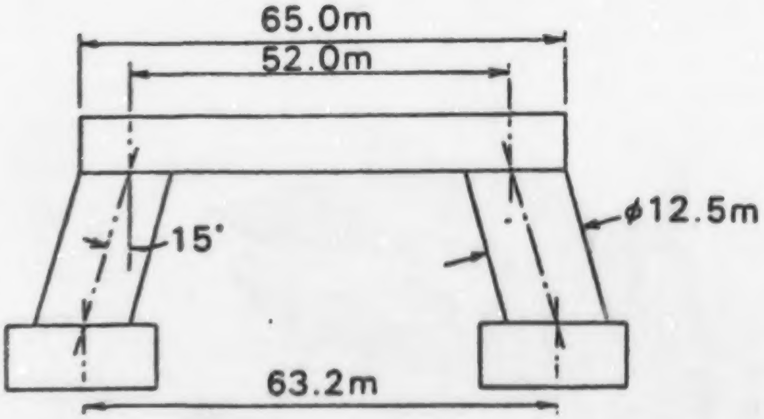
65.0m
52.0m
15°
ϕ12.5m
63.2m

Figure 4.4 Illustration of a Semisubmersible with Inclined Columns.

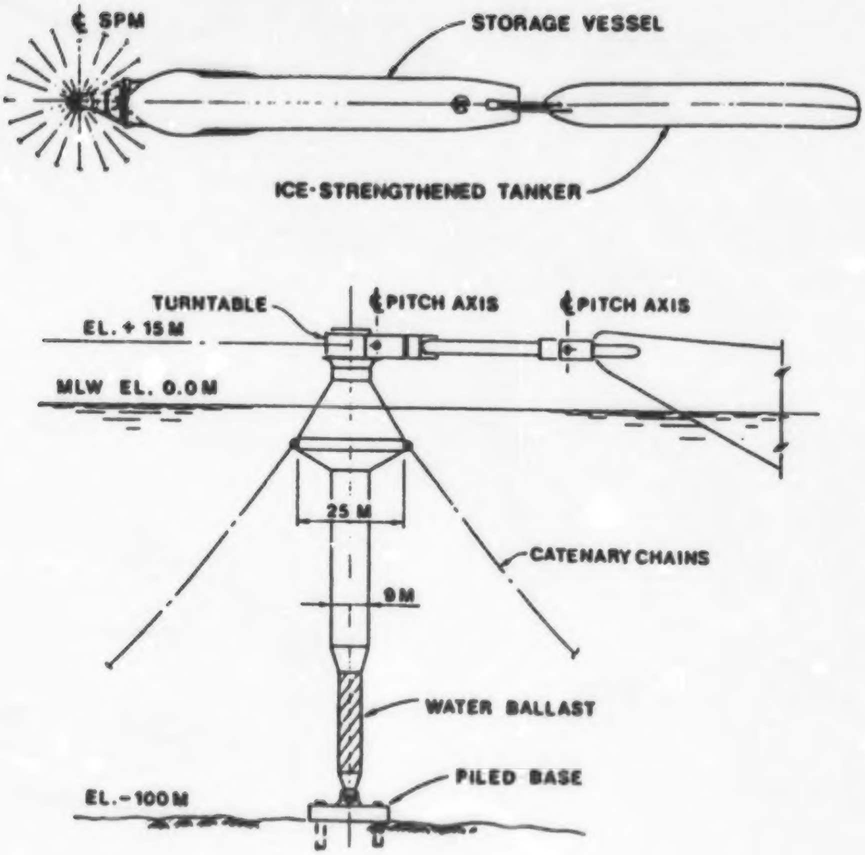
℄ SPM
STORAGE VESSEL
ICE-STRENGTHENED TANKER
TURNTABLE
℄ PITCH AXIS
℄ PITCH AXIS
EL. + 15 M
MLW EL. 0.0 M
25 M
CATENARY CHAINS
9 M
WATER BALLAST
PILED BASE
EL.-100 M

Figure 4.5 Illustration of a Storage Tanker with an Articulated Mooring.

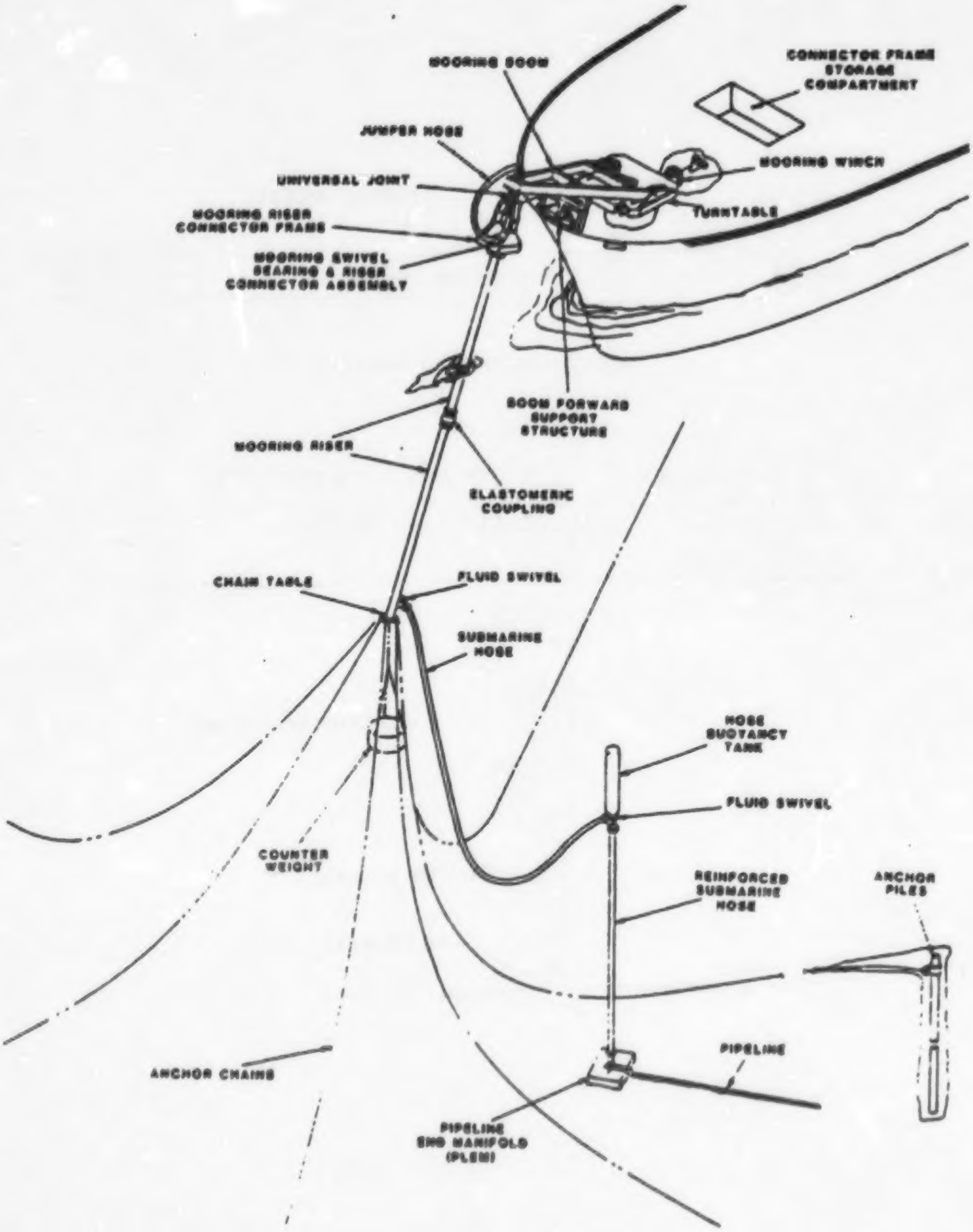
MOORING BOOM
CONNECTOR FRAME STORAGE COMPARTMENT
JUMPER HOSE
UNIVERSAL JOINT
MOORING WINCH
MOORING RISER CONNECTOR FRAME
TURNTABLE
MOORING SWIVEL BEARING & RISER CONNECTOR ASSEMBLY
BOOM FORWARD SUPPORT STRUCTURE
MOORING RISER
ELASTOMERIC COUPLING
CHAIN TABLE
FLUID SWIVEL
SUBMARINE HOSE
HOSE BUOYANCY TANK
FLUID SWIVEL
COUNTER WEIGHT
REINFORCED SUBMARINE HOSE
ANCHOR PILES
PIPELINE
ANCHOR CHAINS
PIPELINE END MANIFOLD (PLEM)

Figure 4.6 Illustration of a Shuttle Tanker with an Articulated Mooring.

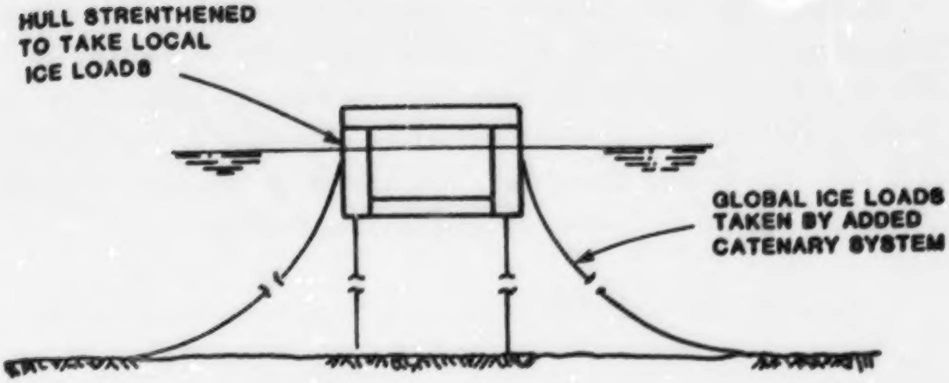
HULL STRENTHENED TO TAKE LOCAL ICE LOADS
GLOBAL ICE LOADS TAKEN BY ADDED CATENARY SYSTEM

Figure 4.7 Illustration of a Tension Leg Platform with Additional Catenary Mooring.

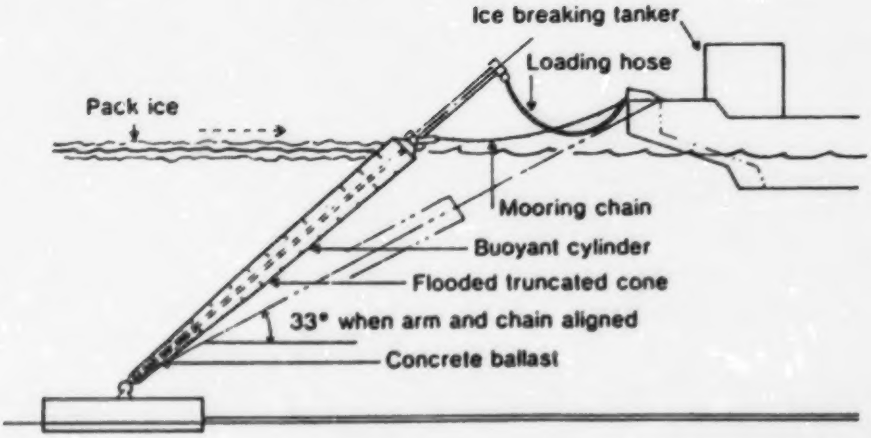
Ice breaking tanker
Loading hose
Pack ice
Mooring chain
Buoyant cylinder
Flooded truncated cone
33° when arm and chain aligned
Concrete ballast

Figure 4.8 Illustration of a Buoyant Articulated Loading Tower.

4.1.3 Ice Types

Although there is every indication that future floating structures may be developed and operate in more severe ice environments, current technology still only allows floating structures to perform in level ice and pack ice of various coverage. In general, it is essential to have an alert system which allows the structure to move off location in an orderly and safe manner when threatened with impact by the more imposing ice features such as multi-year or glacial ice features.

Pack ice and small individual ice pieces are important design ice types for floating structures. The data requirements for the two general types of ice are:

Pack Ice:

- thickness
- strength
- floe sizes
- velocity
- coverage
- jamming potential

Discrete Ice Pieces or Small Floes:

- underwater geometry
- leading edge geometry
- mass
- velocity
- strength

4.1.4 The Ice/Floating Structure Interaction

Intrinsically, the physics and the modes of failure and clearing of ice are the same whether the impeding structure is bottom founded or floating. For instance, if the predominant mode of ice failure is one of crushing, then the force generated on the structure, whether it be fixed or floating, will depend on factors such as the strain rate, the size and the shape of the ice to structure contact area, and the relative strengths of the ice and structure. The main difference between the ice induced behaviour of a floating structure and that of a fixed structure is the relatively large kinematic response of a floating structure. This arises from the compliancy of the mooring system.

The two major force levels required in an analysis of an ice/floating structure interaction are:

- the contact forces born by the local ice resisting elements, and
- the global forces developed by the restraining mooring system.

To describe the development of these forces, it is essential to consider also several other forces as follows:

- the inertial forces of the ice, the structure and their added masses,
- the hydrodynamic damping and drag forces on the ice and the structure,
- wind forces on the ice and the structure, and
- wave forces on the ice and the structure.

The ice and structure respond to these external forces according to the following equations of motion:

ice: $[M_i]\,(\ddot{x}_i) + [C_i]\,(\dot{x}_i) + [D_i]\,(\dot{x}_i^2) + [K_i]\,(x_i) = (F_s) + (F_{i,w\&w})$

structure: $[M_s]\,(\ddot{x}_s) + [C_s]\,(\dot{x}_s) + [D_s]\,(\dot{x}_s^2) + [K_s]\,(x_s)$

$= (F_i) + (F_{s,w\&w}) + (F_m)$

where the subscripts "i" and "s" refer to ice and structure respectively,

$[M]$ = virtual mass (mass + added mass) matrix
$[C]$ = matrix of linear drag coefficients
$[D]$ = matrix of hydrodynamic drag coefficients
$[K]$ = hydrostatic stiffness vector

$(\ddot{x})$ = acceleration vector for surge, sway, heave, roll, pitch, and yaw

$(\dot{x})$ = velocity vector
(x) = displacement vector

(F_i) = vector of ice forces on the structure
(F_s) = vector of structure forces on the ice, equal and opposite to (F_i)
$(F_{w\&w})$ = vector of wind and wave forces
(F_m) = vector of mooring forces

In the following subsection the ice force calculation considerations are described in terms of three basic data sets:

- description of the interaction geometry and ice properties,
- description of the floating structure properties, and
- description of other environmental conditions of current, winds and waves.

4.2 Ice Force Calculation Considerations

4.2.1 Interaction Geometry and Ice Properties

The interaction geometry consists of the direction and the speed of the oncoming ice feature and the orientation of the floating structure with respect to the oncoming ice. In Figure 4.9 the interaction geometry data for a semisubmersible and an SPM (Single Point Mooring) moored ship in pack ice and ice impact conditions are shown.

Ice properties required for a calculation of the ice forces on a floating structure include:

For a pack ice scenario:

1. Sheet ice thickness if the ice pack is a continuous sheet.
2. Ice floe thickness, ice floe diameter and ice coverage if the ice pack is broken.
3. A factor describing the possibility of broken ice arching across the legs of a semisubmersible or the space between the SPM buoy and the ship. This factor is dependent on the percentage of ice coverage as described in of Volume II.
4. The crushing pressure of ice. On a semisubmersible, this includes the maximum crushing pressure on one leg and the average pressure on a number of legs in contact with ice.
5. The flexural strength of ice if the structure surface is sufficiently inclined so that bending failures may be induced in the ice.

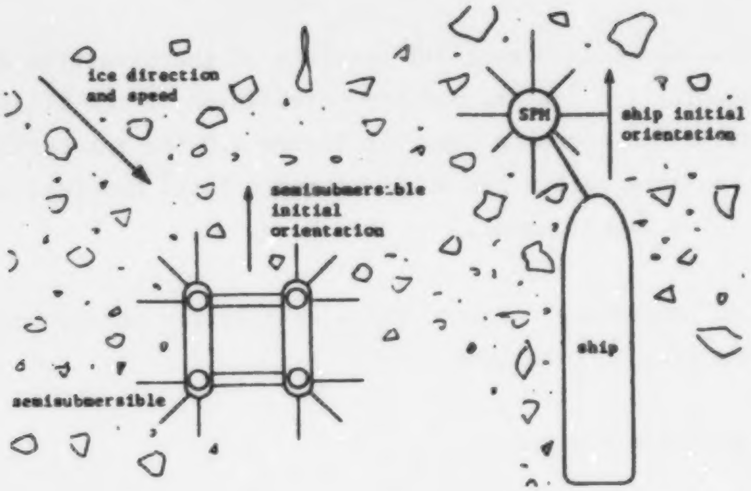
ice direction and speed
semisubmersible initial orientation
semisubmersible
SPM
ship initial orientation
ship

a. Pack ice

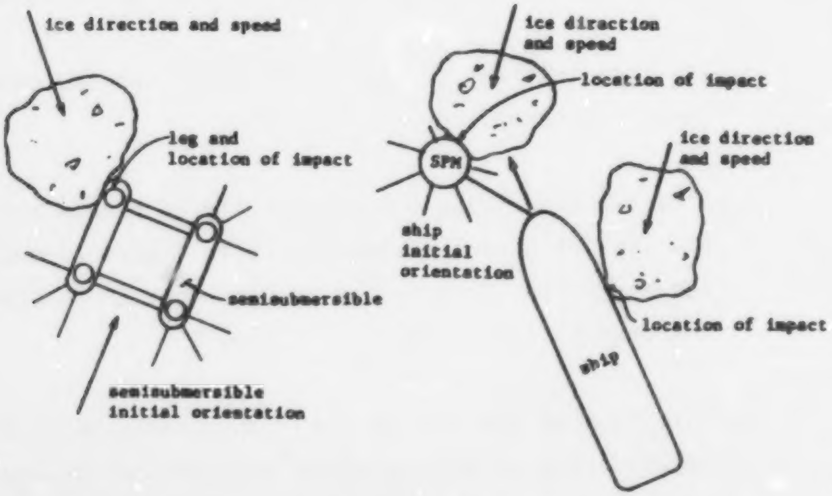
ice direction and speed
leg and location of impact
semisubmersible
semisubmersible initial orientation
ice direction and speed
location of impact
SPM
ship initial orientation
ice direction and speed
location of impact
ship

b. Collision with an individual ice feature

Figure 4.9 Interaction Geometries for Semisubmersibles and SPM (Single Point Mooring) Systems.

6. If the flexural strength of ice is not available, data on brine volume can be used to estimate the flexural strength based on empirical equations.

7. The coefficient of friction between ice and structure.

For an ice impact scenario:

1. The impact ice failure strength parameters. These include coefficients to describe the strain rate dependency, the relation between failure mode and ice contact aspect ratio, the unconfined and confined compressive strengths, and the tensile strength.

2. Ice feature geometry. This includes sail and keel angles, leading edge thickness, as well as overall dimensions.

3. The coefficient of friction between ice and structure.

4. The hydrodynamic surface drag and form drag coefficients:

$$F_{current} = 0.5 \ \rho_w V^2 (C_{d,form} Ap + C_{d,surface} As)$$

where:

$F_{current}$ = hydrodynamic drag force on ice feature,
ρ_w = density of sea water,
V = current speed,
$C_{d,form}$ = form drag coefficient,
Ap = projected area of ice feature in the direction of motion,
$C_{d,surface}$ = surface area drag coefficient, and
As = wetted surface area.

5. The air drag coefficient:

$$F_{wind} = 0.5\ C_{10}\ \rho_a\ V^2\ A$$

where:

F_{wind} = wind force on ice feature,
C_{10} = air drag coefficient,
ρ_a = air density,
V = wind speed, and
A = surface area of the ice feature exposed to the wind.

6. The added mass coefficients. The important added mass directions are the translations and out-of-plane rotations. Expressions for added masses of various geometric shapes are given by Brennen (1982). More complex treatments of analyzing the motion of ice feature in sea states are presented by Kristensen et al., (1983) and Squire, (1983).

4.2.2 Description of the Floating Structure Properties

The properties of the floating structure that require consideration in an ice interaction analysis may be grouped into the following categories:

- inertia
- geometry
- mooring
- hydrodynamics
- wind resistance
- local ice resisting construction details

The first five groups of data relate to the overall motion of the floating structure which ultimately determines the development of the restraining forces in the mooring system. The last group relates to the ice contact force and determines whether the structure would suffer local damage under ice impact. It also influences the strain rate in the ice feature during the collision.

There is a wealth of references on the calculation of the sea state motion of ship-shaped vessels including the recent work by Wichers, (1986). For semisubmersibles, Takagi et al., (1985) gave a comparison of methods for calculating motions of this class of vessels in waves, and Reddy et al., (1982) reported on the calculation of the motion of semisubmersibles in wind, current and waves.

Inertia

Data necessary for the calculation of inertial effects of the floating structure are:

- displacement of the structure,
- the radii of gyration in roll, pitch and yaw, and
- cross product rotational moment of inertia.

Additional information for the evaluation of stability are the locations of the centres of gravity, buoyancy and the metacentres in the longitudinal and the transverse directions.

Geometry

The submerged geometry of the floating structure is required for the consideration of hydrodynamic effects:

- the projected areas and the surface areas, and
- the draft.

The near waterline geometry is required for the determination of the hydrostatics as well as for the determination of the ice failure modes:

- the water plane area and its moment of inertia, and
- the angle that the structure surface makes with the vertical.

Mooring

Lateral restraint of floating structures is provided by catenary moorings to the seabed or by hawsering or yoking to single point moorings. Data descriptions of catenary moorings are

- the stiffness properties of the lines,
- the weight of the lines,
- the pretensioning and the ultimate strength of the lines,
- the location of the fairleads, and
- whether the fairlead is on a turret.

The force analysis of catenary moorings is highly nonlinear, particularly in severe waves when dynamic effects may be significant. Recent progress in this area includes work by Palo (1985).

Hydrostatics and Hydrodynamics

The hydrostatic restoring forces on floating structures are buoyancy forces and can be calculated from the geometry data described above.

Due to the scarcity of field data, the procedures to account for the hydrodynamics of a floating structure are still very much in debate. This section is intended to cite state-of-the-art approaches. Elaboration of specific terms may be found in the references noted.

There are two components in the hydrodynamic force, the drag force imposed by the current and the damping force associated with the influences of the previous histories of motion of the vessel. A methodology for treating hydrodynamic effects on a moored ship that accounts for both the current drag force and the damping of the vessel is given by Wichers (1986). The data requirements for this approach are:

- underwater geometry of the vessel as described above,
- sets of longitudinal, transverse and yaw moment resistance coefficients and surge damping coefficients for drag force and damping force calculations, and
- added mass coefficients, which may be calculated by methods set out by Muga et al., (1977), for inertial force calculations.

Alternatively, the approach described by Muga et al., (1977) requires that the current drag force be calculated independently in a fixed global system and the damping and inertia effects be calculated in the coordinate system of the moving vessel. For the current drag force determination, the document compiled by The Oil Companies International Marine Forum (OCIMF,1976) gives current force coefficients derived from model tests on three types of tankers.

The data requirements for Muga's approach are

- a set of impulse response functions for damping force calculations,and
- a set of constant inertia coefficients for inertial force calculations.

For semisubmersibles, the overall hydrodynamic properties can be approximated by summing the properties of the submerged elements obtained by the method described by Brennen (1982). Other references include experimental results on hydrodynamic coefficients for a range of semisubmersible models presented by Kishev et al., (1985).

Wind Resistance

Wind forces on a ship can be calculated from the method described in the Oil Companies International Marine Forum publication. Force and moment coefficients were developed from data obtained in wind model tests for very large crude carriers.

For semisubmersibles, Sahin et al., (1985) compared empirical methods with wind tunnel testings. They concluded that for preliminary designs, calculations following classification rules such as the ABS (American Bureau of Shipping) or the DnV (Det norske Veritas) rules are acceptable, whereas for economical final designs, wind tunnel testing is preferred.

Local Ice Resisting Construction Details

The properties of the structure in the ice interaction zone affects the ice force felt by the floating structure in essentially two manners:

- the dynamic behaviour of the structure which influences the failure sequence in the ice (Section 5.6 of Volume II), and
- the compliance of the structure which directly limits the attainable ice force.

For a steel floating structure, the information required for the calculation of the dynamic and the compliance properties of the ice zone are:

- the thickness of the hull plate,
- the dimensions of the web and the flange of the plate stiffeners,
- the dimensions of the web and the flange of the web frames,
- the spacings of the plate stiffeners and the web frames,
- the spacing of bulkheads,
- the yield, the ultimate, the buckling strengths and strains of the various structural elements, and
- the strengths of various connections.

The Canadian code containing rules for the design of ice resisting steel hulls is the Canadian Arctic Shipping Pollution Prevention Regulations (CASPPR). Member sizing for hulls subject to ice pressures are based on Schedules E and F of the Arctic Waters Pollution Prevention Act (AWPPA, 1981).

The procedure followed by the CASPPR rules consists of four steps:

1. Define an ice class for the vessel. The AWPPA has a map showing the Arctic zones and the corresponding dates of permitted entry by the various classes of vessel.

2. Define the design ice pressures for each of the three zones of the vessel, namely the bow, the midbody and the stern.

3. Specify a minimum allowable section modulus of the main framing elements and the web frames based on the element spans, the yield strengths and the design ice pressures.

4. Specify a hull plate thickness based on the span, the yield strength and the design ice pressure.

In Table 4.1 a comparison of sizes for selected elements in the midbody of vessels in several ice classes is presented.

The assumed framing layout is:

hull stiffener spacing 400 mm
web frame spacing 1200 mm
web frame span 6480 mm
yield strength 350 Mpa

Table 4.1

Sizes of Selected Elements Based on the
Canadian Arctic Shipping Pollution Prevention Regulations (CASPPR).
Based on the Proposed Framing Layout.

CASPPR Class		1	4	10
Hull plate thickness	(mm)	12	31	37
Flat bar stiffener:				
height	(mm)	119	222	250
thickness	(mm)	13	24	27
Web frame:				
web depth	(mm)	1080	1296	1620
web thickness	(mm)	15	17	20
flange width	(mm)	287	326	383
flange thickness	(mm)	15	17	20

4.2.3 Description of Other Environmental Conditions

In the design of floating structures, environmental conditions other than ice are equally important considerations. Detailed discussions of the forces generated by current, wind and waves are not included here.

Current

The speed and direction of the current with respect to the structure orientation is required. Methods of calculating current drag forces on the floating structure and the ice feature are as described above.

Wind

The speed and direction of the wind with respect to the structure orientation is required. Methods of calculating wind drag forces on the floating structure and the ice feature are as described above.

Waves

The wave amplitude, period and the direction of the wave train are required. State-of-the-art methods of calculating the motions of a vessel in waves are in the references cited above.

4.3 The Interaction of a Bergy Bit with an Arctic Class IV Vessel

The sample analysis is for an interaction between an Arctic Class IV vessel and a bergy bit using the computer software developed for AOGA Project 340, and as generally described in the previous sections of this report.

4.3.1 Vessel

The vessel is an Arctic Waters Pollution Prevention Regulations Class IV 200,000 DWT tanker of length 310 metres. The body plan is shown in Figure 4.10.

The ice zone construction details of the vessel midbody as generated according to AWPPA Class IV specifications are shown in in Table 4.2.

The vessel is turret moored in a water depth of 300 metres. The 0.13 tonne per metre mooring lines are anchored 1000 metres in plan from the fairleads. The effective cross section area and the elastic modulus of the lines are taken to be 9000 mm^2, and 150,000 Mpa respectively. A pretensioning of 150 tonnes is assumed. The turret is located at 30 metres forward from the vessel centre of gravity and is 10 metres in diameter.

The configuration of the vessel and mooring is shown in Figure 4.11.

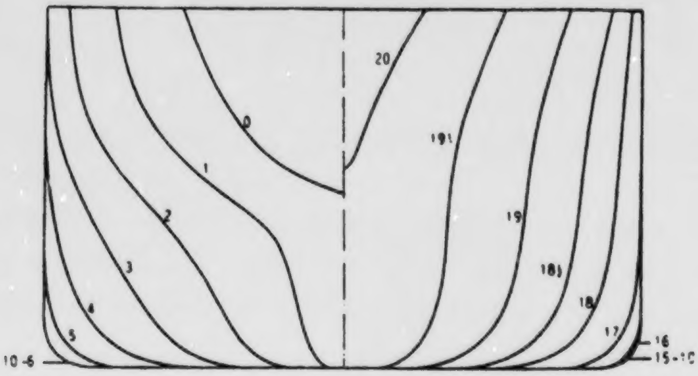
20
0
191
1
2
19
3
181
18
4
17
5
16
10-6
15-10

Figure 4.10 Body Plan of a 200,000 DWT Tanker.

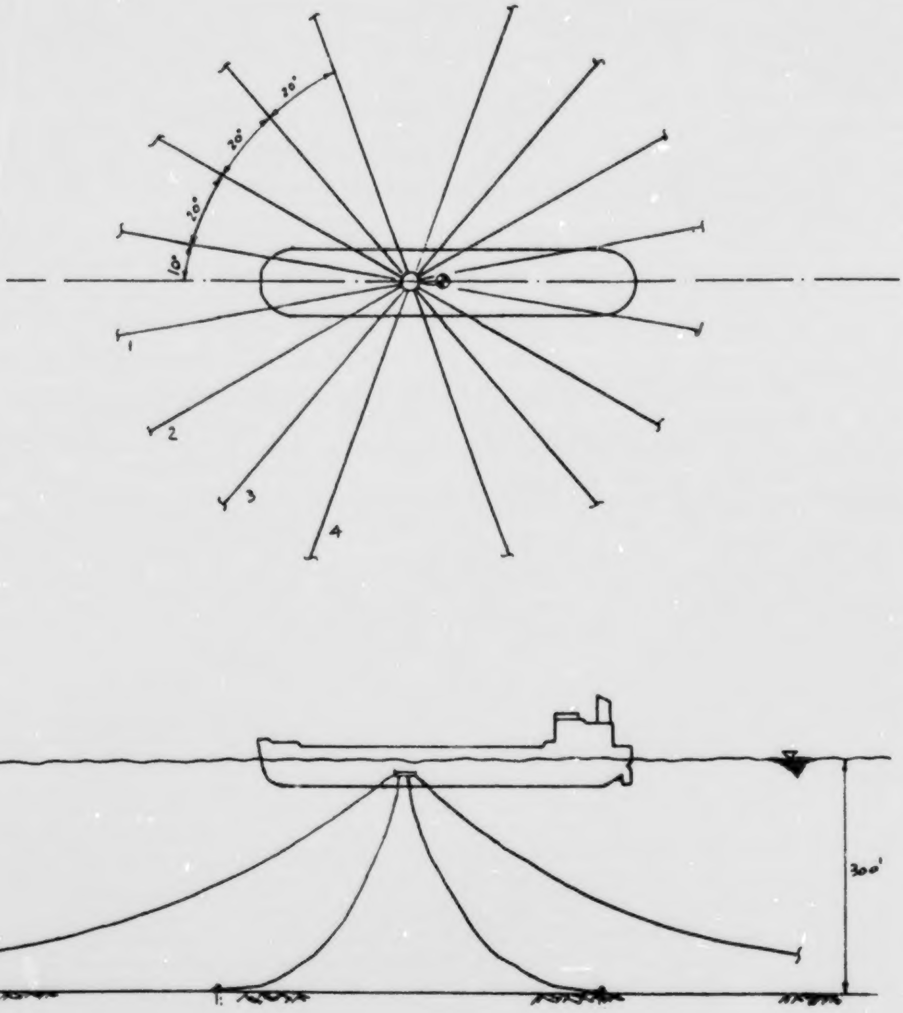
20°
20°
20°
10°
1
2
3
4
300'

Figure 4.11 Configuration of Vessel and Mooring System Used in the Analysis.

Table 4.2

Vessel Midbody Criteria for an Arctic Water Pollution Prevention Regulations Class 4 Vessel

Hull plate	
thickness	16 mm
Hull stiffener	
spacing	200 mm
web thickness	10 mm
web depth	96 mm
minimum section modulus required	32500 mm^3
actual section modulus	34272 mm^3
Web frame	
span	5400 mm
spacing	500 mm
web thickness	11 mm
web depth	1080 mm
flange thickness	11 mm
flange width	211 mm
minimum section modulus required	4643700 mm
actual section modulus	5510500 mm
Yield strength	350 Mpa

4.3.2 Ice

The ice feature is a 20640 tonne glacial ice piece, moving at 1 m/sec at 45 degrees clockwise from the surge direction of the vessel. The impact is on the midbody of the vessel, 30 metres forward of the vessel centre of gravity.

The geometry of the ice feature is shown in Figure 4.12.

The ice strength parameters are as follows:

- Unconfined compressive strength: 7.43 Mpa
- Confined to unconfined compressive strength ratio 1.13
- Tensile strength 1.17 Mpa

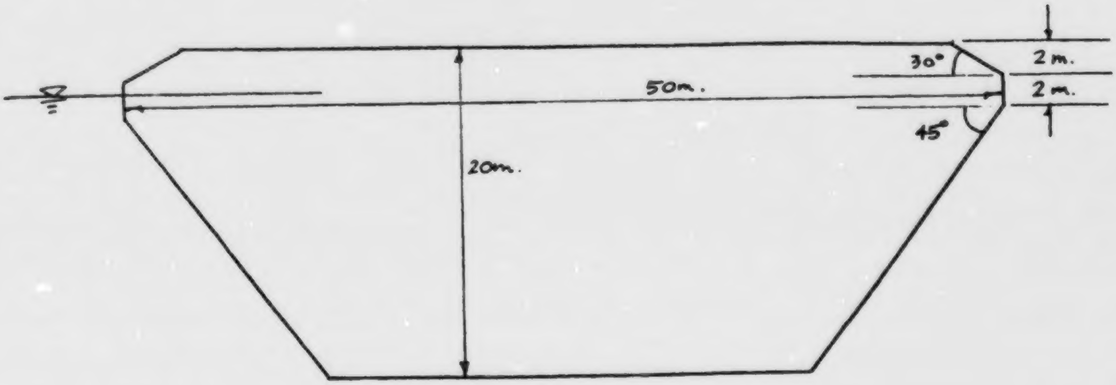
30°
2 m.
50m.
2 m.
45°
20m.

Figure 4.12 Schematic of Ice Feature Used in the Analysis.

For this example the assumed crushing strength dependence on strain rate is as follows:

$$Sc/So = 1.92 + 0.348 \log(\dot{\epsilon}) \quad \text{for } \dot{\epsilon} < 2 \times 10^{-3}$$

$$Sc/So = -0.235 - 0.457 \log(\dot{\epsilon}) \quad \text{for } \dot{\epsilon} > 2 \times 10^{-3}$$

where:

Sc = Crushing strength of ice
So = Crushing strength of ice at $= 2 \times 10^{-3}$
$\dot{\epsilon}$ = strain rate

Note that any variable strength relationship may be input into the analysis and the above relationship has been used here only due to convenience for illustrative purposes.

The friction coefficient between ice and structure is assumed to be 0.3.

4.3.3 Other Environmental Data

Winds, waves and currents are set to zero for this example.

4.3.4 Sample Analysis

The ice/vessel interaction is analyzed by the use of the computer program. The following plots are obtained from the analysis, showing the developments of the local ice/vessel contact force and the global mooring restraint force.

Figures 4.13 and 4.14 show the build-up of the ice contact pressure and force. The collision lasted just short of 1 second, during which the local force normal to the hull reached over 40 MN, developed on an area of 2.3 metres deep by 9 metres wide (Figures 4.15 and 4.16).

Figures 4.17 and 4.18 show the time histories of the global mooring restraining forces on the vessel. The maximum forces were reached some 30 seconds after the collision was over. Note that most of the ice impact force is taken up by the inertial effects and the mooring forces eventually developed were only a small fraction of the maximum ice impact force. Figure 4.19 shows the forces in mooring lines number 1 to 4 (see Figure 4.11).

Figures 4.20 and 4.21 show the time histories of the vessel displacements and velocities. A large portion of the vessel motion occurred after the impact with the ice feature.

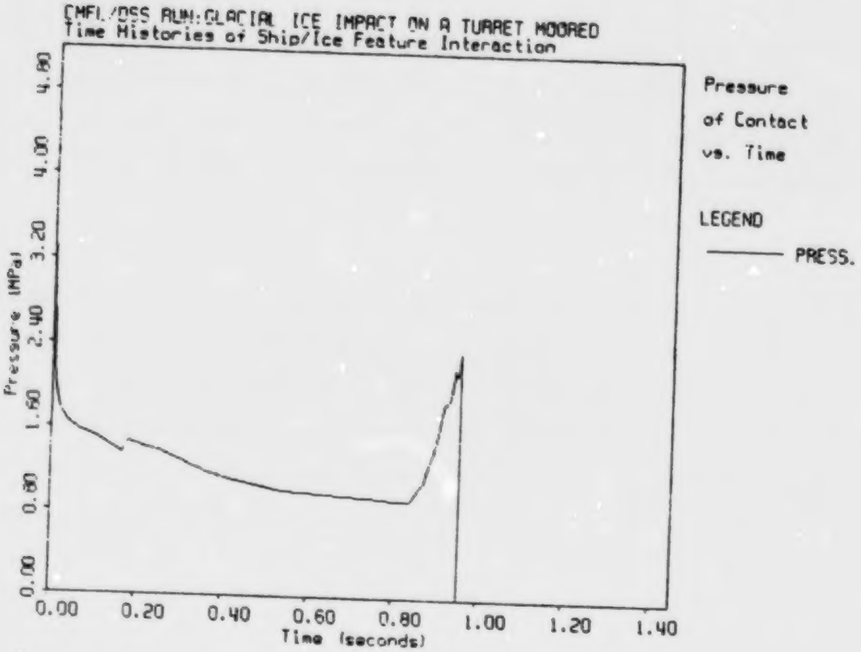

Figure 4.13 Ice/Vessel Contact Pressure.

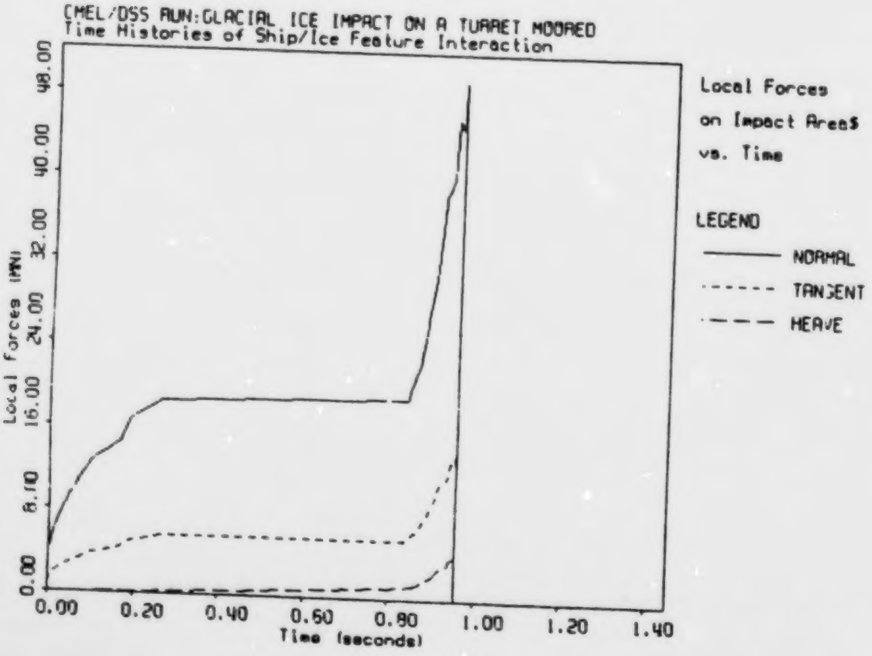

Figure 4.14 Ice/Vessel Contact Force.

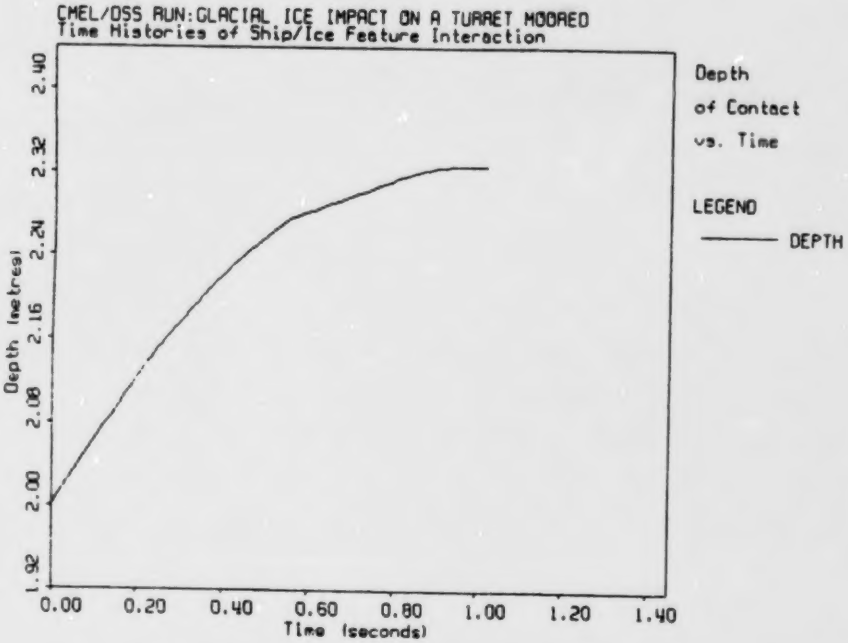

Figure 4.15 Ice/Vessel Contact Depth.

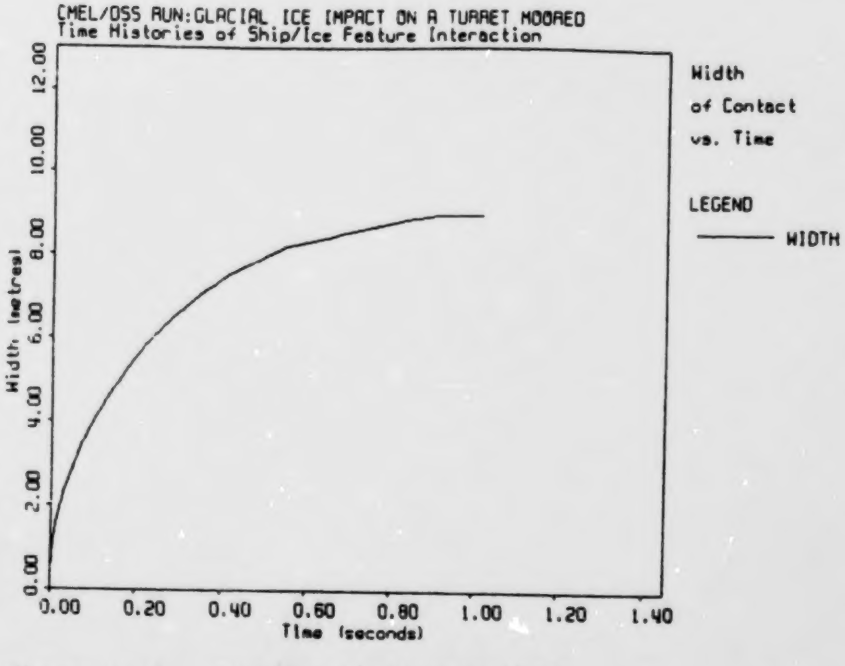

Figure 4.16 Ice/Vessel Contact Width.

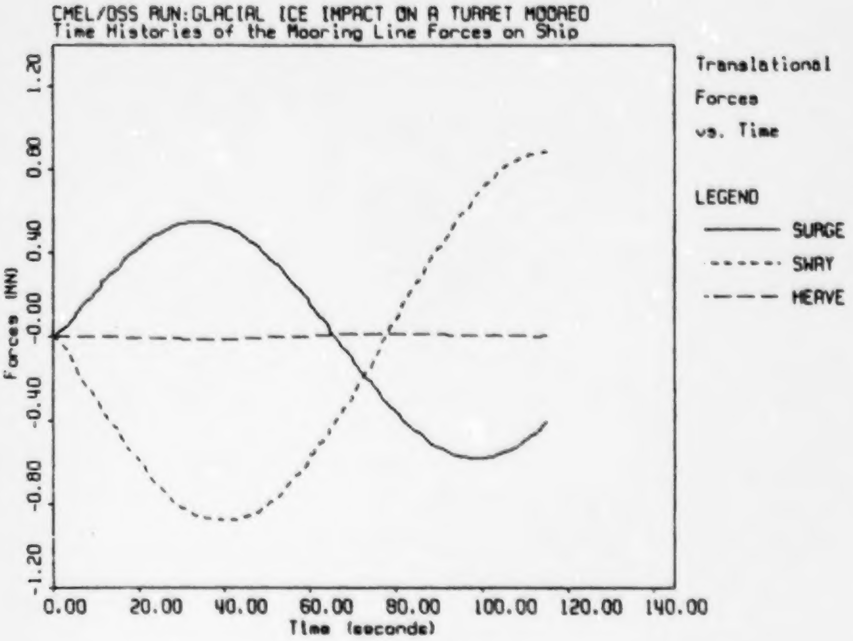

Figure 4.17 Global Translational Mooring Forces.

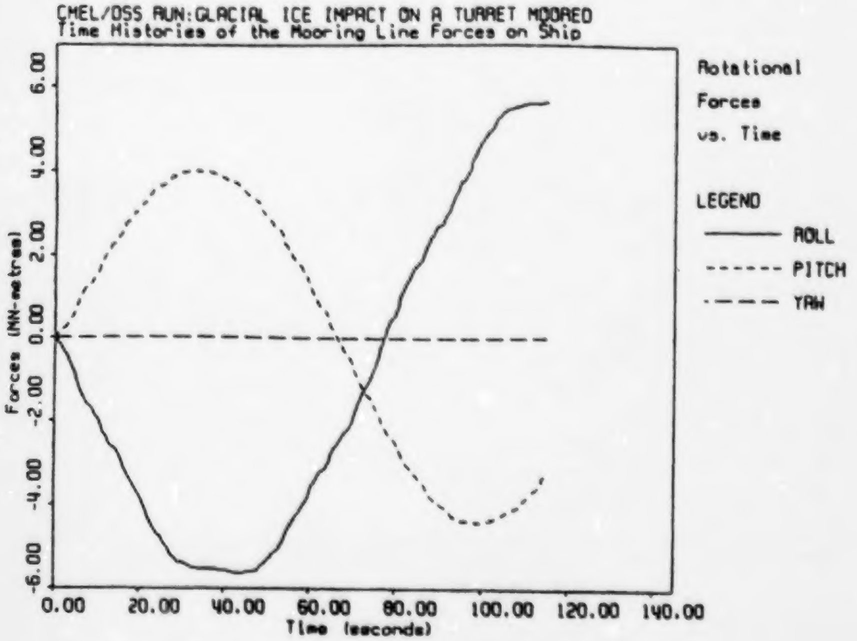

Figure 4.18 Global Rotational Mooring Forces.

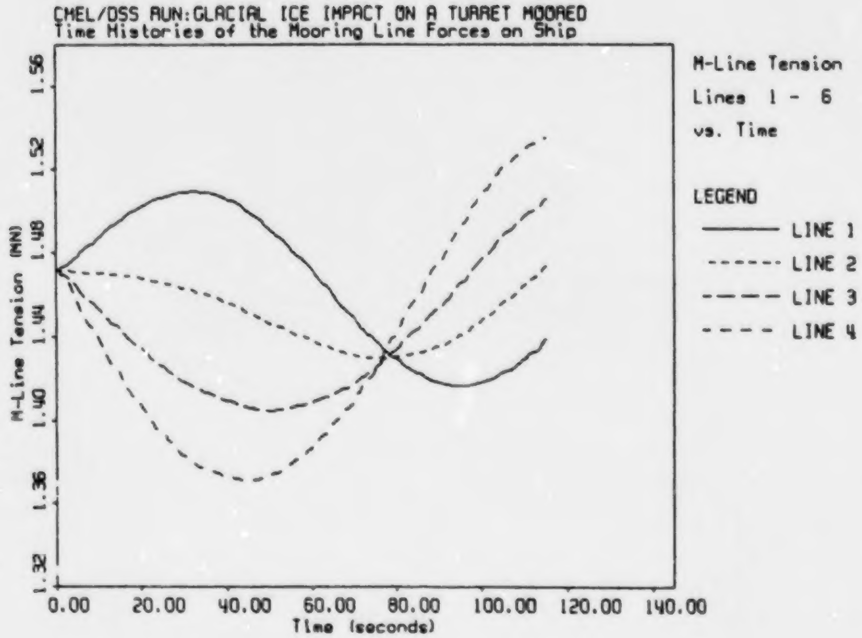

Figure 4.19 Mooring Line Forces.

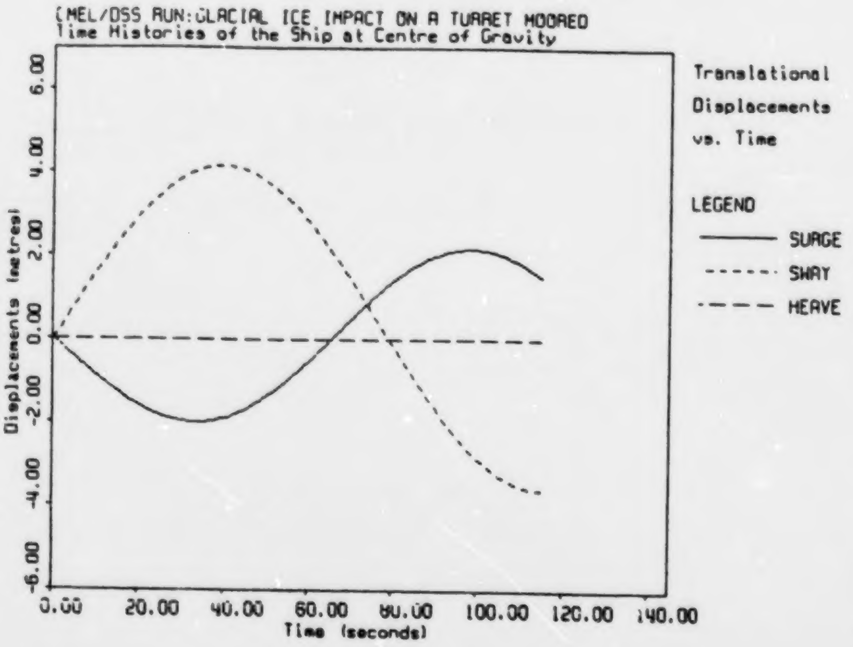

Figure 4.20 Translations of the Vessel.

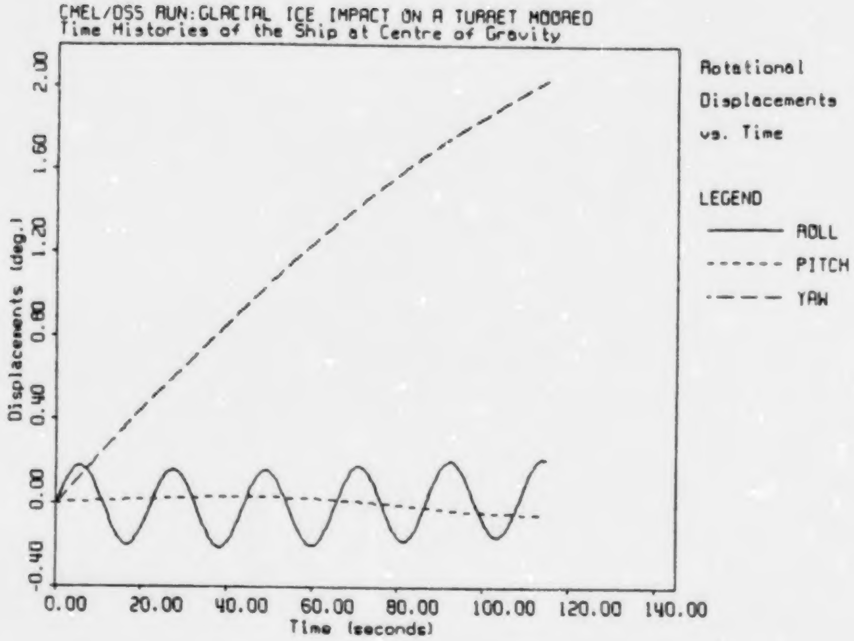

Figure 4.21 Rotations of the Vessel.

5.0 Calculation Procedures for Calculating Ice Forces on Artificial Islands

5.1 General

The design of artificial islands must consider both waves and ice. In this study only the effect of ice on the design of artificial islands is examined.

5.1.1 Types of Artificial Islands

An artificial island is generally constructed of dredged or trucked earth fill, including hybrid structures of combined earthfill and a gravity structures. The following configurations are representative of typical artificial islands:

Sacrificial Beach Artificial Island

- uses large volumes of fill in sacrificial beaches.
- a schematic of a sacrificial beach island is shown in Figure 5.1.

Slope Protected Artificial Island

- uses sandbag or other slope protection against waves.
- a schematic of a slope protected artificial island is shown in Figure 5.2.

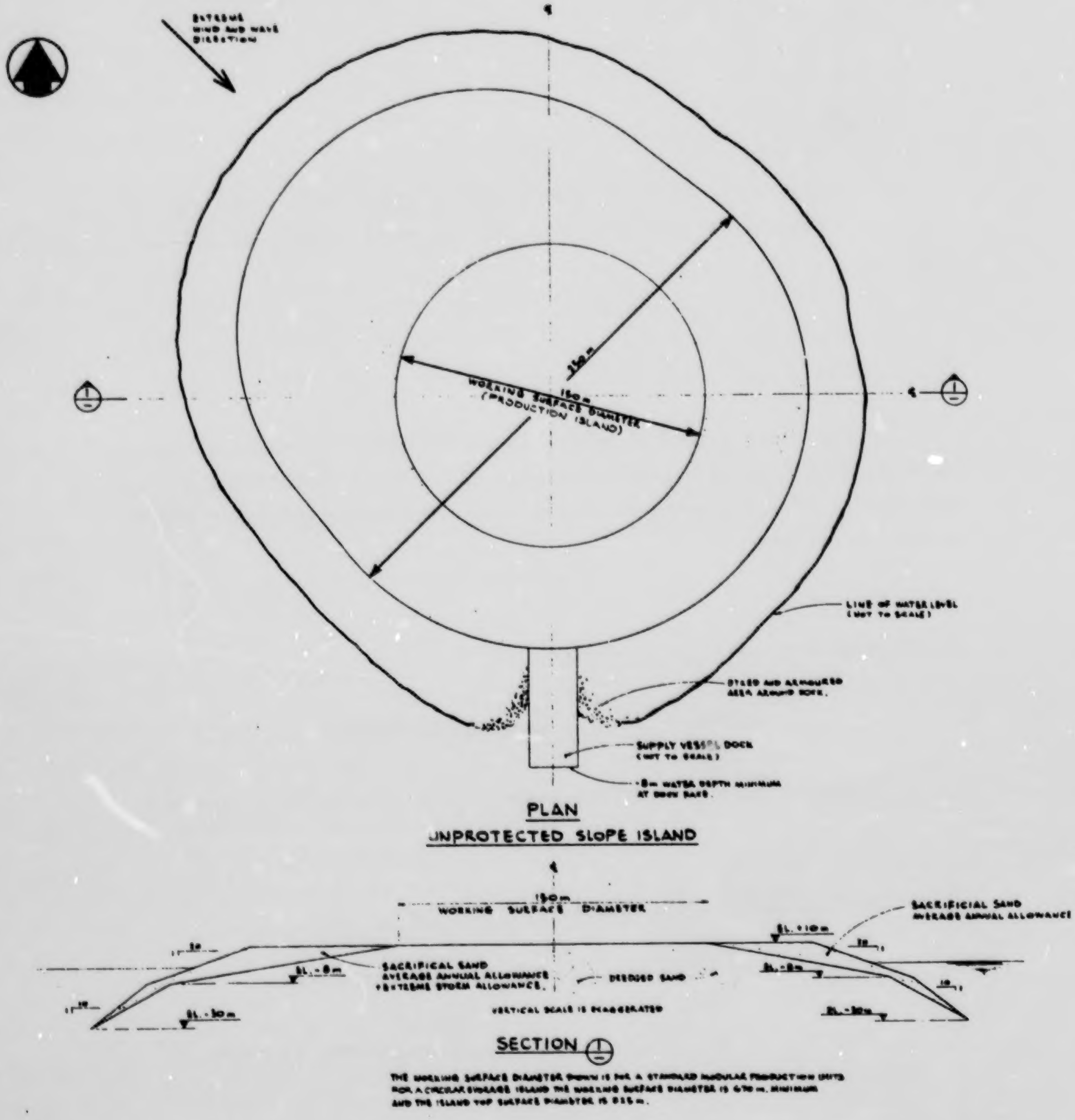
EXTREME WIND AND WAVE DIRECTION
250 m
150 m
WORKING SURFACE DIAMETER (PRODUCTION ISLAND)
LINE OF WATER LEVEL (NOT TO SCALE)
DYKED AND ARMOURED AREA AROUND DOCK.
SUPPLY VESSEL DOCK (NOT TO SCALE)
-8m WATER DEPTH MINIMUM AT DOCK FACE.
PLAN
UNPROTECTED SLOPE ISLAND
150m
WORKING SURFACE DIAMETER
SACRIFICIAL SAND AVERAGE ANNUAL ALLOWANCE
EL. +10m
10 1
EL. -8m
SACRIFICAL SAND AVERAGE ANNUAL ALLOWANCE + EXTREME STORM ALLOWANCE.
DREDGED SAND
10 1
EL. -30m
VERTICAL SCALE IS EXAGGERATED
SECTION
THE WORKING SURFACE DIAMETER SHOWN IS FOR A STANDARD MODULAR PRODUCTION UNITS FOR A CIRCULAR STORAGE ISLAND THE WORKING SURFACE DIAMETER IS 670 m. MINIMUM AND THE ISLAND TOP SURFACE DIAMETER IS 825 m.

Figure 5.1 Schematic of a Sacrificial Beach Artificial Island.

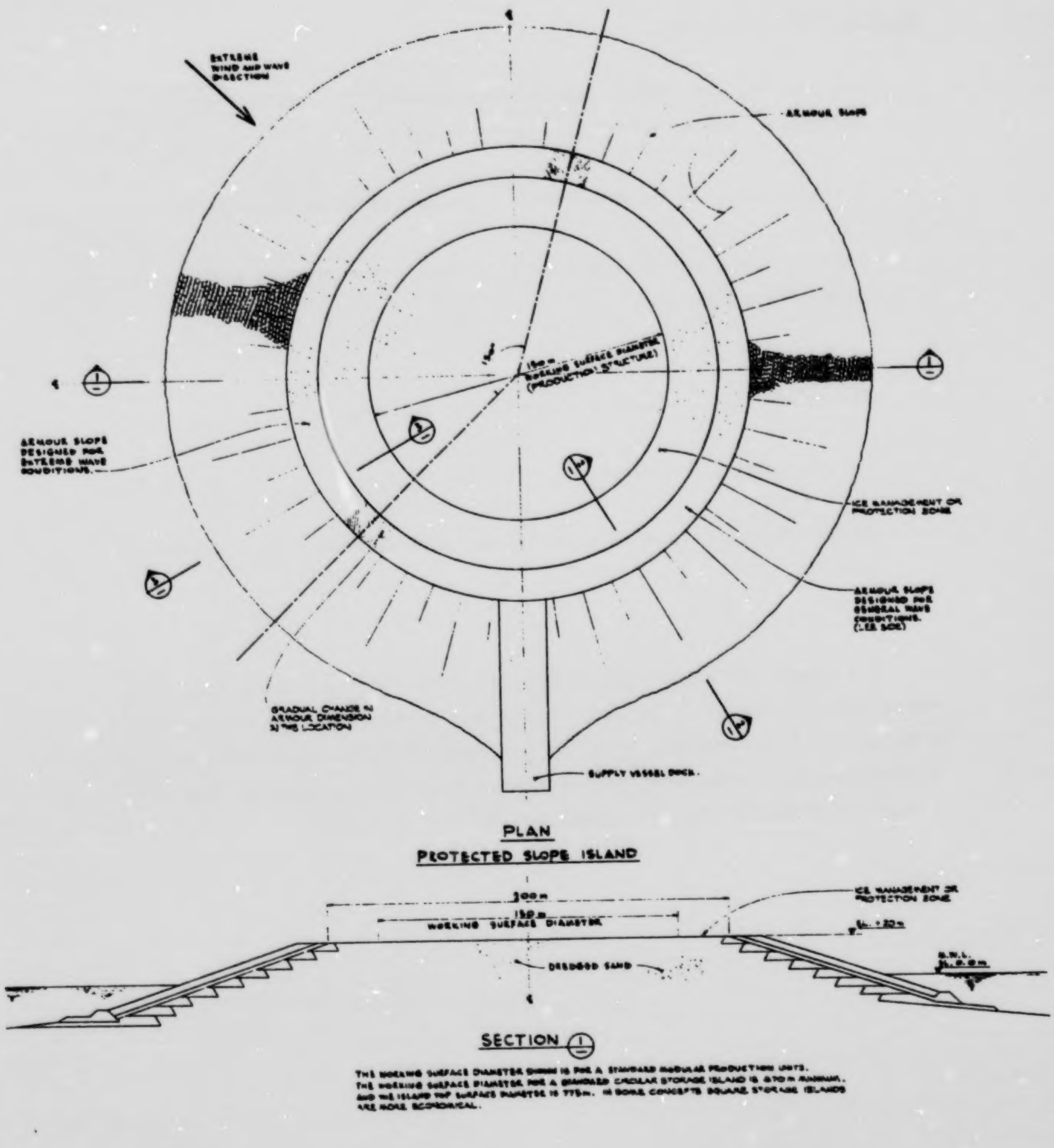
EXTREME WIND AND WAVE DIRECTION
ARMOUR SLOPE
150 m WORKING SURFACE DIAMETER (PRODUCTION STRUCTURE)
ARMOUR SLOPE DESIGNED FOR EXTREME WAVE CONDITIONS.
ICE MANAGEMENT OR PROTECTION ZONE
ARMOUR SLOPE DESIGNED FOR GENERAL WAVE CONDITIONS. (LEE SIDE)
GRADUAL CHANGE IN ARMOUR DIMENSION IN THIS LOCATION
SUPPLY VESSEL DOCK.
PLAN
PROTECTED SLOPE ISLAND
300 m
150 m
WORKING SURFACE DIAMETER
ICE MANAGEMENT OR PROTECTION ZONE
EL. +20 m
S.W.L. EL. 0.0 m
DREDGED SAND
SECTION 1
THE WORKING SURFACE DIAMETER SHOWN IS FOR A STANDARD MODULAR PRODUCTION UNITS.
THE WORKING SURFACE DIAMETER FOR A STANDARD CIRCULAR STORAGE ISLAND IS 670 m MINIMUM.
AND THE ISLAND TOP SURFACE DIAMETER IS 775m. IN SOME CONCEPTS SQUARE STORAGE ISLANDS
ARE MORE ECONOMICAL.

Figure 5.2 Schematic of a Slope Protected Artificial Island.

Caisson Retained Island

- for ice features which contact the berm or the rubble field, this structure behaves as an artificial island.
- a schematic of a caisson retained island is shown in Figure 5.3.
- uses concrete or steel caissons to retain the dredged material at the core of the island.

The island may be used for one of two purposes:

1: exploration (lifetime of one winter),

2: production (lifetime of many summers and winters over a number of years).

The longer return period associated with the production structure means that it should experience higher ice forces than the exploration structure. The structure life and ice features associated with an acceptable risk level are important considerations in determining the design criteria for an artificial island.

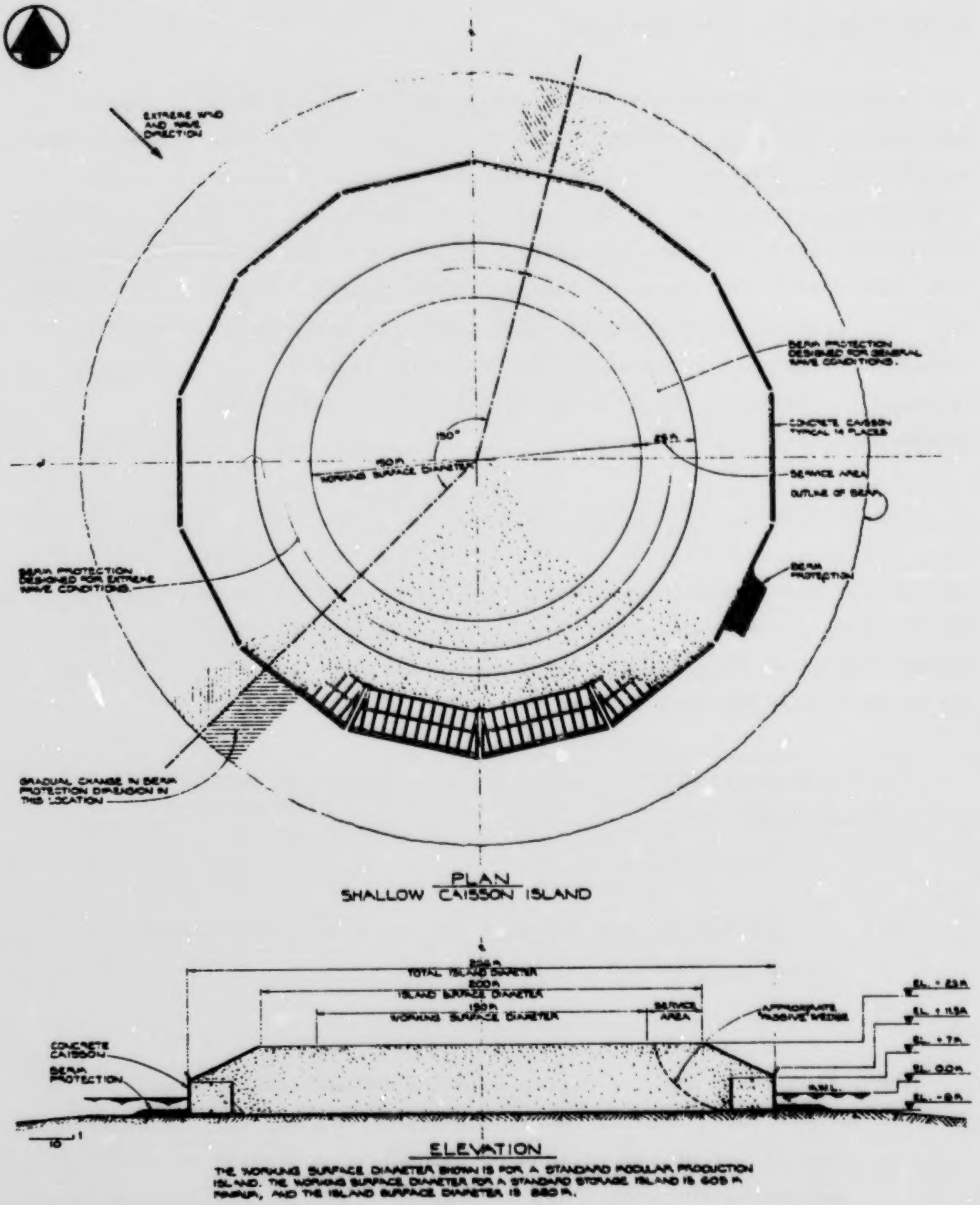
EXTREME WIND AND WAVE DIRECTION
BERM PROTECTION DESIGNED FOR GENERAL WAVE CONDITIONS.
CONCRETE CAISSON TYPICAL 14 PLACES
25 ft
150°
150 ft
WORKING SURFACE DIAMETER
SERVICE AREA
OUTLINE OF BERM
BERM PROTECTION DESIGNED FOR EXTREME WAVE CONDITIONS.
BERM PROTECTION
GRADUAL CHANGE IN BERM PROTECTION DIMENSION IN THIS LOCATION
PLAN
SHALLOW CAISSON ISLAND
TOTAL ISLAND DIAMETER
200 ft
ISLAND SURFACE DIAMETER
150 ft
WORKING SURFACE DIAMETER
SERVICE AREA
APPROXIMATE PASSIVE WEDGE
CONCRETE CAISSON
BERM PROTECTION
EL. + 23 ft
EL. + 11.5 ft
EL. + 7 ft
EL. 0.0 ft
EL. - 8 ft
M.W.L.
10
1
ELEVATION
THE WORKING SURFACE DIAMETER SHOWN IS FOR A STANDARD MODULAR PRODUCTION ISLAND. THE WORKING SURFACE DIAMETER FOR A STANDARD STORAGE ISLAND IS 605 ft MINIMUM, AND THE ISLAND SURFACE DIAMETER IS 880 ft.

Figure 5.3 Schematic of a Caisson Retained Artificial Island.

5.1.2 Geographic Considerations

Artificial islands have been used primarily in the Beaufort Sea as exploration drilling platforms. The first islands were constructed in the early 1970's. They were built in very shallow water, and for some the material was carried out to the location by trucks and placed in holes cut through the ice. To construct islands in deeper water dredging techniques were used. The development of the artificial island concept has continued until the present. The greatest water depth for a non-caisson artificial island structure is 21 metres at the Issungnak location. Islands using caissons to penetrate the waterline are routinely constructed in waterdepths less than 40 metres.

The most recent development in artificial island technology is to use spray ice to economically build structures capable of supporting a drilling rig and the associated infrastructure. This technology is an outgrowth of the flooding concepts developed by Panarctic in the 1970's and the spray ice protection methodology developed in the Canadian and Alaskan Beaufort Sea areas during the past five years.

The ice zones applicable to the installation of an artificial island in the Beaufort Sea are:

Fast ice: Any type of sea ice that remains attached to a shoreline, island, or grounded ice features.

Transition zone: The ice region existing between fast ice and the arctic pack, usually heavily deformed. It may vary in width from hundreds of metres to tens of kilometres depending on seasonal and annual changes. Fast ice may be found in this zone, adjacent to grounded features. The transition zone is also referred to as the shear or Stamukhi zone in the Alaskan Beaufort Sea.

Pack ice: Any area of sea ice other than fast ice. The phrase pack ice usually refers to moving ice.

Active zone: A region in which the ice moves and deforms.

5.1.3 Ice Types and Features to be Considered

Structures constructed in the nearshore area of the Beaufort Sea must be designed to withstand ice loads due to several varieties of ice features to which it may be exposed.

First-Year Ice Feature Types

- first-year, or newly grown sheet ice.
- first-year ice floes.
- rafted or rubbled ice.
- first-year ridges.

Multi-Year Ice Features

- multi-year floes.
- multi-year ridges and hummock fields.
- ice islands and ice island fragments.

The features are described in Chapter 2 of Volume II.

Multi-year features have a smaller probability of entering shallow water.

During the course of the winter a rubble pile may form around the artificial island. When calculating ice forces account must also be taken of the interaction of an ice feature with the rubble pile.

5.1.4 Types of Ice Interactions with Artificial Islands

Several types of failure (or energy dissipation) mechanisms can occur during the interaction of an ice feature and an artificial island. These failure mechanisms must be accounted for during the design phase.

The ice/artificial island interactions to be considered include:

i - Ride-Up: an example of ice ride-up on a sacrificial beach island is shown in Figure 5.4.

ii - Rubble Fields: affect the overall force level and island resistance, as discussed in Section 5.5 of Volume II.

iii - Scour: the underwater portion of the island or berm is susceptible to scouring.

iv - Penetration: the island fill can suffer major displacement and damage.

v - Passive Failure of Caisson Retained Island: room should be left on the working surface to allow for a passive failure behind a caisson, as shown in Figure 5.5.

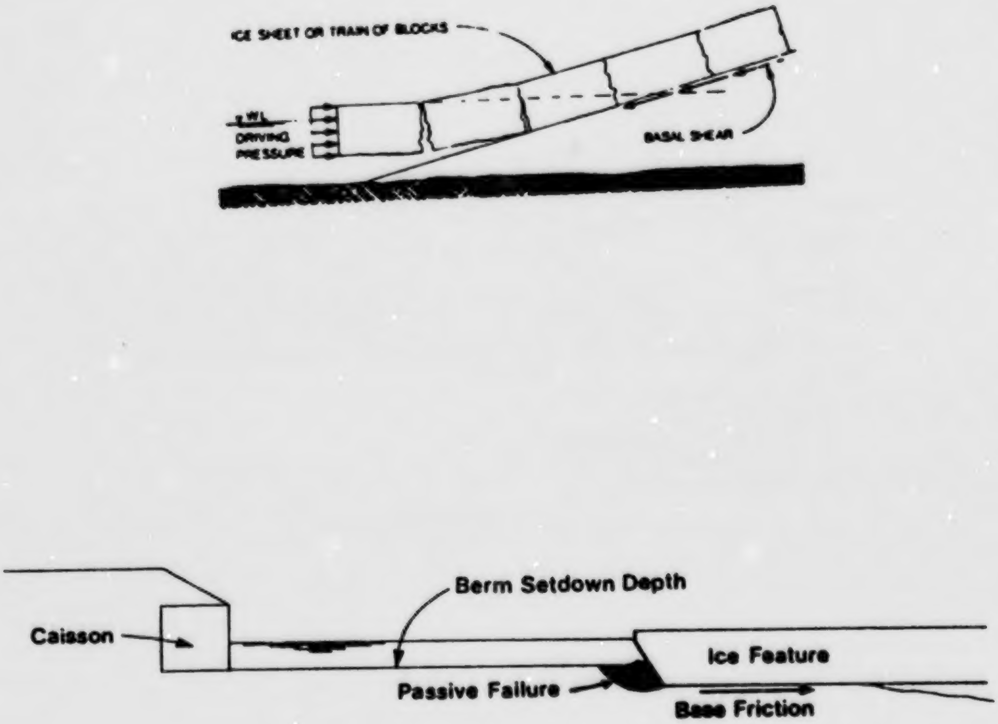
ICE SHEET OR TRAIN OF BLOCKS
WL
DRIVING PRESSURE
BASAL SHEAR
Berm Setdown Depth
Caisson
Ice Feature
Passive Failure
Base Friction

Figure 5.4 Illustrations of Ride-Up and Passive Failure.

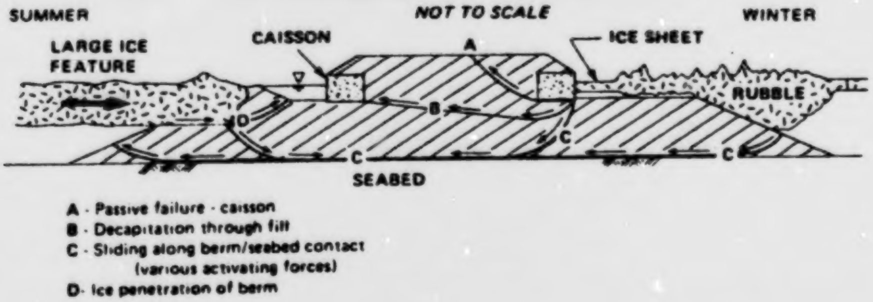
SUMMER
NOT TO SCALE
WINTER
LARGE ICE FEATURE
CAISSON
ICE SHEET
RUBBLE
A
B
C
D
SEABED
A - Passive failure - caisson
B - Decapitation through fill
C - Sliding along berm/seabed contact (various activating forces)
D - Ice penetration of berm

Figure 5.5 Illustrations of Several Failure Mechanisms.

vi - Break-Out Loads: this is due to crushing of late winter sheet ice across the full width of a consolidated rubble field. This is mainly a landfast ice area phenomenon, as perfect contact across the full width of a rubble field can only be achieved by the ice sheet growing in-situ.

vii - Limit Ice Loads: are of three general types:

Limit-Stress: Full envelopment of the structure by the ice, resulting in a maximum ice load.

Limit-Energy: Full envelopment does not occur. During the interaction the ice feature slows down as kinetic energy is dissipated by the failure of the ice. Environmental forces of wind and current drag, and ridge-building decrease the loss of kinetic energy due to their acting in the same direction as the ice features motion. When the ice feature stops, environmental forces continue to act.

Limit-Environmental: When an ice feature is initially at rest against a structure and no ice failure occurs, the load on the structure is limited to the sum of the wind and current drag force vectors and the force vectors exerted on the ice feature by adjacent ice features (if present).

5.2 Example Calculation

5.2.1 Structure

The structure chosen for this example calculation is the slope protected production island shown in Figure 5.6. The dimensions of the structure are:

- diameter of top of island (excluding slope protection)	200 m
- working surface diameter	150 m
- width of ice management zone	25 m
- height of top of island (above mean water level (MWL))	20 m
- diameter of island at MWL	350 m

5.2.2 Location

The structure is assumed to be located in landfast ice in the Canadian Beaufort Sea.

5.2.3 Ice Types and Features

Sheet Ice: calculate break-out loads.

Floes: calculate limit-stress and limit-energy load levels.

Rubble Piles and Rubble Fields: account for the presence of a consolidated rubble field.

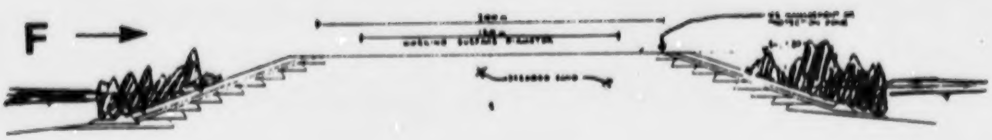

Figure 5.6 Schematic of the Artificial Island Used in the Analysis.

Ice Island: not appropriate for the shallow water, landfast, areas.

Ridges: ridges are not important features in the design of artificial islands, but they are important for deep caisson structures.

The following design criteria, for the landfast ice area, is selected as follows:

Ice type - first year ice.

Ice features - sheet ice/floe/rafted ice.

Ice thickness - 2.2 m (Estimated maximum first-year ice growth in 100 years. A more typical ice growth is between 1.7 and 2.0 metres for the Canadian Beaufort Sea landfast ice zone).

5.2.4 Ice/Artificial Island Interaction

Calculation of Break-Out Ice Load

The global ice force for the "break-out" condition is assumed to govern where:

- the landfast ice moves at the end of the winter season, when the ice sheet thickness is maximum,
- there is perfect contact between the ice sheet and the refrozen rubble,
- the peak ice pressure occurs when the sheet ice just starts to crush, at the so-called transition strain rate,

- simultaneous crushing occurs at the ice sheet/refrozen rubble interface,

The total width of structure is:

- Waterline width of structure	350 m
- Additional width of refrozen rubble, width per side	50 m
- Total island width with rubble	450 m

The failure pressure is calculated by two methods:

1. EIS Ice Failure Pressure Curve (Figure 2.1):

   - Aspect Ratio = 450/2.1 = 205
   - Crushing Pressure = 0.4 MPa

2. Ice Failure Pressure vs. Area Curve (Figure 2.2):

   - Area = 450 x 2.2 = 990 m^2
   - Crushing Pressure = 0.4 MPa

The total force on the island is estimated at:

F = 0.4 x 450 x 2.2 = 396 MN

5.2.5 Summer Floe/Berm Interaction

Illustrated in this example analysis is a summer scenario in which a drifting multi-year ice floe indents into an artificial island.

The multi-year floe is characterized by:

- thickness = 7 m
- diameter = 1 km
- speed = 0.5 m s^{-1}

The kinetic energy of the floe (with say 20% added mass) is approximately 825 MJ.

The indentation analysis is carried out by a computer model (Tseng et al., 1983). The program employs an incremental indentation approach to trace the force build-up and energy dissipation history during the indentation. A configuration of the various forces acting on the ice floe is shown in Figure 5.7.

LIMIT ENERGY ICE FORCE:

The limit-energy ice force is defined as that maximum force experienced by the structure during the time that the original kinetic energy of the ice feature is dissipated. The 825 MJ of original kinetic energy are dissipated completely at a penetration of 15.3 metres. The berm reaction at this penetration is 199 MN. Thus, if the environmental forces were set to zero, the maximum load on the berm would be 199 MN (see Table 5.1).

In reality, current and wind drag alter the limit energy ice force from this value due to the additional input of energy as the velocity of the floe decreases relative to the equilibrium wind and current velocities assumed at the beginning of the interaction.

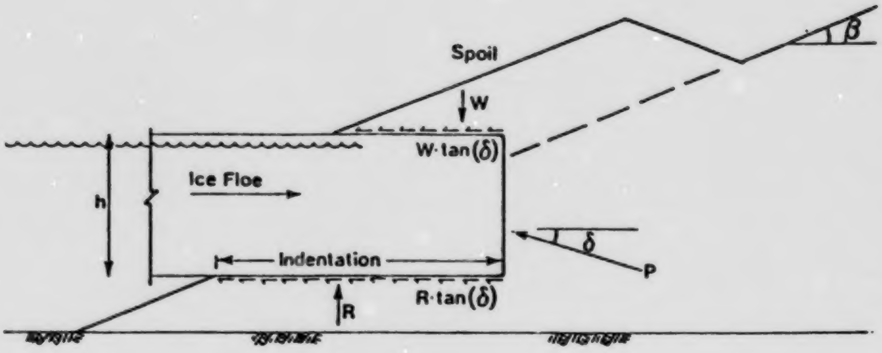
Spoil
β
W
W·tan(δ)
Ice Floe
h
δ
P
Indentation
R·tan(δ)
R

Figure 5.7 Forces Acting on the Ice Floe.

Table 5.1

Output From Ice Floe/Artificial Island Analysis

Indentation (m)	Contact Width (m)	Energy Dissipated (MJ)	Soil Reaction (MN)	Ice Failure Force (MN)
13.0	139.5	446.7	127.0	527.9
⋮				
14.0	144.7	590.0	156.7	547.0
⋮				
15.0	149.6	763.0	189.0	565.0
15.1	150.1	783.5	192.4	567.3
15.2	150.6	803.1	195.8	569.1
15.3	151.0	823.0	199.2	570.9
15.4	151.5	843.3	202.6	572.6
15.5	152.0	863.9	206.1	574.4
15.6	152.4	884.8	209.6	576.2
15.7	152.9	906.1	213.1	578.0
15.8	153.4	927.8	216.7	579.7
⋮				
20.0	171.6	2189.0	386.6	648.5
⋮				
22.0	179.5	3060.0	481.3	678.4
⋮				
24.0	186.9	4128.0	583.0	706.6
⋮				
27.0	197.5	6132.0	750.0	746.3

In Table 5.1 the fifth column in the output is the ice crushing force calculated using the EIS ice failure pressure curve. In this example an indentation of 27 metres would be required for the ice to start crushing at a global force of 746 MN.

For a wind speed of 20 m s^{-1} and a current speed of 0.5 m s^{-1} the wind and current drag forces are 1.23 MN and 0.54 MN respectively. After the floe's forward motion stops the force on the berm would be the sum of these forces, or 1.77 MN. Assuming that this total force acted on the ice floe during the interaction, over 15.3 m penetration 27.1 MJ (15.3 m x 1.77 MN) of added environmental energy would be required to be dissipated. Adding this to the original 825 MJ of energy gives a new total energy to be dissipated of 852 MJ. From Table 5.1 it is seen that this amount of energy would be dissipated at a penetration of 15.45 m, and the new limit energy load on the artificial island would be 204 MN.

In other words the addition of environmental forces of wind and current drag, based on the above assumptions, caused the ice feature analyzed to penetrate an additional 15 cm towards the centre of the structure. This may not seem significant for this example, however the significance of the environmental forces increases dramatically as floe size increases.

References

Acres International Limited, "Northumberland Strait Bridge: Ice Forces Report". Report by Acres International Limited, prepared for Public Works Canada, Draft, March, 1987.

Afanasev, V.P., Y.V. Dolgopolov and Z.I. Shyeishtein, "Ice Pressure on Separate Supporting Structures in the Sea". Draft Translation 346, USACRREL, Hanover, New Hampshire, April, 1972.

Afanasev, V.P., Ice Pressure on Vertical Structures", NRC Technical Translation 1708, Translated by V. Poppe, Translation Section, National Science Library, Ottawa, Ontario, December, 1983. Translated from Transportnoe Strolitel'stvo (3): 47 - 48, 1972.

Alaska Oil and Gas Assosciation Project 340,'Computer Software to Analyze Ice Interaction with Moored Ship-Shaped Vessels', 1987

Arctic Petroleum Operators Association Projoct 180, "Ice Forces on Hans Island: August 1980". Arctic Petroleum Operator's Association Research Project Report No. 180-2, March, 1981.

Arctic Waters Pollution Prevention Act, Ottawa, Ontario, 1981

Bercha, F.G. and J.V. Danys, "Prediction of Ice Forces on Conical Offshore Structures", Marine Science Communications, pp. 365 - 380, 1975.

Bercha, F.G., T.G. Brown and M.S. Cheung, "Local Pressure in Ice-Structure Interactions:, Proceedings, ARCTIC '85, American S-ciety of Civil Engineers, San Francisco, pp. 1243 - 1251, March, 1985.

Bercha, F.G., "Ice Structure Interaction: Engineering Design and Construction Criteria", F.G. Bercha and Associates Report, prepared for Public Works Canada, July, 1976.

Brennen,C. E.,'A Review of Added Mass and Fluid Inertial Forces', Naval Civil Engineering Laboratory,Port Hueneme, California, 1982

Bulow, R. E., S.G. Withee, T. Akaboshi,T. Nawata, and A. Joensuu, 'Inclined Column Semisubmersibl - Design Considerations', OMAE Specialty Symposium, 1986

Canadian Arctic Shipping Pollution Prevention Rules, Ottawa, Ontario, 1985

Cammaert, A.B., T. Kimura, N. Koma, N. Yashima, S. Yano and Matsushima, "Adfreeze Forces on Offshore Platforms", Proceedings of the Fifth Offshore Mechanics and Arctic Engineering Symposium, Tokyo, Japan, Volume 4, pp. 541 - 548, 1986.

Chakraburtty, J.C., H.R. Kivisild, L.H. MacPhie, L.V. Sagriff, T.F. Saunders and H.T. Yan, "Arctic Marine Design and Construction Handbook", Fenco Engineers Inc., Lavalin, Report prepared for the Transportation Development Centre, Montreal, Quebec, September, 1984.

Cormeau, A., I.J. Jordaan and M. Maes, "Development of a Model for Progressive Damage in Ice", Det Norske Veritas Report, prepared for Public Works Canada, 1986.

Croasdale, K.R., and R.W. Marcellus, "Ice and Wave Action on Artificial Islands in the Beaufort Sea", Canadian Journal of Civil Engineering, Volume 5, pp. 98 - 113, 1978.

Croasdale, K.R., N.R. Morgenstern and J.B. Nuttall, "Indentation Tests to Investigate Ice Pressures on Vertical Piers". Journal of Glaciology, Volume 19, No. 81, pp. 301 - 311, 1977.

Croasdale, K.R., "Ice Forces on Fixed, Rigid Structures". In Working Group on Ice Forces on Structures, T. Carstens editor, USACRREL, Hanover, New Hampshire, Special Report 80 - 26, pp. 34 - 106.

Det Norske Veritas,'Rules for the Classification of Mobile Offshore Units', 1984

Gunzelman, S.X.,'Deep Water Bering Sea Development Concepts', Arctic'85, ASCE, 1985

Hnatiuk, J. and B.D. Wright,'Ice Management to Support the Kulluk Drilling Vessel',35th Annual Meeting of the Petroleum Society of CIM, 1984

Hnatiuk, J. and E.E. Felzien, "Performance of Beaudril's New Beaufort Sea Drilling System". Proceedings of the Fifth Offshore Mechanics and Arctic Engineering Symposium, Tokyo, Japan, Volume 4, pp. 183 - 191, 1986.

Hetenyi, M., Beams on Elastic Foundations. University of Michigan Press, Ann Arbor, Michigan, 1946.

Isnard, J.L., "Contribution a l'etude de l'indentation de plaques de glace". These M.Sc., Universite Laval, 1978.

Jordaan, I.J., "Numerical and Finite Element Techniques in Calculation of Ice-Structure Interaction", Third State-of-the-Art Report on Ice Forces, IAHR Ice Symposium, Iowa City, Iowa, 1986.

Korzhavin, K.N., "Action of Ice on Engineering Structures". Report translated by U.S. Joint Publications Research Service for USACRREL, Hanover, New Hampshire, (in the literature this document is referred to also as Korzhavin (1962)), September, 1971.

Kristensen, M. and V.A. Squire,'Modelling of Antarctic Tabular Icebergs in Ocean Waves', Annals of Glaciology 4, 1983

Liljestrom, G. and G. Wilkman,'Semisubmersibles for Arctic Operations',The Society of Naval Architects adn Marine Engineers, Texas Section College Station Meeting, 1984

Kishev, R., A. Ivanov, and L. Pomeranetz, 'On the Practical Evaluation of Hydrodynamic Coefficients of Semisubmersible Platforms, Based on Systematic Model Tests', Behaviour of Offshore Structures, 1985

Loire, R. and W.Y. Chow,'Single Point Moorings for the Bering Sea',Conference Arctic'85, ASCE, 1985

Marcellus, R.W., K.R. Croasdale, N.F.B. Allyn and N.R. Morgernstern, "Analytical Models for Broken Ice Zones", C.M.E.L. Report No. 1038, prepared for Public Works Canada, March, 1986.

Marcellus, R.W., T.B. Morrison, N.F.B. Allyn, K.R. Croasdale, H.S. Iyer and J. Tseng, "Ice Forces on Marine Structures: Volume II", C.M.E.L. Report No. 1046, prepared for Public Works Canada, May, 1987.

Marcellus, R.W., and D.R. Roth, "An Initial Probabilistic Assessment of Ice Loading on Beaufort Sea Structures". Report prepared for the Environmental Impact Statement Partners, April, 1982.

Michel, B. and N. Toussaint, "Mechanism and Theory of Indentation of Ice Plates". Journal of Glaciology, Volume 19, No. 81, pp. 285 - 300, 1977.

Muga, B.J. and M. A. Freeman,'Computer Simulation of Single Point Moorings',OTC, 1977

Oil Companies International Marine Forum,'Prediction of Wind and Current Loads on VLCCS',1976

Padron, D.V., E.H.Y. Han, and M.T. Faeth,'Bering Sea Crude Oil Transportation Systems',Conference Arctic '85,ASCE, 1985

Palo, P.A.,'Development of a General-Purpose Mooring Analysis Capability for the U.S. Navy',Ocean Science and Engineering, 1985

Pilkington, G.R., Oral Presentation at IAHR 1986, Iowa City, Iowa.

Pollack, J., 'Single Point Mooring in Ice Infested Waters', Arctic 85

Prodanovic, A., "Upper Bounds of Ridge Pressure on Structures", Proceedings of the Sixth International Conference on Port and Ocean Engineering Under Arctic Conditions, (POAC '81), Quebec City, Canada, pp. 1288 - 1302, 1981.

Ralston, T.D., "Ice Force Design Considerations for Conical Offshore Structures". Proceedings of the Fifth International Conference on Port and Ocean Engineering Under Arctic Conditions, (POAC '79), Trondheim, Norway, August 13 - 18, Volume 1, pp. 741 - 752, 1979.

Ralston, T.D., "Plastic Limit Analysis of Sheet Ice Loads on Conical Structures". In Physics and Mechanics of Ice, P. Tryde editor, Springer Verlag, Berlin, pp. 289 - 300, 1979.

Ralston, T.D., "Analysis of Ice Sheet Indentation". Proceedings of the IAHR Symposium on Ice Problems, Volume 1, pp. 13 - 31, Lulea, Sweden, August 7 - 9, 1978.

Reddy, D.V., D.B. Muggeridge, A.S.J. Swanidas, M. Ahrockiasmy, J.J. Murray, H. El-Tahan and C.C. Hsiung, "Dynamic Response of Moored Semisubmersibles to Bergy Bit Impact: Irregular Wave, Wind and Current Forces", Proceedings of the Offshore Technology Conference, Houston, Texas, 1982.

Renicke, K.M., and R. Remer, "Procedure for the Determination of Ice Forces". Proceedings of the IAHR Symposium on Ice Problems, Volume 1, pp. 217 - 238, Lulea, Sweden, August 7 - 9, 1978.

Sahin, I. and A. Aybar, "A Survey on Semisubmersible Wind Loads", Ocean Engineering , Volume 12, No. 3, 1985.

Sanderson, T.J.O., "A Pressure-Area Curve for Ice", Proceedings of the IAHR Ice Symposium 1986, Iowa City, Iowa, Volume 2, pp. 361 - 384, 1986.

Sanderson, T.J.O., "Theoretical and Measured Ice Forces on Wide Structures", Proceedings of the IAHR Ice Symposium 1984, Hamburg, West Germany, Volume 4, pp. 151 - 207, August 27 - 31, 1984.

Sjolind, S.-G., "Viscoelastic Buckling of Beams and Plates on Elastic Foundation". Proceedings of the IAHR Ice Symposium 1984, Hamburg, West Germany, Volume 1, pp. 63 - 72, August 27 - 31, 1984.

Sjolind, S.-G., "Visco-Elastic Buckling Analysis of Floating Ice Sheets". Cold Regions Science and Technology, Volume 11, pp. 241 - 246.

Sodhi, D.S., "Flexural and Buckling Failure of Floating Ice Sheets Against Structures", Proceedings of the IAHR Ice Symposium 1986, Iowa City, Iowa, Volume 2, pp. 339 - 359, 1986.

Sodhi, D.S., "Buckling Analysis of Wedge-Shaped Floating Ice Sheets". Proceedings of the Fifth International Conference on Port and Ocean Engineering Under Arctic Conditions, (POAC '79), Trondheim, Norway, August 13 - 18, Volume 1, pp. 797 - 810, 1979.

Sodhi, D.S., F.D. Haynes, K. Kato and K. Hirayama, "Experimental Determiation of the Buckling Loads of Floating Ice Sheets". Annals of Glaciology, Volume 4, pp. 260 - 265.

Squire, V.A., "Numerical Modeling of Realistic Ice Floes in Ocean Waves", Annals of Glaciology, Volume 4, 1983.

Swan Wooster Engineering Company Ltd., "Environmental Impact Statement Study of Production Structures for Beaufort Sea Oilfield Development". Report prepared for the Environmental Impact Statement Partners, 1982.

Takagi, M. S. Arai, S. Takezawa, K. Tanaka and N. Takarada, "A Comparison of Methods for Calculating the Motion of a Semisubmersible", Ocean Engineering, Volume 12, No. 1, 1985.

Tomin, M.J., M.S. Cheung, I.J. Jordaan and A. Cormeau, "Analysis of Failure Modes and Damage Processes of Freshwater Ice In Indentation Tests", Proceedings of the Fifth Offshore Mechanics and Arctic Engineering Symposium (OMAE 86), 1986.

Tseng, J., D.A. Smith and N.F.B. Allyn, "Ice Floe Induced Erosion of Artificial Islands - A Numerical Approach", ACROSES Arctic Regional Workshop, 1983.

Wichers, J.E.W., "Progress in Computer Simulation of Single Point Moored (SPM) Vessels", Proceedings of the Offshore Technology Conference, Houston, Texas, 1986.

Volume

2

Public Works Canada

Architectural and Engineering Services

Travaux publics Canada

Services d'architecture et de génie

Canada

Public Works Canada
Architectural and Engineering Services
Technology

AES/SAG 1-2:88-5v2

ICE FORCES
ON MARINE STRUCTURES
Volume 2 - DISCUSSION

May 1987

Preparation Agency:
C.M.E.L. Enterprises Ltd.

Sponsoring Agency:
Panel for Energy Research
and Development (PERD)
Marine Product Line, Headquarters
Project Manager: M.S. Cheung

The contents of this document represent the views of the authors and are not necessarily the views or policies of the Department of Public Works.

The Minister of Public Works makes no representation or warranty, express or implied, with respect to this publication or the programs or information described in this publication, their quality, merchantability, or fitness for any particular purpose, or their adequacy to produce any particular result. In no event shall the Minister or Her Majesty the Queen in right of Canada, Her employees, servants or agents be legally liable to any person or persons for any damage, whether direct, indirect or consequential, resulting from the use of said publication or the programs or the information contained herein.

Published by Architectural and Engineering Services
Public Works Canada

© Minister of Supply and Services Canada 1988

Cat. No. W62-11/88-5-2E

ISBN 0-662-16285-4

Public Works Canada Travaux publics Canada

DOCUMENT DATA

1. Document Title
ICE FORCES ON MARINE STRUCTURES
Volume 2 - DISCUSSION

2. Control Number
AES/SAG 1-2:88-5v2

3. Date
May 1987

4. Author(s)
R.W. Marcellus, T.B. Morrison, N.F.B. Allyn,
K.R. Croasdale, H.S. Iyer, J. Tseng

5. Consultant's Ref. No.

6. Project Manager
M.S. Cheung

7. Discipline Series No.

8. Preparation Agency and Address
CMEL Enterprises Ltd.
P.O. Box 220
Spencerville, Ontario
KOE 1X0

9. Document Type
Technical Report

10. No. of Pages
436

11. Sponsoring Agency and Address
Panel for Energy Research and Development (PERD)
and Public Works Canada, Marine Product Line
Sir Charles Tupper Bldg., Riverside Drive
OTTAWA, Ontario K1A 0M2

12. PWC File No.
6200-31

13. PWC Project No.
601061

14. Supplementary Notes

15. SSC Publication No.
W62-11/88-5-2E

16. ISBN
0-662-16285-4

17. Abstract

This is Volume 2 of a two-volume report. It contains the backup data and discussion in support of the procedures described in the companion volume entitled Ice Forces on Marine Structures: Volume 1 - Calculations. Volume 2 provides a comprehensive review of state-of-the-art methodologies in current use for estimating the impact of ice forces on various kinds of marine structures.

The report is intended for design engineers who wish to pursue a detailed investigation of the theories and principles behind the guidelines provided in Volume 1. It will also be useful for researchers who wish to define further areas of study. Most of the information now in use derived from laboratory work. Further work is needed to extrapolate to large-scale field test data where other conditions and effects, which are not yet fully understood, come into play.

18. Distribution Statement
Copies are available from:
Documentation Centre
Public Works Canada
Sir Charles Tupper Bldg., Riverside Dr.
Ottawa, Ontario K1A 0M2

19. Keywords
Ice forces; marine caissons; ice/structure interactions

20. Documentation Centre Catalogue No.
MA 101

21. Price
No charge

DPW 2398 (86/09)

Travaux publics Canada   Public Works Canada

FICHE SIGNALÉTIQUE DE DOCUMENT

1. Titre du document

ICE FORCES ON MARINE STRUCTURES
(FORCES EXERCÉES PAR LES GLACES SUR LES OUVRAGES MARITIMES)
Volume 2 - DISCUSSION

2. Numéro de contrôle

AES/SAG 1-2:88-5v2

3. Date

mai 1987

4. Auteur (s)

R.W. Marcellus, T.B. Morrison, N.F.B. Allyn,
K.R. Croasdale, H.S. Iyer, J. Tseng

5. No de réf. du conseil

6. Chargé de projet

M.S. Cheung

7. No de la collection technique

8. Nom et adresse de l'organisme rédacteur

CMEL Enterprises Ltd.
B.P. 220
Spencerville, Ontario
KOE 1X0

9. Type de document

Rapport technique

10. Nombre de page

436

11. Nom et adresse de l'organisme promoteur

Comité de la recherche et du développement
énergétiques et Travaux publics Canada,
Travaux maritimes, Immeuble Sir-Charles-Tupper,
Promenade Riverside, OTTAWA (Ontario) K1A 0M2

12. No de dossier de TPC

6200-31

13. No de projet de TPC

601061

14. Notes

15. No de publication de ASC

W62-11/88-5-2E

16. ISBN

0-662-16285-4

17. Résumé

Volume 2 du rapport en deux volumes. Il renferme les données de référence et les exposés à l'appui du premier volume intitulé Ice Forces on Marine Structures: Volume 1: Calculations. Le volume 2 offre une revue d'ensemble de l'état actuel des connaissance en matière d'évaluation des effets des forces exercées par les glaces sur divers genres d'ouvrages maritimes.

Le rapport s'addresse aux ingénieurs-concepteurs qui mènent une étude détaillée des théories et des principes qui sous-tendent les directives énoncées dans le volume 1. Il peut également servir aux chercheurs qui souhaitent préciser davantage certains secteurs de recherche. La majeure partie des renseignements actuellement utilisés découlent de travaux réalisés en laboratoire. De nouveaux travaux sont nécessaires afin d'extrapoler des données d'essai à pied d'oeuvre de grande envergure dans le cas où d'autres conditions et effets, non encore parfaitement compris, entrent en ligne de compte.

18. Diffusion

Exemplaires disponibles du:
Centre de documentation
Travaux publics Canada
Imm. Sir-Charles-Tupper, Prom. Riverside
OTTAWA, Ontario K1A 0M2

19. Mots clés

Forces exercées par les glaces; caissons; interactions glaces/ouvrages

20. No de catalogue du centre de documentation

MA 101

21 Prix

Sans frais

MTP 2398 (86/09)

PREFACE

This report is one of several reports on research work in the field of marine engineering, indentified and managed by the Marine Product Line and Technology Resources groups of Public Works Canada, with funds provided by the Interdepartmental Panel on Energy Research and Development (PERD).

PERD was established in 1974 to coordinate research on energy by the Federal Government with objectives to provide, in conjunction with efforts in the private sector and the provinces, the technical basis for:

- maintaining oil self-sufficiency over the short term, in view of dwindling conventional supplies;
- developing a diversified energy economy, less dependent on oil and gas in the mid-term; and
- making Canadians less reliant on non-renewable energy sources in the long term.

The research work undertaken by Public Works Canada in Marine Engineering with funds from PERD has been directed particularly toward the following two main topics:

1. Ice/Structure Interaction
2. Construction and Towing of Reinforced Concrete Caissons in the Arctic.

This report is being published with a view to enhancing the technology in the field of Marine Engineering and contributing toward the objectives of PERD.

TABLE OF CONTENTS

PREFACE i

LIST OF FIGURES iii

LIST OF TABLES iv

NOMENCLATURE xviii

1. INTRODUCTION 1-1

2. ICE TYPES AND REGIONS 2-1

2.1 Introduction 2-1
2.2 Ice Types 2-3
2.3 Regional Ice Zones 2-10
2.3.1 Labrador Shelf and Grand Banks 2-11
2.3.2 Davis Strait and Baffin Bay 2-16
2.3.3 Hudson Bay 2-17
2.3.4 The High Arctic Region: The Canadian Archipelago 2-17
2.3.5 The Canadian Beaufort Sea 2-18
2.4 Summary 2-21

3. MECHANICAL PROPERTIES OF ICE 3-1

3.1 Introduction 3-1
3.2 Ice Formation Mechanisms 3-3
3.3 Determination of the Strength of Ice 3-7
3.4 Mechanical Properties of Ice Sheets 3-27
3.4.1 Modulus of Elasticity 3-28
3.4.2 Uniaxial Compressive Strength 3-28
3.4.3 Uniaxial Tensile Strength and Flexural Strength 3-33
3.4.4 Shear Strength o Ice 3-33
3.4.5 Adhesion Strength o Ice 3-36
3.4.6 Poisson's Ratio 3-38
3.5 Mechanical Properties of the Unconsolidated Layers of a Ridge or a Rubble Pile 3-39
3.5.1 Porosity of the Rubble Field of Ridge 3-39
3.5.2 Shear Properties of Partially Consolidated and Unconsolidated Rubble 3-40
3.5.3 Shear Stress Displacement Behaviour of Ice Rubble 3-41
3.6 Summary 3-42

TABLE OF CONTENTS (cont'd)

4. ICE/STRUCTURE INTERACTION: GENERAL LOGIC 4.1

4.1 Introduction 4-1
4.2 Quasi-Static Ice Loads 4-3
4.3 Probabalistic Approaches 4-13
4.4 Other Considerations and General Logic 4-15

5. INTERACTION LOAD THEORY 5-1

5.1 Introduction 5-1
5.2 Ice Interaction with Vertical Sided Structures 5-2
5.2.1 Introduction 5-2
5.2.2 Observed Failure Models 5-5
5.2.2.1 The Behaviour of Ice under Load 5-5
5.2.2.2 Small Scale Brittle Failure 5-6
5.2.2.3 Large Scale Brittle Failure 5-13
5.2.3 Vertical Sided Structure - Ice Load Theories 5-18
5.2.3.1 General 5-18
5.2.3.2 Korzhavin Elastic/Plastic 5-18
5.2.3.3 Multi-Zonal Failure 5-37
5.2.3.4 Large Scale Empirical 5-40
5.2.3.5 Reference Stress 5-49
5.2.3.6 Fracture Mechanics 5-50
5.2.3.7 Discrete Element Method 5-51
5.2.3.8 Critical Delayed Elastic Strain 5-53
5.2.3.9 Damage Modeling 5-55
5.2.4 Scenario Calculations 5-57
5.2.4.1 Introduction 5-57
5.2.4.2 Brittle Failure of First-Year and Multi-Year Ice Sheets Interaction with a Wide Structure 5-59
5.2.4.3 Multi-Year Ridge Interaction with a Wide Structure 5-60
5.2.4.4 First-Year Ridge 5-66
5.2.4.5 The Failure of Ice by Buckling 5-70
5.2.5 Suggested Calculation Procedures - Sea Ice 5-76
5.2.6 Summary 5-77
5.3 Ice Interactions with Sloping Structures 5-78
5.3.1 Types of Structures 5-78
5.3.2 Interaction Scenario for Sloping Structures 5-80
5.3.3 Ice Loads due to Sheet Ice 5-86
5.3.3.1 Historial Overview 5-86
5.3.3.2 Sheet Ice Loads - General Logic 5-87
5.3.3.3 Sheet Ice Loads: Two-Dimensional Theory (Elastic) 5-89

TABLE OF CONTENTS (cont'd)

5.3.3.4 Sheet Ice Loads: Three-Dimensional Theory (Elastic) 5-99
5.3.3.5 Sheet Ice Loads: Three-Dimensional Theory (Plastic) 5-106
5.3.3.6 Sheet Ice Loads - Comparison with Experiments 5-110
5.3.3.7 Sheet Ice Loads - Comparison of Methods 5-116
5.3.3.8 Sheet Ice Loads - Clearing Loads on a Superstructure 5-124
5.3.4 Adfreeze Loads 5-128
5.3.5 Loads on Upward Breaking Structures due to Consolidated Ridges 5-131
5.3.5.1 Introduction 5-131
5.3.5.2 Elasticity Theory 5-132
5.3.5.3 Plasticity Theory 5-135
5.3.5.4 Comparison with Experiments 5-137
5.3.6 Unconsolidated Ridges 5-145
5.3.7 Loads on Downward Breaking Sloping Structures 5-145
5.3.8 Large Scale Flexural Strength of Ice 5-146
5.3.9 Concluding Remarks on the Interaction of Ice with Sloping Structures 5-149
5.4 Ice Interactions with Floating Structures 5-153
5.4.1 Introduction 5-153
5.4.2 Pack Ice Forces 5-160
5.4.2.1 Ice Crushing Loads 5-161
5.4.2.2 Ice Buckling 5-165
5.4.2.3 Ice Jamming 5-170
5.4.2.4 Ice Coverage Effect 5-174
5.4.2.5 Shielding in Pack Ice 5-176
5.4.2.6 Flexural Failure of Ice 5-178
5.4.2.7 Ice Breaker Resistance 5-178
5.4.3 Ice Impact Loads 5-184
5.4.3.1 Ice Impact Force Model 5-185
5.4.3.2 Ice Impact Strength 5-187
5.4.3.3 Effect of Structural Indentation on Ice Impact Force 5-192
5.4.4 Future Work 5-193
5.5 Ice Interactions with Artificial Islands 5-194
5.5.1 Types of Structures 5-194
5.5.2 Landfast Ice Loads 5-196
5.5.3 Rubble Pile Formations and Ride-Up 5-198
5.5.3.1 Ride-Up Observations and Calculations 5-200
5.5.3.2 Pick-Up Observations and Calculations 5-207

TABLE OF CONTENTS (cont'd)

5.5.4 Ice/Rubble/Structure Interaction Loads 5-217
5.5.4.1 Effect of Rubble Fields on Ice Loads 5-217
5.5.4.2 Analysis of Rubble Fields and Spray Ice Conditions 5-220
5.5.4.3 Spray Ice Experience in the Beaufort Sea 5-222
5.5.4.4 Thermodynamics of Rubble and Spray Ice 5-225
5.5.4.5 Rubble Spray Ice Protected Drilling Systems 5-230
5.5.5 Recommendations for Future Work 5-233
5.6 Dynamic Analysis of the Ice/Structure Interaction 5-235
5.6.1 Introduction 5-235
5.6.2 History of the Analysis of Dynamic Ice/Structure Interaction Effects 5-238
5.6.3 Mathematical Models 5-251
5.6.4 Failure Models 5-259
5.6.5 Recommendations for Future Work 5-263
5.7 Local Load Theory 5-264
5.7.1 Introduction 5-264
5.7.2 Analytical Techniques 5-268
5.7.3 Empirical Techniques 5-276

6. SUMMARY AND RECOMMENDATIONS 6-1

LIST OF FIGURES

2.1 Iceberg Sightings - Labrador Sea 2-13

2.2 Labrador Sea Ice Statistics 2-14

2.3 Northwest Passage Ice Conditions 2-19

3.1 Ice Failure Pressure for S_2 Ice at -10°C 3-8

3.2 Unconfined Compressive Strength vs. Strain Rate for a Variety of Brine Volumes and Temperatures 3-9

3.3 Salinity and Texture Procfiles for Multi-Year Ridge (left) and Multi-Year Floe (right) Ice Samples 3-12

3.4 Vertical Salinity and Texture Profile of First-Year Ice 3-13

3.5 Geometry of the Five Frederking Test 3-14

3.6 Illustration of Stress and Strain Histories for Different Testing Machine Stiffness 3-16

3.7 Dependence on Time of Experimentally Observed Stress, Strain, and Theoretical Strain and its Three Components for S_2 Ice of Average Grain Size 4.5 mm at -10°C 3-18

3.8 Formation of the First Cracks:
(a) Total Strain and its Components for Formation of First Cracks
(b) Stress and Temperature Dependence of Creep Strain to the Formation of the First Large Cracks 3-19

3.9 Temperature Dependence of Critical Delayed Strain for the Formation of the First Large Cracks in S_2 Ice of Average Grain Diameter 4.5 mm 3-20

3.10 Time to Cracking for Different Stresses Based on Sinha's Theory and Comparison with Experiment 3-21

3.11 Onset of MicroCracking Activity Based on Acoustic Emission Techniques 3-22

3.12 Theoretical Crack Density versus Strain at -10°C, for an Average Grain Size of 4.5 mm 3-23

LIST OF FIGURES (cont'd)

3.13 Strength versus Brine Volume for Tests Types C and E 3-25

3.14 Failure Envelope for S_2 Ice at Two Different Temperatures 3-26

3.15 Vertical Profiles of Salinity, Density and Air Porosity for Core Samples of First-Year Ice:
(a) In-Situ Measurements at -15°C (Core 1)
(b) Laboratory Measurements at -28°C After Six Months' Storage at -40°C 3-29

3.16 Young's Modulus for Ice as a Function of Porosity 3-30

3.17 Comparison of Flexural and Horizontal Tensile Strength versus the Square Root of the Brine Volume 3-42

3.18 Shear Strength for Various Specimen Orientations as a Function of Total Porosity for Columnar-Grained Sea Ice 3-43

3.19 Adhesion Strength of Ice versus Salinity, Temperature, Stress Rate and Pile Diameter 3-45

4.1 Illustration of the Force-Time History for a Floe/Hans Island Interaction 4-2

4.2 Illustration of Definition of Limit-Stress Load 4-5

4.3 Results from an Analysis of Environmental Loads Acting on an Ice Feature During an Interaction with a Marine Structure 4-6

4.4 Values for the Ridge-Building Foce from Several Studies 4-8

4.5 Illustration of Typical Ranges of Global Loads as a Function of Ridge Building Force 4-9

4.6 Illustration of Crushing, Bending and Rubble Building Failure Modes 4-12

4.7 Flow Chart of Probabilistic Design Load Methodology 4-14

4.8 Floe Chart of Overall Logic for Determining Design Ice Loads 4-16

LIST OF FIGURES (cont'd)

5.2.1 Ice Failing at te Gulf Molikpaq Structure 5-3

5.2.2 Observed Brittle Ice Failure Modes as a Function of Aspect Ratio 5-7

5.2.3 Force-Time Histories of the Different Brittle Ice Failure Modes Observed by Michel and Blanchet Note how the Force-Time History Depends on the Failure Mode 5-8

5.2.4 Observed Brittle Ice Failure Modes Observed by Timco (1986) 5-9

5.2.5 Force-Time Histories of the Different Brittle Ice Failure Modes Observed by Timco. Note how the Force-Time History Depends on the Failure Mode 5-10

5.2.6 Deformation Mode Map Showing Dominant Failure Mode as a Function of Aspect Ratio and Strain Rate 5-12

5.2.7 The Four Fundamental Ice/Structure Failure Modes 5-14

5.2.8 Crushing or Pulverization of Ice into Small Blocks. The Largest Blocks in the Centre of the Photograph have Lengths of About 2 metres 5-16

5.2.9 Illustration of Crushing with Radial and Circumferential Cracking Occurring at the Gulf Molikpaq. Compare with Cases "c" and "d" in Figure 5.2.4 5-17

5.2.10a Illustration o Plane Stress and Plane Strain Geometries 5-23

5.2.10b Yield Surface, Showing Effect of Plane Stress and Plane Strain Confinement Situations 5-23

5.2.11 Illustrations of the Prandtl and Hill Bearing Capacity Velocity Fields 5-26

5.2.12 Out-of-Plane Failure Mechanism 5-28

5.2.13 Values of the Indentation Factor from Several Studies 5-29

LIST OF FIGURES (cont'd)

5.2.14 Different Abutment Shapes: The Ice Load on each will be Different for each, according to the Methodology 5-31

5.2.15 Basis of Statistical Design Stress Reduction for Wide Structures 5-38

5.2.16 Illustration of Difference between Single Zone, Multi-Zone and FIS (empirical) Ice Failure Pressure Theories 5-39

5.2.17 Empirical Peak Ice Failure Pressure Aspect Ratio Relationships, Showing Recently Released Ice Load Measurements for Comparison 5-41

5.2.18 Croasdale's Simplified Universal Ice Pressure Curve 5-46

5.2.19 Failure Pressure as a Function of Area 5-47

5.2.20 Examples of Discrete Element Modeling 5-52

5.2.21 Comparisons of Measured and Calculated Stress at First Crack for Different Ice Types 5-54

5.2.22 Illustration of Damage Progression 5-56

5.2.23 Profile and Plan Views of the Multi-Year Ridge Used in the Scenario 5-61

5.2.24 Detail of Forces Acting on the Structure and the Ridge at the Moment of Breakout 5-64

5.2.25 Force-Time Histories for the Interaction Showing Limit ©tress Load, Breakout Ridge Load and Brittle Failure Load Subsequent to Ridge Breakout 5-65

5.2.26 Croasdale (1980) Shear Failue Analysis of an Unconsolidated Ridge 5-67

5.2.28 Cross-Section of First-Year Ridge Used by Prodanovic 5-69

LIST OF FIGURES (cont'd)

5.2.29	Dimensionless Loads for Crushing and Shearing Failure Modes for a First-Year Ridge	5-69
5.2.30	Comparison of Experimental and Theoretical Buckling Loads	5-71
5.2.31	Illustration of Instability Conditions for Floes in Close Pack Conditions	5-73
5.3.1	Types of Sloping Structures	5-79
5.3.2a	Sheet Ice Failue Mechanisms During Interaction with a Sloping Structure	5-81
5.3.2b	Photo of Ice Breaking on a Conical Structure During a Model Test in the Esso Ice Basin	5-82
5.3.3	Sheet Ice Clearing Around a Sloping Structure	5-83
5.3.4	Consolidated (Multi-Year) Ridge Interaction With a Conical Structure	5-85
5.3.5	General Logic Approach for Calculating Loads on Sloping or Conical Structures	5-88
5.3.6	Initial Interaction Between an Ice Sheet and a Sloping Structure	5-90
5.3.7	Illustration of Frictional Components During the Interaction of Sheet Ice and a Sloping Structure	5-91
5.3.8	Values of the Two Coefficients C_1 and C_2 as a Function of Slope Angle	5-94
5.3.9	Horizontal Force versus Slope Angle and Friction (Simple Two-Dimensional Theory)	5-95
5.3.10	Horizontal Force versus Flexural Strength (Simple Two-Dimensional Theory)	5-97
5.3.11	Illustration of Relative Importance of Ice Ride-Up and Ice Breaking Forces on a Sloping Structure	5-98

LIST OF FIGURES (cont'd)

5.3.12 Three-Dimensional Effects of Ice/Structure Interaction on Sloping Structures 5-100

5.3.13 Summary of Results from Danys and Bercha (1976) 5-102

5.3.14 Illustration o Flow Diagram of APOA 87 Methodology 5-103

5.3.15 Thee-Dimensional Calculation of Ice Forces on a Sloping Structure 5-105

5.3.16 The A and B Coefficients for Ralston's Plastic Analysis 5-107

5.3.17 Horizontal Force versus Ice Thickness for a Narrow Structure Calculated Using Ralston's Theory 5-108

5.3.18 Horizontal Force versus Ice Thickness for a Wide Structure Calculated Using Ralston's Theory 5-109

5.3.19 Comparison of Ralston's Theory with the Results of Test Data Presented in Edwards and Croasdale (1976) 5-111

5.3.20 Comparison of Force Calculated Using Ralston's Theory with Test Results from the Esso Basin 5-113

5.3.21 Comparison of Horizontal Force Calculted by Kim and Kotras (1973) and Semeniuk (1975) with Test Results from Edwards et al., (1974) and Verity (1975) 5-114

5.3.22 Comparison of Horizontal Force Calculated for Wax Model Ice with Test Results 5-115

5.3.23 Peak Ice Force Calculated Using (a) Two-Dimensional Theory and (b) Three-Dimensional Theory, versus as Experimentally Measured Peak Force 5-117

5.3.24 Comparison of Measured and Predicted Loads for Ice Failing against a 45° Upward Breaking Inclined Plane 5-118

5.3.25 Comparison of Loads Calculated for Interaction of Sheet Ice wth a Conical Structure 5-125

LIST OF FIGURES (cont'd)

5.3.26 Illustration of Ride-Up Forces During the Interaction of an Ice Sheet with a Sloping Structure 5-126

5.3.27 Illustration o Horizontal Load on a Wide Structure, and the Load Breakdown into that Acting on the Vertical Portion of the Structure and the Ice Breaking and Ride-Up Portions 5-127

5.3.28 Illustration of Adfreeze Force 5-129

5.3.29 Illustration of First Crack and Hinge Crack Definitions for a Conical Structure 5-133

5.3.30 Illustration of First Crack and Hinge Crack Forces as a Function of the Length of the Ridge, for a Conical Structure 5-136

5.3.31 Vertical Force Comparison between Theory and Experimental Results for Wax Ridge Tests 5-138

5.3.32 Horizontal Force Comparison between Theory and Experimental Results for Wax Ridge Tests 5-139

5.3.33 Vertical Force Comparison between Theory and Experimental Results for Basin Ridge Tests 5-140

5.3.34 Horizontal Force Comparison between Theory and Experimental Results for Wax Ridge Tests 5-141

5.3.35 Horizontal Force Comparison between Theory and Experimental Results for Saline Ridge Tests 5-142

5.3.36 Vertical Force Comparison between Theory and Experimental Results for Saline Ridge Tests 5-143

5.3.37 Vertical and Horizontal Force Comparisons Using the Plasticity Method and the Test Results of Edwards and Abdelnour 5-144

5.3.38 Variation of Flexural Strength of First-Year and Multi-Year Ice as a Function of Cross Sectional Area of the Beam 5-148

LIST OF FIGURES (cont'd)

5.3.39 Comparison of Ice Loads on a Narrow Structure, Showing Loss in Advantage of Sloped Structure as Ice Strength is Reduced 5-152

5.4.1 Gulf Canada's Conical Drilling Unit Kulluk 5-154

5.4.2 Illustration of a Semisubmersible 5-155

5.4.3 Dome Petroleum Drillship Operating in Loose Ice Conditions 5-156

5.4.4 Typical Ice Crushing Force Time Histories 5-162

5.4.5 Coefficient C versus Column Diameter, D, and Aspect Ratio D/t 5-162

5.4.6 Ice Forces versus Aspect Ratio D/t 5-164

5.4.7 Normalized Forces versus Ratio of Centre-to-Centre Distance to Column Diameter 5-166

5.4.8 Normalized Unit Buckling Load versus Ratio of Total Exposed Width of Columns to Characteristic Length 5-167

5.4.9 Illustration of Broken Ice Instability 5-167

5.4.10 Graphical Solution of Dimensionless Instability Forces 5-169

5.4.11 General Layout of Bridge Pier Analysis of Calkins (1978) 5-171

5.4.12 Illustration of Calkin's Data Showing Boundary between Ice Arching and No Ice Arching Conditions 5-172

5.4.13 Illustration of Seven-Column Semisubmersible Geometry 5-173

5.4.14 Measured M.V. Arctic Broken Ice Resistance Comparison with Empirical Predictions 5-175

5.4.15 Illustration of Shielding for a Four-Column Semisubmersible 5-177

LIST OF FIGURES (cont'd)

5.4.16 Illustration of Shielding of a Vessel by a Single Point Mooring Buoy 5-177

5.4.17 Illustration of a Semisubmersible with Downward Breaking Cones 5-179

5.4.18 Illustration of a Semisubmersible with Inclined Colums 5-179

5.4.19 Measured M.V. Arctic Broken Ice Resistance Comparison with Empirical Predictions as a Function of Ice Thickness 5-183

5.4.20 Measured M.V. Arctic Broken Ice Resistance Comparison with Empirical Predictions as a Function of Floe Size 5-183

5.4.21 Pre-Determined Springs in a Ship-Ice Collision Model 5-186

5.4.22 In-Plane Plastic Failure Mechanism for an Ice Floe Impacting a Semisubmersible Column 5-189

5.4.23 Out-Of-Plane Plastic Failure Mechanism for an Ice Floe Impacting on a Semisubmersible Column (Tresca Material) 5-189

5.4.24 Out-Of-Plane Plastic Failure Mechanism for an Ice Floe Impacting on a Semisubmersible Column (Mohn-Coulomb Material) 5-191

5.4.25 Indentation Factor C_1 versus Friction Angle 5-191

5.5.1 Artificial Island Designs 5-195

5.5.2 Rubble Field Formation 5-199

5.5.3 Simple Model of Ice Push or Ride-Up 5-201

5.5.4 Slope Instability Mechanisms 5-204

5.5.5 Island Design Details to Prevent Ride-Up 5-206

5.5.6 Model of Grounded Pile-Up 5-208

5.5.7 Observed Grounded Pile-Ups 5-209

LIST OF FIGURES (cont'd)

5.5.8 Model of an Extruded Grounded Pile-Up 5-210

5.5.9 Observed Extruded Grounded Pile-Up 5-210

5.5.10 Non-Dimensional Height of Pile-Up versus Angle of Pile-Up for Various Friction Coefficients 5-211

5.5.11 Grounded Pile-Up Heights 5-213

5.5.12 Downward Breaking Ridging Mechanisms 5-214

5.5.13 Free Floating Pile-Up Heights 5-215

5.5.14 Effect of Rubble Width 5-218

5.5.15 Illustration o Transfer of Load from Rubble to Foundation 5-218

5.5.16 Illustration of Rubble Growth and Subsequent Block Failure Analysis 5-219

5.5.17 Mars Island Construction Using Stang Monitors 5-223

5.5.18 CIDS Ice Barrier Under Construction 5-224

5.5.19 Illustration of Temperature Distribution in a Rubble Pile 5-226

5.5.20 Illustration of Rubble Field Generator 5-231

5.5.21 Illustration of Using Spray Ice to Ground and Stabilize a Rubble Field 5-232

5.6.1 Ice Force Time History Plots 5-237

5.6.2 Cook Inlet Platform 5-239

5.6.3 Bo-Hai Gulf Platforms 5-240

5.6.4 Norstromsgrund Lighthouse 5-242

5.6.5 Acceleration Envelope for Norstromgrund Lighthouse 5-244

5.6.6 Details from Normstromgrund Lighthouse Acceleration Records 5-245

LIST OF FIGURES (cont'd)

5.6.7 Idealized Saw-Toothed Ice Force Function 5-246

5.6.8 Negative Slope of Ice Strength versus Loading Rate 5-247

5.6.9 The Vibration Isolted Lighthouse Kemi-2, Natural Modes and Frequencies, and Modal Damping Required to Supress Ice Induced Vibrations 5-250

5.6.10 Ice/Structure Interaction Model of Matlock 5-252

5.6.11 Comparison of Computed and Measured Ice Forces 5-255

5.6.12 Total Force on a Pile Calculated Using the Computer Model 5-256

5.6.13 Small Ice Pieces Produced in Crushing 5-257

5.6.14 Pulverization of Ice During Crushing at the Gulf Molikpaq 5-258

5.6.15 Ice Crushing Sequence to Pulverize Ice 5-261

5.6.16 Foce Time History for Sequence in Figure 5.4.15 5-262

5.7.1 Definition of Local Loads 5-265

5.7.2 Brown's Finite Element Model 5-270

5.7.3 The Brian Watts and Associates Probalistic Loads Model for Winter Conditions 5-275

5.7.4 The Brian Watts and Associates Probalistic Loads Model for Summer Conditions 5-275

5.7.5 Sanderson's Empirical Ice Failue Pressure Curve 5-277

5.7.6 Brian Watts and Associates Empirical Failure Pressure Curves for Multi-Year Ice and First-Year Ice 5-280

5.7.7 Iyer's Empirical Ice Failure Pressure Curve 5-285

5.7.8 The Norwegian Research Empirical Ice Failure Pressure Curve 5-284

LIST OF TABLES

3.1 Classification of Selected Fresh Water and Saline Water Ice Types 3-4

3.2 Multi-Year Ice Compressive Strength 3-30

3.3 Iceberg Uniaxial Compressive and Indentation Strengths 3-31

3.4 Rubble Porosity Measurements and Estimates 3-47

3.5 Shear Properties of Ice Rubble 3-48

5.2.1 Chronological Order of Theories Used (and Proposed) to Calculate Ice Loads on Structures 5-19

5.2.2 Comparison of Values for the Indentation Factor (I) from Several Studies 5-25

5.2.3 Values of the Contact Factor, C, from Korzhavin (1971) 5-30

5.2.4 Values of the Shape Coefficient, M, from Soviet Construction Standards and Rules, Moscow, 1983 5-32

5.3.1 Esso Ice Basin Data 5-112

5.3.2 Horizontal Force on Conical Tower Calculated by Ten Methods 5-119

5.3.3 Horizontal Force on a 18 m Diameter Conical Tower 5-122

5.3.4 Horizontal Force on a Wide Conical Structure 5-123

5.5.1 Buckling Strength of a Competent Ice Sheet 5-203

5.7.1 Comparison of Model Results 5-271

5.7.2 Ice Strength Ratio Data from Blanchet (1986) 5-287

5.7.3 Finnish-Swedish Design Ice Loads 5-291

5.7.4 Russian Design Loads 5-292

5.7.5 Canadian Design Ice Loads 5-293

ICE FORCES ON MARINE STRUCTURES

NOMENCLATURE

Chapter 3 Nomenclature

Variable	Definition	Page Number or Figure Number
e	strain	Page 3.3 - 4
e_e	elastic strain	Page 3.3 - 4
e_d	delayed elastic strain	Page 3.3 - 4
e_v	viscous or permanent strain	Page 3.3 - 4
σ_{th}	horizontal tensile strength of ice (MPa)	Figure 3.17
σ_f	flexural strength of ice (MPa)	Figure 3.17
v_b	brine volume	Figure 3.17
τ	shear strength	Figure 3.18
v_t	total porosity (air and brine)	Figure 3.18

Chapter 4 Nomenclature

Variable	Definition	Page Number or Figure Number
F	limit-stress load	Page 4.2 - 2
p	ice failure pressure	Page 4.2 - 2
D	chord width of interaction on structure	Page 4.2 - 2
t	average thickness of ice interacting with the structure	Page 4.2 - 2
F_C	current drag force (MN)	Figure 4.3
F_W	wind drag force (MN)	Figure 4.3
F_{RB}	ridge-building force (MN)	Figure 4.3
X_1	penetration of edge of floe at which point the floe begins to slow down	Figure 4.3
X_2	penetration of edge of floe at which point the floe stops	Figure 4.3
X	distance of penetration of front edge of floe	Page 4.2 - 4
EF_x	total sum of environmental forces acting at a penetration x	Page 4.2 - 4
ΔEK	change of kinetic energy during an increment of penetration dx	Page 4.2 - 4
FS_x	load on the structure at a penetration x	Page 4.2 - 4

Section 5.2 Nomenclature

Variable	Definition	Page Number or Figure Number
V	Ice velocity	Page 5.2 - 6
D	Structure diameter	Page 5.2 - 6
I	Indentation factor	Page 5.2 - 11
C	Contact factor	Page 5.2 - 11
M	Shape factor	Page 5.2 - 11
σ_u	Unconfined crushing pressure	Page 5.2 - 11
X, Y, Z	Horizontal and vertical axes for plane strain and plane stress geometries	Page 5.2 - 12
L	Calculated ice load	Page 5.2 - 17
t	Ice sheet thickness	Page 5.2 - 17
$\dot{\epsilon}$	Strain rate	Page 5.2 - 18
ν	Brine volume	Page 5.2 - 28
ν_o	Reference brine volume (brine volume at which strength of ice becomes zero)	Page 5.2 - 28
ψ	Reference stress coefficient	Page 5.2 - 28
A	Constant	Page 5.2 - 28
Q	Activation energy of ice	Page 5.2 - 28
R	Universal gas constant	Page 5.2 - 28
T	Temperature in °K	Page 5.2 - 28
n	Creep index of ice	Page 5.2 - 28
e_d	Delayed elastic strain	Page 5.2 - 31
E	Young's modulus of ice	Page 5.2 - 31
d	Ice grain diameter	Page 5.2 - 31
d_1	Unit of grain diameter	Page 5.2 - 31
a_T	Constant in Sinha's analysis	Page 5.2 - 31
c_1	Constant in Sinha's analysis	Page 5.2 - 31
b	Constant in Sinha's analysis	Page 5.2 - 31

$\Delta\sigma$	Stress increase per time increment	Page 5.2 - 31
N	Number of time increments	Page 5.2 - 31
t	Time per increment	Page 5.2 - 31
i	Increment index on summation	Page 5.2 - 31
D	Damage coefficient	Page 5.2 - 32
σ_c	Crushing strength of ice based on empirical data	Figure 5.2.24
σ_s	Ice shear strength	Figure 5.2 24
L	Ridge length	Figure 5.2 24
B	Width of ridge	Page 5.2 - 39
t	Keel draft of ridge	Page 5.2 - 39
g	Gravity, 9.1 m/s^2	Page 5.2 - 39
ρ_i	Density of ice	Page 5.2 - 39
ρ_w	Density of water	Page 5.2 - 39
ϕ	Internal angle of friction of the ridge	Page 5.2 - 39
P	Ice load in Prodanovic ridge model	Page 5.2 - 40
C	Cohesion of ice blocks	Page 5.2 - 40
K	Ratio of keel draft to sail height	Page 5.2 - 40
X	Ratio of block to Euler instability	Page 5.2 - 42
f_{ins}	Instability load for blocks	Page 5.2 - 42
f_e	Euler instability load	Page 5.2 - 42
Y	Quotient used in analysis	Page 5.2 - 42
k	Foundation modulus	Page 5.2 - 42
l	Length of block	Page 5.2 - 42
I	Moment of inertia per unit width	Page 5.2 - 42

Section 5.3 Nomenclature

Variable	Definition	Page Number or Figure Number
N	Normal force	Figure 5.3.2a
μ	Coefficient of friction	Figure 5.3.2a
V	Vertical component of force	Figure 5.3.6
H	Horizontal component of force	Figure 5.3.6
α	Slope angle of sloping structure	Figure 5.3.6
t	Ice sheet thickness	Figure 5.3.6
Z	Height of sloping structure above waterline	Figure 5.3.7
wg	Weight of an ice block	Figure 5.3.7
R	Normal force	Figure 5.3.7
σ_f	Flexural strength of ice	Page 5.3 - 7
M_o	Bending moment capacity	Page 5.3 - 7
b	Width of an ice beam	Page 5.3 - 7
l	Characteristic length of ice	Page 5.3 - 8
K	Foundation constant (also denoted k)	Page 5.3 - 8
ρ_w	Density of water	Page 5.3 - 8
g	Gravity	Page 5.3 - 8
E	Young's, or elastic modulus	Page 5.3 - 8
I	Moment of Inertia	Page 5.3 - 8
ρ_i	Density of ice	Page 5.3 - 9
P	Force required to push ice up the slope of the structure	Page 5.3 - 9
C_1	Coefficient in ride-up analysis	Page 5.3 - 10
C_2	Coefficient in ride-up analysis	Page 5.3 - 10

P	Failure force on tip of wedge in the Nevel analysis	Page 5.3 - 12
b_o	Constant describing the width of the wedge in the Nevel analysis	Page 5.3 - 12
a	Distance along the wedge in Nevel analysis	Page 5.3 - 12
l	Characteristic length of a plate in Nevel analysis	Page 5.3 - 12
h	Ice thickness in Frederking analysis	Figure 5.3.15
B	Inclined plane width in Frederking analysis	Figure 5.3.15
V	Ice sheet velocity in Frederking's analysis	Figure 5.3.15
a	Slope angle used in Frederking's analysis	Figure 5.3.15
β	Twice the trapezoidal angle used in Frederking's analysis	Figure 5.3.15
A_1 to A_4	Coefficients in Ralston analysis	Page 5.3 - 15
B_1 and B_2	Coefficients in Ralston analysis	Page 5.3 - 15
D	Conical structure diameter at the waterline	Page 5.3 - 15
D_T	Conical structure diameter at its top	Page 5.3 - 15
φ	Angle of rotation of ice block	Page 5.3 - 20
W	Weight of ice block	Figure 5.3.26
F_H	Horizontal component of force	Figure 5.3.26
F_V	Vertical component of force	Figure 5.3.26
B	Buoyancy	Figure 5.3.26
q	Adfreeze bond or shear strength	Page 5.3 - 21
V_1	Initial vertical force to crack a consolidated ridge	Page 5.3 - 24
y	distance to the surface in tension (for formation of initial crack)	Page 5.3 - 24

V_2	Vertical force to cause hinge cracks to form in a consolidated ridge	Page 5.3 - 25
y	distance to bottom in tension (for formation of hinge cracks)	Page 5.3 - 25
R_V	Vertical force to initiate cracking of a ridge	Figure 5.3.30
R_V	Vertical force to initiate cracking in a ridge of infinite length	Figure 5.3.30
L	Length of ridge	Figure 5.3.30
$A^{\frac{1}{2}}$	Square root of beam section in the determination of large scale flexural strength	Figure 5.3.38

Section 5.4 Nomenclature

Variable	Definition	Page Number or Figure Number
$[M]$	virtual mass (mass + added mass) matrix	Page 5.4 - 3
$[C]$	matrix of linear drag coefficients	Page 5.4 - 3
$[D]$	matrix of hydrodynamic drag coefficients	Page 5.4 - 3
$[K]$	hydrostatic stiffness vector	Page 5.4 - 3
$(\ddot{x})$	acceleration vector for surge, sway, heave, roll, pitch, and yaw	Page 5.4 - 3
$(\dot{x})$	velocity vector	Page 5.4 - 3
(x)	displacement vector	Page 5.4 - 3
(F_i)	vector of ice forces on the structure	Page 5.4 - 3
(F_s)	vector of structure forces on the ice, equal and opposite to (F_i)	Page 5.4 - 3
$(F_{w\&w})$	vector of wind and wave forces	Page 5.4 - 3
(F_m)	vector of mooring forces	Page 5.4 - 3
C	Coefficient of ice crushing from Kato and Sodhi (1983)	Figure 5.4.5
D	Column diameter	Figure 5.4.5
t	Ice sheet thickness	Figure 5.4.5
f	Frequency of ice crushing	Page 5.4 - 7
V	Ice sheet velocity (or vessel speed)	Page 5.4 - 7
F_{mean}	Mean ice crushing force on column	Page 5.4 - 7
F_{max}	Maximum ice crushing force on column	Page 5.4 - 7
σ_{mean}	Mean ice crushing pressure	Page 5.4 - 7
σ_{max}	Maximum ice crushing pressure	Page 5.4 - 7

σ_u	unconfined ice crushing pressure	Page 5.4 - 7
S	Centre to centre spacing of columns	Page 5.4 - 8
f_{ins}	Instability force per unit width for buckling of small floes	Page 5.4 - 8
k	Foundation modulus (unit weight of water)	Page 5.4 - 8
ν	Poisson's ratio	Page 5.4 - 8
R	Ratio used in buckling analysis	Page 5.4 - 8
X	Ratio used in buckling analysis	Page 5.4 - 9
Y	Ratio used in buckling analysis	Page 5.4 - 9
E	Young's modulus of ice	Page 5.4 - 9
l	length of ice pieces	Page 5.4 - 9
I	Moment of inertia per unit width of ice	Page 5.4 - 9
S(0°)	Width orientation between columns of a semisubmersible	Page 5.4 - 10
S(90°)	Length orientation between columns of a semisubmersible	Page 5.4 - 10
B	Width of channel in Calkins analysis	Figure 5.4.11
V_S	Ice drift velocity	Figure 5.4.11
Q_i	Surface ice discharge	Figure 5.4.11
a_i	Diameter of individual floes	Figure 5.4.11
b_1	Clearance between piers	Figure 5.4.11
b_2	Centre spacing of piers	Figure 5.4.11
$\bar{a}$	Average floe size	Figure 5.4.12
D_{long}	Length of semisubmersible	Figure 5.4.13
D_{wide}	Width of semisubmersible	Figure 5.4.13
θ_i	Orientation of ice drift direction with respect to centreline of semisubmersible	Figure 5.4.13

ϕ_0	Outer column diameter	Figure 5.4.13
ϕ_C	Centre column diameter	Figure 5.4.13
ϕ_R	Riser column diameter	Figure 5.4.13
f_b	Blockage factor	Page 5.4 - 11
S_4	Shadow width on Column 4	Figure 5.4.15
W_4	Width of ice interacting with Column 4	Figure 5.4.15
V_i	Velocity of ice	Figure 5.4.16
$R_{\text{sheet ice}}$	Resistance of level sheet ice	Page 5.4 - 15
C_b	Ice breaking coefficient	Page 5.4 - 15
C_s	Ice submerging coefficient	Page 5.4 - 15
C_v	Velocity coefficient	Page 5.4 - 15
C_k	Floe size coefficient	Page 5.4 - 16
$k_i^{s,g}$	Stiffness of growler and ship components	Figure 5.4.21
V_g	Velocity of growler	Figure 5.4.21
Q_n	Normal pressure to cause in-plane failure	Page 5.4 - 20
c	Cohesion of ice	Page 5.4 - 20
P	Normal pressure	Page 5.4 - 20
ϕ	Internal friction	Page 5.4 - 20
ψ	Angle used in analysis	Page 5.4 - 20
α	Angle of inclination of load	Page 5.4 - 20
η	Angle used in analysis	Page 5.4 - 20
θ	Angle used in analysis	Page 5.4 - 20
W	Width of interaction	Figure 5.4.22

Section 5.5 Nomenclature

Variable	Definition	Page Number or Figure Number
W	Weight of pushed ice per unit width	Page 5.5 - 6
ρ_i	Density of ice	Page 5.5 - 6
g	Gravity	Page 5.5 - 6
t	Thickness of the ice sheet	Page 5.5 - 6
x	Horizontal length of ice push	Page 5.5 - 6
θ	Angle of slope up which ice is pushed	Page 5.5 - 6
μ	Ice to slope friction coefficient	Page 5.5 - 6
F_t	Force parallel to slope	Page 5.5 - 6
F_n	Force normal to slope	Page 5.5 - 6
W_t	Weight of ice acting along slope	Page 5.5 - 6
y	Height of front of ice sheet	Page 5.5 - 6
σ_b	Buckling strength of ice sheet	Page 5.5 - 7
K	0.01 MPa/m	Page 5.5 - 7
E	Young's Modulus	Page 5.5 - 7
σ_c	Ice sheet crushing strength	Page 5.5 - 8
σ_t	Ice sheet tensile strength	Page 5.5 - 8
F_{ff}	Free floating ridging force per unit width	Page 5.5 - 10
H_s	Free floating sail height	Page 5.5 - 10
F	Total free floating ridging pressure per unit width	Page 5.5 - 11
H_k	Keel depth below the ice sheet	Page 5.5 - 11
H_s	Sail height above the ice sheet	Page 5.5 - 11
K_p	Passive pressure coefficient	Page 5.5 - 11

γ_s	Porosity of sail	Page 5.5 - 11
γ_k	Porosity of keel	Page 5.5 - 11
μ_s	Ice sheet to sail friction coefficient	Page 5.5 - 11
μ_k	Ice sheet to keel friction coefficient	Page 5.5 - 11
θ	Angle between sail and horizontal	Page 5.5 - 11
ϕ	Angle between keel and horizontal	Page 5.5 - 11
F_{ff}	Conservative free floating ridging force per unit length	Page 5.5 - 11
$F_{structure}$	Force on a structure or artificial island at its waterline	Page 5.5 - 13
F_{ice}	Pack ice force acting on ice rubble surrounding a structure	Page 5.5 - 13
$F_{grounding}$	Force transmitted through the rubble to the berm or seabed	Page 5.5 - 13
μ_{ib}	Coefficient of friction of ice sliding on the berm	Page 5.5 - 14
W	Weight of the sail of the grounded rubble	Page 5.5 - 14
B	Buoyant weight of the keel of the grounded rubble	Page 5.5 - 14
$H_{s,avg.}$	Average sail height of the grounded rubble	Page 5.5 - 14
$H_{k,avg.}$	Average keel depth of the grounded rubble	Page 5.5 - 14
ρ_i	Mass density of ice (0.9 ρ_w)	Page 5.5 - 14
ρ_w	Mass density of water	Page 5.5 - 14
γ_s	Porosity of the sail	Page 5.5 - 14
γ_k	Porosity of the keel	Page 5.5 - 14
A	Waterplane area of the grounded rubble	Page 5.5 - 14
Q_c	Amount of heat conducted through a layer	Page 5.5 - 16
k	Thermal conductivity (W/m°C)	Page 5.5 - 16

t	Ice layer thickness (m)	Page 5.5 - 16
T_b	Temperature at the bottom of the layer (°C)	Page 5.5 - 16
T_s	Temperature at the top of the layer (°C)	Page 5.5 - 16
$k_{sail,\ ice,\ spray\ ice}$	Thermal conductivity for the different ice types (W/m°C)	Page 5.5 - 17
$t_{sail,\ ice,\ spray\ ice}$	Layer thickness (m)	Page 5.5 - 17
T_a	Air temperature (°C)	Page 5.5 - 17
T_b	Freezing temperature of sea water, assumed to be -1.8°C	Page 5.5 - 17
T_0	Temperature at the top of the spray ice (°C)	Page 5.5 - 17
T_1	Temperature at the top of the sail (°C)	Page 5.5 - 17
T_2	Temperature at the bottom of the sail (°C)	Page 5.5 - 17
Q_{thf}	Sensible heat flux	Page 5.5 - 18
ρ_a	Air density, (1.3 kg/m^3)	Page 5.5 - 18
C_p	Specific heat of air at constant pressure (1005 J/kg°C)	Page 5.5 - 18
C_s	Sensible heat transfer coefficient	Page 5.5 - 18
V	Wind speed (m/s)	Page 5.5 - 18
T_a	Air temperature (°C)	Page 5.5 - 18
T_s	Surface temperature (°C)	Page 5.5 - 18
Q_{lr}	Heat flux due to long wave radiation	Page 5.5 - 18
Q_{Ilr}	Incoming long wave radiation	Page 5.5 - 18
ϵ	Emissivity (approximately 1.0 for ice)	Page 5.5 - 18
σ	Stefan-Boltzmann constant (5.67 x 10^{-8} (Wm^{-2}°K^{-4})	Page 5.5 - 18
T_s	Surface temperature (°K)	Page 5.5 - 18

γ_2	Porosity below water line	Page 5.5 - 19
h_{1f}	Latent heat of sea ice	Page 5.5 - 19
dt	Thickness of ice growth	Page 5.5 - 19

Section 5.6 Nomenclature

Variable	Definition	Page Number or Figure Number
v	Velocity of ice	Page 5.6 - 6
t	Thickness of ice	Page 5.6 - 6
f	Frequency of ice crushing	Page 5.6 - 6
k	Stiffness coefficient of structure	Page 5.6 - 6
F	Ice force range	Page 5.6 - 6
[m]	Mass matrix	Page 5.6 - 9
[c]	Matrix of linear drag coefficients	Page 5.6 - 9
[k]	Hydrostatic stiffness matrix	Page 5.6 - 9
$(\ddot{x})$	Acceleration	Page 5.6 - 9
$(\dot{x})$	Velocity	Page 5.6 - 9
(x)	Displacement	Page 5.6 - 9
P(t)	Ice failure pressure	Page 5.6 - 9
$X_c(t)$	Displacement of structure at point of contact of the ice	Page 5.6 - 9
v_i	Velocity of ice	Page 5.6 - 9
P	Length of penetration zone	Page 5.6 - 9
F	Length of failure zone	Page 5.6 - 9
m	Shape factor	Page 5.6 - 10
D	Chord width of interaction zone	Page 5.6 - 10
h	Ice thickness	Page 5.6 - 10
A	Constant relating stress and penetration	Page 5.6 - 10
kcc	Apparent stiffness of ice during the penetration phase	Page 5.6 - 10
Pr(t)	Residual resistance of ice in the failed zone	Page 5.6 - 10

Section 5.7 Nomenclature

Variable	Definition	Page Number or Figure Number
L	Peak ice load	Page 5.7 - 8
I	Indentation factor	Page 5.7 - 8
C	Contact factor	Page 5.7 - 8
M	Shape factor	Page 5.7 - 8
σ_u	unconfined horizontal uniaxial compressive strength of ice	Page 5.7 - 8
D	Chord width of interaction surface	Page 5.7 - 8
t	Average ice thickness at the interaction surface	Page 5.7 - 8
P	Local Pressure	Page 5.7 - 11
A	Area of interaction (= D t)	Page 5.7 - 11
P_{eff}	Effective ice failure pressure	Page 5.7 - 13
P_1	Local ice pressure	Page 5.7 - 14
b_1	horizontal breadth of local load area (= D)	Page 5.7 - 14
h	Maximum "vertical" depth of the total area of the structure in contact with the ice	Page 5.7 - 14
A	Local load area (cm^2)	Page 5.7 - 14
A_o	1.0 cm^2	Page 5.7 - 14
σ_u	Maximum uniaxial crushing strength of the ice	Page 5.7 - 14
K	Confinement coefficient	Page 5.7 - 14

1.0 Introduction

In the last decade increased exploration for conventional energy sources in Canada's North has focused attention on the engineering problems of designing and building large structures in ice covered waters. The interaction of ice with marine structures and the forces generated by various forms of ice have been recognized as major design considerations. Various techniques have been developed for estimating both global and local design ice forces on marine structures and these are presented and reviewed in this report.

This report provides the backup and discussion to a companion report entitled "Ice Forces on Marine Structures, Volume I, Calculation Procedures."

In the next chapter the various ice geometries encountered in selected Canadian marine regions are briefly reviewed.

In Chapter 3 the engineering mechanical properties of ice are reviewed, along with a detailed discussion of testing procedures and the small scale behaviour of ice.

In Chapter 4 an introduction to the general logic for evaluating ice/structure interactions is presented.

The major effort for this study is presented in Chapter 5 where detailed discussions of the interaction load theories for vertical sided, sloping and floating structures, and artificial islands are presented. Sections on ice/structure interaction dynamics and local loads are also included in Chapter 5.

In Chapter 6 a summary of both volumes of this study is provided, along with recommendations to study some of the problems and uncertainties examined in this report.

2.0 Ice Types and Regions

2.1 Introduction

The ice infested regions of Canada are characterized by different environments and different predominant ice types. The mechanical properties of ice also vary over a wide range. In this chapter the different types of ice to which a structure may be exposed for selected regions are examined. References are provided for those requiring more detailed information.

The different types of ice found in Canada's marine environments, reviewed in Section 2.2 have been broken down into eight different types:

- first-year ice floes and landfast ice
- first-year ridges and rubble fields
- second-year floes and ridges
- multi-year floes
- multi-year ridges and hummock fields
- ice islands and ice island fragments
- icebergs and bergy bits
- pack ice

In Section 2.3 the dominant ice types for the following regions are reviewed:

- Labrador Shelf and Grand Banks
- Baffin Bay and Davis Strait
- Hudson Bay
- High Arctic or Canadian Archipelago
- Beaufort Sea

It should be recognized that the information reviewed in this study has a variety of sources. Petroleum company research programs, government agencies (such as Public Works Canada, the National Research Council of Canada, and the Atmospheric Environment Service), and international programs (such as the International Ice Patrol, or the Marginal Ice Zone Experiments MIZEX-type experimental programs) create much of the raw data which has been reviewed during the course of this study.

There are also facilities where data bases of ice information can be accessed to enable users of the system to perform their own studies without having to acquire data, or process raw data manually. Three such facilities are:

1 - Centre for Cold Ocean Resources Engineering (C-CORE) at Memorial University of Newfoundland,

2 - Atmospheric Environment Service (AES), and

3 - Arctic Institute of North America in Calgary.

2.2 Ice Types

In this report the generic ice types found in Canada's marine environments have been broken down into eight different types:

- first-year ice floes and landfast ice
- first-year ridges and rubble fields
- second-year floes and ridges
- multi-year floes
- multi-year ridges and hummock fields
- ice islands and ice island fragments
- icebergs and bergy bits
- pack ice

First-Year Ice Floes and Landfast Ice

A first-year saline ice sheet is an ice sheet which is no more than one year old. First-year ice sheets have a maximum brine concentration by reason of their being newly formed.

The growth of a first-year ice sheet is characterized by a freezing of the surface of the water at a temperature close to -1.8°C (this is depressed from zero due to the salinity of sea water). After the initial layer of ice is formed the subsequent growth is more orderly, which enables columnar crystals of several millimetres to centimetres in diameter to form. Figure 3.4 (in Chapter 3) shows a vertical salinity and texture profile of a first-year ice sheet.

First-year ice sheet thicknesses of one to two metres are common at the end of the winter in the Canadian Arctic. Dependent on where the first-year ice is formed, the ice may occur in the shape of ice floes (generally elliptical ice floes with "effective diameters" ranging from metres to kilometres in the plan dimension), or as landfast ice which is attached to the adjacent shoreline and moves laterally very little throughout the winter.

First-Year Ridges and Rubble Fields

A first-year ridge is a conglomeration of failed pieces of an ice sheet. Ice ridges are formed along a common stressed boundary where the relative movement of two ice features is sufficient to cause brittle failure of one or both of the ice features. Ridges formed by ice floes or sheets moving towards each other are characterized by large ice blocks. Where the ridge is formed by shearing the block sizes are generally smaller.

After ridge formation the water in the voids or spaces between the ice blocks immediately begins to refreeze. The refreezing of the near-waterline portion of the ridge is responsible for a complex structure developing inside the ridge. The top layer above the waterline has an open blocky structure, the portion of the ridge just below the waterline is composed of ice blocks with their interstices frozen. Below the consolidated layer, as the solidly frozen region is called, is a partially consolidated layer where the blocks are frozen together at their contact points.

Rubble fields are of much greater extent than individual ridges, and can be thought of loosely as a close grouping of ridges. Rubble fields are common around artificial islands in the Beaufort Sea where the thin first-year ice is in motion for the first months of the winter. Along the western edge of the Canadian Archipelago first-year rubble piles can consolidate with time to become multi-year hummock fields.

Second-Year Floes and Ridges

A second-year floe is a floe which has survived one winter and one summer. Typically the "birthday" for ice types is October, where ice which has survived until October is said to be a year older. Second-year ice differs from younger ice in one major way - its brine content or salinity is less than that of younger sea ice due to brine drainage.

A second-year ridge, similarly, has survived one summer season, and it too is different in structure than its first-year counterpart. A second-year ridge has a thicker consolidated layer than its first-year counterpart due to refreezing. The bottom form of the older ridge is also different from its younger counterpart. During the summer season the ice at the bottom melts. This causes the formation of another layer, a layer of slush, out of the bottom portions of the partially consolidated layer. The shape of the ridge becomes more rounded compared to the jagged shape of a first-year ridge due to melting and weathering.

Multi-Year Floes

A multi-year floe is a floe which has survived two melt seasons. A multi-year floe, or multi-year ice in general, is characterized by lower salinity than second-year ice.

Multi-Year Ridges and Hummock Fields

Multi-year ridges are ridges that have survived two melt seasons. The shape of the multi-year ridge is more rounded than its second-year counterpart (Wright et al., 1979).

A multi-year hummock field is a conglomeration of multi-year ridges. Specifically, the phrase multi-year hummock field is used for those particular ice features that break off the landfast ice shores of the western Canadian Archipelago and drift towards the Canadian Beaufort Sea. These ice geometries are formed when many shear ridges are formed in groups as the pack ice shears past the landfast ice. The shearing action, and the proximity of the shoreline abating horizontal motion, causes the keels of the ridges to be very deep.

For more details on the characteristics of multi-year hummock fields the reader is referred to DePaoli et al., (1982), which states that the geometric properties of hummock fields are contained in multi-year floe statistics as obtained from under-ice profiles.

Ice Islands and Ice Island Fragments

Ice Islands are thick pieces of landfast ice which grow in the fjords of Northern Ellesmere Island. The ice shelves are created by a complex interaction between sea ice (initiating the stable platform for growth), fresh water runoff from glaciers, and snow accumulation. It is estimated that thousands of years are required before growth can reach 60 metres or so. During the past hundred years or so the ice shelves have decreased in area, and many ice islands have been created. The ice islands generally drift around the Beaufort Gyre when released from their growth place on Ellesmere Island. Ice islands in the Beaufort Gyre melt at an average rate of about one metre per year.

Occasionally, as happened north of Alaska in the early 1960's and 1970's, ice islands can ground out on shoals. The result of such an interaction is usually a partial or complete breakup of the island causing the release of many ice island fragments.

In terms of design criteria an ice island is the most intimidating ice feature of the Arctic Ocean. In the past ice island areas of several hundred square kilometres have been measured, though due to the decay of the ice shelves over the past 80 years new ice islands with areas of more than a hundred square kilometres are not likely.

For an analysis of the probability of an ice island or fragment interacting with a structure, or a general analysis of the characteristics of the ice shelves, the reader is referred to Spedding (1977, APOA 99) and DePaoli et al., (1982). For an analysis of the growth of the ice shelves of Ellesmere Island the reader is referred to Jeffries (1984).

An ice island makes a complete rotation of the Beaufort Gyre approximately once every 10 years, however there is a relatively good chance (probability = 0.7/revolution) of the ice island leaving the Gyre on each circulation. The sum total of the ablation and the escape probability is such that any ice island will not be a constant threat but will periodically threaten an area depending on its original thickness and total ablation.

In DePaoli et al., (1982) the probability of a sizable ice island interacting with an offshore structure in the Canadian Beaufort Sea was estimated. The return period for an interaction at Kopanoar, a location in 60 m water depth, was estimated to be greater than 1000 years.

Icebergs and Bergy Bits

Icebergs are not present in the Arctic Ocean, they are a distinctly eastern arctic phenomenon; icebergs can be found in Baffin Bay, Davis Strait, sometimes in the Northwest Passage, off the Labrador coast, and on the Grand Banks. Bergy bits (icebergs with sizes less than that of a small house) are also found in these regions.

Most icebergs are calved from Greenland glaciers. After calving the icebergs drift northward along the Greenland Coast and westward towards Devon and Baffin Islands. Subsequently they drift down the Labrador current and onto the Grand Banks. The average lifetime of an iceberg, from its calving from the shelves of Greenland to its melting in the Gulf Stream waters south of Newfoundland, is about three years.

Freshwater iceberg ice is quite strong due to low temperatures within tens of centimetres of the outside surface of the iceberg. At the surface of an iceberg the temperature gradient is very high since a new surface is constantly being exposed and the specific heat of ice is large. Parts of icebergs are also made up of compressed ice, possibly thousands of years old.

Pack Ice

The phrase "pack ice" is reserved for the matrix of ice in a local area which completely covers a region. More particularly, "pack ice" is the commonly accepted terminology for moving ice in a region. This is in contrast to "landfast ice", which is ice which is grounded to the shoreline and moves very little.

The composition of "pack ice" varies from region to region as the predominant ice types change. For example, in the Arctic Ocean one collectively refers to the first year ice, ridges, second and multi-year ice and ridges and hummock fields, and ice islands that constitute the ice of the Beaufort Gyre, as pack ice. In the eastern region such as off Baffin Island or Labrador, the matrix of first year ice, ridges, icebergs and bergy bits is referred to as pack ice. The definition relates to the state of motion of ice rather than its composition.

2.3 Regional Ice Zones

In this study five regional ice zones are discussed. These zones are as follows:

- Labrador Shelf and Grand Banks
- Baffin Bay and Davis Strait
- Hudson Bay
- High Arctic
- Beaufort Sea

Chakraburtty et al., (1984), as part of their Arctic Marine Design and Construction Handbook, prepared for the Transportation Development Centre, reviewed the ice characteristics of Canada's marine environments. This section of the report is based on their work, which should be referred to for more detailed information.

In this section of the report the ice characteristics of the different zones are briefly reviewed. For a better description the reader is referred to the Arctic Pilot of Canada. Another review of the ice in the arctic, particularly along tanker routes in the Northwest Passage and in Baffin Bay, can be found in the Beaufort Sea Environmental Impact Statement (Volume 3B). In each of the subsections below, references are provided for those who desire more specific information. The summary presented herein is intended only for the purpose of describing the general ice characteristics.

The arctic regions are characterized by spatial and temporal differences in ice properties. Even over short distances of a few hundred kilometres (especially in the western archipelago) the ice environment can be vastly different. Local geography and latitude are important factors in determining the average ice environment.

2.3.1 Labrador Shelf and Grand Banks

The Labrador Shelf

The dominant ice features of the Labrador Shelf region are first year pack ice, floes, ridges, icebergs and ice islands.

The ice dynamics of the Labrador Shelf is dominated by the Labrador current.

Along the Labrador Shelf thin ice begins to form around the end of November. The landfast ice extends seaward for up to 25 km and interacts with first year pack ice and icebergs which are forced offshore by winds and the current. Depending on the environmental conditions there may or may not be a stretch of open water between the landfast ice and the pack ice (Chakraburtty et al., 1984).

The thickness the ice reaches at maximum is less than that of other zones, being only about 0.5 to 1.0 m in the undeformed state. The dynamics are less fierce than for other areas such as the Beaufort Sea because of the nearby presence of open water. Thus, on average, ridges have less draft than in other zones.

Seaward of the landfast ice a dense pack forms, containing newly formed first-year ice, multi-year floes from the north, icebergs and the occasional ice island or fragment. The pack, at its greatest extent from the Labrador coast, extends east about 300 km.

The zone of greatest iceberg density is in water less than 1000 m deep. The cause of this is the general counter-clockwise water circulation pattern of Baffin Bay and Davis Strait and the Labrador Sea, which forces the icebergs to the shore boundaries of the regions.

The total number of icebergs passing the northern tip of Labrador is about 2500 per year, 1400 of which survive to reach the northern tip of Newfoundland (Gustajtis, 1978).

With water depths of up to 200 m over the general shelf area, large icebergs are capable of encroaching any structures deployed in the region.

Gustajtis (1978) examined in detail iceberg sightings along the Labrador coast. Figure 2.1 shows the spring iceberg concentration in terms of the number of icebergs sighted per two degree square. Figure 2.2 (NORCOR, 1977) shows the maximum sea ice concentrations in February and March for the Labrador Sea. The highest iceberg concentrations occur at approximately the region where the pack ice is close (6 to 8 - 8ths).

Miller and Hotzel (1983) presented estimates of iceberg flux along the Labrador coast. An average flux of about 400 icebergs per year across 48 degrees latitude based on 1900-1979 statistics was documented in Miller and Hotzel.

The Grand Banks

The dominant ice features of the Grand Banks are first-year ice floes and icebergs.

The first-year pack ice rarely extends as far south as the Banks, usually having a southern boundary at 48 degrees North. Any icebergs that do penetrate the Grand Banks are quickly melted as soon as they interact with the Gulf Stream at the southern region of the Banks.

Icebergs are of concern in the design of bottom founded and floating structures on the Grand Banks.

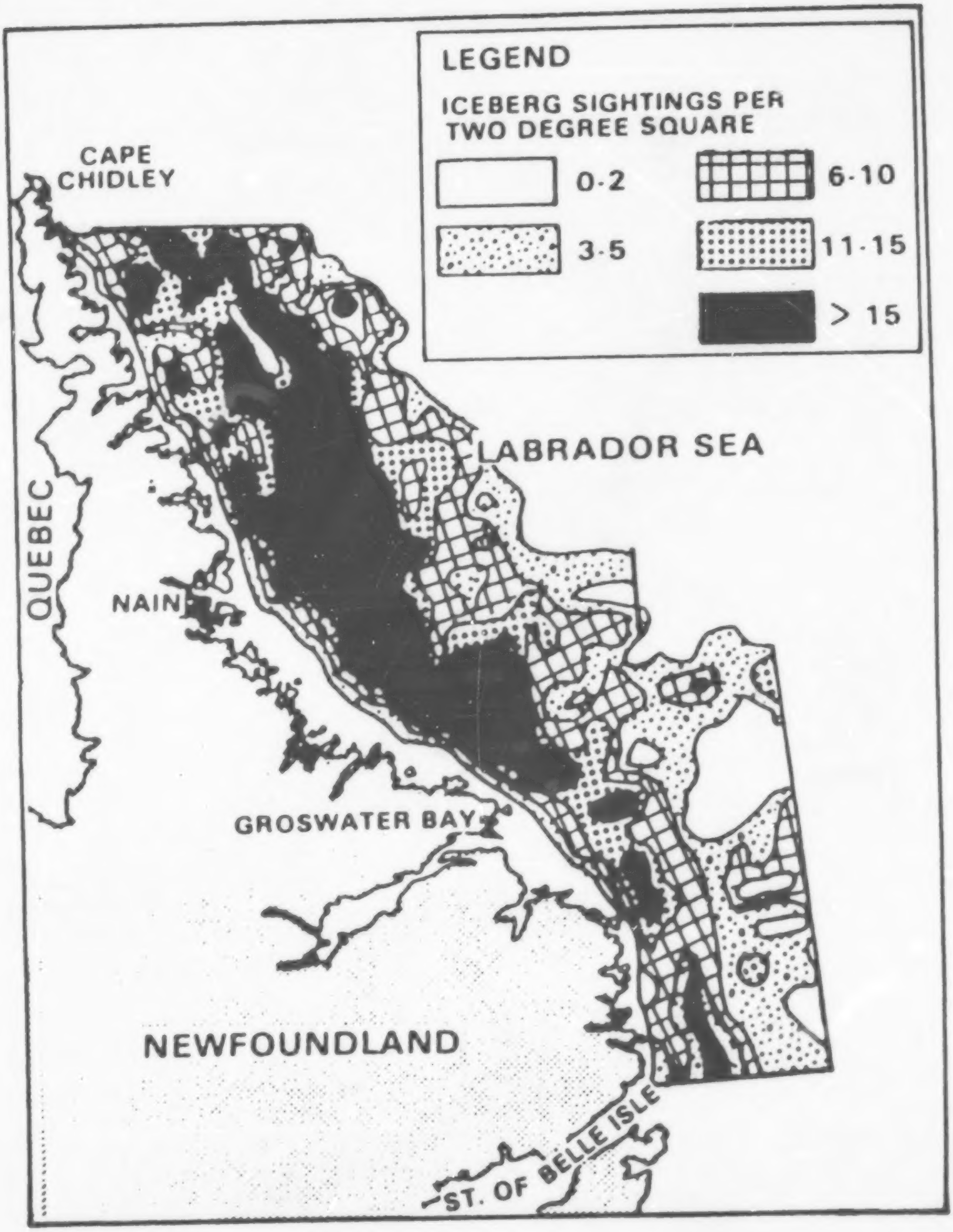
LEGEND
ICEBERG SIGHTINGS PER TWO DEGREE SQUARE
0-2
3-5
6-10
11-15
> 15
CAPE CHIDLEY
LABRADOR SEA
QUEBEC
NAIN
GROSWATER BAY
NEWFOUNDLAND
ST. OF BELLE ISLE

Figure 2.1 Iceberg Sightings - Labrador Sea (Gustajtis, 1977)

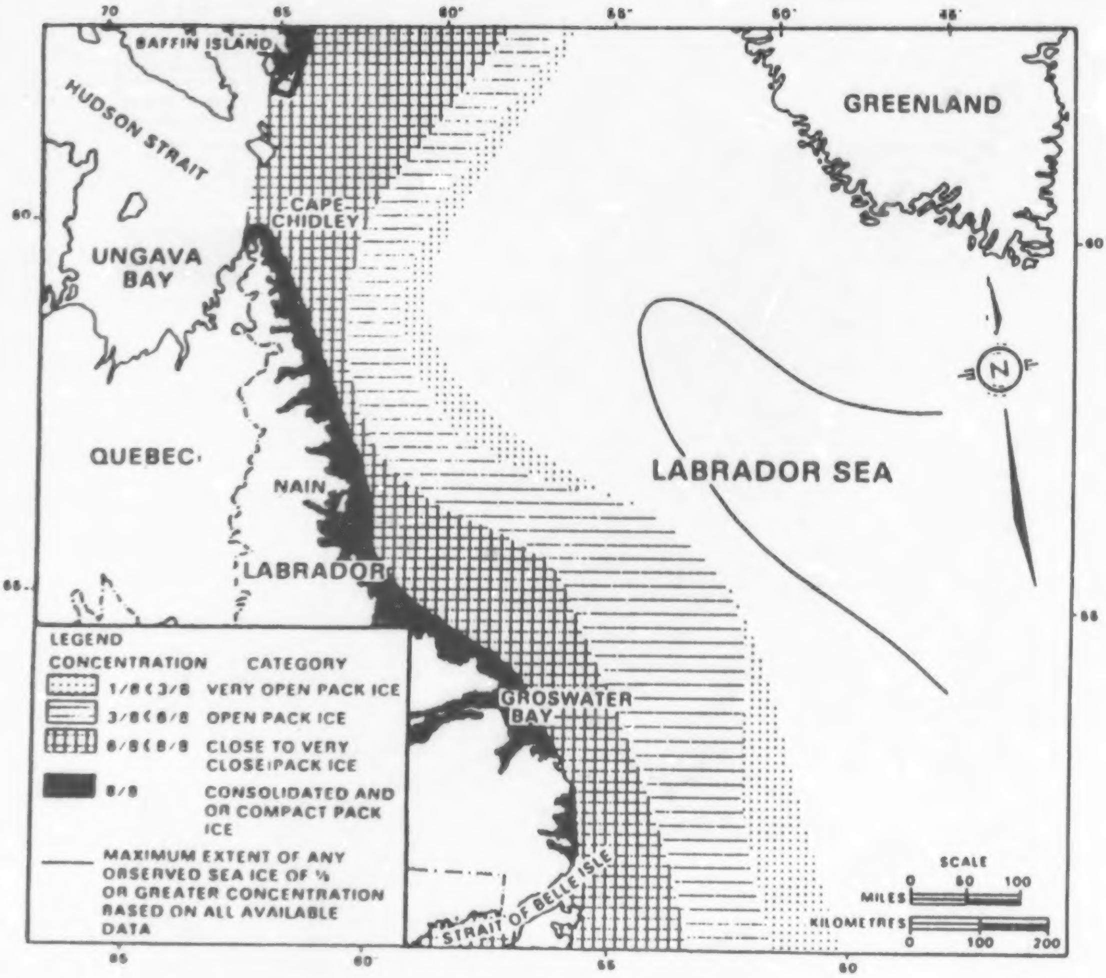
70
65
60°
55°
50°
45°
BAFFIN ISLAND
HUDSON STRAIT
GREENLAND
CAPE CHIDLEY
UNGAVA BAY
QUEBEC
NAIN
LABRADOR
LABRADOR SEA
GROSWATER BAY
STRAIT OF BELLE ISLE
N
60
55
60°
55
LEGEND
CONCENTRATION
CATEGORY
1/8 < 3/8 VERY OPEN PACK ICE
3/8 < 6/8 OPEN PACK ICE
6/8 < 8/8 CLOSE TO VERY CLOSE PACK ICE
8/8 CONSOLIDATED AND OR COMPACT PACK ICE
MAXIMUM EXTENT OF ANY OBSERVED SEA ICE OF ⅛ OR GREATER CONCENTRATION BASED ON ALL AVAILABLE DATA
SCALE
MILES
0
50
100
KILOMETRES
0
100
200
65
60°
55
50

Figure 2.2 Labrador Sea Ice Statistics (NORCOR, 1971)

In contrast to other zones where the influence of pack ice on operations begins in the fall, the influence of pack ice on Grand Banks operations begins in the late winter, usually late February or early March. The spring, from April to June, is the time when icebergs are the most common.

2.3.2 Davis Strait and Baffin Bay

The dominant ice features of this region are large icebergs, first-year and multi-year floes, ridges and pack ice. Ice islands and fragments may also be spotted in this region (more frequently than off Labrador or on the Grand Banks due to the more northerly location and proximity to Ellesmere Island).

The Davis Strait and Baffin Bay region is characterized by more intense pack ice and iceberg presence then the Labrador Shelf. The same counter-clockwise flow that influences the Labrador icebergs exists in this region. The general current flow forces icebergs and ice in general to the closest shoreline. At a maximum, though, the whole interior of Baffin Bay can be covered with dense pack ice.

The shorefast ice forms in late October, a full month before the Labrador shorefast ice, and can reach a thickness of about two metres before melting in the spring.

Multi-year floes can be added to the ice matrix from Lancaster Sound and Jones Sound. Ice islands can be added to the matrix from the Robeson Channel at the northern end of the gap between Greenland and Ellesmere Island. Another way for ice islands to enter Baffin Bay is via the east coast of Greenland and to follow the west Greenland current northwards.

2.3.3 Hudson Bay

Hudson Bay has only one predominant ice type. In contrast to all the other areas discussed herein Hudson Bay can be classified as a first-year ice only regime. The ice begins to form in late October and can reach a mature thickness of nearly two metres in the north, and one and a half metres in the southern portions.

Significant ridging is possible due to the large open area of the Bay. Chakraburtty et. al. (1984) state that average winds during the October to December period are 24 - 30 km/hr, and extreme winds of 80 - 100 km/hr are responsible for extensive ice movements. The large fetch areas available in the bay can easily cause large stresses to build up in the thin ice.

The ice begins breaking up in late May but Hudson Strait forms a bottleneck to movement out of the Bay until late July.

2.3.4 The High Arctic Region: The Canadian Archipelago

The high arctic region extends through all the channels of the Canadian Archipelago with Baffin Bay bordering on the east and the Arctic Ocean on the West. Ellesmere Island is the northern boundary.

The high arctic ice regime is the most extensive of all regions. This region is characterized by a very short melt season, and the environment is conducive to the formation of thick multi-year ice features. The arctic archipelago contains all the generic ice types. First-year ice, multi-year ice, floes of both ice types, hummock fields, and ice islands and icebergs can be found within the borders of the archipelago.

Hummock fields can form along the arctic ocean shores of Banks Island, Prince Patrick Island, Bordon Island, Brock Island, Ellef Ringnes Island and Ellesmere Island.

Figure 2.3 illustrates ice conditions for the proposed tanker routes from the Beaufort Sea to the Labrador Sea (Dickins, 1981). The figure shows the wide variety of ice conditions possible even along the centre region of the Northwest Passage. [For further information on Northwest Passage ice conditions the reader is referred to Dickins (1981), The Pilot of Arctic Canada, and Lindsay (1977).]

2.3.5 The Canadian Beaufort Sea

The ice regime of the Canadian Beaufort Sea is characterized by a near continuous presence of ice of many forms throughout the year. All ice types except icebergs can be found in the Beaufort Sea region. A general description of the Beaufort Sea environment can be found in DePaoli et al., (1982) and Danielewicz and Pilkington (1980). A synthesis of design ice characteristics in the Canadian Beaufort Sea is presented in Morrison and Marcellus (1985).

The dynamics of the Beaufort Sea ice environment are linked to those of the Arctic Ocean. A significant amount of fundamental study of this region has been undertaken for the purposes of determining offshore structure design criteria.

Off the Mackenzie Delta during late September ice begins to freeze in nearshore areas. As the season progresses the frozen area advances seaward and may suffer repeated failures due to movement caused by either winds or currents. Ridges are formed and these may ground out on the shallow continental shelf. By January a stable landfast ice zone is present out to about the 20 metre bathymetric contour. The landfast ice zone generally remains a stable platform until the spring.

The rotation of the Beaufort Gyre is responsible for a continuous clockwise motion of the polar pack ice past the Beaufort Sea. The shearing between the polar pack and the landfast ice is responsible for the creation of the "shear zone", a ridge system set up at the boundary of the moving

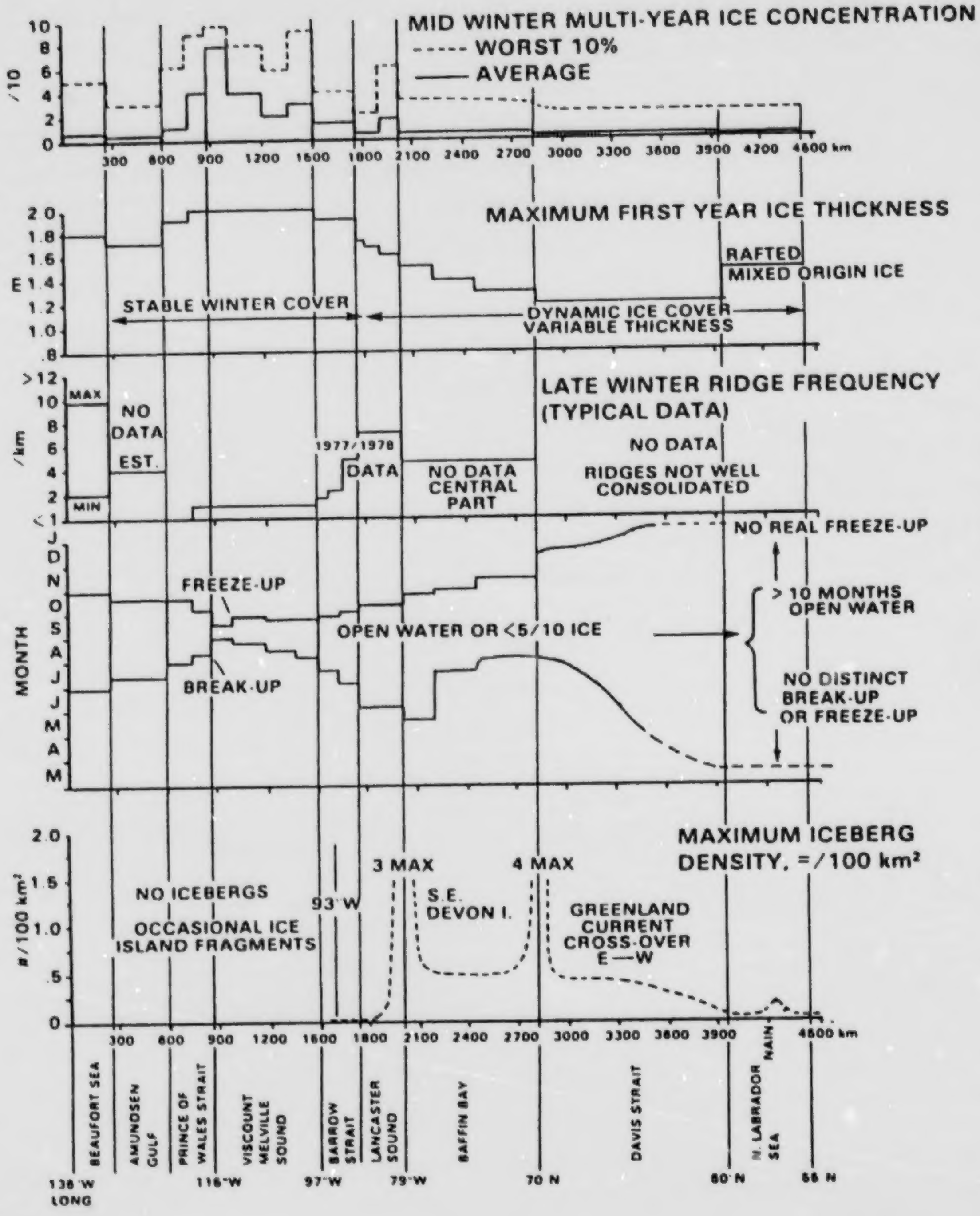

Figure 2.3 Northwest Passage Ice Conditions (Dickins, 1981)

pack ice and the motionless landfast ice. Deep shear ridges serve to anchor the edge of the landfast ice firmly to the seafloor.

As the season progresses the ice thickness in the landfast ice zone grows to about 2 metres before melting (Danielewicz and Pilkington, 1980). Nearshore there is a brief three to four month open water season extending from late June or early July to mid October.

In terms of ice design criteria many features can approach the Beaufort Sea exploration region. These features include multi-year floes and hummock fields and ice islands or ice island fragments. For an examination of these features and probabilities the reader is referred to Marcellus and Morrison (1982) and DePaoli et al., (1982).

2.4 Summary

Each marine region can be characterized by a specific set of probabilistic ice design criteria, which includes ice geometric shapes and sizes, and velocities of interaction. Each of these criteria should be reviewed where a site specific design is considered. General regional statistics are, however, useful and a future synthesis of this regional information may be desirable. As can be seen from the general information supplied in this chapter, such a synthesis is beyond the current scope and would constitute a significant study onto itself.

3.0 Mechanical Properties of Ice

3.1 Introduction

Mechanical properties determine how ice responds under load. Examples of ice mechanical properties of are:

- Young's Modulus
- compressive strength
- tensile strength
- flexural strength
- shear strength
- adhesion strength
- Poisson's ratio

The pertinent mechanical properties of the unconsolidated portions of ridges and rubble fields are:

- porosity of the rubble
- shear properties of the rubble

It is not possible to describe the mechanical properties of ice in a few pages. In this portion of the report only an overview of the mechanical properties is presented.

At this time it is not possible to describe ice, and in particular sea ice, as a material with properties, which will suffice for all design occasions and can be listed in a short table. Ice reacts to forces in non-linear ways and, critically, the reaction of the ice to forces is dependent on many variables.

Ice can be characterized as a material with many different structures, such as crystal size, crystal shape, strength, and void content (both air and brine). The different structures are present because the environmental conditions under which water becomes ice can vary widely.

The two most important characteristics of ice which affect mechanical properties are, first, that ice creeps under load, and second, that ice is extremely brittle.

In Section 3.2 ice formation mechanisms and crystal properties are described.

An introduction to the complexities of determining the mechanical properties of ice is presented in Section 3.3. The discussion is centred around the compressive strength of fresh water and first-year sea ice.

In Section 3.4 data on the compressive strength of multi-year ice and iceberg ice is presented. Other mechanical properties of various ice types are also briefly described.

In Section 3.5 some basic mechanical properties of ice rubble are also described.

3.2 Ice Formation Mechanisms

The formation of ice is examined in detail in a number of references including Weeks (1967), Weeks and Assur (1967) and Michel (1978). Table 3.1 shows the more common crystal structures of sheet ice, based on the scheme popularized by Michel and Ramseier (1971).

The Most Common Types of Ice to Which a Structure is Exposed

The most common types of ice to which a structure will be exposed are briefly reviewed below. In order, these ice types are:

- fresh water ice,
- saline water ice,
- sea ice rubble and ridges, and
- glacial ice.

Fresh Water Ice

River and lake ice is commonly called fresh water ice. The most common type of ice which has to interact with a structure is S_2 ice. S_2 ice can be formed in both fresh water and saline water, and is characterized by small to extra large crystal sizes, and horizontal (but random) orientations of the c-axis.

Fresh water ice contains no brine but can contain air if the water column at formation is turbulent.

Table 3.1
Classification of Selected Fresh Water and Saline Water Ice Types
(From Nadreau and Michel, 1984)

Type		Growing Conditions	Characteristics	Crystal Size	Grain Boundaries	C-Axis
Fresh Water Ice	Sea Ice					
P_1	-	Calm surface, small temperature gradient		L to XL	Irregular	Vertical
P_2	-	Calm surface, large temperature gradient or outside nuclei		M to XL	Tablular needle-like	Random and vertical
P_3	P_{3b}	Agitated surface nucleated from frasil		S to M	Equiaxed tabular	Random
P_4	P_{4b}	Nucleated from snow		S to M	Equiaxed	Random
S_1	-	Grown from P_1	Columnar	L to XL	Irregular	Vertical
S_2	S_{2b}	Grown from P_2, P_3, or P_4 P_{3b} or P_{4b}	Columnar	S to XL	Regular	Horizontal
S_3	S_{3b}	Grown from S_2 or S_{2b}	Columnar	M to XL	Regular	Horizontal and aligned
S_4	S_{4b}	Grown from P_3 or P_{3b}	Congealed Frazil	S to M	Equiaxed tabular	Random
S_5	-	From P_3	Drained frazil low density	S to M	Equiaxed tabular	Random

Crystal Size: small $d < 1$ mm
medium $1 \text{ mm} < d < 5$ mm
large $5 \text{ mm} < d < 20$ mm
extra large $d > 20$ mm

Saline Ice

Saline ice is ice formed from sea water. Saline ice is so called because it contains pockets of brine throughout the ice sheet. As the ice becomes older the salinity decreases.

For details on first-year saline ice growth the reader is referred to Nakawo and Sinha (1984), Nakawo (1983) and Sinha and Nakawo (1981).

Ice Rubble

Ice rubble is the generic name for a zone of broken ice. Well developed ice rubble contains three zones, in order from the top down these layers are: an unsaturated sail made of ice blocks, a consolidated ice sheet, and a partially consolidated layer where the blocks are frozen together where they contact but the voids are not completely frozen.

Glacial Ice

Glacial ice is formed from the compaction of snow under the weight of a deep layer of newer snow. Glacial ice has a reasonably large air content and is quite hard. Icebergs are of glacial origin.

Ice islands are created by a different growth process. Ice islands are calved portions of the ice shelves which used to dominate the fjords at the northern end of Ellesmere Island. The top half of the ice is similar to the top layers of a glacier, being composed of snow layers which are gradually congealing into ice. The bottom half is fresh water ice, which was formed in a particular manner. In some years there is a small open water area between the shelf and the landward end of the fjord. Runoff enters this region and, if enough runoff is present, the water will flow under the ice shelf but above colder salt water. The fresh water is cooled to below it's freezing point at the salt/fresh water interface. The small platlets of ice flow upwards and become part of the underside of the ice shelf. For the past century the ice shelves have been decreasing in area. It is not possible to estimate the time of calving of ice islands with any certainty. At the present time there are two ice islands of diameter approximately 5 km each in the Beaufort Gyre.

3.3 Determination of the Strength of Ice

General

Ice samples obtained in the field have experienced stress, and are therefore said to have a stress history. Samples of ice with no stress history are often called "virgin" ice samples.

The stress history of a sample, coupled with testing uncertainties, introduces scatter into the measurement of the samples properties such as strength, Young's Modulus, etc.

Among the most fundamental properties of an ice sample is its strength. In this section the determination of the strength of ice samples will be discussed. The strength of a sample is defined as that maximum stress the sample can withstand during a test. Ice strength depends strongly on strain rate. Figure 3.1, from Michel and Toussaint (1977), shows results of several studies tests on the strength of S_2 ice as a function of strain rate. The left hand portion of the curve is referred to as the "ductile" failure range. For strain rates in this range cracking occurs at crystal boundaries, but the sample as a whole stays in one piece. The right hand portion of the curve is called the "brittle" failure range. Brittle failure of ice is characterized by cracking and splitting apart of the sample into many pieces. In between the two ranges is a "transition" range where the failure is very complicated, and both brittle and ductile failure can be present in the sample. The indentation coefficients mentioned in the figure are discussed in Section 5.2.

The American Petroleum Institute is preparing a Bulletin on offshore structures. In the latest draft copy (Draft API-2N, 1987), a figure illustrating the dependence of horizontal unconfined compressive strength of first-year sea ice as a function of brine volume and strain rate is presented. The data are reproduced in Figure 3.2.

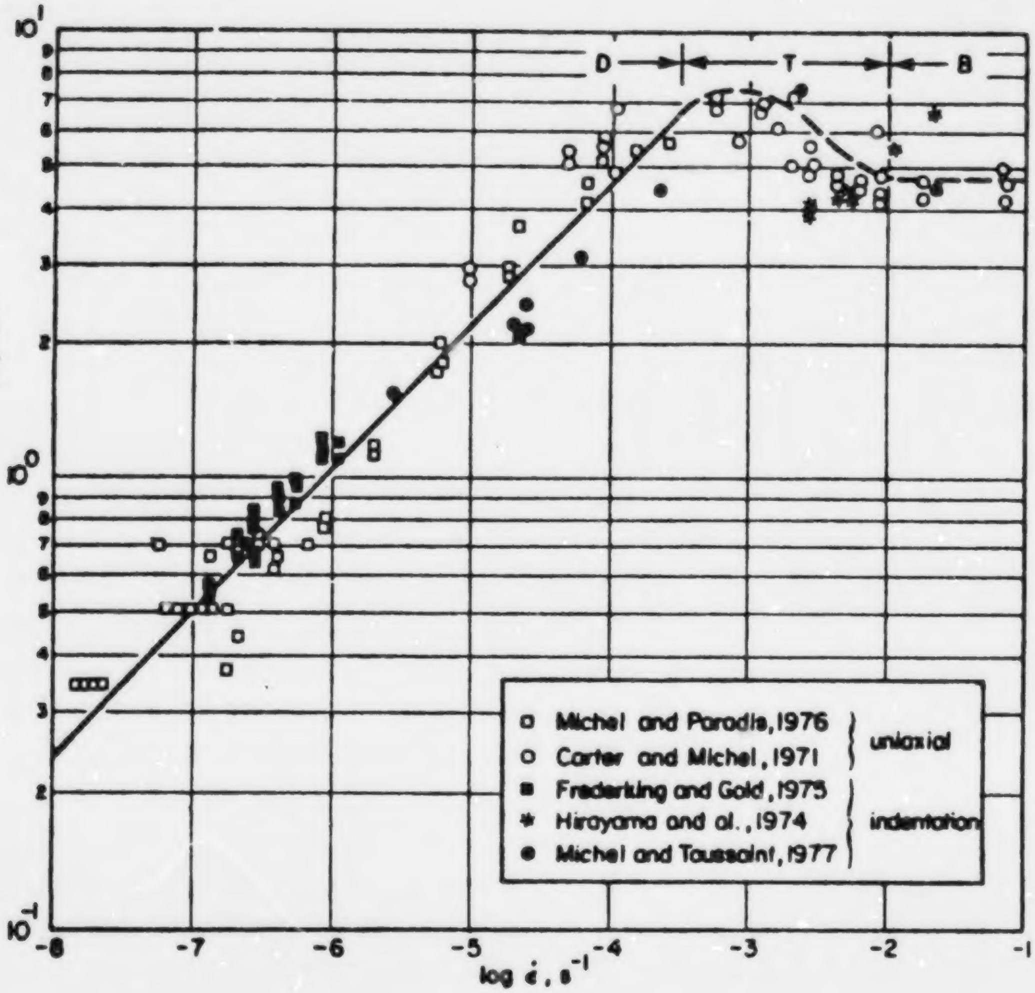

Figure 3.1 Ice Failure Pressure for S_2 Ice at -10°C. (See Michel (1978) For Complete Details).

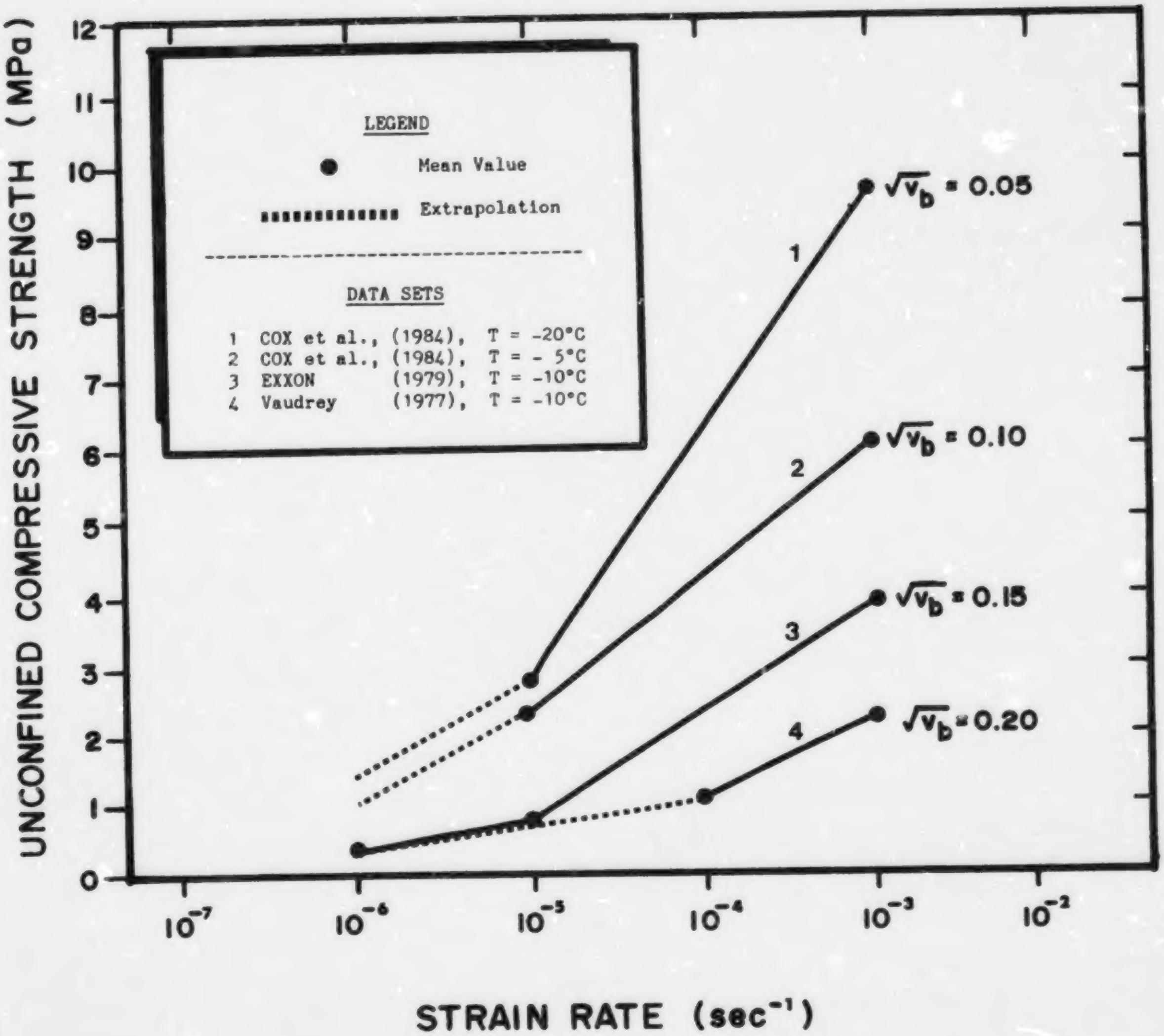

Figure 3.2 Unconfined Compressive Strength vs. Strain Rate For a Variety of Brine Volumes and Temperatures. (American Petroleum Institute Bulletin 2N, Draft, February, 1987).

Similar dependencies on loading rate exist for the other general mechanical properties such as flexural strength, shear strength, adhesion strength, Young's Modulus and Poisson's ratio.

It has become apparent that the data obtained to date on the mechanical properties, presented in Section 3.4, requires further work before a comprehensive understanding of the interrelationships between the significant variables is accomplished.

The mechanical properties of ice depend on the following variables:

- temperature,
- salinity,
- density,
- ice type,
- grain size,
- specimen size,
- loading rate, and
- failure mode.

The major problem that engineers have when conducting ice load analyses is in selecting the appropriate mechanical properties as input for their particular calculations. Size effects, scale effects and field problems such as the variability of mechanical properties as a function of depth in the ice sheet, introduce uncertainties into field data. With a significant effort it is possible to produce good "engineering" numbers, with which to compare the laboratory data (a good consistency check). Often the engineering numbers bear little resemblance to laboratory values, and the phrase "effective" is used to denote a field value, or a value obtained by not taking all of the parameters into account.

Much of the work in Canada on fundamental ice properties has been done by scientists and engineers at Canada's National Research Council, and the reader is referred to their work for further details.

In Figure 3.3 two salinity and texture profiles obtained by Sinha (1986b) are illustrated. The one on the left was obtained in a multi-year ridge; the other sample was obtained in a multi-year floe. It should be noted that the temperature of the samples could vary greatly from the top of the sample to the bottom. There would be a much greater temperature gradient in winter than in summer. During summer the ice can have a temperature close to its melting point throughout its depth.

The ridge sample shows a great variability in its properties. This variability reduces its strength relative to the more perfect sample of multi-year ice on the right of Figure 3.3. The interfaces in the floe at 0.35, 1.52, 2.28, and 3.83 m depth are most likely annual boundaries between growth stages. The complicated structure of the ridge sample implies that accurate modeling of the ridge interacting with a structure is a difficult task.

In comparison to the multi-year samples, Figure 3.4 illustrates a salinity and texture profile for a first-year ice sheet, (Sinha, 1986b). This sample has none of the irregularities of the other two samples. There is disagreement in the industry about whether, in the field, first-year ice is stronger than the multi-year ice illustrated on the right hand side of Figure 3.3. Further study of large scale interactions is needed to resolve the disagreement.

The "strength" of an ice sample is a complicated number to derive. Tests have been proposed to measure the strength in different states of confinement such as shown in Figure 3.5 (Timco and Frederking, 1986). Most often Test C is used, referred to as the "horizontal uniaxial compressive strength" test. Based on the results of the five tests the three-dimensional strength of an ice sample can be determined. This will be examined later in this section.

The testing of an ice sample, per se, is not an easy process. Engineers have in the past used the strain rate as a gauge for documenting the strength of ice. A typical test machine for samples generates a

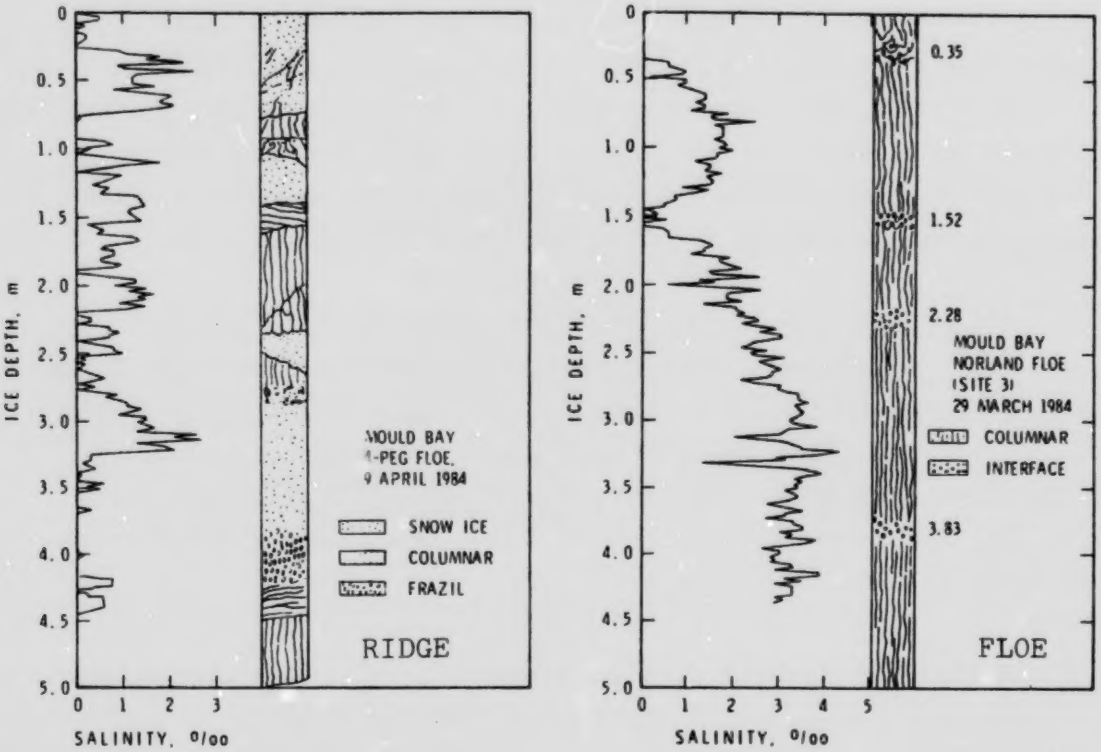

Figure 3.3 Salinity and Texture Profiles for Multi-Year Ridge (left) and Multi-Year Floe (right) Ice Samples (Sinha, 1986b).

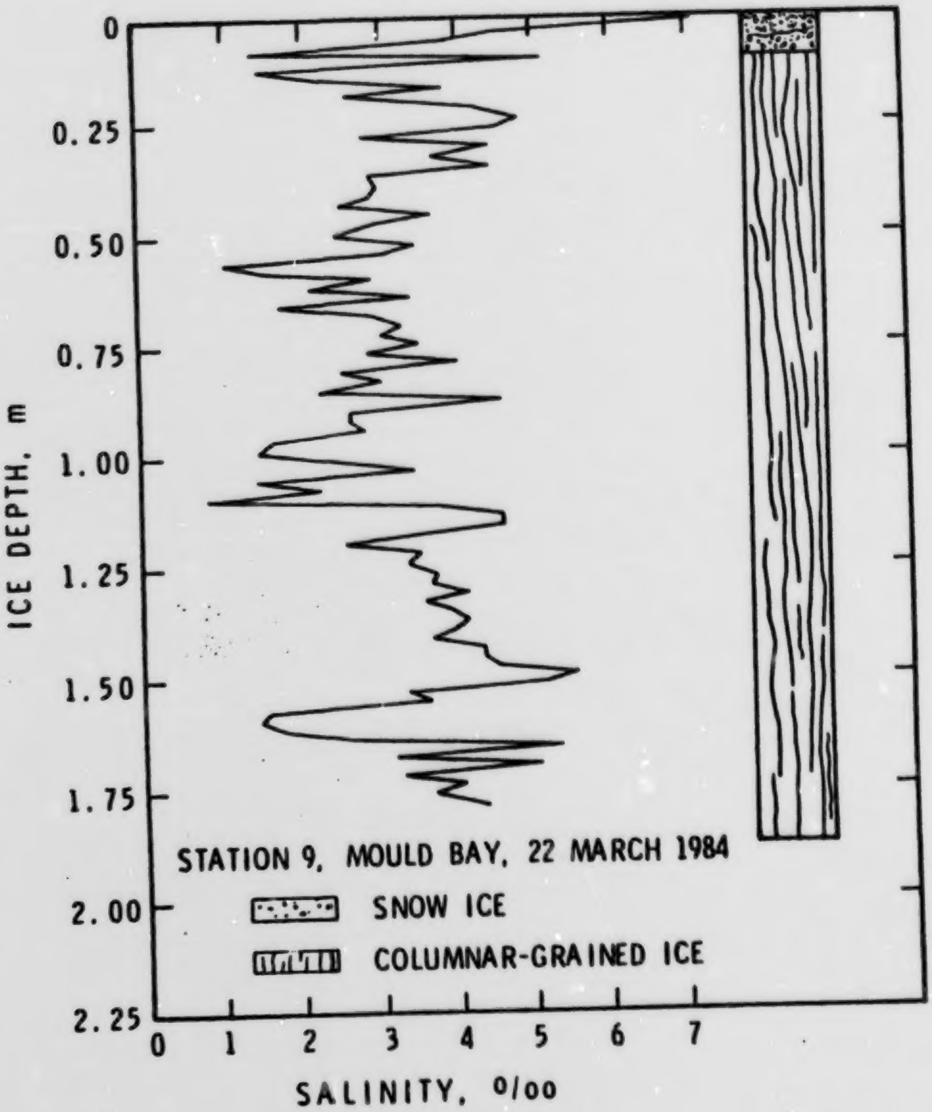

Figure 3.4 Vertical Salinity and Texture Profile of First-Year Ice (Sinha, 1986b).

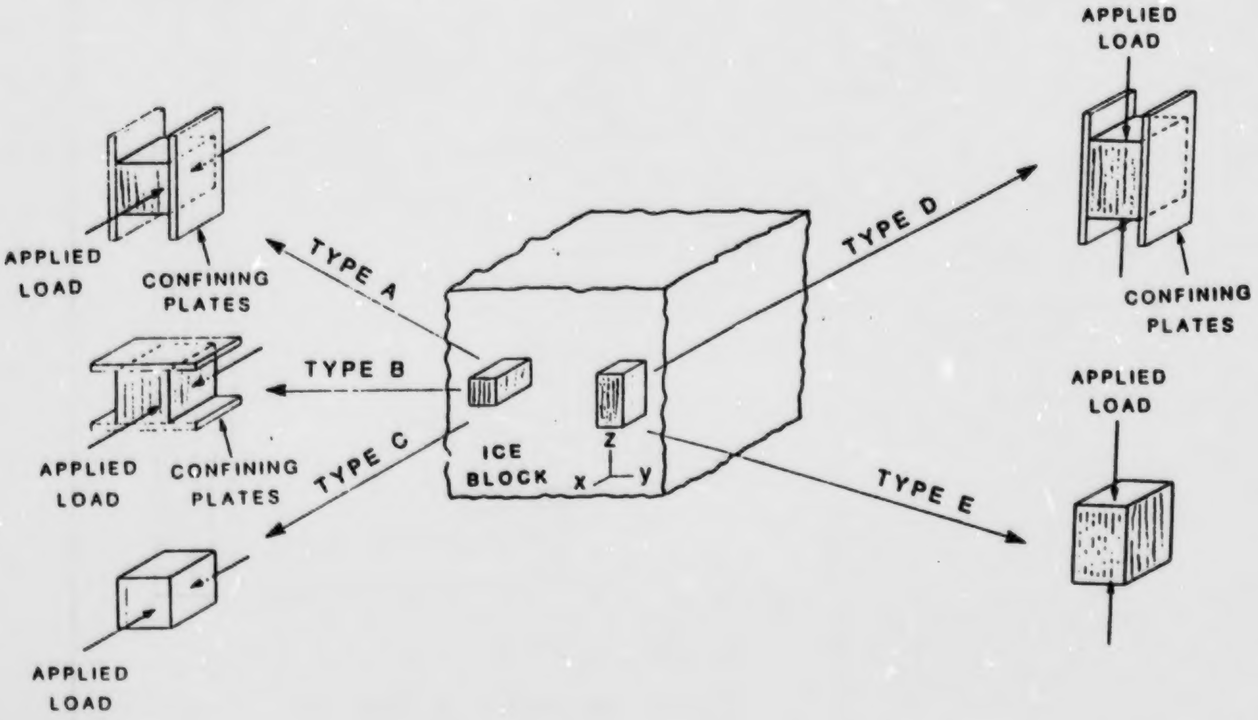
APPLIED LOAD
CONFINING PLATES
TYPE A
TYPE B
APPLIED LOAD
CONFINING PLATES
TYPE C
APPLIED LOAD
ICE BLOCK
z
x
y
TYPE D
APPLIED LOAD
CONFINING PLATES
TYPE E
APPLIED LOAD

Figure 3.5 Geometry of the Five Frederking Tests (Timco and Frederking, 1986).

"constant strain rate" by moving two platens together at a constant "cross-head" rate. It is possible to estimate the strain rate based on the cross-head rate. However, Sinha (1979) has shown that the strain rate in a test, defined using the cross-head rate on a jack, may be significantly different than the strain rate the sample experiences. The stiffness of the test machine has a substantial effect on the response of the machine and sample. Figure 3.6 shows the differences which are possible by comparing a 50 kN machine to a 1 MN machine. Much of the work conducted before about 1975 or 1980 used the estimate of strain rate based on the cross-head rate, which has been shown to be significantly in error (Sinha, 1979). In particular, the bottom illustration in Figure 3.6 shows that the 1 MN test machine strains the sample at a rate much closer to that desired than does the smaller machine. In particular, the smaller machine does not strain the sample at the calculated strain rate until the sample has reached its maximum strength. The "real" strain rate in the sample used in the smaller machine is much smaller than that calculated.

Gold first described the failure of ice, in terms of microcracking during creep tests, in 1972, (Gold, 1972). His observations have been expanded upon by later workers and have been used as a basis for much of the experimentation and theoretical analysis of the ice failure process.

Sinha (1982, 1984a, 1984b) has proposed a theory of the failure process of ice. In his theory the strain in a sample is made up of three components:

$e = e_e + e_d + e_v$,

where the portions of the total strain are:

- elastic strain, e_e
- delayed elastic or time dependent strain, e_d, and
- viscous or permanent strain, e_v.

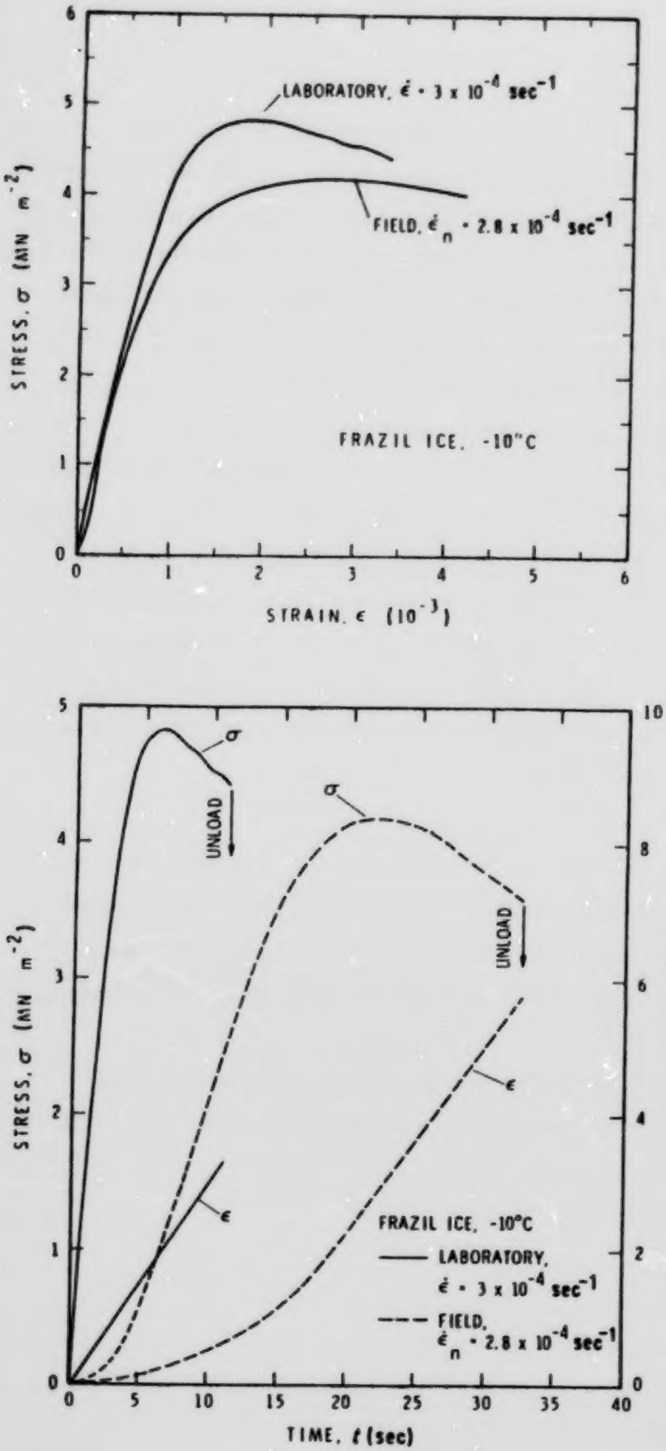

Stress and strain diagrams
for similar loading
conditions in the field
and the laboratory

----- 50 kN

——— 1 MN

Stress and strain histories
for apparently similar
field and laboratory tests

Figure 3.6 Illustration of Stress and Strain Histories for Different Testing Machine Stiffness (Sinha, 1986a).

It is possible to estimate the onset of cracking based on knowledge of the delayed elastic strain, e_d. For a given set of test parameters, and sample characteristics, there is a delayed elastic strain at which microcracking will initiate (Sinha, 1982a). Figure 3.7 shows in detail the response of an ice sample to an applied strain rate, and the theoretical response based on Sinha's equation. For the test shown the critical delayed elastic strain for the onset of microcracking was 10^{-4}.

The term "microcracking" may be misleading. Ice is made up of large crystals compared to other materials. A typical crystal diameter for ice is on the order of a few millimetres, which is typically a thousand times larger than crystals of other materials such as steel. The failure process in these smaller crystalline materials was referred to as microcracking. Microcracking in ice means the formation of cracks at boundaries of crystals. A "microcrack" in ice is typically a millimetre or more in length, i.e. on the order of the crystal diameter.

The formation of large cracks in the ice sample can be calculated with great accuracy. Figure 3.8 shows total strain and its components, stress and temperature dependence of creep strain for the formation of large cracks.

The critical delayed elastic strain as a function of temperature is shown in Figure 3.9, (Sinha, 1984a), and the time to first cracks as a function of different stresses is shown in Figure 3.10, (Sinha, 1984a). After the initiation of cracking, many more cracks appear. It is possible to determine the cracking activity based on acoustic emission techniques. Figure 3.11 shows the progressive failure of the ice sample. The emissions are caused by the formation of cracks.

It is also possible to theoretically calculate the density of cracks as a function of total strain in the sample. Results of some calculations are shown in Figure 3.12.

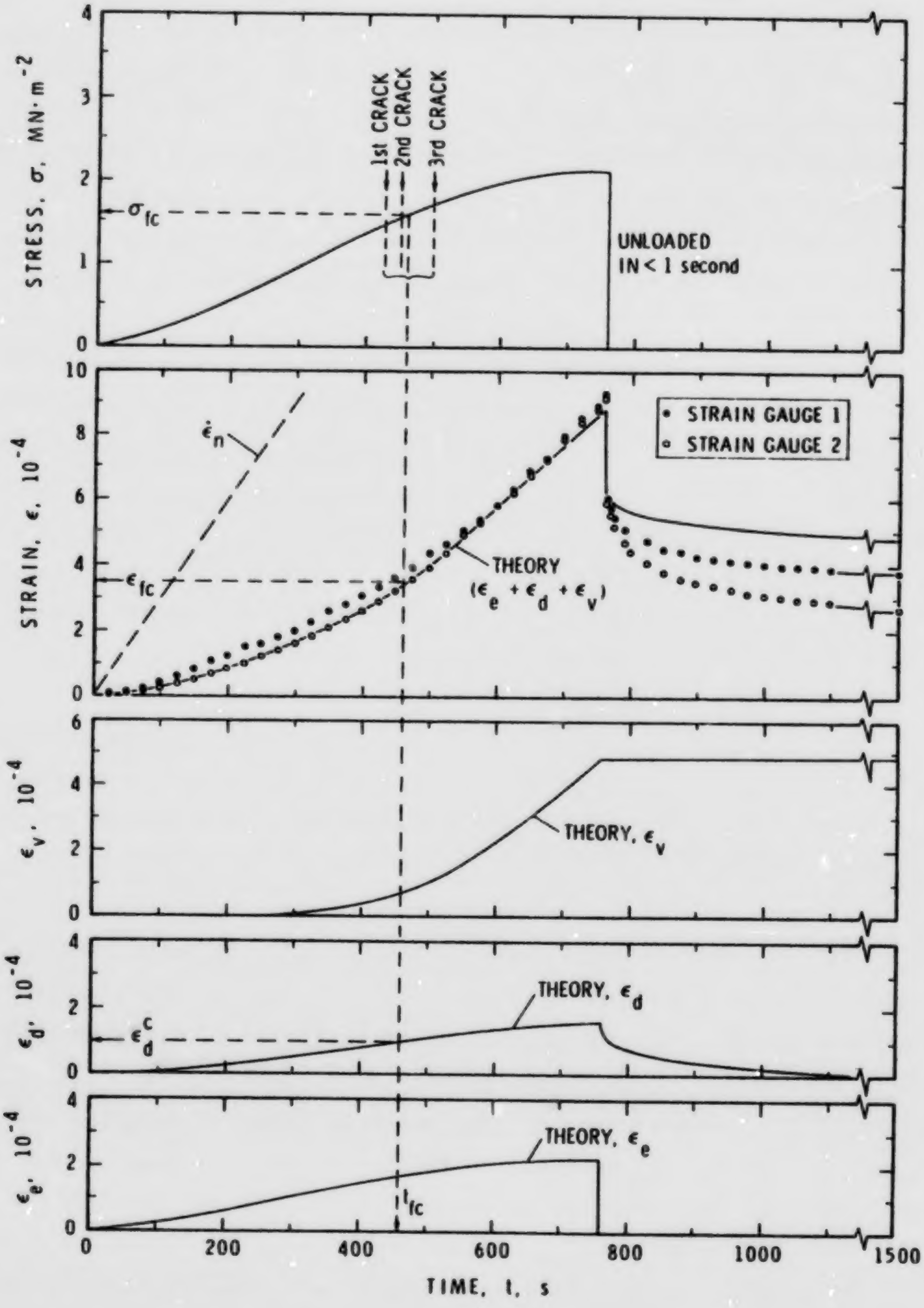

Figure 3.7 Dependence on Time of Experimentally Observed Stress, Strain, and Theoretical Strain and its Three Components for S_2 Ice of Average Grain Size 4.5 mm at -10°C. Constant Cross-Head Rate of 7.5×10^{-4} mm s^{-1} or Strain Rate = 3×10^{-6} s^{-1}.

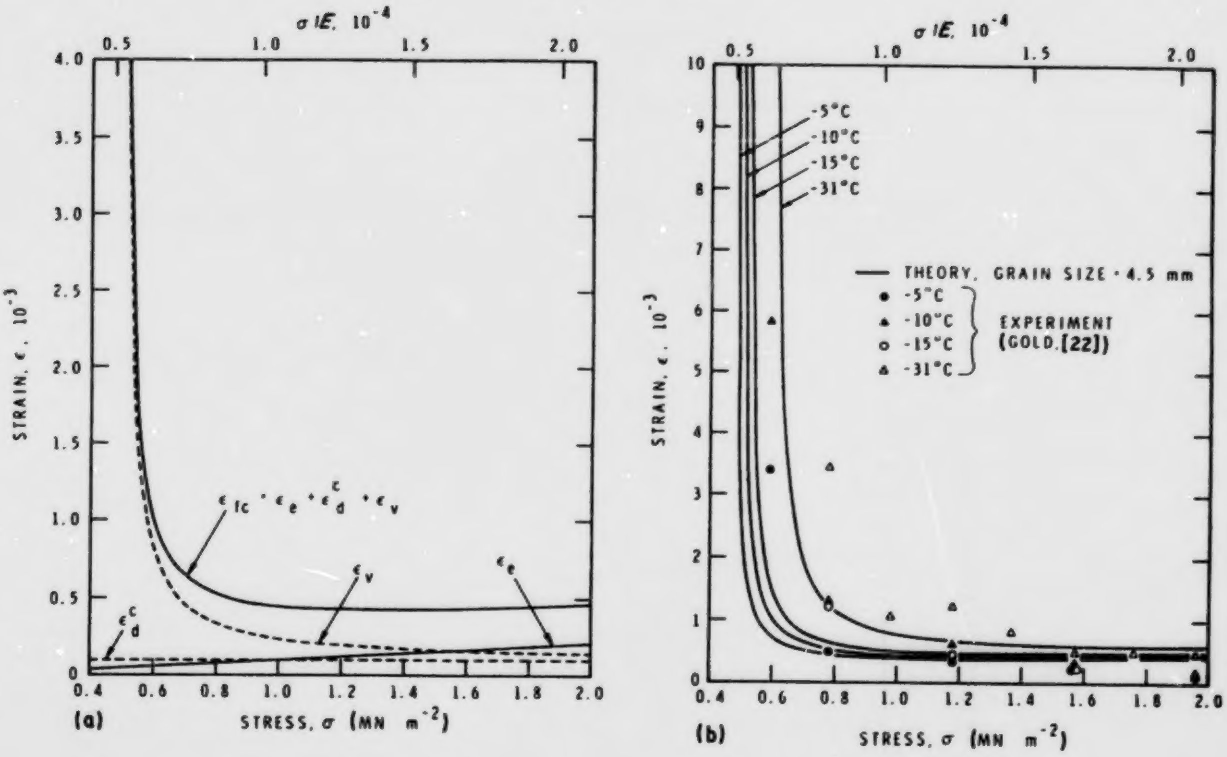

Figure 3.8 Formation of the First Cracks. (a) Total Strain and its Components for Formation of the First Cracks; (b) Stress and Temperature Dependence of Creep Strain to the Formation of the First Large Cracks (Sinha, 1984a).

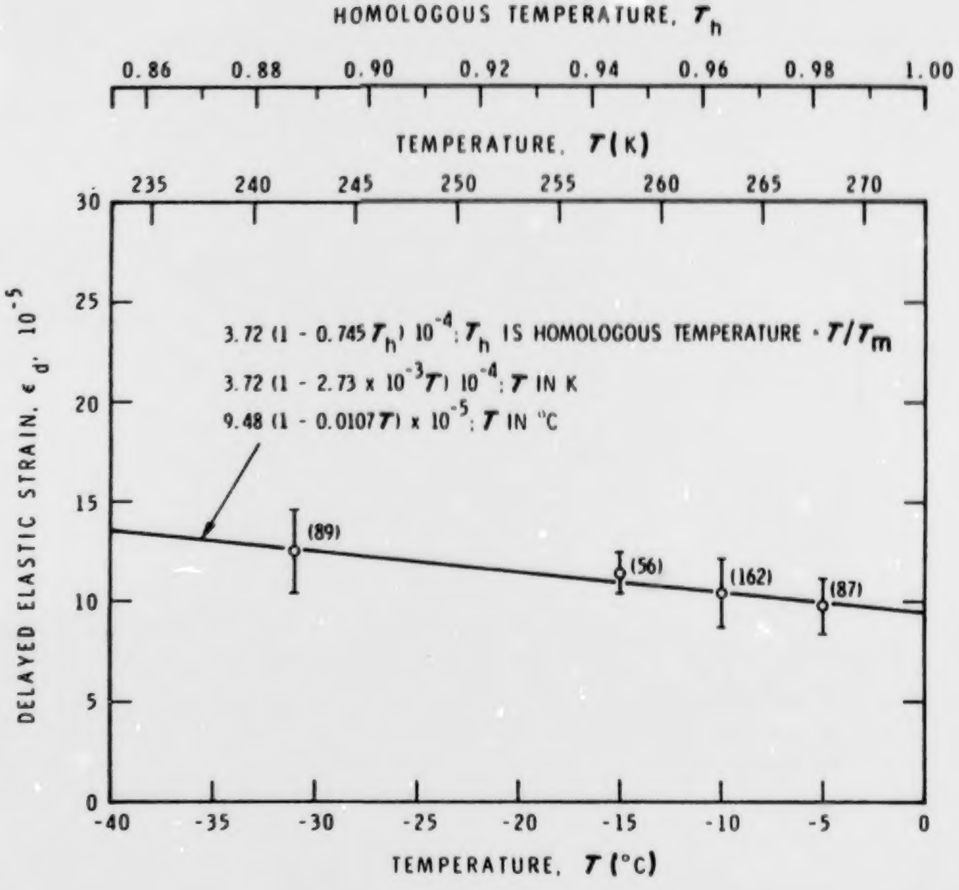

Figure 3.9 Temperature Dependence of Critical Delayed Strain for the Formation of First Large Cracks in S_2 Ice of Average Grain Diameter 4.5 mm. Numbers in Parentheses Indicate Number of Data Points (Sinha, 1984a).

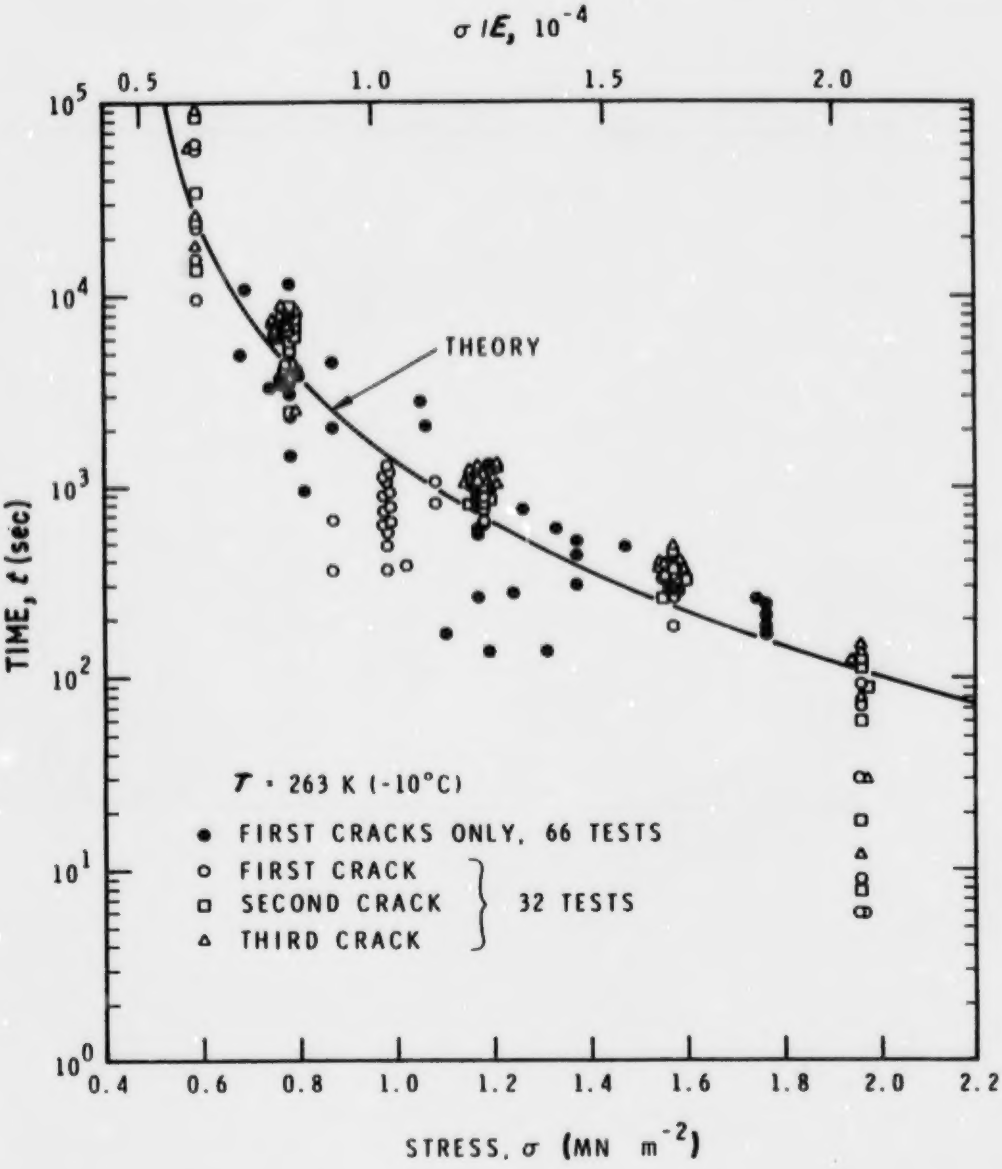

Figure 3.10 Time to Cracking for Different Stresses Based on Sinha's Theory and Comparison With Experiment (Sinha, 1984a).

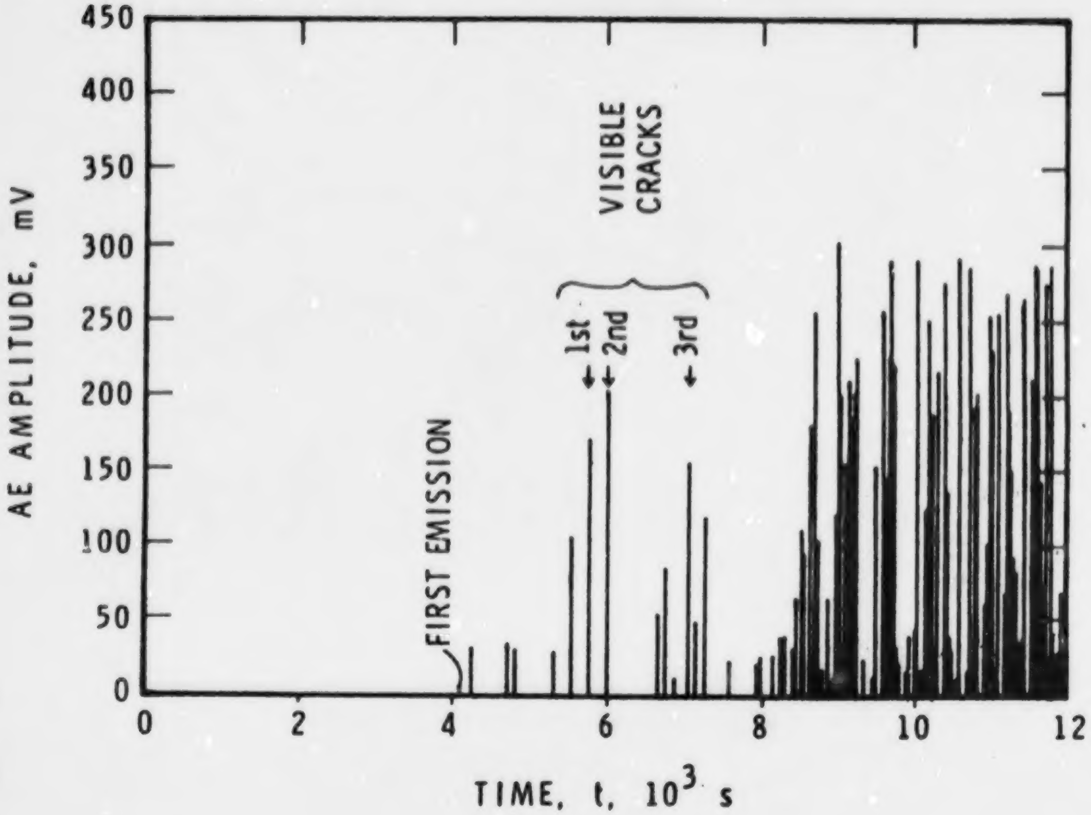

Figure 3.11 Onset of Microcracking Activity Based on Acoustic Emission Techniques (Sinha, 1982b).

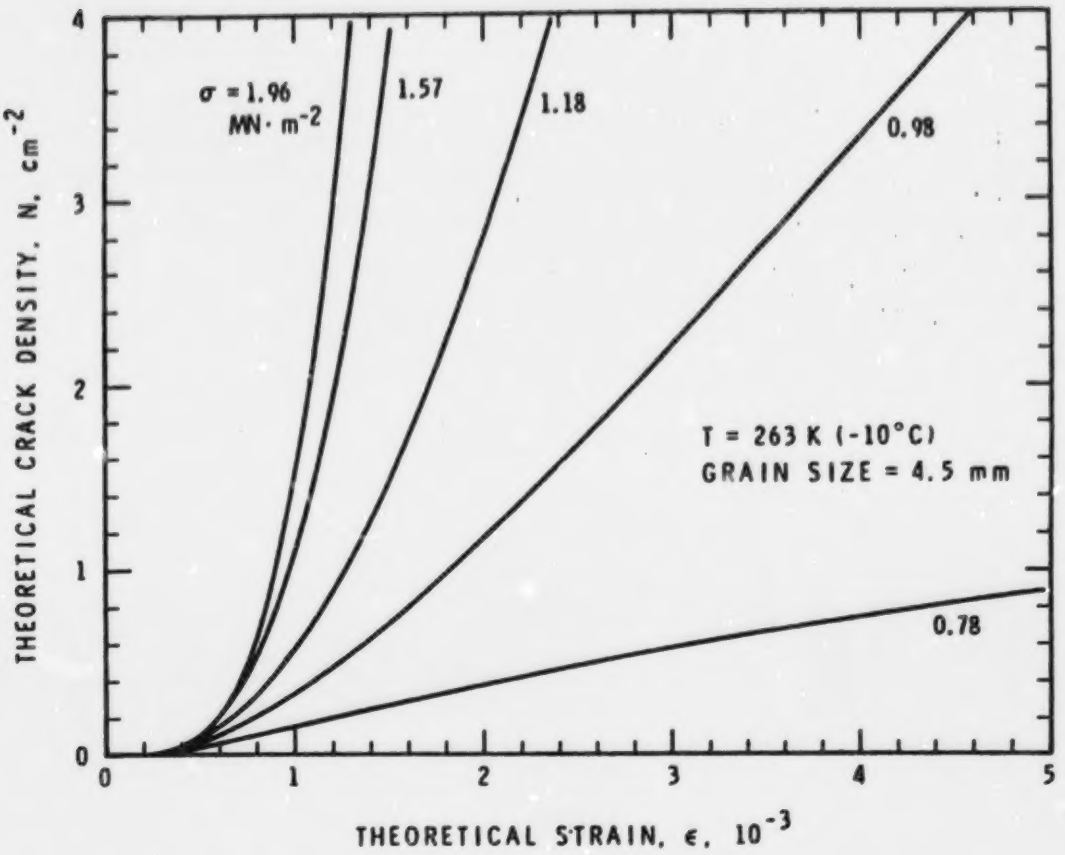

Figure 3.12 Theoretical Crack Density versus Strain at -10°C, for an Average Grain Size of 4.5 mm (Sinha, 1984b).

Of most concern to the engineer is the strength of the ice sample in a variety of situations. Timco and Frederking (1986) have presented failure envelopes for sea ice at two different temperatures. Figure 3.13 shows strength for tests C and E as a function of total porosity. In Figure 3.14 are shown the failure envelopes developed from their tests. Note the change in shape of the envelopes with changing temperature and ice type. For detailed structure load calculations an understanding of how the failure envelopes change as a function of other variables is desirable.

A review of the compressive failure process in ice has been presented in this section. This review has only provided a brief introduction to the failure processes in ice, and the issues involved in going from laboratory data to field scale. In the next sections of this chapter ice mechanical properties in common use are presented.

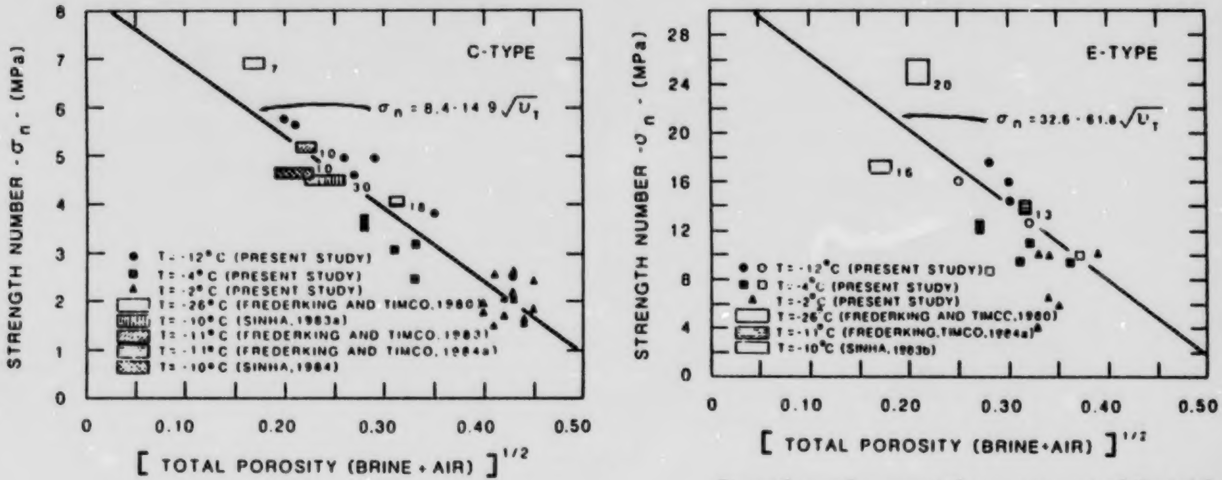

Strength number versus the square root of the total porosity for the present tests for C-type loading. Included on this figure are the envelopes of data from previously published results expressed in terms of the strength number. The number beside each box represents the number of data points for each of these studies.

Strength number versus the square root of the total porosity for the present tests for E-type loading. Included on this figure are the envelopes of data from previously published results expressed in terms of the strength number. The number beside each box represents the number of data points for each of these studies.

Figure 3.13 Strength versus Brine Volume for Tests Types C and E (Timco and Frederking, 1986).

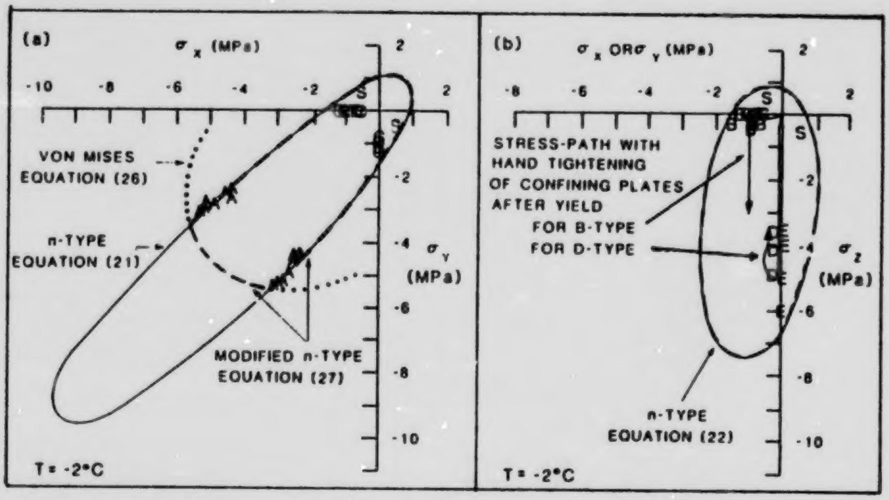

Test results showing points on the failure envelope for columnar sea ice in the (a) x–y plane and (b) *x–z* or *y–z* plane at $\dot{\epsilon}_n = 2 \times 10^{-4}$ s^{-1} and $T = -2$°C. The solid light line represents the fit of the data to an *n*-type yield function. The dotted line represents a fit of a von Mises criterion to the A-type data in 15(a). The heavy dashed line is a modified *n*-type function which gives a good representation of the total failure envelope.

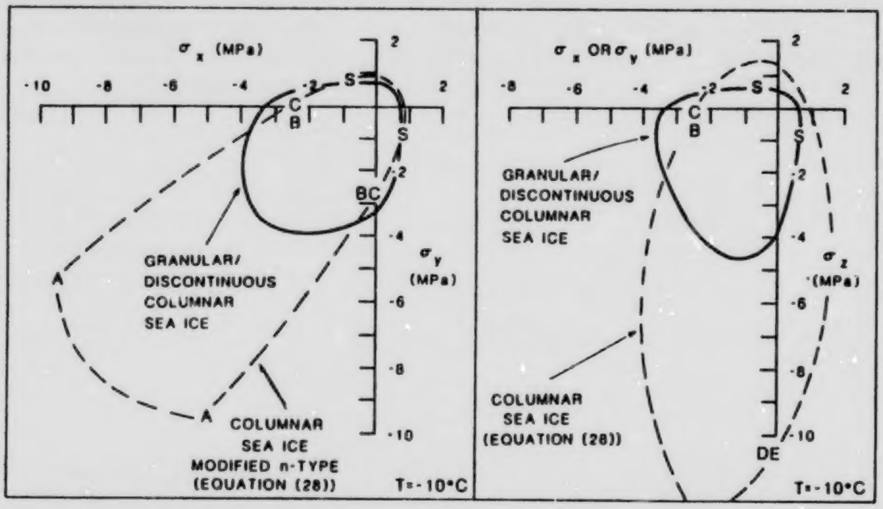

Outline of the failure envelope based on the present and previous tests on columnar sea ice at $\dot{\epsilon}_n = 2 \times 10^{-4}$ s^{-1} and $T = -10$°C. The solid line represent the extent of the failure envelope for granular/discontinuous-columnar sea ice at the same temperature and strain rate.

Figure 3.14 Failure Envelope for S_2 Ice at Two Different Temperatures (Timco and Frederking, 1986).

3.4 Mechanical Properties of Ice Sheets

In this section of the report selected mechanical properties of ice sheets are examined. Due to the lack of a comprehensive understanding of the properties of ice in the field, as discussed in the previous section, and the need to present "engineering solutions" in later chapters, engineering mechanical properties are presented in this section based on currently accepted numbers or relationships. The authors caution the reader, however, that the data presented in this section are subject to ongoing research and future refinement. One alternative source of information on mechanical properties of sea ice can be found in Mellor (1983).

The mechanical properties reviewed in this section include the following (in order of presentation):

- Modulus of Elasticity (Young's Modulus)
- Compressive Strength
    - first-year ice
    - multi-year ice ridges
    - iceberg ice
- Tensile Strength
- Flexural Strength
- Adhesion Strength
- Shear Strength
- Poisson's Ratio

3.4.1 Modulus of Elasticity

The value of E varies significantly with the porosity of an ice sheet. Porosity in consolidated sea ice is usually due to two sources: air bubbles and brine cells. In most research, brine porosity has been measured but air bubble porosity has not. Nakawo (1983) presents vertical profiles of salinity, density and air porosity for core samples of a first-year ice sheet. His results are shown in Figure 3.15. In the past the total porosity due to air bubbles and brine cells has not been used by Canadian and American researchers (Weeks and Assur, 1967; Mellor, 1983). Therefore caution is advised when using porosity values where their definition is not explicit. Most often, brine porosity is meant. Figure 3.16 (from Mellor, 1983) is a plot of Young's modulus vs. porosity. Mellor states that the results of Kohnen (1972), Brown (1963) and Anderson (1958) are perhaps unduly influenced by the fact that they used flexural methods in their tests. Thus, the curves numbered 1, 2, 3 and 5 are expected to be values of the true Young's Modulus as a function of porosity. There is relatively good agreement for data sets 1, 2, 3 and 5 even though two are for brine porosity only, one is for non-saline ice, and the last of the four is for total porosity.

3.4.2 Uniaxial Compressive Strength

In Section 3.3 the compressive strength of fresh water and first-year sea ice, and its measurement, were discussed. Glacial ice and multi-year ice are reviewed here. For completeness it is assumed that ice island ice is similar to glacial ice.

In Table 3.2 the results from a program to measure the strength properties of multi-year ridges are shown. The error bars demonstrate how much variability of ice compressive strength is possible. Note that the ranges are standard deviations and not total ranges.

In Table 3.3 the results of a study to measure the compressive strength properties of iceberg ice are shown.

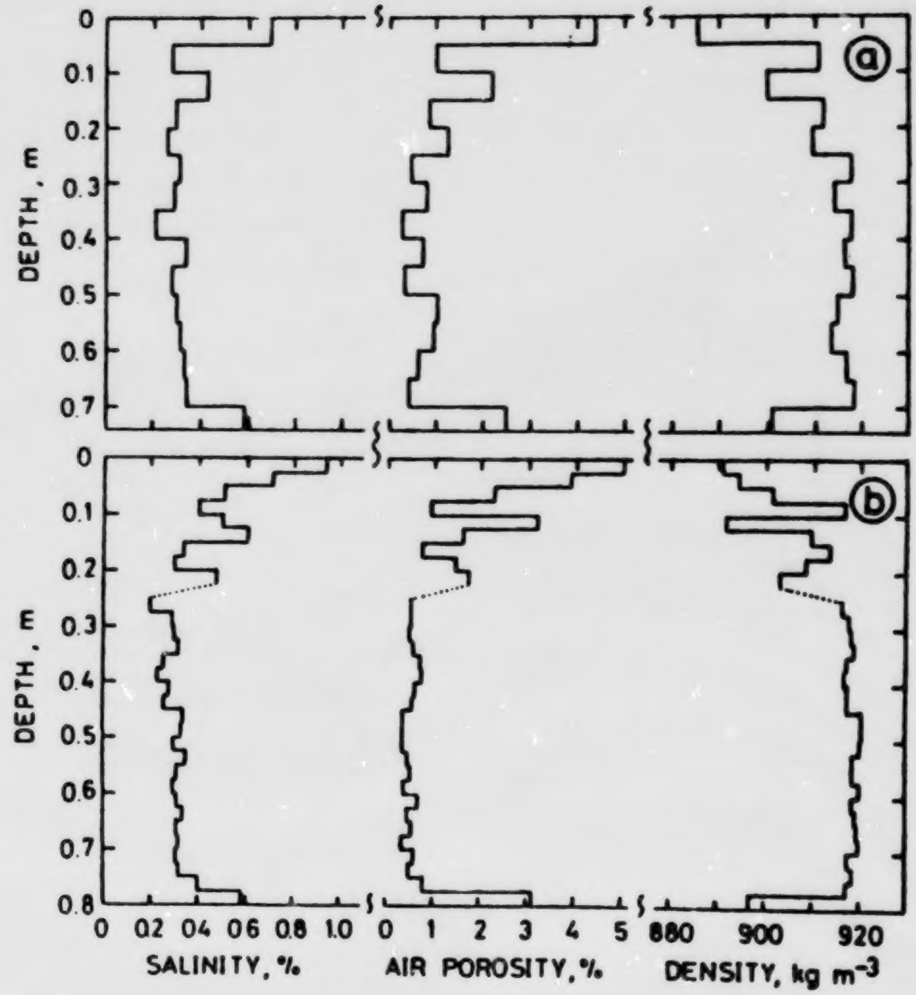

Figure 3.15 Vertical Profiles of Salinity, Density and Air Porosity for Core Samples of First-Year Ice. (a) In-Situ Measurements at -15°C (Core 1); (b) Laboratory Measurements at -28°C After Six Months Storage at -40°C. From Nakawo, 1983.

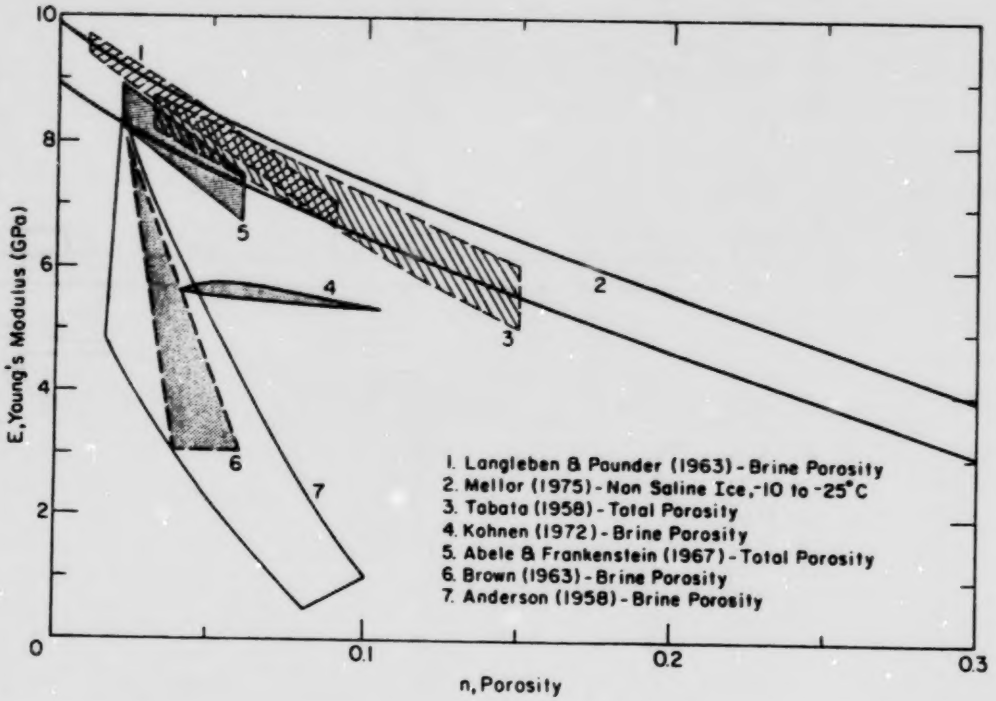

Figure 3.16 Young's Modulus For Ice as a Function of Porosity (Mellor, 1983).

Table 3.2

Multi-year Ice Compressive Strength

(from Cox et al. (1984))

Mean Uniaxial Compressive Strength of Multi-Year Pressure Ridges

Temperature = -5°C

Strain Rate	Mean Compressive Strength	# Samples
1 x 10^{-5}	2.34 ± 1.08 MPa	71 samples
1 x 10^{-3}	6.06 ± 1.63	69 samples

Temperature = -20°C

Strain Rate	Mean Compressive Strength	# Samples
1 x 10^{-5}	2.79 ± 0.69 MPa	41 samples
1 x 10^{-3}	9.63 ± 1.39	41 samples

Table 3.3

Iceberg Uniaxial Compressive and Indentation Strengths El-Tahan et al (1984)

Uniaxial Data (averages from several tests)

Strain Rate	Compressive Strength
8.2×10^{-4}	7.43 MPa
5.9×10^{-3}	6.60
5.8×10^{-2}	6.97

Indentation Test Data
(abstracted from El-Tahan et al (1984)
Cylindrical Indentor radius = 25 mm

Cylindrical Indentor - Unconfined

Strain Rate	Mean Strength (total force divided by area)
4.5×10^{-4}	23.26 MPa
4.4×10^{-3}	30.47
9.6×10^{-2}	23.72

Cylindrical Indentor - Confined

Strain Rate	Mean Strength (total force divided by area)
6.6×10^{-4}	28.43 MPa
4.7×10^{-3}	33.97
3.2×10^{-1}	27.41

In a third set of tests the maximum pressure measured during an impact (velocity between indentor and sample of 2 metres/sec.) was determined. The average pressure of the seven tests was 17.35 MPa, with a total range between 12.46 and 21.63 MPa.

3.4.3 Uniaxial Tensile Strength and Flexural Strength

Vaudry (1977), in a study for the U.S. Navy, measured the values for tensile and flexural strengths of first-year sea ice shown in Figure 3.17.

Frederking and Timco (1983) measured flexural strength of columnar grained sea ice using cantilever beams. For two different relatively thin (40 - 70 mm) ice sheets they obtained values of 660, 740, 860 and 870 kPa from a variety of tests on two different ice sheets. The two lowest numbers are for the first of the two sheets. A significant amount of scatter was reported for both sets of tests.

3.4.4 Shear Strength of an Ice Sheet

Frederking and Timco (1986; 1984) have measured the shear strength of sea ice samples. In their 1984 study, at a temperature of -13°C and a salinity of 4.2% (corresponding to a square root of brine volume = 0.19) they determined an average value of 550 kPa +/- 120 kPa. Horizontal and vertical shear values in the tests had the same value. In the later study they fit shear strength data over a range of porosities (see Figure 3.18).

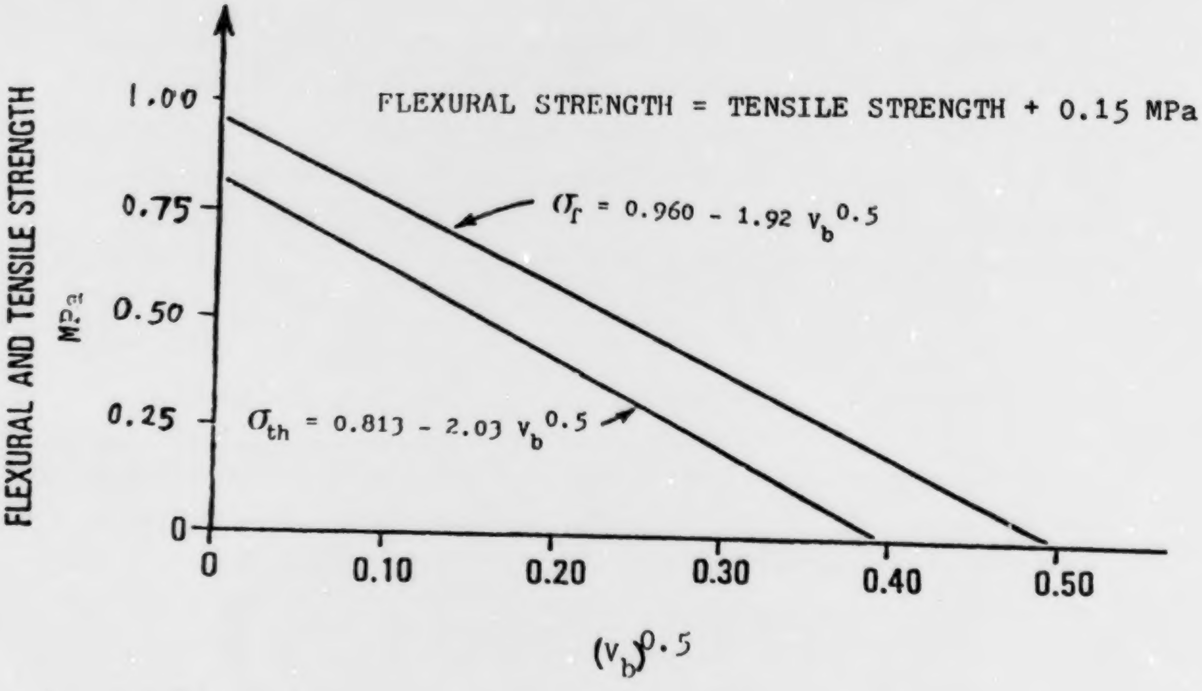

Figure 3.17 Comparison of Flexural and Horizontal Tensile Strength versus the Square Root of the Brine Volume (Vaudry, 1977).

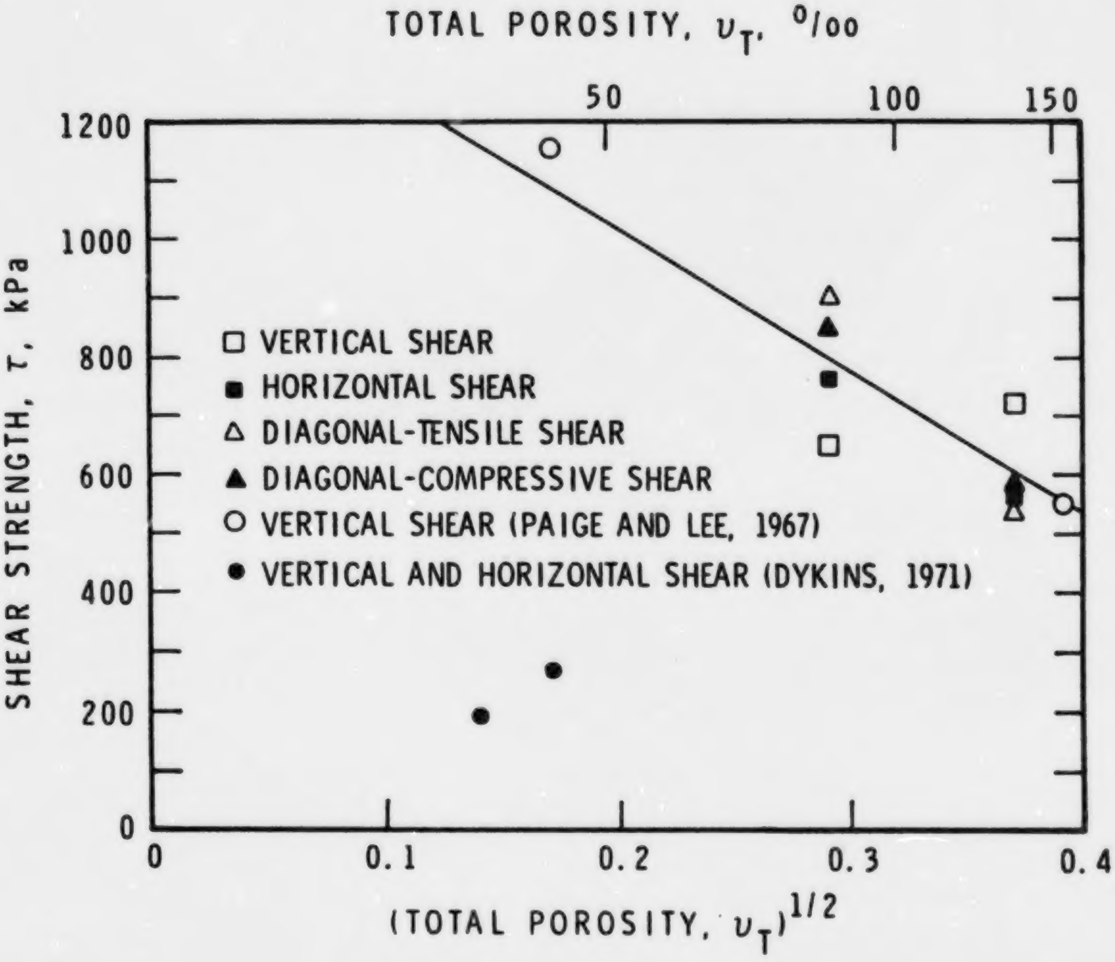

Figure 3.18 Shear Strength for Various Specimen Orientations as a Function of Total Porosity for Columnar-Grained Sea Ice (Frederking and Timco, 1986).

3.4.5 Adhesion Strength of Ice

Cammaert et al (1985) reviewed work on adfreeze strength of several types ice on structures. Some of the variables included in their review are:

- material to which ice is adhered
- ice salinity
- ice temperature
- stress rate
- pile diameter/ice thickness ratio

Figures 3.19 (a to d) show the summary of the data reviewed by Cammaert et al., (1985). The ice type for each study is as follows:

Sackinger (1977):	sea ice
Saeki et al., (1981):	fresh water ice
Oksanen (1983):	sea ice
Arctec (1975):	saline ice
Parameswaran (1981):	fresh water ice

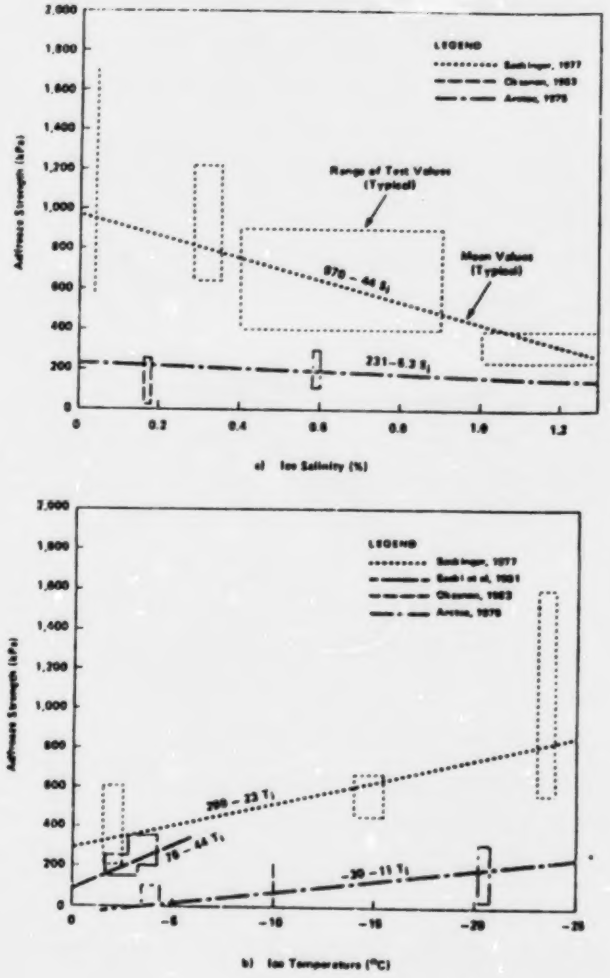

Fig. 2 (a, b)

VARIATION IN ADFREEZE STRENGTH WITH TEST PARAMETERS FROM VARIOUS FIELD AND LABORATORY TESTS

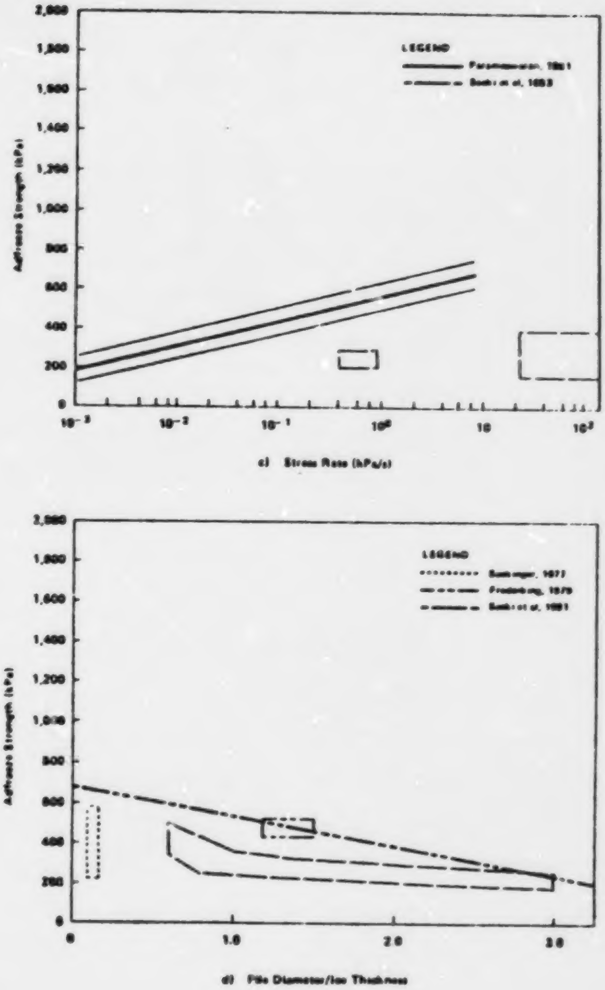

Fig. 2 (c, d)

VARIATION IN ADFREEZE STRENGTH WITH TEST PARAMETERS FROM VARIOUS FIELD AND LABORATORY TESTS

Figure 3.19 Adhesion Strength of Ice versus Salinity, Temperature, Stress Rate and Pile Diameter (Cammaert et al., 1986).

3.4.6 Poisson's Ratio

There are very little data on Poisson's ratio for sea ice; there are some data on Poisson's ratio for fresh water ice. Mellor (1975) illustrated values for Poisson's ratio of fresh water ice as a function of porosity. At a porosity of 0.35 the average of several values for Poisson's ratio was about 0.28. At zero porosity the ratio was about 0.35.

Weeks and Assur (1967) reviewed some data for the Poisson's ratio of sea ice and presented a formula, based on Soviet data, for the variation of Poisson's ratio as a function of temperature. Weeks and Assur used a value of 0.33 from Northwood (1947) in their analysis. Northwood's value is for fresh water ice. In contrast to the Soviet determination of a changing Poisson ratio with temperature, Weeks and Assur point out that Langleben and Pounder (1963) did not discover any variation of Poisson's ratio with changing salinity, temperature or ice type. The latter two researchers recommended a value of 0.295 for Poisson's ratio be used for sea ice.

Sinha has suggested that the term "strain ratio" be used in place of Poisson's ratio for other than elastic analyses. The strain ratio is defined as the ratio of perpendicular to principal strains in a sample. Results presented by Sinha (1986a) show the strain ratio increasing during the compression of samples. He also stated that there are indications that strain ratio values in the range 0.2 may be realistic, meaning that the Poisson's ratio may be significantly lower than the usual "engineering" values of 0.3 for elastic and 0.5 (assuming incompressibility) for plastic modeling. Sinha quoted strain ratio's of 0.88 for tests conducted by Gold (1958) and 1.2 for tests conducted by Exxon (Wang, 1981).

3.5 Mechanical Properties of The Unconsolidated Layers of a Ridge or a Rubble Pile

Introduction

Ice Rubble is a nonhomogeneous material. A cross section through a newly formed ice rubble field around a structure can be separated into an unsaturated layer above the water line and a saturated, partially consolidated layer below. Partial consolidation refers to the fact that there will be some immediate freezing of water near the places where blocks touch because of their reserve of cold. As the season progresses a fully refrozen layer forms at the top of the saturated, partially consolidated layer.

In Marcellus et al. (1986b) for Public Works Canada, the thermal and mechanical properties of ice rubble are examined in detail. The theory for rubble and spray ice freezeback is presented in Section 5.5.4.4.

Generally the rubble has been modeled as a Mohr-Coulomb material.

3.5.1 Porosity of the Rubble Field or Ridge

Porosity within rubble is defined as the ratio of the volume of water and air within the rubble to total volume of rubble. In Table 3.4 are shown measured and estimated ice rubble porosities from various studies. As can be seen from this table, a wide range of values exist within the literature to date.

Table 3.4

Rubble Porosity Measurements and Estimates

Source	Porosity
Kry	0.1 - 0.3
Keinonen and Nyman (1978)	0.32 - 0.37
Prodanovic (1979)	0.38
Weiss et al. (1981)	0.16 - 0.32
Mellor (1983)	0.40
Vivitrat and Kreider	0.1 - 0.3
Mellor (1981)	0.35 in ships tracks

Of interest, Mellor claimed that the porosity in a pressure ridge would be less than that of a rubble field.

3.5.2 Shear Properties of Partially Consolidated and Unconsolidated Rubble

Shear properties of partially consolidated and unconsolidated rubble modeled as a Mohr-Coulomb material can be defined by an angle of internal friction and a value for cohesion. Table 3.5 gives a summary of results from Keinonen and Nyman (1978), Prodanovic (1979) and Weiss et al. (1981), obtained from a review by Hudson (1983). The internal friction angle data shows much scatter, varying from 12 to 53 degrees. If all of the observations can be treated equally, there is no reason to believe the internal friction angle is dependent on the initial ice sheet thickness, though Weiss et al. found a dependence of friction angle on block sizes. More recent work at the University of Alberta used an internal friction angle of 45 degrees.

Table 3.5

Shear Properties of Ice Rubble (From Hudson, 1983)

	Ice Thickness (mm)	Cohesion (kPa)	Friction Angle (degrees)
Keinonen and Nyman (1978)	20	0.26	47
Prodanovic (1979)	38	0.58	53
Weiss et al. (1981)	80	1.4	12
	150	1.8	25
	200	3.7	29

3.5.3 Shear Stress Displacement Behavior of Ice Rubble

Small scale shear box experiments using small rubbled ice pieces conducted by Gale et al. (1985) have shown that shear stress before shear failure increases with horizontal displacement within the rubble itself. From this it can be inferred that the maximum shear resistance within a rubble field will not be attained until a prescribed amount of horizontal displacement of the rubble has occurred. When the rubble has been displaced to a certain extent, (the measurements of Gale et al. do not extend to failure), then failure occurs within the rubble and the shear resistance should peak and then drop slightly and level off.

3.6 Summary

This chapter is much briefer than that required to totally familiarize one with the behaviour of ice under all possible conditions. However, the brevity is felt to be necessary for many reasons, including: the purpose of this report is not to review ice properties, but rather to concentrate on how ice loads on marine structures are currently calculated. As well, a comprehensive and thorough review of ice mechanical properties would take a significant amount of time and would in itself be a large study beyond the current scope. The description of the state of ice requires so many variables that one not familiar with ice as a material would have difficulty selecting numbers appropriate to his or her use.

At this time there is a good understanding of the small scale failure processes in ice. However, there is still much work to be done to extend this understanding to full scale load calculations.

4.0 Ice/Structure Interaction: General Logic

4.1 Introduction

Structures are designed such that when ice moves against them the ice fails. A force is exerted on the structure at the point of contact. The nature and magnitude of the force are governed by many factors, some of which relate to the ice (ice strength and other mechanical properties), and some to the structure (whether it is sloped, vertical sided, floating, and if floating the natural period of vibration, etc.).

In a conceptual sense ice forces are simple to specify. They are governed either by the deformation, failure and clearing of the ice in front of the structure, or by the environmental driving forces on the ice. In both of these situations the magnitude of the ice force is not constant with time. This is especially true in cases where the ice velocity is high enough to cause brittle failure of the ice.

In Figure 4.1 the trace of load versus penetration distance, or time, obtained at Hans Island is shown. Hans Island is a natural rock island located in the Kennedy Channel between Ellesmere Island and Kalaallit Nunaat (Greenland). Knowledge on large scale ice/structure interactions has been obtained during three expeditions to Hans Island in 1980, 1981 and 1983. To date, only the results of the first study (APOA 180) are public; the results of the second study (APOA 181) will be realeased in 1987, and those of the third study (APOA 202) in 1988.

When considering ice forces it is usual to determine the maximum peak ice force and use it as a quasi-static design load. This approach may be appropriate for very massive rigid structures and as a method of designing for overall global stability, however the periodicity of ice forces needs to be considered in terms of dynamic amplification of structural deformation, potential liquifaction of soils, and fatigue life. Also, in certain cases, the deflection of the structure can change the ice failure process and therefore change the level and nature of the ice force. The topic of dynamic ice loads is discussed further in Section 5.6.

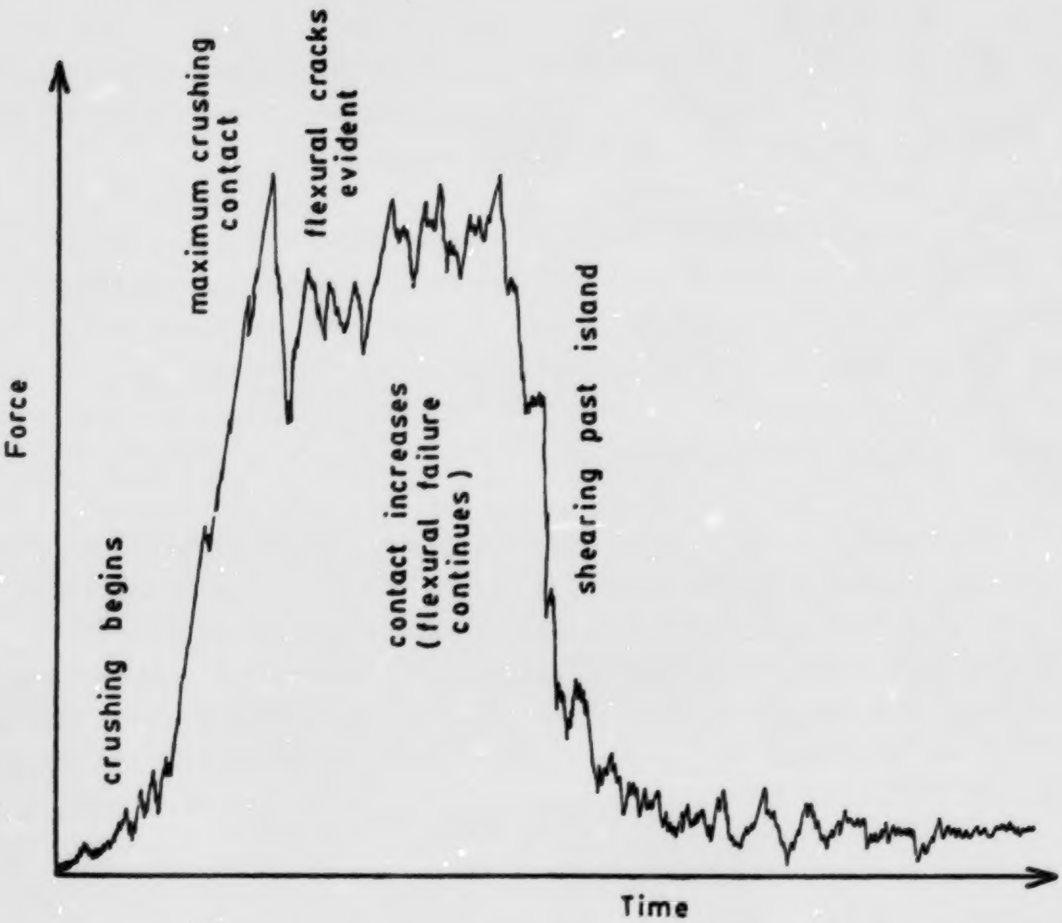

Figure 4.1 Illustration of the Force-Time History for a Floe/Hans Island Interaction (from Danielewicz et al., 1983).

4.2 Quasi-Static Ice Loads

The ice load on a marine structure can be dynamic in cause, (for example, brittle failure of the ice, or flexural failure periodicities, or on a longer time scale, the action of a floe being brought to rest at the structure), but the deformation of the structure and the periodic nature of the ice force are usually not accounted for in determining the peak load.

For any given geographic region three basic interaction scenarios which can be idealized are as follows:

Limit-Stress:	Full envelopment of the structure by the ice, resulting in a maximum ice load.
Limit-Energy:	Full envelopment does not occur. During the interaction the ice feature slows down as kinetic energy is dissipated by the failure of the ice. Environmental forces of wind and current drag, and ridge-building decrease the loss of kinetic energy due to their acting in the same direction as the ice feature's motion. When the ice feature stops, environmental forces are still acting.
Limit Force:	For this scenario the ice adjacent to the structure is stationary prior to the application of limit-environmental forces of wind drag, current drag and ridge-building.

Thin ice sheet/structure interactions are usually of the limit-stress variety. While important to examine in their own right, thin ice sheet/structure interactions are generally not the governing interactions for design except in the case of narrow structures not exposed to the larger ice features.

The limit stress load is that load caused by the deformation and failure of the ice immediately in front of the structure, as shown on Figure 4.2. The limit stress load is expressed as:

$$F = p\,D\,t$$

where: D is the structure diameter,
t is the local ice thickness, and
p is the ice failure pressure (which of course is highly dependent on the mechanical properties of the ice).

The concept of the limit-stress load is based on the assumption that the force F is not large enough to stop the ice feature before the thickest portion of the ice feature fully envelops the structure. If the force F is large enough, then the ice force is limited to that required to overcome the kinetic energy of the ice feature and the work done on the ice feature by the environmental forces acting on the ice feature during the interaction.

In Figure 4.3 are shown some results of a computer program that can model the application of environmental forces during an ice/structure interaction. The environmental forces include the ridge-building force acting across the backside of the ice floe (if present), the wind drag forces acting on the top surface of the ice feature and the current drag forces acting on the bottom of the ice feature. At the beginning of the interaction the ice feature is moving at a velocity in equilibrium with the wind drag, current drag and ridge building forces. As the area of interaction increases the structure is assumed to exert an increasing force on the ice feature as illustrated by the inclined line in Figure 4.3.

The ice feature does not begin to slow down until the force that the structure exerts on the ice feature exceeds the pack ice, or ridge-building forces acting across the backside of the ice feature. As the ice feature slows the wind and current drag forces increase from zero and reach their maximum values when the ice feature comes to rest (i.e. the velocity

LIMIT STRESS

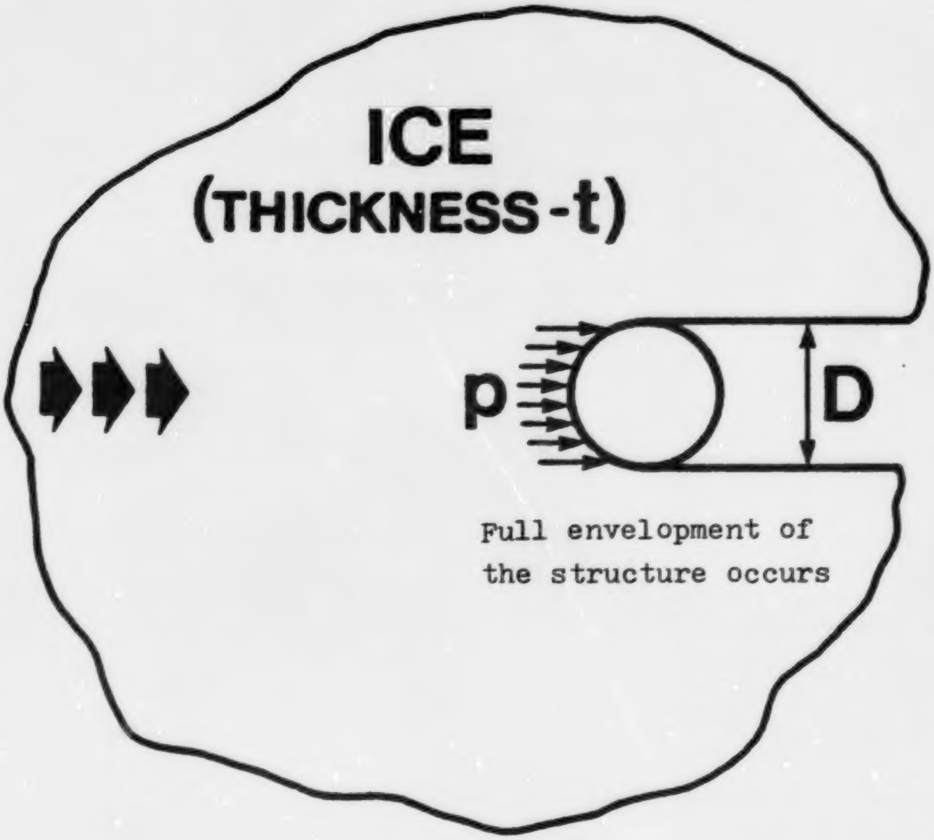
ICE
(THICKNESS-t)
p
D
Full envelopment of the structure occurs

The Limit-Stress load is governed by local ice failure at the structure

Figure 4.2 Illustration of Definition of Limit-Stress Load.

EXAMPLE: ICE FEATURE INITIALLY AT A VELOCITY IN EQUILIBRIUM WITH WIND DRAG AND CURRENT DRAG

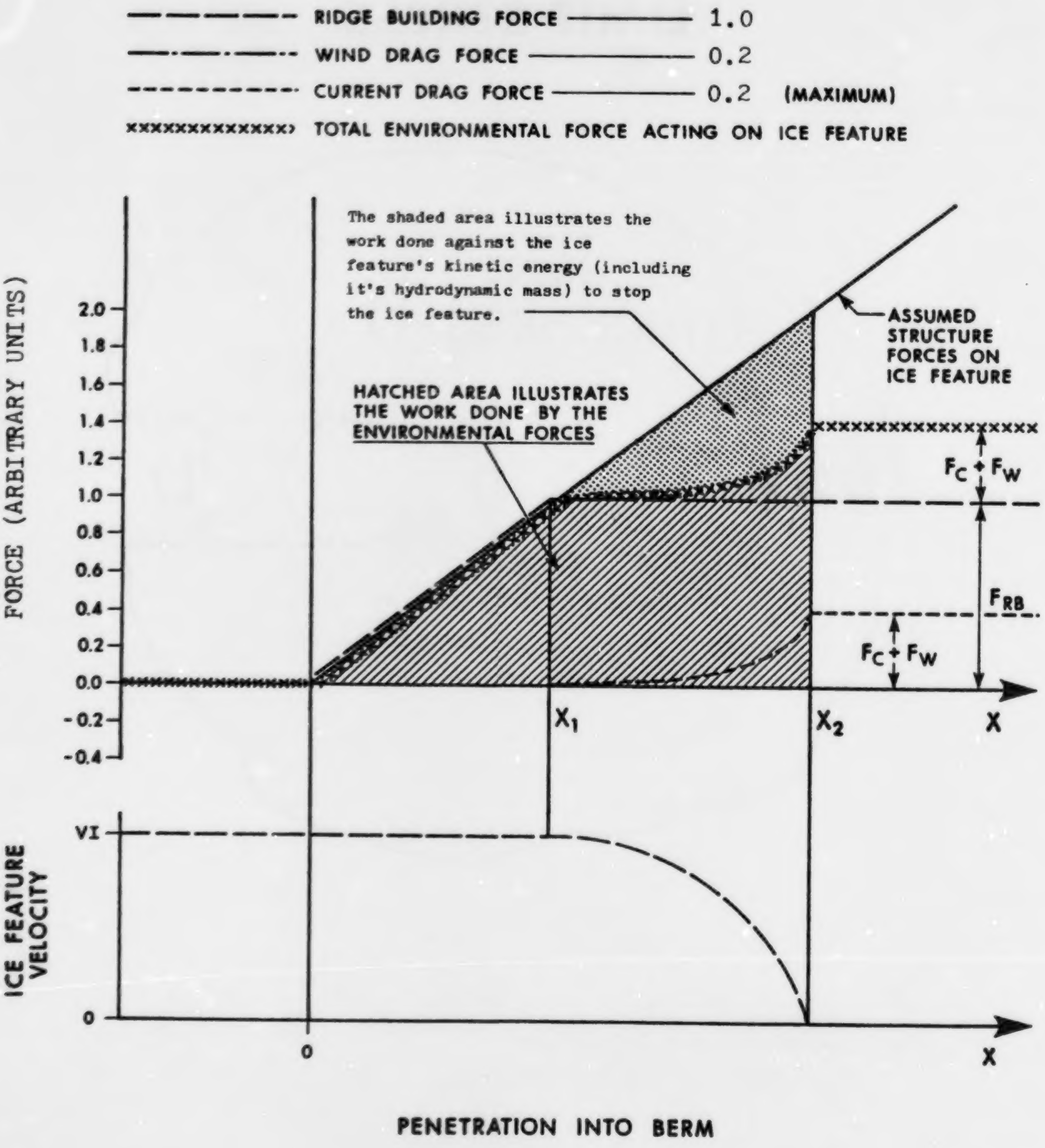

Figure 4.3 Results from an analysis of Environmental Loads Acting on an Ice Feature During an Interaction With a Marine Structure (from Marcellus, 1982).

difference between the wind and current and the ice feature is a maximum when the ice feature comes to rest).

The work done by the environmental forces during the interaction is illustrated by the cross-hatched area in Figure 4.3. The work done against the ice floe kinetic energy (including its added or hydrodynamic mass) to stop the ice feature is also illustrated in the figure. For this particular example the majority of the energy expended on the structure was that required to overcome the environmental forces. This type of interaction would be typical of large ice floes beyond the landfast ice in the Beaufort Sea during the winter months.

If ridge-building forces do not occur during the interaction, then it is obvious from the figure that the load experienced by the structure would be reduced considerably. This type of interaction, where the majority of the work done in stopping the ice feature is done to overcome the ice feature's kinetic energy is more typical of idealized iceberg/structure interactions (eg. Cammaert, Wong and Curtis, 1983).

The types of interactions where the ice features stop before the limit stress ice loads occur are herein termed "Limit Engery Loads".

The ridge-building force is important when the ice feature is surrounded by ice, and does not interact with the structure individually, but rather as part of a larger matrix. Values of the ridge-building force used by several researchers are shown in Figure 4.4.

The important thing about the ridge-building force acting on an ice floe during an interaction is that it may be averaged over several kilometres. Recently, a pilot program to measure typical pack ice forces was carried out in the Beaufort Sea (Croasdale et al., 1986, 1987). The results obtained from the program indicate values less than 10^5 N/m^{-1}. If this is a reasonable upper limit then limit-energy loads for extreme ice feature interactions could be quite a bit less than limit-stress loads (as shown in Figure 4.5).

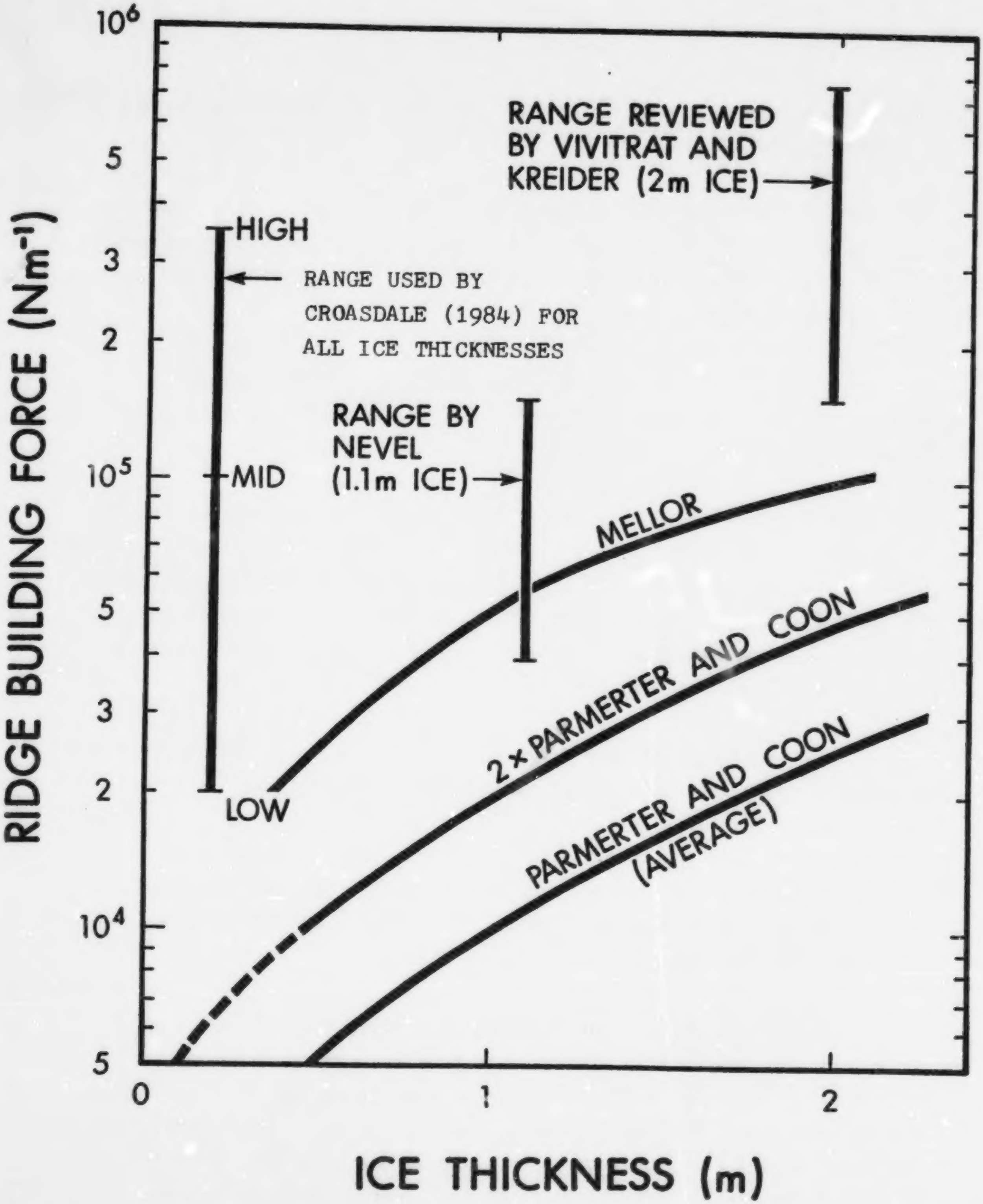

Figure 4.4 Values for the Ridge-Building Force from Several Studies.

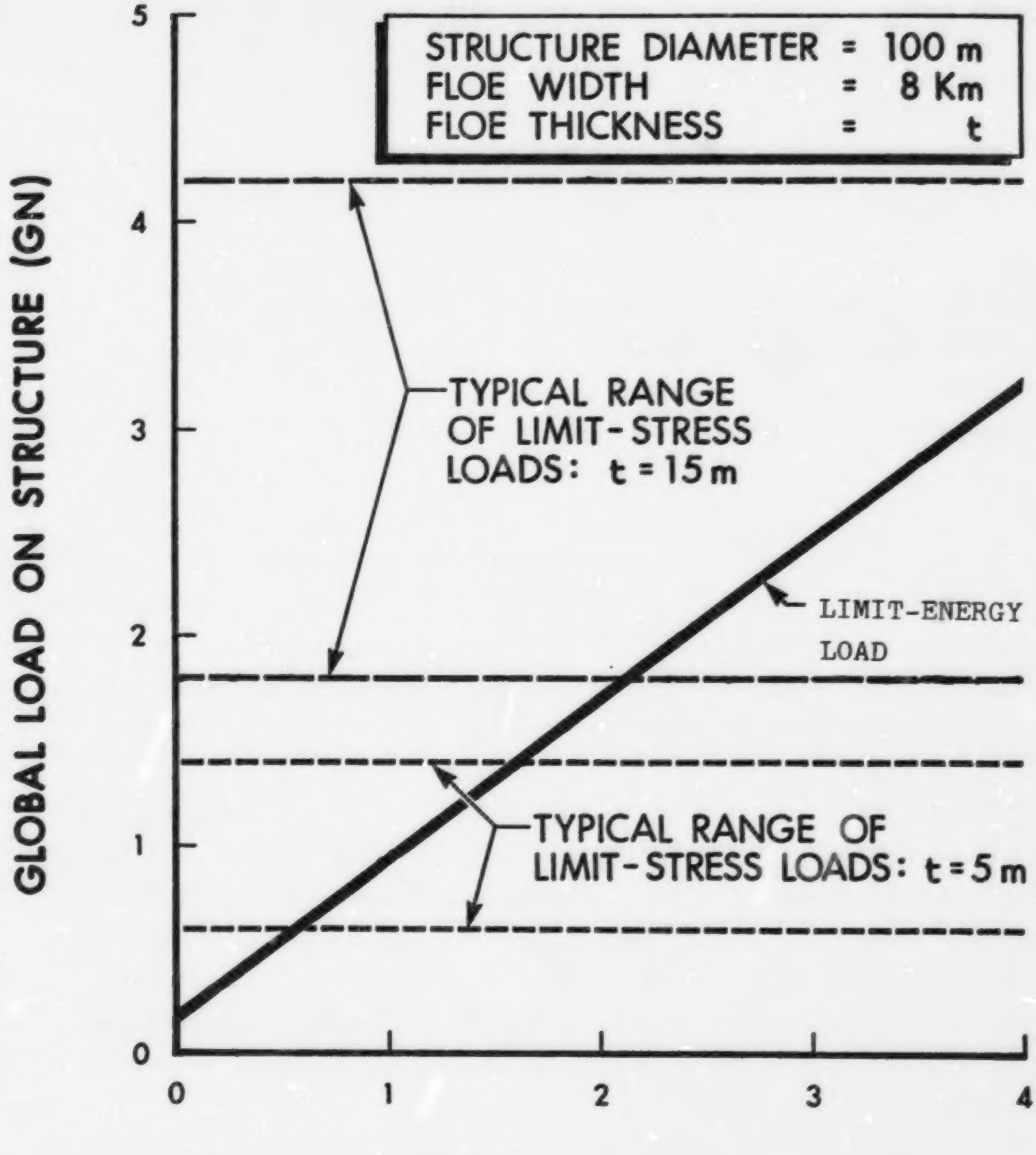

Figure 4.5 Illustration of Typical Ranges of Global Loads as a Function of Ridge Building Force.

Limit energy loads occur when the left and right sides of the following equation are equal and the penetration X (to stop the ice feature) is less than that required to develop the limit stress load.

$$\int_0^X EF_x \, dx + \Delta EK \geqslant \int_0^X FS_x \, dx$$

where:

EF_x = wind drag force + current drag force + ridge-building force,

ΔEK = the change in kinetic energy of the ice feature, including its hydrodynamic mass, and

FS_x = force on the structure at a penetration of X.

The magnitude of FS, the force that the structure exerts on the ice feature, depends on the mode of ice deformation in front of the structure and this has a major influence on the ice load. Among other things, the modes of ice failure are governed by structure shape, structural geometry, strain rate, the state of the ice and the geometry of the ice feature.

From the above equation it is obvious that if the ice feature is at rest at the beginning of the interaction, the ΔEK term is zero and the load on the structure is equal to the environmental forces (the "Limit-Force" condition). In order for the limit-stress scenario situation to develop from an ice feature which is initially at rest against the structure, movement of the ice feature towards the structure would be required and some of the energy expended by the environmental forces would go into accelerating the ice feature.

At high loading rates ice moving against a vertical-faced structure will generally fail in crushing; however, if the ice is thin it may fail in buckling. Ice moving against a sloping structure will fail in bending unless it is frozen to it. Calculations for ice forces have to recognise these various failure modes (see Figure 4.6).

It is also important to recognize that broken ice does not just disappear. It is either carried around the structure by the moving ice or it collects in front of the structure. Clearing forces have to be recognized, particularly for sloping structures. Furthermore, for wide structures the ice cannot usually clear and piles up in front. This ice rubble can significantly affect the ice failure mode and the resulting ice forces.

For example, consider a caisson retained island resting on an underwater soil berm (Figure 4.6). Initially, the ice moving against the sloping caisson will fail in bending; however, for a typical 100 m wide structure the ice will not clear around the structure and a rubble pile will form. Where the depth to the top of the berm is small the rubble is likely to become grounded on the underwater berm and, therefore, the active failure zone moves from the structure to the outside of the ice rubble. Obviously the ice load is now controlled by failure at the outside of the rubble and the shape of the structure has no influence on either the failure mode or the ice force. The effect of ice rubble is an important consideration in ice force calculations as discussed in Chapter 5.

The berm can also cause thick ice ice features to be slowed by grounding. The forces created by deformation of the soil berm and uplift of the floe will dissipate the ice feature's momentum and thereby reduce the potential force on the structure.

Different methods for estimating the loads for various structure and ice feature shapes are presented in detail in Chapter 5. The estimates, however, must recognize the probabilistic aspects of the interactions.

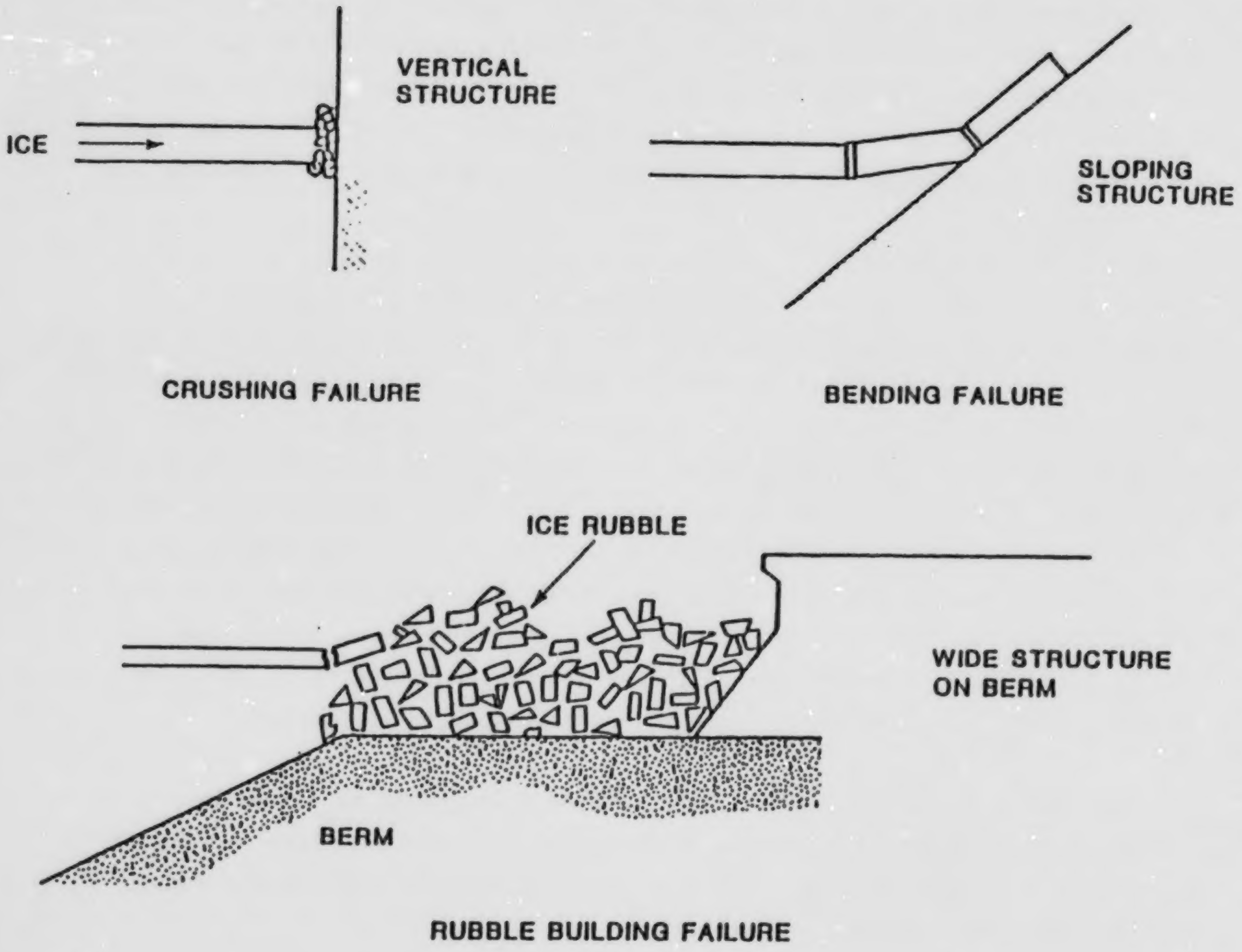
VERTICAL STRUCTURE
ICE
CRUSHING FAILURE
SLOPING STRUCTURE
BENDING FAILURE
ICE RUBBLE
WIDE STRUCTURE ON BERM
BERM
RUBBLE BUILDING FAILURE

Figure 4.6 Illustration of Crushing, Bending and Rubble Building Failure Modes (Croasdale and Person, 1984).

4.3 Probabilistic Approaches

Ice, being a natural material, has mechanical properties which vary. The issue of which value of ice strength to include into an ice force prediction is one which can be treated statistically (eg. Bercha, 1979). However, in addition to ice strength, there are other parameters in the ice force prediction which can also have large variability. For example in the limit-stress condition, ice thickness is a required input and can be treated statistically. In the limit-energy situation, the floe size, velocity and environmental forces are additional inputs. In the limit-environmental force situation only the environmental forces are additional inputs.

It is obvious that in any deterministic load calculation, if the worst values of each of the input parameters are combined, then a very conservative ice load value will result. It is for this reason that methods have been developed to treat ice loads in a probabilistic framework.

Such approaches have been developed by Wheeler (1981), Marcellus (1982), Allyn et al., (1985), Marcellus et al, (1986), Jordaan et al. (1986), and Vivitrat et al., (1985).

A general framework for the probabilistic approach is shown in Figure 4.7.

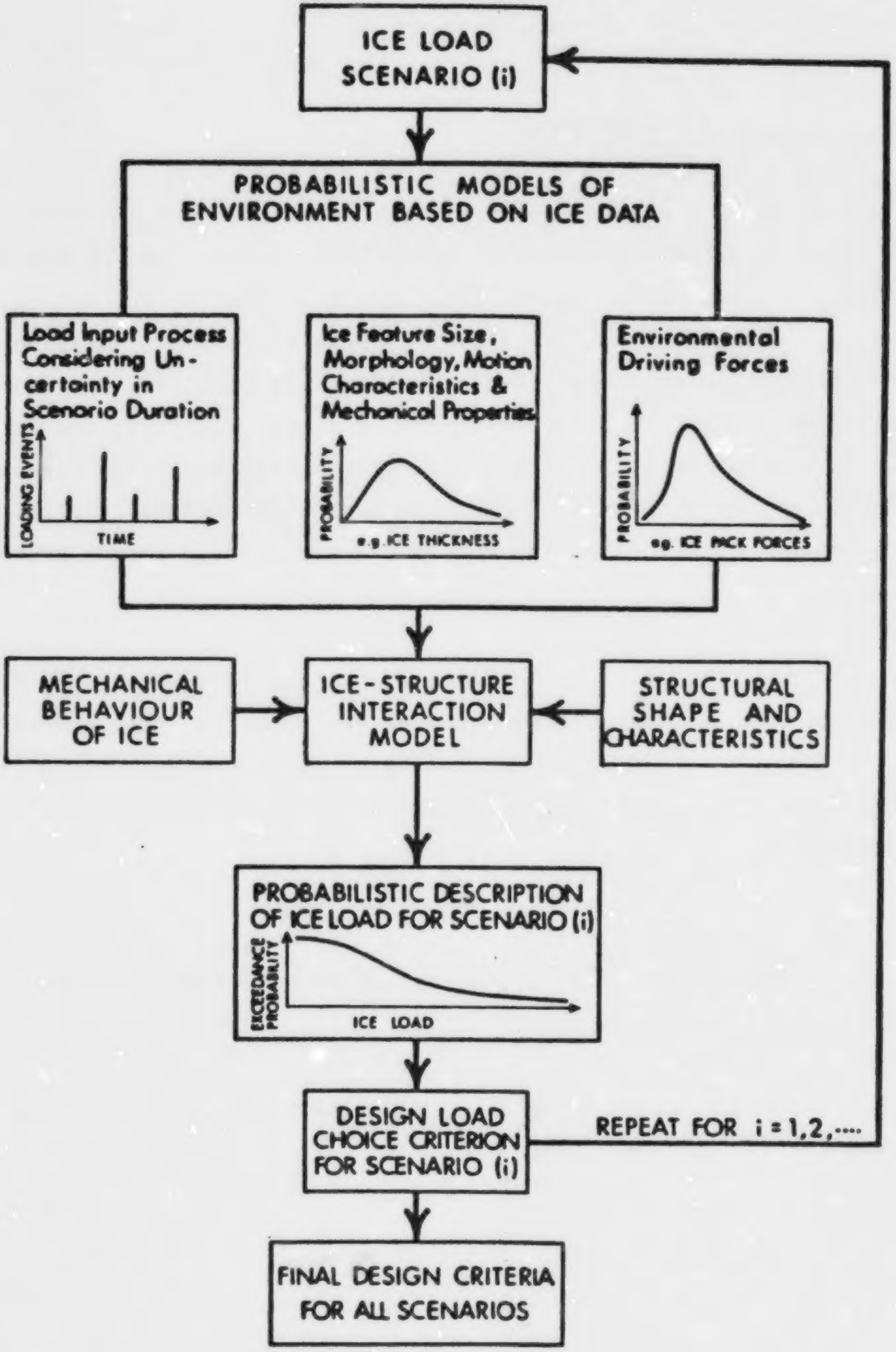
ICE LOAD SCENARIO (i)
PROBABILISTIC MODELS OF ENVIRONMENT BASED ON ICE DATA
Load Input Process Considering Uncertainty in Scenario Duration
LOADING EVENTS
TIME
Ice Feature Size, Morphology, Motion Characteristics & Mechanical Properties
PROBABILITY
e.g. ICE THICKNESS
Environmental Driving Forces
PROBABILITY
eg. ICE PACK FORCES
MECHANICAL BEHAVIOUR OF ICE
ICE-STRUCTURE INTERACTION MODEL
STRUCTURAL SHAPE AND CHARACTERISTICS
PROBABILISTIC DESCRIPTION OF ICE LOAD FOR SCENARIO (i)
EXCEEDANCE PROBABILITY
ICE LOAD
DESIGN LOAD CHOICE CRITERION FOR SCENARIO (i)
REPEAT FOR i = 1,2,....
FINAL DESIGN CRITERIA FOR ALL SCENARIOS

Figure 4.7 Flow Chart of Probabilistic Design Load Methodology. (Jordaan, 1985).

4.4 Other Considerations and General Logic

The general logic for estimating ice loads is shown in Figure 4.8. The geographical location for the structure obviously influences the values to be selected for ice feature geoemtries, the velocities and the driving forces. The geometry of the structure, influenced partly by other parameters such as ice feature geometry and strength, will determine ice failure modes that are preliminary to load calculations using various ice load models. Ice loads can be calculated for selected ice feature values, and as such, might be termed deterministic. In contrast, if ice feature statistics are integrated with the ice load models in a probabilistic model, e.g. a Monte Carlo simulation, then probabilstic ice loads can be calculated. Finally, other load considerations such as local ice pressures, ice ride-up and pile-up evaluations can be treated in a similar fashion.

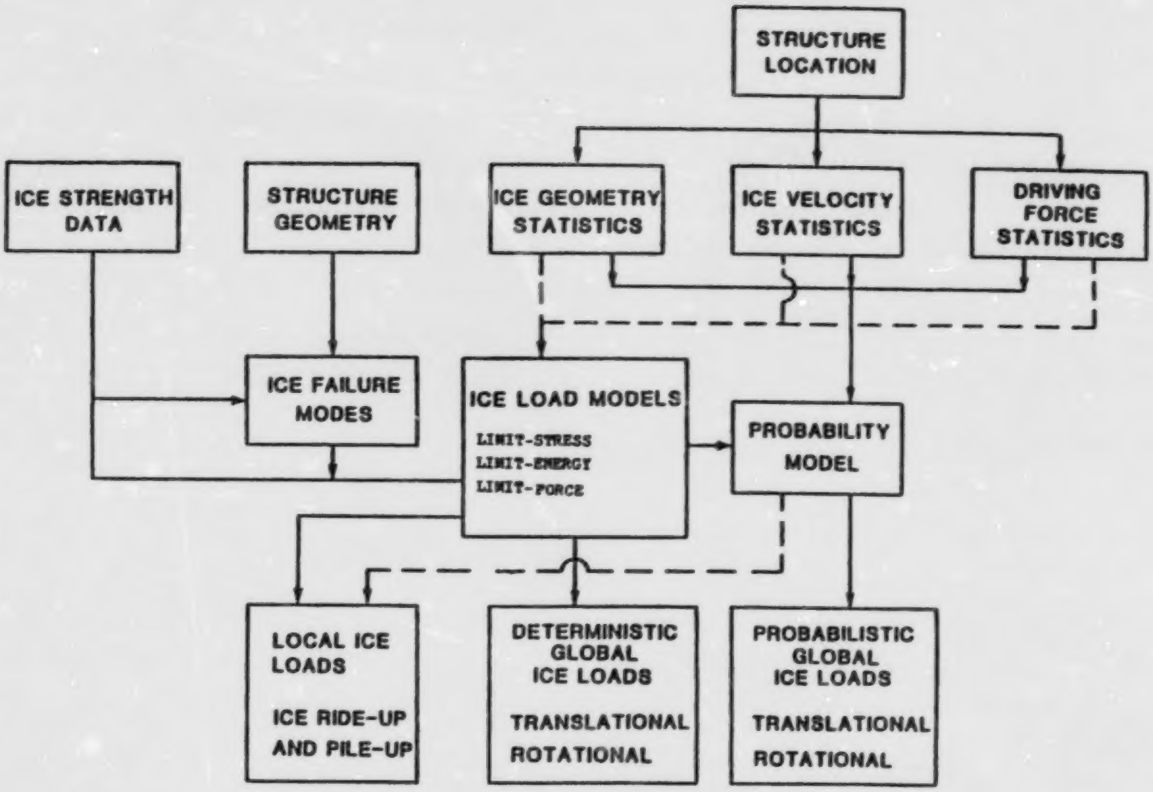
STRUCTURE LOCATION
ICE STRENGTH DATA
STRUCTURE GEOMETRY
ICE GEOMETRY STATISTICS
ICE VELOCITY STATISTICS
DRIVING FORCE STATISTICS
ICE FAILURE MODES
ICE LOAD MODELS
LIMIT-STRESS
LIMIT-ENERGY
LIMIT-FORCE
PROBABILITY MODEL
LOCAL ICE LOADS
ICE RIDE-UP AND PILE-UP
DETERMINISTIC GLOBAL ICE LOADS
TRANSLATIONAL
ROTATIONAL
PROBABILISTIC GLOBAL ICE LOADS
TRANSLATIONAL
ROTATIONAL

Figure 4.8 Flow Chart of Overall Logic for Determining Design Ice Loads (Croasdale and Person, 1984).

5.0 Interaction Load Theory

5.1 Introduction

Methodologies for calculating ice loads on structures are presented in this chapter. The chapter is divided into six sections following this introduction.

In Section 5.2 a review of ice failing against a vertical sided structure is presented. This is followed by an examination of ice failing against a sloping structure. In comparison to a vertical structure where the failure is predominantly by crushing, a properly designed sloping structure causes the ice to fail in bending. The loads caused by bending failure are generally less than for crushing, however, for certain conditions, reviewed in Section 5.3, the sloping structure offers no advantage over a vertical sided structure.

Next, in Section 5.4 interactions of ice features with floating structures are examined. The load scenarios for floating structures differ from vertically sided or sloping gravity structures in that the movement and response of the structure has to be evaluated.

The last generic structure type presented in this chapter is the artificial island type structure (Section 5.5). For the purposes of this report an artificial island is defined as a structure around which a rubble pile is expected to form during the winter months. The term artificial island also includes sand and gravel bermed structures.

The discussions on the different ice failure modes and structure types are followed by discussions on the dynamic response of a structure in Section 5.6 and local ice loads in Section 5.7.

5.2 Ice Interactions With Vertical Sided Structures

5.2.1 Introduction

In Figure 5.2.1 a photograph of the rubble created during an interaction between a ridge and Gulf Canada's Molikpaq structure is presented. Measured multi-year ice ridge loads up to 500 MN have been reported for this structure.

In the remainder of this section a review of the current state-of-the-art for calculating ice loads on vertical sided structures, such as the Molikpaq, is provided.

In Subsection 5.2.2 a review of observed ice failure modes is presented.

In Subsection 5.2.3 the detailed review of the methodologies used to estimate ice loads on vertical sided structures is presented.

Subsection 5.2.4 contains example calculations for a number of different ice/structure interaction scenarios. Covered in the example calculations are:

- an analysis of the interaction of a multi-year ridge with a structure,
- an analysis of an unconsolidated ridge with a structure, and
- analyses of buckling of both ice sheets and small floes of ice,

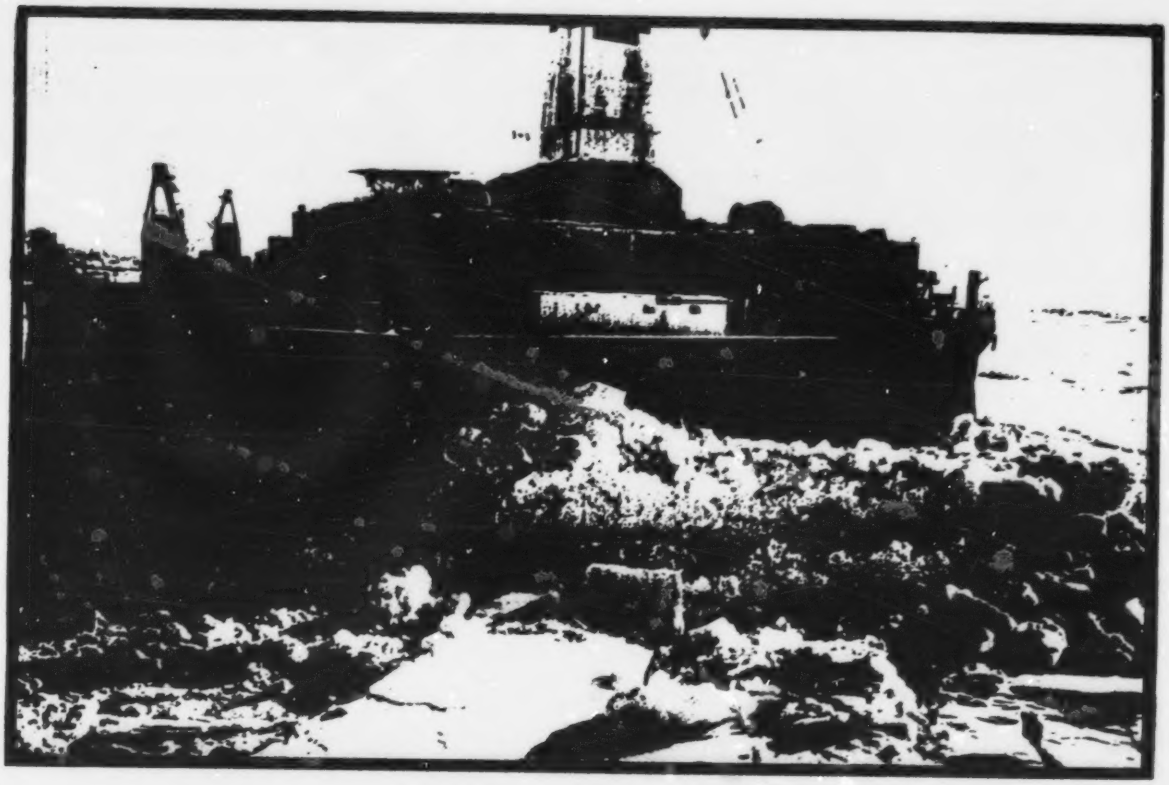

Figure 5.2.1 Ice Failing at the Gulf Molikpaq Structure (photo courtesy Gulf Canada).

Subsequent to the presentation of the scenario calculations a summary of suggested calculation procedures is presented in Subsection 5.2.5.

The interaction of icebergs with vertical sided structures is not specifically reviewed in this section of the report. The estimate of loads exerted on large structures due to the interaction with a large iceberg is equal to the product of an assumed failure pressure and an area of interaction. Failure pressure data have been presented in Chapter 3. For reviews of large iceberg/structure interactions the reader is referred to the work by Cammaert and Tsinker (1981), Cammaert et al. (1983) and Bass et al. (1985).

5.2.2 Observed Failure Modes

5.2.2.1 The Behaviour of Ice Under Load

At low loading rates all ice behaves in a ductile fashion as illustrated in Chapter 3. In a purely ductile mode the ice flows around immovable obstacles in its path. As the loading rate increases the ice failure mode changes from ductile to brittle. The transition occurs at a peak stress in the ice for the given loading conditions.

The addition of brine pockets or channels and air bubbles into the ice matrix reduces the strength of the ice, and both brine and air content should be taken into account when estimating the failure stress for the ice. The structure of the ice also affects its strength.

Sea ice is typically composed of a mixture of granular ice crystals and columnar ice crystals. When typical sea ice first forms the surface crystals are normally granular. After an initial growth of granular crystals the ice normally grows in vertical columnar crystals. After a full winter's growth a first-year ice sheet in the Canadian arctic will have a thickness of approximately 2.0 metres. Of this thickness the top 10 or 15 cm will be granular in texture.

Iceberg ice is also granular ice, however its strength can not be compared directly with sea ice due to the different formation mechanisms. Iceberg ice is fresh water ice which contains significantly more air than sea ice.

Ice creeps at all stresses. At the highest strain or stress rates the ice will fracture before significant creep can take place. In landfast ice conditions in the Beaufort Sea the loading rates are generally low enough such that brittle failure may not occur, and the ice will flow in a ductile manner around a fixed structure throughout most of the winter.

In the laboratory it has been determined that cracks will appear in stressed ice when the delayed elastic strain in the ice sheet equals some predetermined critical value (Sinha, 1982).

The behaviour of the ice in the brittle range is essentially elastic. Microcracks in front of an indentor have been observed to be aligned along maximum shear stress trajectories (Timco, 1986; Tomin et al., 1985).

5.2.2.2 Small Scale Brittle Failure

Laboratory tests have shown that in the brittle range sheet ice, in particular columnar S_2 ice, can fail in a great variety of modes.

Michel and Blanchet (1983)

Michel and Blanchet (1983) presented illustrations of the failure modes observed in their tests, and these are reproduced in Figure 5.2.2. Force-time histories of some of the tests are shown in Figure 5.2.3. The force-time history of the interaction is seen to be highly dependent on the failure mode observed during the interaction, i.e. the loading depends on the mode of failure.

Timco (1986)

Timco (1986) repeated the Michel and Blanchet tests and observed the same phenomenon. In Figures 5.2.4 and 5.2.5 are shown the force-time histories and observed modes of failure of the ice used in the tests. Comparing the latter two figures with those of the Michel and Blanchet tests it is seen that basically the same phenomenon were observed in both sets of tests.

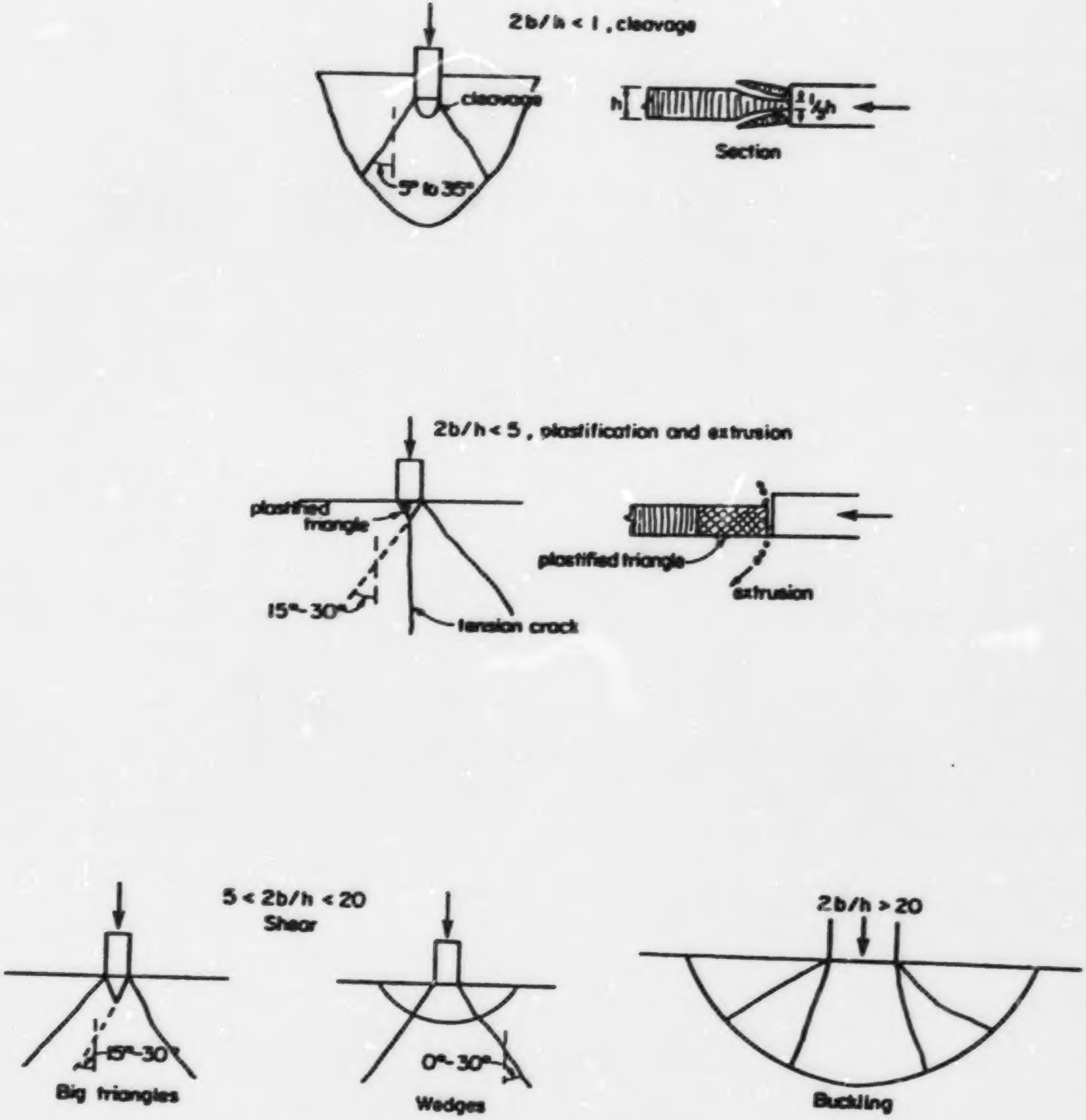
2b/h < 1, cleavage
cleavage
5° to 35°
h
1/3 h
Section
2b/h < 5, plastification and extrusion
plastified triangle
15°–30°
tension crack
plastified triangle
extrusion
5 < 2b/h < 20
Shear
15°–30°
Big triangles
0°–30°
Wedges
2b/h > 20
Buckling

Figure 5.2.2 Observed Brittle Ice Failure Modes as a Function of Aspect Ratio, (from Michel and Blanchet, 1983).

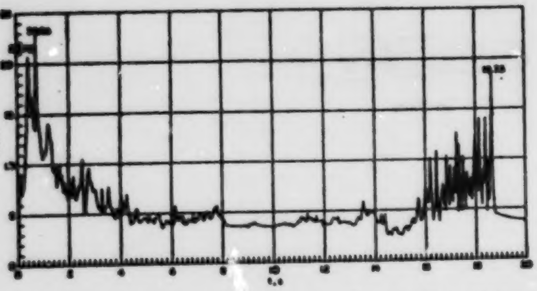

Recording of loads for an ice sheet failing by cleavage (test 1).

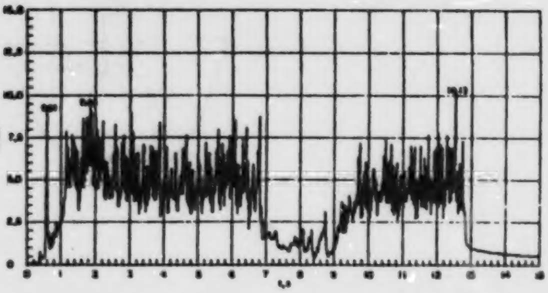

Recording of loads for an ice sheet failing by formation of plastified triangles and extrusion (test 2).

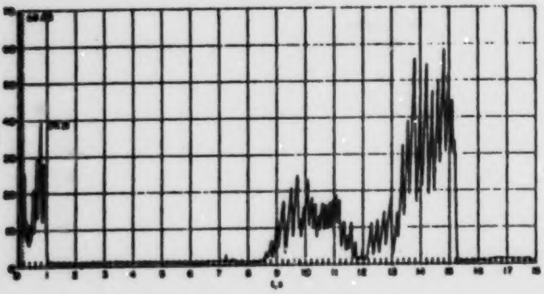

Recording of loads for an ice sheet failing by shear with wedge formation and secondary buckling (test 5).

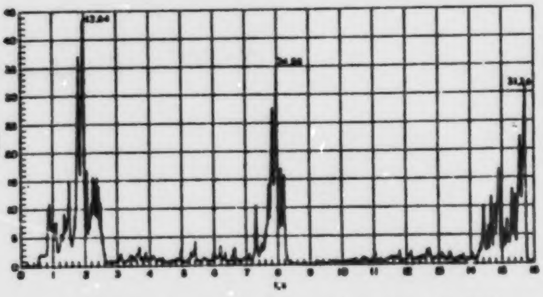

Recording of loads for an ice sheet failing by shear with the formation of large triangles (test 8).

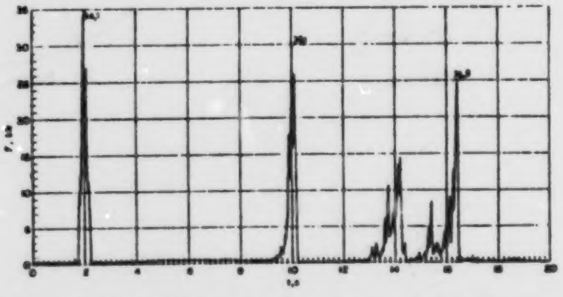

Recording of loads for an ice sheet failing by successive buckling of wedges (test 27).

Figure 5.2.3 Force-Time Histories of the Different Brittle Ice Failure Modes observed by Michel and Blanchet. Note How the Force-Time History Depends on the Failure Mode.

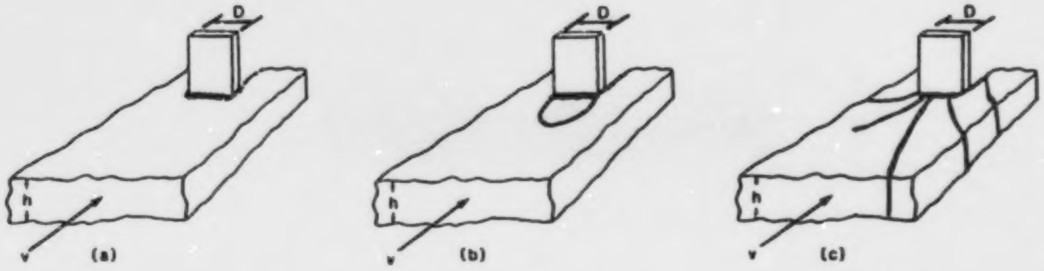

CRUSHING (c)

CRUSHING WITH SPALLING (s)

CRUSHING WITH RADIAL CRACKING (r)

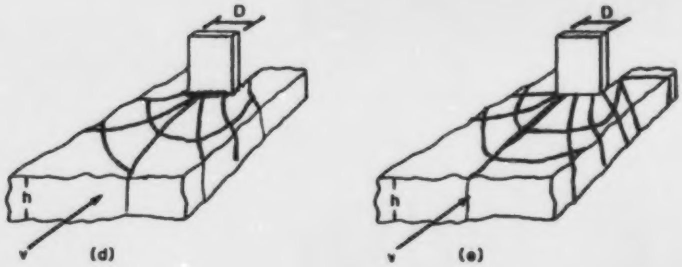

CRUSHING WITH RADIAL AND CIRCUMFERENTIAL CRACKING (m)

RADIAL AND CIRCUMFERENTIAL CRACKING WITH BUCKLING (b)

Figure 5.2.4 Observed Brittle Ice Failure Modes Observed by Timco (1986).

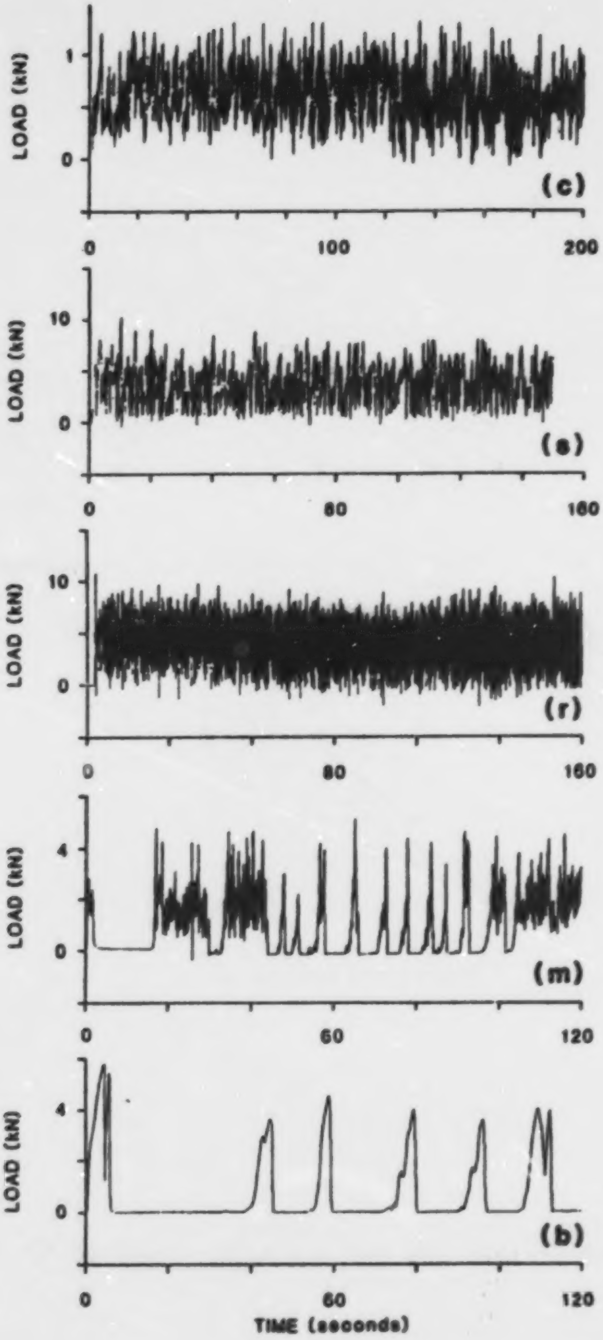

THE LOADS SHOWN IN THIS FIGURE ARE NOT FOR ICE SHEETS OF THE SAME THICKNESS AND CAN NOT BE COMPARED.

Figure 5.2.5 Force-Time Histories of the Different Brittle Ice Failure Modes Observed by Timco. Note How the Force-Time History Depends on the Failure Mode.

It is possible to categorize the observed failure mode as a function of interaction characteristics. In Figure 5.2.6 the dominant failure mode is shown as a function of strain rate (calculated here as v/2D, where v is the ice velocity, and D is the indentor width), and aspect ratio (D/t, where t is the thickness of the ice sheet). This characterization is referred to as a "deformation mode map".

Kry (1981)

Some indentation test data are available for medium scale situations. Kry (1981) reviews indentation test data obtained both in the laboratory and at Eagle Lake, a natural lake about 50 km east of Calgary. The tests are examined in detail in APOA 106.

Three weeks before tests were to commence, large areas of ice, 8 m x 7.6 m, were removed from the natural ice sheet. Refreezing of the water was initiated by seeding the open water areas. The natural ice sheet was about 0.6 m thick.

S_2 ice grew in the ponds, and was 0.25 m thick at testing time. The large size of the ponds enabled indentor penetrations of 3.7 m. The reaction to the loads was passed to the thicker natural ice sheet.

Three major failure modes were observed in the laboratory tests, referred to by Kry (in order of strain rate), as ductile, ductile flaking and brittle flaking. Only ductile flaking was observed in the Eagle Lake tests.

In the laboratory tests the highest stresses were observed during ductile failure, however, ductile flaking was examined in greater detail due to it being the only observed failure mode for the lake tests.

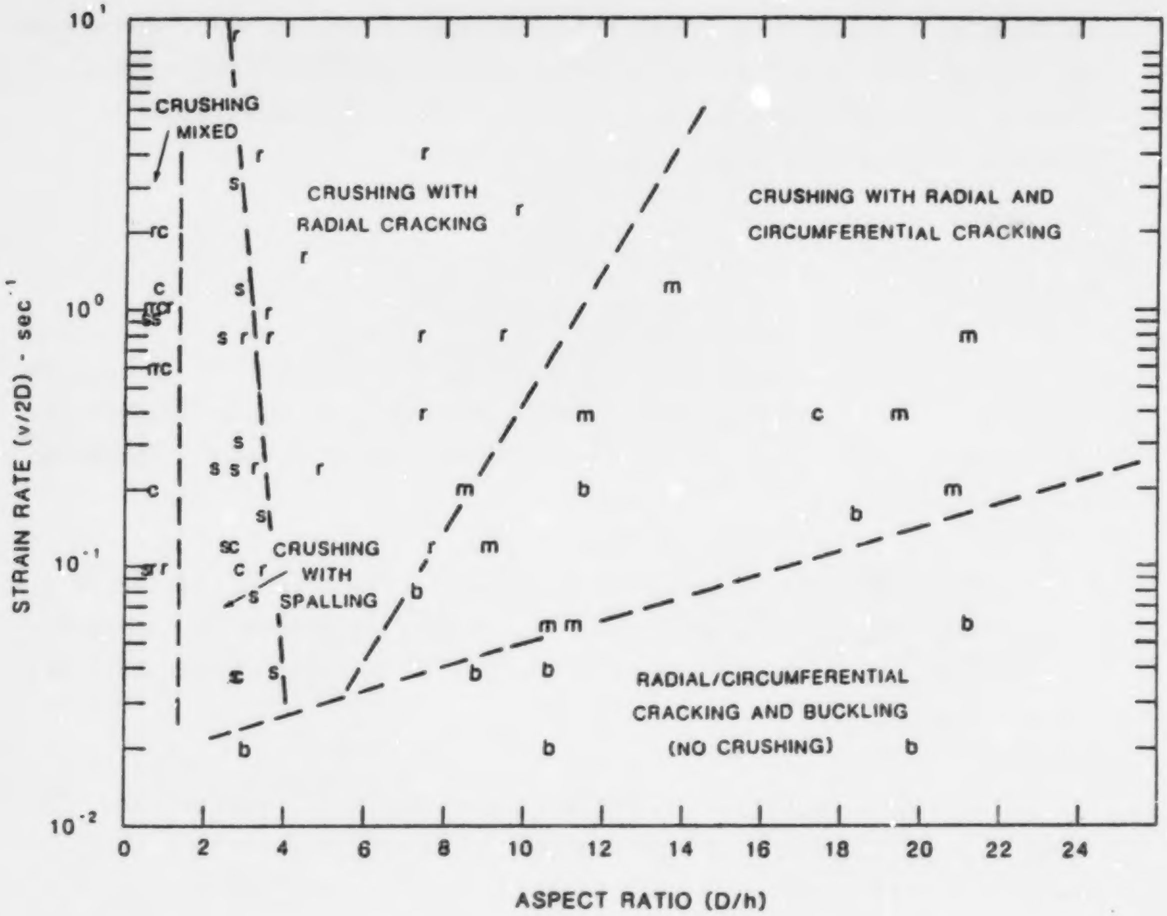

Figure 5.2.6 Deformation Mode Map Showing Dominant Failure Mode as a Function of Aspect Ratio and Strain Rate (Timco, 1986)

Both in the laboratory, and at Eagle Lake, the spalling failures typically had thicknesses of 1/4 to 2/3 the ice sheet thickness, extended 2 to 3 ice sheet thicknesses away from the indentor, and had a width of 2 to 3 ice sheet thicknesses.

The indentor had a diameter of 1.2 m, and was semi-circular in shape. The ice sheet was 27 cm thick during the tests. Penetration rates from 0.2 to 10 mm s^{-1} were used in the field tests. The aspect ratio was about 4.4, and strain rates (based on v/2D) were in the range of 8×10^{-5} s^{-1} to 4.2×10^{-3} s^{-1}.

Further study is required in order to characterize alternate failure modes onto a deformation mode map for lower strain rates. Further study is also necessary in order to determine the relationship of size on the observed failure mode.

5.2.2.3 Large Scale Brittle Failure

On the large scale, brittle failure of ice can be quite spectacular. Four primary failure modes that occur around shallow water artificial islands in the Beaufort Sea are shown in Figure 5.2.7.

Flexure, the failure of an ice sheet by bending due to contact with a sloping obstruction, is discussed in detail in Section 5.3.

Rubble formation, for which one particular type of failure is shown in Figure 5.2.7, is discussed in Section 5.5.

Buckling is a result of in-plane compressive stresses exceeding the limits of elastic stability in an ice sheet. In principal, buckling is an instability that leads to a failure rather than a true failure mode itself. Buckling is discussed in the Section 5.2.4.5.

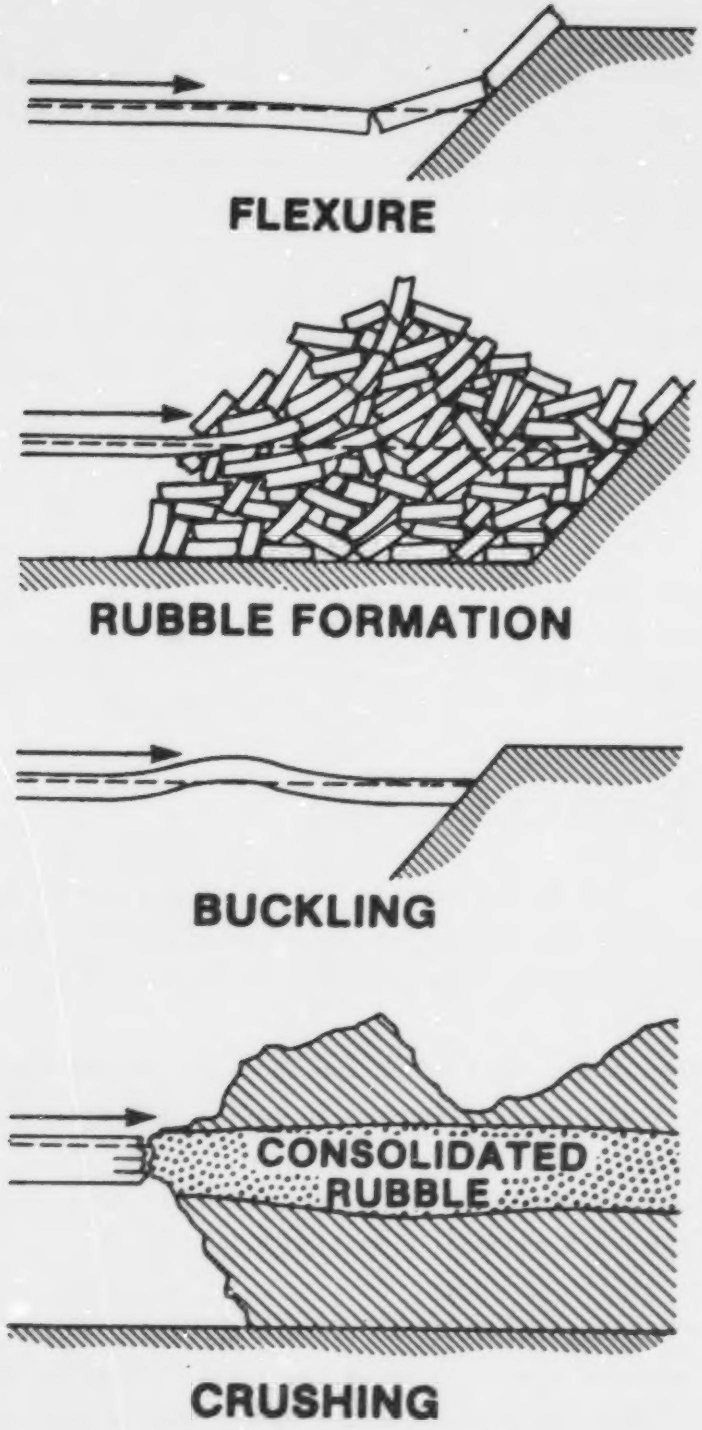

FLEXURE

RUBBLE FORMATION

BUCKLING

CRUSHING

CONSOLIDATED
RUBBLE

Figure 5.2.7 The four fundamental ice/structure failure modes (Kry, 1980)

Crushing is the loss of in-plane load bearing capacity and the structural integrity of the ice due to compressive stresses (Kry, 1980). Crushing is the term generally associated with the pulverization of the ice in the failure zone (Figure 5.2.8). On a larger scale, radial and circumferential cracking, and floe splitting may limit the load by local crushing alone (see Figure 5.2.9).

In Subsection 5.2.3 ice load theories which have been proposed to reproduce observed ice failure modes are presented and discussed.

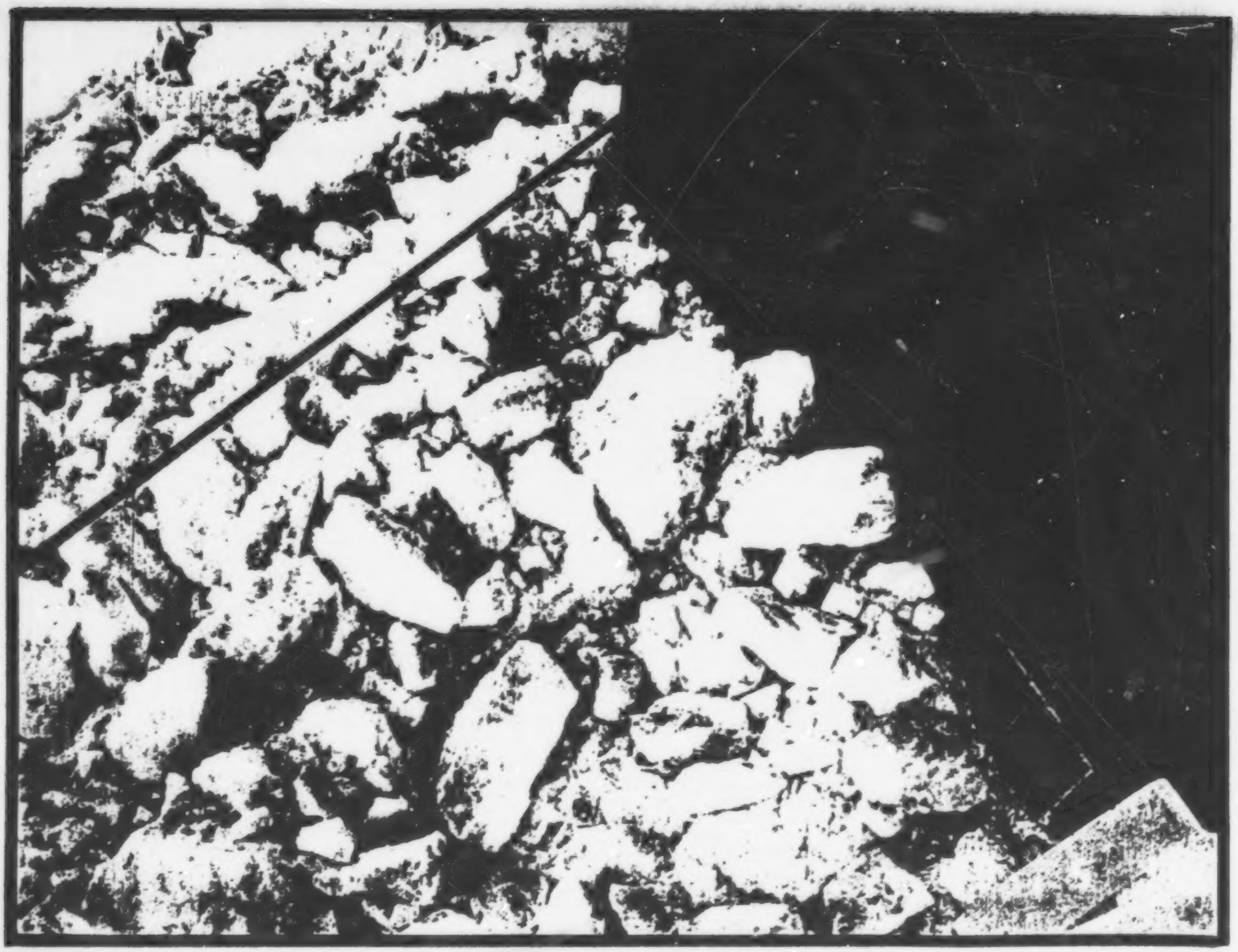

Figure 5.2.8 Crushing or Pulverization of Ice Into Small Blocks. The Largest Blocks in the Centre of the Photograph have Lengths of About 2 metres. (Photograph Courtesy Gulf Canada).

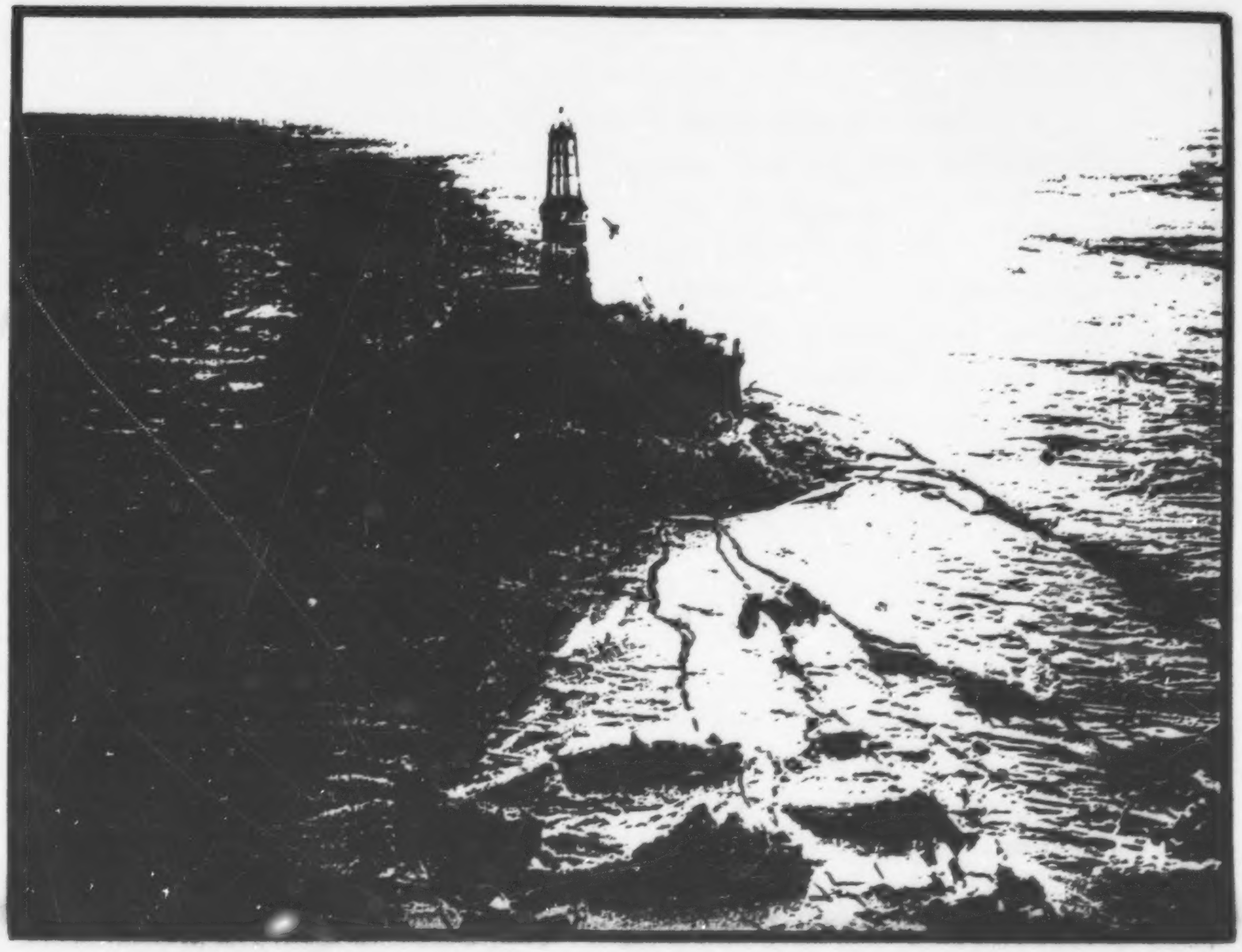

Figure 5.2.9 Illustration of Crushing With Radial and Circumferential Cracking Occurring at the Gulf Molikpaq. Compare with Cases "c" and "d" in Figure 5.2.4 (Photograph Courtesy Gulf Canada).

5.2.3 Vertical Sided Structure - Ice Load Theories

5.2.3.1 General

In Table 5.2.1 an ordering of theories or methodologies proposed to calculate ice loads on structures is presented.

Many of the theories developed during the 1980's require extensive computer modeling for application to structure design. In this respect the theories are not easily adjustable for different structure shapes. As well, most of the published (or public) literature deals only with ice sheet/structure interactions. Application of the theories to complicated ridge/structure geometries necessitates computer analysis.

5.2.3.2 Korzhavin/Elastic-Plastic

A significant number of ice load calculations are based on the "Korzhavin Equation" or "Korzhavin Methodology". Korzhavin, at the Siberian Branch of the USSR Academy of Sciences wrote, in 1962, a work detailing their methodology of determining the forces ice imposed on structures. This work was translated in 1971 by U.S.A. CRREL and has since been distributed widely.

Korzhavin developed an empirical equation which was (and still is) used to calculate the force imposed by ice, failing by crushing, against structures with a wide variety of characteristics. In order to account for the variability in structure characteristics the equation included coefficients for shape, contact between the ice and the structure, and for confinement (or indentation).

The equation also included a velocity (or strain rate) function, to calculate differences in ice failure pressure when the velocity of the floe was not equal to 1 m s^{-1}. Later research would show that the velocity

Table 5.2.1

Chronological Order of Theories Used (and Proposed) to Calculate Ice Loads on Structures

Introduction Date	Generic Name of Theory	Representative Reference(s)
1960's or earlier	Korzhavin Methodology	Korzhavin, (1971) Afanas'ev (1972)
Early and Mid 1970's	Elastic - Plastic	Morgernstern and Nuttall (1971) Croasdale et al., (1977) Ralston, (1978) Reinicke and Remer, (1978)
Late 1970's	Multi-Zonal Failure	Kry, (1978)
Early 1980's	Large Scale Empirical	Marcellus and Croasdale, (1984)
	Reference Stress	Ponter et al., (1983) Sanderson, (1984)
	Fracture Mechanics	Palmer et al., (1983)
Mid 1980's	Fracture Mechanics	Tomin et al., (1985)
	Discrete Element Method	Hocking et al., (1985a,b)
	Critical Delayed Elastic Strain	Sinha (1985) Sanderson and Child (1986)
	Damage Modeling	Cormeau et al., (1986)

dependence was actually reversed from that determined by Korzhavin. Only when a full ice failure pressure vs. strain rate curve concept developed by Michel and Toussaint (1976) became available did it become obvious that Korzhavin's measurements were at a critical portion of the failure pressure curve where the slope was opposite to that at strain rates different from those analyzed by Korzhavin. In fact Korzhavin measured a decreasing failure pressure with increasing velocity of impact of floes against bridge piers. Placed on the Michel and Toussaint unconfined compressive strength curve, Figure 3.1, Korzhavin's measurements would be at a strain rate greater than 10^{-3} s^{-1}.

The Korzhavin methodology is usually the starting point for calculating ice loads on narrow structures.

General Theory for Crushing on Narrow Structures

At high loading rates, ice fails in a brittle fashion. At lower strain rates the ice fails in a ductile manner. The brittle failure pressure is intimately related to the size of the zone over which the ice is failing. The "size" aspect of the crushing pressure is examined in Section 5.2.3.4. In this section the discussion will concentrate on examining the engineering analysis of ice failure theories.

At full envelopment of a structure (and not including any environmental parameters), the force the ice exerts on it can be determined from:

Force = Pressure x Width x Thickness

where: Pressure = the failure pressure,
width = the width of the structure, and
thickness = the thickness of the ice.

In the Korzhavin Methodology the determination of the crushing pressure is made from:

$$\text{Pressure} = I\ C\ M\ \sigma_u$$

where: I = the indentation factor,
C = the contact factor,
M = the shape factor, and
σ_u = the unconfined crushing pressure.

The formula is identical to Korzhavin's formula except the velocity (or strain rate) term has been removed. Instead of incorporating a velocity term it is thought to be more appropriate to include the strain rate dependence in the value for the unconfined crushing pressure, or to use one representative value in place of a strain rate dependence. This method of replacing Korzhavin's velocity term has gained general acceptance throughout the industry and the modified equation has come to be known as the Korzhavin Methodology. Timco (1986), API Bulletin 2N and Acres (1987) are three representative studies which use the equation in the above form.

The reason the calculation of the crushing pressure is represented as the above formula is that the three factors I, C and M each have a well defined effect on the pressure.

Confined Strength

Sea ice subject to confinement has an apparent peak strength much greater than the uniaxial unconfined strength. The coefficients developed by Korzhavin were created to transform the unconfined compressive strength into an appropriate value to use for calculating ice loads.

The Geometrical Problem of the Indentation Factor: Plane Strain and Plane Stress Analyses

The coordinates are described as follows: X and Y are the axes of the horizontal plane and Z is the vertical axis. There exist two different situations of stress or strain which are relevant to the problem at hand, which are are described as "plane strain" and "plane stress", see Figure 5.2.10a.

The phrase "plane strain" refers to the situation where the material is not allowed to strain in the Z direction, or in other words, the material is confined in the Z direction. The net strain in the Z direction is therefore zero. Note that this does not necessarily mean that the stress in the Z direction is zero; the stress in the ice in the Z direction can be very large.

In contrast to plane strain, a plane stress situation occurs when the material is stressed in the X and Y planes but not the Z direction, and is unconfined in the Z direction. In this situation the material is capable of straining in the Z direction but there is no net effect because there is no confinement and the material simply moves out of the way.

The plane strain and plane stress situations are relevant to ice/structure interaction mechanics because they are the limiting situations used in the calculation of the indentation factor.

The ice becomes confined in the vertical direction when the ratio of the interaction width to the ice sheet thickness is small, as occurs in local crushing at a bridge pier for example. In the limit the thickness of the ice sheet becomes very large. The ice failure pressures are high since, as measured in laboratory tests (Figure 5.2.10b) the material can withstand more pressure before failure occurs if it is confined. This situation is a plane strain situation, and forms the high pressure end of the failure pressure curve for ice. The indentation factor is large which means that the effective, or observed failure pressure is many times what the unconfined failure pressure would be expected to be.

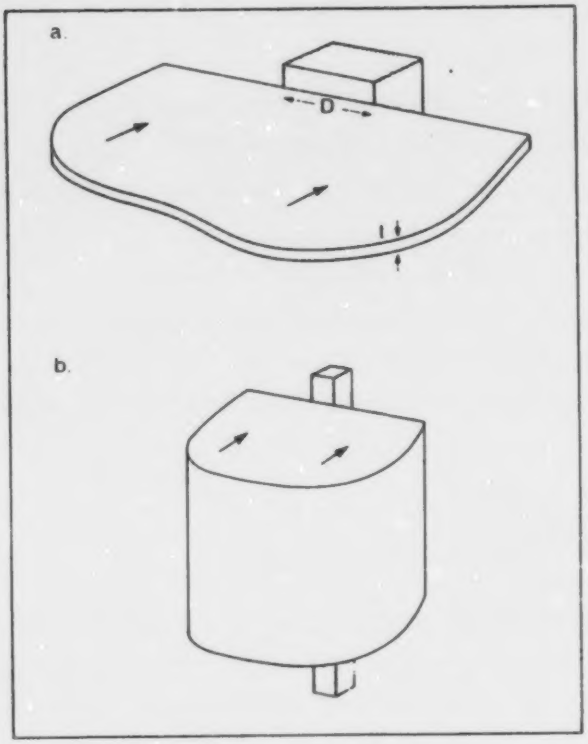

(a) plane stress conditions, where $D >> t$.

(b) plane strain conditions, where $D << t$.

Figure 5.2.10a Illustration of Plane Stress and Plane Strain Geometries.

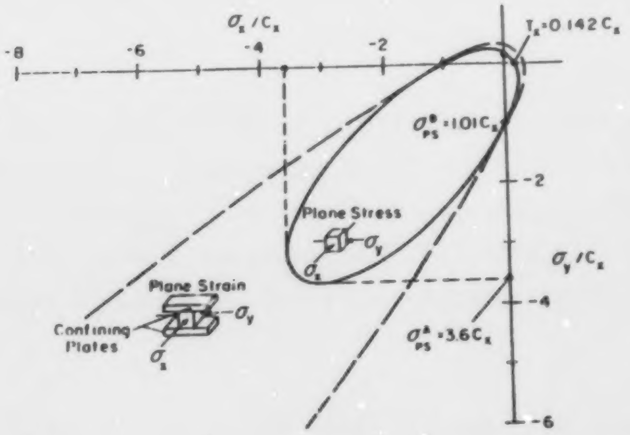

Figure 5.2.10b Yield Surface, Showing Effect of Plane Stress and Plane Strain Confinement Situations.

In the limit of ice sheet thickness going to zero the confinement in the vertical direction is also reduced to zero. This is referred to as a plane stress situation, and is at the lower end of the indentation factor curve. In this situation it is easier for the ice interacting with the structure to move relative to ice above or below it in the sheet, therefore the failure stress of the ice is effectively reduced in comparison to the previous case. For this case the observed failure pressure can still be higher than that expected from unconfined laboratory measurements.

The Indentation Factor: I

The indentation factor represents the effect of the confinement of the ice sample on the compressive strength. It is a dimensionless number, and is the ratio of the observed failure pressure to the measured unconfined compressive strength for the same ice sample (i.e. for a sample the same crystal size, temperature, brine content or salinity, and so on).

There are many different ways to calculate the value of I. Table 5.2.2 shows the values for I calculated in nine studies. Note that different material properties have been used, as well as failure mechanisms.

It is possible to calculate I based on elastic-plastic models (Croasdale et al., 1977). The first calculations of I were simple analytical representations capable of being figured out by hand, but the latest papers (Ralston, 1978; Reinicke and Remer, 1978) used finite element modeling and complicated yield functions to represent the ice failure.

In Figure 5.2.11 the two plane strain (or in-plane) failure models used in most of the studies are illustrated. The Prandtl and Hill bearing capacity models yield different values of I due to their modeling a different failure mechanism.

Table 5.2.2

Comparison of Values for the Indentation Factor (I) from Several Different Studies

Study	Type of Failure	Failure Mechanism	Indentation Factor		Notes
Croasdale et al. (1977)	ductile ($7.5\text{x}10^{-5}$ to $4.4\text{x}10^{-3}$ s^{-1})	Tresca	Prandtl Indentor (perfectly plastic)	Upper bound	I = 2.57 (maximum, decreasing with increasing D/t ratio)
			Elastic (?)	Lower bound	I = 1.00 (constant)
Michel and Toussaint (1977)	ductile	Huber-von Mises	Hill Indentor (perfectly plastic)	Upper bound	I = 2.97 (plane strain)
Michel (1978) also Imard (1978)	brittle (> $2.3\text{x}10^{-2}$)	Tresca	Pure elastic deformation	exact	I = 1.57 (constant)
Korzhavin (1962)	ductile		Pure elastic deformation	exact	I = 2.5 (Maximum, decreasing with floe size if floe width less than 15 times structure width. For a given constant D/t ratio, the value of I is as given above. In the end result the value of I does indeed depend on D/t, but Korzhavin cancels the factor of D/t for computational ease.)
Afanasev et al. (1971) and Afanasev (1972)			Prandtl Indentor		I = $[\,5\,(t/D) + 1\,]^{\frac{1}{2}}$ for D/t > 1 (For 0.1 < D/t < 1.0 interpolate assuming that at the boundaries I = 4.0 and 2.5 respectively, based on Prandtl stress calculation at ice/structure interface.)
Ralston (1978)	crushing	4-parameter von-Mises	Hill Indentor		I = 4.47 (upper bound, plane strain, D/t = 0.0) 3.37 (lower bound, plane strain, D/t = 0.0) 3.28 (upper bound, plane stress, D/t = large) 2.98 (lower bound, plane stress, D/t = large) (4-parameter von Mises yield criteria accounts for inequality of tensile and compressive strengths, sensitivity to hydrostatic pressure, and anisotropy (Frederking Test A and B strengths). Note: 2-dimensional analysis only).
Reinicke and Remer (1978)	crushing	3-parameter von-Mises	Hill Indentor		I = 5.13 (plane strain, upper bound, constant) I = $[\,1.4 + 0.97\,(D/t)^{-1}\,]$ (3-dimensional upper bound, same shearing mechanism as Croasdale et al., 1977)
			plane strain	lower bound	I = 1.4 (all values of D/t) I = 4.69 (D/t = 0.0) (3-parameter von Mises yield criteria accounts for inequality of tensile and compressive strengths, and sensitivity to hydrostatic pressure. The material can be modeled as compacting during failure, but anisotropy can not be taken into account.)

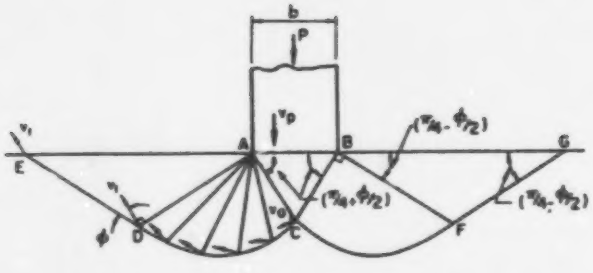
b
P
v_p
v_1
A
B
G
E
$(\pi/4 - \phi/2)$
v_1
$(\pi/4 + \phi/2)$
$(\pi/4 - \phi/2)$
v_0
ϕ
D
C
F

Prandtl Model of In-Plane Bearing Capacity

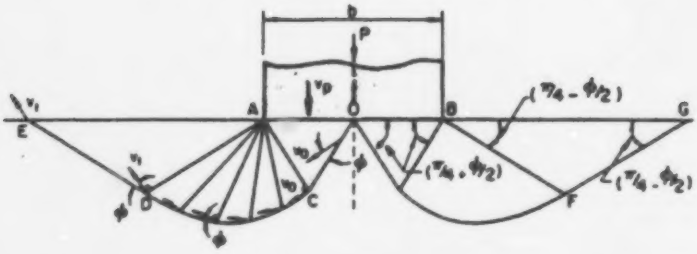
b
P
v_p
v_1
A
O
B
G
E
$(\pi/4 - \phi/2)$
v_0
v_1
ϕ
$(\pi/4 + \phi/2)$
$(\pi/4 - \phi/2)$
v_0
ϕ
D
C
F
ϕ

Hill Model of In-Plane Bearing Capacity

Figure 5.2.11 Illustrations of the Prandtl and Hill Bearing Capacity Velocity Fields.

A three-dimensional model of the failure of ice in an out-of-plane situation is illustrated in Figure 5.2.12.

A wide variety of estimates of I are possible. In Figure 5.2.13 graphs of I from several different studies are shown. The results of Ralston are particularly significant since they are being used in the API Bulletin 2N on Guidelines for Offshore Structures (1987 draft). For columnar ice Ralston (1978) predicted I values of 3 at a minimum for all aspect ratio's. Many of the other researchers have minimum I values of approximately 1. The major difference for the value of I is related to the assumption of ice structure (i.e. whether the ice is isotropic (granular) or anisotropic (columnar)).

The Contact Factor: C

The contact factor, C, is used to take into account the fact that the ice sheet will not be in contact with the structure over the whole width of the structure. The value of C is equal to 1.0 for perfect contact between the ice and the structure, and is of lessor magnitude for imperfect contact. To some extent the setting of C less than 1 accounts for the brittle nature of the ice and non-simultaneous failures.

Contact factors can be used where the indentation factor was calculated using plasticity theory. The usefulness of plasticity theory is that the boundary conditions are strictly defined based on full contact. The incorporation of a contact factor is somewhat of a empirical change in the failure pressure.

Korzhavin gave values of C dependent on the velocity of the ice as shown in Table 5.2.3.

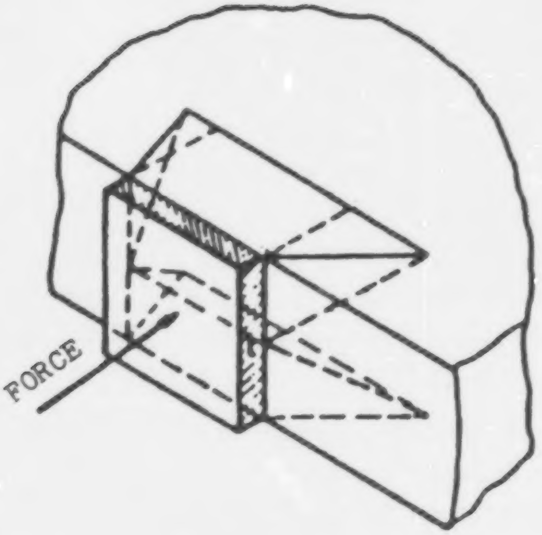

Figure 5.2.12 Out-of-Plane Failure Mechanism, (Reinicke and Remer, 1978).

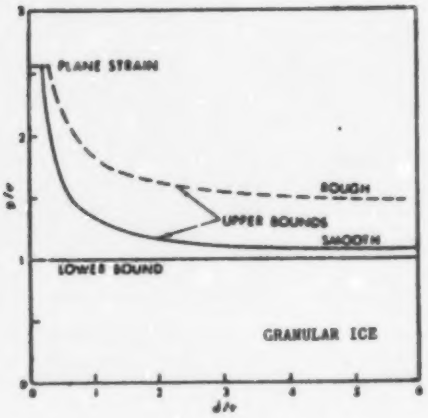

Croasdale et al., 1977

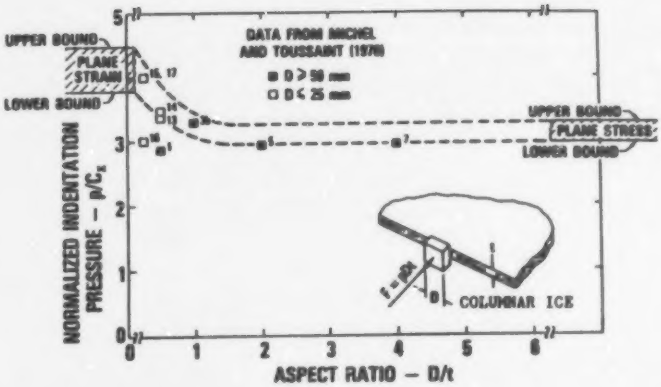

Ralston 1978

Data Points are from Michel
and Toussaint, 1977

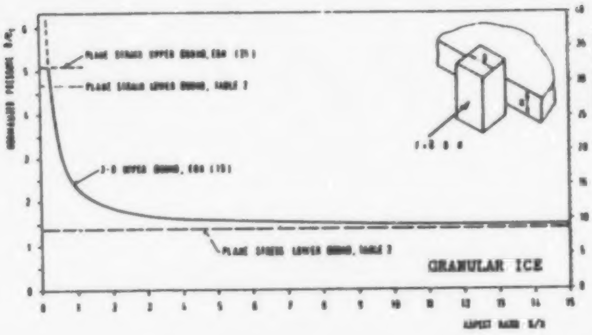

Reinicke and Remer, 1978

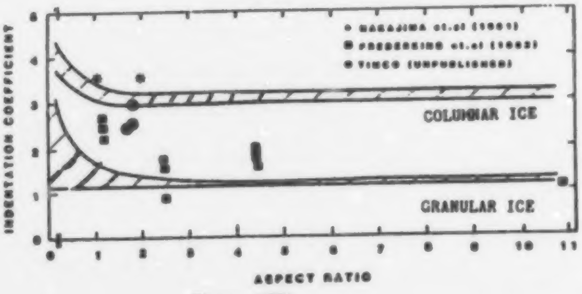

Timco, 1984

Shaded Areas Show Theoretical
Limits for Columnar and
Granular Ice

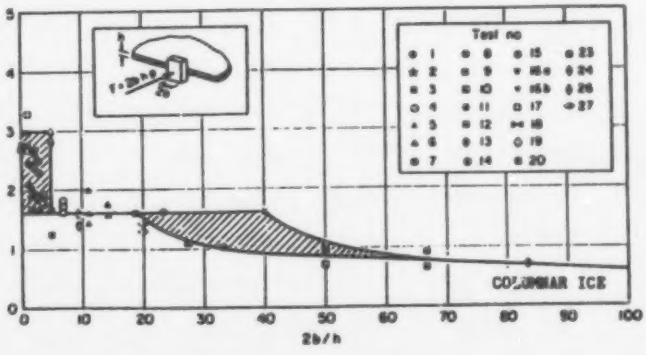

Michel and Blanchet, 1983

Figure 5.2.13 Values of The Indentation Factor from Several Studies.

Table 5.2.3

Values of the Contact Factor, C, From Korzhavin (1971)

Width of Support (interaction width) (m)	Velocity of Floe Movement (m/s)		
	0.5	1.0	2.0
3 - 5	0.70	0.60	0.50
6 - 8	0.60	0.50	0.40

The Shape Factor: M

The failure pressure depends, as well, on the shape of the interaction surface (see Figure 5.2.14).

Where the indentation factor was calculated using plasticity theory the influence of the shape of the indentor would have been taken into account during the determination of I. It so happens that the Morgernstern and Nuttall (1972), Croasdale et al., (1977), Ralston (1978) and Reinicke and Remer (1978) indentation factors were calculated for flat indentors. To be proper, when it is desired to calculate the pressure on a non-flat indentor, the actual shape of the indentor should be used in the calculation of I, and therefore I would not require modification based on the shape of the indentor.

The shape factor M takes into account the difference between a "flat wall" structure and structures of other shapes. Table 5.2.4 shows values of the shape coefficient from SNiP 2.06.04-82, the Soviet Construction Standards and Rules, Moscow, 1983.

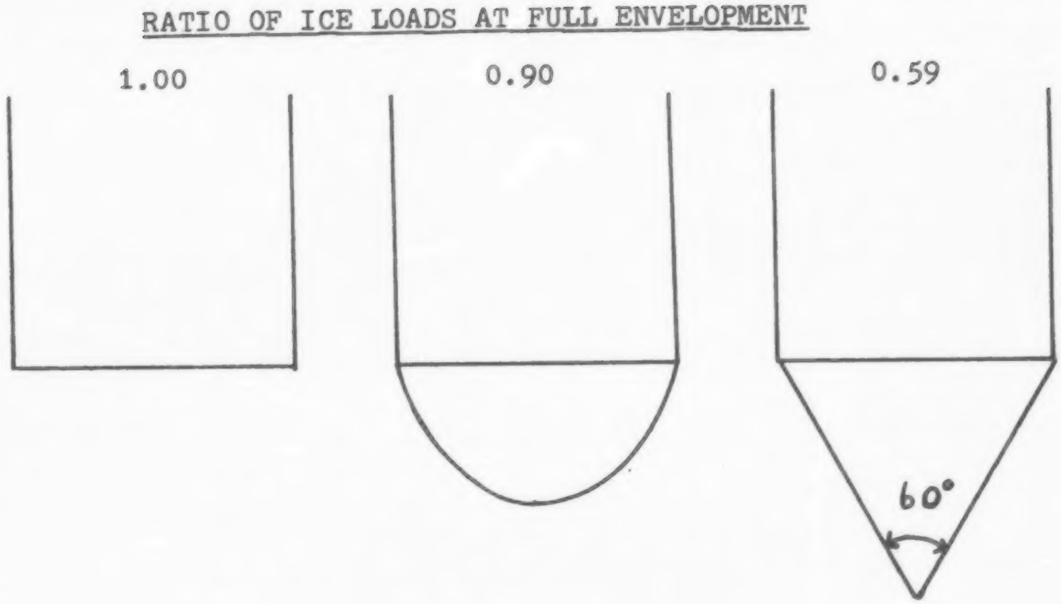
RATIO OF ICE LOADS AT FULL ENVELOPMENT
1.00
0.90
0.59
60°

Figure 5.2.14 Different Abutment Shapes: The Ice Load on Each Will Be Different for Each One According to the Korzhavin Methodology.

Table 5.2.4

Values of the Shape Coefficient, From Soviet Construction Standards and Rules, Moscow, 1983.

Coefficient	Polyhedron (semi-circle)	Rectangle i.e. flat	Triangle with open angle in the horizontal plane (degrees)					
			45	60	75	90	120	150
M_1	0.90	1.00	0.54	0.59	0.64	0.69	0.77	1.00

Illustration of Use of the Korzhavin Methodology

Consider a structure which will be exposed to both ice sheet ductile failure loads and impacts from quickly moving floes. Timco (1986) has presented such an example, modeling the interaction of ice with a leg of a semisubmersible. Timco's example will be briefly reviewed here. Note that some of the notation has been changed slightly for conformity with the rest of this report.

Ductile Failure of an Ice Sheet Against a 1 m Diameter Circular Structure

In the ductile mode Timco uses the following form of the Korzhavin equation:

$$L = C\ M\ I\ D\ t\ \sigma_u$$

where:

C = contact coefficient,
M = shape coefficient,
I = indentation factor,
D = diameter of leg of submersible,
t = ice sheet thickness, and
σ_u = uniaxial unconfined compressive strength of ice at the strain rate of interest.

Due to the low strain rate the ice fails in a ductile manner and the contact coefficient is set equal to 1.0, i.e. the ice and leg are in perfect contact. The shape coefficient is set to 0.9, from Table 5.2.4, for a semicircular interaction surface. For D = 1.0 m and t = 0.35 m, I is determined to be 1.2 based on a D/t (aspect) ratio of 3, and assuming the ice is granular (see Timco's graph in Figure 5.2.13). Note that the surface has been assumed to be rough, or highly frictional.

As well, it should be realized that the strain rate appropriate for use is not exactly known. Ralston (1979) recommends the use of the ratio V/2D for the strain rate. The uniaxial compressive strength is selected based on the strain rate calculated.

For a given creep strain rate Wang (1979) determined that the following equation could be used to represent granular ice.

$$\sigma_u = 30\ \dot{\epsilon}^{0.22}$$

where

σ_u is in MPa, and

$\dot{\epsilon}$, the strain rate, is in units of s^{-1}.

For a velocity of 0.3 m/hr and a 1 m diameter column a strain rate of [V/2D = (0.3 m/hr / 2 m) / 3600 s/hr =] $4.2 \times 10^{-5}\ s^{-1}$ is determined. Based on this strain rate a strength of [$30 \times (4.2 \times 10^{-5}\ s^{-1})^{0.22}$ =] 3.3 MPa is determined.

Inputting these values into the Korzhavin equation, a load on the leg of 1.0 MN is obtained.

Note that in this example granular ice was assumed to interact with the leg. If columnar ice were assumed to interact with the leg the strength would be approximately two-thirds that of 3.3 MPa, or 2.2 MPa (Sanderson, 1984). Using Ralston's value for the indentation factor, the apparent strength would be equal to 2.2 MPa multiplied by a factor of 3, for a resulting strength of 6.6 MPa. The load on the leg would then be 2.3 MN, or a factor of over two greater than calculated for granular ice.

The difference in the two loads is critical, and serves to illustrate the subtlety of the ice failure process and how the failure pressures depend critically on the ice crystal structure.

Brittle Failure of an Ice Sheet Against a 1 m Diameter Circular Structure

For a brittle failure three values in the Korzhavin equation change.

The contact factor is not equal to 1 but is less. The reduction in the contact factor accounts for the lack of perfect contact and non-simultaneous failure of ice at the ice/structure surface.

The other factor which changes is the strength of the ice. In this case a predetermined or estimated strain rate is not used, but rather a representative maximum ice strength is used.

Timco (1986) points out that the values of I calculated by Afanasev et al. (1973) are frequently used.

$I = [\ 5\ (t/D) + 1\ ]^{\frac{1}{2}}$ for $1 < D/t < 6$, and

$I = 4 - 1.55\ (D/t)$ for $D/t < 1$.

The contact factor is included in the determination of I in this case. A nominal, or maximum, ice strength value is used. Typically the strength is on the order of a few MPa, usually greater than 2 but less than 4.

The above I values are based on columnar ice.

Summary of the use of the Korzhavin Methodology

The Korzhavin Methodology gained popularity by use by offshore designers before large scale empirical data were obtained. For small scale structures, perhaps having widths less than 10 times the ice sheet thickness, use of the Korzhavin Methodology may still be appropriate. For larger structures, on the order of island size (50 m width or greater), empirical measurements of ice loads are used to calculate loads on a structure.

Semi-submersible legs, bridge piers, and local load calculations are three applications where the methodology continues to be used.

The assumptions input into the Korzhavin Methodology are important. The researcher has at hand several recommendations for each of the coefficients and the strength of the ice. The ice type modeled should not be treated lightly due to the significant change in the estimated ice loads. The reader should be careful to determine small differences in methodology between different researchers, such as incorporation of the contact coefficient into the indentation factor calculation, as done by Afanasev et al. (1973).

The use of the elastic-plastic methodology is not as widespread as it was a decade ago. The indentation factors calculated using the upper bound/lower bound plastic methodologies are in current use, however there are two major problems with the elastic-plastic modeling:

- ice is not a plastic material, and

- the elastic-plastic methodology over predicts large scale ice failure pressures when small scale laboratory failure pressure data are used.

Often "more modern" methodologies for brittle failure such as the discrete element technique of computer modeling, (Hocking et al., 1985a,b; Williams et al., 1986), fracture mechanics (Palmer et al., 1983), or the damage philosophy (Cormeau et al., 1986) are offered as possible alternatives.

5.2.3.3 Multi-Zonal Failure

An ice zone is defined as a region where the ice acts as a unit. Neill (1976) showed that a zone had a width of four or five times the ice sheet thickness.

Observations of ice crushing against artificial islands constructed by Esso indicated that the crushing failure of ice against the islands did not occur in a unified manner but, rather, consisted of crushing of individual zones along the ice/structure boundary.

When ice interacts with small size indentors, the distribution of the load on the indentor can have a very high standard deviation due to the fluctuating nature of the process. In his theory Kry (1978, 1980) modeled the interaction of an ice sheet and a structure as made up of many statistically independent individual zones of failure, each with the same statistical distribution of load with distance of penetration (Figure 5.2.15).

When the individual load distributions are statistically summed to produce a total load, the result is that the average failure stress of the ice interacting with the structure is equal to the average failure stress of an individual zone, and the standard deviation of the average stress is much less than the standard deviation of the stress of an individual zone (see Figure 5.2.16). Statistical theory shows us that the mean of many zones would be equal to that of the individual zone, and, more importantly, the standard deviation of the failure pressure decreases as the square root of the number of zones. This result is significant in that the probability of a pressure over the whole interaction zone approaching the highest values observed in one zone is significantly reduced and the peak global design load is also reduced.

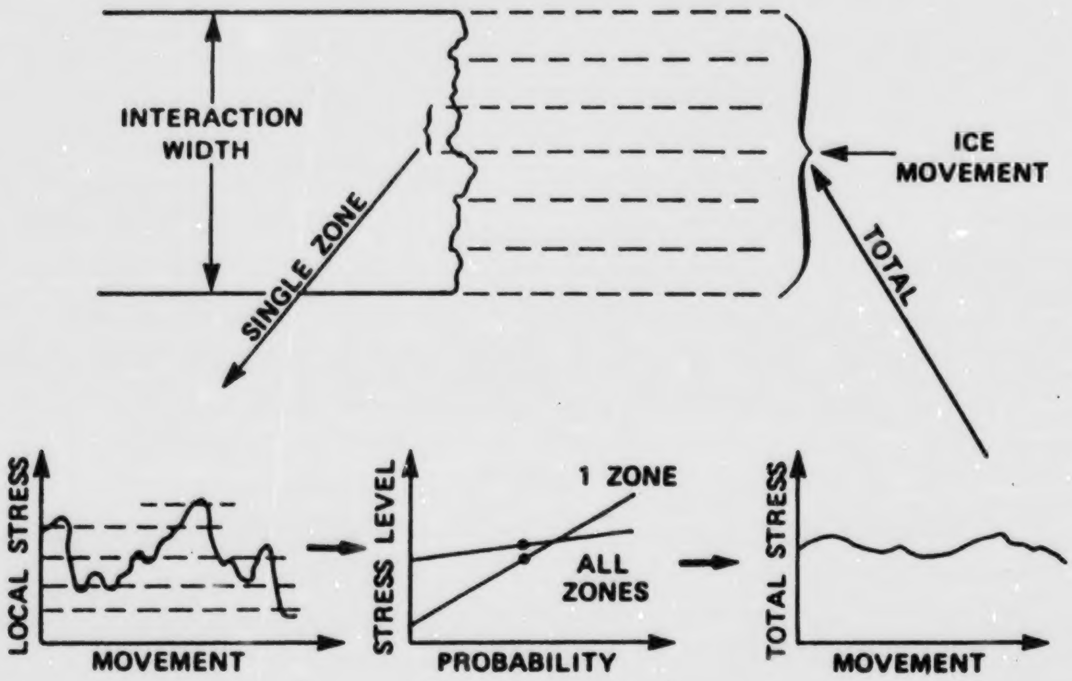
INTERACTION WIDTH
SINGLE ZONE
ICE MOVEMENT
TOTAL
LOCAL STRESS
MOVEMENT
STRESS LEVEL
1 ZONE
ALL ZONES
PROBABILITY
TOTAL STRESS
MOVEMENT

Figure 5.2.15 Basis of Statistical Design Stress Reduction for Wide Structures, (from Kry, 1980).

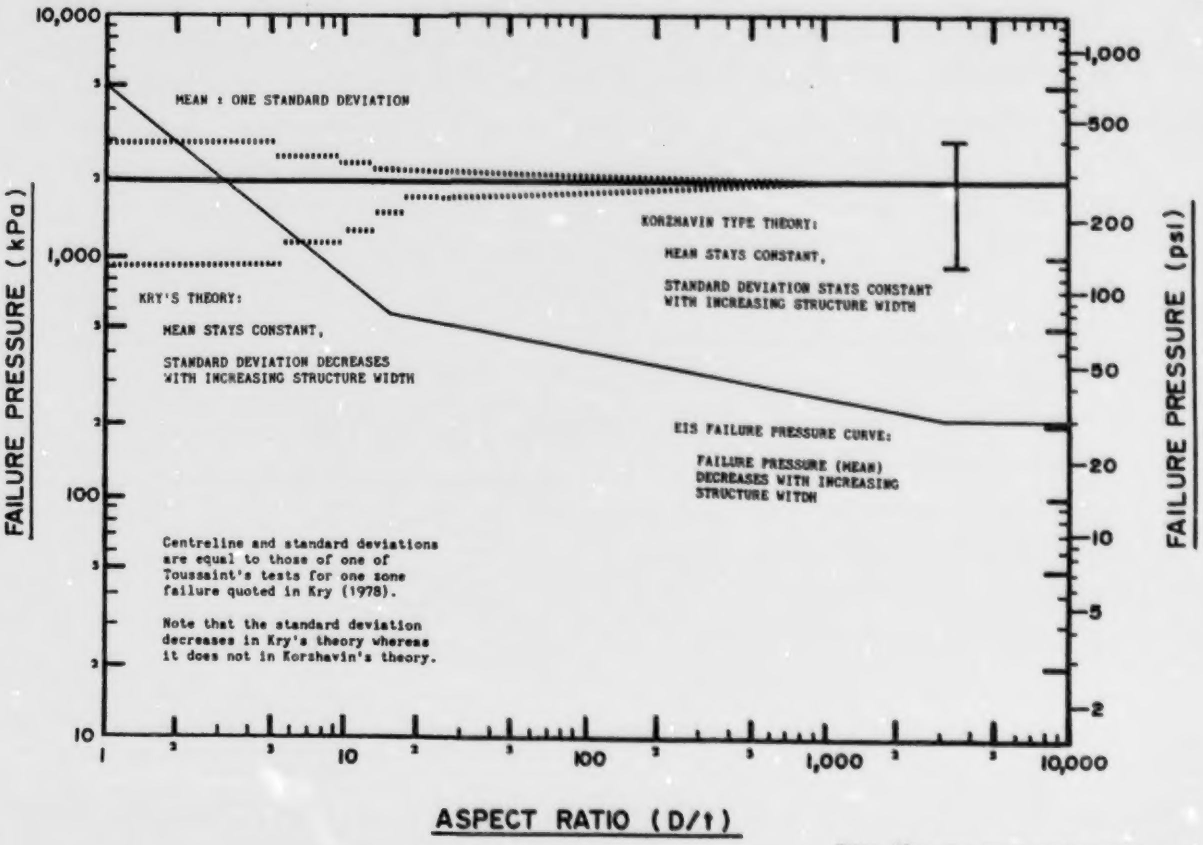

Note: D/t = structure width/ice thickness

Figure 5.2.16 Illustration of Difference Between Single Zone, Multi-Zone and EIS (empirical) Ice Failure Pressure Theories.

5.2.3.4 Large Scale Empirical

As part of the submission on offshore structures for the 1982 Environmental Impact Statement for the Beaufort Sea (EIS) Dome Petroleum, Esso Resources Canada and Gulf Canada Resources, reviewed in detail the available data on ice failure pressures. The peak failure pressure data was used in mathematical models of the ice/structure interaction on a large scale. The estimated peak failure pressure relationship to aspect ratio for multi-year ice is presented in Figure 5.2.17. The data points on the graph are discussed below.

The peak failure pressure relationship is used as an empirical representation of multi-year ice failure stress, which accounts for all manner of brittle ice failure modes. The failure pressure is a function of many variables, and can be written as:

Failure Stress = f(strain rate, temperature, age, porosity, confinement, indentation factor, contact factor, shape factor, mixture of ice states within the sheet or ridge, and so on)

The failure stress of multi-year ice, multi-year ridges and hummock fields, are all represented by the EIS failure pressure aspect ratio relationship. Cold ice is assumed. In this manner the failure pressure determined using the graph should be conservative for summer interactions, and directly applicable for winter interactions.

The graph shown in Figure 5.2.17 has been used in ice load calculations since 1981.

The graph is a plot of failure pressure vs. aspect ratio. The aspect ratio is equal to the chord length D of the interaction zone divided by the average ice thickness in the zone. At low values of aspect ratio local effects govern. At the highest values ridge building effects are expected to govern. Ridge building effects were represented by the constant failure pressure of 200 kPa, for aspect ratio's greater than 3000 (or 3 km for 1 m

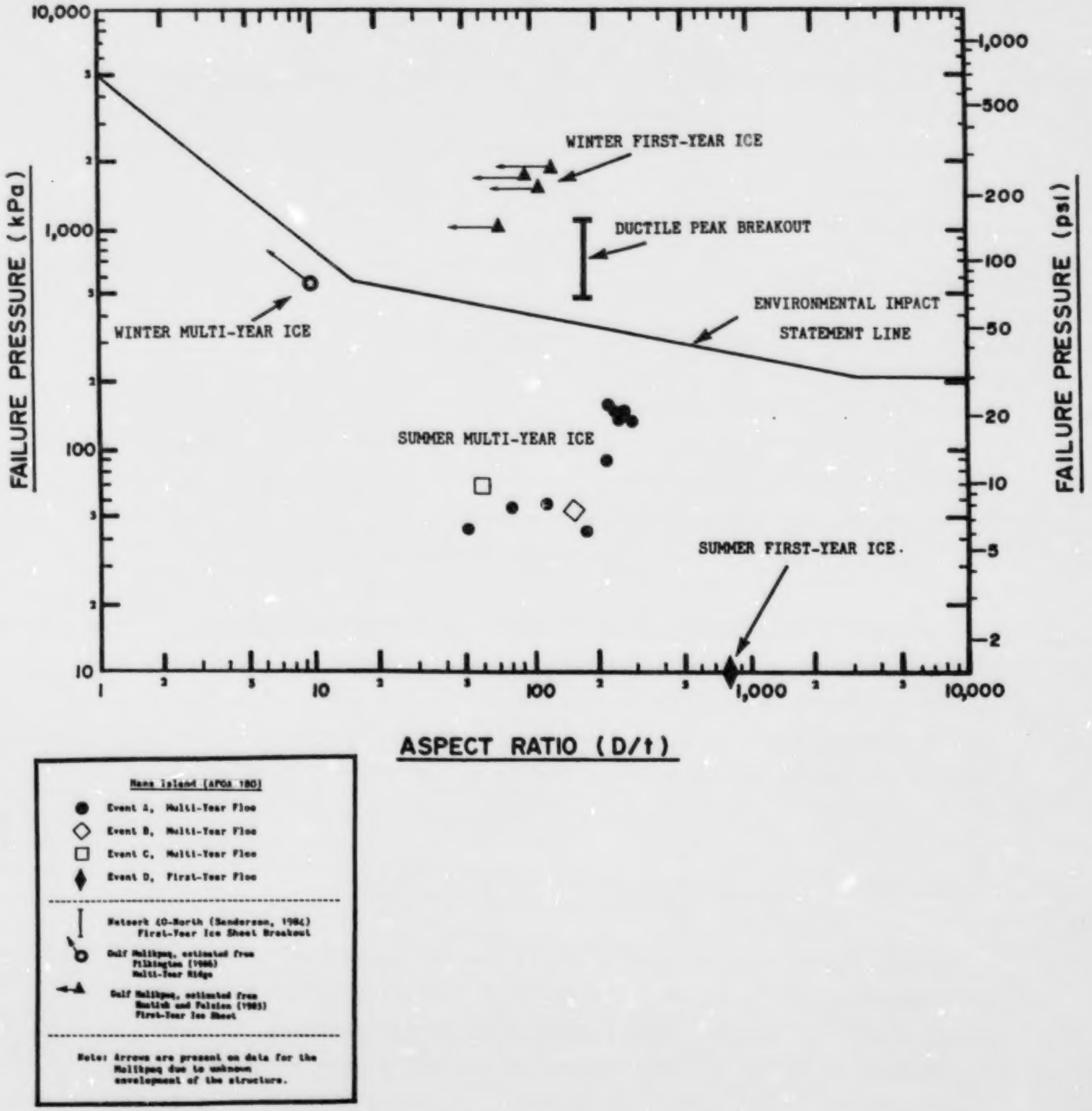

Figure 5.2.17 Empirical Peak Ice Failure Pressure Aspect Ratio Relationships, Showing Recently Released Ice Load Measurements for Comparison.

thick ice). This can be compared to the Croasdale et al. (1986) expected ridge-building force value of less than 100 kPa (for a 1 metre thick ice sheet).

For confined situations, at very small aspect ratio's, the failure pressure is expected to be in the range of many MPa. As the aspect ratio becomes larger, the confinement decreases, and therefore so does the failure pressure. The theory underlying the failure pressure curve is examined in more detail below.

Multi-Year Ridge Impact with Molikpaq Structure

Gulf has reported global ice loads on their Molikpaq structure of 0.5 GN (Pilkington, 1986) The feature which generated this load was apparently a 10 m thick multi-year ridge. Assuming full envelopment of the structure by the ridge, a failure pressure of 0.56 MPa can be estimated. The point is plotted on the graph at an aspect ratio of 9.0.

The upward slanting arrow indicates that the point at D/t = 9.0, and failure pressure = 0.56 MPa, may not be exact. It is not known whether full envelopment of the structure by the ridge occurred. Assuming the load was the same, it can be shown that the ice failure pressure would follow a path along the direction shown by the arrow for lower D/t ratios.

First-Year Ice Sheet Loads Measured on the Molikpaq

Hnatiuk and Felzien (1985) listed four measured loads for interactions of first-year ice sheets and the Molikpaq. It is possible to use average first-year ice thickness data presented in Danielewicz and Pilkington (1980) to estimate the thickness of the ice on the days events took place at the Molikpaq. Using these thickness estimates, it is then possible to estimate the ice failure pressures for the loads quoted by Hnatiuk and Felzien. On Figure 5.2.17 the arrows on the winter first-year ice points reflect the assumption of full envelopment.

Hans Island Study, APOA 180

Hans Island is an island in the Kennedy Channel located between Ellesmere Island and Kalaallit Nunaat (the new official name for Greenland).

Expeditions to Hans Island to examine large scale multi-year ice floe interactions took place in 1980, 1981 and 1983. The results of the latter two expeditions are still proprietary.

The first of the three Hans Island study reports has recently been released. The report (APOA 180) documents the methods used to determine the loads ice floes exerted on Hans Island during interactions. The many dots on Figure 5.2.17 are points calculated based on the data provided in APOA 180. During the study measurements were obtained for four floe/island interactions. Event "A" yielded the most information, whereas the three other events yielded one measurement per interaction.

The second Hans Island study (APOA 181) is due for release around July of 1987.

Netserk F-40 North

Sanderson (1984) reviewed loads exerted by a first-year ice sheet interacting with the Esso artificial island Netserk F-40, and this data is also shown on Figure 5.2.17.

Size Effect

Ice loads on wide structures are not as high as would be calculated using small scale data. A calculation will serve to highlight this point.

Consider a structure 90 m wide, being impacted by a columnar ice sheet of thickness 1 m, typical to a first-year arctic ice sheet and similar to the observations of Hnatiuk and Felzien (1985). The other parameters are as follows:

Parameter	Value	Reference
Indentation Factor	3	Ralston Graph, Figure 5.2.13
Velocity of ice sheet V	0.5 m/s	Given
Structure Diameter D	90 m	Similar to Gulf Molikpaq
Approximate strain rate	$V/2D = 2.8 \times 10^{-3}$	Calculated
Peak failure pressure based on salinity of 5 ppt and a temperature of -10°C	3.4 MPa	(Figure 3.2)
Contact factor	0.3	Range of probable contact factors would be from about 0.3 to 0.6.
Shape factor	0.9	Semi-circular structure
Calculated failure pressure	2.75 MPa	$3.4 \times 3.0 \times 0.3 \times 0.9 = 2.75$ MPa If a larger contact factor is used the failure pressure increases.
Aspect ratio	$D/t = 90$	Width / ice thickness

On Figure 5.2.17 the calculated failure pressure, at an aspect ratio of 90, and a failure pressure of 2.75 MPa, is above the measured value of approximately 1.75 MPa for winter first-year ice. The reduction in loads on the large scale is an important aspect of the feasibility of large structures.

The Croasdale Simplified Universal Ice Pressure Curve

Croasdale (1983) discussed the decrease in failure pressure with increasing size of interaction zone, and presented a conceptual rational for the size effect (see Figure 5.2.18). Croasdale's graph does not yield specific ice pressures but rather proposed a rational to explain why the crushing pressure decreases with the aspect ratio (D/t), width or area of loading. It also emphasizes that different ice failure processes may control at different aspect ratios, widths or areas.

The Brittle Foam Analogy, Square Root of Interaction Area Theory of Ashby et al. (1986)

The statistical model proposed by Kry did not yield a rule-of-thumb for how the load decreased as a function of the ice/structure interaction geometry. Ashby et al. (1986), state in contrast, that if their admittedly simple theory is somewhat valid, the average failure stress should decrease as the square-root of the interaction area. Support for a decrease in failure pressure as the square-root of the area is shown in Figure 5.2.19, from Sanderson, (1986).

Ashby et al., (1986) state that, in the past, it has been the rule rather than the exception to model a size effect using "flaw theory", meaning that the reduction in strength of the material is not modeled as a material parameter, but rather as the result of flaws within the material reducing the overall strength. With the latest measurements of full scale loads (such has Hans Island, artificial island, and

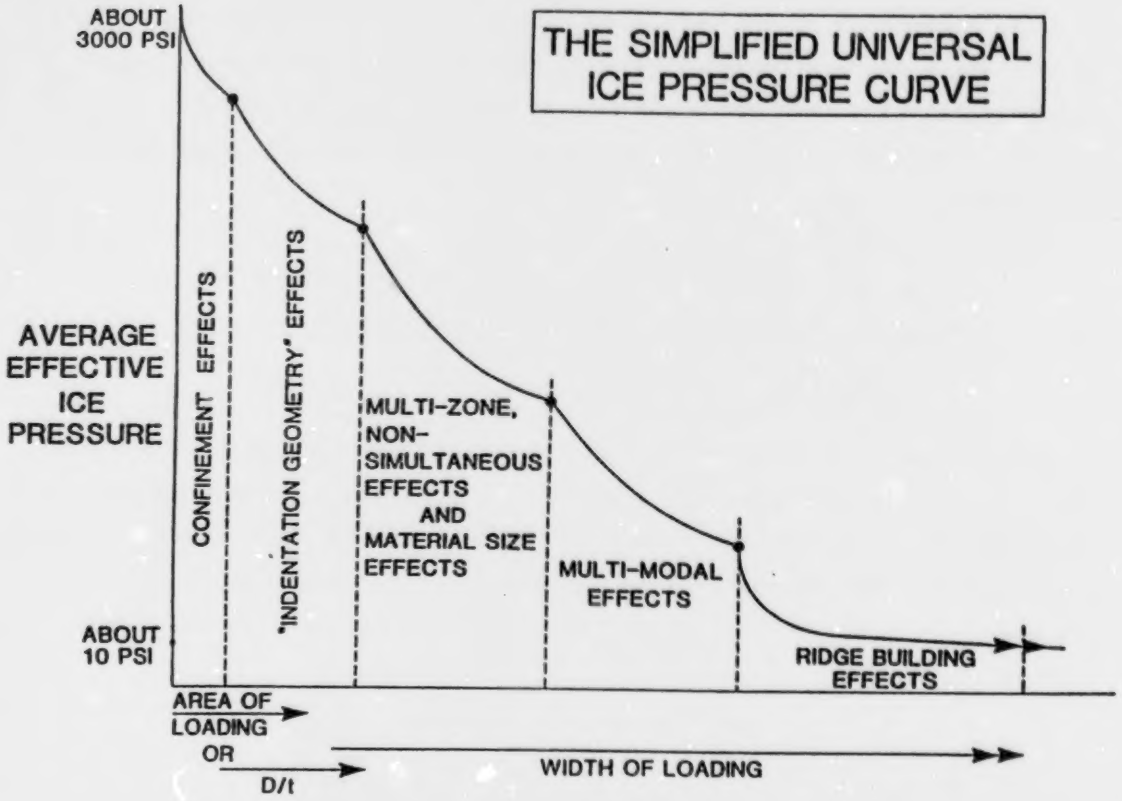

Figure 5.2.18 Croasdale's Simplified Universal Ice Pressure Curve.

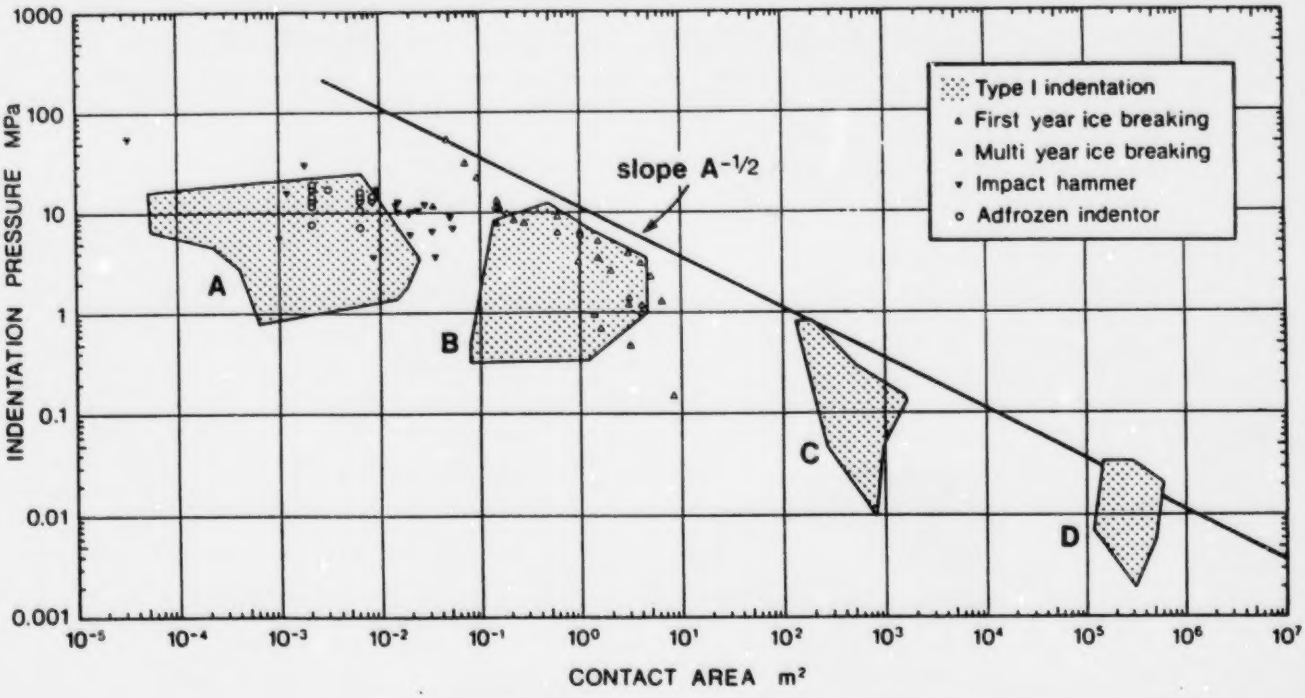

General trend of pressure-area curve, with data groups.

A: Laboratory tests

B: Medium-scale in situ tests, lighthouses and bridge piers

C: Full-scale Arctic islands and structures

D: Meso-scale models.

Figure 5.2.19 Failure Pressure as a Function of Area (Sanderson, 1986).

proprietary data sets) at hand it became obvious that the size of the flaws necessary to reduce the strength by the amount observed were very large. Ashby et al. advocate a non-simultaneous failure theory based on a simple statistical model and some brittle material tests.

The State-of-the-Art of the Understanding of the Size Effect

There is substantial evidence for the failure stress of ice to decrease dramatically when the area (or size) of the interaction is large.

The information reviewed in this section have several important results, two of which are:

- When ice interacts with a wide structure the failure stress of the ice in the brittle mode is less than that determined from small scale tests.

- Alternative mechanisms to "flaw" theory, where the reduced stress is due to cracks already present in the ice, have been proposed which are physically pleasing, and in one case yielded a rule-of-thumb for how the failure stress should decrease with an increase in area of interaction.

- The empirical treatment of large-scale data is currently the only reliable method available of predicting design ice loads.

From the data presented in Figure 5.2.17 the first-year ice data of Hnatiuk and Felzien shows first-year ice having a greater failure pressure than multi-year ice. The failure pressure calculated based on the Hnatiuk and Felzien data are based on full envelopment of the Molikpaq, which is 90 m wide. This assumption may not be correct. If the ice is assumed to have acted diagonally across the structure the width would be greater, as would be the aspect ratio, and the difference would be larger. There is disagreement in the industry as to whether first-year ice is stronger (i.e.

has a greater failure pressure) than multi-year ice.

It is important to emphasize that although first-year columnar ice may have a higher failure pressure than multi-year ice, the loads are much less for first-year ice since the thickness is less.

A design peak first-year ice failure pressure for artificial island structures located in the Canadian Beaufort Sea which has been used in the past is 1.75 MPa (250 psi). The value of 1.75 MPa is very close to those values calculated based on the Molikpaq data from Hnatiuk and Felzien (1985).

5.2.3.5 Reference Stress

The Reference Stress Method is a continuum mechanics approach to the calculation of ice loads (Ponter et al., 1983; Sanderson, 1984). The Reference Stress Method is a familiar technique used to study materials which creep. The indentation factor I represents the change from unconfined to confined ice state, however it can not be compared directly with the indentation factors calculated using plasticity theory or in the Korzhavin Methodology.

One uncertainty with the Reference Stress Method to date is that the failure pressure of the ice is not limited by an upper bound. The failure pressure increases indefinitely with increasing velocity.

The formula used to determine a load on a structure is:

$$L = I\ D\ t\ [\ 1 - (\nu / \nu_o)^{\frac{1}{2}}\ ]\ (V/I\ \psi\ D\ \ A\ \ \exp[-Q/RT]\ )^{1/n}$$

where:

L = total load,

I = indentation factor,

D = chord width of interaction,

t = ice sheet thickness,

ν = brine volume,

ν_o = reference brine volume (brine volume at which strength of ice becomes zero),

V = ice velocity,

ψ = reference stress coefficient,

A = constant,

Q = activation energy,

R = Universal gas constant,

T = Temperature in °K, and

n = creep index.

The reader is referred to the papers above for a more detailed discussion of the method.

5.2.3.6 Fracture Mechanics

Fracture mechanics is the study of the nucleation and propagation of cracks in a material based upon the physical properties of the material. Given nucleation and propagation models, the theory of fracture mechanics can be used to determine the forces which the material can sustain.

Fracture mechanics can incorporate both linear and non-linear models. Tomin et al., (1986) have shown that for the analysis of global ice fracture, linear fracture mechanics is sufficient. However, for local modeling of the ice failure process they determined that models of progressive damage, where the elastic shear resistance is degraded, were more appropriate.

The science of fracture mechanics is well advanced, and sophisticated computer models can be brought to bear on ice problems. The importance of fracture mechanics has been known for several years, however it was only in 1983 that Palmer et al., (1983) illustrated the significance of the load reducing large scale cracking occurring during an ice/structure interaction. They state that their treatment of radial cracking confirmed that very low loads were capable of propagating cracks to long distances.

5.2.3.7 Discrete Element Method

The discrete element modeling procedure incorporates discrete fracturing and large discontinuous motion into the analysis of a material which is breaking into pieces. In essence the motion and forces on each broken piece are incorporated into the analysis and each piece is followed throughout its motion.

Hocking et al., (1985a) state:

> In the discrete element method, each element is considered as a distinct body which communicates with its surrounding elements via face, edge, and corner interaction forces which change as the bodies move and deform. The connectivity of element to element is computed automatically in the program.

In Figure 5.2.20a an illustration of the motion of pieces of ice during the progress of a compression test is presented. The methodology, as implemented, would follow the motion of the individual pieces and would calculate the force between the pieces as a function of time.

In Figure 5.2.20b a simple illustration of the interaction of an ice sheet with a vertical sided structure is presented.

The use of the discrete element method requires extensive use of computational resources and, since the associated costs are great, the use of the discrete element method has not been as widespread as would be expected. Further, this methodology requires an accurate input of mechanical properties which, as illustrated in Chapter 3, are not as clear cut as would be hoped.

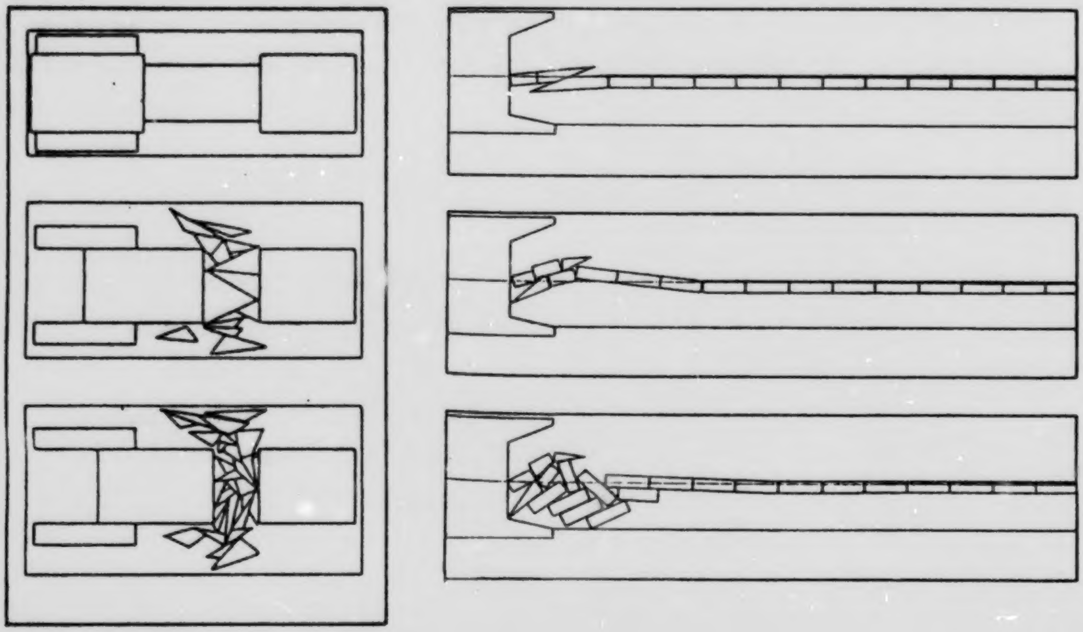

a) Discrete element analysis of compression failure of an ice sample (Hocking et al., 1985a).

b) Discrete element analysis of an ice floe interacting with a vertical sided structure (Hocking et al., 1985b).

Figure 5.2.20 Examples of Discrete Element Modeling.

5.2.3.8 Critical Delayed Elastic Strain

Failure of the ice sheet will occur, it is proposed, when the delayed elastic strain in the ice sheet equals some predetermined critical value. Sinha (1983) presented the following equation to determine the value of the delayed elastic strain for a constant stress rate:

$$e_d = \frac{c_1}{E} \frac{d_1}{d} \sum_{i=1}^{N+1} \Delta\sigma \left(1 - \exp\left[- (a_T [N + 1 - i] \Delta t)^b \right]\right)$$

where:

E = Young's modulus (9.5 GPa),

d = the grain diameter of the columnar crystals of ice,

d_1 = unit of grain diameter (e.g. 1 mm for grain sizes in mm),

a_T = 2.5×10^{-4} s^{-1} at T = -10°C,

c_1 = 9

b = 0.34

$\Delta\sigma$ = stress increase per time increment,

N = number of time increments, and

Δt = time per increment.

For a columnar crystal size of 4.5 mm and a temperature of -10°C Sinha (1982) determined that first cracks occurred when the delayed elastic strain exceeded 1.04×10^{-4}.

Based on Sinha's delayed elastic strain criteria Sanderson and Child (1986) determined the stress at first crack based upon stress rate. Their results are shown as the lines on Figure 5.2.21. The modification to sea ice was obtained by modifying the net stress using the formula of Frankenstein and Garner (1967) to estimate brine volume based on a salinity of 7 ppt.

Also shown on the figure are measurements of laboratory ice and multi-year ice obtained by Sinha (1985). The multi-year ice samples had salinities of either 0.5 ppt or 1.5 ppt. The preferred c-axis of the ice

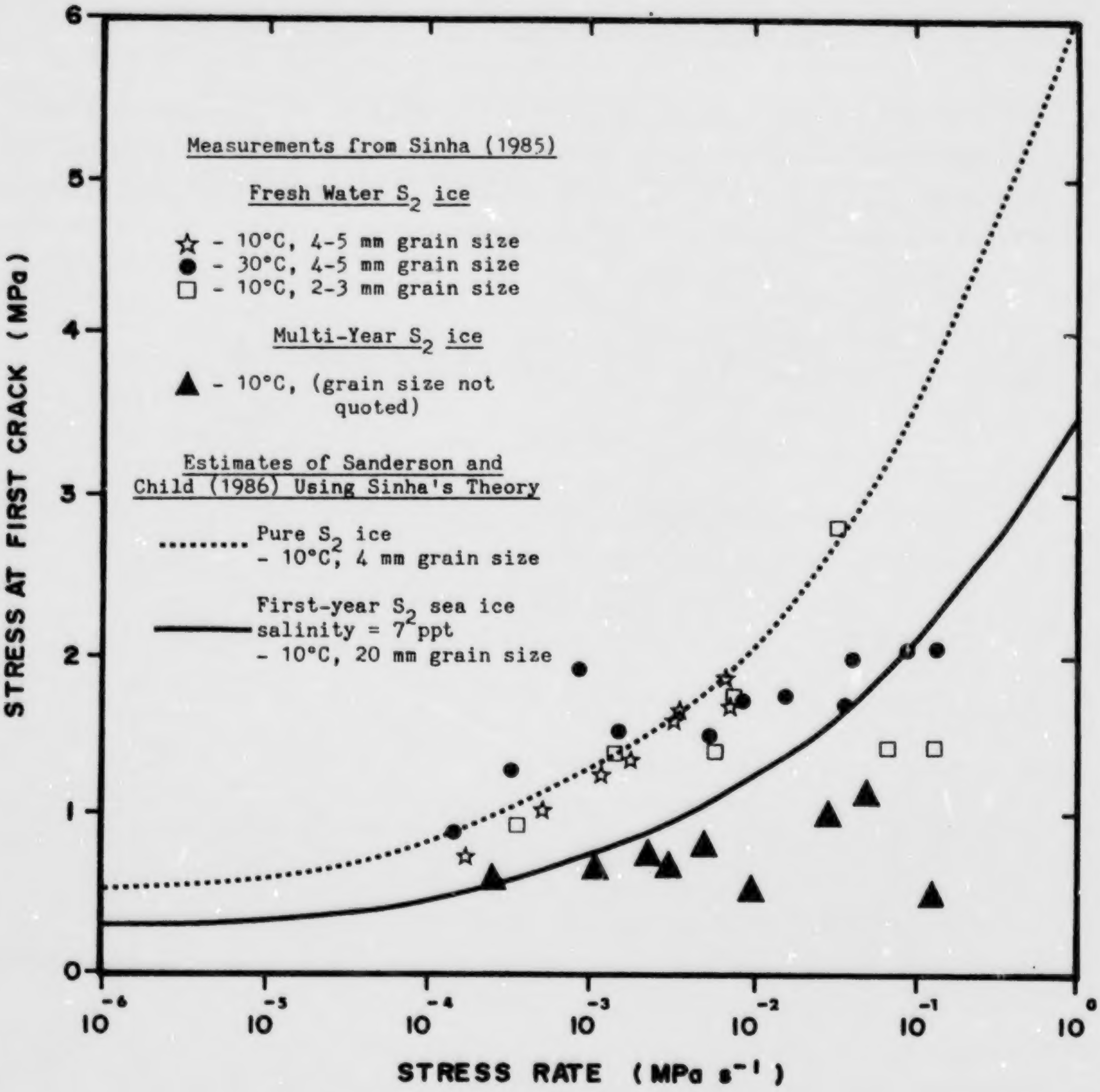

Figure 5.2.21 Comparisons of Measured and Calculated Stress at First Crack for Different Ice Types.

was horizontal and has a preferred direction. During tests the preferred direction of the c-axis was oriented parallel to the applied stress.

The data at Netserk reviewed by Sanderson (1984) showed stress rates between 10^{-5} kPa s^{-1} and 3.5×10^{-5} kPa s^{-1}. For these stress rates the maximum stress expected based on Sinha's theory would be approximately 0.65 MPa for pure S_2 ice and 0.40 MPa for first-year sea ice. Immediately after the peak stress measurements at Netserk the stress dropped to zero on one panel and to about 0.35 MPa on the other panel. Sanderson and Child suggest it is quite reasonable that the falling stress was associated with crack formation and that the observations support the theory as much as can be expected.

Sinha's theory is an important basis for other types of modeling such as the damage modeling technique, examined in the next subsection.

5.2.3.9 Damage Modeling

The premise of damage theory modeling is to describe the degradation of properties of a material in terms of a scalar variable, D, which can vary between 0 and 1. When D is zero the material is virgin; a D value of 1 indicates the material is fully damaged. The behaviour of the material is usually described in terms of the damage rate, which can be either coupled (depend to some extent on D) or can be uncoupled (no dependence of the rate on the damage at any given time). Cormeau et al., (1986) discuss the damage modeling technique in detail in their report. For a briefer review the reader is referred to the paper by Tomin et al., (1986).

In Figure 5.2.22 an illustration of the progressive damage of the ice in front of an indentor is presented.

While still in the preliminary stage, the technique shows promise for ice related work.

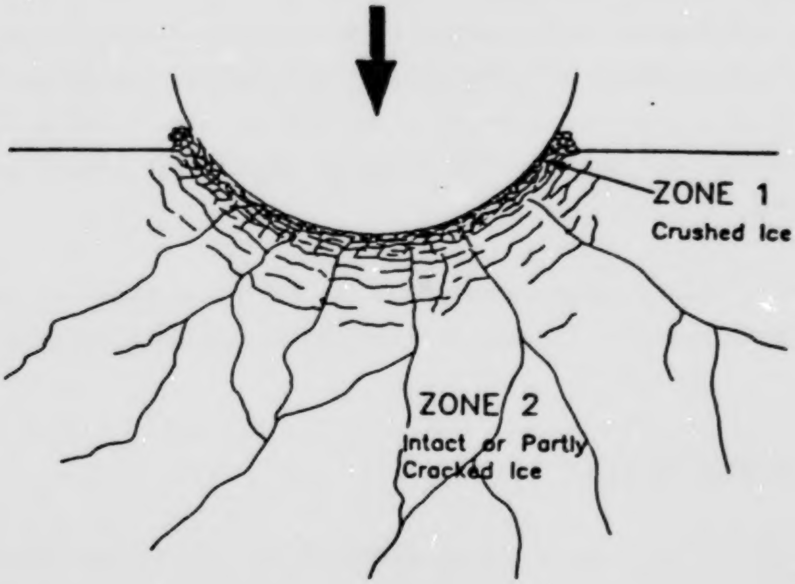
ZONE 1
Crushed Ice
ZONE 2
Intact or Partly
Cracked Ice

Figure 5.2.22 Illustration of Damage Progression (Cormeau et al., 1986).

5.2.4 Scenario Calculations

5.2.4.1 Introduction

In this subsection ice load calculations on a scale more appropriate for larger marine structures are reviewed. Narrow structures are not examined; the scenario calculations are mainly concerned with wide structures, of which the Gulf Molikpaq is a typical example.

The Korzhavin Methodology is widely used where narrow structure design is considered. Where possible the results should be compared with full scale ice data. The Korzhavin Methodology and calculation procedures have been reviewed in Subsection 5.2.3.2. The use of this methodology for estimating ice loads on wide structures is not recommended.

Loads due to large iceberg/structure interactions are not reviewed here. For calculations of large iceberg/structure loads the reader is referred to Cammaert and Tsinker (1981), Cammaert et al. (1983) and Bass et al. (1985).

Loads due to small iceberg/structure interactions are reviewed in Section 5.4, under ice interactions with floating structures.

The four different scenario calculations presented in this subsection are as follows:

- brittle failure of first-year and multi-year ice sheets interacting with a wide structure,
- brittle failure of a multi-year ridge interacting with a wide structure,
- brittle failure of a first-year ridge interacting with a wide structure,

- buckling failure of first-year ice sheets and small first-year floes interacting with a wide structure.

Where it is desired to determine the load on a structure due to brittle failure of ice sheets or consolidated ridges, or even icebergs for that matter, the objective of the analysis is to determine the product of the area of interaction and an assumed failure pressure.

For wide structures and first-year columnar sea ice, a failure pressure of 1.75 MPa independent of geometry is recommended.

For iceberg ice the use of the failure pressure data reviewed in Chapter 3 is recommended as a preliminary guide only.

For multi-year ice one can advocate either the area relationship of Sanderson (1986) shown as Figure 5.2.19 or the empirical aspect ratio dependent (i.e. geometry dependent) failure pressure line shown on Figure 5.2.17.

5.2.4.2 Brittle Failure of First-Year and Multi-Year Ice Sheets Interacting with a Wide Structure

First-Year Ice Sheet Loads

For a first-year Beaufort Sea ice sheet failing in a brittle crushing manner against a 100 m wide structure, the ice load would be approximately 2 m x 100 m x 1.75 MPa = 350 MN.

Multi-Year Ice Sheet Loads

The ice load exerted on a structure due to the interaction with a multi-year ice floe is equal to the product of the chord width of the interaction surface, the average thickness of the floe at the interaction surface, and a failure pressure determined from the empirical data based on the ratio of D/t.

Consider the interaction of a typical multi-year floe with a square shaped structure of sides of length 100 metres. The average thickness of the floe at the edge is assumed to be 4 metres.

The D/t ratio is equal to 25, and from Figure 5.2.17 an estimated failure pressure of 500 kPa (70 psi) is determined.

The area of interaction is 400 m^2, therefore the load is equal to 200 MN. This value is 60% that exerted on the same structure by a first-year ice sheet of thickness 2 metres. Using the pressure-area relationship in Figure 5.2.19 at 400 m^2 the upper bound failure pressure is 600 kPa, which would give a total load on the structure of 240 MN.

5.2.4.3 Multi-Year Ridge Interaction With a Wide Structure

This example was chosen not to represent typical conditions, per se, but rather to illustrate that "ice crushing" may not be the design load for a wide structure. The following example shows that many factors can affect the interaction scenario, and in particular shows that shearing on a large scale, with transfer of crushing from the ridge/structure interface to the ridge/floe interface can significantly reduce the load.

Example Calculation: The "End-On" Ridge Scenario

The end-on ridge situation refers to the situation illustrated in Figure 5.2.23. The structure is impacted by a nearly square ridge or hummock field.

The parameters in this example calculation are:

Environmental:

Water depth: 35 m
Wind speed: 12.5 m/s
Current speed: 0.50 m/s

Structure:

Octagonal in shape, width: 100 m

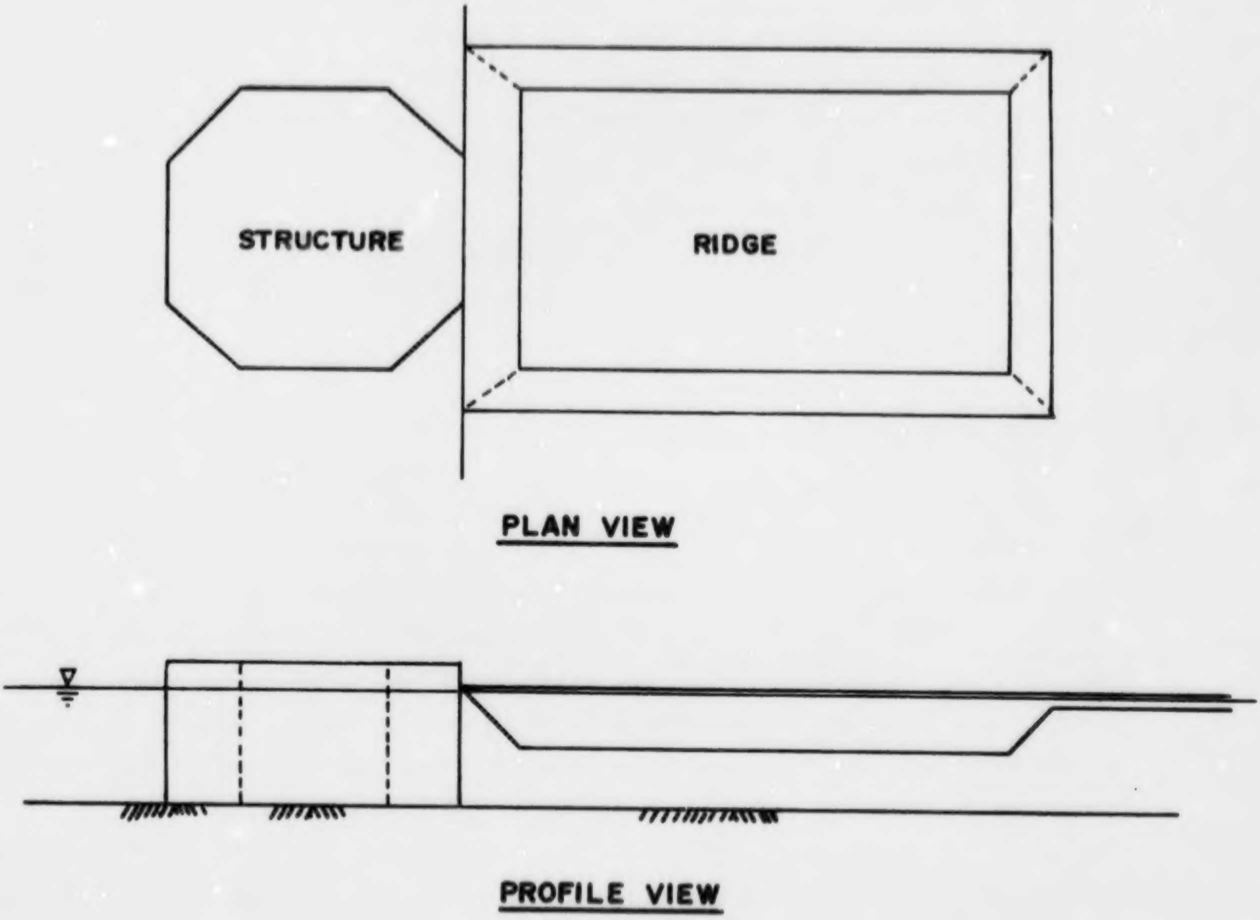
STRUCTURE
RIDGE
PLAN VIEW
PROFILE VIEW

Figure 5.2.23 Profile and Plan Views of the Multi-Year Ridge Used in the Scenario.

Ice Floe:

Shape:	circular
Diameter:	10 km
Average thickness:	5 m
Maximum ridge thickness:	20 m
Ridge dimensions at top:	130 m x 200 m
Ridge dimensions at bottom:	100 m x 165 m
Angle at ridge leading edge:	45° to horizontal
Initial floe velocity:	0.50 m/s
Assumed multi-year ridge ice strength:	Large Scale Empirical (Figure 5.2.17)

The Interaction Scenario

The object of the analysis is to determine the load the ice feature described above exerts on the vertically sided structure. If the crushing load at the ridge/structure interface is great enough it is possible for the ice to shear along the edges of the ridge, and for crushing to be initiated in the thinner ice at the backside of the ridge. The ridge thus stops moving towards the structure and becomes separate from the floe. The floe shears past the ridge and structure, and the load exerted on the structure is that of crushing at the backside of the ridge.

If the possibility of the ridge breaking out of the floe is not included in the analysis the ultimate load on the structure is caused by full envelopment of the ridge at about 45 m penetration. The load, of the limit stress variety, is 2.6 GN.

The ridge breakout scenario is responsible for a reduction in the load which the structure must bear. The "breakout" load is calculated by determining the force necessary to shear the ridge out of the floe and to initiate crushing at the backside of the floe.

In the example above the crushing load at the backside of the ridge is calculated as 360 MN (D/t ratio of 130/5=26, for a crushing pressure of 0.55 MPa from Figure 5.2.17. To initiate crushing, a "breakout factor" of 2.0 is used, which means that to initiate crushing a load of 720 MN is necessary.

The shearing force is calculated by multiplying the area of ice sheared by an assumed shear strength of the ice (0.5 MPa). The area is calculated as 5 m thickness x 200 m length = 1000 m^2. The force per side is calculated as 500 MN; that for both sides is 1.0 GN.

Therefore, when the load caused by crushing at the ridge/structure interface is greater than the breakout load (1000 MN + 2.0 x 360 MN) of 1.72 GN, breakout will occur, the sides of the ridge will shear, the crushing at the structure/ridge interface will stop, and crushing at a load of 360 MN will begin at the backside of the ridge.

The initial conditions are shown in Figure 5.2.23. The conditions at breakout of the ridge are shown in Figure 5.2.24, and Figure 5.2.25 is a plot of the load versus penetration for both scenarios.

As part of the design process examples such as that presented above are included in the analysis of ice loading conditions.

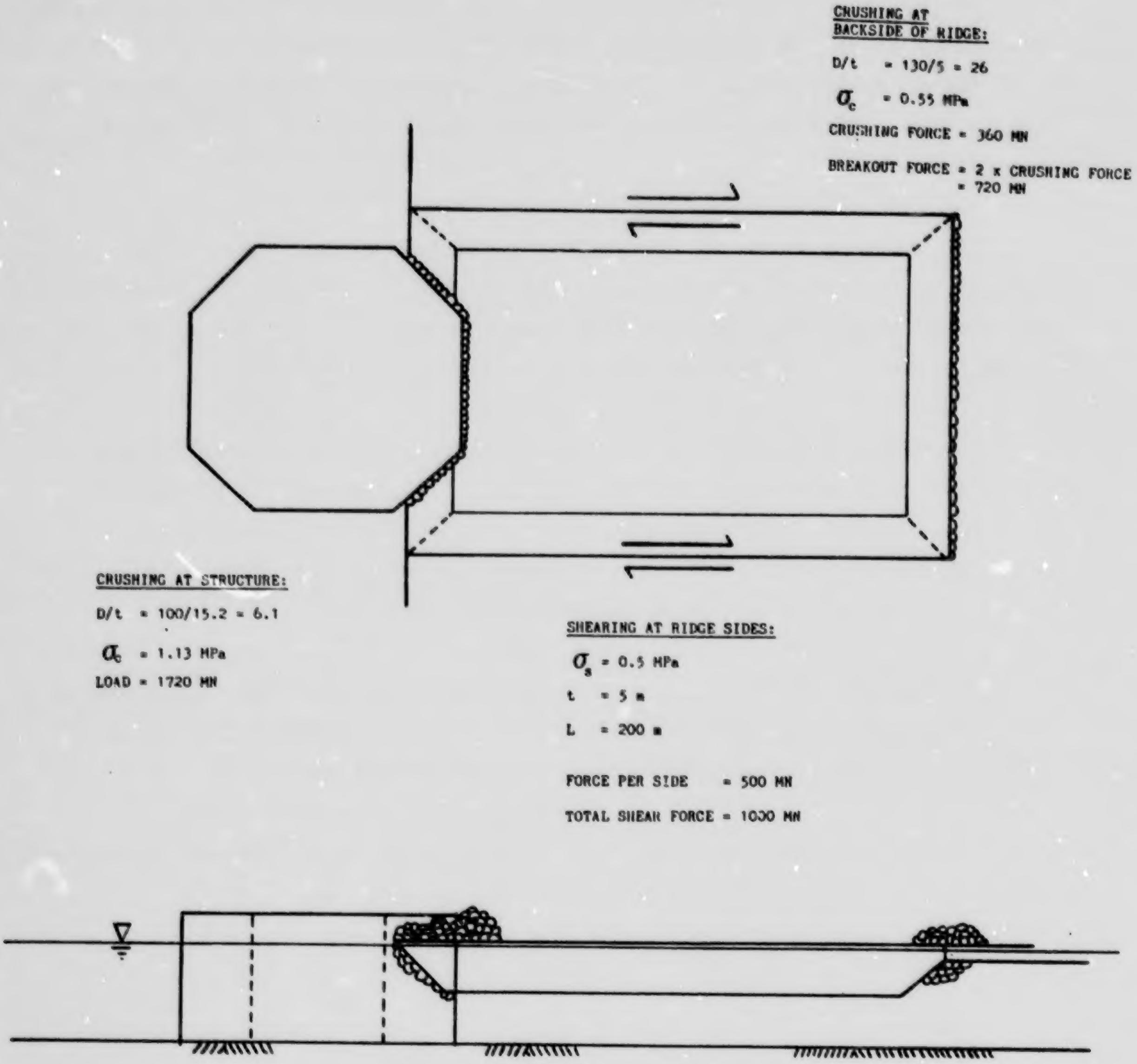
CRUSHING AT BACKSIDE OF RIDGE:
D/t = 130/5 = 26
σ_c = 0.55 MPa
CRUSHING FORCE = 360 MN
BREAKOUT FORCE = 2 x CRUSHING FORCE = 720 MN
CRUSHING AT STRUCTURE:
D/t = 100/15.2 = 6.1
σ_c = 1.13 MPa
LOAD = 1720 MN
SHEARING AT RIDGE SIDES:
σ_s = 0.5 MPa
t = 5 m
L = 200 m
FORCE PER SIDE = 500 MN
TOTAL SHEAR FORCE = 1000 MN

Figure 5.2.24 Detail of Forces Acting on the Structure and the Ridge at the Moment of Breakout.

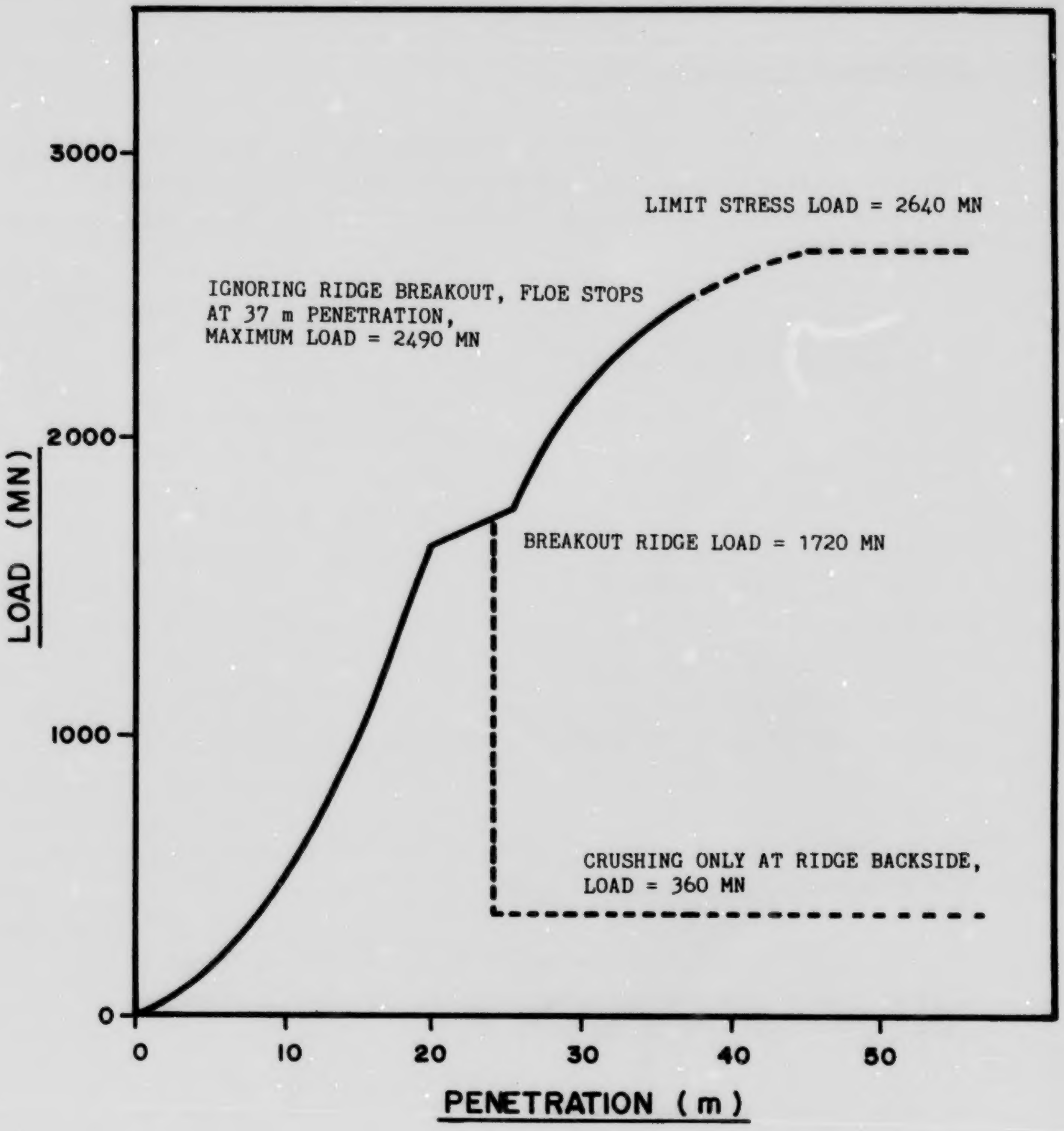

Figure 5.2.25 Force-Time Histories for the Interaction Showing Limit Stress Load, Breakout Ridge Load and Brittle Failure Load Subsequent to Ridge Breakout.

5.2.4.4 First Year Ridge

The Croasdale Ridge Shear Model

Based on a simple shear failure Croasdale (1980) proposed the following formula for the load on a structure during the interaction with a first-year (unconsolidated) ridge. The assumed failure mode is shown in Figure 5.2.26.

$$L = \frac{2\ B\ t^{2}}{3} \left(\rho_w - \rho_i \right) g \tan \left(\phi \right)$$

where:

B = the width of the ridge,
t = the keel draft of the ridge,
g = 9.81 m/s',
ρ_i = density of ice,
ρ_w = density of water, and
= the internal angle of friction of the ridge.

The influence of the sail is ignored. The keel is assumed to be acted upon by buoyancy, gravity and friction.

The load L is that load exerted on the structure as a "plug" of the ridge is sheared from the remaining portions. The load is therefore independent of the width of the structure.

With reference to the next model, it is possible to include the presence of a consolidated layer in Croasdale's model by assuming the ice at the ice/structure interface crushes at a failure pressure of 1.75 MPa.

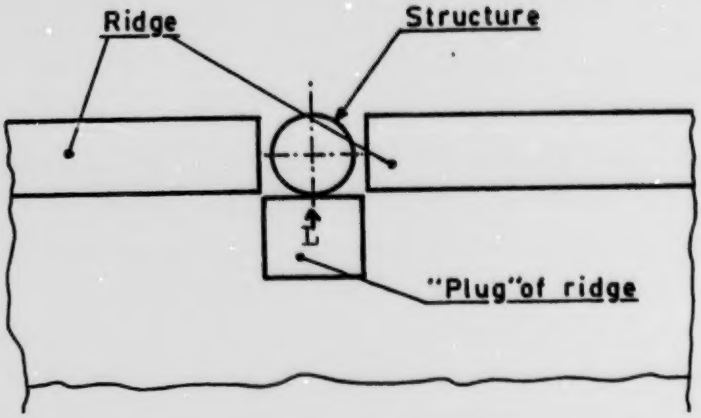
Ridge
Structure
L
"Plug"of ridge

Figure 5.2.26 Croasdale (1980) Shear Failure Analysis of an Unconsolidated Ridge.

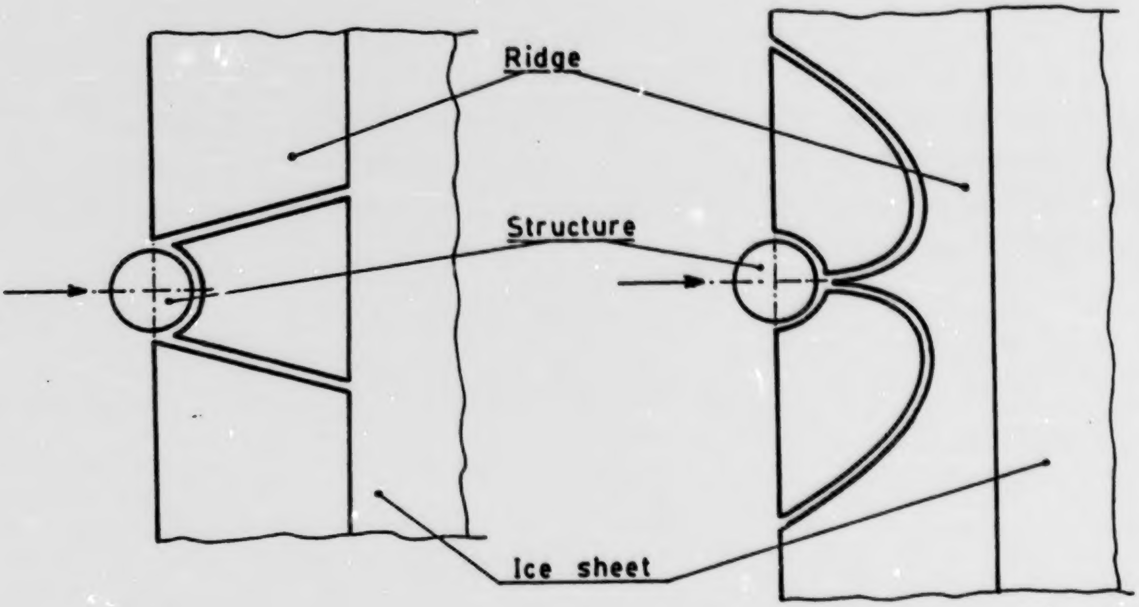
Ridge
Structure
Ice sheet

(a) Shear

(b) Crushing

Figure 5.2.27 Prodanovic (1981) Shearing and Bearing Capacity Type Failure Modes for Ridges.

The Prodanovic Bearing Capacity Model

In this model Prodanovic (1981) included the capability for a consolidated layer to be present at the upper portions of the ridge. The consolidated layer and blocky portions of the ridge are assumed to fail separately, and the total load equal to their sum.

A Prandtl indentor (or velocity field) was modeled by Prodanovic. Aside for the usual assumptions of isotropy and homogeneity in the blocky portion of the ridge, the ridge's strength was assumed to increase directly with confinement.

In Figure 5.2.27 failure modes of the ridge used by Prodanovic (1980) are shown. A profile of the ridge is shown in Figure 5.2.28, and a dimensionless load analysis diagram is shown in Figure 5.2.29. In Figure 5.2.29, P is the load, C is the cohesion of the blocks, D is the diameter of the structure and K is the ratio of keel depth below the ice sheet to sail height above the ice sheet. Recall that the ice sheet failure is calculated using other methods such as the large scale empirical data shown on Figure 5.2.17.

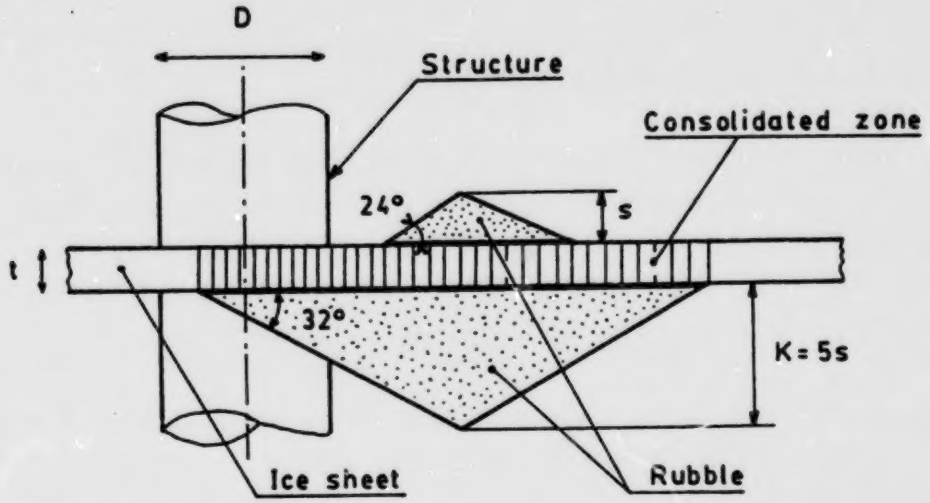
D
Structure
Consolidated zone
24°
s
t
32°
K = 5s
Ice sheet
Rubble

Figure 5.2.28 Cross-Section of First-Year Ridge Used by Prodanovic.

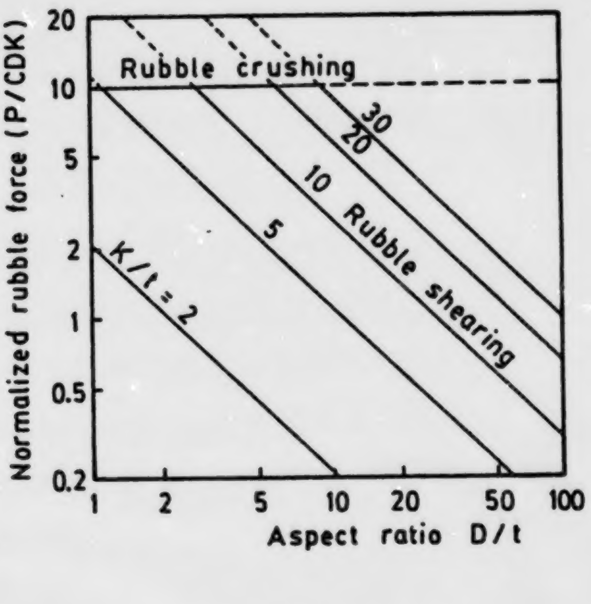

Figure 5.2.29 Dimensionless Loads for Crushing and Shearing Failure Modes for a First-Year Ridge, (from Prodanovic, 1981).

5.2.4.5 The Failure of Ice by Buckling

There are three distinct types of buckling failure of ice appropriate for structure design considerations. An ice sheet can fail by large scale buckling, be it by elastic criteria such as at a high strain rate, or by creep. As well, small floes in close pack conditions can buckle, and load floating vessels such as drillships, or semisubmersibles.

In this section of the report buckling by creep will not be examined. The reader is referred to Sjolind (1984, 1985) for a viscoelastic buckling analysis of beams and plates resting on elastic foundations. For structures located within ice experiencing low loading rates (ductile) creep buckling may be a primary load limiting mechanism at play.

Buckling of a Single Ice Sheet

In Figure 5.2.30, from Sodhi (1986), prepared for the Third IAHR State-of-the-Art Report on Ice Loading on Offshore Structures, is presented a dimensionless plot of theory and experimental results on buckling ice loads on structures. The hinged and frictionless conditions are end conditions for the ice. The calculations are based on beams on elastic foundations.

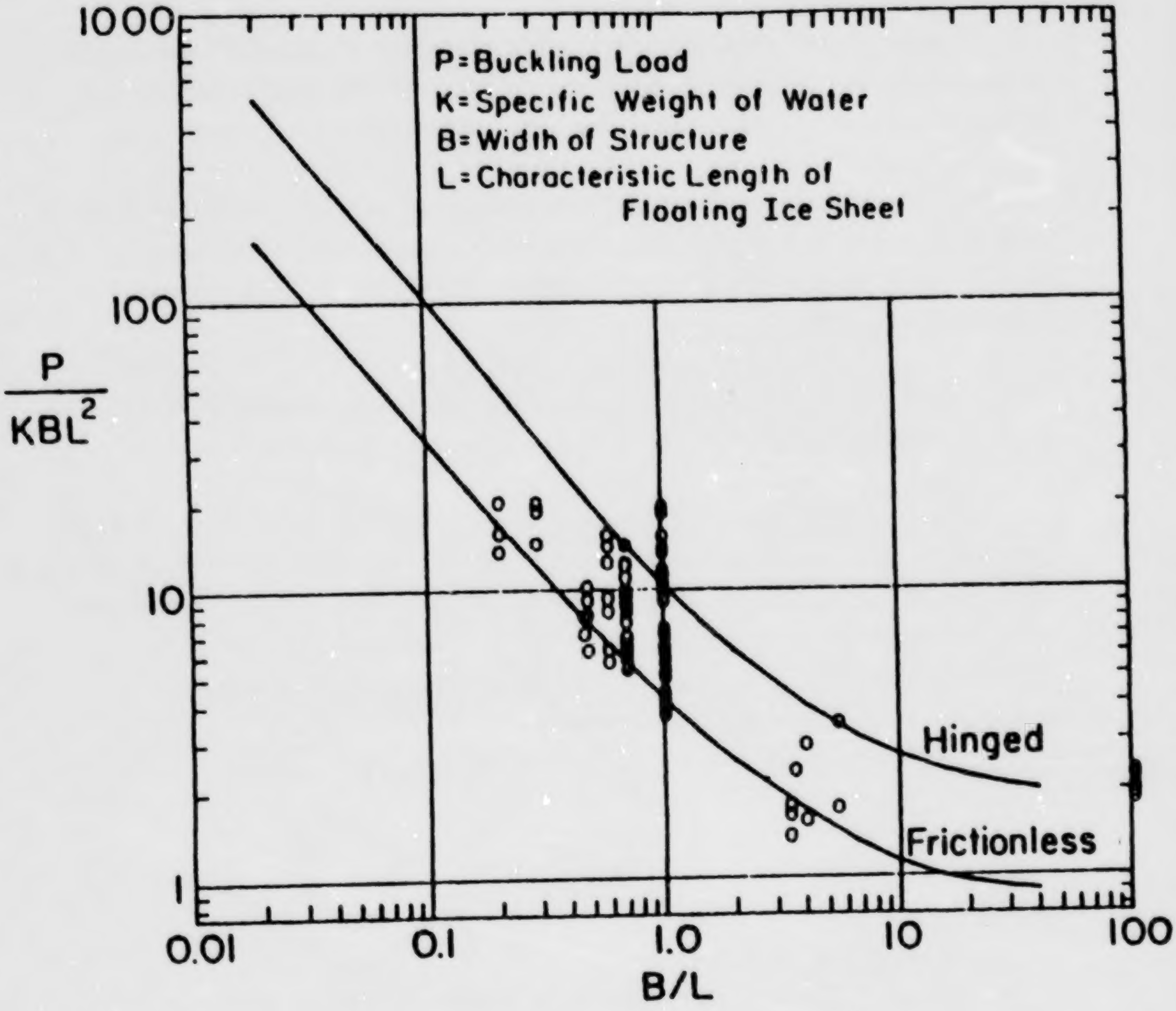

Figure 5.2.30 Comparison of Experimental and Theoretical Buckling Loads.
Heavy Lines: Theoretical Results from Sodhi (1979);
Circles: Experimental Results (Sodhi et al., 1983).

Buckling of a Collection of Floes

Hetenyi (1946) examined the elastic stability of straight bars. His calculations can be used to calculate the instability load caused by out-of-plane buckling of floes in close pack conditions.

The instability stress for floes calculated here is most often used in analyzing loads on the legs of semisubmersibles or other floating structures such as a drill ship, where the structure can not withstand large global loads.

A plot of the conditions for elastic instability in bars resting on an elastic foundation is shown in dimensionless form in Figure 5.2.16

As the full theory is given in Hetenyi (1946), only a summary will be reviewed here. The bars can deflect in one of two ways; the ends of the bars can both move in the same direction as the floes buckle, or they can move in opposite directions. The former situation is referred to as symmetrical buckling, and the latter, antisymmetrical buckling. New variables X and Y are defined as follows:

$X = f_{ins} / f_e$
= ratio of instability load to Euler load, and

where:
f_{ins} = instability load, and
f_e = l'/pi' E I, the Euler load for a hinged-end bar of length l and flexural rigidity EI.

$Y = [k\ l^4 / E\ I]^{\frac{1}{2}}$

where:
k = foundation modulus,
l = length of bar,
E = Young's Modulus, and
I = Moment of Inertia per unit width, $t^3/12$.

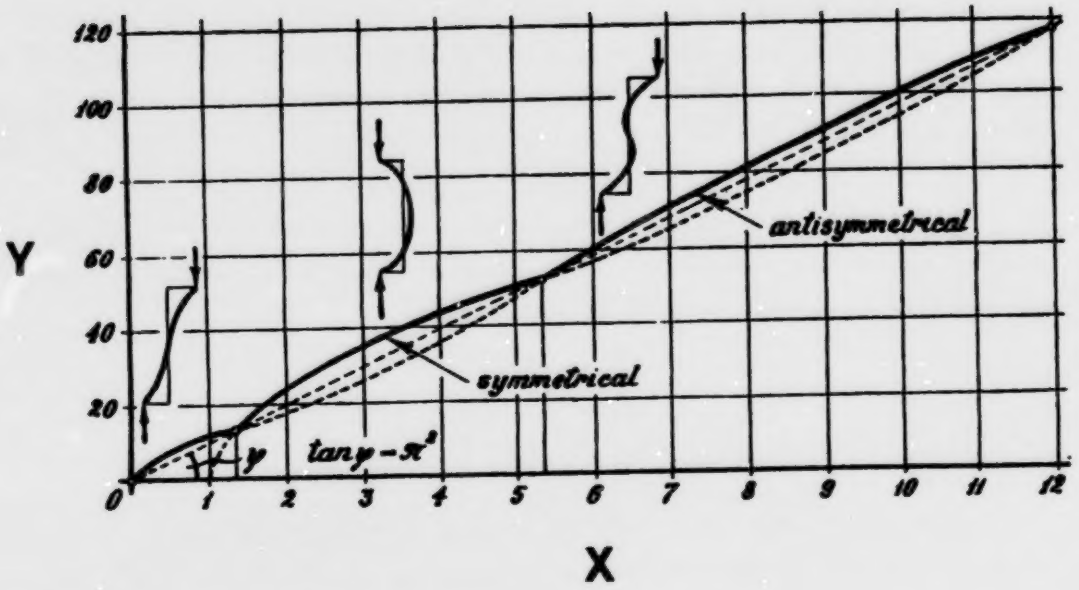

Figure 5.2.31 Illustration of Instability Conditions for Floes in Close Pack Conditions (Hetenyi, 1946).

The objective is to determine the quotient f_{ins}/f_e (the ratio of instability load to Euler buckling load). Thus, Y must be determined first. For an accurate determination of the load, and a determination of which way the floes will buckle the graph in Figure 5.2.31 should be referred to, however, it should be noted that an approximate estimate of the load can be obtained by dividing Y by 10. The straight dotted line in the figure has a slope of pi², which is close to 10 (i.e. the slope of the instability curve approximates the critical conditions for buckling of a semi-infinite beam). Where more accuracy is necessary, the thick continuous line is to be used in the calculations.

Note that most realistic conditions such as that illustrated below yield Y values very close to zero. In cases such as these it is more appropriate to divide Y by 10 to estimate X.

Example Calculation of Floes Buckling

Consider floes about 2 metres square, with a thickness of 30 cm. The instability load is determined to be about 80 kN per metre width. For a semi-submersible leg of width about 10 metres the load would be 80 tonnes; for a drillship with a length of about 100 m, the load would be 800 tonnes.

Close Pack Ice Conditions: Calculation of Out-of-Plane Instability Load Conditions Based on Buckling

floe shape, $l \times l$ = 2 m x 2 m
thickness, t = 0.3 m

Young's Modulus, E = 7000 MPa
foundation modulus, k = 0.01 MN/m^3
Moment of Inertia per unit width, I, = $t^3/12$

Euler Buckling:

$f_e = l^2 / pi^2\ E\ I = 40$ MN/m

$Y = [k\ l^4/E\ I]^{\frac{1}{2}} = 0.02$

Calculation of Instability Load:

$f_{ins} = Y\ f_e / 10 = 0.08$ MN/m width
= 80 kN/m width

5.2.5 Suggested Calculation Procedures - Sea Ice

Multi-Year Ice Floes and Ridges

Wide Structures Only

- Determine chord width and average thickness of interaction surface to estimate the D/t ratio. Based on the value of D/t estimate the failure pressure based on the large scale empirical estimates in Figure 5.2.17. The product of the failure pressure, chord width and average thickness is equal to the load on the structure. The pressure-area line in Figure 5.2.19 can also be used as a reference, (also see Section 5.7 on local pressures).

First-Year Ice Sheets

Wide Structures

- Determine the product of chord width and ice thickness and multiply by 1.75 MPa (250 psi) to determine the first-year ice sheet load.

First-Year Ridges

Wide Structures

- Use Croasdale shearing model, or Prodanovic bearing capacity model to determine failure of unconsolidated portions of the ridge. Add to those values the product of chord width, thickness and assumed failure pressure of 1.75 MPa.

Narrow Structures

- Use of a Korzhavin-type methodology is recommended for consolidated ice failing against narrow structures.

5.2.6 Summary

- Small scale brittle failure is complex, but can be described using an empirical "deformation mode map". On the small scale the brittle failure process is characterized by crushing, spalling, radial and circumferential cracking, and buckling.

- The small scale brittle failure processes are observed on the large scale.

- Ice load theories, such as the Korzhavin Methodology and others documented in the mid 1970's, were used to estimate large scale structure loads when full scale empirical data were not available.

- Later measurements showed that the large scale ice loads were less than those estimated based on the smaller scale theories. On the large scale the Korzhavin Methodology is not used.

- The use of empirical data has become the norm when it is desired to estimate ice loads on large vertical sided structures.

- As of late sophisticated analytical models are available which incorporate both simple and complicated failure mechanisms.

5.3 Ice Interactions With Sloping Structures

5.3.1 Types of Structures

Sloping structures are often chosen over vertical structures due to the perceived belief that the ice forces will be lower. Whether this is true depends on many factors, including; the relative ice strength in the crushing and bending failure modes; the ice thickness and morphology; and in particular the structure geometry. Relevant structure parameters can be listed as:

- slope angle,
- ice to structure friction,
- water depth,
- structure width,
- superstructure geometry, and
- whether the slope is upward breaking or downward breaking.

In general, with respect to predicting ice loads, structures can be categorized as being of the following types:

- conical structures with a relatively narrow superstructure,
- sloping structures with a wide superstructure, and
- downward breaking sloping structures.

These three categories of sloping structures are shown conceptually in Figure 5.3.1.

As will be discussed later, the main difference in the way ice forces are generated on these three categories of structures relates to the differences in the ice clearing loads.

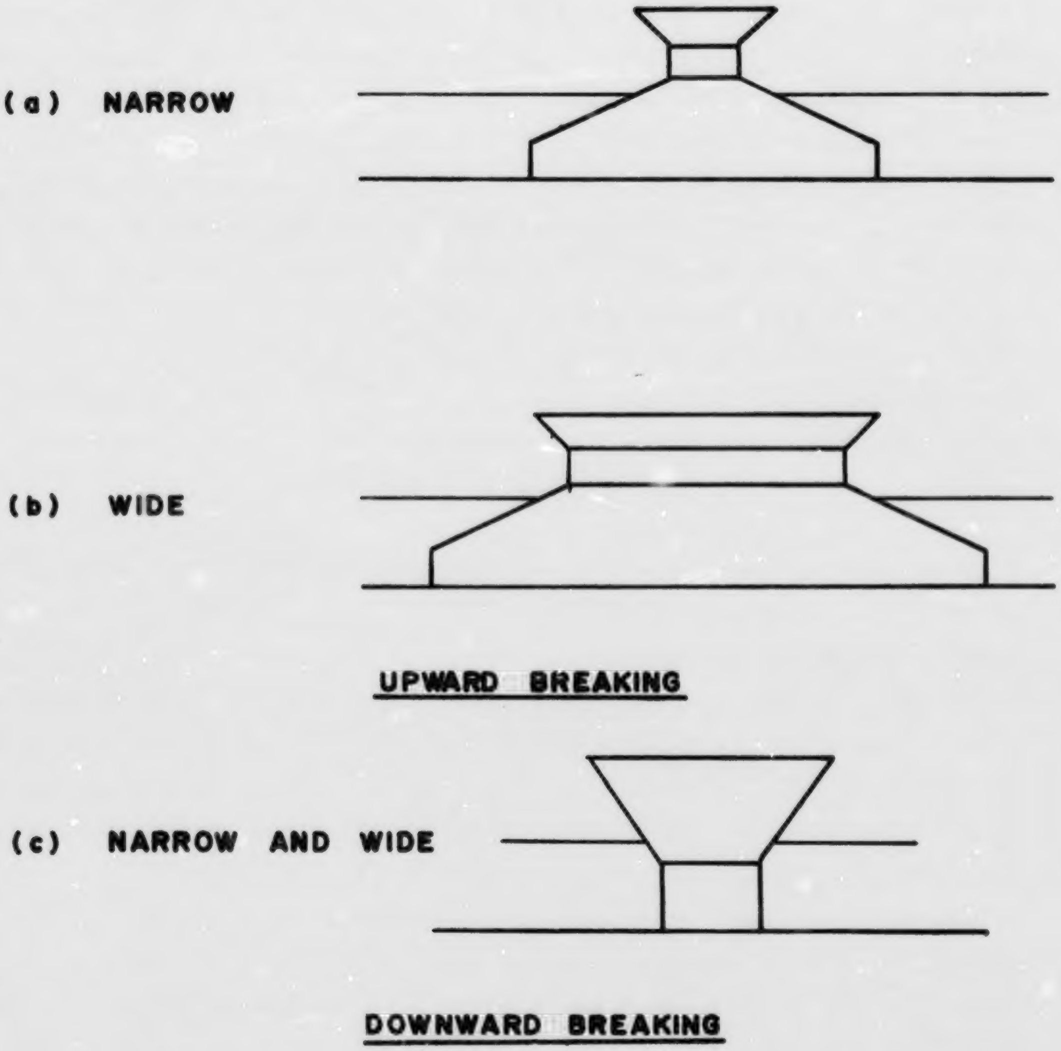
(a) NARROW
(b) WIDE
UPWARD BREAKING
(c) NARROW AND WIDE
DOWNWARD BREAKING

Figure 5.3.1 Types of Sloping Structures

5.3.2 Interaction Scenarios for Sloping Structures

(a) Sheet Ice

Consider the simple case of sheet ice advancing on a sloping structure (Figure 5.3.2a). As the ice contacts the structure, local crushing occurs (on the underside of the ice sheet for an upward breaking slope). This local crushing creates a force normal to the interface, and if relative upward movement occurs, there will also be a friction force acting along the slope. The normal and friction force components create an out-of-plane force which creates bending in the ice sheet. As the ice sheet continues to advance the out-of-plane force increases until bending failure of the advancing ice sheet occurs (Figure 5.3.2b). The bending failure is analogous to a bearing capacity failure of an ice sheet. Initially radial cracks are formed and then a circumferential crack leads to complete failure of the ice at some distance from the leading edge.

Once the ice sheet has failed, the advancing ice continues to push the broken pieces against the structure. Experience with real structures and model tests indicates that the broken ice pieces ride-up the slope of the structure as illustrated conceptually in Figure 5.3.3. There are kinematic and frictional forces associated with the ice ride-up which create loads on the structure and must be accounted for in the ice force calculations. Furthermore, the geometry of the structure above the waterline (or below the waterline for downward breaking structures) has a significant influence on the way the broken ice clears around the structure. As can be appreciated from Figure 5.3.3., on a cone with a relatively narrow superstructure the ice can clear sideways. On a wide structure the ice may get turned back on itself, creating additional ice on the slope of the structure, which may lead to ice rubble creation in front of the structure, which may in turn inhibit simple bending failure of the advancing ice against the slope of the structure. For thick ice, significant ice ride-up forces can be created on the vertical superstructure which must be accounted for in design.

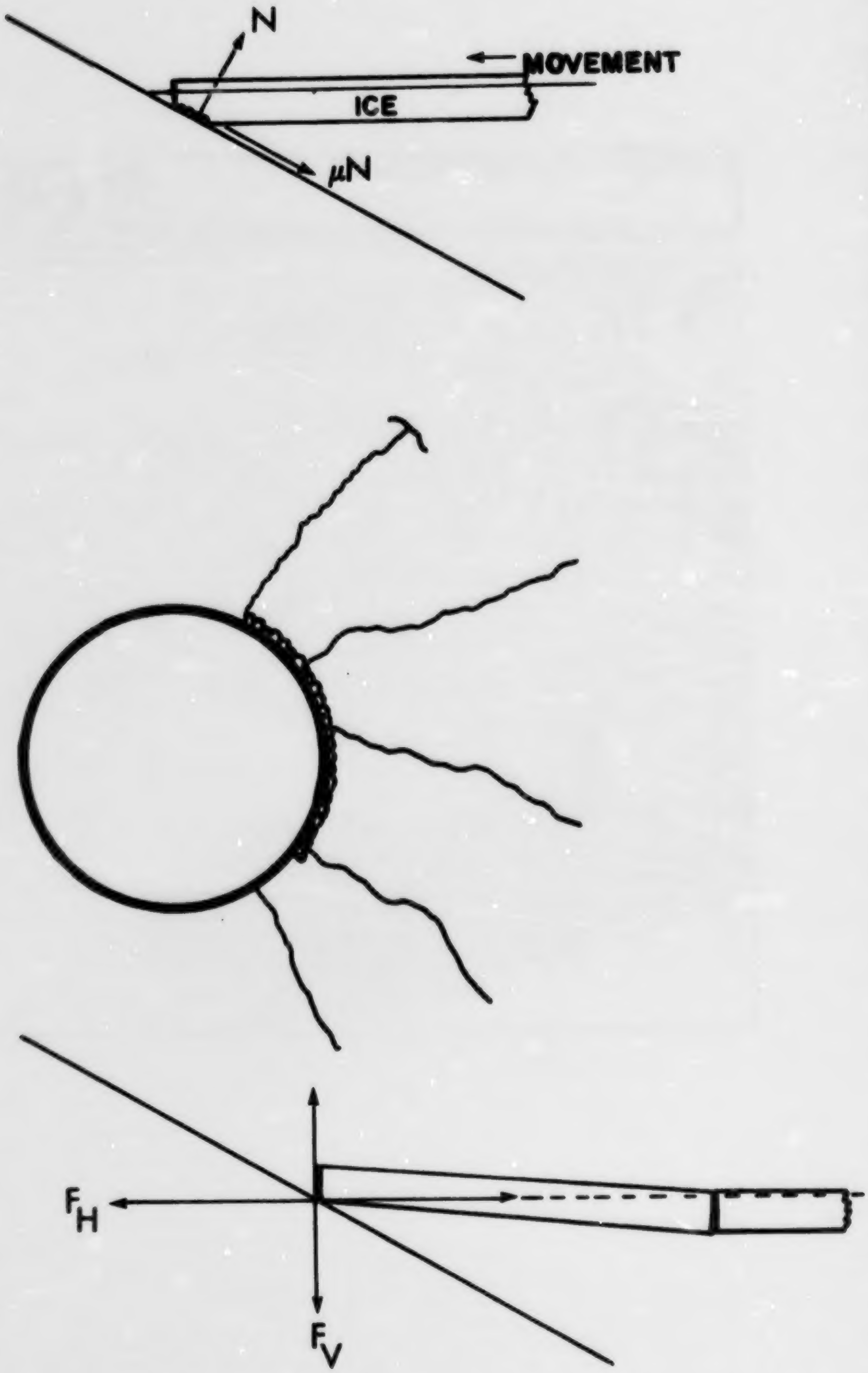

- INITIAL CRUSHING GENERATES OUT-OF-PLANE FORCE
- BENDING FAILURE CAUSED BY OUT-OF-PLANE FORCE
- RADIAL CRACKS
- CIRCUMFERENTIAL CRACKS LIMIT ULTIMATE LOAD

Figure 5.3.2a Sheet Ice Failure Mechanisms During Interaction With a Sloping Structure

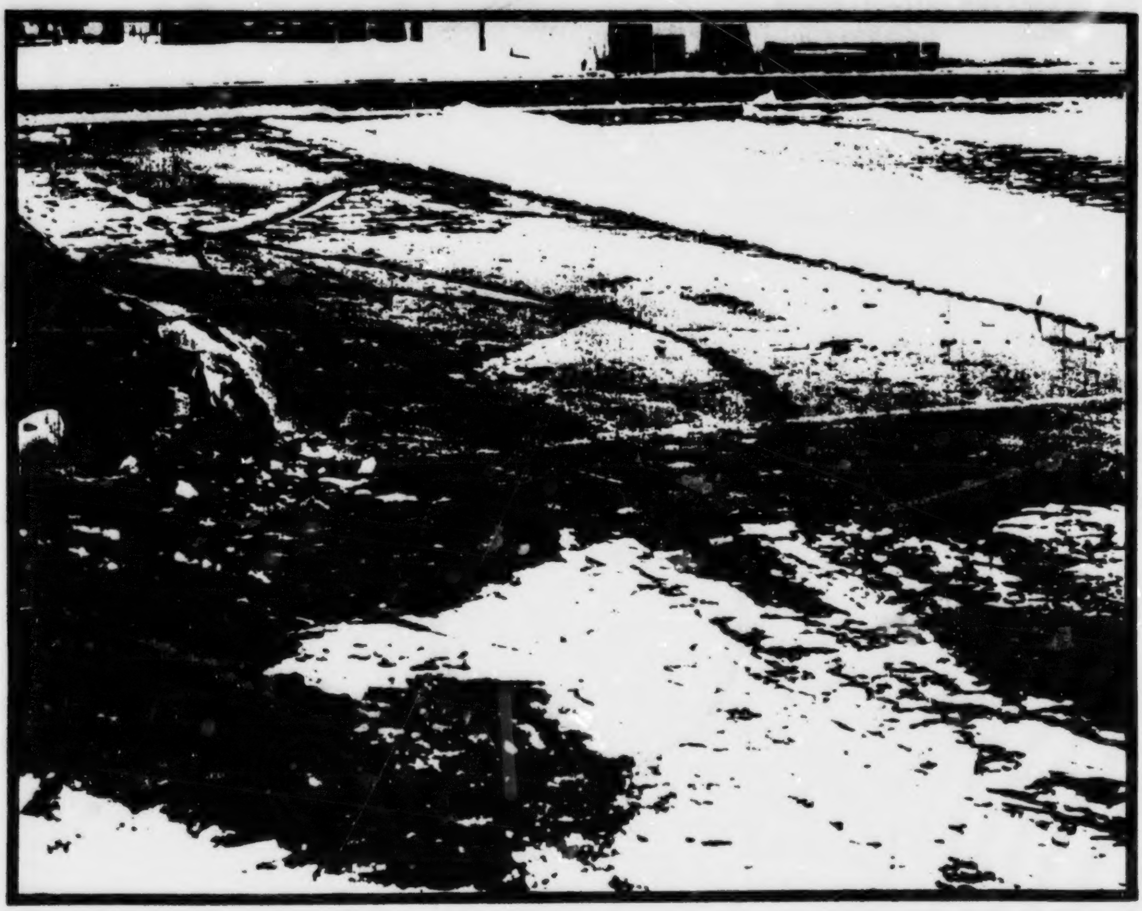

Figure 5.3.2.b Photo of Ice Breaking on a Conical Structure During a Model Test in the Esso Ice Basin (courtesy of Esso Resources)

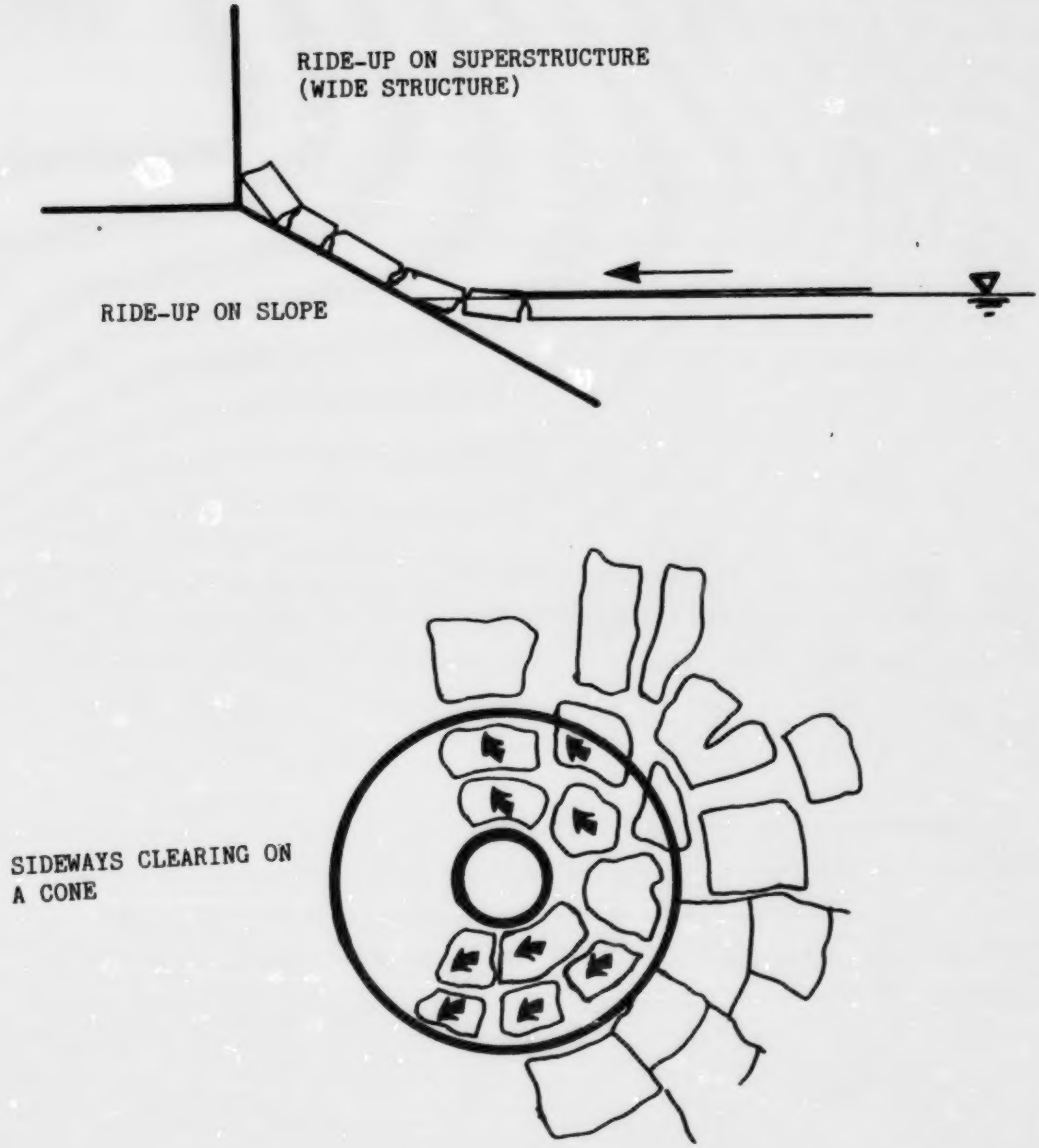
RIDE-UP ON SUPERSTRUCTURE
(WIDE STRUCTURE)
RIDE-UP ON SLOPE
SIDEWAYS CLEARING ON
A CONE

Figure 5.3.3 Sheet Ice Clearing Around a Sloping Structure

On a downward breaking structure it is expected that the clearing forces will be lower due to the weight of ice in water being less than that in air. The reduction in clearing forces is the main advantage of a downward breaking structure.

In ice force calculations it is generally assumed that as the ice motion progresses the subsequent ice breaking sequences occur with the slope of the structure already covered with ice blocks. In this scenario the ice breaking load has to be added to the ice clearing load.

A potential disadvantage of sloping structures is the freezing of the ice sheet to the structure during periods when the ice is not moving. This condition is known as adfreeze and has to be considered. Adfreeze forces can be reduced by local heating or by the use of anti-adfreeze coatings.

(b) Ice Ridges

Consolidated (multi-year) ridges may be considered to act as beam-like local thickening in the ice sheet. For these features, the interaction is similar to sheet ice except that the ice failure mode is conceptualized as the out-of-plane failure of an ice beam, as shown in Figure 5.3.4 for a ridge parallel to the edge of a floe.

Unconsolidated ridges (first-year) can be treated as an accumulation of granular material. For these features a sloping structure appears to offer little advantage over a vertical structure, since the ridge will deform in a manner as to eliminate any advantages gained by having the sloping structure in the first place.

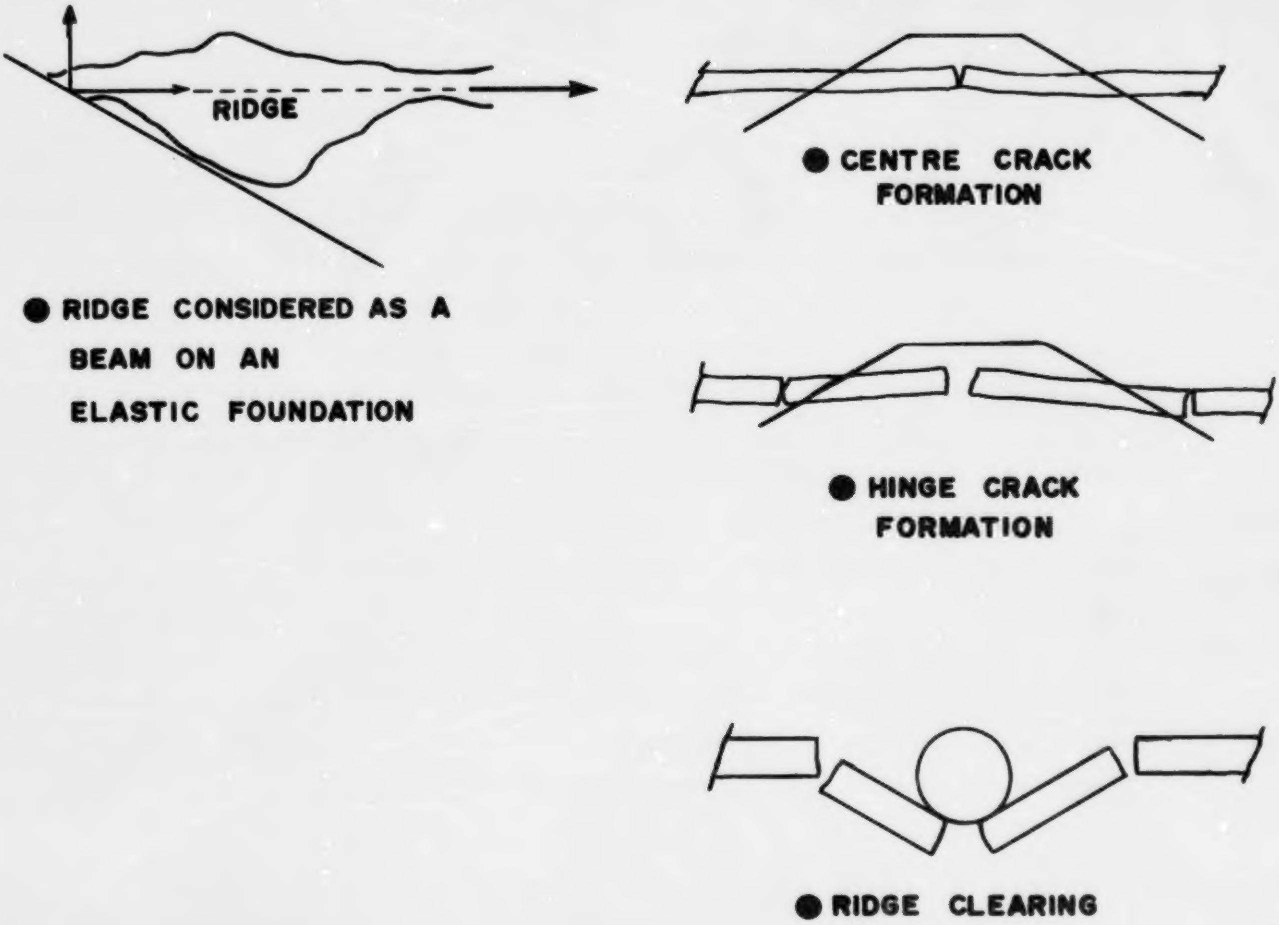
RIDGE
● RIDGE CONSIDERED AS A BEAM ON AN ELASTIC FOUNDATION
● CENTRE CRACK FORMATION
● HINGE CRACK FORMATION
● RIDGE CLEARING

Figure 5.3.4 Consolidated (Multi-Year) Ridge Interaction With a Conical Structure

5.3.3 Ice Loads due to Sheet Ice

5.3.3.1 Historical Overview

Early work by Korzhavin, Afanas'ev and Danys was primarily in relation to sloping bridge piers, and has been comprehensively reviewed by Neill (1976), and also by Michel (1970). The early approaches were mostly empirical and did not account for ice ride-up forces.

In the early 1970's the oil industry began examining conical structures for arctic offshore oil exploration. This stimulated extensive model testing (Edwards and Croasdale, 1976) and the parallel development of analytical models. The math models were based on analyzing the breaking of ice sheets on elastic foundations and were an adaptation of the bearing capacity analyses of Nevel (1972). In addition to ice breaking, the math models also accounted for ice ride-up and adfreeze (Kim and Kotras, 1973). The analytical models developed were later incorporated into a comprehensive computer program (Semeniuk, 1975). About the same time Bercha and Danys developed similar approaches (e.g. Bercha and Danys, 1975).

All the above approaches were based on the theory of elastic plates on elastic foundations. An alternative analysis using plasticity theory was developed by Ralston (1977). He demonstrated good agreement with the early model tests.

Between 1973 and 1976, Esso conducted a comprehensive series of small-prototype tests on a conical structure of diameter 3.3 m at the waterline. The tests were used to calibrate the analytical models for both sheet-ice and ice ridges (e.g. Verity, 1975).

As part of an IAHR State-of-the-Art review of ice forces on structures, Croasdale (1980) reviewed all methods in the public domain up until 1978, and also used simple 2-dimensional theory to demonstrate the relative importance of the influencing parameters.

Croasdale et al. (1978) published theories for ice ride-up on sloping beaches. The theory demonstrated the possibility of a jamming mechanism against a steeper section of the slope.

In the late 1970's Schwarz and Frederking (1978) conducted further model tests; in parallel Frederking developed an analysis for ice acting on a flat-faced inclined structure. The analysis took account of ice breaking, rotational forces, hydrodynamic forces, inertia forces and sliding. Also about the same time Tryde (1977) conducted model tests on a wedge shaped pier and developed an empirical approach. Sorenson (1978) conducted a thorough analysis of the dynamic interaction between ice and a sloping face.

More recently, Timco (1984) and Frederking and Timco (1985) conducted a comprehensive set of model tests on a wide inclined structure and compared the results with theory.

5.3.3.2 Sheet Ice Loads - General Logic

The general approach to predicting sheet ice loads on a conical or sloping structure is shown in Figure 5.3.5. The design ice load will be the lower of either the adfreeze force or the sum of the ice breaking and ice clearing forces. The ice breaking forces are determined from the failure of a plate on an elastic foundation using either an elastic-brittle or a plasticity approach. An important input parameter is the large-scale flexural strength of the ice (this will be discussed later). The ice clearing forces should account for buoyancy and gravity forces, rotation, friction and inertia. The interaction of advancing ice blocks with the superstructure also has to be considered.

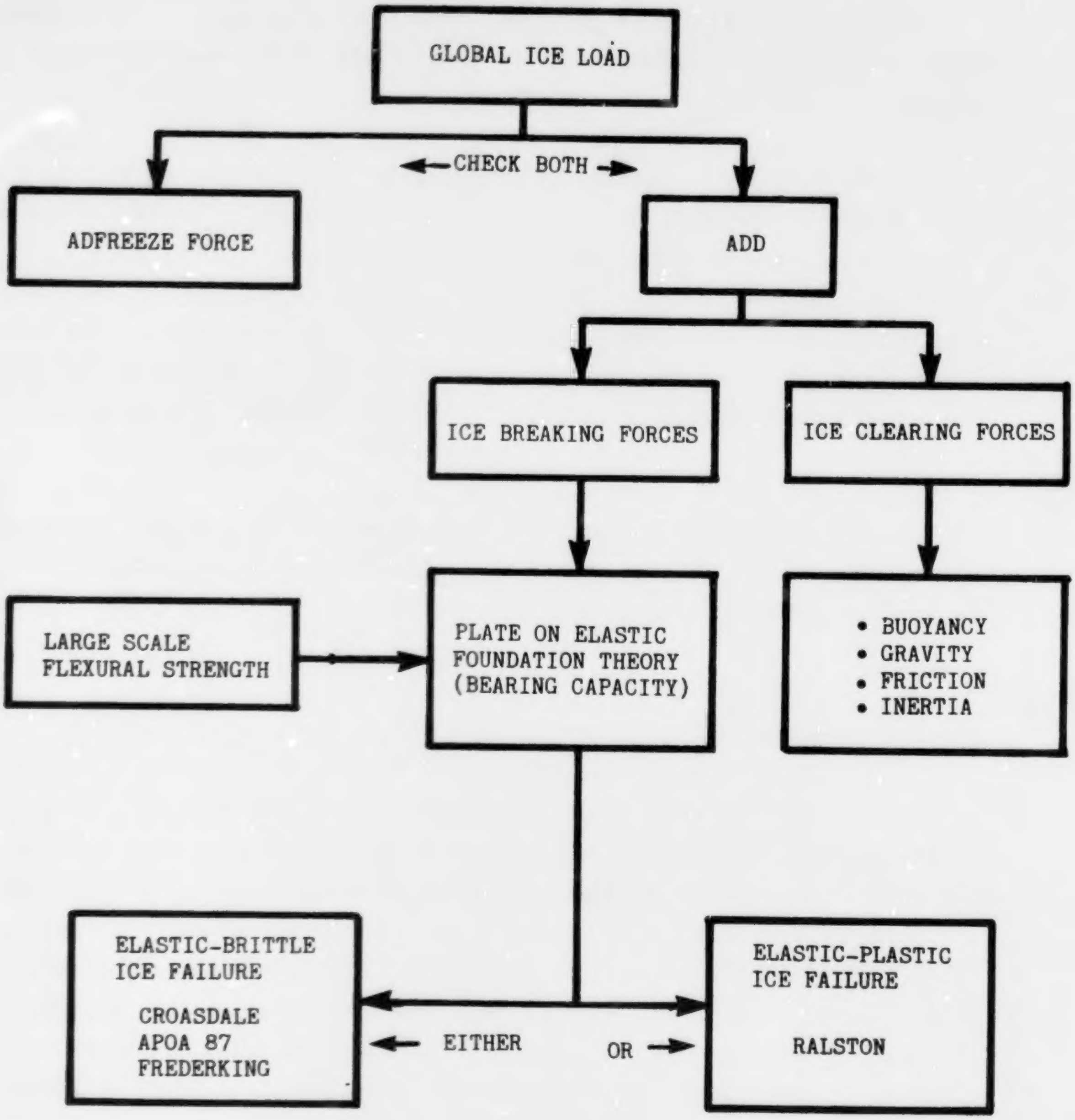
GLOBAL ICE LOAD
CHECK BOTH
ADFREEZE FORCE
ADD
ICE BREAKING FORCES
ICE CLEARING FORCES
LARGE SCALE FLEXURAL STRENGTH
PLATE ON ELASTIC FOUNDATION THEORY (BEARING CAPACITY)
• BUOYANCY
• GRAVITY
• FRICTION
• INERTIA
ELASTIC-BRITTLE ICE FAILURE
CROASDALE
APOA 87
FREDERKING
EITHER
OR
ELASTIC-PLASTIC ICE FAILURE
RALSTON

Figure 5.3.5 General Logic Approach for Calculating Loads on Sloping or Conical Structures

5.3.3.3 Sheet Ice Loads: Two-Dimensional Theory (Elastic)

Theory based on two-dimensional analysis has been presented and discussed by Croasdale (1980). It is useful to review some of the early work due to the insight into the types of forces involved and the influence of various parameters which can be obtained.

The following extract is an abridged version of that presented in Croasdale (1980).

Consider the simplified two-dimensional system shown in Figure 5.3.6. As the advancing ice sheet first encounters the sloping structure, local crushing occurs on the underside of the ice sheet. The local crushing causes an interaction force normal to the structure surface. In addition, due to the motion of the ice sheet relative to the surface, a frictional force is also generated.

The normal and tangential forces can be resolved into vertical and horizontal components V and H acting at the centre of the crushed area. In the simple two-dimensional model shown in Figure 5.3.6, the forces acting on the ice will be V, H, gravity and buoyancy; the latter can be considered as that due to an elastic foundation.

As the ice sheet continues to advance the crushed area will increase, causing V and H to increase. If the driving force is large enough, V and H will continue to increase until the ice fails in bending. For a properly designed sloping structure the ice should fail in bending.

Except for very steep structures the effect of H on the bending failure of the ice can be ignored. The ice sheet then behaves as a beam or plate on an elastic foundation. The load V to fail the ice sheet governs the initial lateral load on the structure. Subsequent loads are generally higher because of the additional load required to push the ice pieces up the slope (Figure 5.3.7).

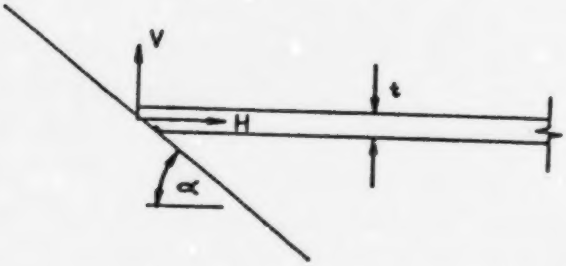

FORCES ACTING ON ICE

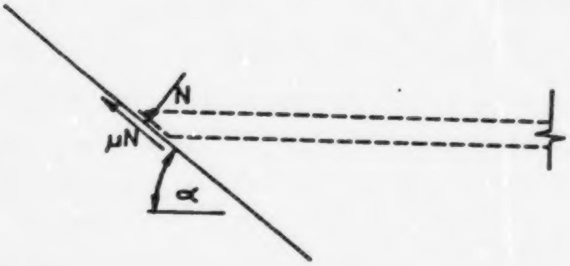

FORCES ON STRUCTURE

Figure 5.3.6 Initial Interaction Between an Ice Sheet and a Sloping Structure

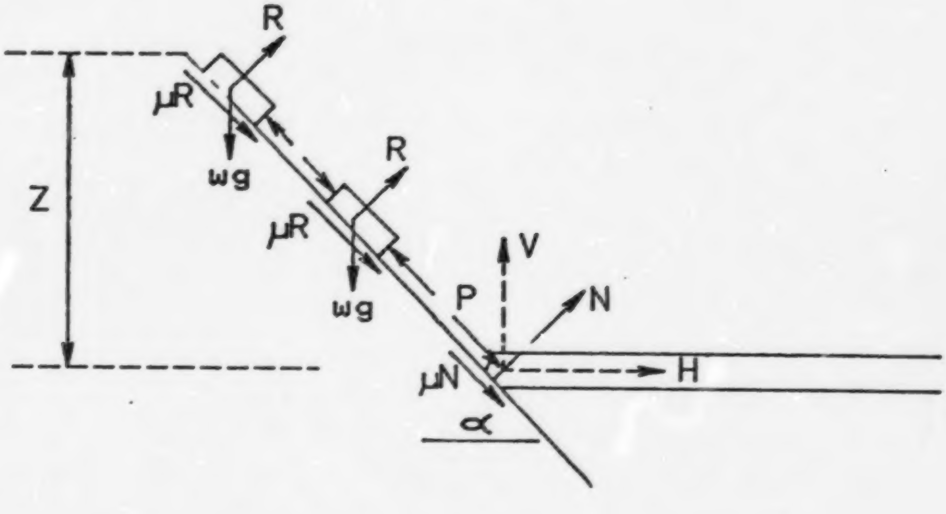
R
μR
wg
R
Z
μR
wg
V
P
N
H
μN
α

Figure 5.3.7 Illustration of Frictional Components During the Interaction of Sheet Ice and a Sloping Structure

The horizontal force per unit width calculated in Equation 5.3.1.7 can be thought of as the component required to break the advancing ice. For subsequent interactions a component is also required to push the ice up the slope. The force system in this latter case is shown in Figure 5.3.7.

P is the force required to push the ice up the slope, and can be calculated as:

$$P = \frac{Z}{\sin(\alpha)} t\, b\, \rho_i\, g\, (\sin(\alpha) + \cos(\alpha)) \qquad \text{...Eqn. 5.3.1.8}$$

where Z is the height reached by the ice on the slope, and ρ_i is the density of the ice, then,

$$H = (V + P\sin(\alpha)) \frac{(\sin(\alpha) + \mu\cos(\alpha))}{(\cos(\alpha) - \mu\sin(\alpha))} + P\cos(\alpha)$$

...Eqn. 5.3.1.9

substituting for V and P gives

$$\frac{H}{b} = 0.68\, \sigma_f\, (\rho_w\, g\, t^5/E)^{\frac{1}{4}} \frac{\sin(\alpha) + \mu\cos(\alpha)}{\cos(\alpha) - \mu\sin(\alpha)} +$$

$$+ Z\, t\, \rho_i\, g\, \frac{[\sin(\alpha) + \mu\cos(\alpha)]^2}{\cos(\alpha) - \mu\sin(\alpha)} + \frac{\sin(\alpha) + \mu\cos(\alpha)}{\tan(\alpha)}$$

...Eqn. 5.3.1.10

Equation 5.3.1.10 is similar to equation 5.3.1.7 except for the additional term. The equation can be simplified to:

$$\frac{H}{b} = \sigma_f \left(\rho_w \, g \, t^5/E \right)^{\frac{1}{4}} C_1 + Z \, t \, \rho_i \, g \, C_2 \qquad \text{...Eqn. 5.3.11}$$

where C_1 and C_2 are functions only of α and μ. Values for the coefficients C_1 and C_2 are plotted in Figure 5.3.8 for typical values of α and μ.

In the simple two-dimensional theory given above, the first term can be considered to be the force necessary to break the ice, and the second term can be considered to be the force necessary to push the ice pieces up the sloping structure. As a two-dimensional theory it might be considered accurate for a very wide structure, but as will be discussed later it is probably inaccurate for narrow structures. For structures which are narrow relative to the characteristic length (approximately 15 times the ice thickness for t = 1.0 m and E = 7 GPa, and 11 times the ice thickness for t = 0.3 m and E = 7 GPa) the zone of ice failure will be wider than the structure itself, also most of the ice pieces will not necessarily ride-up the structure but move around it. Nevertheless it will be useful to discuss the importance of some of the key parameters in the context of the simple two-dimensional theory.

Effect of Friction and Slope Angle

In Figure 5.3.9 the effect of friction and slope angle is shown for a structure with a 5 m freeboard, an ice sheet thickness of 1 m, and a flexural strength of 700 kPa. It can be seen that the effect of friction and slope angle becomes significant above an angle of 45°. For a structure with an angle of 55° the horizontal ice force increases from 125 kN m^{-1} for $\mu = 0.1$, to 450 kN m^{-1} for $\mu = 0.5$. For steep angles and high friction the ice may fail in crushing rather than bending. The results shown in

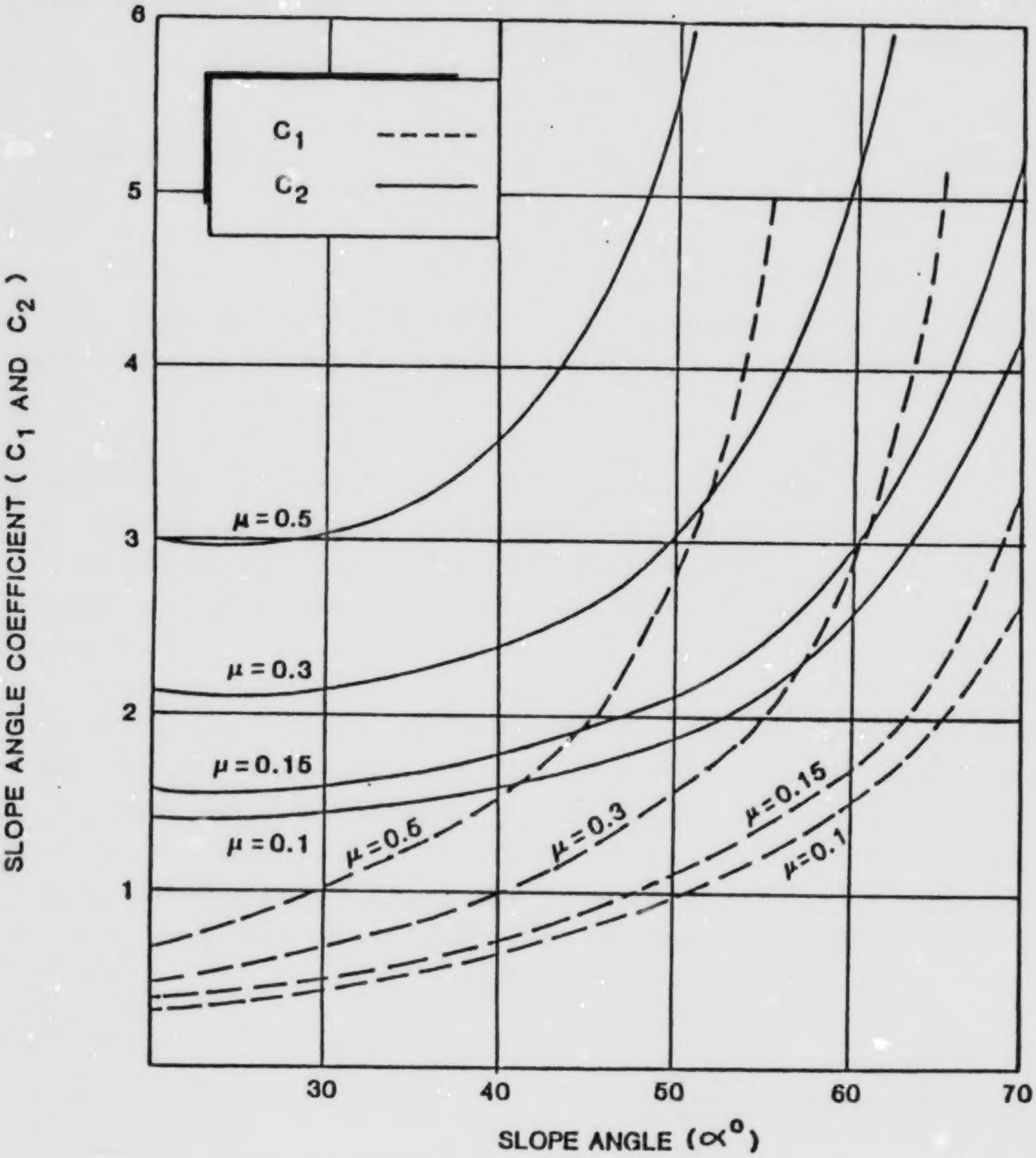

Figure 5.3.8 Values of the Two Coefficients C_1 and C_2 as a Function of Slope Angle

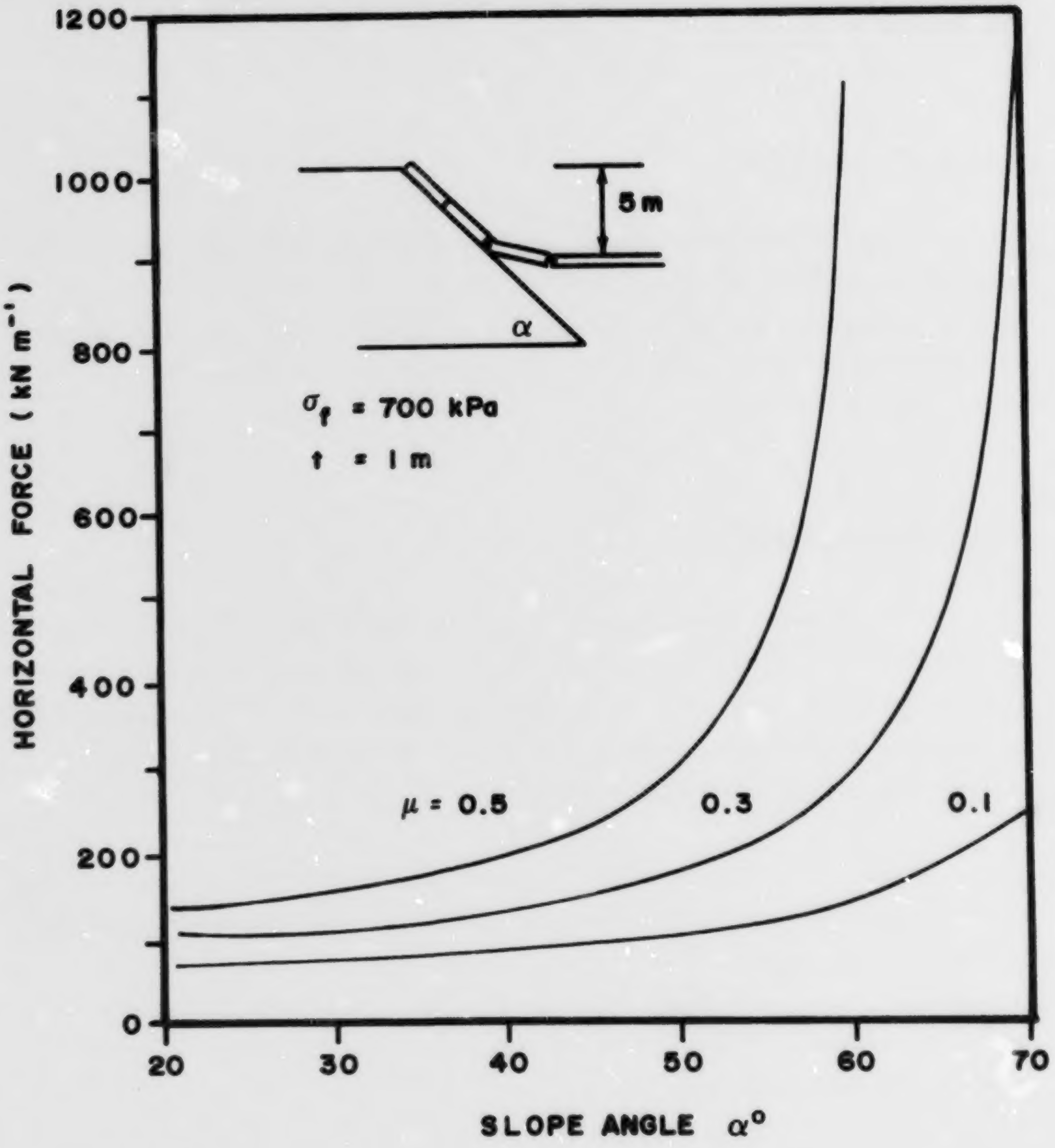

Figure 5.3.9 Horizontal Force versus Slope Angle and Friction (Simple Two-Dimensional Theory)

Figure 5.3.9 emphasize the need to maintain smooth surfaces on sloping structures so that ice forces are minimized. Even for very shallow angled structures high friction can increase loads significantly. Other investigators (Bercha and Danys, 1977; Ralston, 1977) have also shown the importance of friction.

Effect of Ice Strength

The ice strength affects the ice breaking component but not the ride-up component. As shown in Figure 5.3.10, in the two-dimensional elastic analysis, the ride-up force in a typical interaction is larger than the breaking force, so the effect of ice strength on total force is not as significant as one might suppose. This will be discussed later.

Effect of Ice Thickness

Ice thickness is probably the most significant parameter affecting ice forces on sloping structures. In the simple two-dimensional analysis the ice breaking component is proportional to $t^{1.25}$ and the ride-up force is directly proportional to t. The effect of thickness for a typical interaction is shown in Figure 5.3.11.

Again, it is interesting to note from Figure 5.3.10 that the ice ride-up force is larger than the ice breaking force. However as already discussed, this observation can only be considered relevant to two-dimensional theory as might be applicable to a very wide structure. For a narrow structure, the ice breaking component will be larger and the ice ride-up component smaller.

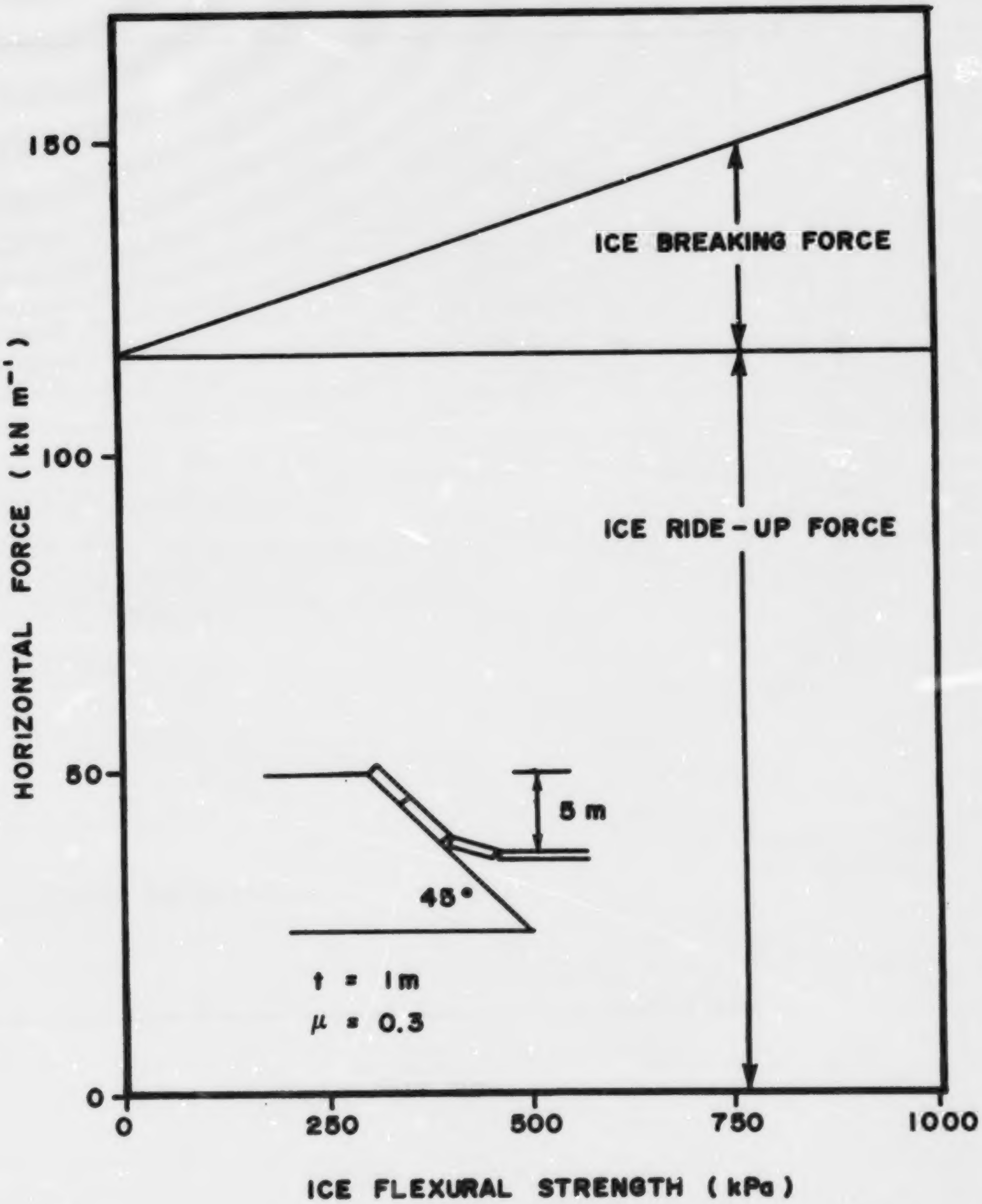

Figure 5.3.10 Horizontal Force versus Flexural Strength (Simple Two-Dimensional Theory)

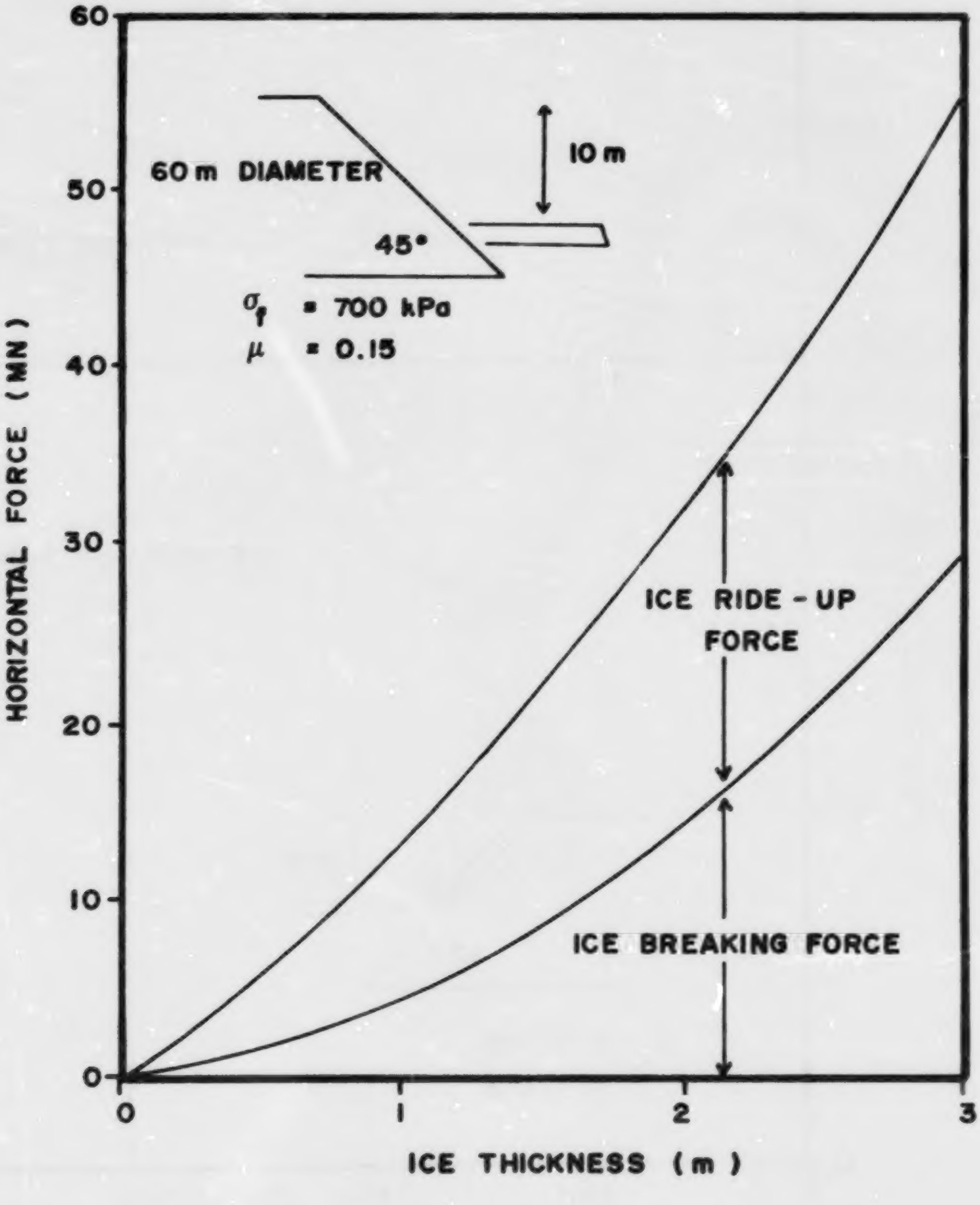

Figure 5.3.11 Illustration of Relative Importance of Ice Ride-Up and Ice Breaking Forces on a Sloping Structure

5.3.3.4 Sheet Ice Loads:Three-Dimensional Theory (Elastic)

In a three-dimensional situation, the same forces and mechanisms of ride-up apply but the zone of failure extends wider than the structure width. This effect is illustrated conceptually in Figure 5.3.12.

Croasdale (1980) suggested the simple correction of adjusting the two-dimensional force by the ratio of the length of the circumferential crack divided by the structure width, i.e. multiplying the ice breaking portion of equation 5.3.11 by $(1 + \frac{1}{4} \pi^2 l / b)$. However other investigators have conducted more rigorous analyses of the three-dimensional problem.

For the ice breaking component, the simple beam theory is replaced by plate-on-elastic foundation theory. Nevel (1972) proposed an equation for the ultimate failure of ice plates which can be applied to forces on sloping structures.

On a conical structure the problem reduces to calculation of the forces necessary to fail a series of ice wedges formed by radial cracking of the ice as it advances against the cone (see Figure 5.3.12).

Nevel's (1972) equation for the force to fail these wedges is given as:

$$\frac{6P}{b_o \sigma_f t^2} = 1.05 + 2.00 (a/l) + 0.50 (a/l)^3$$

...Eqn. 5.3.12

where P is the failure force on the tip of the wedge, σ_f is the ice flexural strength, t is the ice thickness, a is the distance from the tip of the wedge over which it is loaded, b_o is a constant defining the width

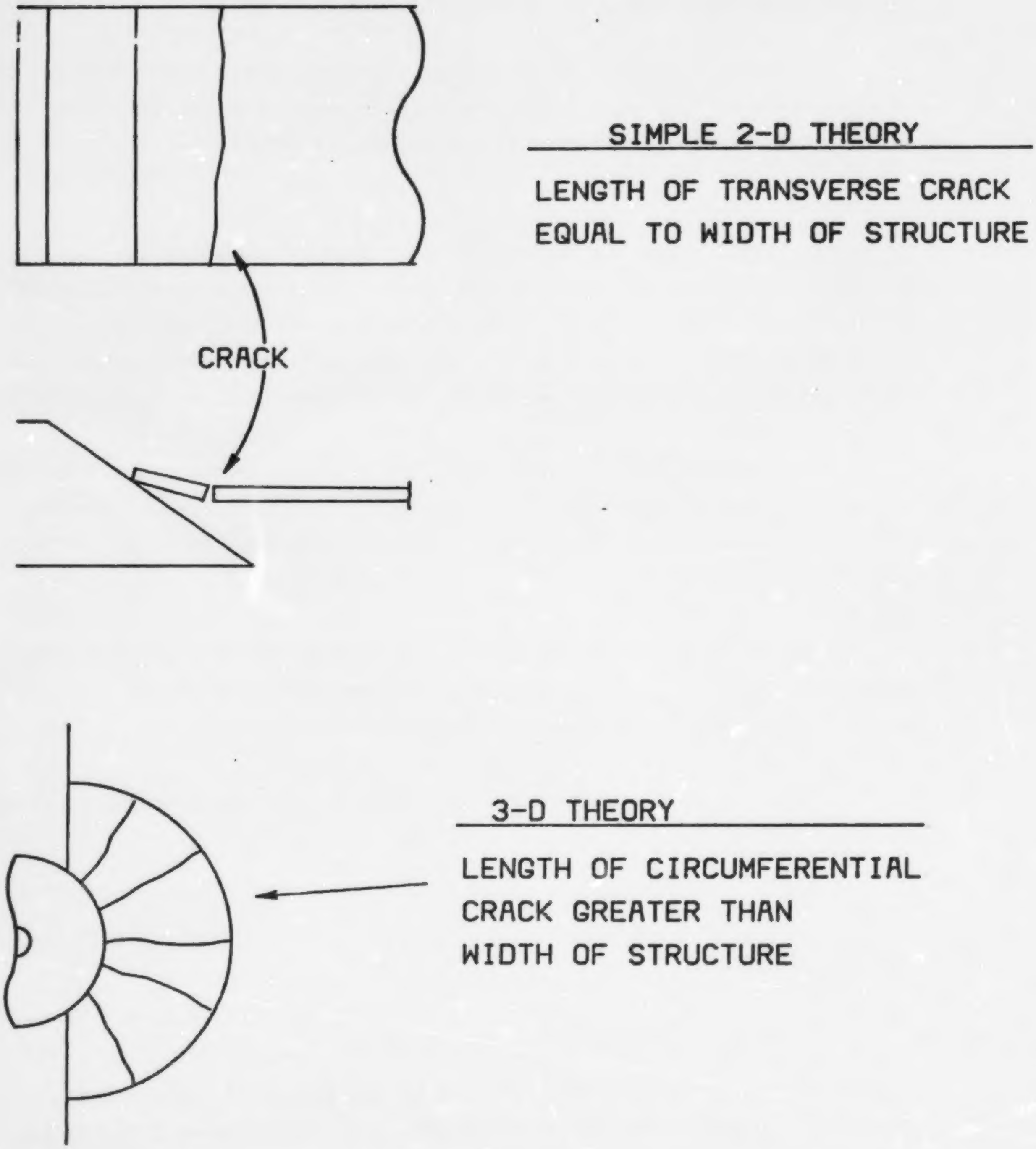
SIMPLE 2-D THEORY
LENGTH OF TRANSVERSE CRACK EQUAL TO WIDTH OF STRUCTURE
CRACK
3-D THEORY
LENGTH OF CIRCUMFERENTIAL CRACK GREATER THAN WIDTH OF STRUCTURE

Figure 5.3.12 Three-Dimensional Effects of Ice/Structure Interaction on Sloping Structures

of the wedge (b) in the equation

$$b = b_o \chi \qquad \text{...Eqn. 5.3.13}$$

where χ is the distance along the wedge, b_o is a constant and l is the characteristic length for the plate given by

$$l = [\ E\ t^3 \ /\ 12\ \rho_w\ g\ ]^{\frac{1}{4}} \qquad \text{...Eqn. 5.3.14}$$

Danys and Bercha (1976) have made use of the above theory to present an elastic analysis for the ice breaking component of the ice force on a conical structure. Their results are repeated here in Figure 5.3.13 for structures with waterline diameters up to 10.7 m (35 ft) subject to ice 0.91 m (3 ft) thick.

Danys and Bercha (1976) have also analyzed the effect of in-plane compressive stresses on the flexural failure of the ice sheet. For steep, rough structures the effect can be significant and increases the horizontal force.

Kim and Kotras (1973) also used Nevel's theories in the mathematical model they developed for Imperial Oil as part of APOA 57. Their work was later incorporated into a comprehensive computer program (Semeniuk, 1975, also known as APOA 87). The flow diagram for the program is shown in Figure 5.3.14. It can be seen from the flow diagram that the method is comprehensive and calculates loads associated with initial radial cracks, circumferential cracks, ride-up, adfreeze and loads due to ridges embedded in the ice sheet. Results obtained from the computer program will be discussed later.

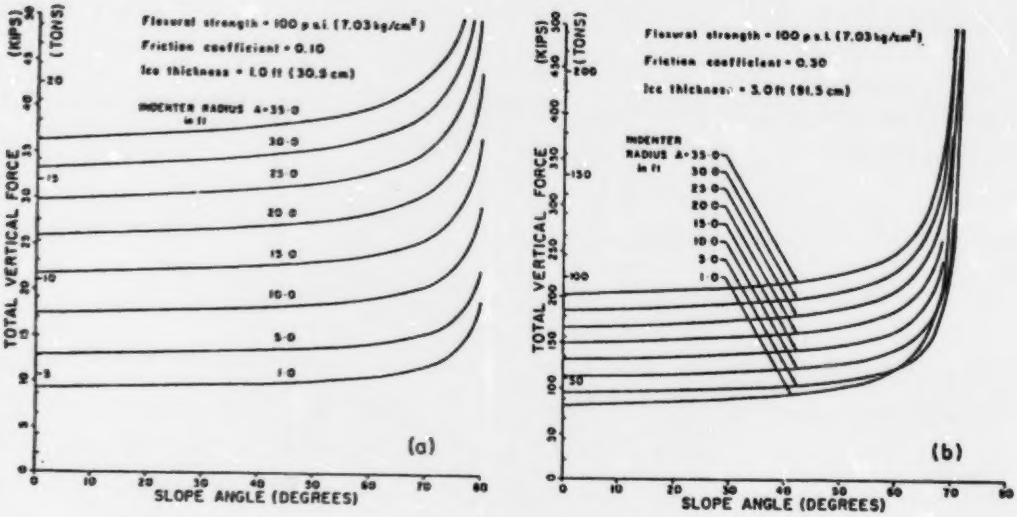

Vertical force vs slope angle and indenter radius A for constant flexural strength, friction and ice thickness. (Kip = 1000 lbs.), (Danys and Bercha 1976).

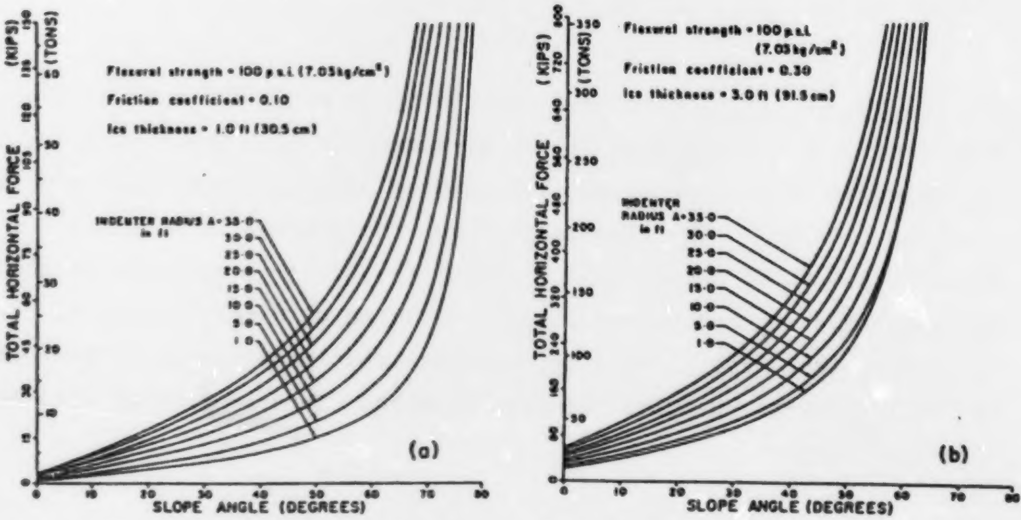

Horizontal force vs slope angle and indenter radius A for constant flexural strength, friction and ice thickness. (Kip = 1000 lbs.), (Danys and Bercha 1976).

Figure 5.3.13 Summary of Results from Danys and Bercha (1976)
(From Danys and Bercha, 1976)

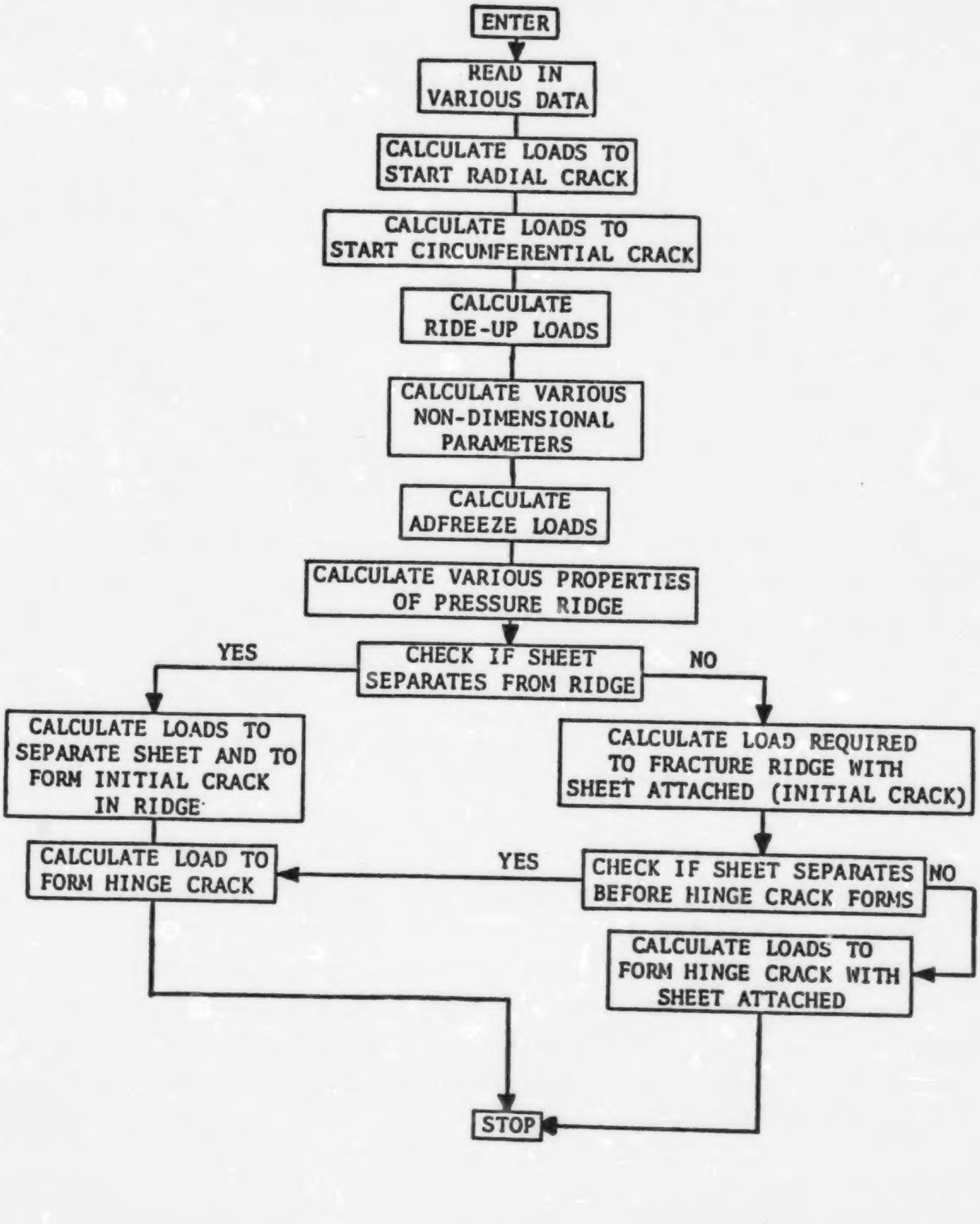
ENTER
READ IN VARIOUS DATA
CALCULATE LOADS TO START RADIAL CRACK
CALCULATE LOADS TO START CIRCUMFERENTIAL CRACK
CALCULATE RIDE-UP LOADS
CALCULATE VARIOUS NON-DIMENSIONAL PARAMETERS
CALCULATE ADFREEZE LOADS
CALCULATE VARIOUS PROPERTIES OF PRESSURE RIDGE
CHECK IF SHEET SEPARATES FROM RIDGE
YES
NO
CALCULATE LOADS TO SEPARATE SHEET AND TO FORM INITIAL CRACK IN RIDGE
CALCULATE LOAD REQUIRED TO FRACTURE RIDGE WITH SHEET ATTACHED (INITIAL CRACK)
CALCULATE LOAD TO FORM HINGE CRACK
YES
CHECK IF SHEET SEPARATES BEFORE HINGE CRACK FORMS
NO
CALCULATE LOADS TO FORM HINGE CRACK WITH SHEET ATTACHED
STOP

Figure 5.3.14 Illustration of Flow Diagram of APOA 87 Methodology (after Semeniuk, 1975)

Frederking (1979) developed a three-dimensional analysis for sheet ice acting on an inclined plane, also based on the theory of plates on an elastic foundation, and assuming elastic-brittle properties for the ice. Frederking developed load equations for the following effects:

- ice breaking, both radial and circumferential cracks,
- rotation of the ice pieces after breaking,
- ride-up (or sliding), and
- hydrodynamic and inertial forces.

The reader is referred to Frederking (1979) for the actual equations governing each of the above contributions to the ice load.

In subsequent model tests (e.g. Frederking and Timco, 1985), the theory was compared to experiments (and this comparison will be discussed later).

The relative magnitude of the various ice load contributions, based on small scale model tests, is illustrated in Figure 5.3.15. The relative magnitudes of the breaking and sliding (ride-up) contributions are similar to the analyses of others. However, in Frederking's analysis the rotation contribution is also significant; is this realistic? In calculating the rotation component it was assumed the piece size length was some function of the characteristic length and remained constant as the ice piece was lifted out of the water. In large scale tests (e.g. as conducted in the Esso basin) it was apparent that secondary failures of the ice took place as rotation occurred. The secondary failures resulted in smaller ice pieces which lead to smaller rotation forces. Therefore the rotation force as computed by Frederking is likely conservative and caution is advised. It can also be argued that rotation and breaking forces can not be added, due to rotation of a previously broken ice piece having to occur before the ice can again be broken as it contacts the structure.

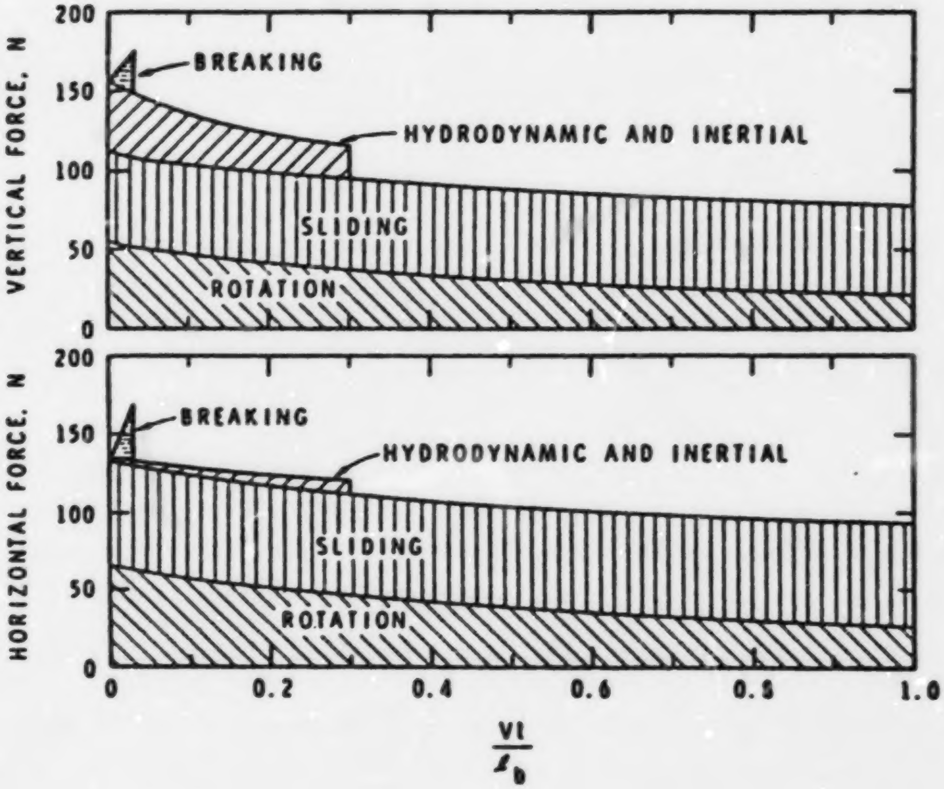

Force variations for the case $h = 40$ mm, $B = 0.75$ m, $V = 0.5\ \mathrm{m{\cdot}s^{-1}}$, $\alpha = \pi/4$, $E = 40$ MPa, $\sigma_f^* = 20$ kPa, $\mu = 0.1$, $\beta = \pi/3$

Figure 5.3.15 Three-Dimensional Calculation of Ice Forces on a Sloping Structure (from Frederking, 1979)

5.3.3.5 Sheet Ice Loads: Three-Dimensional Theory (Plastic)

An approach for ice forces on a conical structure using plastic limit analysis has been proposed by Ralston (1977). His results can be expressed as equations for H and V:

$$H = A_4\,[A_1\,\sigma_f\,t^2 + A_2\,\rho_w\,g\,t\,D^2 + A_3\,\rho_w\,g\,t\,(D^2 - D_T^2)]$$

$$V = B_1\,H + B_2\,\rho_w\,g\,t\,(D^2 - D_T^2) \qquad \text{...Eqn.'s 5.3.15}$$

where D_T is the top diameter and D is the waterline diameter. A_1 and A_2 are coefficients dependent on $\rho_w.g.D^2/\sigma_f.t$, and A_3, A_4, B_1 and B_2 are coefficients dependent on the cone angle α and friction μ. Values for the coefficients are reproduced in Figure 5.3.16.

It should be noted that Ralston's analysis included both the forces due to ice ride-up and ice breaking. In the horizontal force portion of Eqn.'s 5.3.15 the first two terms are due to ice breaking and the third term results from the ice pieces sliding over the surface of the cone.

It is of interest to note that for narrow structures Ralston's theory predicts the ride-up component to be small compared with the ice breaking component, as shown in Figure 5.3.17. For wide structures the ice ride-up component becomes a larger part of the total force, as shown in Figure 5.3.18.

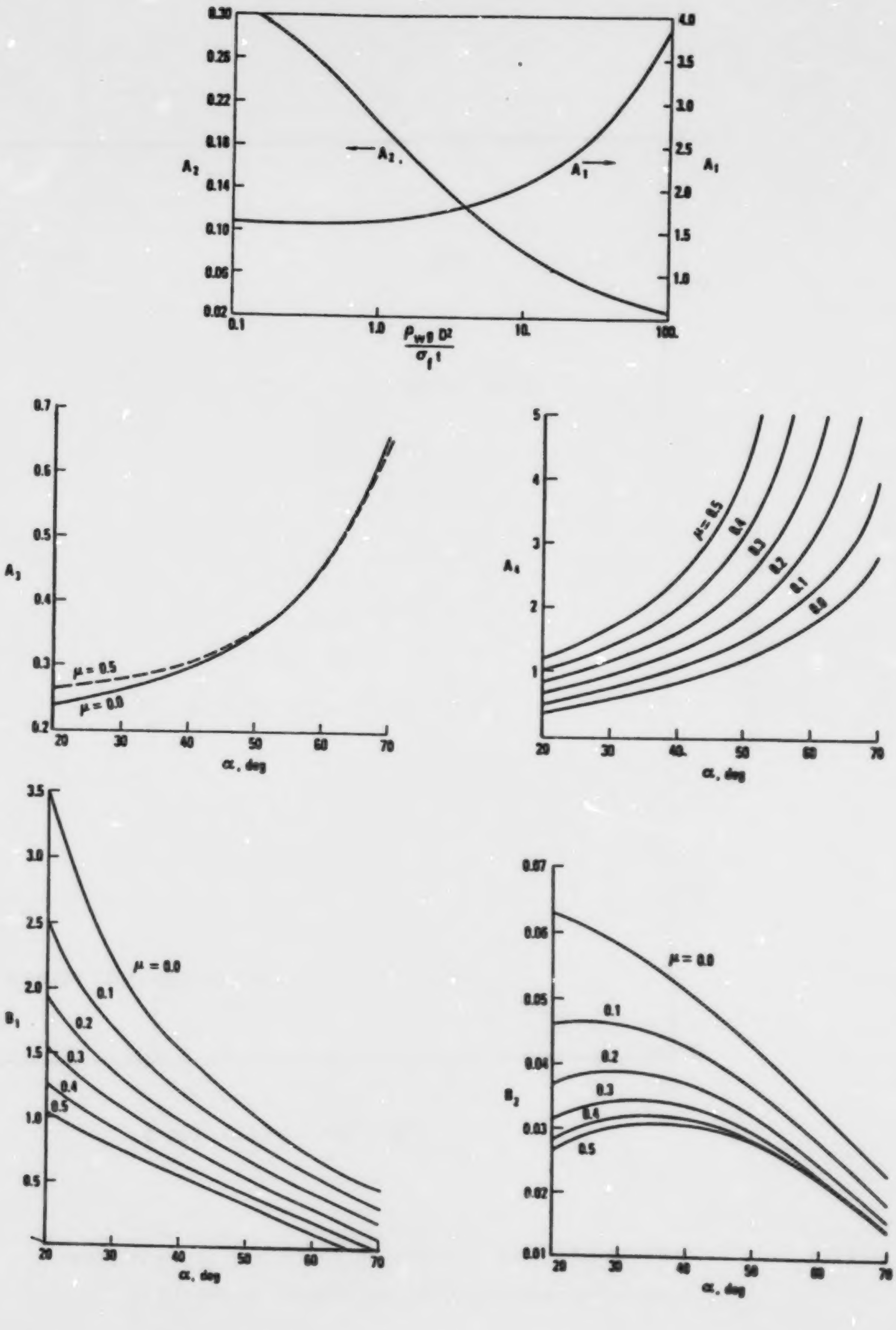

Figure 5.3.16 The A and B Coefficients for Ralston's Plastic Analysis (from Ralston, 1977)

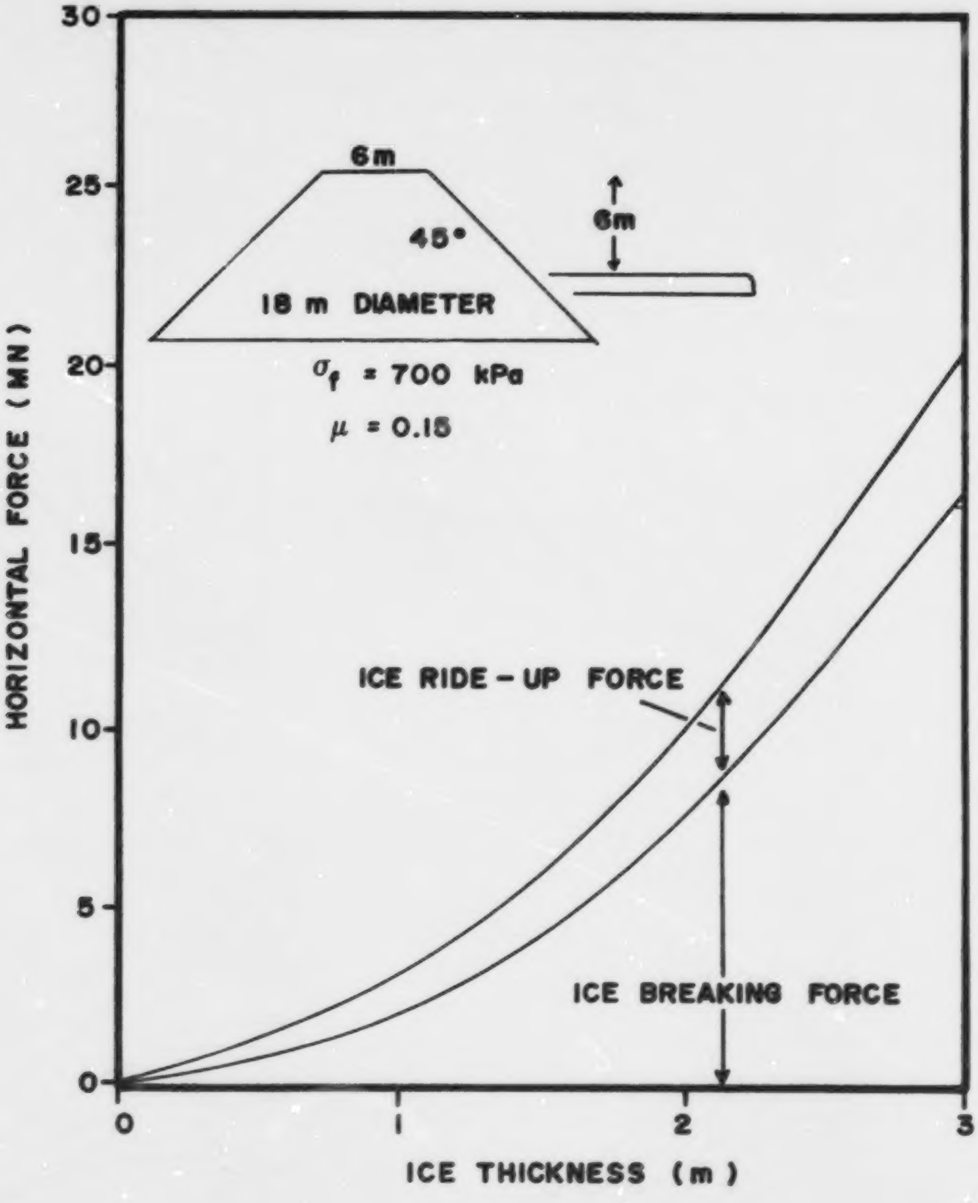

Figure 5.3.17 Horizontal Force versus Ice Thickness for a Narrow Structure Calculated Using Ralston's Theory

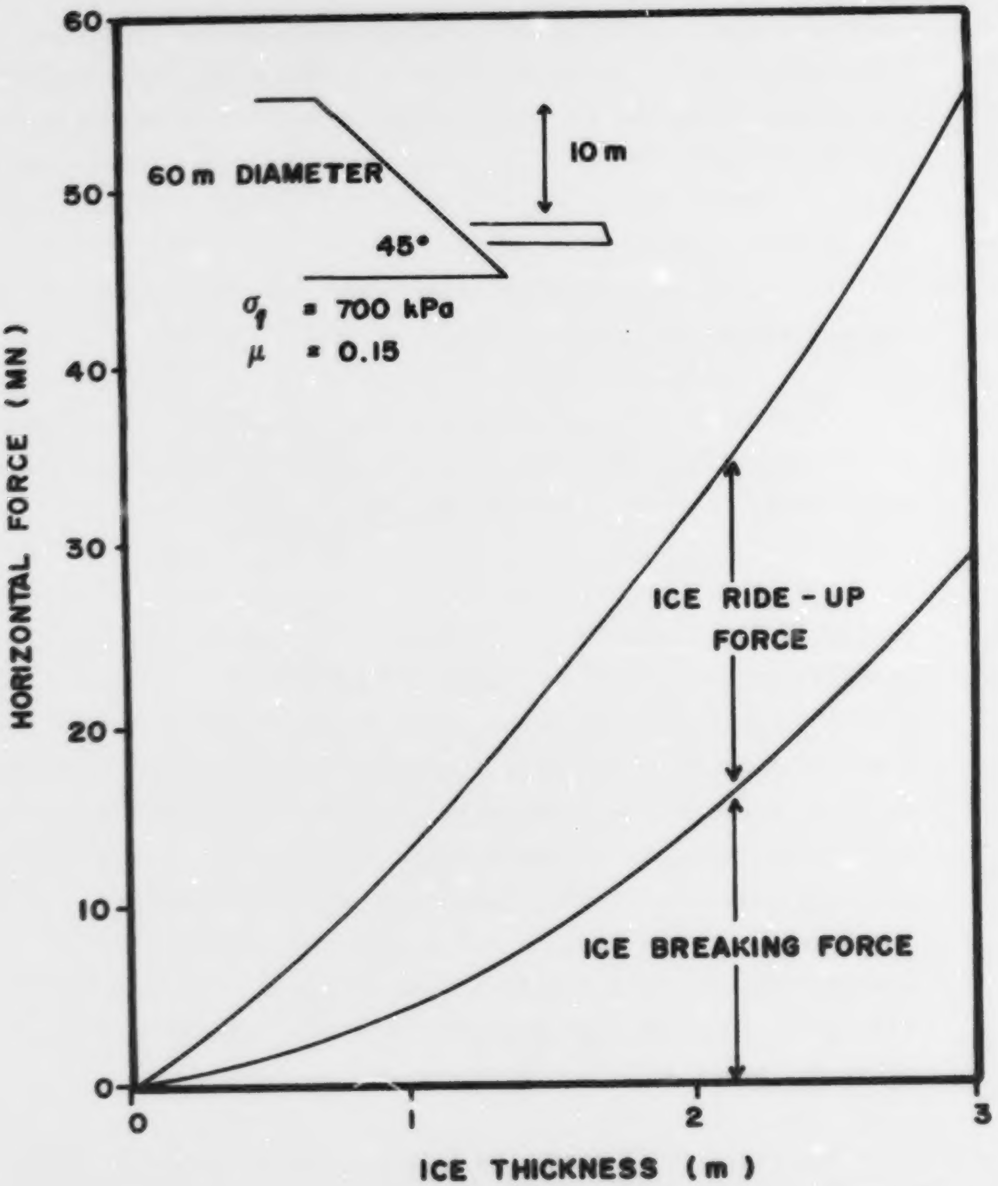

Figure 5.3.18 Horizontal Force versus Ice Thickness for a Wide Structure Calculated Using Ralston's Theory (after Croasdale, 1980)

5.3.3.6 Sheet Ice Loads - Comparison With Experiments

In 1970 small-scale model tests were conducted using saline model ice in Arctec's model basin; the results were reported by Edwards and Croasdale (1976). Subsequently, additional model tests using synthetic ice (wax) were conducted for the purpose of validating math models (Edwards et al., 1974). About the same time, small-prototype experiments using a conical structure 3.05 m (10 ft) in diameter, and ice up to 45 cm (19 in) thick were conducted (see Verity, 1975, APOA 65 and APOA 82). The results from these early experiments have been compared with theory by various investigators.

Ralston (1977) compared his theory with results from Edwards and Croasdale (1976). This comparison showed good agreement between theory and experiment, as demonstrated in Figure 5.3.19.

Kry (1980) compared Ralston's theory with the results obtained by Verity (1975) in the Esso ice basin. The results from the tests which were compared to theory are tabulated in Table 5.3.1. Using the test parameters from the table, Ralston's theory was used to predict peak forces for each run. To provide an estimate of uncertainty associated with the calculated values, an overestimate was made by assuming the friction coefficient was 0.2 (rather than the measured value of 0.13). An underestimate was made by assuming that the ice clearing forces were only half those calculated by the model (corresponding to ice pieces covering only half of the cone surface when the peak breaking force occurred. The comparison is shown in Figure 5.3.20. The theory shows reasonable agreement with the experimental data, but tends to be conservative.

Semeniuk (1975) conducted a comprehensive comparison of three-dimensional elastic theory (Kim and Kotras, 1973; Semeniuk, 1975) with experimental data from Edwards et al. (1974) and Verity (1975). Typical comparisons are shown as Figures 5.3.21 and 5.3.22. The results show some scatter, but reasonably good agreement.

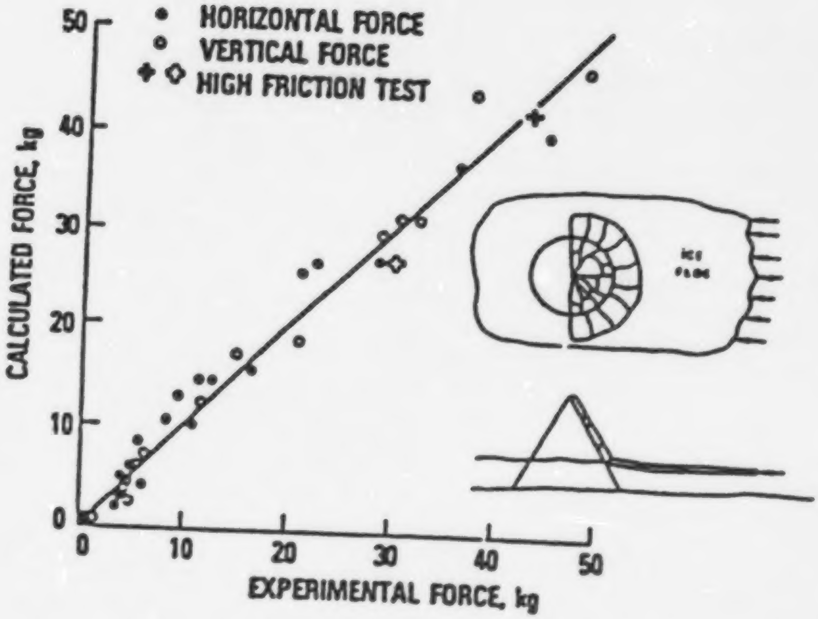

Figure 5.3.19 Comparison of Ralston's Theory with the Results of Test Data Presented in Edwards and Croasdale (1976), (after Ralston, 1977)

Table 5.3.1 Esso Ice Basin Data

Run Number	Ice Thickness (m)	Flexural Strength (MPa)	Horizontal Force (kN)	Number of Force Peaks
1	0.0681	0.210	3.46 ± 1.3	2
2	0.132	0.495	23.7 ± 5.7	10
3	0.191	0.495	34.3 ± 4.6	4
4	0.235	0.218	30.5 ± 6.1	14
5	0.155	0.477	11.8 ± 5.3	8
6	0.155	0.477	17.0 ± 2.6	8
7	0.153	0.477	12.6 ± 2.1	3
8	0.141	0.238	12.5 ± 1.4	37
9	0.135	0.238	13.8 ± 1.1	8
10	0.135	0.238	16.1 ± 1.8	18
11	0.146	0.238	16.1 ± 0.3	2

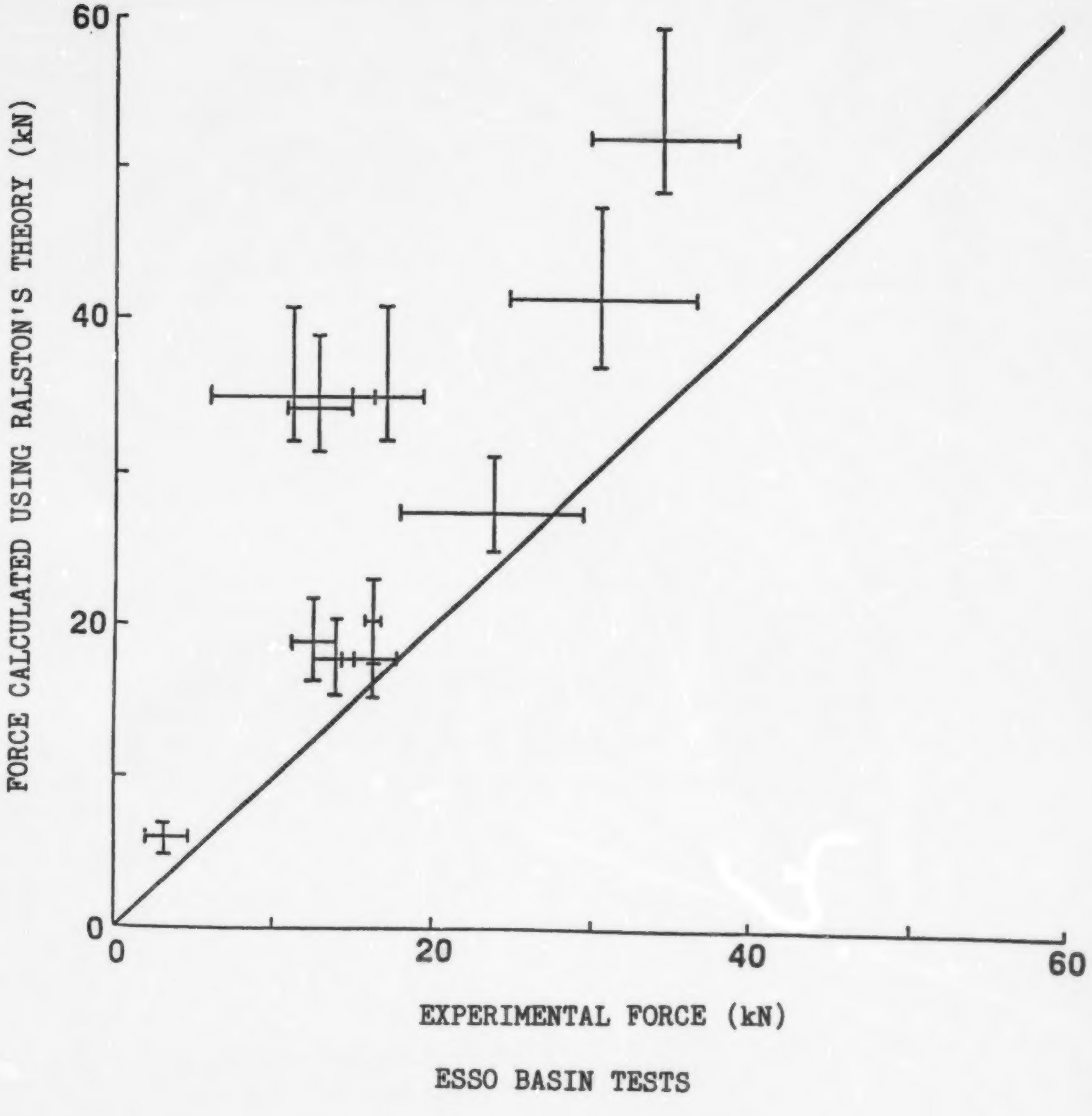

Figure 5.3.20 Comparison of Force Calculated Using Ralston's Theory with Test Results from the Esso Basin (after Kry, 1980)

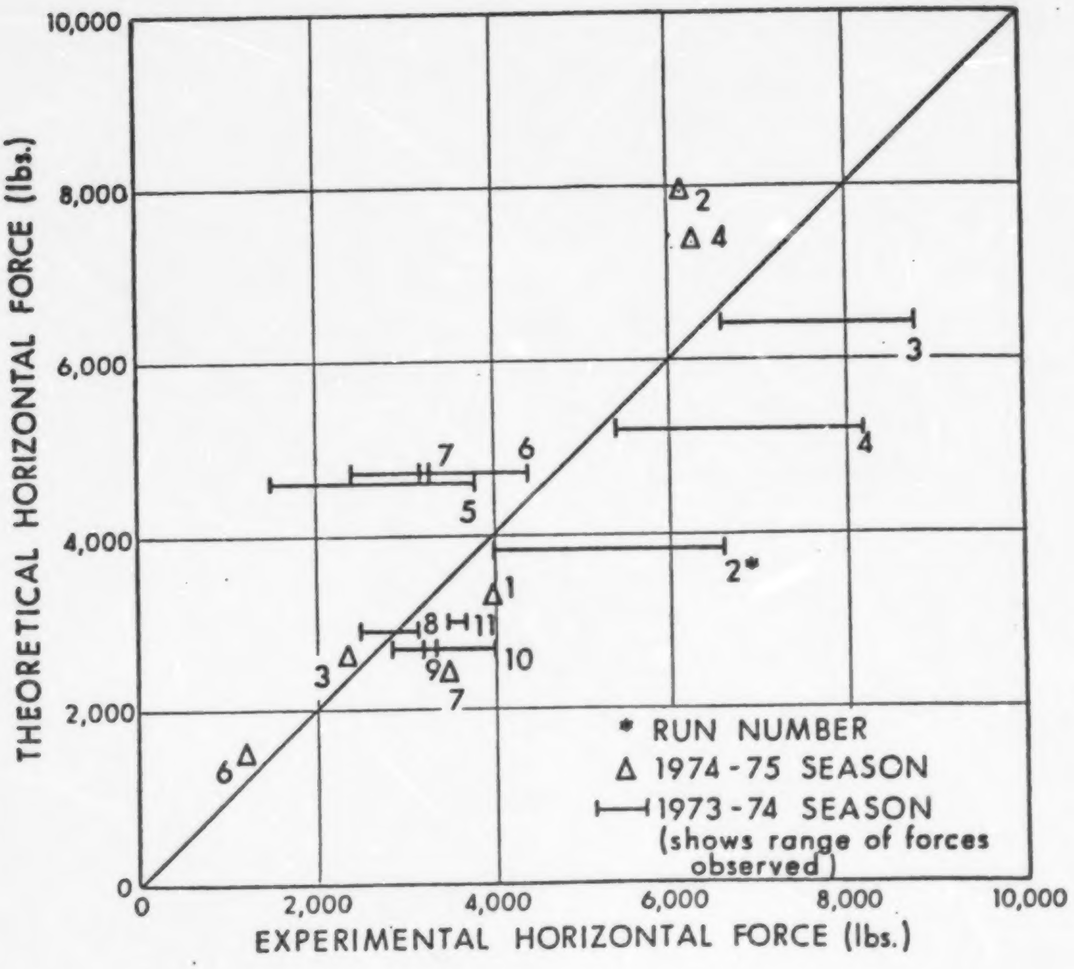

Figure 5.3.21 Comparison of Horizontal Force Calculated by Kim and Kotras (1973) and Seminuk (1975) with Test Results from the Esso Basin (Edwards et al., 1974; Verity, 1975). (after Semeniuk, 1975)

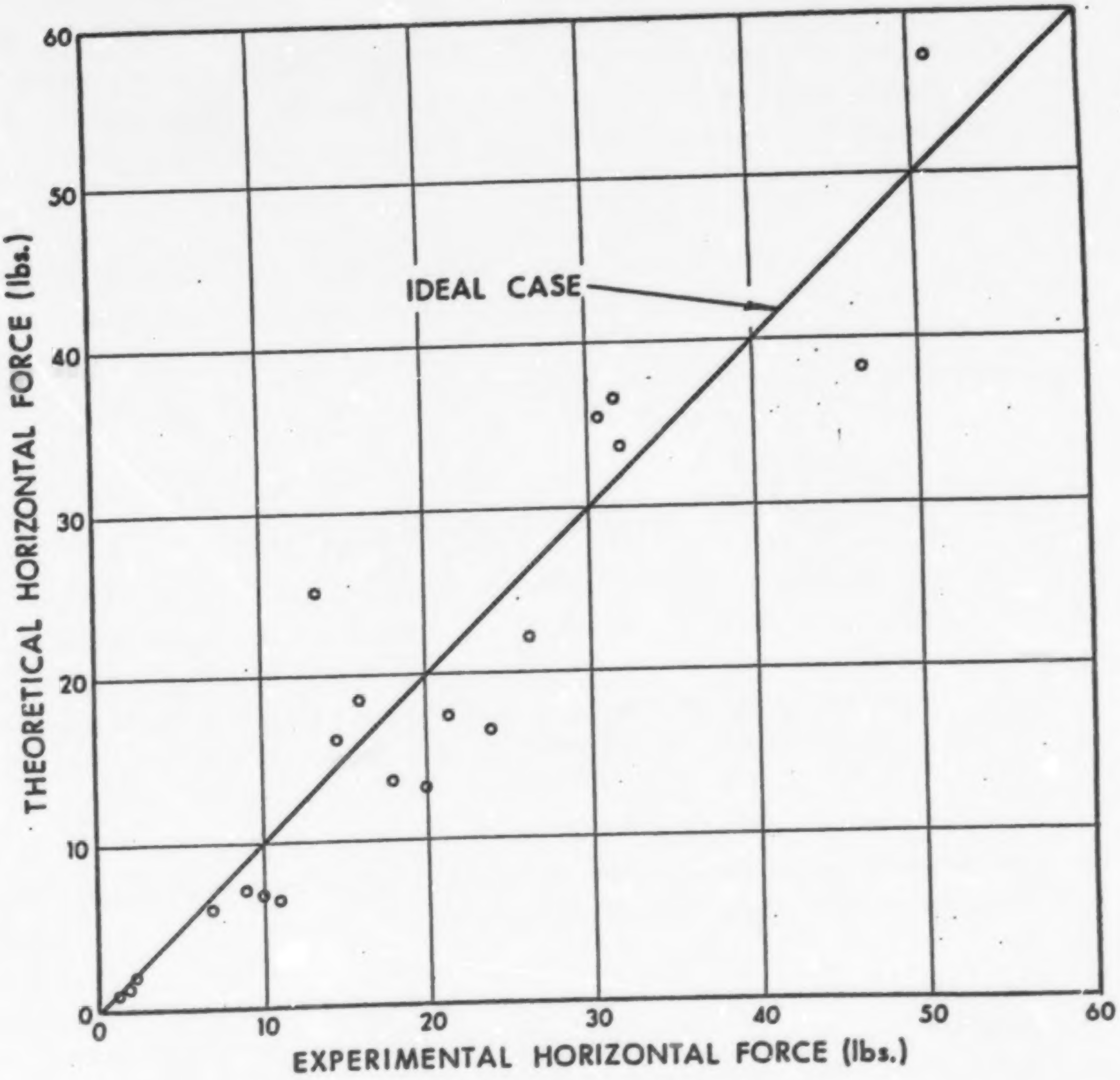

Figure 5.3.22 Comparison of Horizontal Force Calculated for Wax Model Ice with Test Results (after Semeniuk, 1975)

Timco (1984) conducted a series of model tests on an upward-breaking 45°inclined plane using carbamide (urea) model ice. The structure was 0.3 m wide. He compared his results with Croasdale's (1980) two-dimensional theory and with Frederking's (1979) three-dimensional theory. The results are shown in Figure 5.3.23. Both theories tended to under predict the experimental values. Not surprisingly, the three-dimensional theory gave better agreement.

Additional comparison of theory and experiment were made by Frederking and Timco (1985). They also compared breaking, rotation and sliding loads. In their experiments, agreement was quite good, with theory generally over predicting by about 20% (see Figure 5.3.24).

5.3.3.7 Sheet Ice Loads - Comparison of Methods

In his review of ice forces on piers and piles, Neill (1976) used an example of a 3.05 m (10 ft) diameter conical tower to compare various methods for ice forces on sloping structures. Croasdale (1980) extended this comparison to include the methods of Ralston, Croasdale, Bercha and others. The comparison is shown in Table 5.3.2.

An immediate observation from the forces shown in Table 5.3.2 is that all the more recent formulae and correlations generally give higher forces than the methods originally listed by Neill.

None of the original formulae listed by Neill took account of friction, but even if the friction is set to zero the formulae of Bercha and Ralston still yield higher forces than the first four methods. Although not stated directly, it is implied that the three-dimensional models of Bercha and Ralston assumed simultaneous failure of the ice across the width of the structure, and this perhaps represents an upper bound. For example in Bercha's model the ice force is derived assuming all the loaded ice wedges fail simultaneously. If in fact they do not, then presumably the peak ice breaking force will be lower.

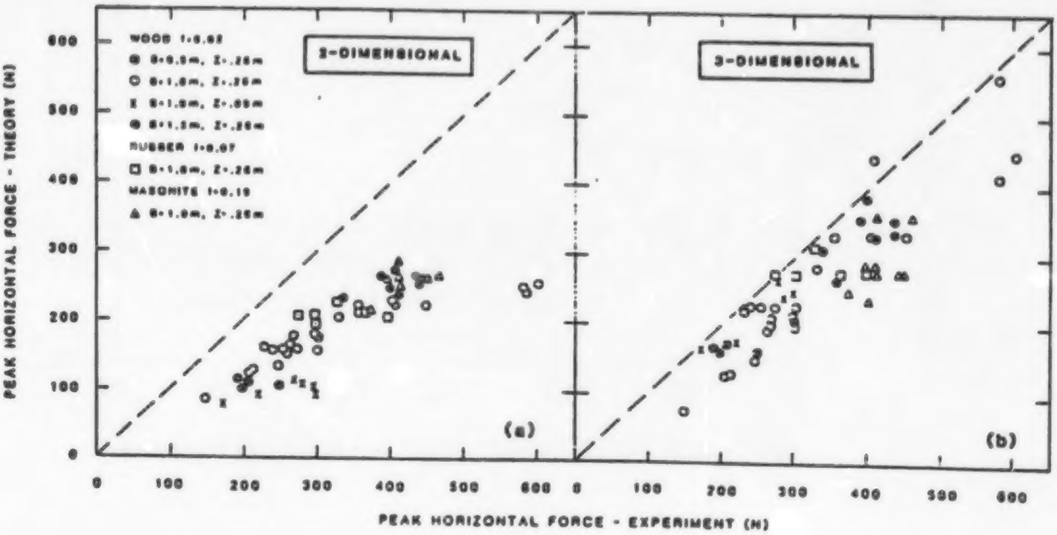

Figure 5.3.23 Peak Ice Force Calculated Using (a): Two-Dimensional Theory and (b) Three-Dimensional Theory, versus an Experimentally Measured Peak Force (after Timco, 1984)

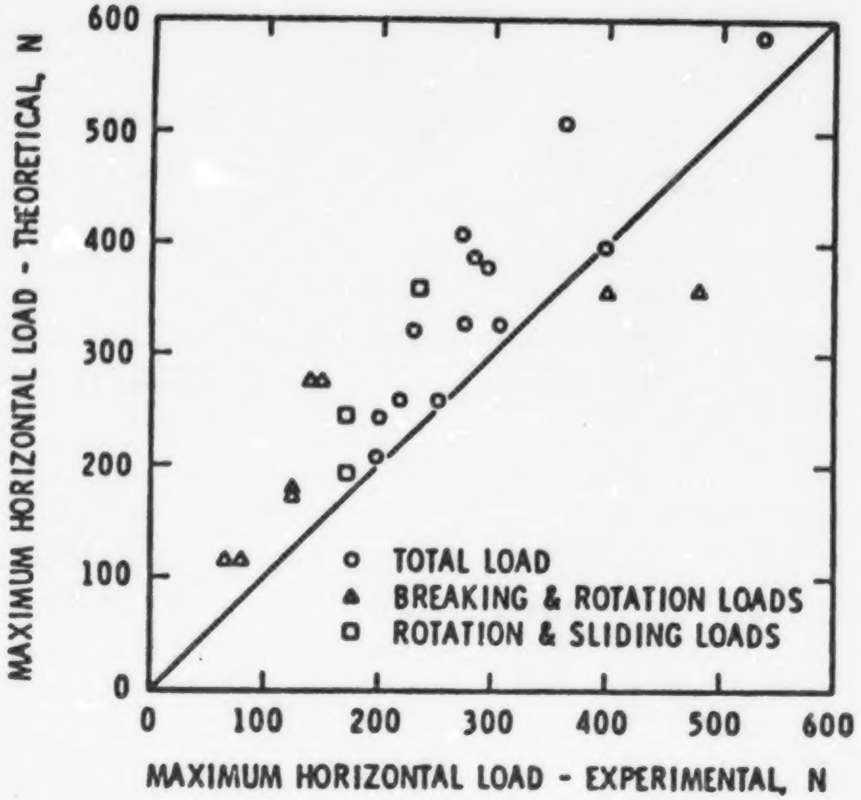

Figure 5.3.24 Comparison of Measured and Predicted Loads for Ice Failing Against a 45° Upward Breaking Inclined Plane (after Frederking and Timco, 1985)

Table 5.3.2
Horizontal Force on Conical Tower Calculated by Ten Methods

ASSUMPTIONS: D = 3.05 m (10 feet)
t = 0.91 m (3 feet)
crushing strength = 1.05 MPa (150 psi)
Poisson's Ratio = 0.33
Modulus of Elasticity = 7 GPa (1 x 10^6 psi)
angle of cone = 45 degrees
freeboard = 1.53 m (5 feet)

Source of Formula	Breaking Force (kN)	Ride-Up Force (kN)	Total Force (kN)
Afanasev et al. (1971)	694	---	694
Dany's Procedure as reported in Neill (1976)	249	126	375
USSR Code SN 76-66 (Appendix 2)	543	---	543
Korzhavin's Formula	463	---	463
Bercha and Dany's (1975)			
friction = 0.0	954	---	954
friction = 0.15	1335	---	1335
Ralston			
friction = 0.0	1400	---	1400
friction = 0.15	1964	---	1964
Edward and Croasdale	1384	150	1534
Simple 2-D Theory friction = 0.15	84	70	154
Simple 2-D Theory (Adjusted) friction = 0.15	1200	70	1270
Tryde (Sloping Wedge)			
E = 7000 MPa	485	---	485
E = 200 MPa	1200	---	1200
Crushing Force strength = 2.8 MPa (400 psi) k = 0.5	3886	---	3886
Crushing Force strength = 4.2 MPa (600 psi) k = 0.5	5829	---	5829

It is of interest to note that the model data of Edwards and Croasdale, if extrapolated to this example, gives forces comparable with those predicted by Bercha and Ralston. This fact lends support to the validity of their predictions.

As expected, the simple two-dimensional theory under predicts the ice breaking component. This is because the structure width is small compared with the characteristic length of the ice sheet. If the two-dimensional force is adjusted by the ratio of the length of the circumferential crack to the structure width, then the force predicted by the two-dimensional theory agrees quite well with the methods of Bercha and Danys (1975) and Ralston (1977). The length of the circumferential crack is about $\frac{1}{4}\pi^2 l$ where l is the characteristic length as defined by Equation 5.3.14.

Also, based on Table 5.3.2 it is seen that, even using the most conservative predictions, the forces on the conical tower are significantly less than typical crushing forces on a cylindrical structure of the same diameter.

Finally, it is seen that for narrow conical structures the ride-up force is small compared to the ice breaking force.

Until better test data are available, designers would be wise to use the most conservative prediction techniques (e.g. Ralston, Bercha and Danys, or the adjusted two-dimensional theory).

Bercha's Example: Conical Structure With a Waterline Diameter of 18.3 m

To examine the results for a wider structure consider the example of an 18.3 m diameter cone, with the other variables as defined in Table 5.3.3. This is the largest diameter structure considered by Bercha and Danys (1975).

Again, the Ralston formula predicts the highest force, but the ice breaking force is in reasonably close agreement with Bercha and Danys.

The most significant point about the data presented in Table 5.3.3 is that the ice ride-up or clearing forces are now quite large. The simple two-dimensional theory probably over predicts the ride-up force but both the correlations of Ralston and Edwards and Croasdale suggest ride-up forces of around 1 MN. Clearly for a structure of this width the ride-up forces can not be ignored.

A Wide Sloping Structure

The horizontal forces acting on a structure 60 m wide are compared in Table 5.3.4. In this case only forces derived using the Ralston formula and simple two-dimensional theory are compared. The agreement for total force is quite good, but the two-dimensional theory consistently predicts lower ice breaking forces than ride-up forces. This is to be expected for the reasons already discussed in Section 5.3.3.3, i.e. that for narrow structures the zone of failure is wider than the structure, therefore the ice pieces do not ride-up but move to the side.

Again the ice ride-up or clearing forces are very significant and can not be ignored for such a wide structure. Perhaps more importantly the actual clearing mechanism needs to be further addressed when considering such wide structures, especially interactions with the superstructure.

As a further comparison between elasticity and plasticity methods, calculations by four methods for a full scale cone structure are performed.

Table 5.3.3
Horizontal Force on a 18.3 m Diameter Conical Tower
(Bercha's Example)

ASSUMPTIONS:
D = 18.3 m (60 feet)
t = 0.91 m (3 feet)
crushing strength = 0.70 MPa (100 psi)
Poisson's Ratio = 0.33

Modulus of Elasticity = 7 GPa (1×10^6 psi)
angle of cone = 45 degrees
freeboard = 6.1 m (20 feet)
friction coefficient = 0.15

Source of Formula	Breaking Force (kN)	Ride-Up Force (kN)	Total Force (kN)
Bercha and Danys (1975)	1558	---	1558
Ralston (1977)	1964	1196	3160
Simple 2-D Theory	355	1896	2251
Simple 2-D Theory (Adjusted)	845	1896	2741
Afanasev et al. (1971)	711	---	711
Edwards and Croasdale (1977)	922	900	1822

Table 5.3.4 Horizontal Force on Wide Conical Structure

ASSUMPTIONS:
D = 60.0 m (200 feet)
crushing strength = 0.70 MPa (100 psi)
Modulus of Elasticity = 7 GPa (1×10^6 psi)
angle of cone = 45 degrees
freeboard = 10 m (33 feet)
friction coefficient = 0.15

Source of Formula	Ice Thickness (m)	Breaking Force (kN)	Ride-Up Force (kN)	Total Force (kN)
Ralston (1977)	0.5	1574	4385	5959
Simple 2-D Theory	0.5	559	5625	6184
Ralston (1977)	1.0	4822	8770	13592
Simple 2-D Theory	1.0	1330	11250	12580
Ralston (1977)	2.0	14855	17540	32395
Simple 2-D Theory	2.0	3162	22500	25662

The results of this comparison are shown in Figure 5.3.25.

It should be noted that the Frederking and Timco method is actually derived for an inclined plane and not a cone. Also, the rotation term has been added directly to the breaking and ride-up terms. As discussed previously, the breaking and rotation terms should not be added as they occur sequentially. Also it is considered that the piece size assumed in the rotation term is too large, hence the rotation component is probably very conservative.

5.3.3.8 Sheet Ice Loads - Clearing Loads on a Superstructure

If a sloping structure has a wide superstructure and it is subject to thick ice interaction, then forces on the vertical portion of the superstructure, above the sloping face, have to be considered. Theoretically, the kind of interaction which might occur is shown conceptually in Figure 5.3.26.

In this situation, a simple equation for H (ignoring buoyancy) can be written as:

$$H = 3 \rho_i t^2 \frac{1.5 \cos(\varphi) + 0.5 \sin(\varphi)}{3 \sin(\varphi) - \cos(\varphi) - \mu[3 \cos(\varphi) + \sin(\varphi)]}$$

...Eqn. 5.3.16

The contribution and relative magnitude of this load on a wide structure is shown in Figure 5.3.27. For thick ice, the load is almost equal to the loads due to breaking and ride-up on the lower slope. Furthermore the total load approaches typical global ice crushing loads, which implies that the advantage of a sloping structure has been lost.

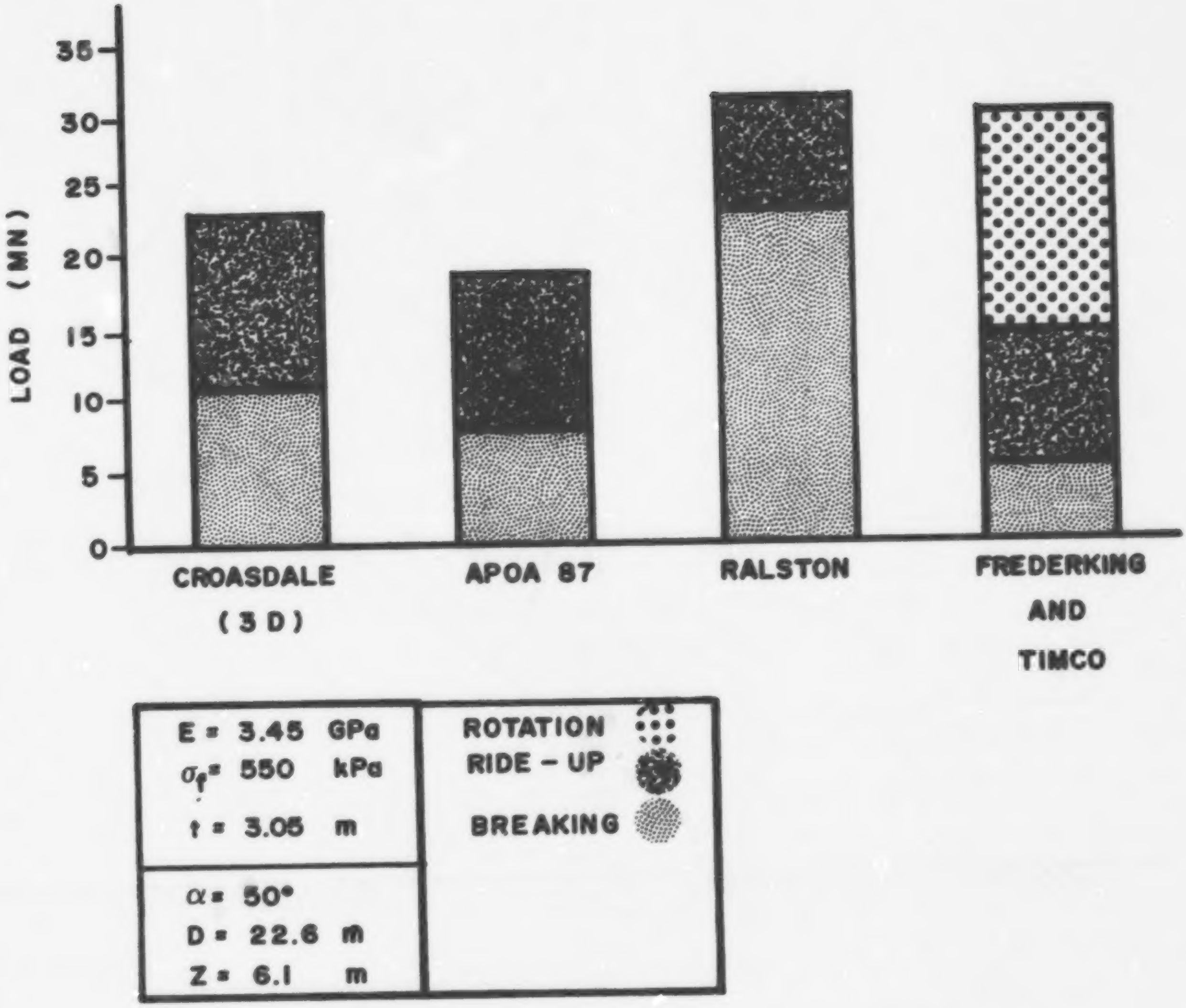

Figure 5.3.25 Comparison of Loads Calculated for Interaction of Sheet Ice With a Conical Structure

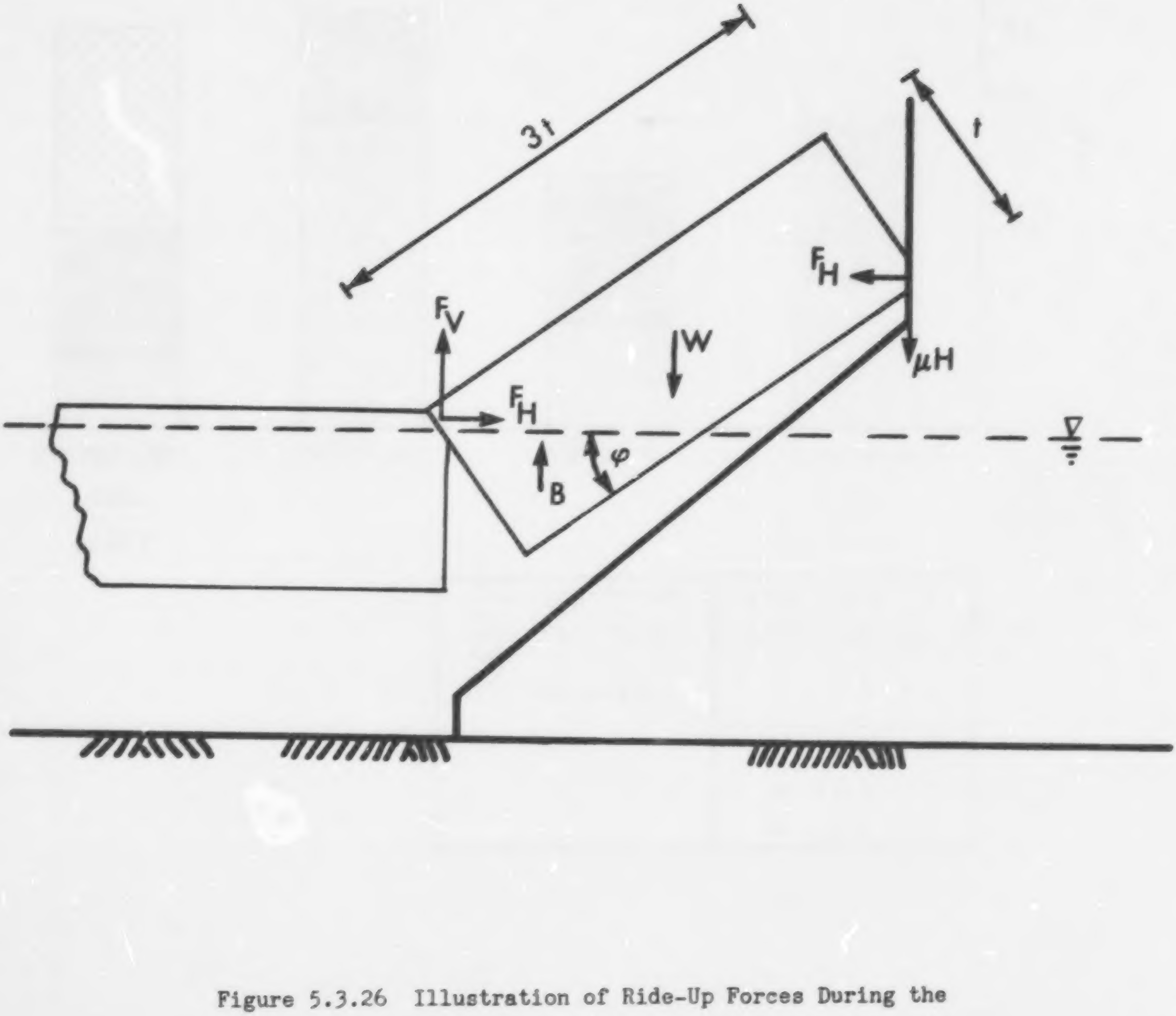
3t
t
F_H
F_V
W
μH
F_H
B
φ

Figure 5.3.26 Illustration of Ride-Up Forces During the Interaction of an Ice Sheet With a Sloping Structure

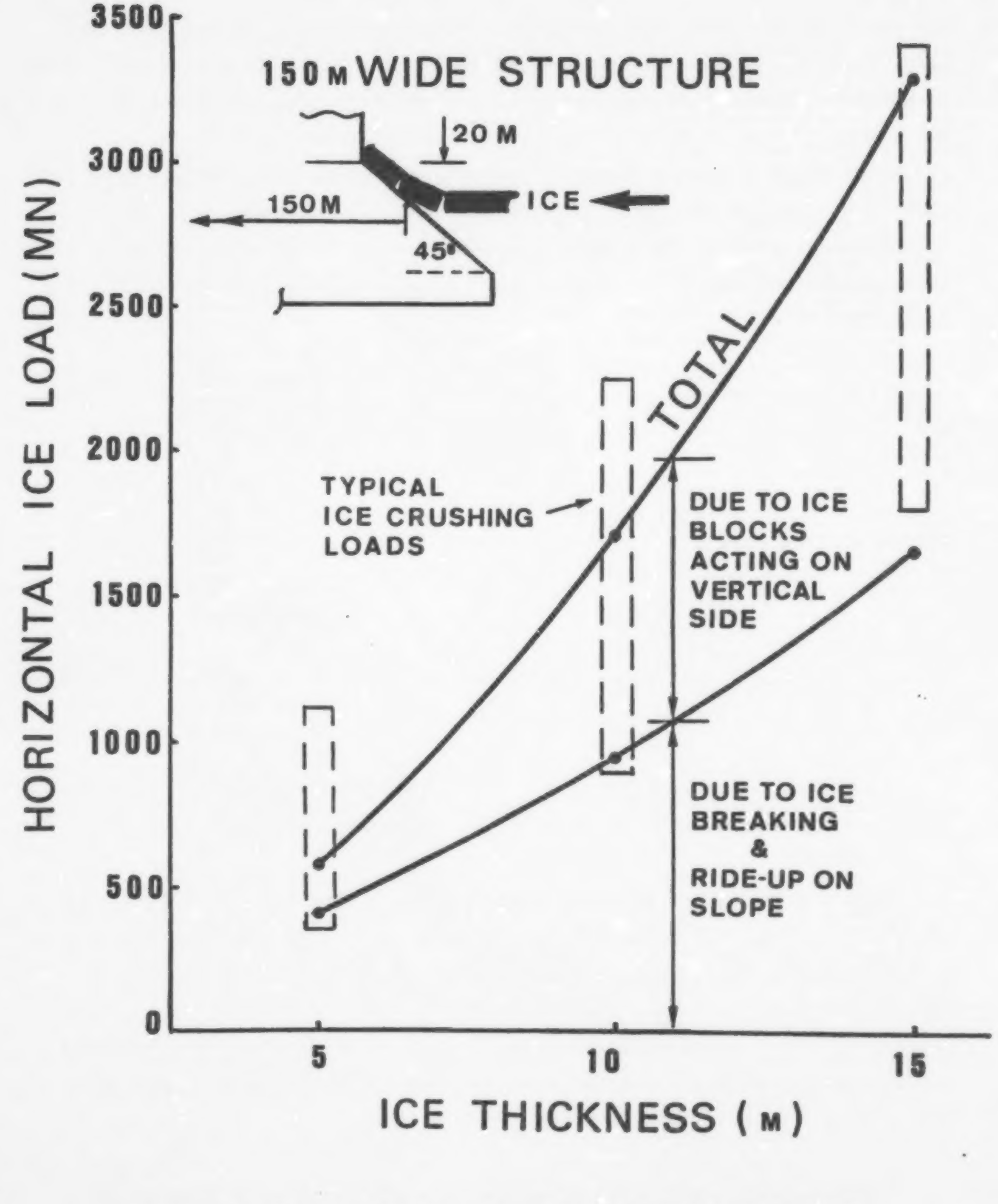

Figure 5.3.27 Illustration of Horizontal Load on a Wide Structure, and the Load Breakdown into that Acting on the Vertical Portion of the Structure and the Ice Breaking and Ride-up Portions

5.3.4 Adfreeze Loads

In the nearshore arctic environment the ice surrounding a structure can remain stationary long enough for the ice to freeze to the structure. Also, vertical motions of the ice due to tidal action can be so small that an adfreeze bond can develop between the ice sheet and the structure. Once the ice sheet starts to move again, sliding motion between ice and structure first requires breaking the adfreeze bond. For certain types of sloping structures the force required to fail the adfreeze bond can be significantly greater than the force needed to fail the ice in bending. In these situations the force to fail the adfreeze bond can become the design force for the structure.

In the arrangement shown in Figure 5.3.28 the adfreeze force is given by:

$$\text{Adfreeze force} = \frac{\pi\, t\, q\, D}{\sin(\alpha)\cos(\alpha)} \qquad \text{...Eqn. 5.3.17}$$

where t is the ice thickness, α is the slope angle, D is the structure diameter and q is the adfreeze bond strength.

Adfreeze loads, accounting for ice pieces frozen onto the slope of the structure were calculated in APOA 57 (see Semeniuk, 1975).

With regard to the adfreeze shear strength (see Section 3.3.5), there have been several strength studies performed on laboratory samples, usually on a very small scale, and usually at high strain rates. The range of values obtained from these studies is quite wide. For example, Sackinger (1977) measured about 0.5 MPa with uncoated steel at -15°C and 0.4 ppt salinity; but at higher temperatures the adfreeze strength was less.

Oksanen (1983) performed adhesion strength tests on a variety of

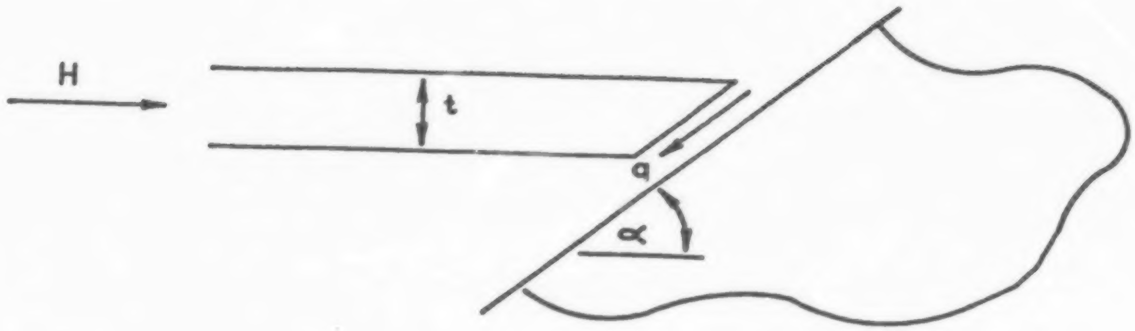

Figure 5.3.28 Illustration of Adfreeze Force

materials at three temperatures (-5, -10 and -15°C) but with fresh ice. For steel he measured 0.46 MPa at all temperatures. With an Intertuf Epoxy, 0.13 MPa, and PTFE, 0.07 MPa.

Saeki et al., (1981) measured adhesion strengths for steel, concrete, painted steel and corroded steel for sea ice at -2.0°C. Typical values for clean steel were in the range 100 to 300 kPa (14 psi to 42 psi), for painted steel much lower, and for corroded steel in the range of 400 to 560kPa (56 to 80 psi).

Finally, work was done by Arctec Canada in 1975 (APOA 85) to investigate adfreeze strengths on urethane coated steel. The study indicated that at -5°C, the maximum adfreeze strength was 400 kPa (54 psi) with fresh water, and only 18 kPa (2.6 psi) at 6 ppt salinity.

Most adfreeze strength values are quoted (and measured) at high strain rates. In landfast ice areas, however, ice movement events start at slow strain rates, even if eventually quite high movement rates occur. This movement pattern is usually recognized when calculating forces against a vertical structure by associating low strain rate ice strength with a contact factor of 1.0 (see Section 5.2.3.2 for a discussion of the contact factor). Subsequent higher strain rates have associated with them lower contact factors; the implication being that break-out has occurred at the slow strain rates (with associated lower ice strength).

This approach can be used in considering adfreeze forces. For example it might be assumed that the adfreeze bond is broken at strain rates as low as 10^{-5} or 10^{-6} s^{-1}. What is known about adfreeze strengths at these strain rates? No actual test data are available but perhaps one can synthesize a relationship by assuming that adfreeze shear strength varies as a function of strain rate in the same way that uniaxial compressive strength does.

Such an approach was developed by Croasdale (1984). Based on a conservative adfreeze strength of 700 kPa (100 psi) at high strain rates, the corresponding value at low strain rates was about 100 kPa (or 15 psi).

5.3.5 Loads on Upward Breaking Conical Structures due to Consolidated Ridges

5.3.5.1 Introduction

Solid multi-year (consolidated) ridges occur within the polar ice and represent a severe loading condition for arctic offshore structures. Multi-year ridges up to 15-20 m thick are not uncommon and are fully consolidated.

Early approaches assumed that ridges could be treated as simple beams on elastic foundations. Solutions for an infinitely long ridge, acting broadside on a structure were published by Croasdale (1975). More sophisticated mathematical modeling, extensive physical modeling, and experiments in the Esso ice basin took place in the 1970's. An elastic ridge model accounting for break-out from the adjacent sheet was developed in APOA 57 and was computerized in APOA 87. Recent work by Marcellus et al., (1986) concentrates on ridges which may interact with bermed structures for any orientation of ridge within the floe.

In 1978, Lewis and Croasdale (1978) published results from early model tests. Semeniuk (1975) compared the theoretical model developed in APOA 57 with experiments conducted in model tanks and in the Esso basin.

Abdelnour (1981) published results from extensive ridge modeling for Esso in APOA 86. He compared the results with elastic theory.

Wang (1984) published results of model tests conducted for Exxon in AOGA 96 and he compared the results with a theory based on the principles of plasticity.

5.3.5.2 Elasticity Theory

As a first approximation multi-year ridges can be considered as floating beams infinitely long. Failure loads can be calculated using the theory of elastic beams on elastic foundations (Hetenyi, 1946; Croasdale, 1975).

Observations of ridge/structure interaction in model tests (Lewis and Croasdale, 1978) indicates that the ridge usually fails first with a centre crack at the point of interaction with the structure (see Figure 5.3.29). Using simple beam theory the vertical load necessary to cause this initial crack is given by

$$V_1 = \frac{4 I \sigma_f}{y l} \qquad \text{...Eqn. 5.3.18}$$

where I is the second moment of area of the ridge cross section about its neutral axis, σ_f is the ice flexural strength, y is the distance to the surface in tension (in the case of an upward-breaking structure this is the top surface), and l is the characteristic length given by

$$l = [4 E I / \rho_i g b]^{\frac{1}{4}} \qquad \text{...Eqn. 5.3.19}$$

where b is the width of the ridge.

Although when the first centre crack has occurred the ridge can be considered broken, it can not pass around the structure without further breaking. Again, observations of tests indicate that the subsequent interaction mechanism is the formation of hinge cracks as shown in Figure 5.3.29. The vertical force to cause the hinge cracks is calculated

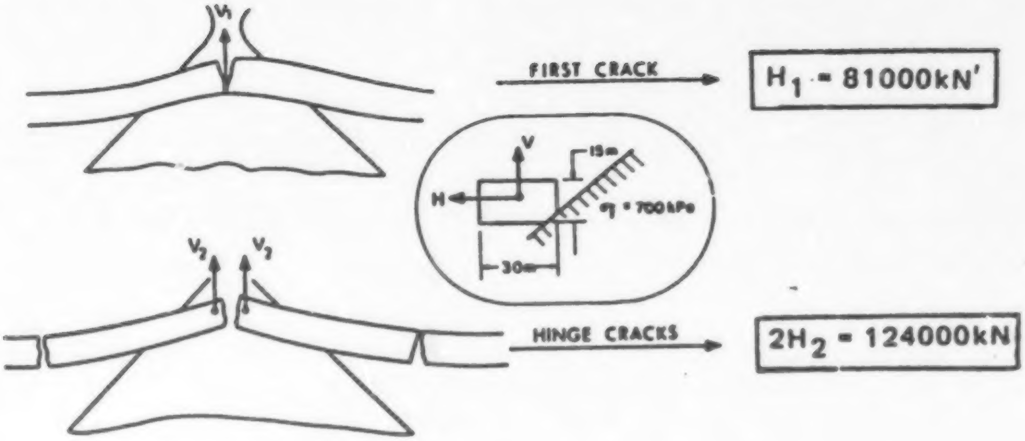
V1
FIRST CRACK
H1 = 81000kN'
V
15m
H
σf = 700kPa
30m
V2
V2
HINGE CRACKS
2H2 = 124000kN

Figure 5.3.29 Illustration of First Crack and Hinge Crack Definitions for a Conical Structure (after Croasdale, 1975, 1980)

by considering the simultaneous failure of two semi-infinite beams on elastic foundations, that is:

$$V_2 = \frac{6.17\ I\ \sigma_f}{y\ l} \qquad \text{...Eqn. 5.3.20}$$

In this case y is the distance from the neutral axis to the bottom of the ridge.

It will be noted from Equation 5.3.20 that the formation of the hinge cracks will generally cause greater loads on a structure than the load due to the initial crack.

For a ridge 15 m deep and 30 m wide, with a flexural strength of 700 kPa and an elastic modulus of 7 GPa, the vertical force to create the initial crack is 18.74 MN whereas the force to create the two hinge cracks is 28.9 MN.

The corresponding horizontal forces depend on the cone angle and ice-to-structure friction, that is:

$$H_1 = V_1 \frac{\sin(\alpha) + \mu\cos(\alpha)}{\cos(\alpha) - \mu\sin(\alpha)}$$

$$H_2 = V_2 \frac{\sin(\alpha) + \mu\cos(\alpha)}{\cos(\alpha) - \mu\sin(\alpha)}$$

...Eqn.'s 5.3.21

More sophisticated analyses of ridge loads can be performed using a more realistic ridge cross-section to calculate I and y and by incorporating torsion and shear stress. Also, the equations given above are for an infinitely long ridge. Ralston (1977) has pointed out that shorter ridges can cause greater loads than infinitely long ridges. The relationship derived by Ralston showing the effect of ridge length is reproduced in Figure 5.3.30. Obviously as the ridge gets shorter there is more chance of other interactions taking place. The ridge may simply rotate or the ice sheet may fail at the backside of the ridge (as has been incorporated in recent models of ridge/structure and ridge/berm interactions). Therefore, Figure 5.3.30 should be used with care.

A more sophisticated analysis accounting for the attached ice sheet, ridge shape and length was developed by Kim and Kotras (1973) and included in the computer program by Semeniuk (1975).

5.3.5.3 Plasticity Theory

Wang (1984) published a theory for ridges on cones based on the upper bound limit analysis and plasticity theory. The method accounts for ridge bending, attached ice sheet bending, ridge and ice sheet weight (or buoyancy) and friction between the ridge and cone. The author claims that the approach is more conservative than the elasticity method and gives better agreement with experiments. Unfortunately, the plasticity methods can not easily be reduced to a few sample equations for illustrative purposes. Wang does not provide details in his paper, and refers the reader to AOGA 96 for more information.

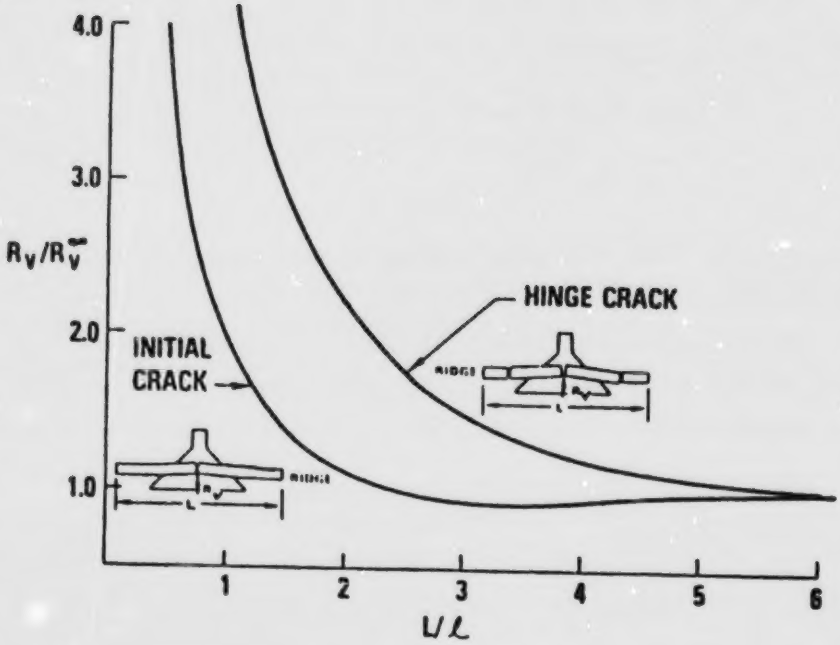

Figure 5.3.30 Illustration of First Crack and Hinge Crack Forces as a Function of the Length of the Ridge, for a Conical Structure (after Ralston, 1977)

5.3.5.4 Comparison With Experiments

Semeniuk (1975) conducted a comprehensive comparison between elastic theory and the model tests and ice basin experiments conducted up until that time. Some of these comparisons are shown in Figures 5.3.31 to 5.3.36. Semeniuk concluded that large scatter in the physical property data from the experiments created problems in comparing theory with experiment. He noted a difference of up to 27% for the horizontal ridge forces between theory and experiments with synthetic ice, although the vertical forces were in better agreement (suggesting problems in measuring the friction coefficient). In general, he suggests that elastic theory under predicts ridge forces by about 20%.

Other comparisons of theory with experiment for ridge loads have been published by Lewis and Croasdale (1978) and Abdelnour (1981).

Wang (1984) showed comparison of calculated forces using the plasticity approach, with previous experiments. He concludes that the plasticity approach gives better agreement than the elasticity method (see Figure 5.3.37).

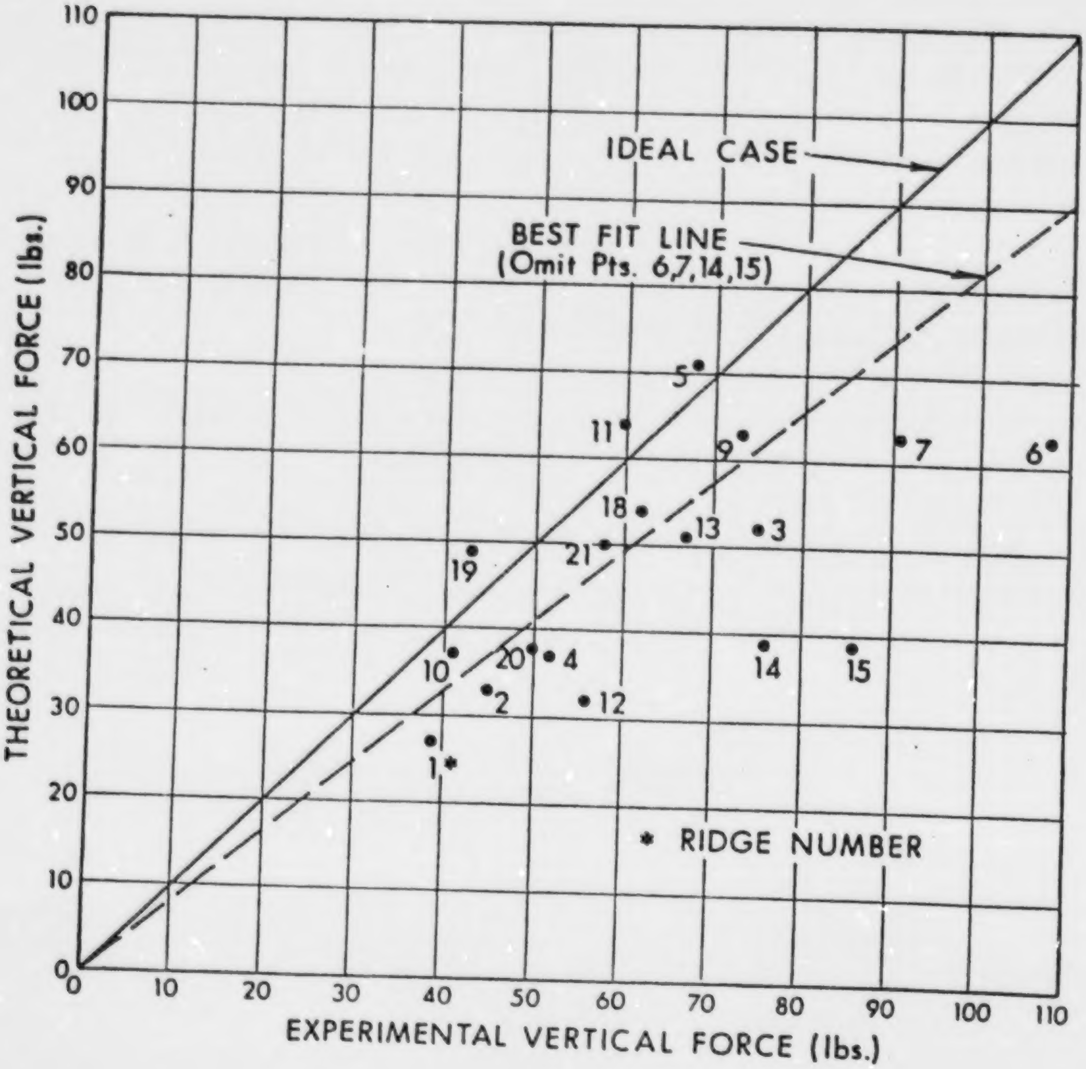

Figure 5.3.31 Vertical Force Comparison Between Theory and Experimental Results for Wax Ridge Tests (after Semeniuk, 1975)

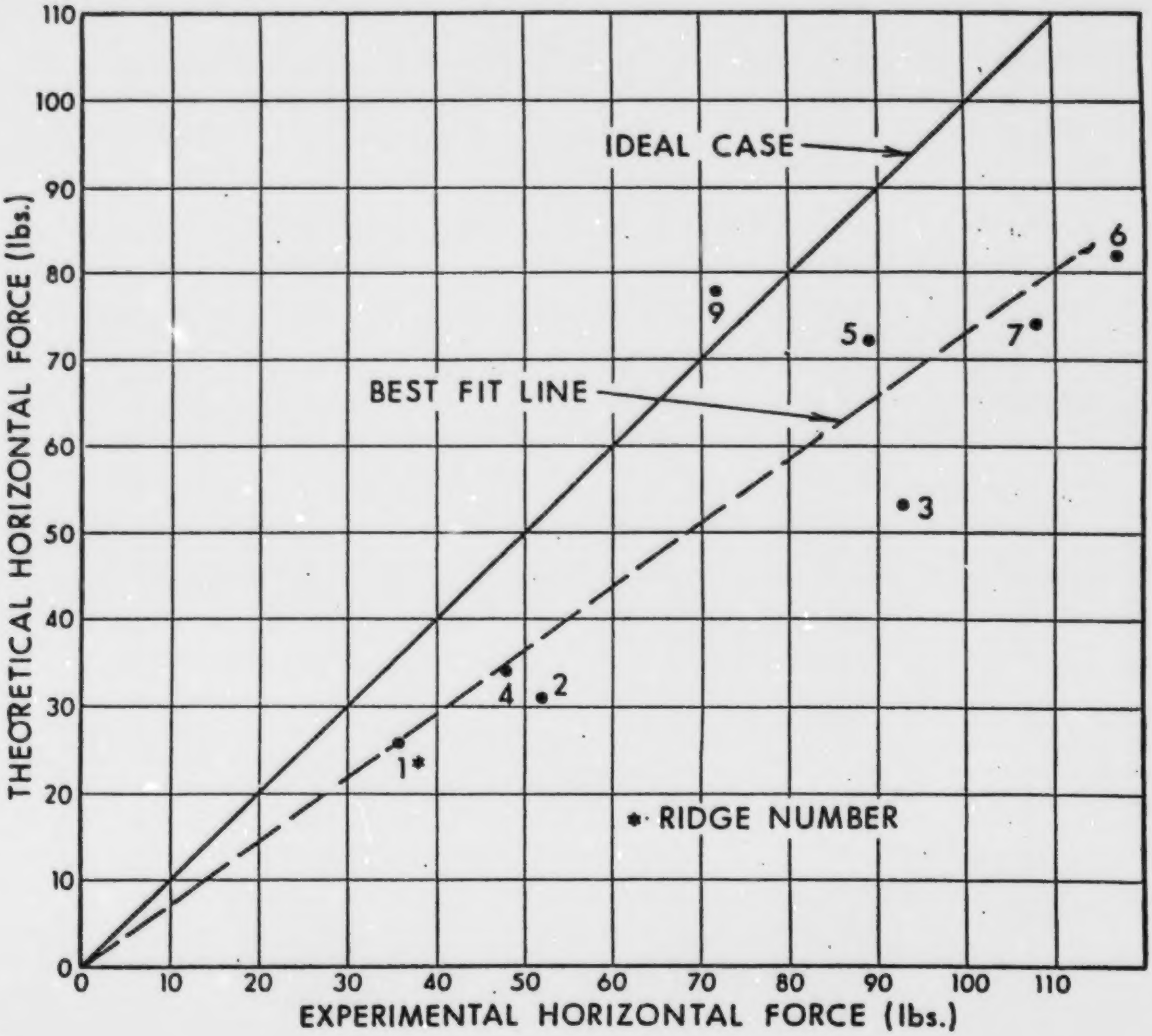

Figure 5.3.32 Horizontal Force Comparison Between Theory and Experimental Results for Wax Ridge Tests (after Semeniuk, 1975)

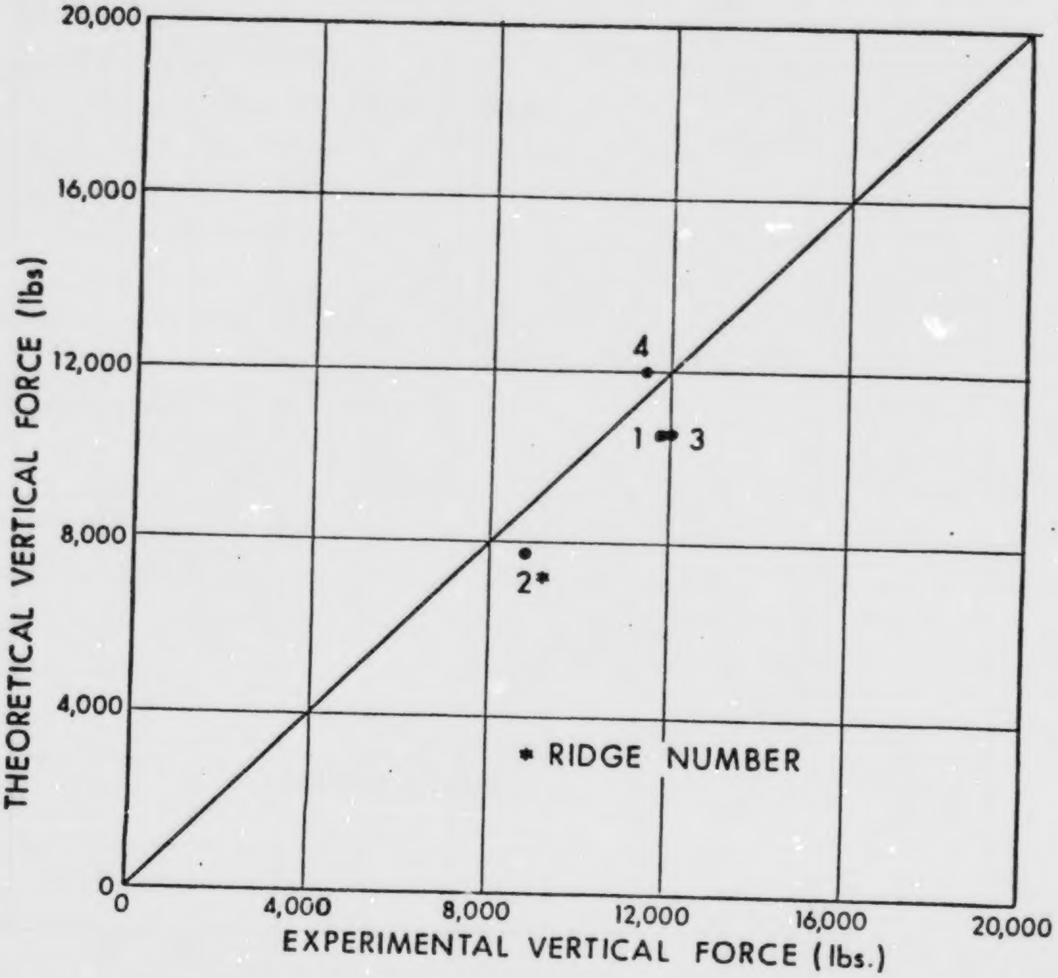

Figure 5.3.33 Vertical Force Comparison Between Theory and Experimental Results for Basin Ridge Tests (after Semeniuk, 1975)

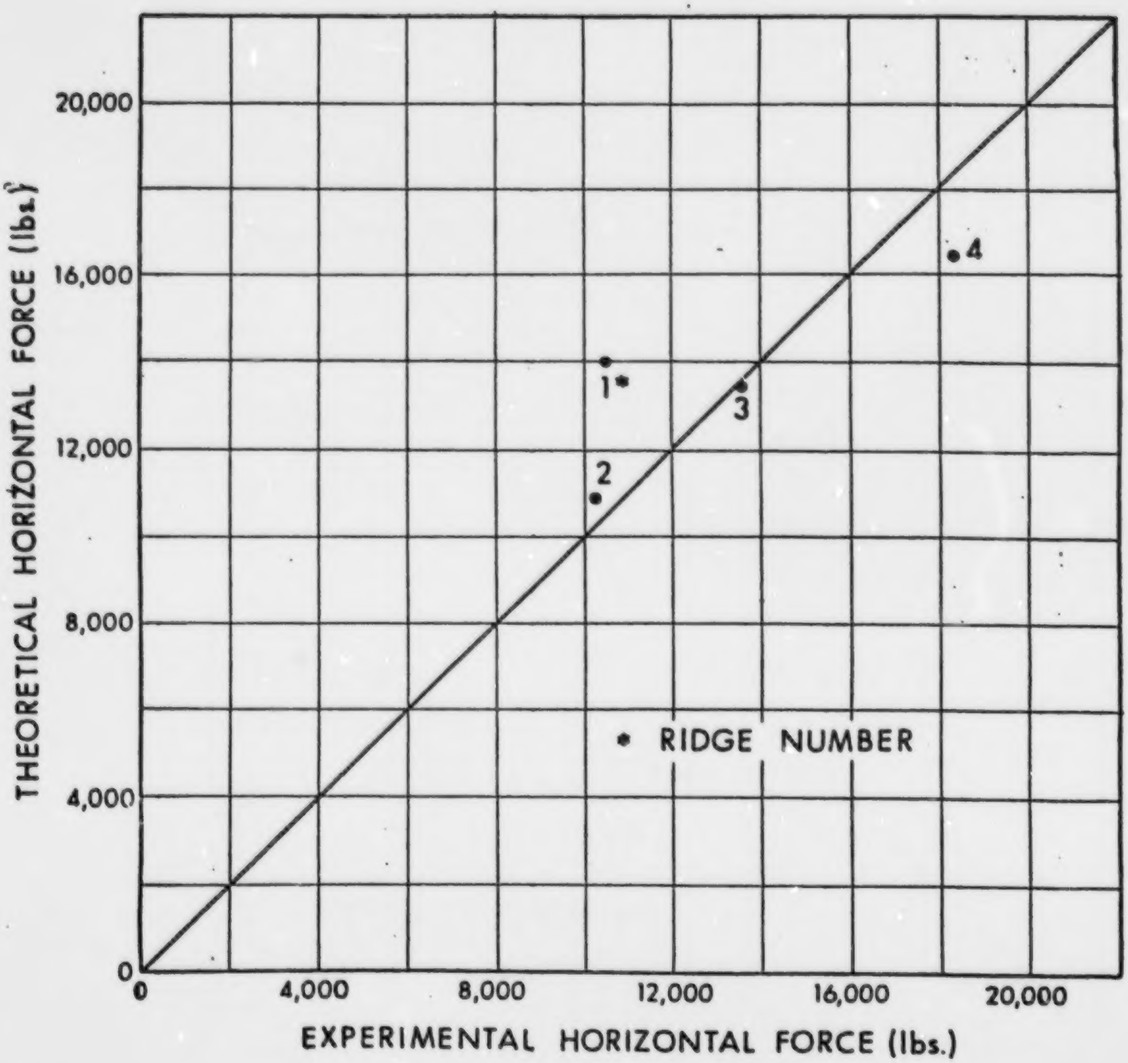

Figure 5.3.34 Horizontal Force Comparison Between Theory and Experimental Results for Basin Ridge Tests (after Semeniuk, 1975)

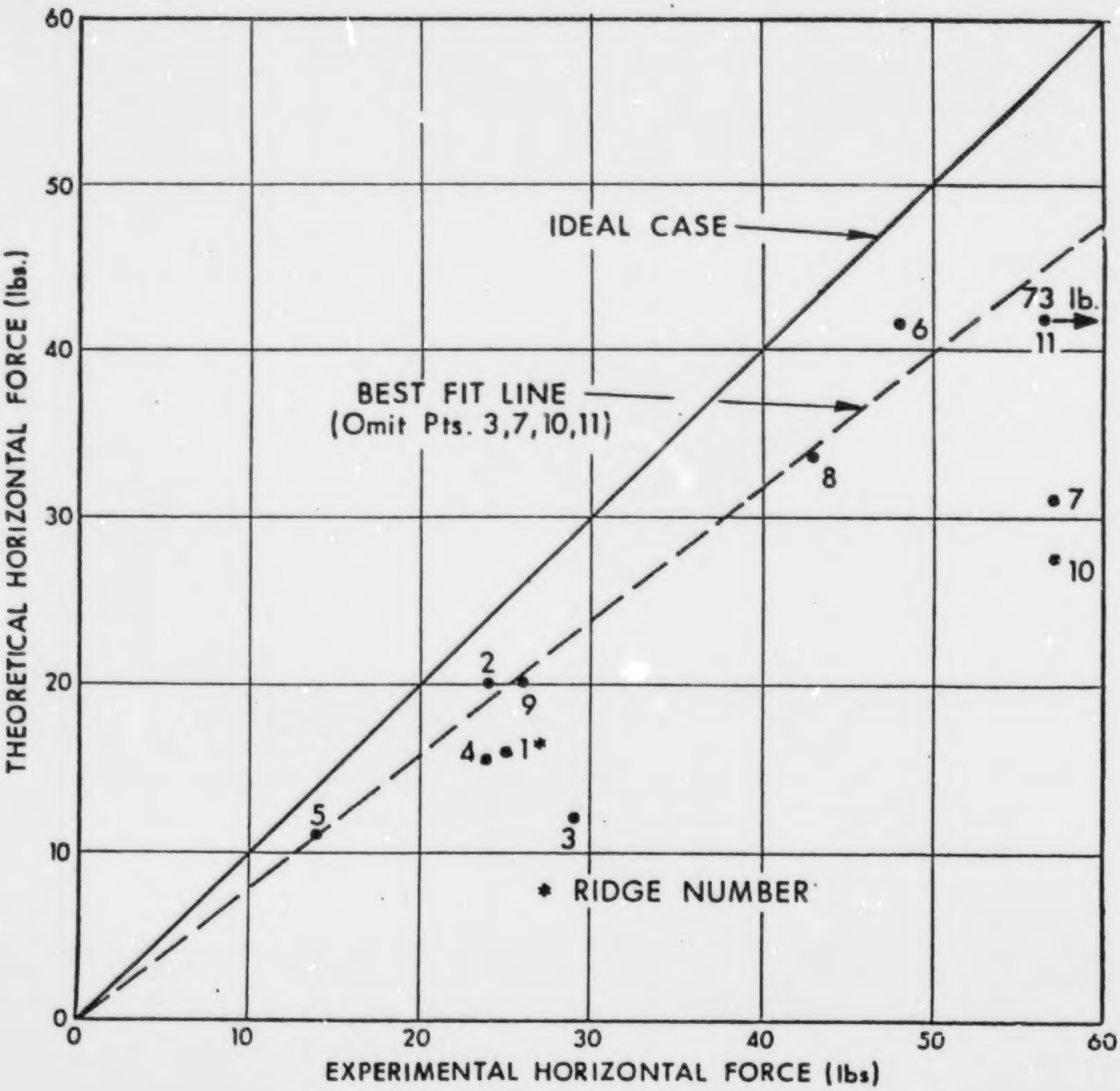

Figure 5.3.35 Horizontal Force Comparison Between Theory and Experimental Results for Saline Ridge Tests (after Semeniuk, 1975)

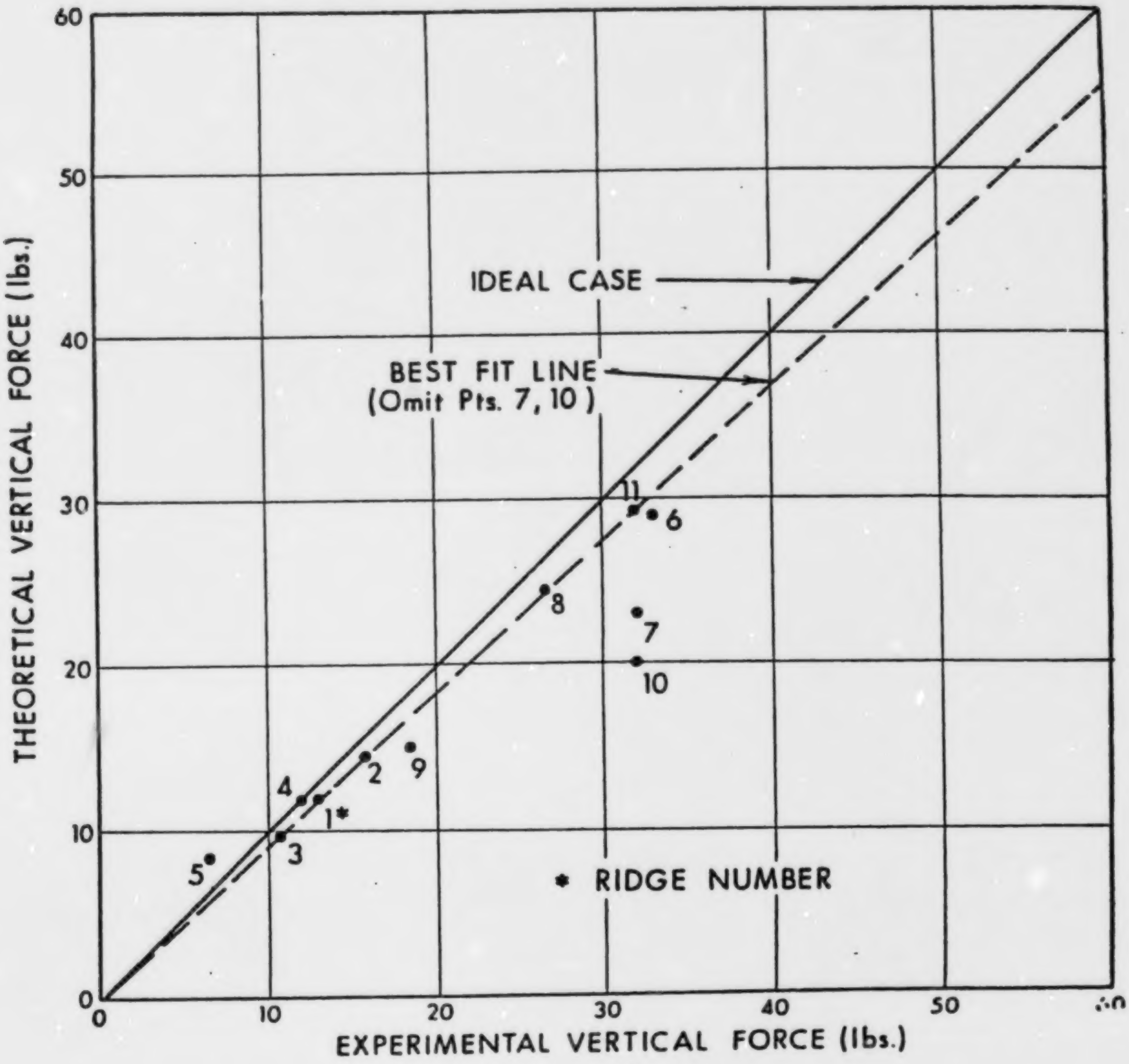

Figure 5.3.36 Vertical Force Comparison Between Theory and Experimental Results for Saline Ridge Tests (after Semeniuk, 1975)

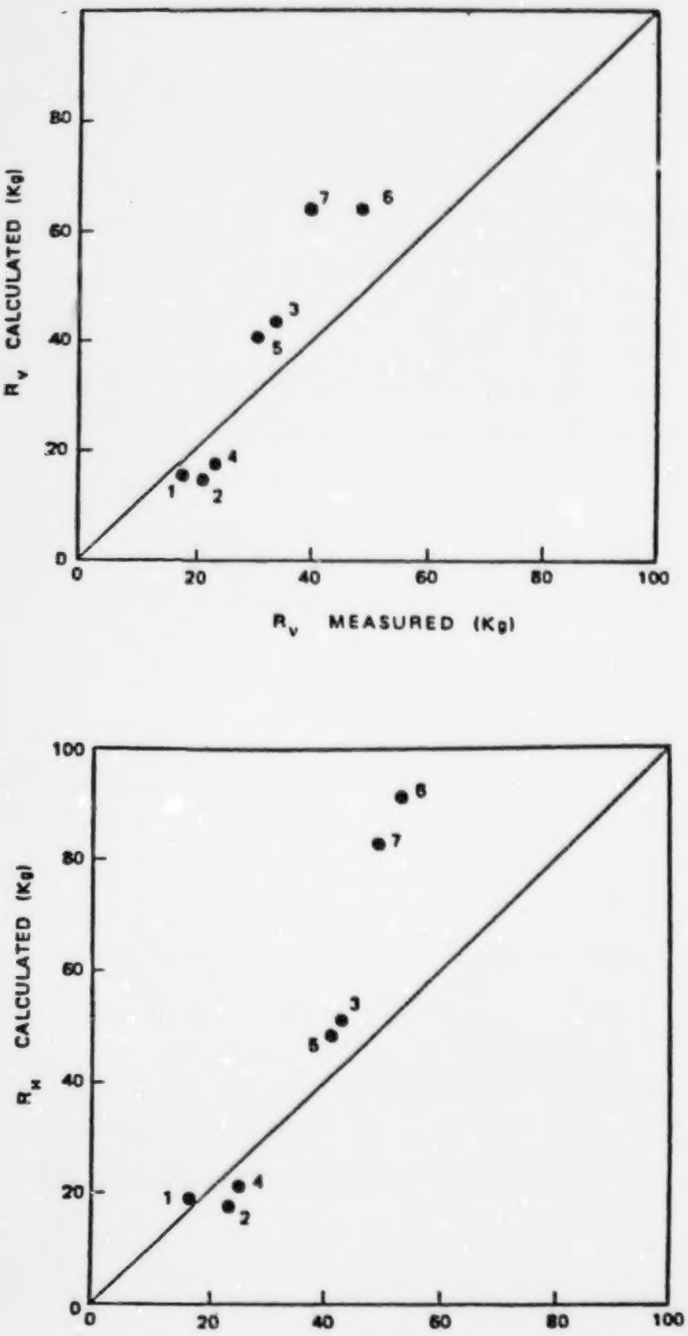

Figure 5.3.37 Vertical and Horizontal Force Comparisons Using the Plasticity Method and the Test Results of Edwards and Abdelnour (1975). (after Wang, 1984)

5.3.6 Unconsolidated Ridges

Newly formed first-year ridges are essentially unconsolidated accumulations of ice rubble held together by friction, gravity and buoyancy forces. Their interaction with a sloping structure will therefore be quite different than for consolidated ridges. Ice forces due to first-year ridges can be expected to be much lower than for the same thickness of a multi-year ridge.

Only approximate theories exist to treat ice rubble (or first-year ridge action) on structures. These are reviewed in Section 5.2 for vertical structures. Sloping structures offer no advantage over vertical structures in terms of lowering the loads due to unconsolidated ice rubble. It is suggested that at this time, the approximate methods developed for vertical structures (e.g. Croasdale, 1980) also be used for sloping structures.

5.3.7 Loads on Downward Breaking Sloping Structures

Downward breaking cones have been analyzed by Ralston (1979). His analysis indicates that ice failing against a downward breaking cone does so at lower ice loads than upward breaking. He points out that this is primarily due to the clearing forces (ride-up or ride-down) being less. The reason for this is that the effective "weight" of the ice pieces below water is only about one tenth of their effective "weight" above water.

Formulae used for upward-breaking structures, described in Section 5.3.3, can be used for downward-breaking structures as long as the ride-up term is suitably modified. This is done by changing the term for ice density (ρ_i) to (ρ_w - ρ_i), where ρ_w is the water density. The effect of this modification is to reduce the clearing loads by a factor of about 10.

Other differences which might be accounted for include:

- the difference in flexural strength of the ice between upward and downward breaking,
- the difference in ice-to-structure friction, recognizing that the upper surface of the ice usually has a snow layer.

Very little experimental data exists on downward breaking structures. Some preliminary expressions were reported by Abdelnour (1981) and Gerwick and Jahns (1979). In both cases the experiments indicated reductions in forces by about a factor of two, compared with upward breaking.

5.3.8 Large-Scale Flexural Strength of Ice

When considering the appropriate value to use for ice flexural strength in ice loading equations, it is necessary to recognize that ice flexural strength can vary as a function of:

- salinity and temperature distribution,
- strain rate,
- crystal structure, and
- the size of the ice beam (or thickness of the ice sheet).

Whether the same flexural strength should be used for upward breaking and downward breaking will depend on the salinity and temperature profiles through the ice. In this context it is also necessary to recognize that moment capacity is perhaps more relevant than flexural strength, since the position of the neutral-axis within the ice will also vary with salinity and temperature profiles.

The issue of size effects in flexural failure is important because most full-scale situations will involve ice features much larger than have been tested in the measurement of flexural strength. It is not clear whether a size effect exists in flexural failure. The flexural strength values discussed in the literature show a range from nearly zero to about 3.5 MPa (500 psi), but it is clear that the high values have been obtained from small scale tests.

This trend is confirmed by plotting the data obtained by Gladwell (1977) and Kry (1975) in which samples of the same ice were tested at various beam sizes (see Figure 5.3.38). The results indicate that for large beams a flexural strength value of 700 kPa (100 psi) or less would be appropriate. The results also show that multi-year sea ice appears to be weaker than low salinity columnar sea ice. The appropriate value of flexural strength to use in ice load calculations for typical multi-year ice features, with cross sections 10 to 500 times greater than the largest tests to date, is still an issue for speculation.

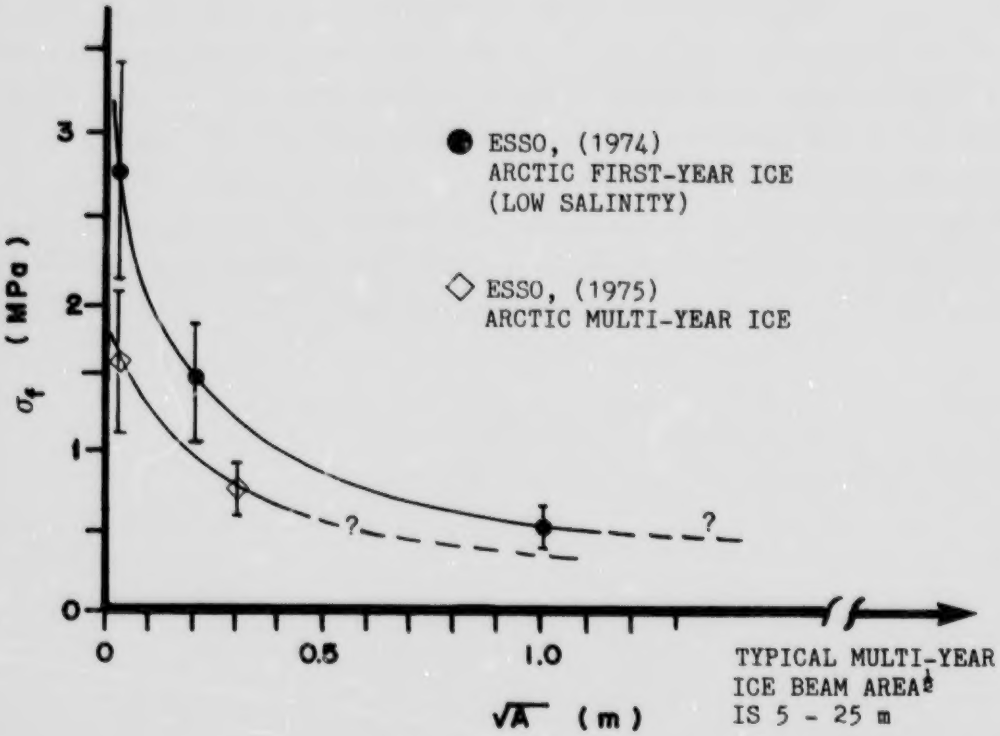

Figure 5.3.38 Variation of Flexural Strength of First-Year and Multi-Year Ice as a Function of Cross Sectional Area of the Beam (after Croasdale, 1985)

5.3.9 Concluding Remarks on the Interaction of Ice With Sloping Structures

In concluding this section on ice forces on sloping structures, the reader is referred back to the overall logic shown as Figure 5.3.5. The logic shown has to be applied in any consideration of ice interaction with sloping structures.

Sloping structures are configured to fail advancing ice in bending. The forces on sloping structures have been studied using theoretical models and physical models. This work has led to predictive methods for loads on sloping structures, but no large-scale data are available to qualify these methods. It has been shown however that theoretical methods such as developed by Ralston (1977) agree quite well with physical model test data (Kry, 1980). An important factor to recognize in ice interaction with sloping structures is that the global force is made up of an ice-breaking component and an ice-clearing component. Typically, the ice clearing or ride-up component can be similar in magnitude to the ice breaking component, as illustrated in Figure 5.3.11.

In addition, other factors have to be recognized in the design of sloping structures, such as:

- If the ice is stationary for some period then it may freeze to the structure. This bond has to be broken before the ice can fail in bending. The adfreeze failure load can be as high as the crushing load unless special precautions are taken to reduce it by special coatings.

- The ice will ride-up the surface of the slope. All surfaces subject to ice may have to be designed for high local ice pressures. Deflectors may be needed to prevent ice encroaching on the working surface.

- Ice riding-up the side of a wide structure will probably fall back on the advancing ice and interfere with the simple flexural failure mode. The rubble field so formed will "hide" the structure geometry from the advancing ice and the loads on the outside of the rubble will be the same regardless of whether the structure is sloped or vertical.

Physical model tests indicate that narrow conical structures allow the ice to clear around them quite well. Little experimental work has been done to investigate ice clearing mechanisms in front of a wide sloping structure. Furthermore it has been shown using simple ride-up math models that high forces can be exerted on the upper vertical faces of wide structures due to thick ice jamming against them.

Recent publications relating to ice action on sloping structures have mostly been concerned with physical test data. Timco (1984) compares experimental ice forces on a 0.3 m wide model with values calculated using Frederking's (1979) three-dimensional (elastic) theory. Timco concludes that the theoretical model under predicts peak horizontal forces by about 20%. Wang (1984) and Abdelnour (1981) compared math models and physical model tests for ice ridges acting on a conical structure. Wang shows that a math model using plastic limit analysis gives better agreement with the tests than one based on elastic-brittle ice characteristics.

The major perceived advantage of a sloping structure is to minimize the ice forces associated with extreme ice features which might act on the structure during its lifetime.

In Figure 5.3.27 typical ice crushing loads on a 150 m wide structure are shown. Note that as the ice thickness increases, the apparent advantage of a sloping structure diminishes (i.e. for a 10 m thick ice feature the total load is at the midpoint of the range of crushing loads whereas for a 15 m thick ice feature the total load is at the maximum of the range of crushing loads).

If the structure is made narrower however, and shaped in the form of a cone, then the clearing forces are proportionally less and the potential advantage over a vertical sided structure is increased as shown in Figure 5.3.39.

It should not be forgotten though that the loads on the conical structure are less sensitive to ice strength. The broken lines in Figure 5.3.39 show the effect of reducing ice strength by 50%. In this case the difference between ice forces on the sloping and vertical sided structures is narrowed.

Further work on ridges which do not impact the sloping structure broadside is recommended.

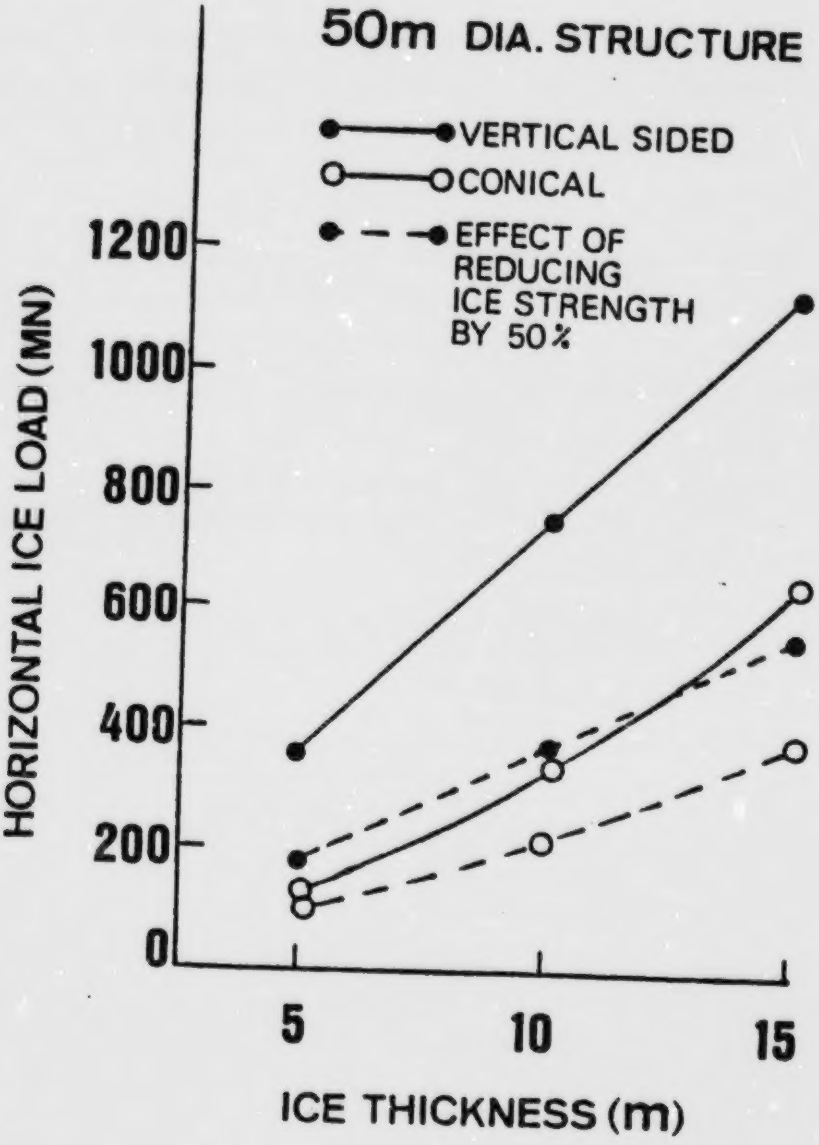

Figure 5.3.39 Comparison of Ice Loads on a Narrow Structure, Showing Loss in Advantage of Sloped Structure as Ice Strength is Reduced (after Croasdale, 1985)

5.4 Ice Interactions With Floating Structures

5.4.1 Introduction

In contrast to gravity based structures floating structures maintain their position by transferring load to the seafloor via mooring lines or by using dynamic positioning. This indicates that floating structures are not capable of sustaining interactions with large ice features such as multi-year floes, ridges, or large icebergs and ice islands. Floating structures may offer advantages which more than offset their inability to cope with the more hostile ice features. They can be used in locations where it may not be possible to construct a gravity based structure such as offshore Labrador or on the Grand Banks due to prohibitive construction costs. In fact, Petro Canada and partners have recently announced that they are going to continue work on developing the Terra Nova field (on the Grand Banks) using a floating production structure scenario.

The most significant development in floating structure design for ice infested environments is Gulf Canada's Conical Drilling Unit Kulluk, shown in Figure 5.4.1. Two other types of floating structures are shown in Figure 5.4.2 (a semisubmersible) and Figure 5.4.3 (a Dome Petroleum Drillship operating in the Beaufort Sea)

Portability is a main key to the usefulness of a floating structure. A program is mounted whereby ice features which can be deflected from the region of the structure are removed (such as the iceberg towing programs of the East Coast Operators). If an ice feature of too great a size encroaches the structure, a procedure is initiated whereby a calm move from the site away from the ice feature is undertaken. The advantage of moving compensates for not having to design an immobile platform for large ice features.

Therefore, the ice design characteristics for floating structures are radically different than for the other types of structures. Thin first-year ice sheets, thin ice floes, bergy bits, and broken pack ice zones form

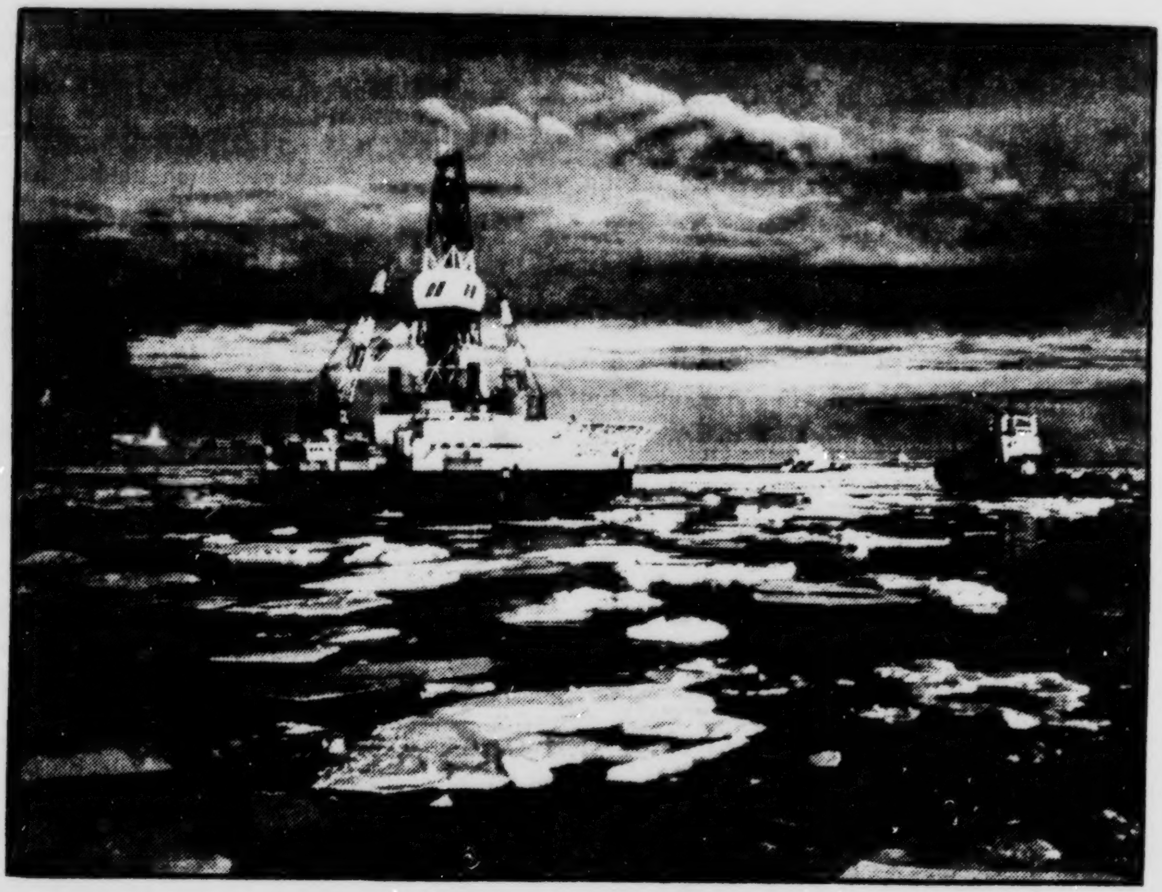

Figure 5.4.1 Gulf Canada's Conical Drilling Unit Kulluk (courtesy Gulf Canada)

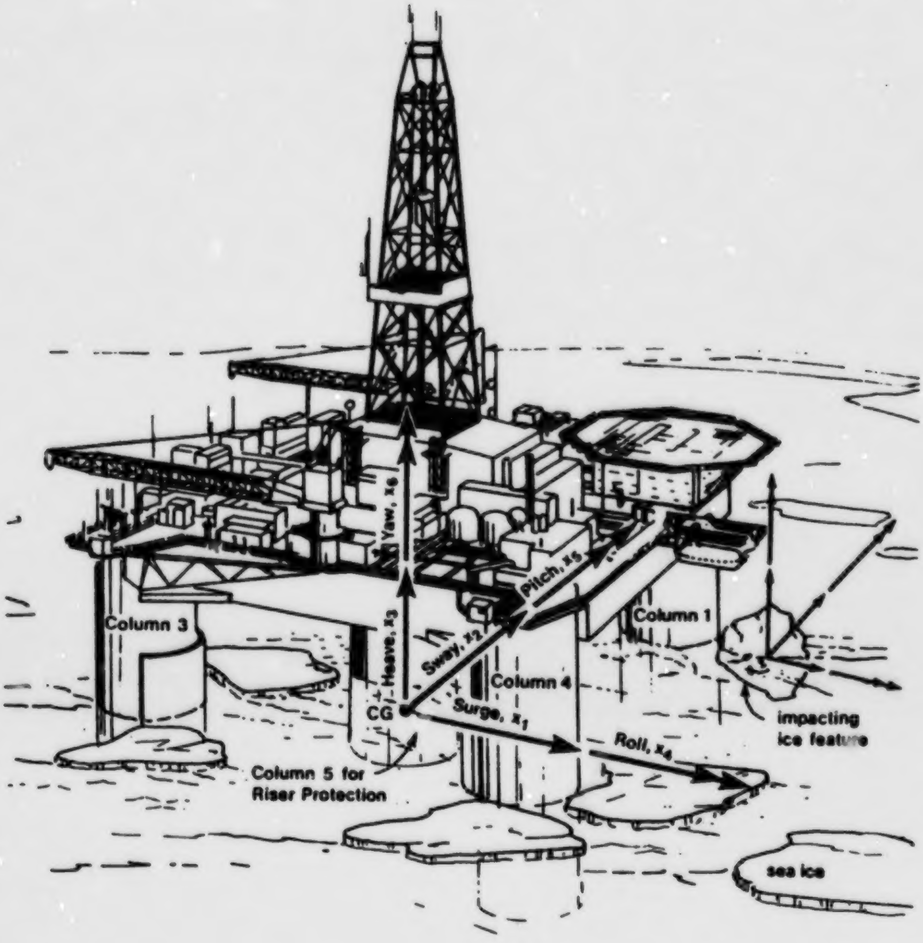
Yaw, x_6
Heave, x_3
Pitch, x_5
Sway, x_2
Column 3
Column 1
Column 4
CG
Surge, x_1
Roll, x_4
impacting ice feature
Column 5 for Riser Protection
sea ice

Figure 5.4.2 Illustration of a Semisubmersible

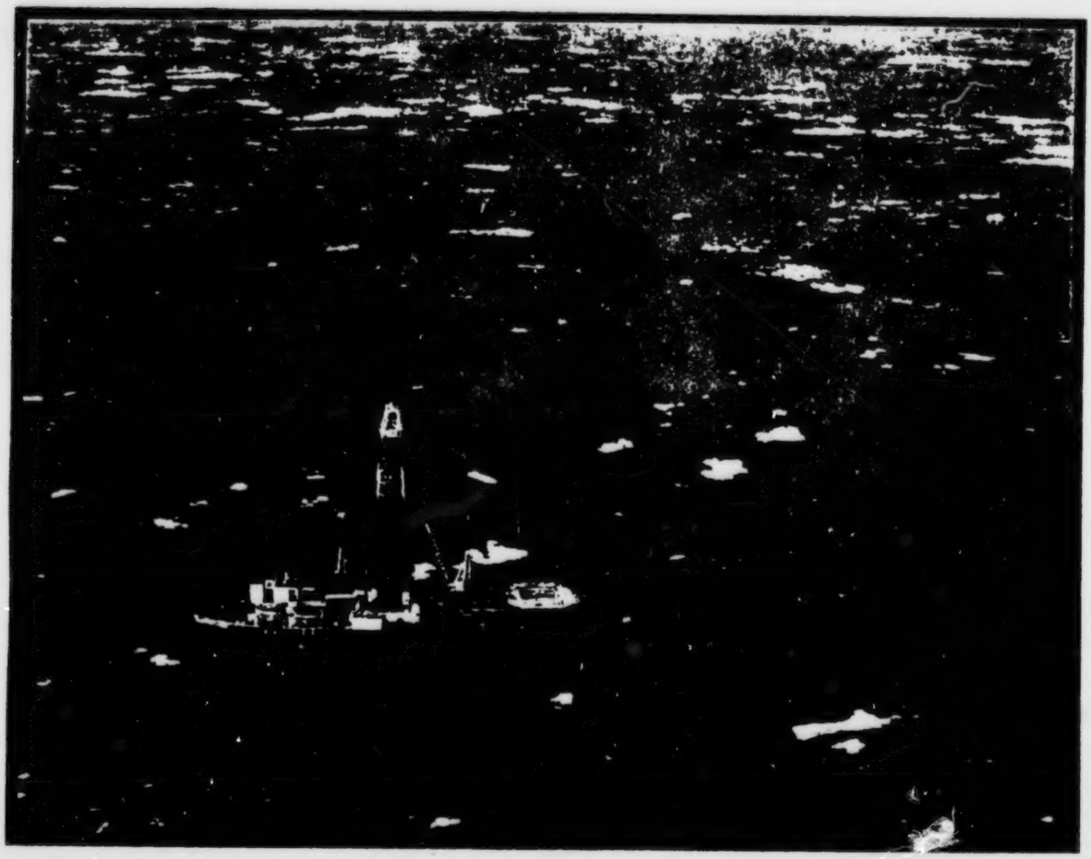

Figure 5.4.3 Dome Petroleum Drillship Operating in Loose Ice Conditions (Gary Watson Photography, Calgary)

the ice design criteria. In contrast to ice strengthened semisubmersibles, the Gulf Kulluk can withstand more close-in pack ice and thicker first-year ice with the support of an ice management program (e.g. icebreakers and supply ships breaking the ice into small sized pieces upstream of the Kulluk). In fact, the Kulluk has set records for earliest floating structure and latest floating structure operating in the Beaufort Sea.

Intrinsically, the physics and the modes of failure and clearing of ice are the same whether the impeding structure is bottom founded or floating. For instance, if the predominant mode of ice failure is one of crushing, then the force generated on the structure, whether it be fixed or floating, will depend on factors such as the strain rate, the size and the shape of the ice to structure contact area, and the relative strengths of the ice and structure. The main difference between the ice induced behaviour of a floating structure and that of a fixed structure is the relatively large kinematic response of a floating structure. This arises from the compliancy of the mooring system.

The two major force considerations for the interaction between ice and a floating structure are the contact forces born by the local ice resisting elements and the forces developed by the mooring system. To see how the local structural loads relate to the global mooring loads, it is essential to consider a number of forces acting during an ice/floating structure interaction. These forces are:

- the interactive force between the contacting ice and the structure (which accounts for ice failure and clearing modes),

- the inertial forces of the ice and the structure virtual masses, - the hydrodynamic forces on the ice and the structure,

- the hydrostatic forces on the ice and the structure,

- the wind and wave forces on the ice and the structure, and

- the mooring forces on the structure.

The ice and structure respond to these external forces according to the following equations of motion:

$$\text{ice:}\quad [M_i]\,(\dot{x}_i^{\cdot}) + [C_i]\,(\dot{x}_i) + [D_i]\,(\dot{x}_i^2) + [K_i]\,(x_i) = (F_s) + (F_{i,w\&w})$$

$$\text{structure:}\quad [M_s]\,(\dot{x}_s^{\cdot}) + [C_s]\,(\dot{x}_s) + [D_s]\,(\dot{x}_s^2) + [K_s]\,(x_s) = (F_i) + (F_{s,w\&w}) + (F_m)$$

...Eqn.'s 5.4.1

where the subscripts "i" and "s" refer to ice and structure respectively,

$[M]$ = virtual mass (mass + added mass) matrix
$[C]$ = matrix of linear drag coefficients
$[D]$ = matrix of hydrodynamic drag coefficients
$[K]$ = hydrostatic stiffness vector

$(\dot{x}^{\cdot})$ = acceleration vector for surge, sway, heave, roll, pitch, and yaw

$(\dot{x})$ = velocity vector
(x) = displacement vector

(F_i) = vector of ice forces on the structure
(F_s) = vector of structure forces on the ice, equal and opposite to (F_i)
$(F_{w\&w})$ = vector of wind and wave forces
(F_m) = vector of mooring forces

It is convenient to categorize the ice/floating structure interaction as follows:

- pack ice (continuous sheet or broken ice coverage) moving against the floating structure (Section 5.4.2).
- an individual ice piece impacting the floating structure in open water (Section 5.4.3).

In the pack ice scenario, the ice/structure interactive force is of a long duration nature whereas in the ice impact scenario, the interactive force builds up and diminishes quickly, typically in a fraction of a second. The potential modes of pack ice failure include:

- crushing; can be ductile or brittle in nature, depending on the strain rate,
- buckling; can be sheet ice buckling or block instability in broken pack ice,
- jamming; blocks of ice may jam between the columns of a semi-submersible and cause the pack ice to fail across the exposed width of the rig,
- flexure; if the floating structure is slope sided at the waterline, it can induce flexural failure in the pack ice, in an upward or downward mode,

The following factors influence the pack ice force levels:

- ice coverage effects; in broken ice, the ice force increases with increasing sea surface coverage by ice,

- shielding; various columns of a semi-submersible can be shielded, depending on the angle of ice attack, and a ship-shaped vessel can be shielded by a single point mooring (SPM),

- ship resistance; the pack ice force on a ship (such as a tanker type floating structure).

5.4.2 Pack Ice Forces

Pack ice forces are those forces exerted on a floating structure by the motion of small floes that constitute the local pack ice. Much of the work on pack ice forces is empirical in nature, and is based on model tests or bridge pier studies (where the general geometries of the interaction are similar).

Experimental studies by Matsuishi et al., (1986), Machemehl (1987), Szeto et al., (1987), and others have given empirical model measurements of interactive force between model pack ice and model floating structures. While these studies provide visual data to further the understanding of the pack ice/floating structure interaction, by themselves they do not easily enable the user to perform methodical calculations of pack ice forces on floating structures. In a pack ice scenario, the ice force fluctuates at periods much smaller than the natural period of the floating structure lateral motion, i.e. the time scale of the interaction is on the order of fractions of a second or less whereas the general motion of the vessel occurs in many seconds. Thus, for the most part it is possible to use fixed structure force calculations in place of more complicated analyses such as Equation's 5.4.1.

Several analytical/numerical studies have been undertaken by the industry on ice forces on floating structures. The most recent studies include Alaska Oil and Gas Association (AOGA) projects 201, 309 and 340. The first involved the development of a mathematical model of ice forces on a semisubmersible. The latter two projects were for the development of computer software for the analysis of ice forces on semisubmersibles, single point moorings and moored ship-shaped vessels. These computer programs may be regarded as the state-of-the-art numerical tools for the calculation of ice forces on floating structures. Brief descriptions of these are given in Section 5.4.4.

5.4.2.1 Ice Crushing Loads

The modes of ice failure for ice crushing on a floating structure are intrinsically the same as those for ice crushing on a fixed structure. The time histories of the ice force variation, however, are different due to the motion of the floating structure, which affects the strain rate of crushing.

The various modes of ice crushing failure are presented in Section 5.2. The effects of the motion of the structure on ice crushing are discussed in Section 5.6.2. This section concentrates on the crushing of ice on the multiple legs of a semisubmersible. Ice crushing against wide floating structures such as the Kulluk or a ship is inappropriate due to the fact that the high loads that would be induced would break the mooring lines, so the vessel would leave the site beforehand.

Studies of the crushing of ice on vertical columns in close proximity include Timco and Pratte (1985) and Kato and Sodhi (1983). In the Third State-of-the-Art Report on Ice Forces for IAHR, presented at IAHR 1986, Timco reviewed ice forces on multi-legged structures. Kato and Sodhi based their findings on data collected on the crushing of synthetic ice on pairs of cylinders. Typical recorded ice force histories are shown in Figure 5.4.4.

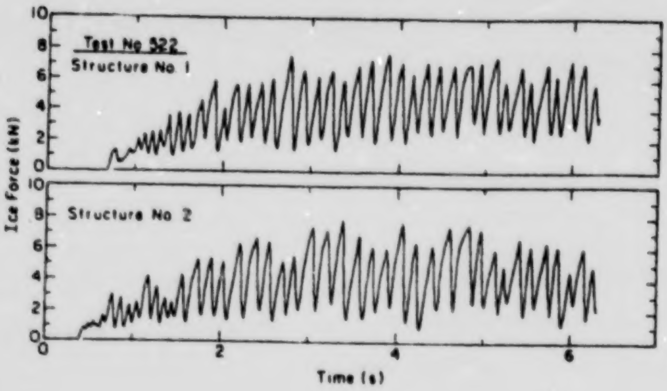

Figure 5.4.4 Typical Ice Crushing Force Time Histories (Kato and Sodhi, 1983)

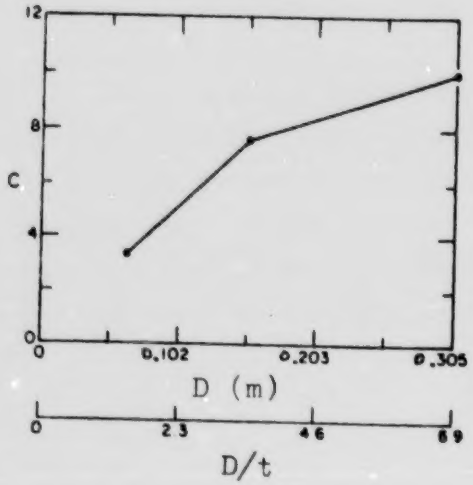

Figure 5.4.5 Coefficient C versus Column Diameter, D, and Aspect Ratio D/t (Kato and Sodhi, 1983)

Kato and Sodhi proposed an expression for the crushing force frequency in terms of the aspect ratio of ice contact and the speed of ice:

$$f = C\ V / t \qquad \text{...Eqn. 5.4.2}$$

where:

f = frequency in cycles/second

V = ice speed in metres/second

t = ice sheet thickness in metres

C = coefficient as a function of column diameter, D (in metres) as given in Figure 5.4.5.

The ice force fluctuation periods are in the order of fractions of a second. These short periods are several orders of magnitude smaller than the periods of lateral motion of typical moored semisubmersibles and drillships. Hence for the purpose of calculating the displacement of the typical moored floating structure under continuous ice crushing, the time average of the ice crushing force can be justifiably used. The average and the peak forces on a single column have been measured by Kato and Sodhi, who proposed the following quantification:

$$F_{mean} = \sigma_{mean}\ (5\ (t/D) + 1)^{\frac{1}{2}}\ t\ D$$

$$F_{max} = \sigma_{max}\ (5\ (t/D) + 1)^{\frac{1}{2}}\ t\ D \qquad \text{...Eqn.'s 5.4.3}$$

where:

t = ice thickness in metres

D = column diameter in metres

σ_{mean} = mean crushing pressure in Mpa = $1.36\ \sigma_u$

σ_{max} = maximum crushing pressure in Mpa = $2.33\ \sigma_u$

σ_u = unconfined crushing strength of ice in Mpa.

The relationships between the aspect ratio and F_{mean} and F_{max} are shown in Figure 5.4.6.

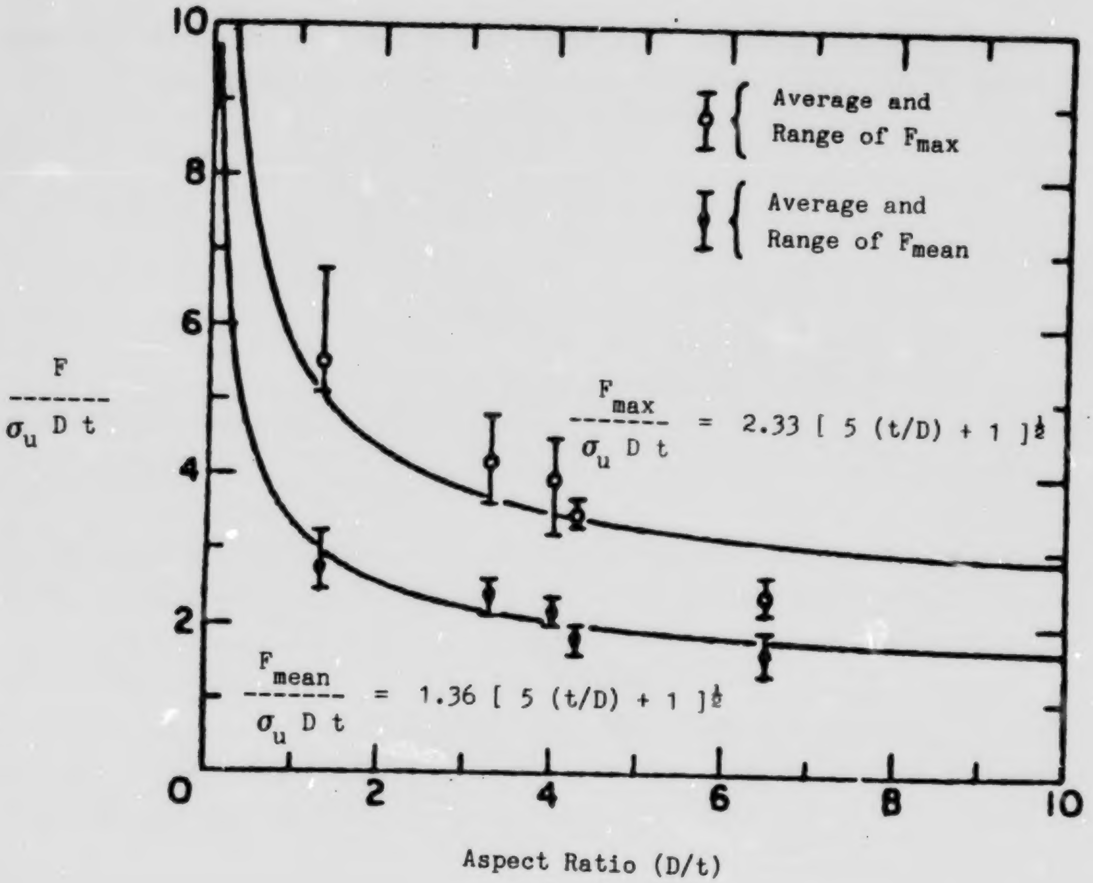

Notation has been changed slightly for conformity with this report.

Figure 5.4.6 Ice Forces versus Aspect Ratio D/t (Kato and Sodhi, 1983)

The effects of the close proximity of another column was recorded for both the average and the peak forces and are shown in Figure 5.4.7 where:

S = centre-to-centre spacing between columns measured perpendicular to ice movement direction in metres

$f_{mean} = F_{mean} / [1.36 \, (5 \, (t/D) + 1)^{\frac{1}{2}} \, \sigma_u \, t \, D]$

$f_{max} = F_{max} / [2.33 \, (5 \, (t/D) + 1)^{\frac{1}{2}} \, \sigma_u \, t \, D]$

...Eqn.'s 5.4.4

It is apparent from the plots in Figure 5.4.7 that for S/D less than 2, the ratio of average to peak force intensity is about one half, and for S/D greater than 4 to 5, the individual columns reacted independently against the ice crushing action.

5.4.2.2 Ice Buckling

The buckling of ice may be a governing force mechanism on a floating structure if the ice thickness is very small. For sheet ice the critical force per unit length to cause buckling is given by:

$f_{ins} = k \, l^2 \, R$ ...Eqn. 5.4.5

where:
k = unit weight of water in MN/m^3
l = characteristic length of ice sheet = $[E \, (1 - \nu^2) \, t^3 / 3 \, k]^{\frac{1}{4}}$
E = Young's modulus of ice in Mpa
ν = Poisson's ratio of ice
t = ice sheet thickness
R = the ratio given in Figure 5.4.8, from Kato and Sodhi (1983).

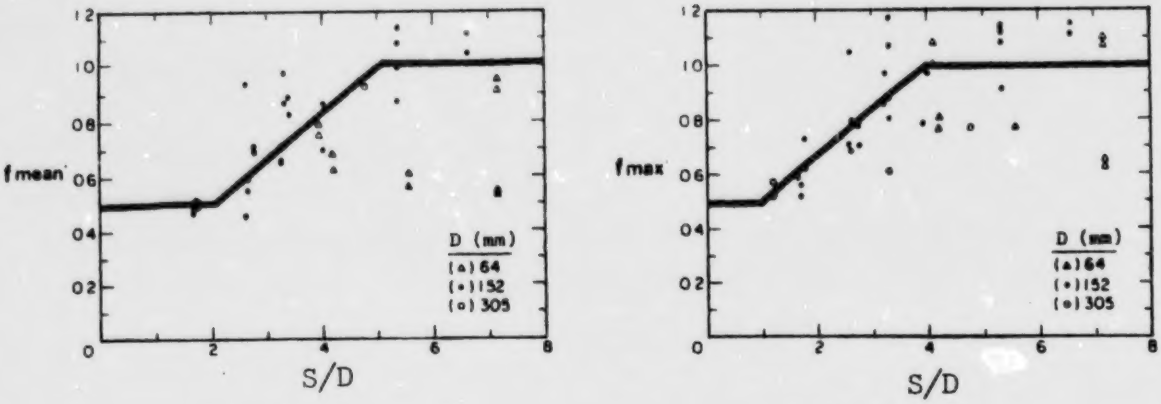

a.) Mean Forces

b.) Maximum Forces

Figure 5.4.7 Normalized Forces versus Ratio of Centre-to-Centre Distance to Column Diameter (S/D) (Kato and Sodhi, 1983)

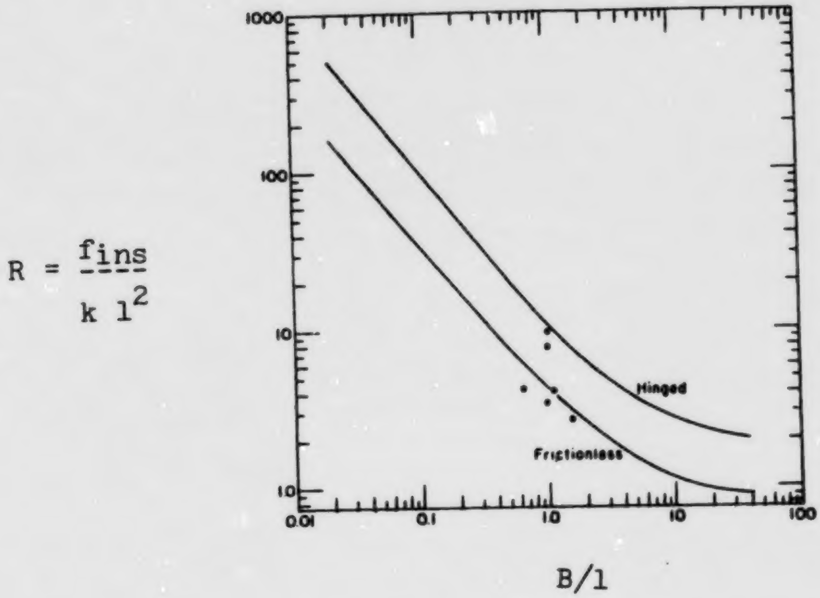

Figure 5.4.8 Normalized Unit Buckling Load versus Ratio of Total Exposed Width of Columns to Characteristic Length

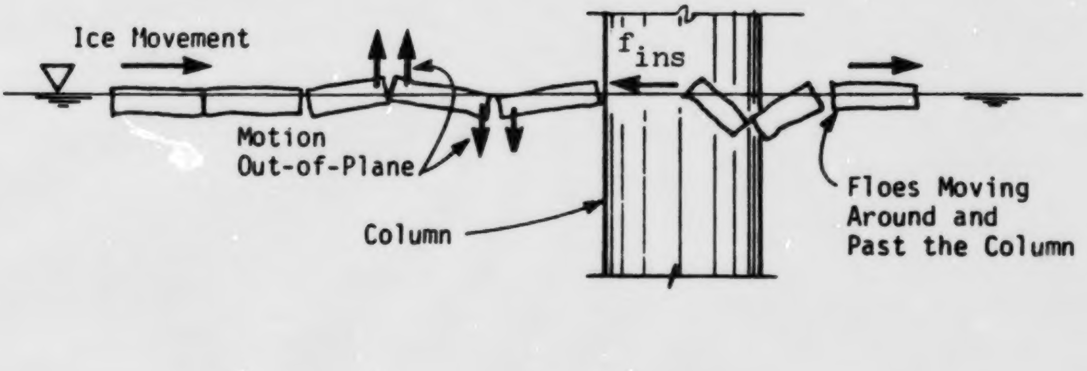
Ice Movement
f_{ins}
Motion Out-of-Plane
Column
Floes Moving Around and Past the Column

Figure 5.4.9 Illustration of Broken Ice Instability

For broken ice pieces, the force to cause them to buckle and rotate out-of-plane is much smaller. This mechanism, shown in Figure 5.4.9, would typically govern the ice force exerted on a floating structure in a broken ice cover.

The theory of stability on elastic foundation developed by Hetenyi (1946) provides a basis for the calculation of the force required to cause the instability of the ice pieces in calm water. The unstable condition is given by the following expressions:

$$\frac{\sin \frac{1}{2}\,[2\,Y + \pi^2\,X]^{\frac{1}{2}}}{\mathrm{Sinh}\,\frac{1}{2}\,[2\,Y - \pi^2\,X]^{\frac{1}{2}}} = \mp\,\frac{(Y - \pi^2\,X)\,[2\,Y + \pi^2\,X]^{\frac{1}{2}}}{(Y + \pi^2\,X)\,[2\,Y - \pi^2\,X]^{\frac{1}{2}}}$$

$X = f_{ins}\ l^2 / (\pi^2\ E\ I)$

$Y = [k\ l^4 / E\ I]^{\frac{1}{2}}$

...Eqn.'s 5.4.6

where:

f_{ins} = critical or buckling force per unit width of ice in MN/m,
E = elastic modulus of ice MPa,
I = moment of inertia per unit width of ice = $t^3/12$,
k = density of water in MN/m^3, and
l = length of ice piece in metres.

The solution to this expression requires numerical iterations and is shown graphically in Figure 5.4.10.

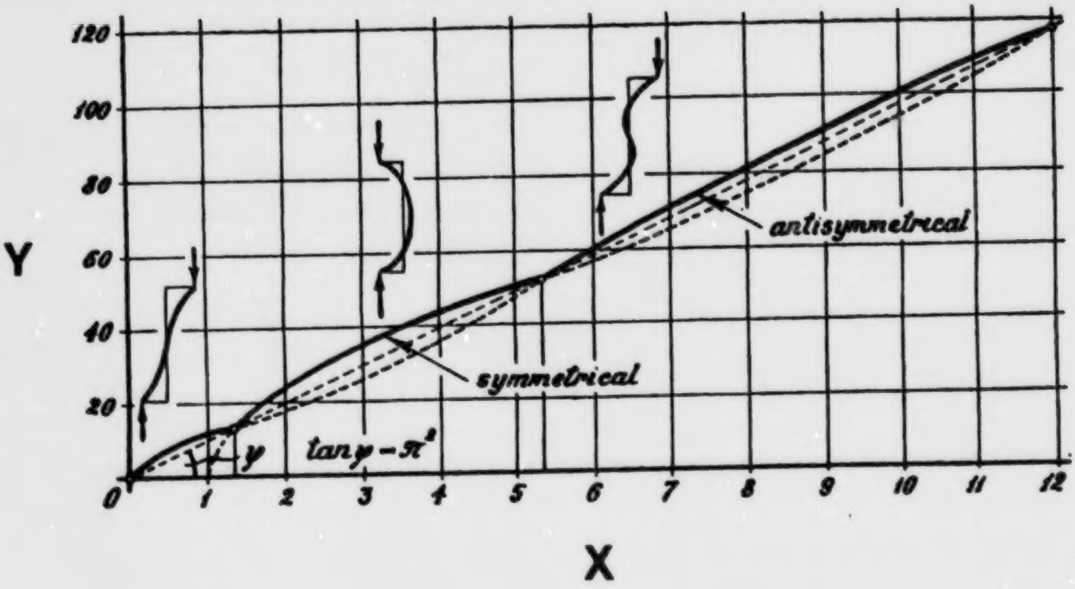

Figure 5.4.10 Graphical Solution of Dimensionless Instability Forces

The width over which the unit width buckling force is applied is the greater of:

- the exposed width of the structure (if for a semisubmersible there is ice jamming among the columns, this would be the exposed width of the ice jam), or
- the diameter of the ice piece.

In a pack ice zone it is possible for pieces of ice to become lodged inside the legs of a semisubmersible or piled structure. In this case, if the pack ice is moving, it is possible for a jamming situation to occur. Jamming is examined in detail in the next section.

5.4.2.3 Ice Jamming

The consideration for jamming of broken ice among the columns of a semisubmersible or between a drillship and a single point mooring buoy is based on tests reported by Calkins (1978). Figure 5.4.11 shows the layout of tests by Calkins to investigate the arching of ice floes between bridge piers.

A dimensionless plot of ice concentration versus the ratio of average floe diameter to clear spacing is suggested by Calkins to define the boundary between the regimes of possible ice-arching and possibility of ice-arching, as shown in Figure 5.4.12.

The definition of clear spacing is taken to be the spacing perpendicular to the ice floe movement. The concept of clear spacing is illustrated in Figure 5.4.13 for a seven-column semisubmersible. There are two types of spacings - S(0°) and S(90°) which are important to the analysis. These two distances relate to the spacing between legs of the semisubmersible relative to the axis of symmetry that passes through the

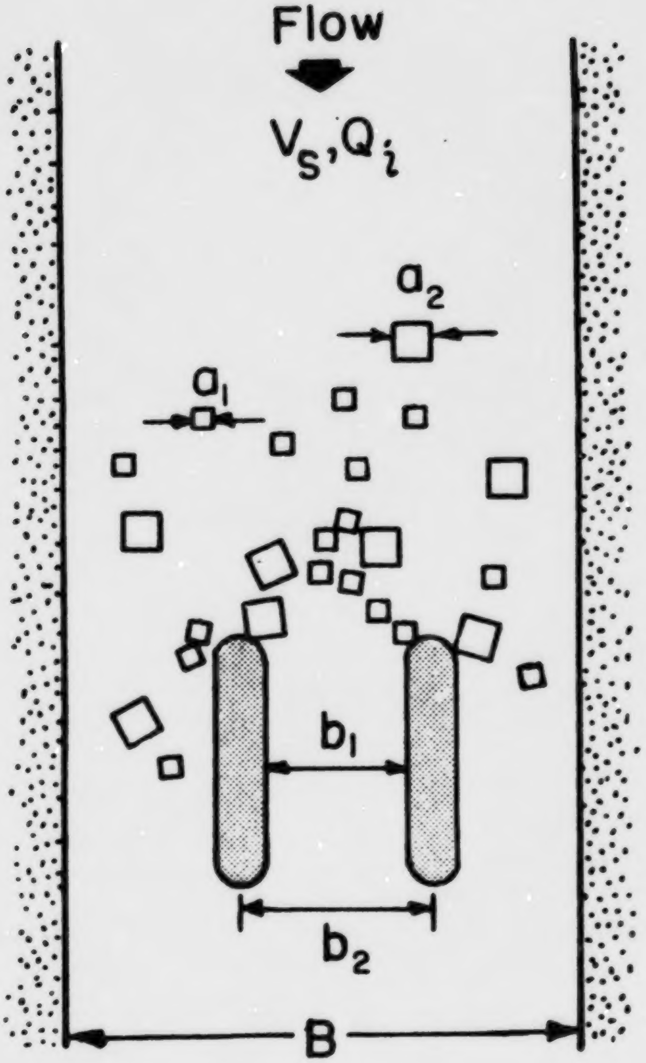
Flow
V_s, Q_i
a_2
a_1
b_1
b_2
B

Figure 5.4.11 General Layout of Bridge Pier Analysis of Calkins (1978)

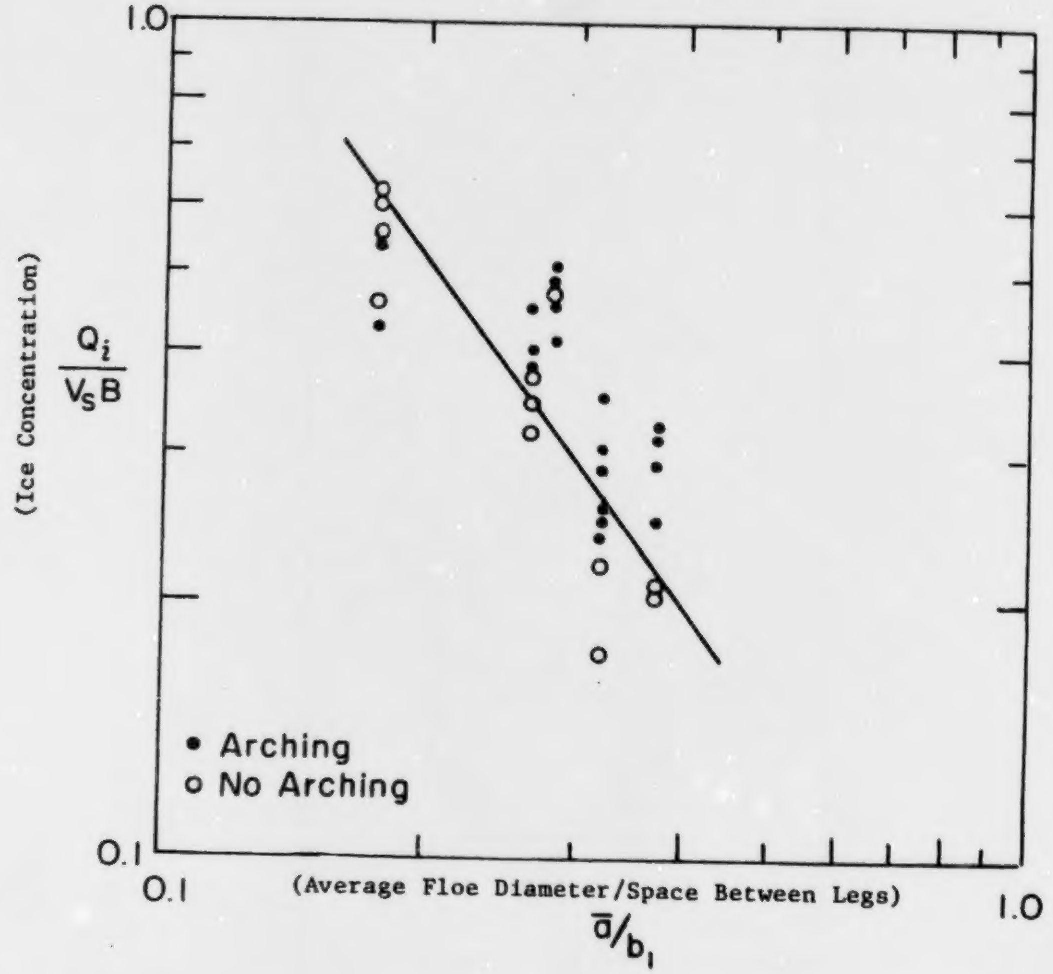

Figure 5.4.12 Illustration of Calkin's Data Showing Boundary Between Ice Arching and No Ice Arching Conditions (Calkins, 1978)

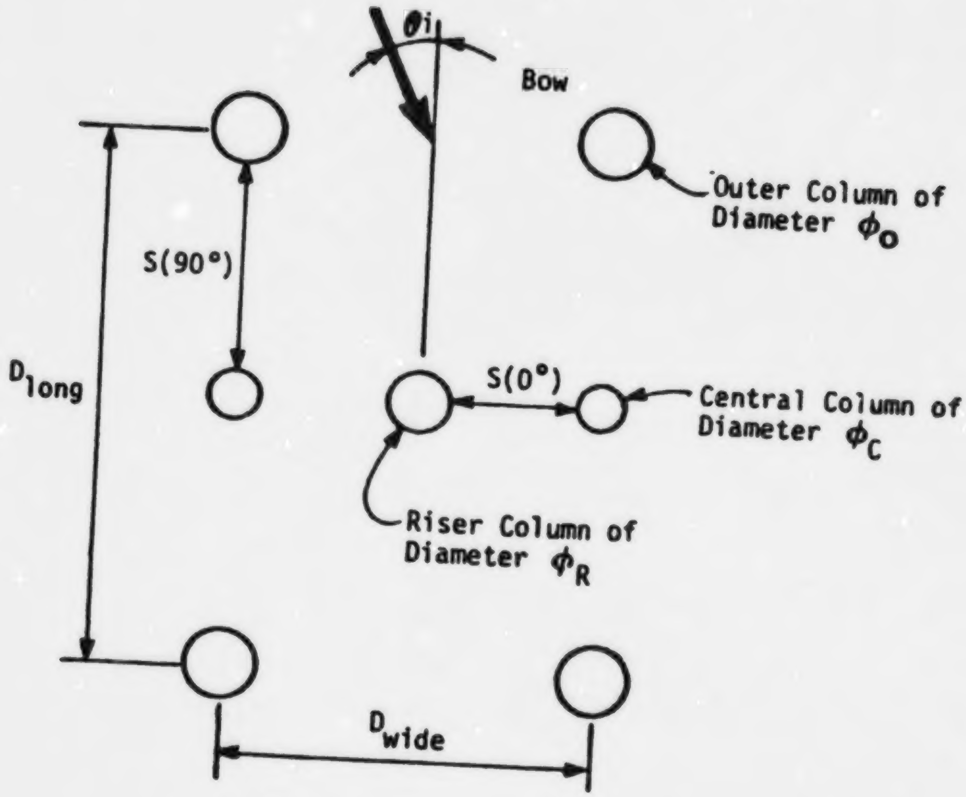
θi
Bow
Outer Column of Diameter ϕ_O
S(90°)
D_{long}
S(0°)
Central Column of Diameter ϕ_C
Riser Column of Diameter ϕ_R
D_{wide}

Figure 5.4.13 Illustration of Seven-Column Semisubmersible Geometry

semisubmersible widthwise. The clear spacing is given as the maximum spacing along either the width orientation of the vessel or the length orientation of the vessel.

S = maximum of:

width orientation gap: $S(0°)\ (\cos(\theta)_i)\ (1 - f_b)$, or
length orientation gap: $S(90°)\ (\sin(\theta)_i)\ (1 - f_b)$

...Eqn.'s 5.4.7

where:

f_b = blockage factor between 0 and 1,
= 0 if there are no braces at the waterline,
= 0.5 if there is one brace midway between the columns at the waterline
= 1.0 if there are many braces at the waterline which effectively block any ice floes from passing between the columns.

5.4.2.4 Ice Coverage Effect

It is possible to quantify ice loads expected when a field of broken ice is passing by a structure. This situation is analogous to that of a vessel transiting a series of floes, and empirical relations have been developed relating the average resistance experienced by the vessel and the local ice coverage. A study for Transport Canada in 1984 on the performance of the Arctic Class 4 bulk carrier M.V. Arctic gave a plot of ice resistance versus ice coverage, which is reproduced in Figure 5.4.14. Note that the average size of the floes must be smaller than the size of the vessel for these relations to be useful.

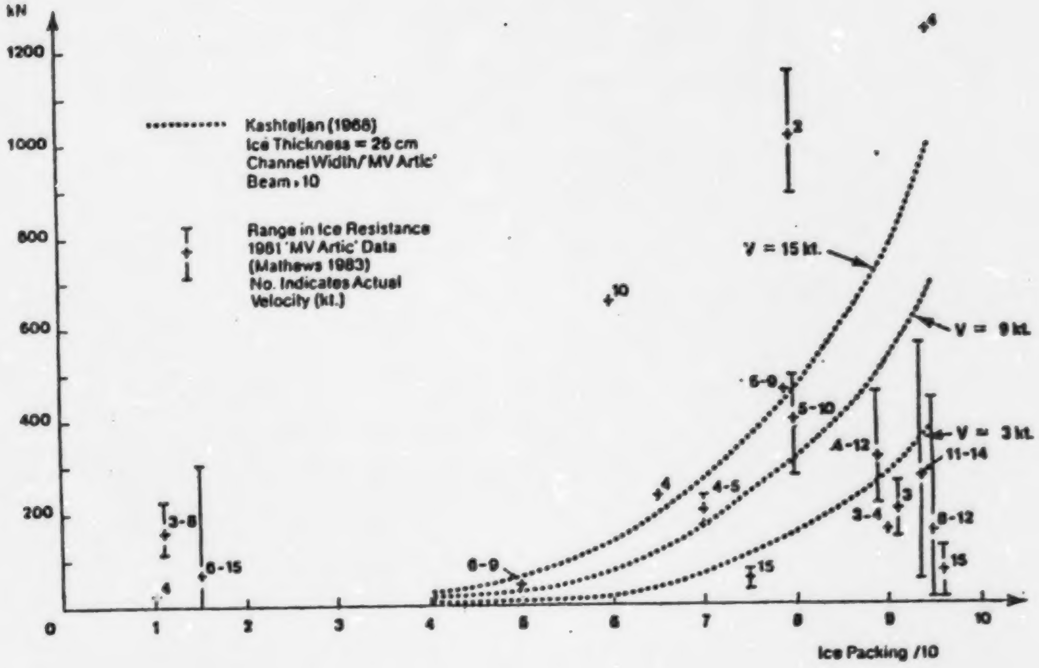

Figure 5.4.14 Measured M.V. Arctic Broken Ice Resistance Comparison with Empirical Predictions

Several conclusions may be drawn from the M.V. Arctic data:

- ice cover of 9/10 or higher provides necessary lateral confinement in the ice pack to produce the maximum ice
- at an ice cover of 7.5/10, the ice force is about one-half the value at 9/10 or higher cover.
- at an ice cover of 6/10, the ice force is about one-quarter the value at 9/10 or higher cover.
- at an ice cover of 4/10, the global ice force is essentially zero as individual floes will readily deflect and rotate around the floating structural elements.

5.4.2.5 Shielding in Pack Ice

When a thin ice sheet is interacting with a semisubmersible it is possible that one of the columns shields a column downstream from the ice. Thus, not all of the columns are necessarily exposed to the ice, and the total load on the vessel is less than would otherwise be expected. An example of shielding is illustrated in Figure 5.4.15 for a 4 column semisubmersible.

Similarly, a vessel moored in pack ice can be shielded by a single point mooring device (SPM) buoy. The partial shielding of a vessel by an SPM is shown in Figure 5.4.16.

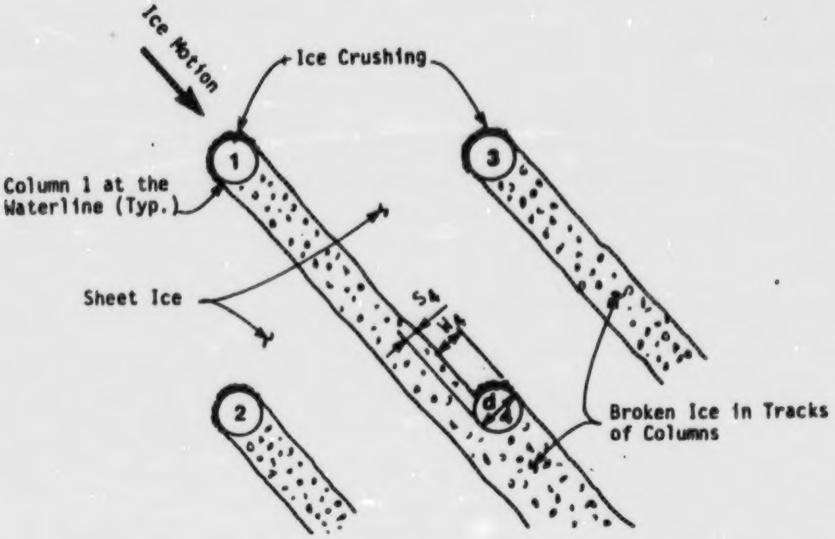
Ice Motion
Ice Crushing
1
3
2
Column 1 at the Waterline (Typ.)
Sheet Ice
S4
W4
d4
Broken Ice in Tracks of Columns

Figure 5.4.15 Illustration of Shielding for a Four-Column Semisubmersible

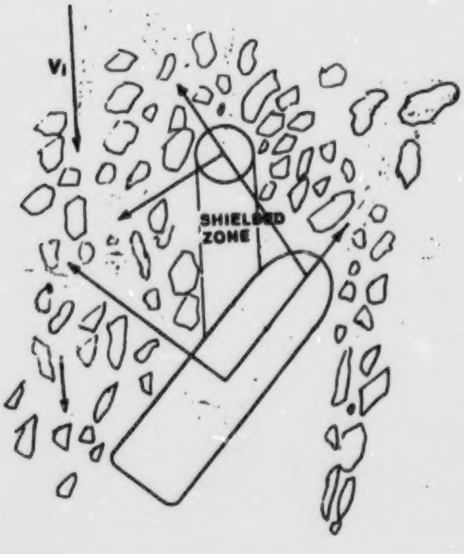
Vi
SHIELDED ZONE

Figure 5.4.16 Illustration of Shielding of a Vessel by a Single Point Mooring Buoy

5.4.2.6 Flexural Failure of Ice

Examples of floating structures that may cause flexural failures in ice include vessel hulls that are sufficiently flared, loading towers and semisubmersibles with columns equipped with a cone or themselves inclined at the waterline. A model semisubmersible equipped with downward breaking cones from Corona et al., (1983) is shown in Figure 5.4.17.
A semisubmersible design with inclined columns from Bulow et al., (1986) is shown in Figure 5.4.18.

The interaction ice load theories for sloping structures are generally covered in Section 5.3. Vessels with ice breaker characteristics also cause flexural failure in the ice and this is elaborated upon in the next section.

5.4.2.7 Ice Breaker Resistance

Ship resistance studies can be used to estimate forces on moored vessels. The reader should be aware that the comparison may not be exact due to the characteristics of a moored vessel being different from those of a moving vessel.

As well, the use of ship resistance theory is only strictly appropriate for motion of the ice parallel to the length of the vessel.

The hull of the vessel may be optimized for ice motion parallel to the length of the vessel (i.e. for forward motion if the vessel is moving). Often, hulls for stationary vessels are strengthened only, and not optimized.

For completeness sake a brief review of a study prepared for Transport Canada is included in this report.

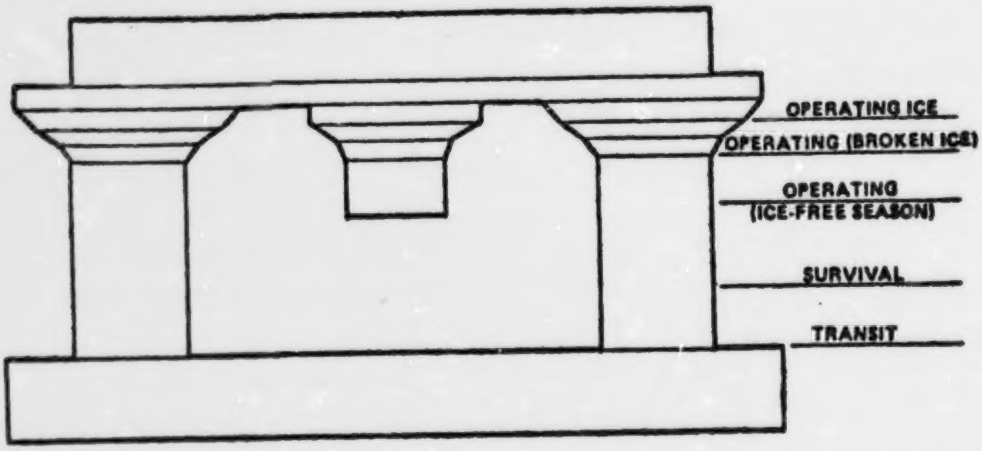
OPERATING ICE
OPERATING (BROKEN ICE)
OPERATING
(ICE-FREE SEASON)
SURVIVAL
TRANSIT

Figure 5.4.17 Illustration of a Semisubmersible with Downward Breaking Cones

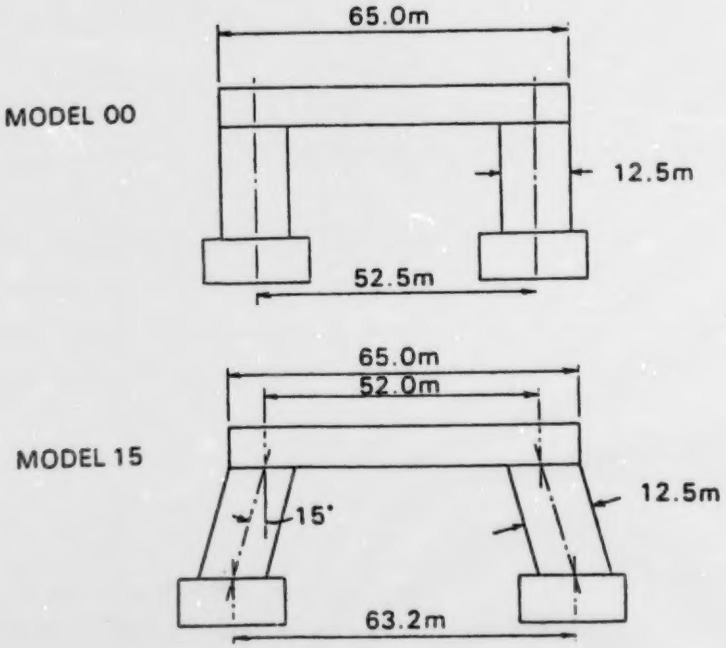
65.0m
MODEL 00
12.5m
52.5m
65.0m
52.0m
MODEL 15
15°
12.5m
63.2m

Figure 5.4.18 Illustration of a Semisubmersible with Inclined Columns

A vessel in pack ice coming from the bow interacts with the ice in very much the same way as an icebreaker transiting an ice pack. The M.V. Arctic report prepared for Transport Canada in 1984 summarizes the latest theories and field tests for the ice resistance of the Class 4 vessel transiting level sheet ice and broken ice in a range of coverage.

Several points in the Transport Canada report are worth noting as they illustrate the state-of-the-art in ice breaker resistance equations:

1. The actual selection of parameters forming the terms in the ice resistance equation is still very much in debate. For instance, there is some evidence that both the waterline length and the draft of the ship should be included in the equations.

2. The equations only include a term for ice breaking in flexure, whereas some ice crushing at the shoulders and buckling of ice pieces would inevitably occur. Also, the elastic modulus of ice is an essential factor in ice bending and, therefore, in the resistance caused by ice breaking in bending. However, the equations do not include the elastic modulus of ice as a variable.

3. The hull/ice friction plays an important part of vessel ice resistance. The frictional effect depends very much on the shape of the bow, in particular, the vertical flare at the shoulders where the vessel approaches her maximum beam. If the flare angle is too steep, the ice will have difficulty in sliding down the hull to fail in bending, and will instead jam and crush at the shoulders.

4. The reliability of test results from model testing in artificial saline ice has been questioned, for it is virtually impossible with ordinary saline ice to satisfy the laws of similarity simultaneously for both the strength and

the elastic modulus of ice. Therefore, model adjustment methods are required and there remains some doubt regarding their validity. The recent introduction of carbamide and EGADS ice, which are claimed to satisfy the similarity laws for ice modeling better, may solve some modeling problems, but it is certain that analytical judgement will be needed for the interpretation of test results.

It is evident that a general method of predicting ice loads on vessels of various shapes is yet to be developed. Equations for ice resistance calculations, therefore, are only valid for the range of available test data. In general, for all vessels, the resistance equation for level sheet ice would be:

$$R_{\text{sheet ice}} = C_b \ \sigma_f \ t^2 + C_s \ t + C_v \ V \ t^{1.5} \qquad \text{...Eqn. 5.4.9}$$

where:

C_b = ice breaking coefficient,
C_s = ice submerging coefficient, and
C_v = velocity coefficient.

In general the above equation contains three terms - the first is an ice breaking term, the second is an ice submerging term, and the last term is a velocity term.

The following expression for resistance in sheet ice was obtained from the M.V. Arctic data:

$$R_{\text{sheet ice}} = 3.33 \times 10^{-3} \ \sigma_f \ t^2 + 0.169 \ t + 0.241 \ V \ t^{1.5} \ \text{(MN)} \qquad \text{...Eqn. 5.4.8}$$

where:

σ_f = ice flexural strength in Mpa,
t = sheet ice thickness in metres, and
V = vessel speed in m/s.

A dynamic ice/hull friction coefficient of 0.1 is assumed for the Inerta 160 hull coating.

For general floe conditions and the time of year the study was conducted, it was concluded in the M.V. Arctic report that it was realistic to quantify the ice resistance of the vessel in broken ice by the relationship suggested by Kashteljan et al., (1968):

$$R_{floes} = (C_k + 0.5\, V^{1.3})\, t^{1.2} \qquad \text{...Eqn. 5.4.10}$$

where:

t = ice thickness (80 to 200) cm,

V = average vessel speed (0.5 to 13) knots, and

C_k = empirical coefficient based on floe sizes, approximately equal to 1.0.

Equation 5.4.10 represents a time averaged resistance, and it becomes increasingly coarse as the floe size increases and coverage decreases when bursts of ice breaking occur. Figures 5.4.19 and 5.4.20 show the predicted ice resistance variations with ice thickness and size.

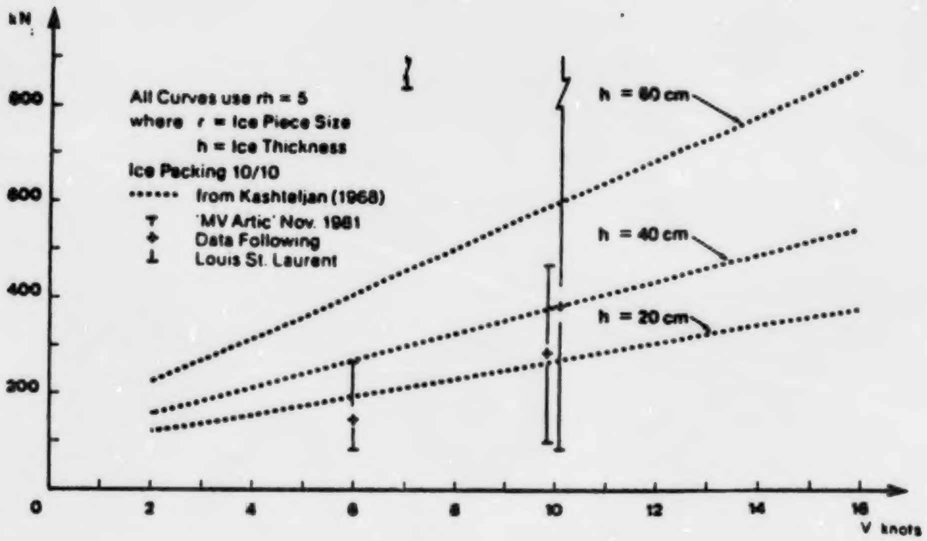

Figure 5.4.19 Measured M.V. Arctic Broken Ice Resistance Comparison with Empirical Predictions as a Function of Ice Thickness

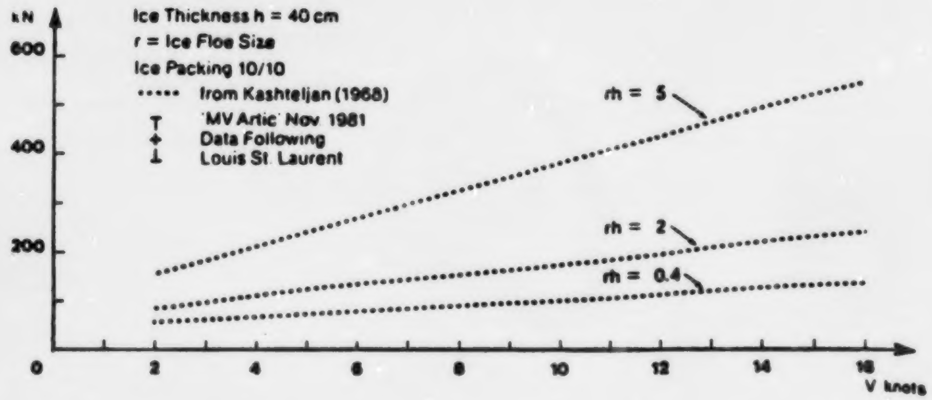

Figure 5.4.20 Measured M.V. Arctic Broken Ice Resistance Comparison with Empirical Predictions as a Function of Floe Size

5.4.3 Ice Impact Loads

Ice impact loads are caused by different ice features in each of the different regions. In the the Beaufort Sea impacts between structures and free floating first-year and multi-year ice features are possible. In the arctic archipelago structures may be impacted by first-year and multi-year ice features, icebergs and ice islands. In Hudson Bay a structure is exposed to first-year ice features. In Baffin Bay and Davis Strait structures are exposed to first-year ice features, multi-year ice features, and icebergs. In the subarctic marginal ice areas such as the Grand Banks, ice impacts may range from first and multi-year ice features to icebergs.

Depending on the relative velocity between the impacting ice feature and the floating structure, the masses and the added masses of the colliding bodies, and the geometry of the contact zone, a force will be produced between the ice feature and the floating structure, accelerating each body. The interaction of the colliding bodies is governed by the equations of motion for each body, taking into account all the forces acting which includes hydrodynamic, wind, mooring, inertial and the interactive ice force.

The ice impact force is an equilibrium force between the ice failing and the structure yielding. In this section of the report the analytic modeling of dynamic ice/structure interactions is examined.

5.4.3.1 Ice Impact Force Model

Since the scenario of an ice feature impacting a floating structure is dynamic in nature, an analytical model of the impact force generated between the colliding bodies should recognize the need to describe the magnitude of this force in terms of the relative positions and velocity of approach of the bodies.

Experimental studies by El-Tahan et al., (1985) and Swamidas (1986) were undertaken in parallel with analytical models similar to the type described above. Good agreement was found between the analytical and experimental models over the limited range of investigation.

Early modeling by Cammaert et al., (1983) presented a single degree of freedom (SDOF) model for a semisubmersible with the impact force modeled by a pre-calculated input to the SDOF model. Later works by Kitami et al., (1984) and Acres (1983) on ice impacts on semisubmersibles and Koehler and Jorgenson (1985) on ice impacts on ship-shaped vessels included the mass of the ice feature in the impact analysis. To accomplish this, "force-penetration" curves accounting for ice crushing and structural yielding were first determined and then modeled by non-linear springs linking the masses of the ice feature and the vessel in a multi-degree-of-freedom model. The shortcoming of the pre-determined spring system is obvious: the springs themselves were determined by an assumed sequence of events in an ice/indentor interaction, whereas a dynamic ice impact would probably generate a different sequence of events in the ice/vessel interaction. Figure 5.4.21 shows the pre-determined modeling of the interactive springs in a ship-ice collision model (Koehler and Jorgenson).

More recent work in two AOGA joint industry projects in 1986 and 1987 resulted in numerical models in which the ice/structure interactive force is calculated as a function of the relative kinematics between the ice and the floating structure during the course of an impact scenario. This ice force depends on a number of related factors:

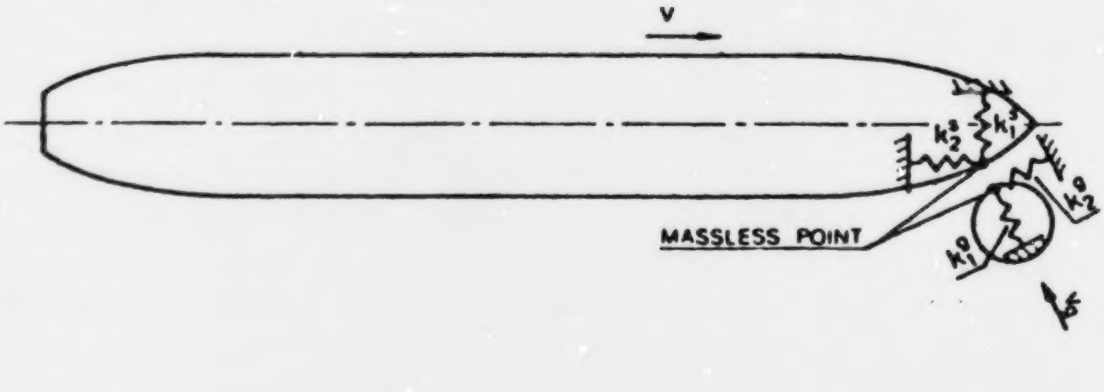
V
k_2^s
k_1^s
MASSLESS POINT
k_2^o
k_1^o
V_o

Figure 5.4.21 Pre-Determined Springs in a Ship-Ice Collision Model

- the relative location between the ice feature and the floating structure: This determines the size and shape of the ice/structure contact area, which affects the failure mode of the ice and the available resisting structural strength.
- the relative speed and direction of approach between the surfaces of contact: This affects the strain rate in the ice and in the structure. The strength of the ice is strain rate dependent (see earlier sections and Section 5.4.3.2) and the rupture strain of the structure is also strain rate dependent (see Section 5.4.3.3).

In this model, the impact ice force time history, the force versus indentation for the ice and the force versus indentation for the structure can be generated simultaneously for the ice/structure collision being analyzed.

5.4.3.2 Ice Impact Strength

The strengths of sea ice and glacial ice are briefly described in Chapter 3. This section of the report contains a review of the theories used for the calculation of ice forces based on ice strengths and a recapitulation of the relevant factors affecting ice strengths.

The compressive strength of ice is a function of temperature and strain rate, and in the case of sea-ice, brine volume. For an ice impact analysis, the variation of strength with strain rate is of the most interest.

Test data on the strain rate dependency of ice compressive strength show that there is a tendency for the strength to increase with strain rate up to a so-called "transition" strain rate at about 10^{-3} s^{-1}.

Most of the available data to date on strain rate dependence of the ice compressive strength are results of constant strain rate tests. In an ice impact, however, the strain rate varies from high brittle failure strain rates to low plastic failure strain rates. Future work on the effect of varying strain rate during ice indentation can help to clarify the use of the present day strength data in a solution to the ice impact analysis.

At strain rates higher than the transition strain rate, the failure mode of ice is of a brittle nature. At strain rates lower than the transition strain rate, the failure mode of ice takes on a ductile nature. Depending on the aspect ratio of the contact area, an ice floe may fail in an in-plane (Figure 5.4.22) or in an out-of-plane manner (Figure 5.4.23).

For the in-plane failure mechanism, upper bound plasticity solutions such as that advanced by Ralston (1978) are readily found in the literature. In particular, for the case where a relatively straight edged ice floe hitting, say, a semisubmersible column at an oblique angle, an adaptation of the theory by Meyherhof (1953) gives an upper bound plasticity solution. Consider the failure mechanism shown in Figure 5.4.22.

Using Meherhof's theory the normal pressure Q_n to cause failure is given by the solution to the following simultaneous equations:

$$Q_n = (c + P \tan(\phi)) [(\sin (2 \psi - \phi) + \sin(\phi)] / \cos(\phi) + P$$

$$Q_n = (c + P \tan(\phi)) [\cos(2 \psi - \phi) + \cot(\alpha)] / \cos(\phi)$$

...Eqn.'s 5.4.11

where:

$$P = [c (1 + \sin(\phi)) e^{2 \theta \tan(\phi)} - c] / \tan(\phi)$$

$$\theta = 3 \pi / 4 + \phi/2 - c$$

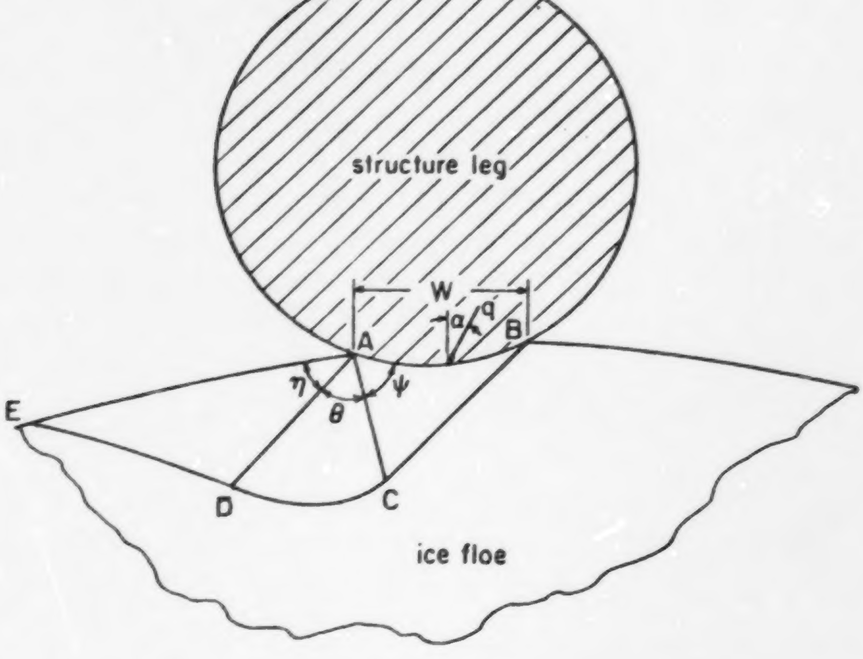
structure leg
W
α
q
A
B
η
θ
ψ
E
D
C
ice floe

Figure 5.4.22 In-Plane Plastic Failure Mechanism for an Ice Floe Impacting a Semisubmersible Column

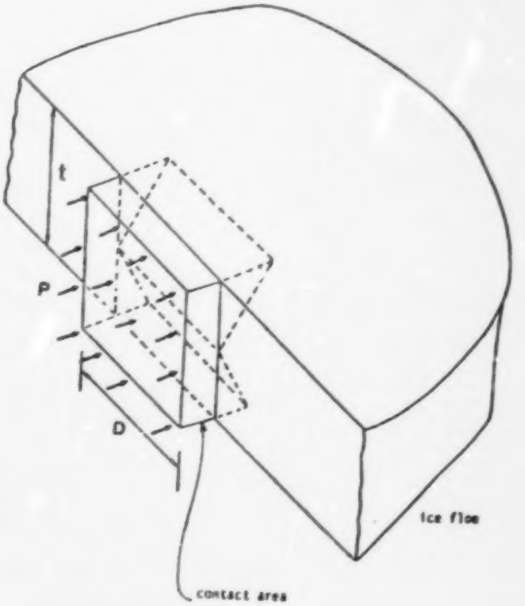
t
P
D
ice floe
contact area

Figure 5.4.23 Out-Of-Plane Palstic Failure Mechanism for an Ice Floe Impacting a Semisubmersible Column (Tresca Material)

The ice properties c, unit cohesion and ϕ, the angle of internal friction, may be for a Tresca or a Coulomb type material.

For the out-of-plane mechanism, the upper bound plasticity solutions described in Coon et al (1984) are applicable for impacts that are perpendicular to the flat face of the ice floe as shown in Figures 5.4.23 and 5.4.24 for Tresca and Coulomb materials respectively.

The normal stress, Q_n, to cause failure is given by:

$Q_n = \sigma_c (1.0 + 0.35\, t / D)$ for a Tresca material and
$Q_n = \sigma_u (1.0 + C_1(\phi)\, t / D)$ for a Coulomb material

where:

σ_u = unconfined compressive strength
σ_c = compressive strength under high confining pressures
t = height of contact area
D = width of contact area and
C_1 = as defined in Figure 5.4.25.

For oblique impacts, the failure mechanism will most likely be different. There does not seem to be a readily available solution in the literature for an oblique angle.

With respect to the selection of the material behaviour model, the minimum pressure should be used from the Coulomb and Tresca material models.

The upper bound plasticity solutions described above are merely applications to the particular problem of ice floe failure of a more general and rigorous plasticity solution method. In this method, a yield surface describing the behaviour of ice under different confinement and an associated flow rule would be used. However, noting the inhomogeneity of

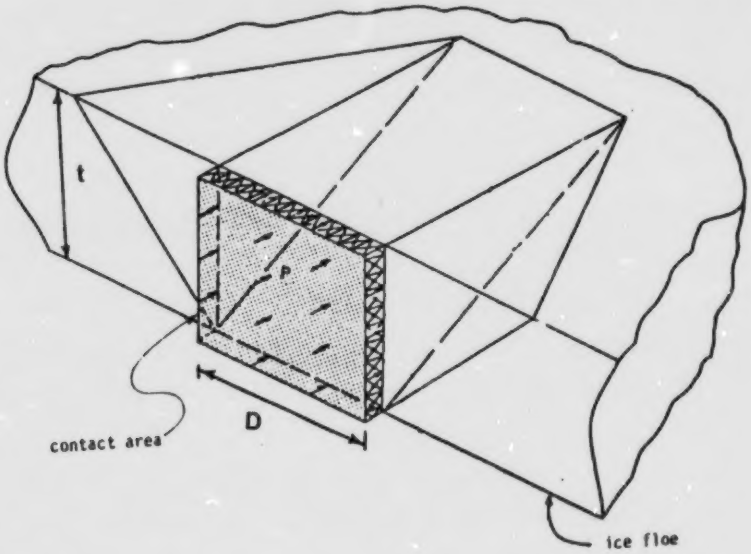
t
P
D
contact area
ice floe

Figure 5.4.24 Out-Of-Plane Plastic Failure Mechanism for an Ice Floe Impacting a Semisubmersible Column (Mohr-Coulomb Material)

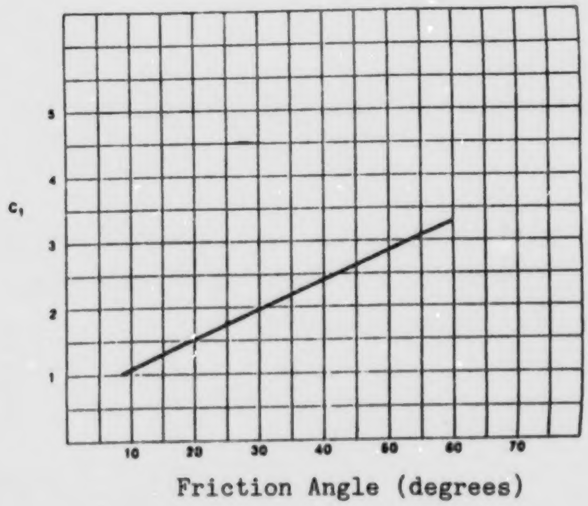

Figure 5.4.25 Indentation Factor C_1 versus Friction Angle

naturally occurring ice features, it is evident that any plasticity solution must take into consideration factors such as the occurrences of different ice growth orientations, the change in the ice crystal structure with depth in an ice sheet, and the unevenness in the ice thickness and leading surface.

5.4.3.3 Effect of Structural Indentation on Ice Impact Force

A yielding indentor affects the relative velocity between the indentor surface and the impacting ice. This phenomenon is discussed in Section 5.6 on the effects of the motion of the structure on the crushing of ice.

It suffices to mention here that the determination of structural plastic indentation requires the consideration of a number of factors including:

- the plastic and buckling behaviour of the various structural elements such as the hull plate, the hull stiffeners, the web frames or the ring stiffeners, the bulkheads, the decks and the various connections,

- the rupture strain at critical locations on these structural elements, and

- the load distribution mechanisms among these structural elements.

Applications of structural mechanics in plastic behaviour include the work by Zayas et al., (1985) on semisubmersible columns and the work by Wierzbicki et al., (1984) on vessel hulls.

5.4.4 Future Work

Most of the current state-of-the-art techniques of evaluating ice/floating structure interaction have drawn on empirical data from tests performed on fixed structures. To further the understanding of the ice/floating structure interaction, future work should therefore include desk and field studies on:

- pack ice jamming, clearing and rubble accumulation in a full range of wave, current and wind climate.
- hydrodynamics of ice impacting a floating structure, that is when two bodies are accelerating in close proximity.
- material behaviour of natural occurring ice under impact (brittle failure) conditions.
- integrate analytical and experimental studies by cross calibration and compilation.

5.5 Ice Interactions With Artificial Islands

5.5.1 Types of Structures

In this report an artificial island is defined as a structure which will, during the course of a winter, have a stationary rubble pile around it. This definition encompasses sacrificial beach islands, sandbag retained islands, and caisson type structures on berms where the depth to the top of the berm is such that ice will ground out and initiate rubble pile formation.

Relevant artificial island parameters include:

- top surface diameter,
- distance to the top of the berm (for caisson structures),
- slope of waterline penetrating portion of island, and
- local grounding frequency (or anchoring capability) of rubble.

In Figure 5.5.1 three different artificial island designs are illustrated.

A sacrificial beach island is designed with a large beach or shallow sloped region surrounding the working surface. Thin ice grounds out on the beach and rubble formation is initiated. During the summer wave energy is dissipated on the beach.

A sand-bag retained island uses sandbags on a steep slope to dissipate wave action. The volume of material is less than that required for a sacrificial island.

The third type of island illustrated in Figure 5.5.1 is a caisson retained island. Building on the principle of the sand-bag retained island, caissons are used to penetrate the waterline. The caissons are typically placed on a subsea berm, though in shallower water it is possible to place the caissons on a modified portion of the seabed.

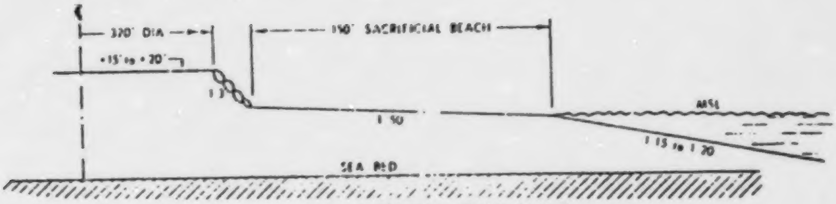
320' DIA
150' SACRIFICIAL BEACH
+15' to +20'
1:3
1:50
MSL
1:15 to 1:20
SEA BED

SACRIFICIAL BEACH ISLAND

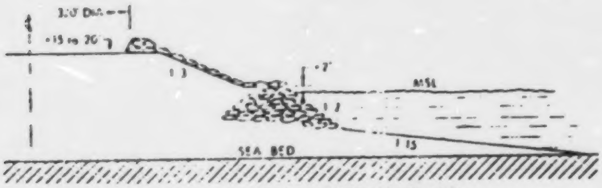
320' DIA
+15 to 20'
1:3
+7'
MSL
1:2
1:15
SEA BED

SAND-BAG RETAINED ISLAND

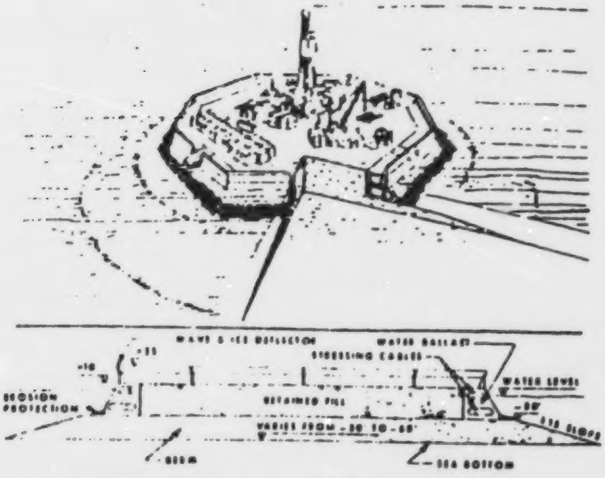
WAVE & ICE DEFLECTOR
WATER BALLAST
STRESSING CABLES
WATER LEVEL
EROSION PROTECTION
RETAINED FILL
VARIES FROM -30 TO -60'
BERM
SEA BOTTOM

caisson retained island

Figure 5.5.1 Artificial Island Designs

5.5.2 Landfast Ice Loads

The Labrador coast, Baffin Bay and Davis Strait, Arctic Archipelago and Beaufort Sea regions all exhibit landfast ice zones. A landfast ice zone is a band of ice near the shoreline which, during the winter, is anchored to the shoreline. Ridges ground out in the shallow water and abate large scale motion in this zone. In the arctic archipelago the landfast ice situation is different from the other areas due to the possibility of the ice surviving the summer melt season. Much of the archipelago shoreline can be classified as a "multi-year landfast ice area" in contrast to the other areas which are seasonal or first-year landfast ice areas. For structural design account must be taken of the possibility of landfast ice surrounding the structure.

There are several types of action which may induce loading on a structure located in a landfast ice zone. The two most common are:

- build-up of stresses due to wind action over the landfast ice zone area, and

- thermal expansion loads caused by temperature changes.

Landfast ice loads are treated as low strain rate events due to the stress in the ice sheet building up over a reasonable length of time compared to more typical events such as a floe impacting a structure.

The landfast ice itself may move short distances during the course of a winter. Typical motions are on the order of less than a few metres with greater probability of movement closer to the outer edge of the landfast ice. During these motions significant ice events have been observed in the Beaufort Sea.

As part of general ice research programs, petroleum companies exploring in the Beaufort Sea developed technology whereby ice stresses could be measured in-situ. Some of the earliest data from the in-situ ice pressure sensors have recently become public.

A summary of the early data was presented by Sanderson (1984) as follows:

Adgo P - 25

- failure stress was estimated to be greater than 0.83 ± 0.07 MPa (120 psi).
- movement was less than 6 cm in 6 hours, i.e. at low ductile rates

Netserk F - 40

- In-situ stress panels measured stresses of up to 1.1 MPa (160 psi).
- Ice velocity was on the order of tenths of metres per hour (ranging from 0.0 m/hr to about 0.4 m/hr).

Netserk B - 44

- 0.6 to 0.8 MPa (85 to 115 psi), peak at 1.5 MPa (220 psi)

Arnak L - 30

- typical stresses were about 0.35 MPa (50 psi), with a peaks in the range of 1.1 to 1.35 MPa (160 psi to 190 psi).

Note that Sanderson has applied calibration factors to some of the data so the numbers above may not exactly match those in the original work.

Shallow water artificial islands in the Beaufort Sea have been designed for ice failure stresses of approximately 1.75 MPa (250 psi). Many years of operating experience have shown that this level is adequate and may be conservative. Unfortunately, even with winter long programs in effect, the ice rarely interacts with a structure in a situation where one would expect a maximum stress to occur. No artificial islands designed to 1.75 MPa have failed to date. First-year ice sheet stresses close to 1.75 MPa have been recorded on the Molikpaq beyond the landfast ice in the Beaufort Sea.

5.5.3 Rubble Pile Formations and Ride-Up

Rubble formations, extensive three dimensional accumulations of sea ice fragments, are comprised of blocks of ice with a more or less random orientation. Rubble fields form around most offshore structures located in a dynamic ice environment. Typically, they form when the parent sheet ice encounters a wide obstruction such as an artificial island or offshore structure, and the sheet ice is broken up into blocks which accumulate to form a rubble field, such as shown in Figure 5.5.2.

The influence of rubble fields is multi-fold:

i) they change the ice failure mode,

ii) they change the force intensity transmitted to the structure at the water-line,

iii) they influence detailed design considerations such as access to the structure, water intake, design of structure height, ice deflector strength and geometry, etc.,

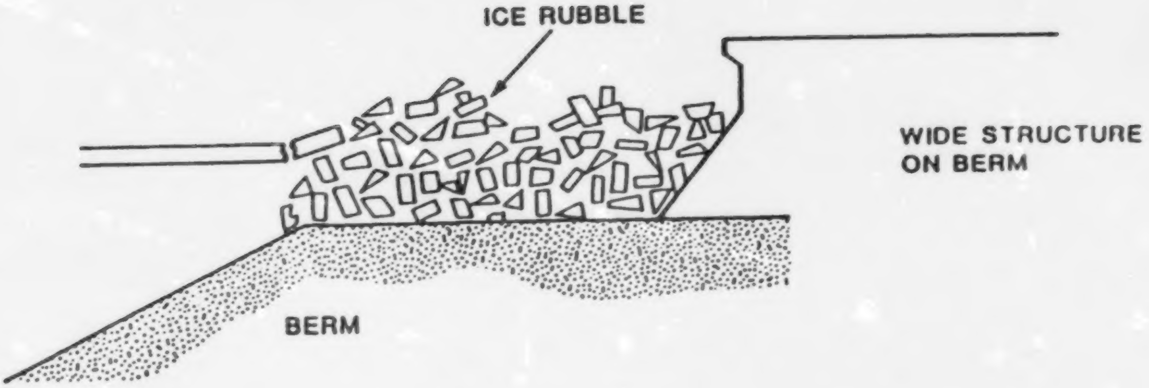
ICE RUBBLE
WIDE STRUCTURE
ON BERM
BERM

Figure 5.5.2 Rubble Field Formation (Croasdale, 1985)

iv) they offer use as a platform for storing supplies, acting as a base for spraying an ice pad for relief wells or exploration drilling purposes, and

v) they offer use as a construction material when created artificially.

The first two points are discussed later in this section. The latter three points are not examined in this report, except to say that the third and fourth points influence scheduling and detailed design considerations, while the fifth point offers a potential for exploiting natural ice as a construction material.

The extent and influence of rubble fields is a function primarily of water depth, ice thickness, ice movements, strength properties of the ice and geometry of the structure.

5.5.3.1 Ride-Up Observations and Calculations

Ice ride-up on a slope can occur if the slope is shallow, and if the parent ice sheet is intact, and, possibly, warm or pliable so that it can bend without fracturing. Sun Oil, for example, experienced early winter ride-up onto the working surfaces of their artificial islands in shallow water in the Mackenzie River delta area of the Canadian Beaufort Sea, as did Esso Resources at Issungnak artificial island when the ice sheet was 0.7 to 0.8 m thick during a December 17-20, 1979 storm (Shinde, 1981). An "ice push" of about 150 m was documented by Taylor (1978) on Somerset Island. A simple model of ice push or ride-up is shown in Figure 5.5.3.

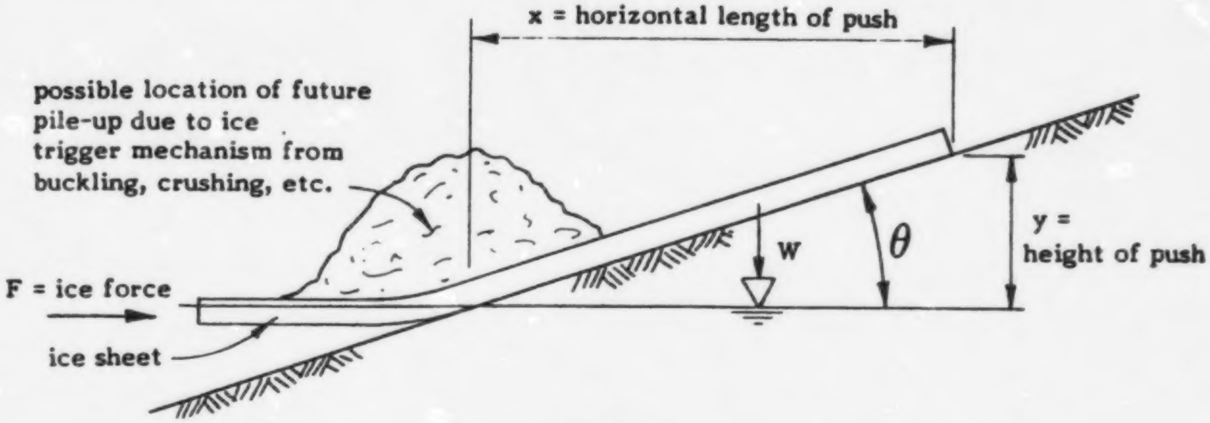
x = horizontal length of push
possible location of future pile-up due to ice trigger mechanism from buckling, crushing, etc.
W
θ
y = height of push
F = ice force
ice sheet

a. Geometry

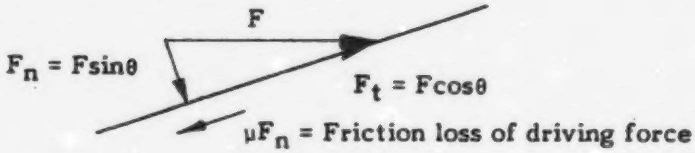
F
F_n = Fsinθ
F_t = Fcosθ
μF_n = Friction loss of driving force

b. Resolution of Driving Force

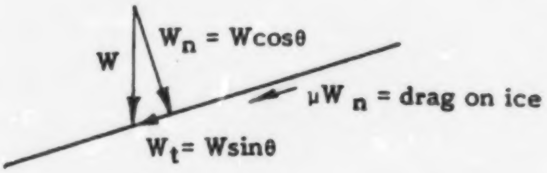
W
W_n = Wcosθ
μW_n = drag on ice
W_t= Wsinθ

c. Resolution of Weight of Ice

Figure 5.5.3 Simple Model of Ice Push or Ride-up

The weight, W, of the pushed ice, per unit width, is:

$$W = \rho_i \; g \; t \; x \; / \; \cos(\theta) \qquad \text{... Eqn. 5.5.1}$$

where:

ρ_i = density of ice, 915 kg/m^3,
g = 9.81 m/sec^2,
t = thickness of ice sheet,
x = horizontal length of push, and
θ = slope angle.

The force equilibrium equation is:

$$F_t - \mu F_n = W_t + \mu W_n \qquad \text{... Eqn. 5.5.2}$$

which can be solved for the horizontal length of push, x:

$$x = (F \; / \; \rho_i \; g) \cos(\theta) \; [\; 1 - \mu \tan(\theta) \;] \; / \; [\; \tan(\theta) + \mu \;] \qquad \text{... Eqn. 5.5.3}$$

The height of ride-up, y, is:

$$y = (F \; / \; \rho_i \; g) \sin(\theta) \; [\; 1 - \mu \tan(\theta) \;] \; / \; [\; \tan(\theta) + \mu \;] \qquad \text{... Eqn. 5.5.4}$$

The limiting ice force, F, is a function of:

- the crushing strength of ice,
- the flexural strength of ice,
- the buckling strength of ice, and so the integrity of the ice, (i.e., whether it is fractured or competent).

A discussion of pile-up heights and driving forces is given in several references, including Allyn (1980) and Cox et al., (1983). Table 5.5.1 gives the buckling strengths of competent ice sheets of varying thickness (Allyn, 1980).

Buckling strength is calculated using Equation 5.5.5.

$$\sigma_b = (K\ E\ (1 - \nu^2)\ t\ /\ 12)^{\frac{1}{2}}\ (\text{MPa}) \qquad \text{... Eqn. 5.5.5}$$

Table 5.5.1 Buckling Strength of a Competent Ice Sheet

t	σ_b	
.05 m	.242 MPa	(35 psi)
.1	.342	(50)
.5	.764	(111)
1	1.08	(157)
2	1.53	(222)
3	1.87	(271)

Note: $K = .01$ MPa/m; $E\ (1 - \nu^2) = 1400$ MPa

For a buckling strength of about 0.7 MPa (100 psi), an ice sheet thickness of 0.5 m, a friction coefficient of 0.6 (for sand construction) and a slope of 10°, the length of ice push is calculated as:

$x = 85$ m

Thus, for the high arctic, where the ice is thicker and stronger, ice push or ride-up lengths similar to those observed by Taylor (1978), in the order of 150 m, can be expected. Methods of reducing ride-up by inducing instability at a slope change have been examined in a model test study (Rosenegger, 1981), as shown in Figure 5.5.4 and and in the field "tank

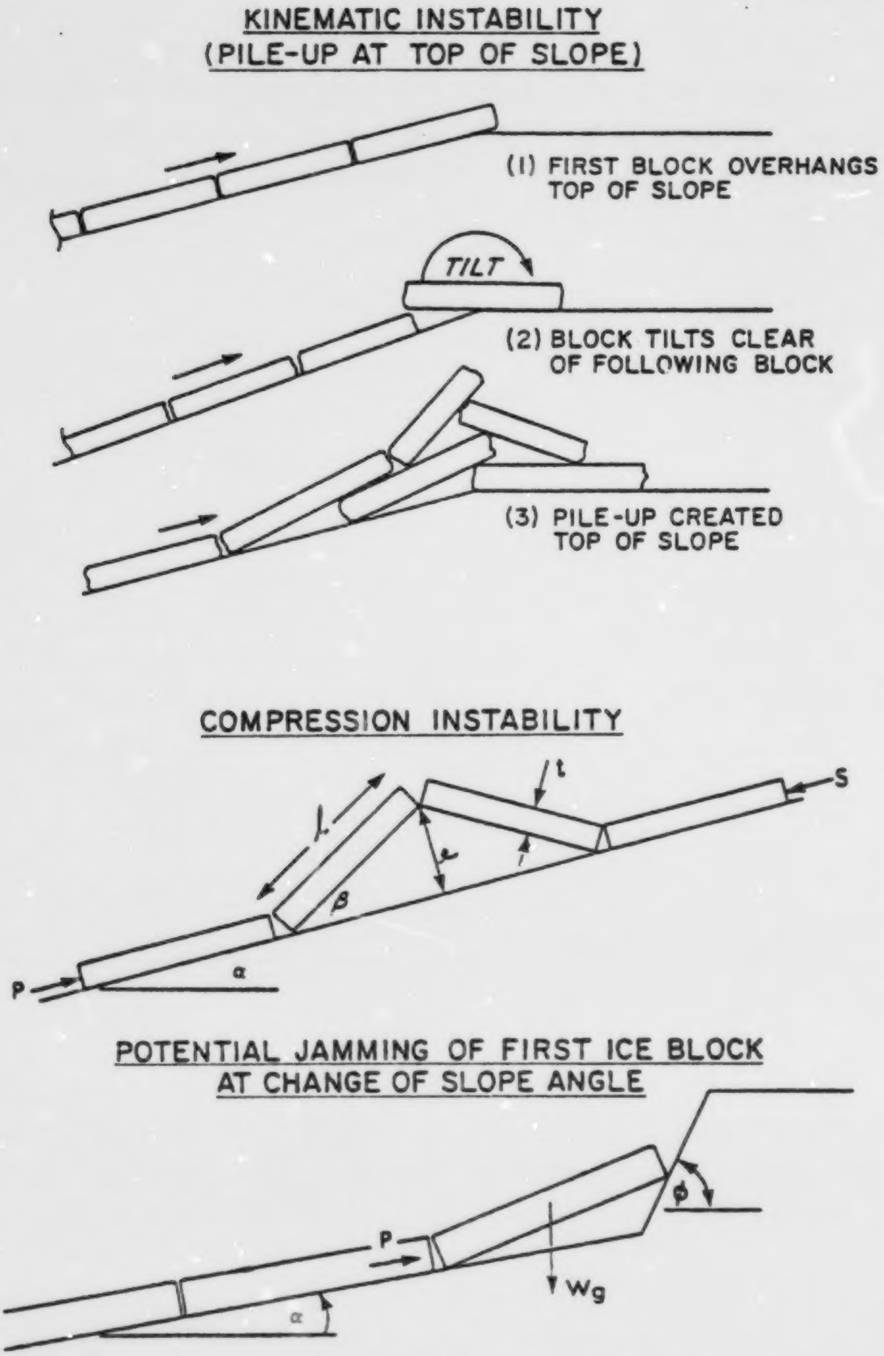
KINEMATIC INSTABILITY (PILE-UP AT TOP OF SLOPE)

COMPRESSION INSTABILITY

POTENTIAL JAMMING OF FIRST ICE BLOCK AT CHANGE OF SLOPE ANGLE

(1) FIRST BLOCK OVERHANGS TOP OF SLOPE
TILT
(2) BLOCK TILTS CLEAR OF FOLLOWING BLOCK
(3) PILE-UP CREATED TOP OF SLOPE
t
S
l
e
i
β
P
α
P
φ
Wg
α

Figure 5.5.4 Slope Instability Mechanisms (Croasdale et al., 1978)

traps" have been placed on the slopes of the barrier islands in the Alaskan Beaufort Sea (Vaudrey and Potter, 1981). Proposed designs to prevent ride-up are shown in Figure 5.5.5 (Croasdale et al., 1978).

For a highly fractured ice sheet, the driving force necessary to induce buckling can be calculated using Hetenyi's theory (1946) for finite length beams on an elastic foundation, which has been adapted to ice mechanics by Allyn (1980). The driving force in a fractured ice sheet, comprised of individual floes, is very much dependent on the characteristic size of the ice blocks or floes, but may be an order of magnitude lower than the driving force for a competent ice sheet.

For a competent ice sheet, a limit mechanism to ride-up and pile-up is derived in detail in Allyn (1980), and essentially occurs when the crushing strength is reached in the top fiber of the floe, and the tensile strength is reached in the bottom fibre of the floe. The associated driving force is:

$$F = t (\sigma_c - \sigma_t) / 2 \qquad \text{...Eqn. 5.5.6}$$

where:

t = floe thickness,

σ_c = crushing strength, (a function of temperature and salinity), and

σ_t = tensile strength, (a function of temperature and salinity).

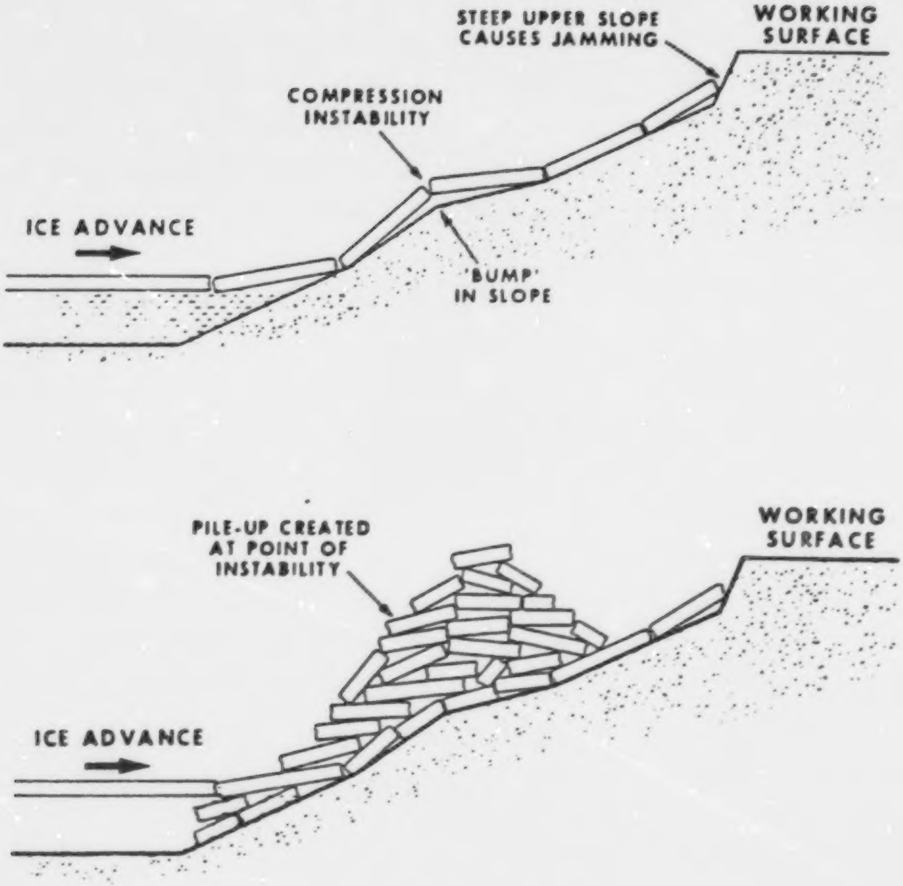
STEEP UPPER SLOPE CAUSES JAMMING
WORKING SURFACE
COMPRESSION INSTABILITY
ICE ADVANCE
'BUMP' IN SLOPE
PILE-UP CREATED AT POINT OF INSTABILITY
WORKING SURFACE
ICE ADVANCE

Figure 5.5.5 Island Design Details to Prevent Ride-up (Croasdale et al., 1978)

5.5.3.2 Pile-up Observations and Calculations

There are essentially two types of pile-ups:

- grounded, and
- free floating.

The pile-up mechanisms and driving forces are totally different for grounded and free floating pile-ups. Furthermore, the ice/rubble interactions vary for each type of pile-up, both spatially and with time. For reasons of complexity, as no one theory can explain all of the observed phenomena, the ice engineer must exercise considerable judgment when calculating pile-up heights and driving forces.

Grounded pile-up formations can be very spectacular, and pile-up heights of 30 m have been observed (Taylor, 1978). A ride-up mechanism developed by Allyn (1980) is shown in Figure 5.5.6, a field example of which is shown in Figure 5.5.7 from Taylor (1978).

Less frequently, but certainly not less spectacularly, are pile-ups formed by an extrusion process as shown in Figures 5.5.8 and 5.5.9 (Hudson et al., 1981; Hudson, 1983).

The model of grounded pile-up heights proposed by Allyn (1980) is readily amenable to a closed form theoretical solution, and the pile-up heights are plotted in non-dimensional form in Figure 5.5.10, which is a plot of the angle function in Equation 5.5.4, versus angle of pile-up and for varying friction coefficient.

The effect of ice thickness, temperature and salinity were investigated by Allyn and Charpentier (1982), with the theories of Ryvlin (1974) and Colbeck (1980) used to produce the curve shown in Figure 5.5.11.

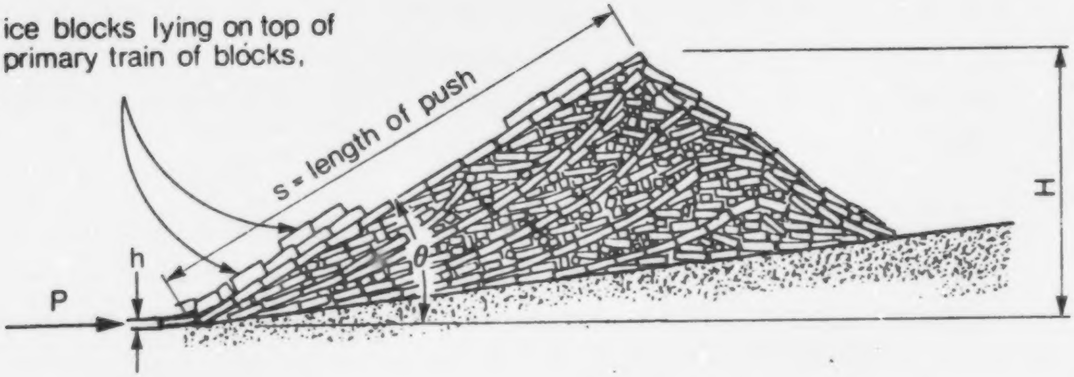
ice blocks lying on top of
primary train of blocks,
s = length of push
h
P
θ
H

Figure 5.5.6 Model of Grounded Pile-up (after Allyn, 1980)

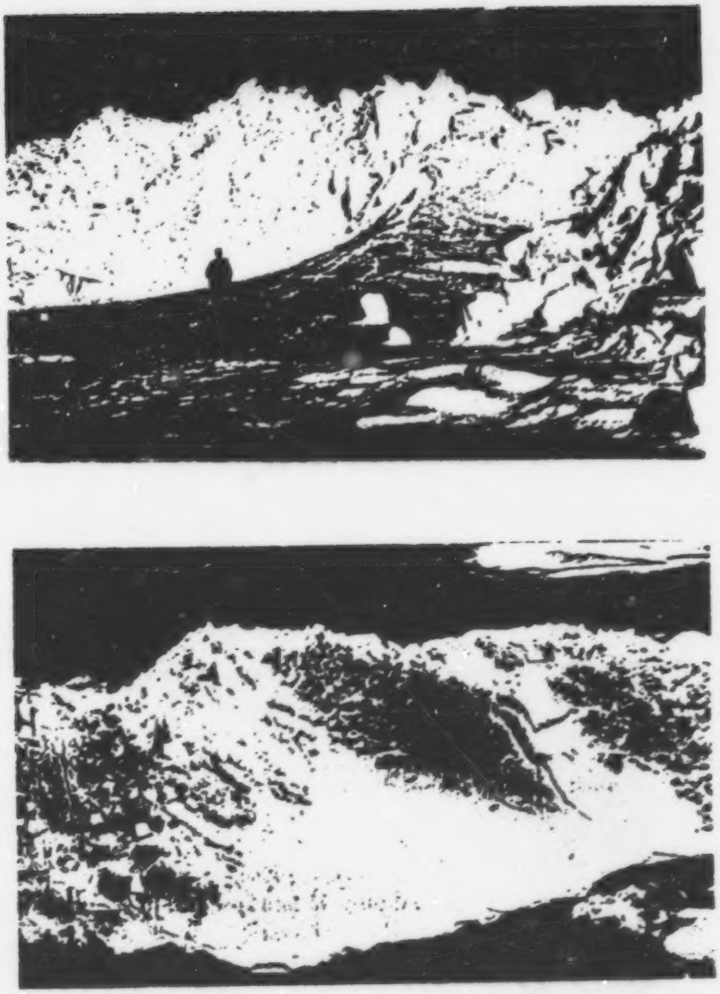

Figure 5.5.7 Observed Grounded Pile-Ups (after Taylor, 1978)

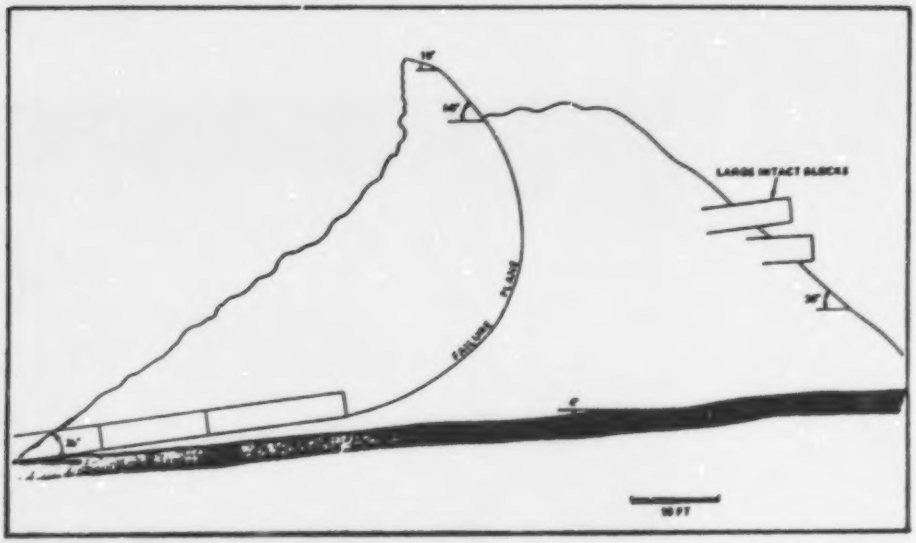
LARGE INTACT BLOCKS
FAILURE PLANE
10 FT

Figure 5.5.8 Model of an Extruded Grounded Pile-Up
(Hudson et al., 1981)

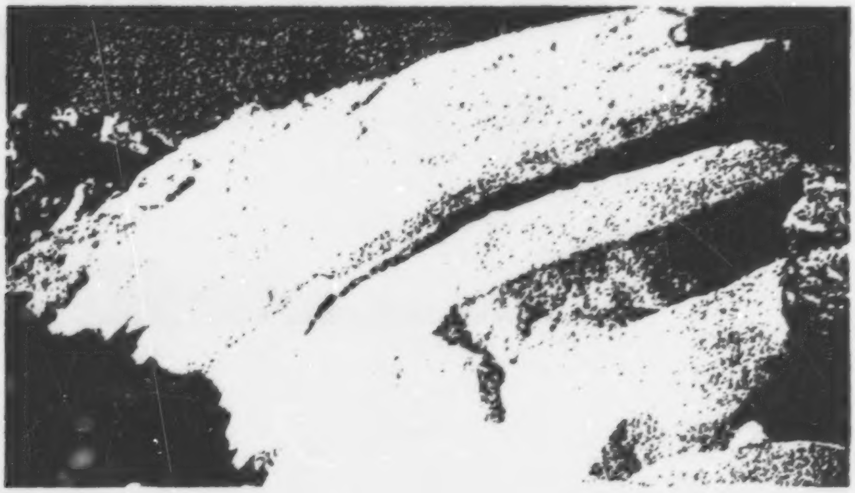

Figure 5.5.9 Observed Extruded Grounded Pile-Up
(Hudson 1983)

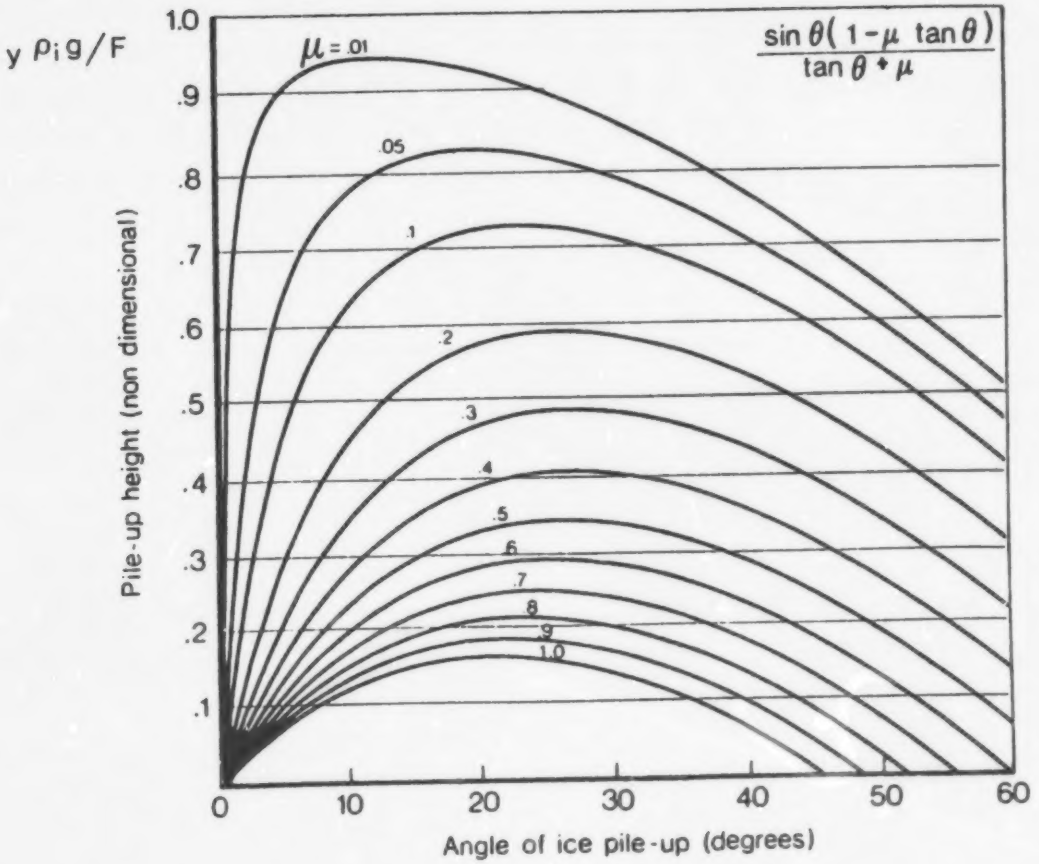

Figure 5.5.10 Non-Dimensional Height of Pile-Up versus Angle of Pile-Up for Various Friction Coefficients (Allyn, 1980)

The data in Figure 5.5.11 has been used in the design of ice deflectors, notably for Gulf Canada's Molikpaq (Bruce et al., 1982), where the top of the deflector is about 14 m above water level. The deflector is sloped seaward to turn back higher pile-ups generated from thick multi-year ice, which minimizes the probability of blocks of ice overtopping the deflector. The deflector was model tested for effectiveness in both ice and wave tanks.

Free floating rubble piles, or ridges, are generally formed from flexural failure of the ice sheet, due principally to unbalanced loads and moments on the sheet. This is due to offsets in the sail and keel of the ridged ice (Parmerter and Coon, 1977 and 1973). An example of free floating ridging is shown in Figure 5.5.12 (Allyn and Wasilewski, 1979).

Free floating pile-up heights are shown in Figure 5.5.13.

The limit free floating ridging force derived by Parmerter and Coon (1973) using energy methods, is:

$$F_{ff} = \tfrac{1}{2} \rho_i \, g \, t \, H_s \qquad \text{...Eqn. 5.5.7}$$

where:

F_{ff} = conservative free floating ridging force per unit length, and
H_s = free floating sail height.

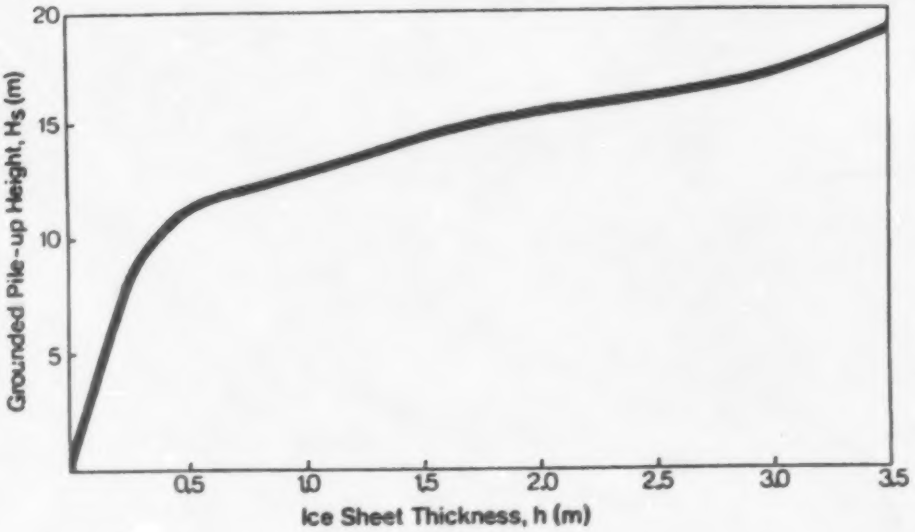

Figure 5.5.11 Grounded Pile-Up Heights
(Allyn and Charpentier, 1982)

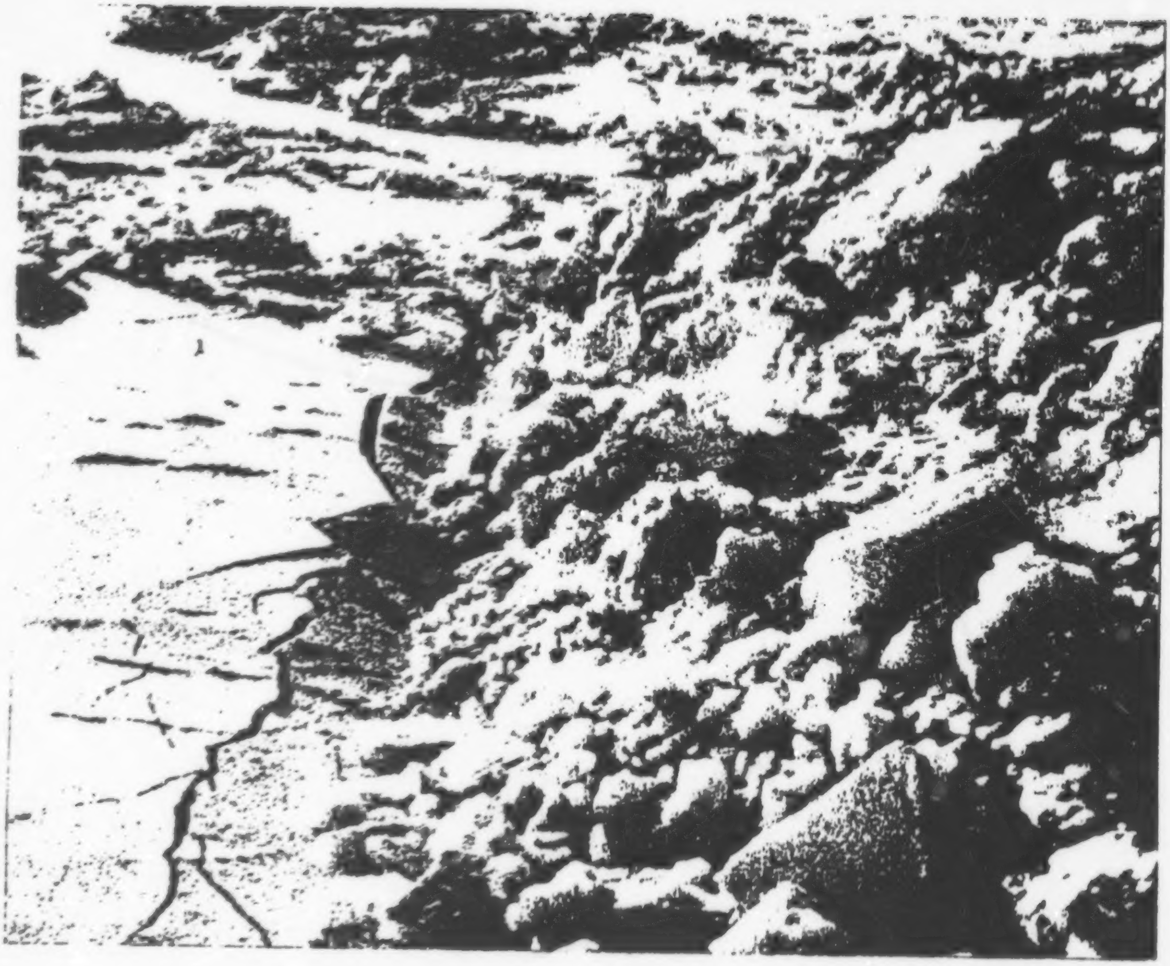

Figure 5.5.12 Downward Breaking Ridging Mechanisms
(Allyn and Wasilewski, 1979)

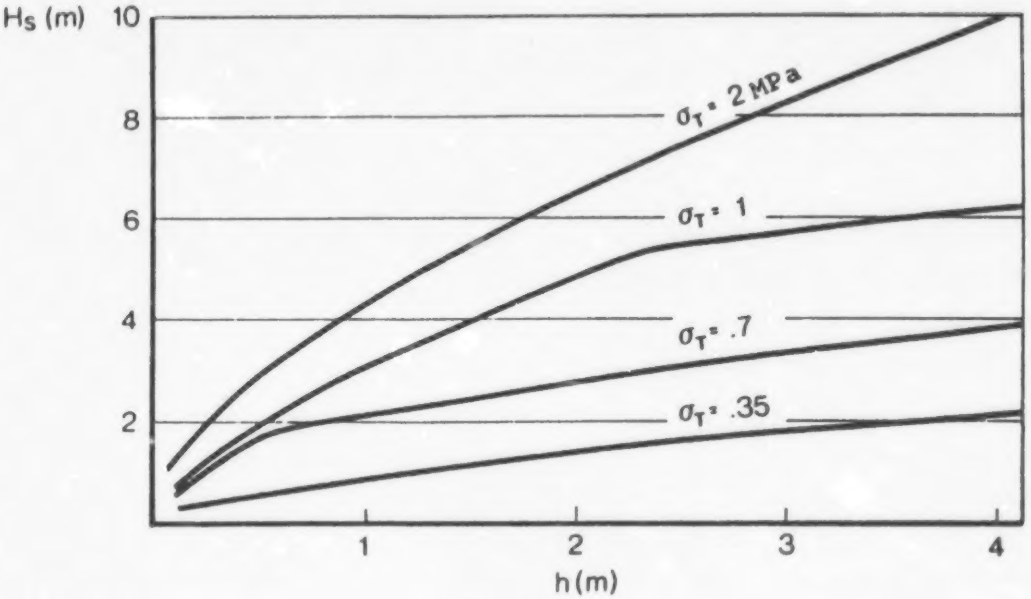

Figure 5.5.13 Free Floating Pile-Up Heights
(Parmerter and Coon, 1973)

The force calculated using Equation 5.5.7 is conservative in the sense that the process is reversible without losses. Allyn and Charpentier (1982) have included the nonconservative forces of friction and passive pressure:

$$F = \tfrac{1}{2}\rho_i\, g\, H_s^2 \left[\gamma_s \left(\mu_s \cot(\theta) + 2\, K_p \frac{t}{Hs}\right) + \frac{H_k}{H} \gamma_k\, \mu_k \cot(\phi) \right] + F_{ff} \qquad \text{...Eqn. 5.5.8}$$

where:

F = total free floating ridging pressure per unit width,

t = thickness of parent ice sheet or floe,

H_k = keel depth below the ice sheet,

H_s = sail height above the ice sheet,

K_p = passive pressure coefficient,

γ_s = porosity of sail,

γ_k = porosity of keel,

μ_s = ice sheet to sail friction coefficient,

μ_k = ice sheet to keel friction coefficient,

θ = angle between sail and horizontal,

ϕ = angle between keel and horizontal, and

F_{ff} = conservative free floating ridging force per unit length.

5.5.4 Ice/Rubble/Structure Interaction Loads

5.5.4.1 Effect of Rubble Fields on Ice Loads

The main influences on the loads transmitted to a structure surrounded by an ice rubble field are:

i. The rubble field is at least as wide as the structure, as shown in Figure 5.5.14 and so can potentially attract more load. The rubble field will tend to induce principally a flexural failure in the ice sheet, with perhaps some crushing and buckling - depending on the thickness of the sheet ice and the extent of consolidation (Kry, 1980).

ii. The rubble field may be grounded over part of its extent, and this will transmit load to the berm or seabed, as shown in Figure 5.5.15.

In dynamic ice conditions, the rubble field can continually change due to:

- accumulation of new rubble upstream of the existing rubble, and
- failure of large blocks of rubble from the sides of the rubble field, more or less perpendicular to the ice movement direction.

The accumulation and failure mechanisms are illustrated in Figure 5.5.16.

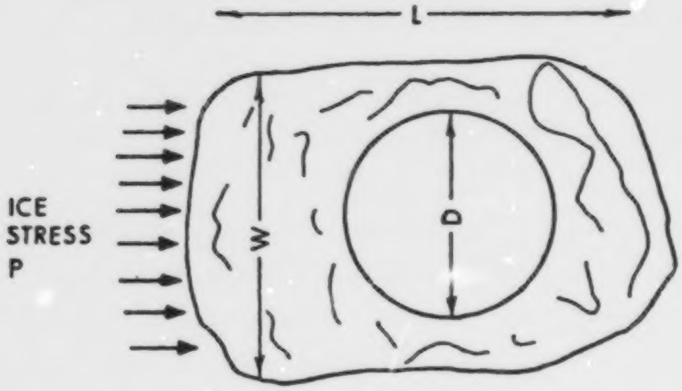
L
ICE
STRESS
P
W
D

Figure 5.5.14 Effect of Rubble Width
(Croasdale and Marcellus, 1978)

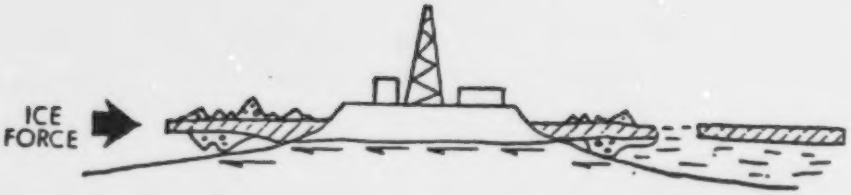

Figure 5.5.15 Illustration of Transfer of Load from Rubble to Foundation (Croasdale and Marcellus, 1978)

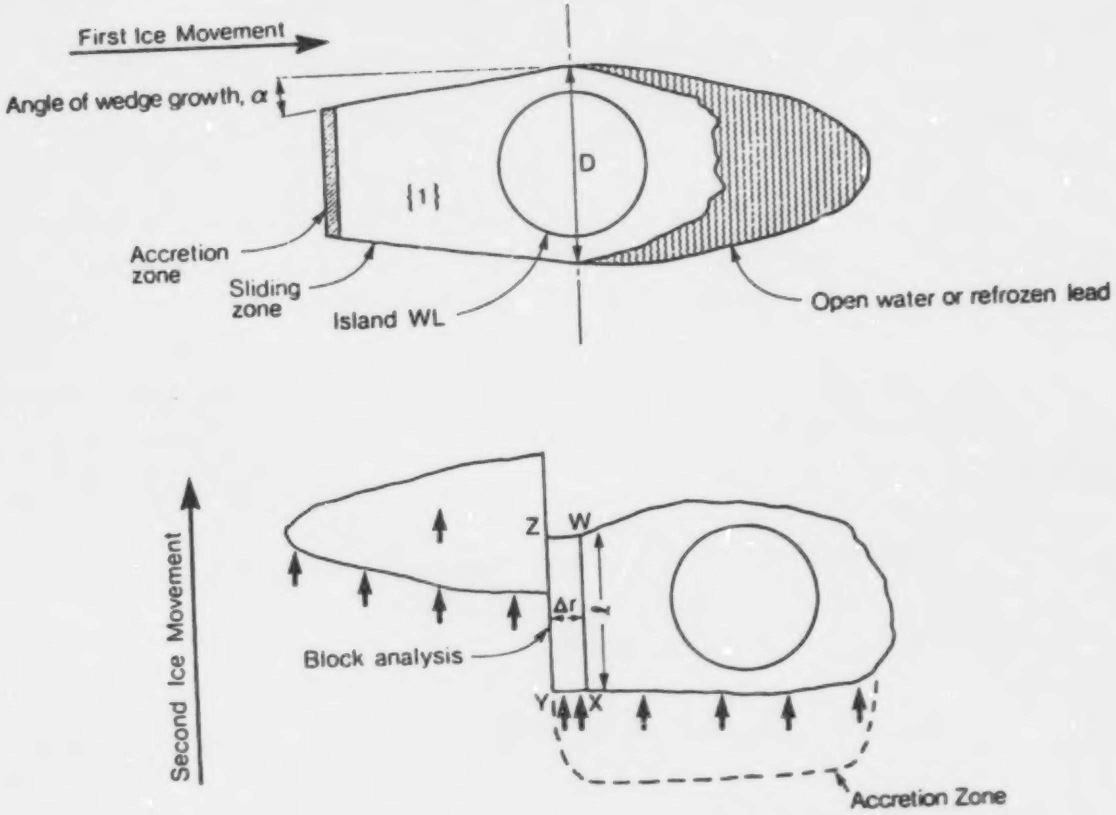
First Ice Movement
Angle of wedge growth, α
D
{1}
Accretion zone
Sliding zone
Island WL
Open water or refrozen lead
Second Ice Movement
Z
W
Δr
ℓ
Block analysis
Y
X
Accretion Zone

Figure 5.5.16 Illustration of Rubble Growth and Subsequent Block Failure Analysis (Allyn and Charpentier, 1982)

5.5.4.2 Analysis of Rubble Fields and Spray Ice Construction

The load transmitted to a structure, or an artificial island at its waterline, is the difference between the force exerted by the pack ice on the rubble field and the force transmitted to the seabed or berm by the grounded portion of the rubble field.

$$F_{structure} = F_{ice} - F_{grounding} \qquad \text{... Eqn. 5.5.9}$$

where:

$F_{structure}$ = force on a structure or artificial island at its waterline
F_{ice} = pack ice force on the rubble (Eqn.'s 5.5.5 and 5.5.6)
$F_{grounding}$ = force transmitted through the rubble to the berm or seabed.

To analyze a continually changing rubble field, Swan Wooster developed a computer program (Allyn and Charpentier, 1982) which automatically accounts for:

- ice movement velocity and direction,
- changing ice sheet thickness,
- consolidation or refreezing of the voids below the water level,
- grounding of the rubble and dissipation of the pack ice forces, and
- breakout forces in the Arctic Spring/Summer (which are calculated if the area has been landfast), using crushing loads from the large scale empirical curve (Environmental Impact Statement) presented in Section 5.2.

The maximum force that can be transmitted through the grounded rubble to the seabed can be calculated assuming a frictional material:

$$F_{grounding} = \mu_{ib} (W - B) \qquad \text{... Eqn. 5.5.10}$$

where:

μ_{ib} = coefficient of friction of ice sliding on the berm,

W = weight of the sail of the grounded rubble,

$$= H_{s,avg} \rho_i g \gamma_s A, \qquad \text{... Eqn. 5.5.11}$$

B = buoyant weight of the keel of the grounded rubble,

$$= H_{k,avg} (\rho_w - \rho_i) g \gamma_k A, \qquad \text{... Eqn. 5.5.12}$$

$H_{s,avg}$ = average sail height of the grounded rubble,
$H_{k,avg}$ = average keel depth of the grounded rubble,
ρ_i = mass density of ice (0.9 ρ_w),
ρ_w = mass density of water,
g = 9.81 m/sec^2,
γ_s = porosity of the sail,
γ_k = porosity of the keel, and
A = waterplane area of the grounded rubble.

If the outer extent of the rubble is unconsolidated and free floating where it interacts with the pack ice, then the unit load is quite low. Otherwise, grounded ridging pressures, or even crushing pressures during a break-out event, can be expected. These forces are calculated using the program which has three analysis routines:

i. a rubble field simulation routine for simulating rubble fields in dynamic ice conditions,

ii. a spray ice island simulator, which simulates the building of a spray ice island in landfast ice conditions, and

iii. a combined rubble field and spray ice simulation, where the spray ice is used to weigh down the rubble field and so achieve a grounded rubble field earlier than is otherwise possible.

5.5.4.3 Spray Ice Experience in the Beaufort Sea

Spray ice has been used on the shoulders of artificial islands to build relief well pads (Kemp, 1984), as well as for the creation of a drilling island in the landfast ice at 8 m water depth in Harrison Bay (Funegard et al., 1987), and as a protective ring around the CIDS structure in about 15 m of water in the Alaskan Beaufort Sea (Jahns et al., 1986).

The spraying at Mars Island is shown in Figure 5.5.17, while the CIDS barrier is shown in Figure 5.5.18 (from the POAC 1987 brochure) while under construction using a high volume Thure-Eureka monitor. The main advantages of spraying, as opposed to flooding, is that there is a much larger increase in surface area for droplets compared with ponded ice, and the spray monitor can cover a large island surface area by continually adjusting the vertical and sweep angles.

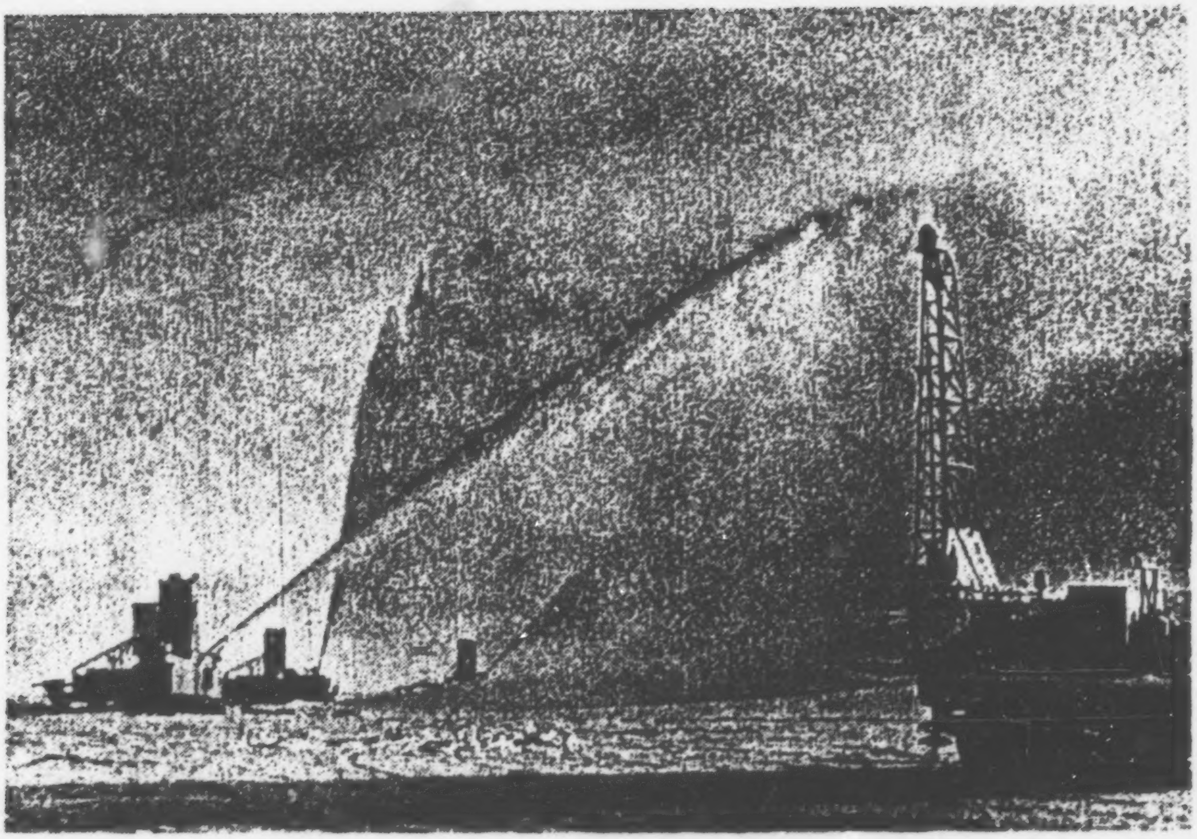

Figure 5.5.17 Mars Island Construction Using Stang Monitors (Golder, 1986)

[illegible]

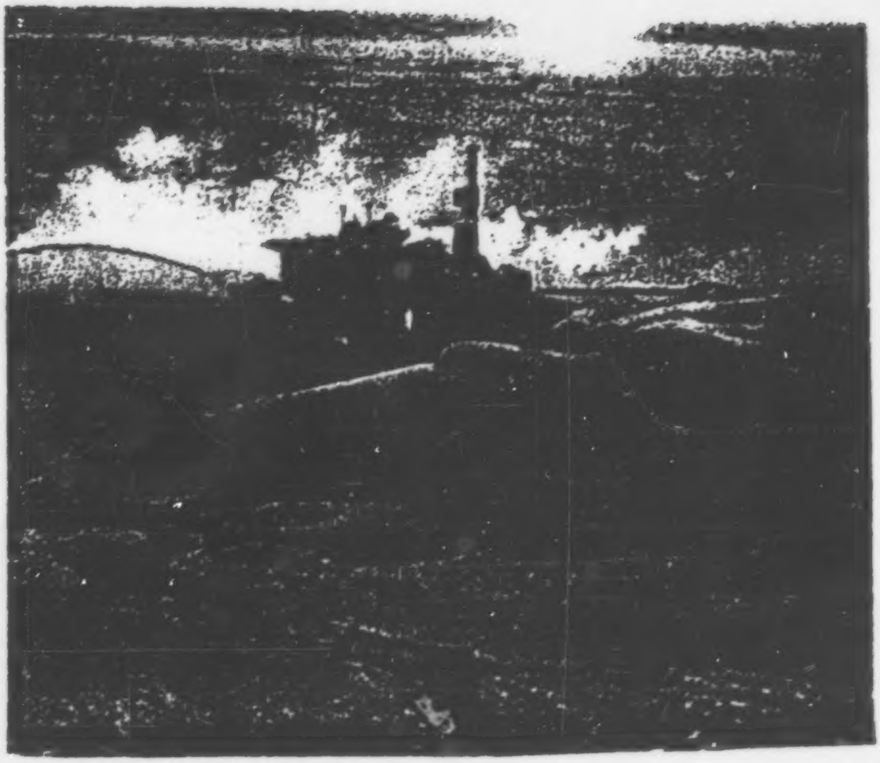

Figure 5.5.18 CIDS Ice Barrier Under Construction

5.5.4.4 Thermodynamics of Rubble and Spray Ice

The thermodynamics of rubble and spray ice can be analyzed using a computer program which was developed for Public Works Canada by Marcellus et al., (1986). The program analyzes the consolidation or refreezing of the ice mass, and includes the effects of various horizontal layers.

The program treats four layers within the broken ice zone as follows:

1. Spray ice or snow
2. Unsaturated broken ice layer above the water line (i.e. sail)
3. Fully refrozen or consolidated layer below the water line
4. Partially refrozen saturated layer below the fully consolidated layer

The temperature distribution through these layers is shown in Figure 5.5.19.

Conduction of Heat Through Ice

Conduction through one layer (Q_c) can be formulated using steady-state conduction theory, i.e.

$$Q_c = (T_b - T_c)\ k\ /\ t \qquad \text{... Eqn. 5.5.13}$$

where:

k = the thermal conductivity (W/m°C),
t = ice layer thickness (m),
T_b = the temperature at the bottom of the layer (°C), and
T_s = the temperature at the top of the layer (°C).

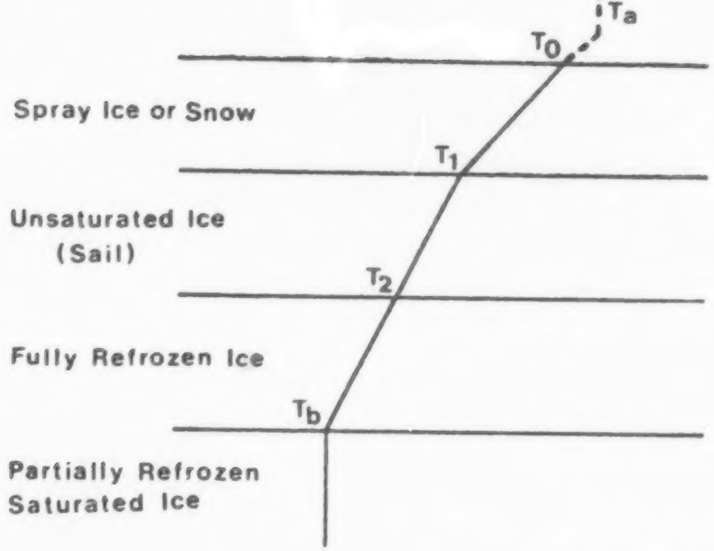
Ta
T0
Spray Ice or Snow
T1
Unsaturated Ice
(Sail)
T2
Fully Refrozen Ice
Tb
Partially Refrozen
Saturated Ice

Figure 5.5.19 Illustration of Temperature Distribution in a Rubble Pile

For the steady state condition, the conductions through the spray ice layer, sail and consolidated ice are the same at each time step:

$$Q_c = \text{conduction through ice} = (T_b - T_2)\, k_{ice} / t_{ice}$$

$$= \text{conduction through sail} = (T_2 - T_1)\, k_{sail} / t_{sail}$$

$$= \text{conduction through spray ice} = (T_1 - T_0)\, k_{spray\ ice} / t_{spray\ ice} \quad \text{...Eqn.'s 5.5.14}$$

where:

$k_{sail,\ ice,\ spray\ ice}$ = thermal conductivity for the different ice types (W/m°C),
$t_{sail,\ ice,\ spray\ ice}$ = layer thickness (m),
T_a = user specified air temperature (°C),
T_b = freezing temperature of sea water, assumed to be -1.8°C,
T_0 = temperature at the top of the spray ice (°C),
T_1 = temperature at the top of the sail (°C), and
T_2 = temperature at the bottom of the sail (°C).

Sensible Heat Flux:

The transfer of heat from the surface layer into the air above it with a wind blowing is a forced convection phenomenon. With no wind it is analogous to natural convection from a horizontal surface.

In micro-meteorology, a simple approach to heat flow from the earth's surface to the air is used, and is quoted by Maykut (1978):

$$Q_{thf} = \rho_a C_p C_s V (T_a - T_s) \qquad \text{... Eqn. 5.5.3.7}$$

where:

ρ_a = the air density, (1.3 kg/m^3),
C_p = the specific heat of air at constant pressure (1005 J/kg°C),
C_s = a sensible heat transfer coefficient,
V = the wind speed (m/s),
T_a = the air temperature (°C), and
T_s = the surface temperature (°C).

Long Wave Radiation

The heat flux due to long wave radiation (Q_{lr}) is expressed as:

$$Q_{lr} = Q_{Ilr} - \epsilon \sigma T_s^4 \qquad \text{... Eqn. 5.5.16}$$

where:

Q_{Ilr} = the incoming long wave radiation,
ϵ = the emissivity (approximately 1.0 for ice),
σ = the Stefan-Boltzmann constant (5.67 x 10^{-8} (Wm^{-2}°K^{-4}), and
T_s = the surface temperature (°K).

Heat Balance

In the steady state condition the heat transfer from the ice surface to the atmosphere is equal to the conduction of heat through each layer of ice, i.e.

Heat Conducted = Sensible Heat Flux + Long Wave Radiation

therefore

$$Q_c = \rho_a C_p C_s V (T_a - T_0) + \epsilon \sigma T_0^4 - Q_{Ilr}$$

$$= (T_1 - T_0) k_{spray\ ice} / t_{spray\ ice}$$

$$= (T_2 - T_1) k_{sail} / t_{sail}$$

$$= (T_b - T_2) k_{ice} / t_{ice} \qquad \text{...Eqn.'s 5.5.17}$$

Equations 5.5.17 are solved to determine the total heat transfer and the temperature profile through the ice.

Knowing the total heat transfer, the rate of freezing of new ice is calculated from the following equation:

$$Q_c = Q_{lat} = \rho_i \gamma_2 h_{lf} dt \qquad \text{...Eqn. 5.5.18}$$

where:

ρ_i = density of ice,
γ_2 = porosity below water line,
h_{lf} = latent heat of sea ice, and
dt = thickness of ice growth.

5.5.4.5 Rubble Spray Ice Protected Drilling Systems

It has been recognized that spray ice construction by itself is only feasible in the shallower, landfast conditions of the Beaufort Sea. It has also been recognized that in the deeper water, dynamic ice condition environment, there is the potential to use combined rubble and spray ice construction.

The following figures show the conceptual application of a rubble protected drilling system which combines rubble and spray ice:

- Figure 5.5.20 shows a rubble field grounded upstream of a steel framed rubble generator in about 20 m of water in dynamic ice conditions.
- Figure 5.5.21 shows how spraying can be used to help ground the rubble ice.

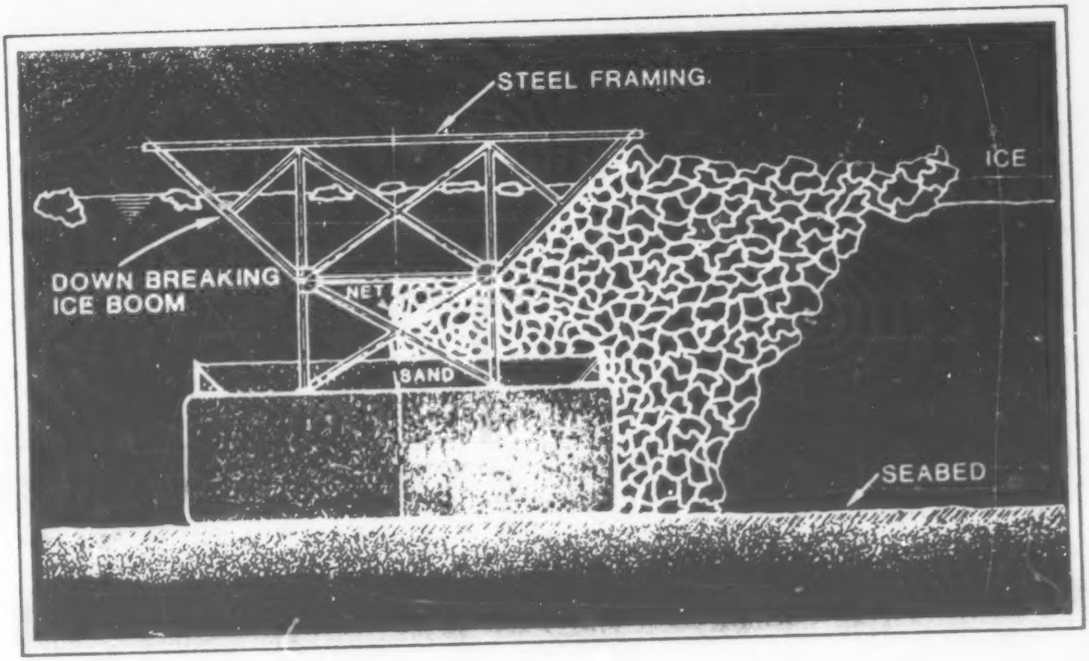
STEEL FRAMING
ICE
DOWN BREAKING ICE BOOM
NET
SAND
SEABED

Figure 5.5.20 Illustration of Rubble Field Generator

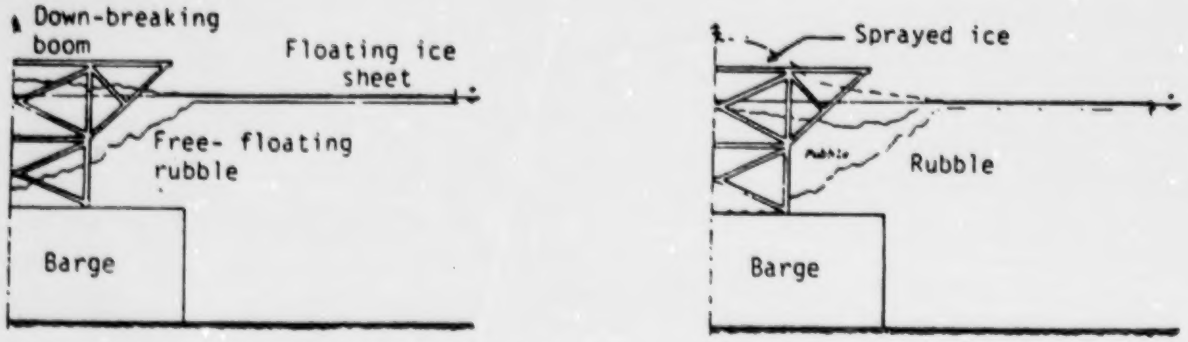
Down-breaking boom
Floating ice sheet
Free- floating rubble
Barge
Sprayed ice
Rubble
Rubble
Barge

a) Free-floating Rubble Forms from Thin Ice

b) Rubble Begins to Ground on Barge

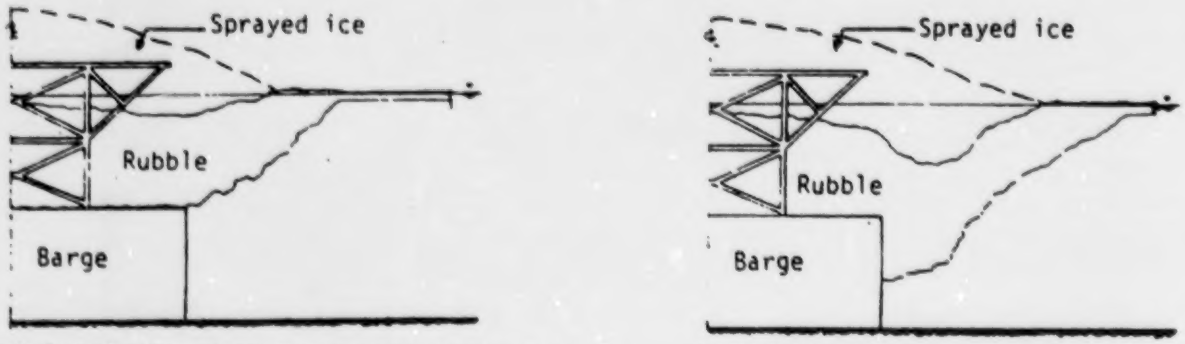
Sprayed ice
Rubble
Barge
Sprayed ice
Rubble
Barge

c) Rubble Grounded Out to the Edge of the Barge

d) Additional Surcharge from Sprayed Ice Providing Enough Downward Load to Sink Free-floating Rubble at the Edge of the Barge

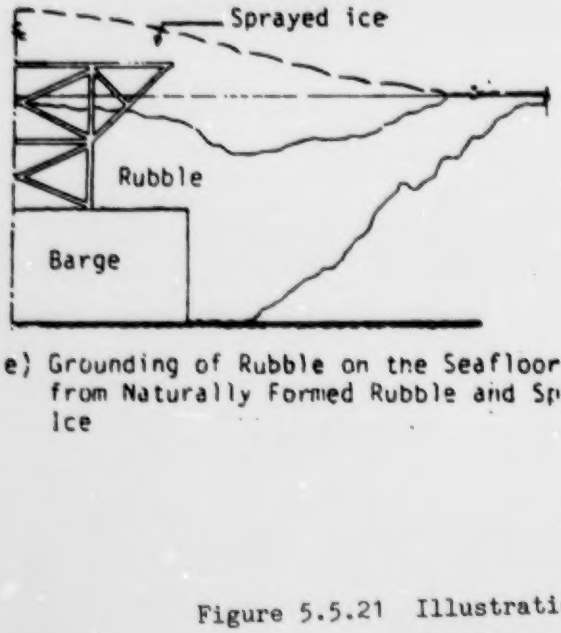
Sprayed ice
Rubble
Barge

e) Grounding of Rubble on the Seafloor from Naturally Formed Rubble and Sprayed Ice

Figure 5.5.21 Illustration of Using Spray Ice to Ground and Stabilize a Rubble Field

5.5.5 Recommendations for Future Work

1. Rubble Fields Around Deep Caisson Structures/Cut-off Grounding Depth

It is now known that rubble fields will clear around deep, narrow structures, even when the rubble is grounded immediately in front of the structure at a water depth of about 20 m. On the other hand, it is known that rubble fields will form on natural shoals (McGonical et al., 1986) with a minimum water depth of 16 m. To understand the mechanics governing the following phenomena:

1. clearing around deep caisson structures,
2. cut-off grounding depth, i.e. when grounded rubble becomes free floating rubble as the water depth is increased,

it is recommended that further sturdy, including new theoretical developments and field observations, be carried-out.

2. Rubble Properties

Most of the properties of rubble, such as:

- cohesion, and
- internal friction angle

are taken from model ice. It is recommended that more field tests, such as those reviewed in Croasdale (1986), be conducted to measure these properties and others, in-situ, so that the simulation models will have more accurate input and result in more accurate rubble field and force transmission calculations.

3. Deep Water Rubble/Spray Ice Structures

It has been demonstrated that spray ice island construction can be used for exploration drilling in 8 m of water in the Beaufort Sea (Funegard et al., 1987), where ice cover is stable. It is possible that cheap rubble generating structures can be used to initiate rubble fields in dynamic ice conditions in deeper water, in the order of 20 m to 30 m, and that spray ice can then be used to stabilize the rubble. Further work, including a full scale field test, is recommended to prove this concept.

4. Spray Ice Production Platforms

To date, spray and flooded ice platforms have only been used for exploration in the Beaufort Sea. It is recommended that studies, conceptual designs, and field tests, be implemented to determine methods of extending the life of ice structures so they can be used as production structures.

5.6 Dynamic Analysis of the Ice/Structure Interaction

5.6.1 Introduction

During recent years the consideration of the dynamic structural response in an Arctic pack ice environment has become of more concern to engineers. At the moment it is difficult to reduce the scientific results to definite design procedures or formulae in regard to dynamic design. However, it has become clear that any current or future design should make specific consideration of the potential for dynamic effects. Consequently, there is currently considerable interest in advancing our understanding of the dynamic effects of ice-structure interaction.

The structure response is said to be dynamic when the inertia forces in the structure and/or ice are of significant magnitude, compared to the stiffness restoring forces and the ice-structure interaction forces. Three principal types of continuous vibrations of structures in ice have been observed:

i. A random type of vibration, which is similar to random vibrations occurring in many other types of structures. The ice is failing in brittle crushing, with small pieces of ice produced. Predominant periods may still be observed.

ii. A periodic oscillation type, which may occur when good ice/structure contact is maintained and the ice deforms somewhat plastically over a part of the cycle. The oscillating mass then includes an effective mass of the ice, while the stiffness is only that of the structure.

iii. A ratcheting type, characterized by a relatively slow build-up of deflections, followed by a more rapid spring-back motion. At this stage, the ice is virtually stopped or is stopping.

Examples of force versus time histories for the three types of vibrations are shown in Figure 5.6.1 (from Blenkarn, 1970). There have been different opinions regarding the effect of the structure or the periodicity of the ice crushing forces. Peyton (1966) measured the ice forces against some of the oil platforms in Cook Inlet which indicated a periodicity in the ice crushing of approximately 1 Hz. Even though the natural period of the structures was approximetly 1 Hz, Peyton concluded that it was the result of a natural property of the ice.

Single-pile bottom founded structures with little internal damping, as well as flexible multi-pile jacket structures exhibit the most pronounced dynamic effects. Maattanen (1980) states that structures which have natural frequencies between 0.5 and 15 Hz may exhibit problems with ice-induced vibrations.

For vertical structures dynamic effects due to bending and buckling failures may be significant, as well as the dependence of brittle failure pressure on strain rate. Mass, stiffness and damping characteristics of the structure must be included in an analysis. As well, the influence of water, ice to structure friction and the foundation must be taken into account.

More recent work suggests that the dynamic response of the structure does indeed effect the resulting ice force. The most recent work (Maattanen, 1983; Eranti et al., 1981) recognizes the dependence of ice strength on loading rate; the loading rate is directly dependent on the deformation rate between the ice and structure at the contact zone. Thus, there is a closed loop between the ice and the structure, and it is possible to solve for the force/deformation history based on the physical properties of the ice and the structure.

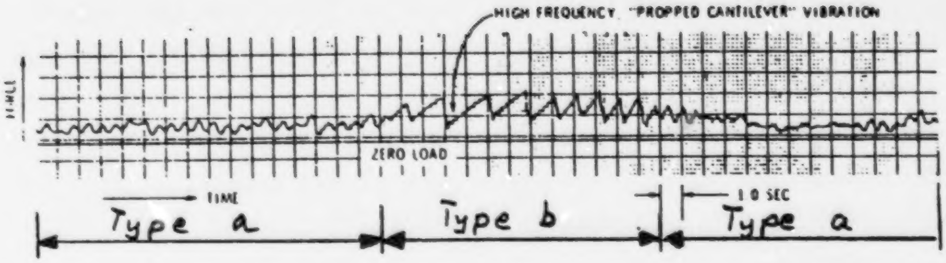

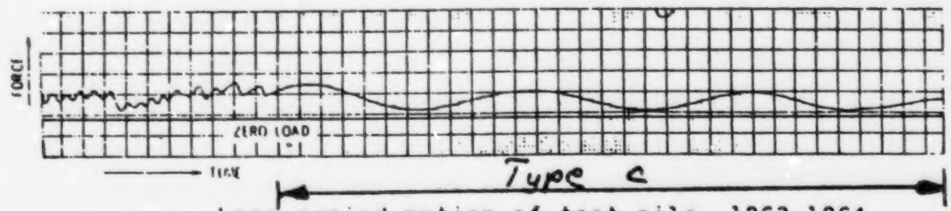

- Long period motion of test pile, 1963-1964.

Type a: Random Vibrations (High Velocities)

b: Periodic Oscillations (Intermediate Velocities)

c: Ratcheting Vibrations (Slow Velocities)

Figure 5.6.1 Ice Force Time History Plots (Blenkarn, 1970)

5.6.2 History of the Analysis of Dynamic Ice/Structure Interaction Effects

The occurrence of structural vibrations due to ice crushing was first studied for the Cook Inlet oil fields. The production structures selected for that environment were generally slender steel jacket structures with very clean cross-sections through the tidal zone. An example of a structure with 4 columns only piercing the water surface, and with exterior bracing below the water level where it will not usually contact the ice, is shown in Figure 5.6.2 (Blenkarn, 1970).

Ice-structure dynamics was also studied for bridge piers (Neill, 1976), Baltic Sea lighthouses (joint Norwegian Study, 1980), and the Bohai Gulf oil fields offshore China (Jizu et al., 1983). In the Bohai Gulf there have been two failures of jacket-type structures similar to the one shown on Figure 5.6.3 (Jizu et al., 1981), and there is currently a considerable amount of effort being directed at developing new design criteria. Much of this work is being funded by the Canadian Government and uses the expertise of Canadian personnel. More recently the vibrations of the highly instrumented Molikpaq exploration drilling structure have been reported.

The Molikpaq results are very important for the following reasons:

i. The Molikpaq is relatively wide, about 100 m at the waterline, and as such would not normally be expected to exhibit dynamic effects due to its large size.

ii. The vibrations appear to be a complex combination of ice crushing and soil/structure vibrations.

iii. The Molikpaq is highly instrumented, so the structure motions and stresses are well documented.

iv. The Molikpaq is manned with ice observers who recorded ice thickness, ice properties and modes of ice failure.

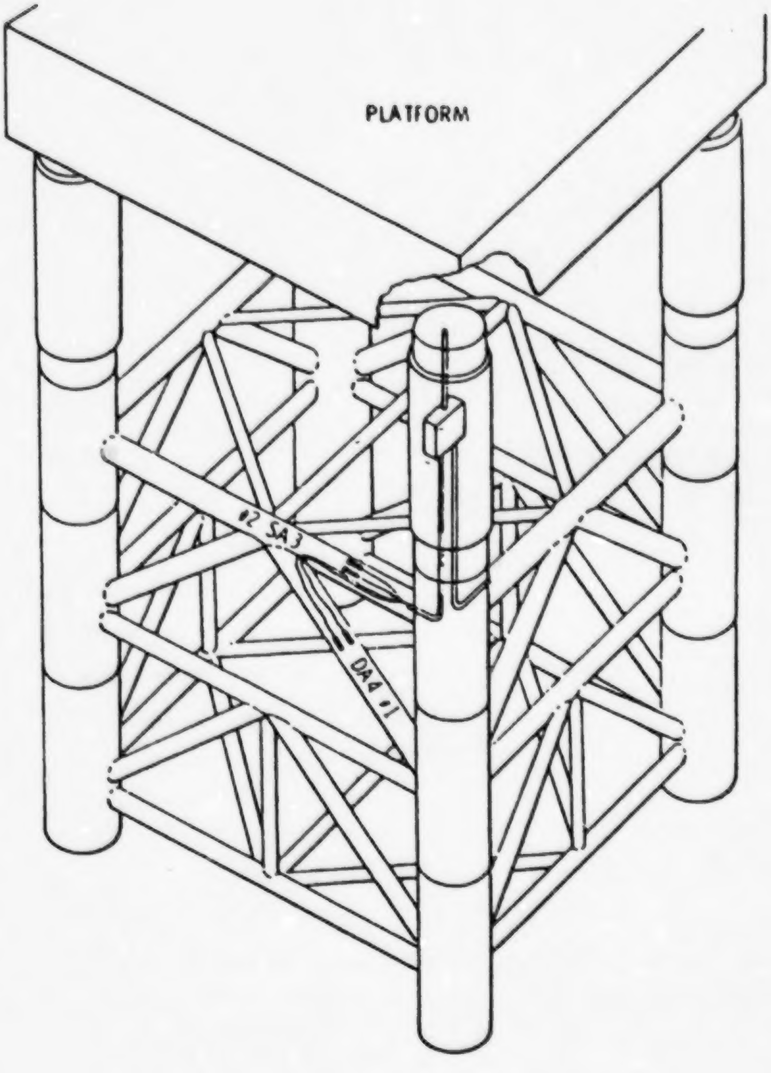
PLATFORM
#2 SA3
DA4 #1

Figure 5.6.2 Cook Inlet Platform (Blenkarn, 1970)

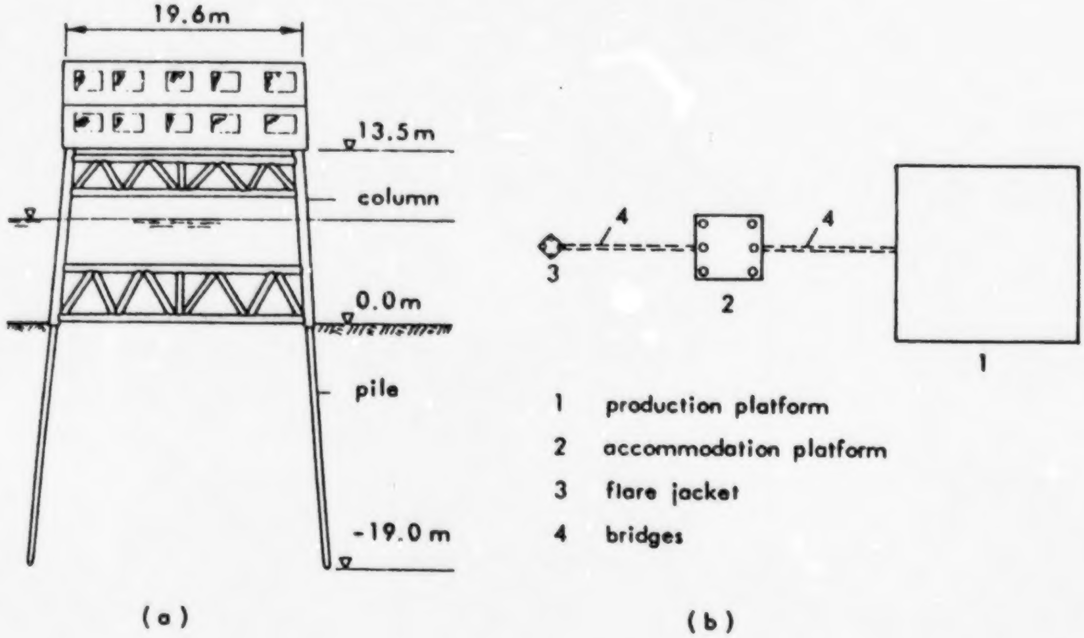
19.6m
13.5m
column
0.0m
pile
-19.0 m
4
4
3
2
1
1 production platform
2 accommodation platform
3 flare jacket
4 bridges
(a)
(b)

Figure 5.6.3 Bo-Hai Gulf Platforms (Jitu, 1981)

In view of the uncertainty which presently exists regarding the physical reasons for dynamic excitation of structures in ice, it is difficult to give specific criteria on whether dynamic structure response will occur. It is even more difficult to give reliable quantitative criteria for the magnitudes of the stresses caused by structure vibrations. Until recently, the best option appeared to be for the designer to be aware of the possibility of dynamic structure response, and avoid, or at least analyze very carefully, designs where dynamic response is a possibility.

For future designs, however, a more exact analysis of dynamic effects will be necessary in order to provide economical structures that satisfy the required performance criteria. To date, a number of slender bottom-founded steel lighthouses have been installed along the coast of Finland. These structures avoid the effects of self-induced vibrations through the concept of vibration isolation; this required the use of detailed computer and scale-model simulations to predict the full scale performance. In Canada, it will be necessary to advance the art of dynamic design to be able to accurately predict the response of structures in conditions as severe as the Beaufort Sea.

The structures where dynamic response have been of importance and even caused structural failures are very slender pile-type structures, e.g. lighthouses and piers in the Gulf of Bothnia. These structures had natural frequencies in the order of magnitude of 1 Hz and the dynamic response occurred mostly in solid ice floes. It is thought that for pile-like structures with natural frequencies which are lower than 1-2 Hz, the possibility of dynamic response should be considered.

Ice induced vibrations of offshore lighthouse structures in the Baltic have been studied for more than ten years both in Sweden and in Finland. In 1973, the lighthouse Norstromsgrund (Figure 5.6.4) in the Gulf of Bothnia, was equipped with accelerometers in order to collect data for analyzing the nature of rather strong structural vibrations, which had been observed from time to time during periods of ice drift.

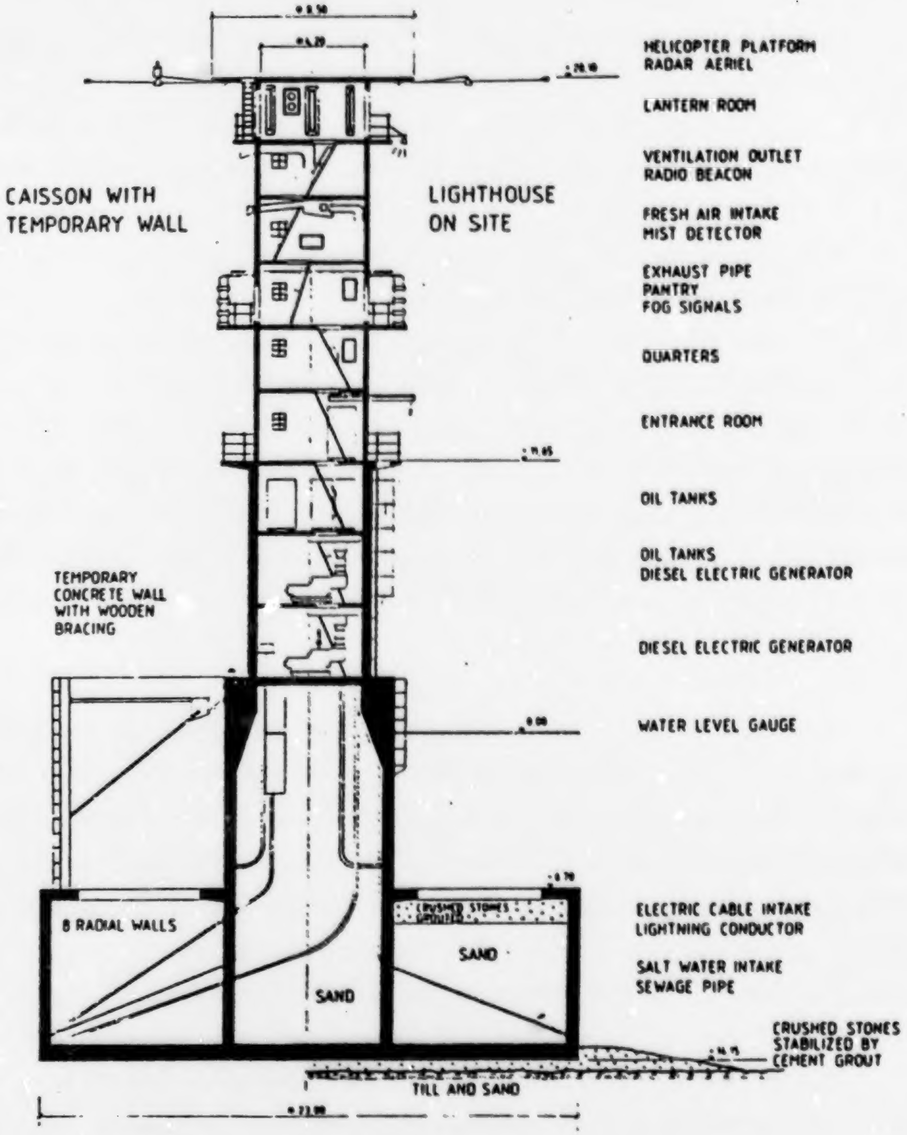
HELICOPTER PLATFORM
RADAR AERIEL
LANTERN ROOM
VENTILATION OUTLET
RADIO BEACON
CAISSON WITH
TEMPORARY WALL
LIGHTHOUSE
ON SITE
FRESH AIR INTAKE
MIST DETECTOR
EXHAUST PIPE
PANTRY
FOG SIGNALS
QUARTERS
ENTRANCE ROOM
OIL TANKS
OIL TANKS
DIESEL ELECTRIC GENERATOR
TEMPORARY
CONCRETE WALL
WITH WOODEN
BRACING
DIESEL ELECTRIC GENERATOR
WATER LEVEL GAUGE
8 RADIAL WALLS
CRUSHED STONES
GROUTED
SAND
SAND
ELECTRIC CABLE INTAKE
LIGHTNING CONDUCTOR
SALT WATER INTAKE
SEWAGE PIPE
CRUSHED STONES
STABILIZED BY
CEMENT GROUT
TILL AND SAND

Figure 5.6.4 Norstromsgrund Lighthouse
(Norwegian Research Project, 1981)

An example of recorded accelerations is shown in Figure 5.6.5. As with other sequences of strong vibrations recorded during the observation period, the record is characterized by typical resonance vibrations, which is still more clearly demonstrated by the details shown in Figure 5.6.6. The first detailed increment (between 10-12 s) constitutes an example of increasing resonance vibrations and the second increment (14-16 s) demonstrates stationary resonance vibrations.

The frequency is very close to the natural frequency of the first mode of structural vibration: that of a cantilever beam with some rotation of the base due to elastic deformation of the sea bed material. The time history of the periodic ice force can be described, using some simplifications, by the "saw-toothed" curve in Figure 5.6.7. This is discussed further below.

Another reason for the potential excitation of marine structures in an ice environment is related to the negative slope for ice crushing strength at relatively high loading rates, as shown on Figure 5.6.8. The negative slope gives a negative contribution to the structural damping (i.e. the negative slope means the oscillations will increase in magnitude, thus the phrase "negative damping"). Negative damping may make the structure dynamically unstable for small oscillations. The non-linear character of the ice/structure system will probably result in the system executing stable limit cycles with large amplitude, however the effect is to pump energy into the structural system.

It appears from laboratory measurements in ice tanks and from the field measurements of slender lighthouse structures that the frequency of ice failure against a pile is related to the ice movement velocity, at least for low values of the velocity. However, at higher velocities the ice failure frequency will tend to lock onto one of the natural structural frequencies of the pile. Several methods for predicting the response of a structure in ice have been proposed (Kivisild, 1969; Maattanen, 1983; Eranti et al., 1981) so that it is feasible to make reasonable estimates of the response of pile-type structures.

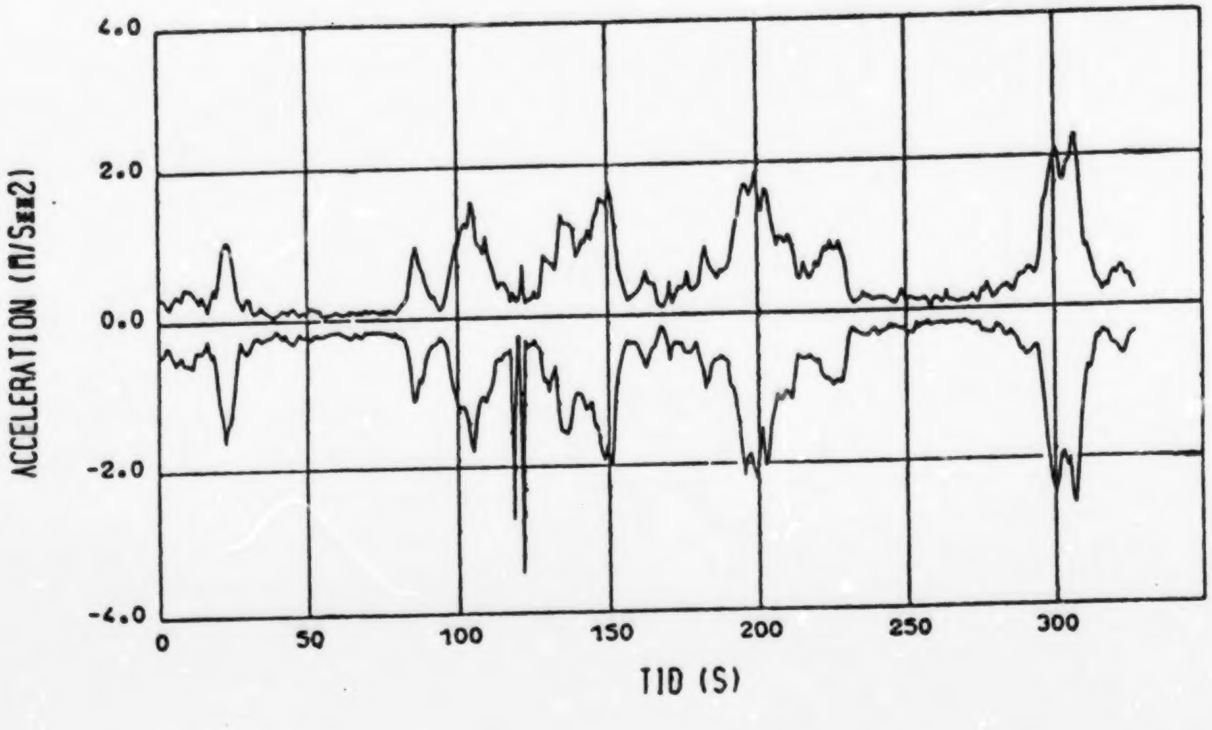

Figure 5.6.5 Acceleration Envelope for Norstrumgrund Lighthouse (Norwegian Research Project, 1981)

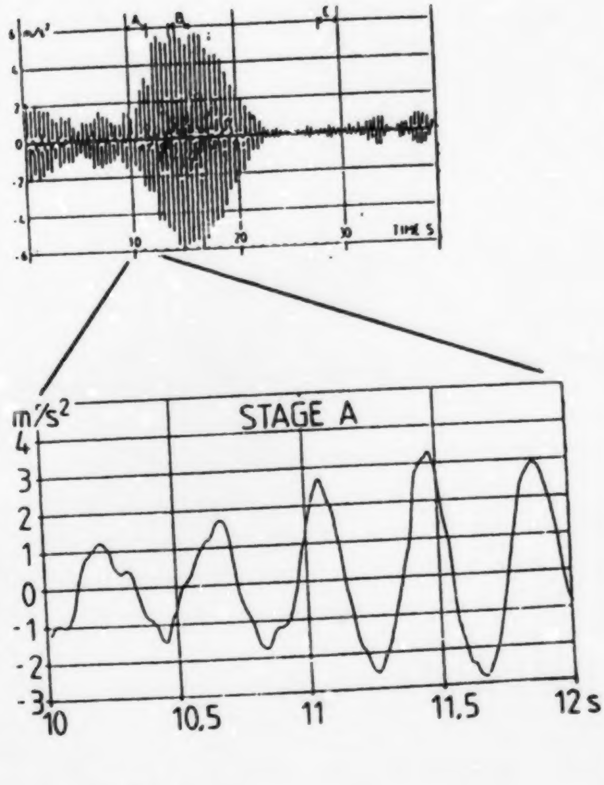

Figure 5.6.6 Details from Norstrumgrund Lighthouse Acceleration Records (Norwegian Research Project, 1981)

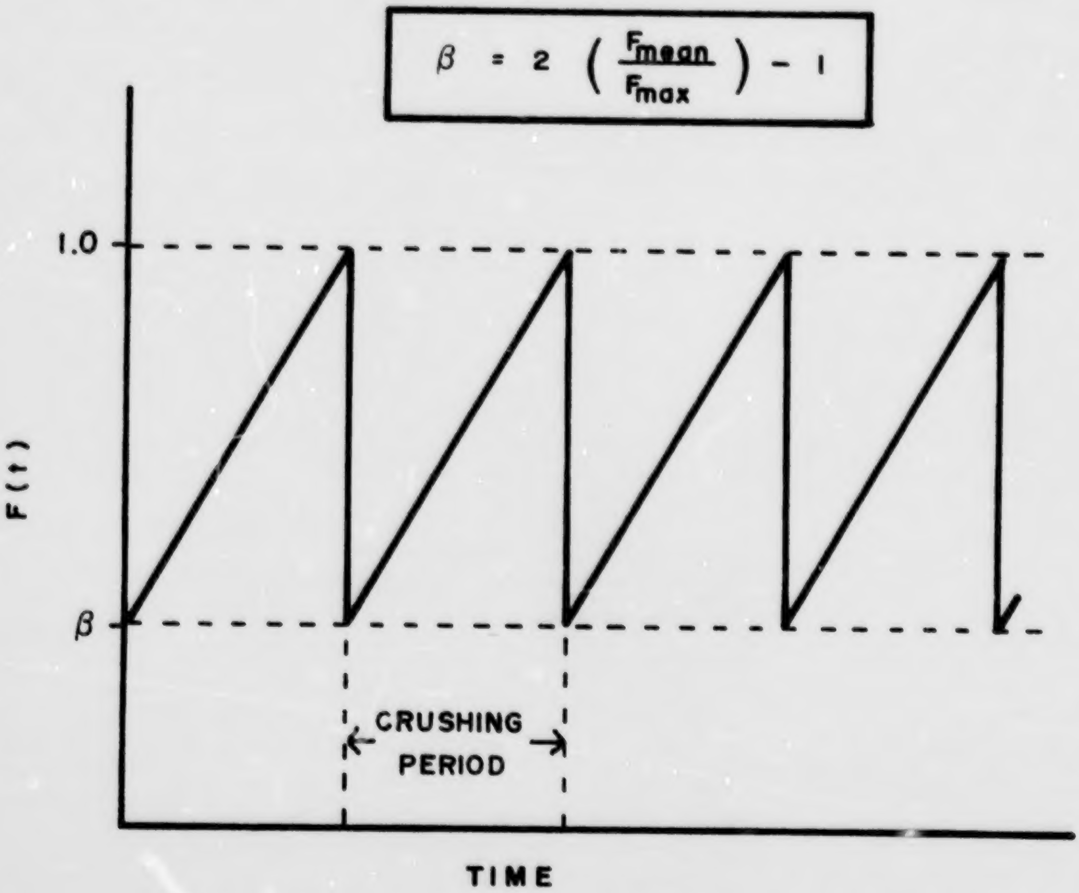

Figure 5.6.7 Idealized Saw-Toothed Ice Force Function (Daoud and Lee, 1986)

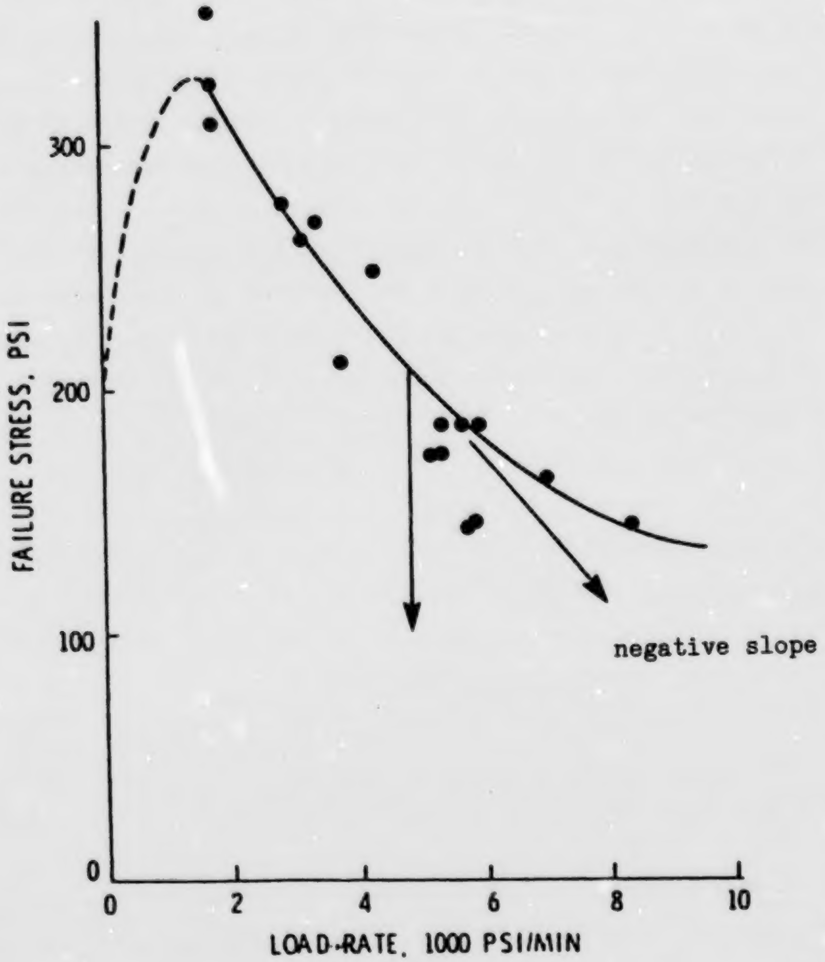

Peyton's compressive strength data.

Figure 5.6.8 Negative Slope of Ice Strength versus Loading Rate (Blenkarn, 1970)

Maattanen has reported that for model tests on cantilever pile structures, a saw-tooth like ice force (and displacement) pattern occurs at low velocities, and that there is a direct relationship betwen the ice crushing frequency and the ice velocity. Maattanen also reported that at higher ice velocities the crushing frequency tended to lock onto one of the natural modes of the structure. The maximum ice forces were generally recorded at low velocities, but also occured more randomly at the higher velocity ranges. This may have been due to the fact that pile deflection rates were high enough that ductile loading rates were occuring at ice velocities that would normally induce brittle loading rates. Generally, it was found that if resonance occured, it was the severest loading condition during ice crushing.

With regard to the crushing frequencies, there are currently two methods reported; Neill (1976) notes that the failure or damage zone in the ice sheet (or size of an individual piece) is generally between 20-50% of the ice thickness. From this it is simple to deduce that the frequency is in the range shown in Equation 5.6.1.

$$2\,v/t < f < 5\,v/t \qquad \text{...Eqn. 5.6.1}$$

Maattanen has found this equation to be satisfactory at the low end of the ice velocity range, but failing when dynamically unstable modes are induced at intermediate or higher ice velocities. Maattenan himself has suggested that the length of ice that is crushed during each cycle is equal to the elastic displacement of the structure. This leads to the equation:

$$f = \frac{k\,v}{F} \qquad \text{...Eqn. 5.6.2}$$

where k is the stiffness coefficient of the structure, and F is the ice force range. Laboratory results from his work indicate crushing frequencies that are consistently less than predicted by this equation, however, when the stiffness of the closed-loop system was taken into account better agreement resulted. Hence, it is considered to be a reasonable method for estimating the ice crushing frequency at intermediate and higher velocities.

A good example of the current state-of-the-art of dyanmic analysis and design in sub-arctic areas is reflected in the installation of vibration isolated steel lighthouses in the Finnish waters of the Gulf of Bothnia.

The design of these structures recognizes that dyanmic instability can be induced in flexible structures under ice crushing forces. This is a result of the negative damping effects created by the reduction of the strength at increasing loading rates; this causes the structural response to promote itself during dyanmic ice/structure interaction. The concept of vibration isolation is to vary the structural properties in a manner that ensures that some of the natural modes are made dynamically stable. Figure 5.6.9 shows the Kemi-2 lighthouse with its natural modes and frequencies, together with the model damping required to suppress vibrations. It can be seen that for modes 1, 2 and 4 the structure can be rendered dynamically stable since a maximum of 0.36% positive damping is required to suppress the effects of ice induced negative damping. Although the third mode is unstable due to the structure shape, there is practically no dyanmic response in the superstructure. The field experience for this type of flexible structure is good, however it is interesting to note that the magnitude of negative damping has been found to be larger than expected from laboratory results, and it is estimated that between 5-15% positive model damping is necessary to totally suppress ice induced resonant vibrations.

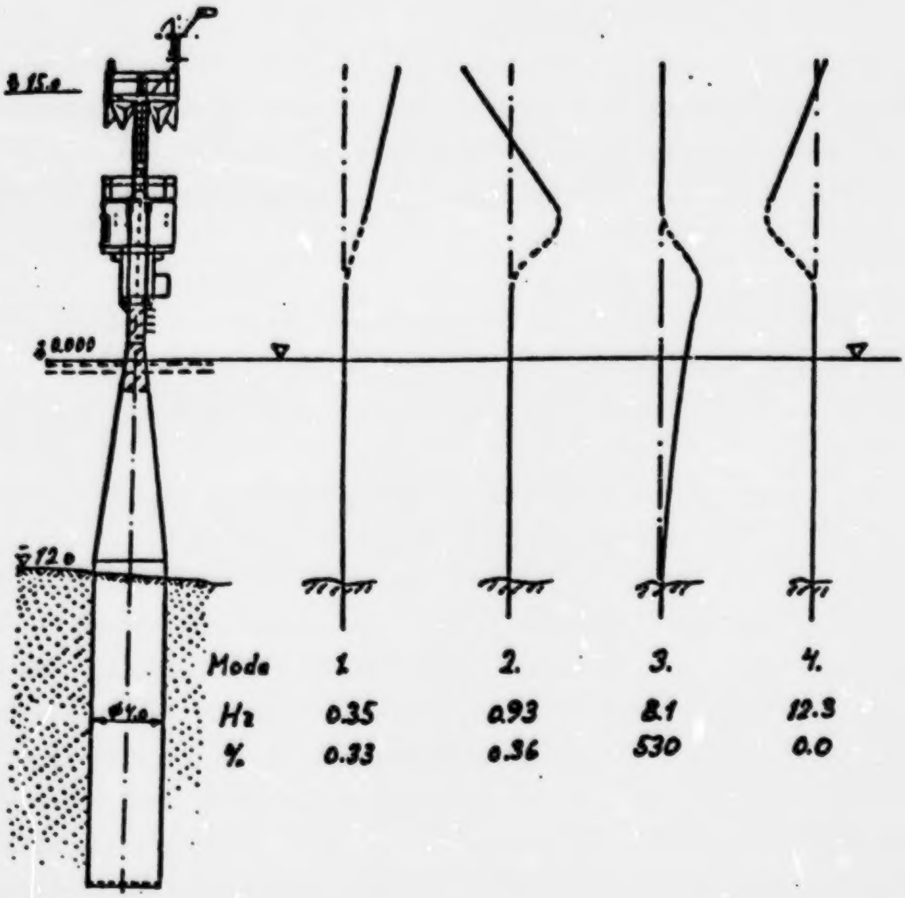
±15.0
±0.000
-12.0
Ø4.0
Mode 1 2. 3. 4.
Hz 0.35 0.93 8.1 12.3
% 0.33 0.36 530 0.0

Figure 5.6.9 The Vibration Isolated Lighthouse Kemi-2, Natural Modes and Frequencies, and Modal Damping Required to Supress Ice Induced Vibrations (Maattanen)

5.6.3 Mathematical Models

The most successful mathematical models of ice/structure interaction have incorporated both the nonlinearities of ice crushing, and the principal structural characteristics namely:

Ice Nonlinearities

- progressive failure,
- strain-rate dependent crushing strength, and
- characteristic sizes of failed ice.

Principal Structural Characteristics

- structural stiffness,
- structural damping, and
- mass.

The first important ice-structure dynamics model (Matlock, 1970) incorporated most of the above features in a computer model that replaced the ice with an innovative structural failure model made up of elastic/brittle piles mounted on a cart, that simulated a ramp function (Matlock, 1971). The idealized model is shown in Figure 5.6.10a, and sample results are shown in Figure 5.6.10b.

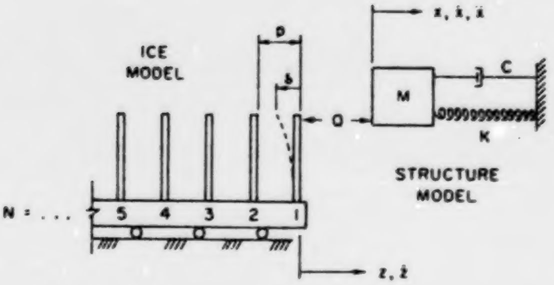
ICE MODEL
D
δ
Q
M
C
K
x, ẋ, ẍ
STRUCTURE MODEL
N = . . .
5
4
3
2
1
z, ż

(a) Mechanical Analogue of Ice and Structure

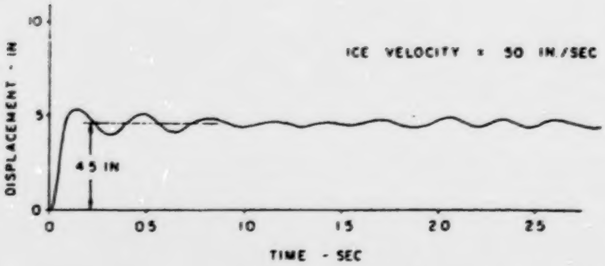

(a) HIGH VELOCITY ICE

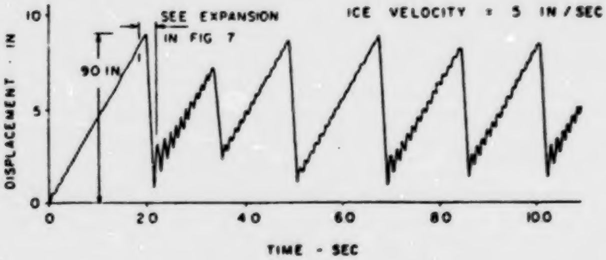

(b) LOW VELOCITY ICE

(b) Displacements for High and Low Velocities of Ice

Figure 5.6.10 Ice/Structure Interaction Model of Matlock (1970)

Eranti et al., (1981) have developed an analysis technique for modeling the dynamic ice interaction with narrow vertical structures that has been found to have practical application for a designer. The method is a step by step procedure, using model shape analysis, which involves two basic phases: Firstly, there occurs a penetration phase which is limited by a random loading rate dependent ice strength; and secondly, a failure phase which calculates the dimension of the failure zone as a function of the critical force. Eranti writes the general equation of motion for a structure:

$$[m]\{\ddot{x}\} + [c]\{\dot{x}\} + [k]\{x\} = \{P(t)\}$$

...Eqn. 5.6.3

It is then assumed that the penetration into the ice is proportional to the stress or force. This can be described by the equation:

$$Xc(t) = (\int v_i(t)dt - \Sigma_j (P_j + F_j) - \frac{Pc(t)}{mhD} A \qquad \text{...Eqn. 5.6.4}$$

Xc is the displacement of the structure at the point of contact with the ice, v_i is the ice velocity, and P and F are the lengths of the penetration and failure zones. A is the constant used to relate stress and penetration. These two equations can be combined to provide the equation of motion for the penetration phase:

$$[m]\{\ddot{x}\} + [c]\{\dot{x}\} + ([k] + [kcc])\{x\} = \{P_o(t)\} + \{P_c(t)\} \qquad \text{...Eqn. 5.6.5}$$

Vectors with a subscript c are zero except for a generally non-zero term at the contact point between the ice and the structure.
The term kcc (= mDh/A) represents the apparant stiffness of the ice during the penetration phase.

A similar procedure is used to calculate the dynamic response after the critial ice force is reached. The length of the failed or damaged zone is defined by Equation 5.6.6.

$$F = \frac{P c r}{m D h} B \qquad \text{...Eqn. 5.6.6}$$

The equation of motion can be written as:

$$[m]\{\ddot{x}\} + [c]\{\dot{x}\} + [k]\{x\} = \{P_o(t)\} + \{Pr(t)\} \qquad \text{...Eqn. 5.6.7}$$

Pr(t) is the residual resistance of the ice in the failed zone. A computer program has been used to solve equations (1) and (2), with a typical result of the force/time history shown on Figure 5.6.12.

A more advanced model was developed by Swan Wooster (1987) which incorporates the observed smaller pieces of ice shown in Figure 5.6.13 for a Cook Inlet structure and Figure 5.6.14 for the Molikpaq. The equation of motion is similar to equations 5.6.5 and 5.6.7 above, however, a hydrodynamic damping term involving the square of the velocity term has been included.

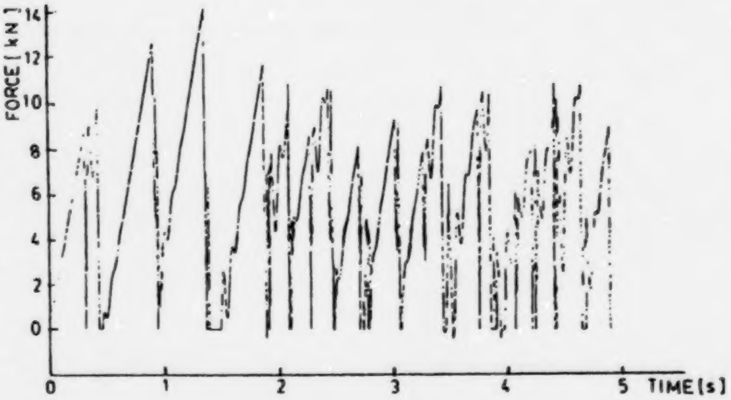

a. Computed Ice Force

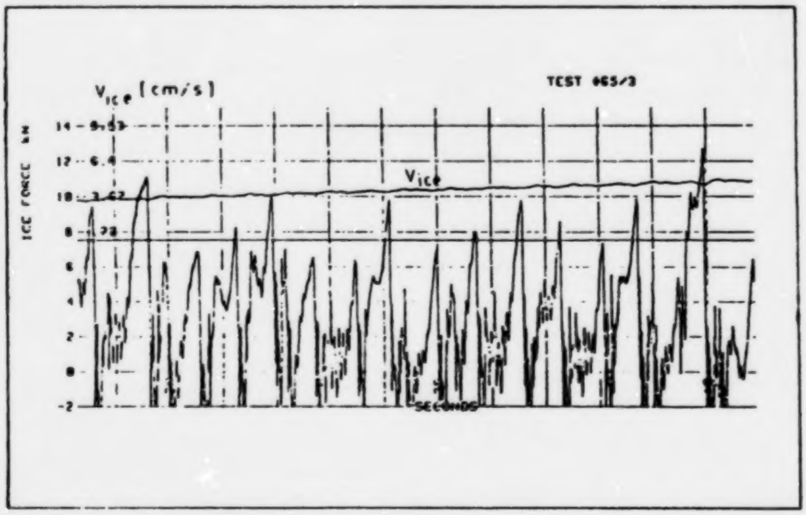

b. Measured Ice Force

Figure 5.6.11 Comparison of Computed and Measured Ice Forces (Eranti et al., 1981)

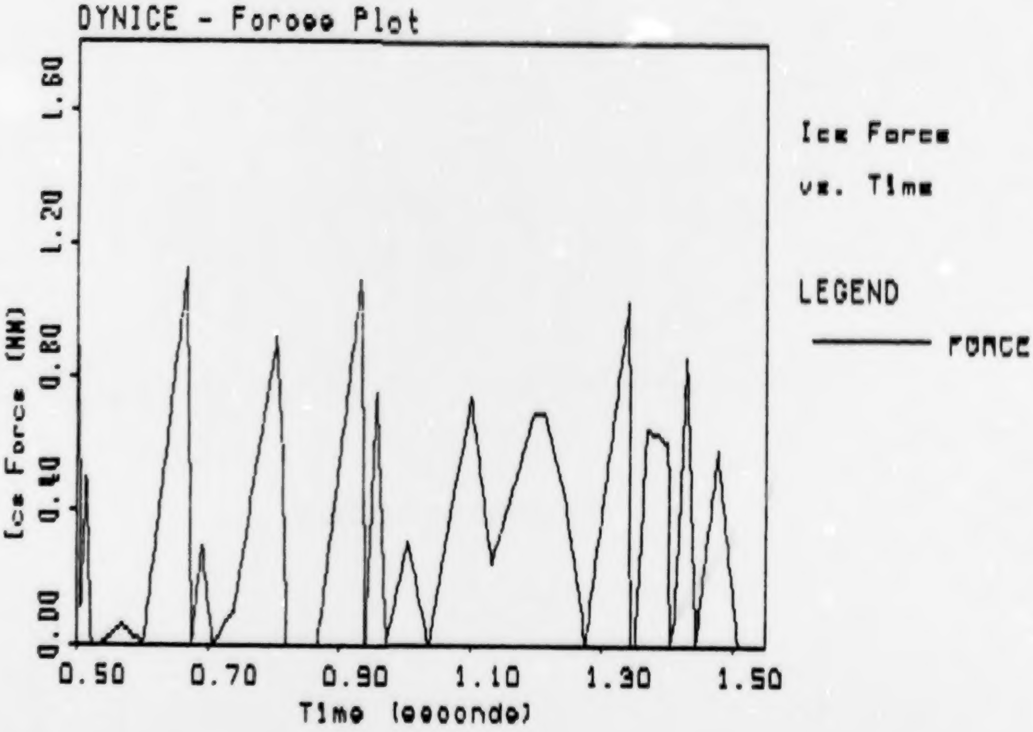

Figure 5.6.12 Total Force on a Pile Calculated Using the Computer Model

Figure 5.6.13 Small Ice Pieces Produced in Crushing (Carlile, 1969)

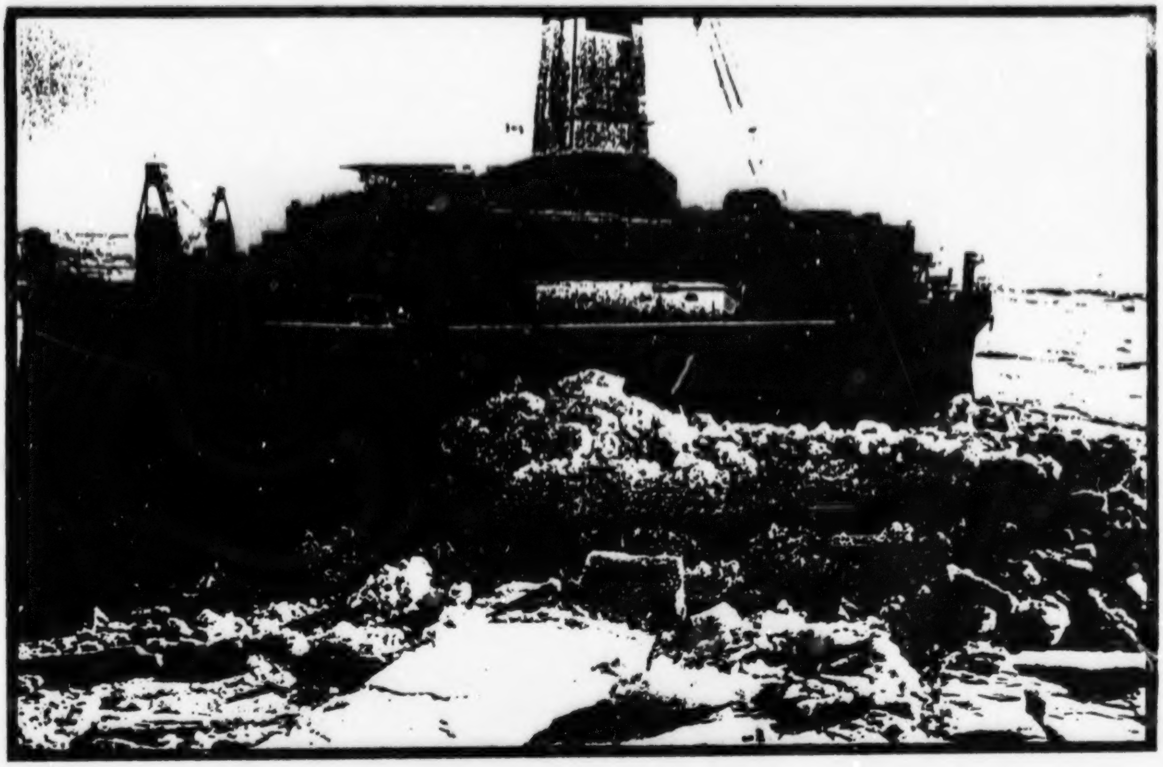

Figure 5.6.14 Pulverization of Ice During Crushing at the Gulf Molikpaq

5.6.4 Failure Models

The majority of mathematical ice failure models that have been developed are upper bound models that calculate peak ice forces (e.g. Coon et al., 1984). Although these models may be useful for structural design calculations, or for calculating a single peak load (see Section 5.4), they are of limited use in predicting the dynamic response, and do not necessarily even provide a realistic prediction of the sustained static loading effects.

Jordaan (1986) has reviewed the numerical techniques that can be applied to the ice-structure interaction, from which it is clear that there is a need for models that better reflect the actual failure processes involved. The results from recent large scale ice-structure interactions, such as with the Gulf Molikpaq in 1986, indicate that both large and small ice features are pulverized at the structure interface. Classical continuum mechanics cannot adequately represent this behaviour and other techniques are required. Continuum damage models have been applied to sea ice (Ting and Sunder, 1985; Karr, 1985), whereby a scalar variable between 0 and 1 is used to describe the degree of damage. Once the ice is pulverized during penetration, it then behaves as a viscoplastic material and has flow properties. However the failure surfaces associated with the virgin ice are not appropriate for a viscoelastic analysis of the pulverized ice. Jordaan (1986) has proposed that new techniques be adopted using Eulerian formulations (i.e. flow).

For strutural dynamics excitation, the ice failure model must be very realistic, even down to the microcracking scale. As a first requirement, a model must exhibit some periodicity and the early work of Matlock (1970) used a train of vertical cantilever elements with elastic/brittle failure properties to represent a saw-tooth force history. Some of the more important items that need be considered in a dynamic model are:

- strain or loading rate sensitivity,
- statistial strength effects, and
- non-simultaneous failure.

The force transmitted to the structure is also a function of the actual contact area which is, in turn, a function of the failure process. This failure process is shown schematically in Figure 5.6.15 with the associated force time history shown on Figure 5.6.16.

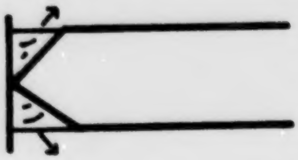

a. INITIAL BREAKOUT

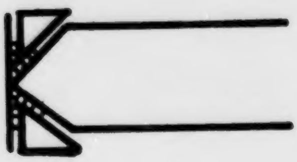

b. CRUSHING

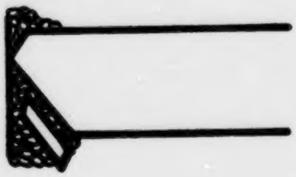

c. SECONDARY BREAKING

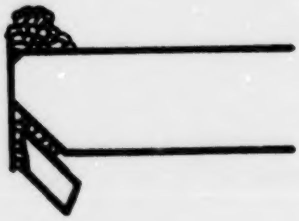

d. CRUSHING

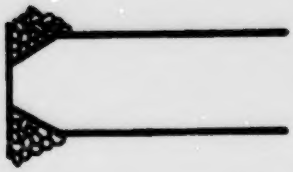

e. FLAKING / CRUSHING

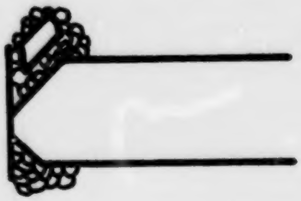

f. CRUSHING

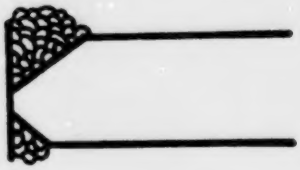

g. FLAKING / CRUSHING

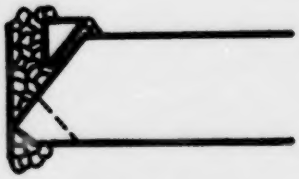

h. CRUSHING

Figure 5.6.15 Ice Crushing Sequence to Pulverize Ice

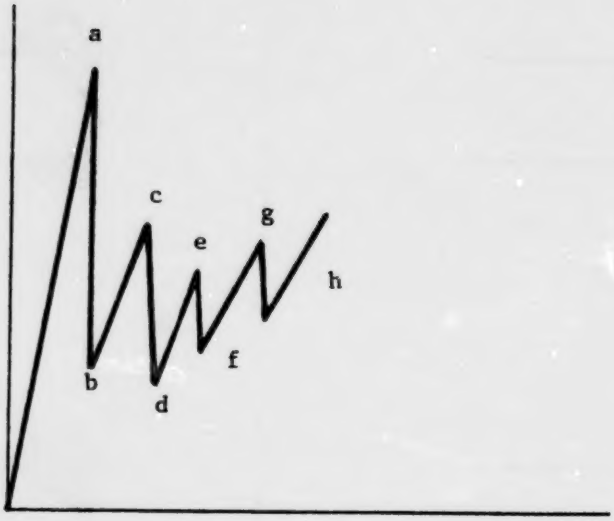

Figure 5.6.16 Force Time History for Sequence in Figure 5.4.15

5.6.5 Recommendations for Future Work

The understanding of the ice failure process on both the large and small scale has increased significantly in recent years, however there remains the need to develop good numerical models with which to predict the ice-structure response. Much of the early work on dynamic effects has concentrated on vertical pile-type structures with relatively narrow cross-sections. The recent experience with the Gulf Molikpaq structure has demonstrated the importance of accounting for dynamic effects on large, gravity structures. Some of the most important research topics that should be considered for future work are:

- development of damage models to represent the failure process of crushing or pulverization on the local scale,
- inclusion of non-simultanteous effects on large structures with a wide waterplane section,
- inclusion of statistical effects to represent the major variables such as ice strength, and
- determination of the effect of global fracture on both the global and local loads.

5.7 Local Load Theory

5.7.1 Introduction

As mentioned earlier, ice loads can be divided into two categories, global loads and local loads. Global load is the total force that an ice feature exerts on a structure and is used primarily for the foundation design. Since ice does not fail at a uniform pressure across the complete contact area between the structure and the ice feature, higher than average pressures over smaller areas can be exerted locally on the structure.

Figure 5.7.1 shows the pressure distributions at the contact between ice and the structure wall, indicating the high local pressures for cold brittle ice. The pressures correspond to those in indentation tests and confined compression tests. These pressures are referred to as local loads or pressures. The tributary areas (supporting areas for the local pressures) are generally large and the local loads are sometimes referred to as semi-local loads.

Because of the tributary area considerations, local pressures are usually considered in terms of pressure versus contact area and investigations are carried out with focus on these parameters. In the past it has been postulated that the design ice pressure decreases as the loaded area increases. This is said to be due to: (1) the effect of scale, and (2) non-simultaneous occurrences of peak pressure along the contact area.

Local ice pressures are a function of the ice type, temperature, salinity, geometry of the ice feature, geometry of the structure and rate of loading. All these factors affect the failure behaviour in ice which can be described as ductile (continuum) or brittle. Loading at a low strain rate results in a ductile failure and at a higher strain rate the ice fails in a brittle manner. Determination of local pressures for design involves ice strengths under various confinement conditions and ice/structure contact areas which are considerably larger than the sizes normally considered in the basic strength testing of ice. Materials have

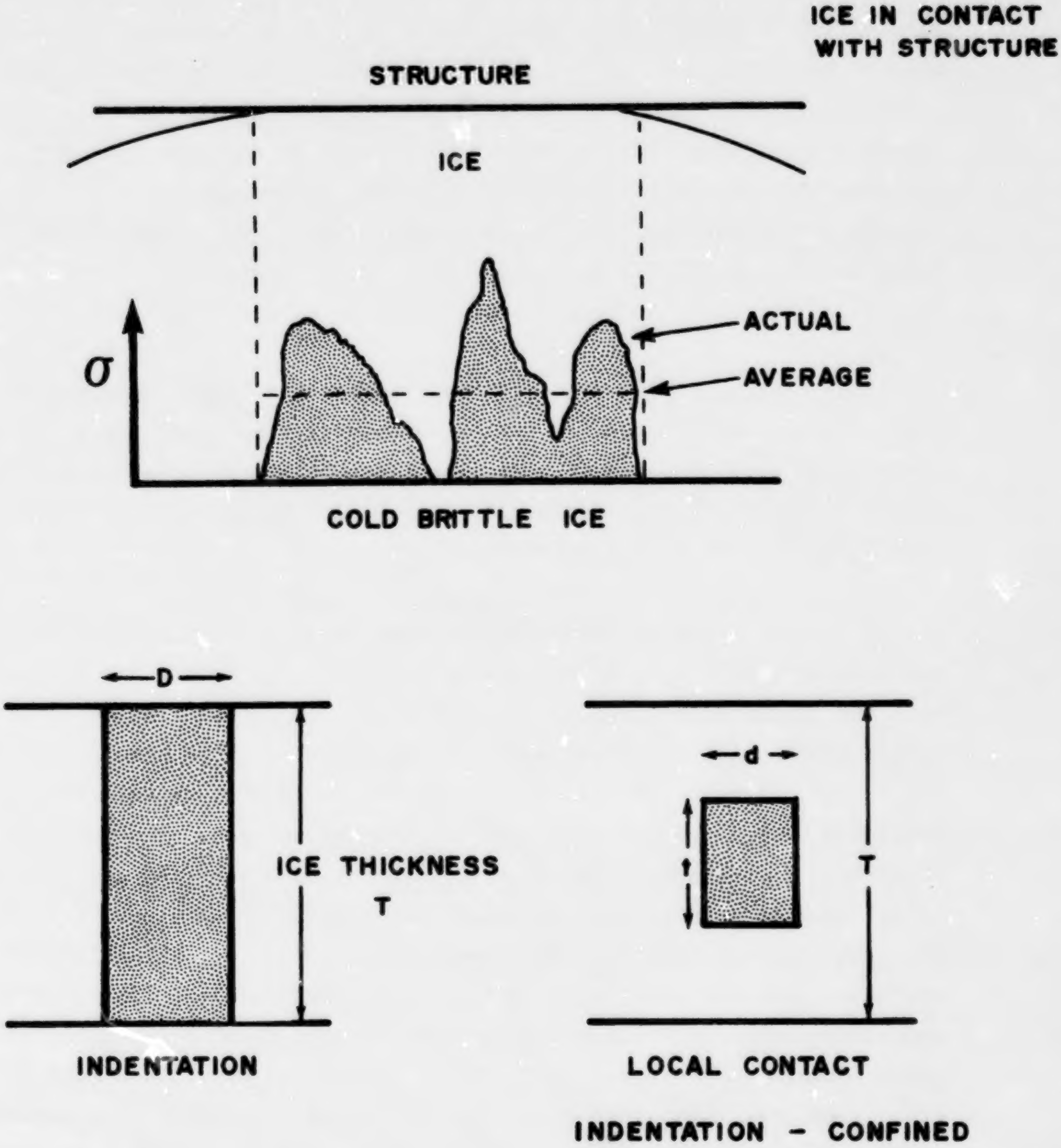
ICE IN CONTACT
WITH STRUCTURE
STRUCTURE
ICE
σ
ACTUAL
AVERAGE
COLD BRITTLE ICE
D
ICE THICKNESS
T
INDENTATION
d
t
T
LOCAL CONTACT
INDENTATION - CONFINED

Figure 5.7.1 Definition of Local Loads

been known to exhibit lower strengths with increase in size. This behaviour is termed size effect or scale effect. A good discussion of the size effect is presented in Iyer (1983). A ductile behaviour in ice is said to be independent of the scale effect as opposed to brittle failure which occurs as a result of flaws and stress concentrations. The scale effect noticed with brittle failure is said to be the result of the statistical distribution of flaws. However, other theories also have been postulated for scale effect (Ashby et al., 1986). The scale effect is not fully understood and due to lack of full scale experimental results, it has been found difficult to relate small scale to large scale tests.

Chen and Lee (1986) discusse the results of a large scale ice strength test at slow strain rates (10^{-5} s^{-1}) on natural first-year ice sheet and the results were compared with small scale laboratory tests. The tests did not indicate any scale effect. This may be due to the ductile behaviour resulting from the slow strain rate.

A review of the various selection processes for local ice pressures has been carried out by Bruen et al., (1982). This review has indicated that the existing technology for local pressures is far from satisfactory. Design codes exist for floating structures such as ships and ice breakers, but large differences exist between the various design codes. Very few published design procedures exist for fixed structures. The purely analytical approaches, proposed now, have not been verified and they are useful more to predict qualitative trends then anything else. The experimental data base is very limited to establish any reliable empirical approach. The available data is related to small scale cylindrical indentors and large scale values are established from these small scale data. Local ice pressures result from various ice conditions such as first-year ice, multi-year ice floes and ridges, icebergs, ice islands, and rubble piles with and without consolidated zones. Also, the design ice pressures against an ice face should take into account the nature of the ice zone, the transition zone above and the underwater zone below the ice zone. The compliance of the structure also affects the local pressure variations.

At present, there are no codes, nor guidelines for the selection of local pressures for design of offshore structures. This is largely left to the individual owners and engineers.

5.7.2 Analytical Techniques

The available analytical techniques can be classified as closed form solutions, deterministic numerical techniques such as the finite element (Bercha and Associates, 1985; Bercha et al., 1985), discrete element modeling techniques (Hocking et al., 1985a,b), and probabilistic models (Vivitrat and Slomski, 1983). Only closed form and finite element techniques have been applied so far of the prediction of local ice pressures. The discrete element model is a new technique and is still under further development. Because of the enormous computation time needed even with the most powerful computer, the discrete element technique is prohibitively expensive and has not yet been applied to local ice pressure problems.

The following section presents the basic details of a finite element approach applied to the determination of local ice pressures and an approach based on probabilistic considerations using Monte Carlo simulation.

Tom Brown's Model (Bercha, Brown and Cheung, 1985)

Explicit dependence of localized contact pressure on ice and structural stiffness has been known to affect significantly the local pressure distributions and magnitudes. This reference presents two models for the determination of the local pressure. The first model is a 2-D analytical (numerical) model based on simplifying assumptions regarding ice stiffness and strength providing a quasi static distribution of local pressures (Figure 5.7.2). The second model is a 3-D finite element model which utilizes an n-type yield function to describe the failure of ice in biaxial or uniaxial states of stress. The structural response can be elastic or inelastic.

The approximate model is a finite element idealization of the local geometry of the structure with ice modelled as a series of non-linear one dimensional elements. The effects of confinement are considered by assuming a state of plane strain for the ice, the yield stress for the interior elements as three times the uniaxial strength and for that of the edge elements the same as the uniaxial strength.

The advanced finite element model is a non-linear 3-D idealization.

In addition, a closed form solution using conservation of energy during impact was also applied.

The three methods were applied to a case of sheet ice impinging between the diaphrams of a concrete wall and the results have been presented in Table 5.7.1.

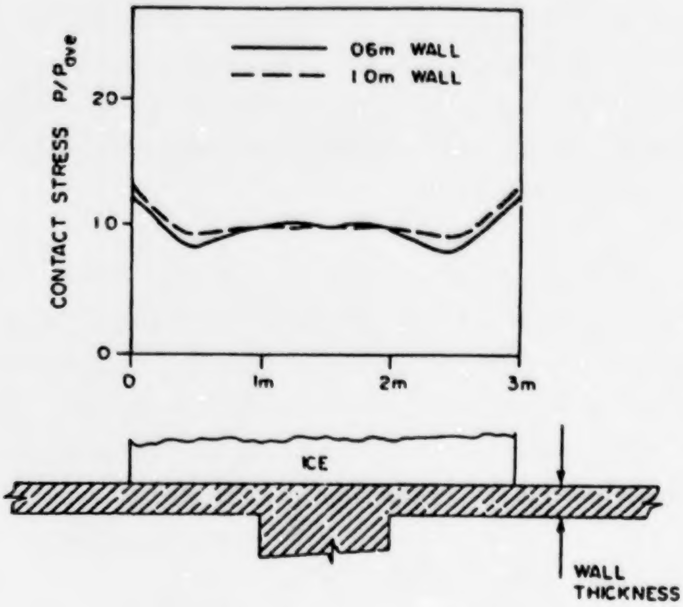

Figure 5.7.2 Brown's Finite Element Model

Table 5.7.1 Comparison of Model Results
Ratio of Maximum Stress to Uniaxial Ice Crushing Strength

	Example 1		Example 2	
	1.0 m Wall	0.6 m Wall	1.0 m Wall	0.6 m Wall
Closed Form	1.0	1.0	1.0	1.0
Approximate Numerical Model	3.0	3.0	3.0	3.0
Advanced Finite Element Model: von-Mises Yield	1.84	2.01	1.98	2.20
Advanced Finite Element Model: Tension Cracking	1.55	2.01	1.65	2.05

The conclusions of the Brown study are:

1 - The closed form solutions for local load prediction are inadequate.

2 - The finite element models can be used as tools to realistically predict the pressures.

3 - More realistic rheological modeliing of ice is required for better prediction of the local loads.

A full description of the technique and the results of investigations of several cases have been presented in Bercha et al., (1985).

The finite element models are quite complex and improvements in the following areas are needed:

1 - Use of proper failure criteria in the model.

2 - Development of finite elements with better ice characterization including strain rate dependence and brittle and ductile failure modes.

3 - Development of ice/structure interface elements which include modeling of friction and adfreeze.

4 - Incorporation of scale factor in the yield function and ice strength values. Not much test data exists on scale factor. This factor may lead to reduction in local loads. This has, however, to be verified.

5 - Currently, analyses indicate design pressures of about 1.5 to 3.0 times the uniaxial compressive strengths. This may be highly conservative and may lead to uneconomical designs.

The Brian Watt and Associates Probabilistic Methods (Vivitrat and Slomski, 1983; Slomski and Vivitrat, 1983)

In this reference probabilistic procedures for the determination of local design pressures as a function of contact areas for winter ice interactions are presented. The approach depends on a computerized simulation procedure based on Monte Carlo technique which considers probabilistic distributions for first-year and multi-year ice thicknesses, floe diameter and velocity. The load is calculated using the Korzhavin Methodology:

$$L = I\ C\ M\ \sigma_u\ D\ t$$

where:

L = the load,

I = the indentation factor,

C = the contact factor,

M = the shape factor,

σ_u = the unconfined horizontal uniaxial compressive strength of the ice,

D = the chord width of the interaction surface, and

t = the average ice thickness.

Note that the nomenclature has been changed slightly for purposes of conformity with this report.

The authors claim that there is no consistent effect of the aspect ratio, but the size of the loaded area has a significant effect on the pressure. The peak pressure L is assumed to be a function of temperature and strain rate. The relationship is based on 103 small scale laboratory indentation tests. The indentation factor I is taken as 3.0. The contact factor is taken as 0.3, and the shape factor M is taken equal to 1.0 since a flat wall interaction is being modeled.

Using a computer program, about 20,000 events were simulated. Both first-year and multi-year ice interactions were considered, including pack ice driving forces. The results are presented in Figure 5.7.3. Figure 5.7.4 shows results of a similar probabilistic approach for summer load impacts.

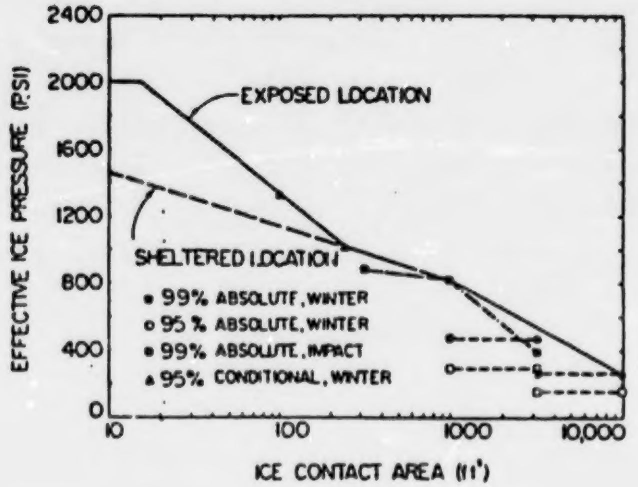

Figure 5.7.3 The Brian Watts and Associates Probabilistic Loads Model for Winter Conditions

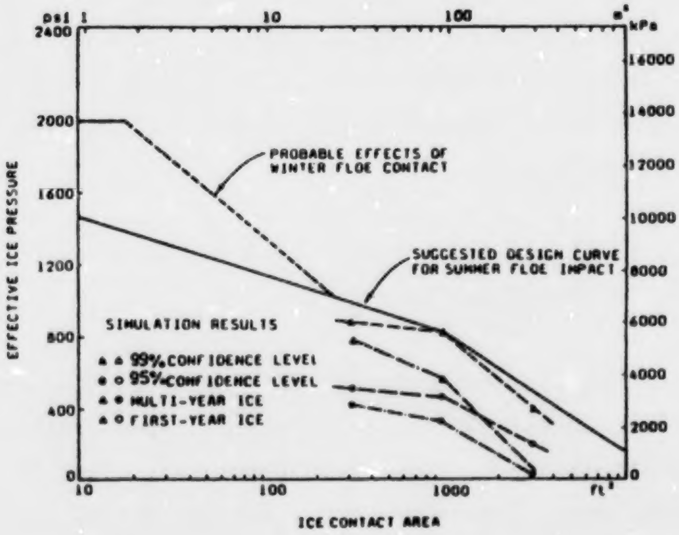

Figure 5.7.4 The Brian Watts and Associates Probabilistic Loads Model for Summer Conditions

5.7.3 Empirical Techniques

As empirical techniques, the procedures of Sanderson (1986), Brian Watts (Bruen et al., 1982), Iyer (1983), the Norwegian Research Centre (1981), and Blanchet (1986) can be mentioned. All these procedures use the results of small scale indentation tests, laboratory and in-situ tests, and tests on ice breakers and lighthouses, and publicly available offshore structures and islands. In the following the essential details of these techniques are presented.

Sanderson's Empirical Curve

Sanderson (1986) presents very briefly the results of investigations carried out by himself into the publicly available field data on ice pressures. The results are presented in Figure 5.7.5, which shows effective pressures as a function of contact area.

A Type I interaction occurs when D is much greater than t. The reader is referred to Sanderson's work for more details. All data is for indentation testing, and the range of results includes tests on fresh water, first-year and multi-year ice. Data include measurements from the laboratory, in-situ indentation, icebreakers, lighthouses, offshore structures and islands.

The curve in Figure 5.7.5 is not intended as a design curve, but to illustrate the following two points:

1 - Scatter of results, owing to variability of loading conditions (e.g. plane strain, plane stress, axisymmetry, aspect ratio, impact, constant displacement rate and temperature), types of ice (e.g. first-year, multi-year, laboratory ice), and ice properties (e.g. grain size, salinity, and crystallography).

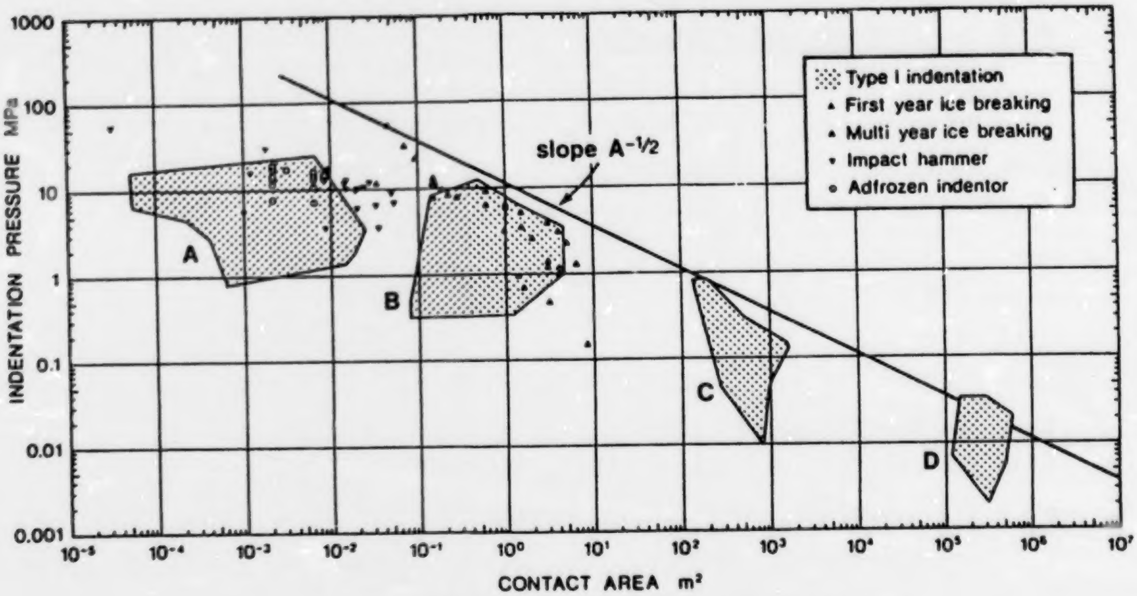

General trend of pressure-area curve, with data groups.

A: *Laboratory tests*

B: *Medium-scale in situ tests, lighthouses and bridge piers*

C: *Full-scale Arctic islands and structures*

D: *Meso-scale models.*

Figure 5.7.5 Sanderson's Empirical Ice Failure Pressure Curve

2 - Strong dependence of pressure on contact area: peak typically 10 to 25 MPa, while over areas of 100 m^2 they are typically less than 1 MPa.

A large body of confidential data exists which has not been used in the compilation of this curve.

Brian Watts Empirical Procedure

Bruen et al., (1982) presented a treatment of the local pressure problem in an analogous manner to the indentation problem. The local pressure is given using the Korzhavin Methodology:

$$P = L / A = M\ I\ C\ \sigma_u$$

where:

L = the total applied force,
A = the area of application (the product of D and t),
σ_u = the unconfined compressive strength,
I = the indentation factor,
C = the contact factor, and
M = the shape factor.

The following values have been assumed in the development of the pressure-area empirical curves:

1 - Unconfined compressive strength is taken as the value at the transition strain rate of $10^{-3}\ s^{-1}$, this being considered as the maximum.

2 - Confinement is considered in terms of the "indentation factor" I and the "shape factor" M. I is taken as 3.0. Assuming the ice to be granular, M is assumed to be given by the following expression from Afanasev (1971):

$$M = [\ 5\ (\ t/D\ ) + 1\ ]^{\frac{1}{2}}$$

where t is the ice sheet thickness and D is the chord length of the width of the interaction.

Caution is warranted when using the results of Bruen et al., (1982). The interpretation of Bruen et al., (1982) appears to differ from that of other researchers. Afanasev (1971) uses values of 0.9 or 1.0 for the shape factor, M, following the Korzhavin (1971) use of M. The formula above is Afanasev's for I, interpreted as an indentation factor which is to account for confinement. The double multiplication appears in choosing an "indentation factor" of 3.0 and a "shape factor" given by the above formula. One should use one or the other for I; M is given as 0.9 for a circular interaction zone, or 1.0 for a flat wall.

Brittle behaviour is considered in terms of the contact factor C. This considers non-simultaneous failure aspect of the loaded area of the ice and is assumed to be equal to 0.3.

Using the above information and assumptions, interactions with various thicknesses of first-year and multi-year ice with different radii of curvature for the ice were analyzed and two upper bound "design" curves have been proposed, one for each ice type (see Figure 5.7.6).

The authors admit that the above criteria is only an interim solution. The brittle behaviour has not been properly characterized by taking into account temperature and strain rate effects. The values for large contact areas beyond about 4.5 m^2 (50 ft^2) need to be verified by field observations.

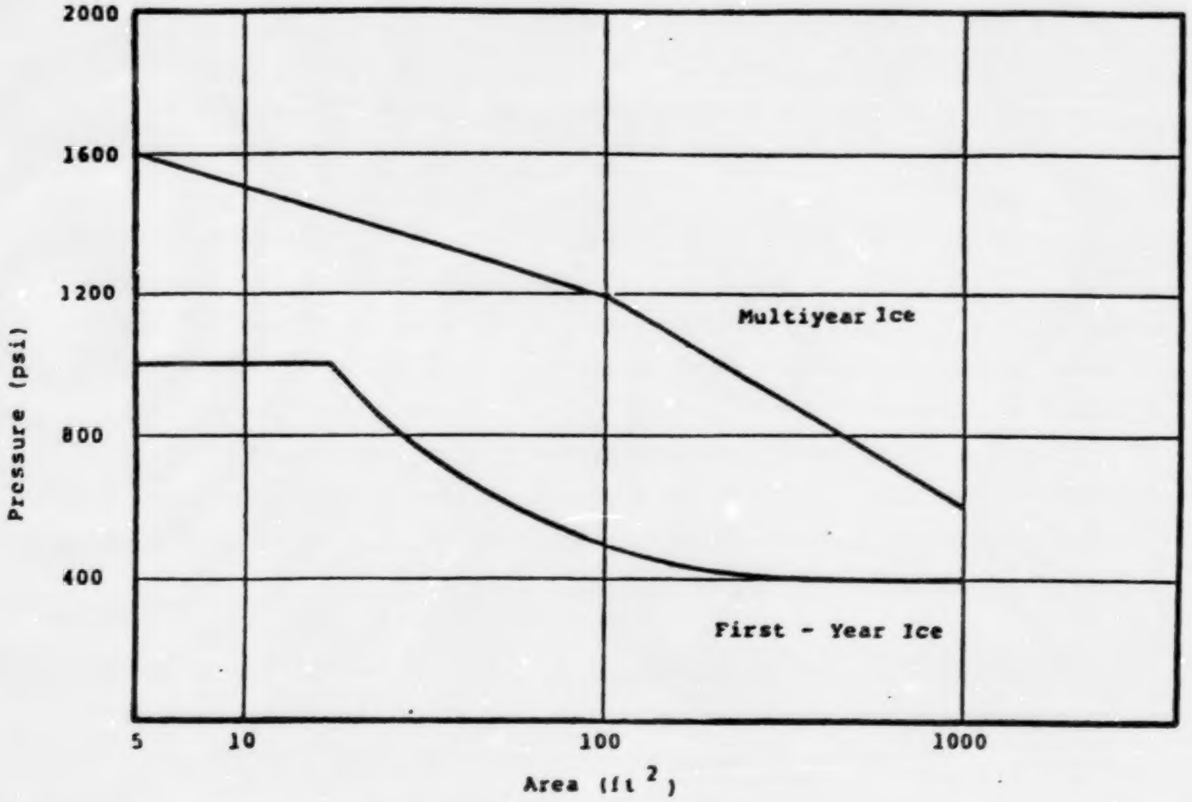

Figure 5.7.6 Brian Watts and Associates Empirical Failure Pressure Curves for Multi-Year Ice and First-Year Ice

Iyer's Model

The approach of Iyer (1983) is an empirical approach based on the results of small indentation tests. Prior to fully enveloping the structure, contact is locally established between the ice and the structure. The local pressure will be a function of the aspect ratio D/t and the contact area. Figure 5.7.7 shows the curve of failure pressure versus contact area for various values of D/t. These curves have been established based on all the available large scale APOA (Arctic Petroleum Operator's Association) projects (No.'s 1, 9, 52, 66 and 93). An empirical relationship of the following form has been established:

$$P_{eff} = 6.8\ (D\ t)^{-0.3}$$

where the product of D and t is the tributary area (in metres) and P_{eff} is the effective pressure in MPa.

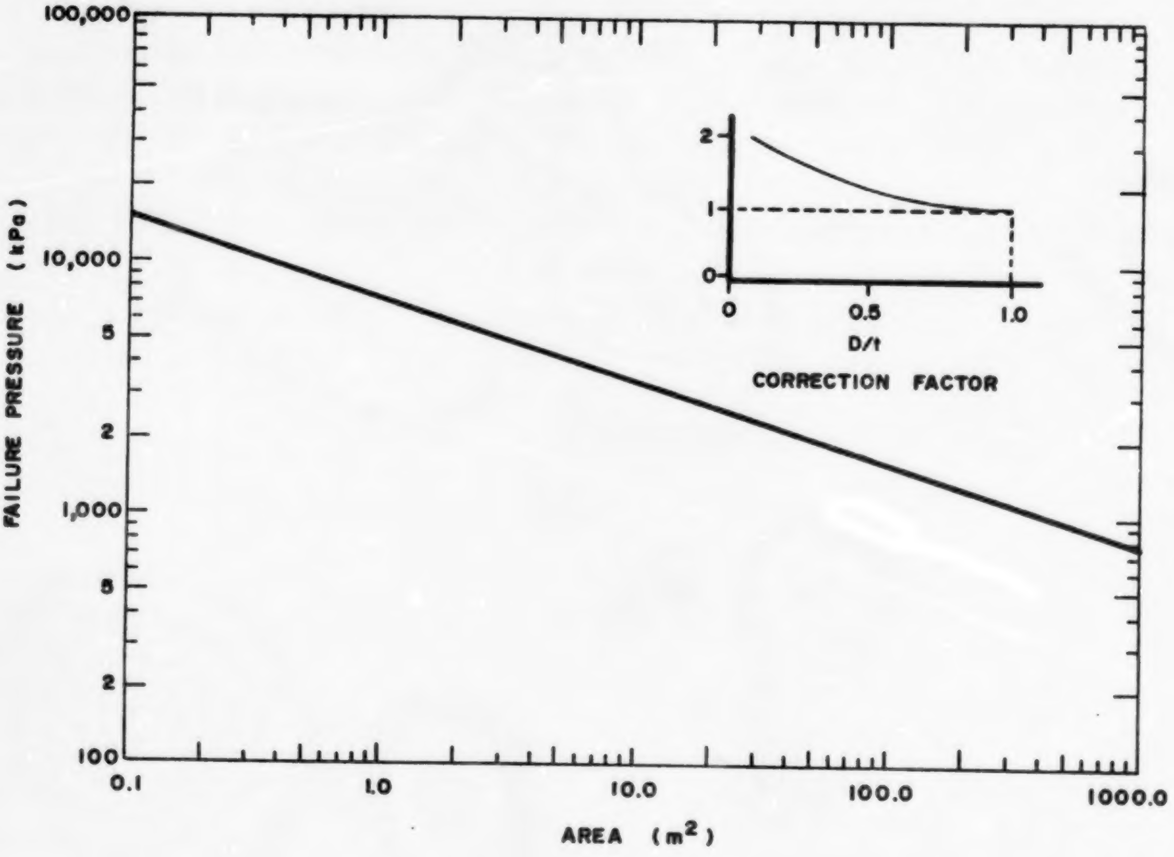

Figure 5.7.7 Iyer's Empirical Ice Failure Pressure Curve

Norwegian Research (Norwegian Research Report, 1981)

This reference presents an empirical expression for the prediction of local ice loads. This is based on model tests of multi-year ridges with vertical sided structures. It is mentioned that this formula can be applied to any kind of ice/structure interaction case.

The local loads on the structure can be determined using the following formula:

$$P_1 = 2 \, [\ 1 + b_1/h)^{-0.6}\ ] \, [\ (A/A_o)^{-0.165}\ ] \ \sigma_u$$

where:

P_1 = the local ice pressure,

b_1 = the horizontal breadth of the local load area,

h = the extreme "vertical" depth of the total area of the structure in contact with the ice,

A = the local load area in cm^2,

A_o = 1.0 cm^2, and

σ_u = the maximum uniaxial crushing strength of ice.

The interpretation of the parameters b_1 and h is illustrated in Figure 5.7.8. The relevance of making use of the parameters b_1 and h is based on the assumption that the structure will experience the highest pressure when crushing takes place simultaneously only over the local load area. Still, under these conditions the presence of the structure will prevent any "plastic" flow of the ice normal to the interaction plane over the complete area in contact with the ice, resulting in a strong confinement of the portion actually being crushed.

The effect on the pressure of the confinement of the ice or the multi-axial state of stress under which crushing takes place, is represented by:

$$K_\sigma = 2 \, [\ 1 + (b_1/h)^{-0.6}\ ]$$

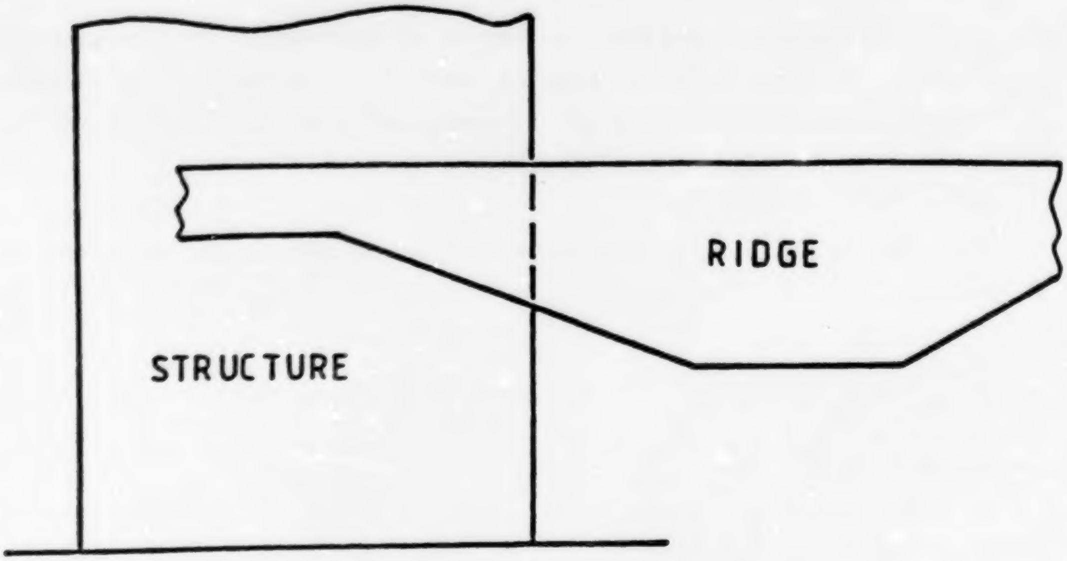
RIDGE
STRUCTURE

$$P = 6 \left[\left(A/A_o \right)^{-0.165} \right] \sigma_u$$

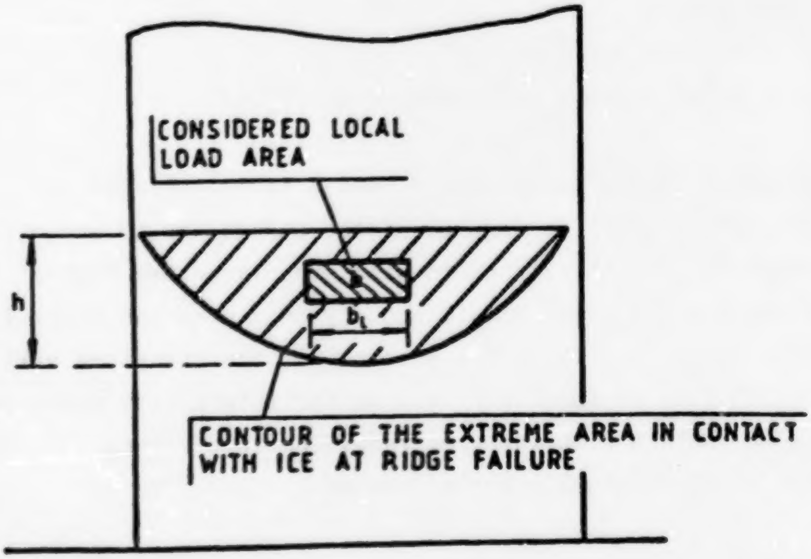
CONSIDERED LOCAL LOAD AREA
h
b_L
CONTOUR OF THE EXTREME AREA IN CONTACT WITH ICE AT RIDGE FAILURE

Figure 5.7.8 The Norwegian Research Empirical Ice Failure Pressure Curve

Model tests and theoretical evaluations indicate that K should not be taken to be greater than 6.0.

For h/b_1 greater than 3.0 the formula for the local loads is given by:

$$P_1 = 6 \; [\; (A/A_o)^{-0.165} \;] \; \sigma_u$$

This represents the "extreme" local ice pressure to which a structure may be exposed.

Blanchet's Empirical Relationships

Blanchet (1986) presents the results of the investigations on the variations of the local failure pressure with depth through first-year and multi-year ice. The distributions are related to several parameters, such as salinity, temperature, ice type, location of the ice pressure area through the thickness, thickness, density, crack and flaw distributions. It should be noted that the results are quite empirical in nature and are based on variation of ice strength with these individual parameters. The results give an understanding of the variation of the localized pressures within the tributary area defining the contact. Table5.7.2 presents the results for 8 metre thick multi-year ice and 2 metre thick first-year ice. An element at the centre of the ice sheet is assumed to be fully confined with a degree of confinement of unity.

This empirical procedure does not take into account the actual failure of the ice within the contact area and the structural stiffness. The results are expected to be very conservative because of the way the pressures are estimated within the contact area.

Table 5.7.2: Ice Strength Ratio Data from Blanchet (1986)

Granular/ Columnar Ice	Depth (m)	Temperature		Type of Ice	Salinity	Confinement	Combined Strength Ratio	
		S	W	S & W	S & W	S & W	S	W
Multi-Year	0.0	0.63	1.30	1.0	1.30	0.50	0.41	0.85
	2.0	0.84	1.12	1.0	1.14	0.92	0.88	1.17
	4.0	1.00	1.00	1.0	1.00	1.00	1.00	1.00
	6.0	0.88	0.78	1.0	0.92	0.90	0.74	0.66
	8.0	0.63	0.46	1.0	0.85	0.50	0.27	0.20
First-Year	0.0	0.58	1.25	1.30	0.72	0.43	0.23	0.50
	0.5	0.92	1.10	1.15	0.88	0.90	0.84	1.00
	1.0	1.00	1.00	1.00	1.00	1.00	1.00	1.00
	1.5	0.97	1.70	0.96	0.78	0.90	0.65	0.47
	2.0	0.90	0.42	0.91	0.65	0.43	0.23	0.11

NOTE: S stands for summer, and W stands for winter measurements.

Floating Vessels

There is another class of marine structures; the floating vessels such as the Gulf Kulluk, the ship shapes, the icebreakers and supply vessels. As explained above, design requirements developed by various classification societies, the Finnish/Swedish Ice Class Rules, the USSR Register of Shipping, and the Canadian Arctic Shipping Pollution Prevention Regulations are worth mentioning. The Norwegian Research Report (1979) presents a detailed discussion of theses requirements. Tables 5.7.3 to 5.7.5 present summaries of these regulations. Mathematical models to determine the ice loads due to impact of various ice features are also presented in the 1979 Norwegian Research Report. All these regulations rely on ice pressures determined without direct consideration of ice characteristics or failure modes. It is also questionable whether these regulations can be applied to moored vessels.

Conclusions

1 - There are no well defined design guidelines for the selection of local pressures. The choice is left to the discretion of the engineer or the designer.

2 - The existing models, both analytical and empirical, suffer from various limitations. Most of the approaches are expected to lead to very conservative values. This is to be verified by full scale measurements.

3 - The current philosophy of some engineers is that minor local damages resulting from improper selection of local pressures can be tolerated provided the local damages do not affect the operation of the marine structure and do not lead to any catastrophic failure.

Example of Calculation of Local Loads

Given a frame spacing of 2.5 m and an ice thickness of 8.0 m, calculate the local load.

Spacing of frames	2.5 m
Ice thickness	8.0 m
Tributary area	$2.5 \times 8 = 20\ m^2$

Empirical Calculations

1. Brian Watt: Probability

winter multi-year ice	12 MPa maximum
summer multi-year ice	9 MPa maximum

2. Sanderson 3 MPa maximum

3. Brian Watt: Empirical

winter multi-year ice	7 MPa maximum
summer multi-year ice	3 MPa maximum

4. Iyer

   D/t = 1.0; Local pressure = 2.7 MPa
   D/t = 2.5/8.0 = 0.31
   contact area = 1.6

   Pressure = 2.7 x 1.6 = 4.3 MPa

5. Norwegian Research

$$P = 6\ [\ (A/A_o)^{-0.165}\ ]\ \sigma_u$$

$$= 6\ [\ \frac{(20 \times 100 \times 100)}{1}^{-0.165}\ ]\ \sigma_u$$

$$= 0.133\ \sigma_u$$

assuming uniaxial strength of ice = 10 MPa, then
P = 0.133 x 10 = 1.33 MPa

6. Blanchet's Approach

   Select the 8 m thick multi-year floe
   average of combined strengths = 0.776
   confined strength = 30 x 0.78 = 23 MPa
   effective pressure on contact area = 23 MPa

Analytical Calculations

Tom Brown's Analytical Approach

1 - closed form solution: effective pressure = 10 MPa
(assumed as a small scale unconfined value)

2 - Approximate Numerical Approach
effective strength = confined strength
= 3 x 10 MPa = 30 MPa

3 - Finite Element

maximum pressure = 2.20 x uniaxial strength
= 2.20 x 10 MPa
= 22 MPa

$P_{max}/P_{ave} = 1.25$

Effective Pressure = 22/1.25 = 18 MPa

This example shows that there is a wide divergence among the results obtained using the different approaches discussed. The local pressure can vary anywhere from 1.33 MPa to 23 MPa. The empirical approaches of Brian Watt, Sanderson and Iyer give values which are within a range of 3 to 7 MPa.

In summary, the values obtained are shown below:

Example: Frame spacing of 2.5 m, and an ice thickness of 8.0 m

1.	Tom Brown's Analytical Approach:	
	Closed Form:	10 MPa
	Approximate:	30
	Finite Element:	18
2.	Brian Watt	
	Probabilistic	12
	Empirical	7
3.	Sanderson Empirical	3
4.	Iyer	4.3
5.	Norwegian	1.3
6.	Blanchet	23

Table 5.7.3 Finnish-Swedish Design Ice Loads

Ice Class	Load on Plating and Frames (kp/cm^2)	Propulsion Power SHP
1 A Super	$p_b = 6.4 + 0.73\ k < 16.5$	$SHP = 0.40\,\Delta + 1500$
	$p_m = 5.7 + 0.21\ k < 8.6$	$SHP < 25500$
	$p_s = 4.6 + 0.13\ k < 6.3$	
1 A	$p_b = 5.8 + 0.64\ k < 15.0$	$SHP = 0.35\,\Delta + 1000$
	$p_m = 4.6 + 0.14\ k < 6.9$	$SHP < 22000$
	$p_s = 3.5 + 0.09\ k < 4.6$	
1 B	$p_b = 5.2 + 0.55\ k < 13.5$	$SHP = 0.30\,\Delta + 500$
	$p_m = 4.6 + 0.07\ k < 4.6$	$SHP < 18500$
	$p_s = 2.4 + 0.05\ k < 2.9$	
1 C	$p_b = 4.6 + 0.46\ k < 12.0$	$SHP = 0.25\,\Delta$
	$p_m = 2.4$	$SHP < 15000$
	$p_s = 1.2$	

$$k = \frac{1}{1000} (\Delta\ SHP)^{0.5}$$

Δ = displacement of ship in tons

p = ice pressure (kp/cm^2) [kilogram pressure / cm^2]

index: b = bow,
m = midbody
s = stern

Table 5.7.4 Russian Design Codes

Ice Class	Load on Plating	Load on Frames
UL	$p_b = 0.0144\ L\ (1 + \frac{2\ L}{1000})\ \alpha_1^{4/5} \mu_1$	$q_b = 1.2\ L\ (1 + \frac{2\ L}{1000}) \alpha_2^{4/5}\ \mu_2$
	$p_m = \frac{L}{10} - 1.5 > 7.5$	$q_m = 4.55\ L > 500$
	$p_s = p_m$	$q_s = q_m$
L 1	$p_b = 0.00865\ L\ (1 + \frac{2\ L}{1000})\ \alpha_1^{4/5}\ \mu_1$	$q_b = 0.55\ L\ (1 + \frac{2\ L}{1000})\ \alpha_2^{4/5}\ \mu_2$
	$p_m = \frac{L}{10} - 3.5 > 4.5$	$q_m = 3.0\ L > 270$
	$p_s = p_m$	$q_s = q_m$
L 2	Loads Not Specified (incorporated in strength requirements)	
L 3	Loads Not Specified (incorporated in strength requirements)	

PLATES:

ζ	11 and less	20	30	40
μ_1	1.00	0.97	0.90	0.82

ζ = angle between the tangent to the frame and the vertical line on the level of the summer load waterline in the section located at 0.1 L from the forward perpendicular, in degrees.

α_1 = angle between tangent to the waterline and the longitudinal plane at 0.1 L aft of forward perpendicular.

FRAMES:

β	8 and less	10	12	14	16	18
μ_2	1.00	0.87	0.78	0.72	0.66	0.62

β = angle between the tangent to the frame and the vertical line on the level of the summer load waterline in the section located at 0.2 L from the forward perpendicular, in degrees.

μ_2 = angle between tangent to the waterline and the longitudinal plane at 0.2 L aft of forward perpendicular.

L = ship length (metres)
b = bow
m = midbody
s = stern

p = ice pressure on plates (kp/cm^2)
q = "horizontal" line ice load on frames (kp/cm)

Table 5.7.5 Canadian Design Ice Loads

Ice Class	Load on Plating and Main Frames (kp/cm^2) bow	midbody	stern
1	17.6	7.0	7.0
1 A	28.1	18.3	22.9
2	42.2	28.1	33.2
3	56.2	37.3	46.4
4	70.3	46.4	57.7
6	84.4	57.2	66.1
7	98.4	59.8	73.8
8	105.7	66.8	84.4
10	105.7	66.8	84.4

Ice Class	Load on Stringers and Web Frames Supporting Main Frames (kp/cm^2) bow	midbody	stern
1	6.0	-	-
1 A	6.8	5.5	6.0
2	9.0	6.8	3.2
3	10.9	8.2	9.6
4	13.7	9.6	10.9
6	19.1	12.3	14.9
7	21.8	13.6	16.4
8	27.3	16.4	20.5
10	45.0	19.1	21.8

6.0 Summary and Recommendations

In this volume of the study a rather lengthy review of the current state-of-the-art for calculating ice forces on offshore structures has been presented. The length of this document is in direct proportion to the alternative methodologies currently in use or proposed for calculating ice loads. In this regard it goes without saying that some uncertainty in the calculations exists. This uncertainty relates primarily in the prediction of the behaviour of the material under different loading conditions.

The alternative methods for calculating ice loads on marine structures, as described in this volume, are basically alternative methods for predicting the behaviour of ice under different loading conditions; as such none of the models have been successful in predicting the behaviour of ice under all loading conditions. Currently the only reliable method for accurately predicting ice forces on marine structures is to use large scale empirical data for ice of the same "state" as that predicted for design. Similar large scale data is generally not available and extrapolation from ice behavioural data at different scale or ice of a different state is required. In comparison to the current uncertainties, reasonably accurate estimates of upper bound static ice forces can be made. Additional empirical data is desirable and as such the collection and synthesis of large scale empirical data is recommended as future work.

The approach to using an upper bound ice force as a quasi-static design load is appropriate for very massive rigid structures and as a method of designing for overall global stability.

The periodicity of ice forces should also be considered in terms of dynamic amplification of structure deformation, potential liquefaction of the soils, and fatigue life. In certain cases, the deflection of the structure can change the ice failure process and therefore change the level and nature of the ice force. The dynamic response of a structure to applied ice loads is an area requiring sophisticated modelling efforts and as such is recommended as an area for future research.

Regional Ice Statistics

In Chapter 2 the various ice geometries encountered in selected Canadian marine regions are briefly reviewed. Each region can be characterized by a specific set of general probabilistic ice design criteria, which includes geometries, velocities of interaction, and driving forces. Each of the criteria should be reviewed in detail when a site specific design is considered. General regional statistics are, however, useful and a future synthesis of this regional information may be desirable.

The Mechanical Properties of Ice and Failure Modes

A complete and comprehensive description of the dependencies of ice mechanical properties on the variance in the state of the ice is not available at this time. Ice shows a strong dependence on loading rate, porosity and temperature. A complete description of these dependencies is, however, not available. Further work on establishing the dependence of ice strength on the various physical parameters is definitely recommended.

Further work on establishing the dependence of ice failure modes on variance in the state of the ice is also recommended.

Interaction Scenarios

In regards to understanding the general logic for ice/structure interactions, sufficient knowledge exists in the industry to quantify the probabilities of occurrence of alternative interaction scenarios. Site specific data is required to establish the design interaction scenarios for proposed installations.

Vertical Sided Structures

For calculating ice forces on narrow vertical sided structures engineers often resort to a procedure referred to in this report as the Korzhavin Methodology. The empirical procedure breaks down the load calculation into an equation consisting of four parts: a strength for the ice, and coefficients for: the indentation or confinement of the ice, the contact of the ice and the structure, and the shape of the ice/structure interaction surface.

For wide structures engineers often use empirically derived failure pressures when calculating ice forces. In this report two empirical relations for the large scale failure pressure of ice have been presented. One represents the failure pressure as a function of the aspect ratio while the other represents the failure pressure as a function of the area of the interaction at the ice/structure interface.

With respect to empirical data, a comprehensive set of field data is still not available for all possible structure sizes and ice states. There therefore is a need to consolidate the useful measured ice force data and to develop a mechanism for readily including future measurements into an empirical ice force/ice pressure/ice state data base.

The sophisticated numerical models of ice/vertical sided structure interactions suffer from the lack of a complete description of the variance of ice mechanical properties and failure modes with the variance in loading conditions and ice states.

Sloping Structures

The global ice force on sloping structures is made up of two parts: the ice breaking component and the ice clearing component. Typically the ice clearing or ride-up component can be similar in magnitude to the ice breaking component.

Important considerations in the design of sloping structures are: the friction between the structure and the ice during the ride-up, the clearing mechanism and the adfreeze bond created between stationary ice and the side of the structure. Careful attention has to be paid to all of these aspects such that the ice loads do not become prohibitively large and the advantages of a sloping structure are lost.

Floating Structures

A floating structure is different from a bottom founded structure in one fundamental way - the resilience of the structure depends on the mechanism used to maintain the structure position. As well, a floating structure will not be able to sustain the same level of ice loading conditions as a bottom founded structure.

With the recent developments in ice force, ship and semisubmersible technology it is possible to consider development scenario's where a floating structure is used in ice infested waters.

The technology used to determine the loads on the floating structure is exactly the same as for vertical or sloping structures, however the structure response to the load now becomes an important aspect of the interaction.

Artificial Islands

In this study an artificial island is a structure which will most likely be surrounded by ice rubble during the course of the winter. In the Canadian Beaufort Sea artificial islands have been constructed of sand and/or gravel, or have consisted of sand berms upon which caissons are placed.

When a thick ice feature interacts with a sand or gravel artificial island its energy is dissipated by physically moving the sand or gravel and creating a spoil pile in front of the ice feature. Normally, for thin ice features the ice failure mode is that of rubble building.

During the winter months the ice rubble refreezes at the waterline. In most areas the currents and tidal action is sufficient to prevent the formation of an adfreeze bond between the rubble and the surrounding ice sheets, floes, etc.

At present there is only a small amount of empirical data on the properties of ice rubble, and programs to measure these properties in the field in detail are recommended.

Ice Loading Dynamics

Usually the term "dynamics" has been used to encompass only the dynamic response of a floating structure to an applied short term ice load. In the recent past the term has been broadened to include the dynamic response of gravity structures to an applied loading condition, and the dynamics of the failure of ice as it interacts with a structure.

The actual dynamics of the coupling of ice and structure responses to the ice/structure interaction has been a fertile field for study for many years. The description of the interaction is complicated by the number of variables which must be taken into account. Only recently has the state-of-the-art developed to such an extent that it has become possible to study in detail the ice and structure responses to the given loading condition. Recent experience with large gravity structures in the Canadian Beaufort Sea indicates that the dynamics of the interaction can have an important effect on the response of the structure. The dynamics of ice/structure interactions, therefore, is something which should be addressed during the design phase.

The understanding of the ice failure process on both the large and small scale has increased significantly in recent years, however there remains the need to develop good numerical models with which to predict the ice-structure response. Much of the early work on dynamic effects has concentrated on vertical pile-type structures with relatively narrow cross-sections. The recent experience with the Gulf Molikpaq structure has demonstrated the importance of accounting for dynamic effects on large, gravity structures. Some of the most important research topics that should be considered for future work are:

- development of damage models to represent the failure process of crushing or pulverization on the local scale,
- inclusion of non-simultaneous effects on large structures with a wide waterplane section,
- inclusion of statistical effects to represent the major variables such as ice strength, and
- determination of the effect of global fracture on both the global and local loads.

Local Ice Loads

It has been stated that the strength of ice depends on the size of the ice under a loading condition. The average strength of ice acting over a large area of a structure is less than the strength of ice measured in the laboratory. In terms of global stability the large scale ice failure pressure is important. In terms of structure member design the local failure pressure of ice is important.

To date there are no well defined design guidelines for the selection of local pressures. The choice of which model to use is left to the discretion of the engineer or the designer. Both analytical and empirical models suffer from various limitations. Most of the approaches are expected to lead to very conservative local load values. It is recommended that the current models be compared to future full scale measurements.

The current design philosophy of some engineers is that minor local damages resulting from improper selection of local pressures can be tolerated provided the local damages do not affect the operation of the marine structure and do not lead to any catastrophic failure.

General

There are at present "real" engineering differences in estimated ice loads on structures, based on the method used by the engineer to estimate the load. In comparison to other engineering disciplines where standard methodologies are used for determining solutions to standard problems, ice mechanics is different due to there being significant differences in methodologies, and such fundamental properties as compressive strength, bending capacity, and scale effect. Engineering interpretation based on experience and judgment is an important aspect of the calculation of ice loads on marine structures.

One should be aware of the potential wide disparity in ice loads calculated by different methods. The best procedure is to calculate the ice load by a variety of methods, examine the differences in the loads and the probable reasons for the differences, and use engineering judgment to estimate the appropriate load.

A significant amount of fundamental ice research remains. This research includes the effect of size of sample on the fundamental strength parameters, and the interrelationship between the physical properties of the ice and the mechanical properties. The full parameterization of the strength of ice under as wide a variety of conditions possible should as well be examined.

Recent developments of modelling ice damage should be continued in order to fully develop a theory of the damage progression in ice as it interacts and fails against a structure. Coincidental structure response should be examined to enable the prediction of dynamic loads and better quantification of force-time histories.

ICE FORCES ON MARINE STRUCTURES

References

Abdelnour, R., "Model Tests of Multi-Year Pressure Ridges Moving Onto Conical Structures", Proceedings of the International Association of Hydraulic Research Symposium on Ice, Quebec City, 1981.

Acres International Ltd., "Influence of Small Icebergs on Semisubmersibles", Report prepared for the Petroleum Directorate, Government of Newfoundland, 1983.

Acres International Ltd., "Northumberland Strait Bridge: Ice Forces Report", Draft copy of Acres International Ltd. Report prepared for Public Works Canada, March, 1987.

Afanasev, V.P., Y.V. Dolgopolov, and Z.I. Shvaishstein, "Ice Pressure on Individual Marine Structures", in Ice Physics and Ice Engineering, ed. G.N. Yakovlev, Leningrad, U.S.S.R. Translated by Israel Program for Scientific Translation, Jerusalem, Israel, 1973.

Afanasev, V.P., "Ice Pressure on Vertical Structures", NRC Technical Translation 1708, Translated by V. Poppe, Translation Section, National Science Library, Ottawa, Ontario, December, 1973. Translated from Transportnoe Strolitel'stvo (3): 47 - 48, 1972.

Alaska Oil and Gas Association Project 96, "Model Tests and Analysis of Multi-Year Pressure Ridges Failing Against a 45° Cone", 1979.

Alaska Oil and Gas Association Project 201, "Interaction of Ice Cover with a Semisubmersible Drilling Unit", 1983.

Alaska Oil and Gas Association project 309, "Computer Software to Analyze Ice Interaction with Semisubmersibles", 1986.

Alaska Oil and Gas Association project 340, "Computer Software to Analyze Ice Interaction with Moored Ship-shaped Vessels", 1987.

Allyn, N. "Keynote Address on Global and Local Ice Loads Including Dynamic Effects", Ice/Structure Interaction State-of-the-art Research Needs Workshop, Calgary, 1986.

Allyn, N. and Tseng, J., "Computer Software to Analyze Ice Interaction with Semisubmersibles", Arctic Offshore Technology Conference, (AOTC '86), 1986.

Allyn, N. and B.R. Wasilewski, "Some Influences of Ice Rubble Field Formations Around Artificial Islands in Deep Water", Proceedings of the Fifth International Conference on Port and Ocean Engineering under Arctic Conditions (POAC '79), Trondheim, Norway, August, 1979.

Allyn, N., "Ice Pile-Up Around Offshore Structures in the Beaufort Sea", NRC Workshop on Sea Ice Ridging and Pile-Up, Calgary, October, 1980.

Allyn, N.F.B. and K. Charpentier, "Modeling Ice Rubble Fields Around Arctic Offshore Structures", Offshore Technology Conference, Houston, May, 1982.

American Petroleum Institute, "American Petroleum Institute Planning, Designing and Constructing Fixed Offshore Structures in Ice Environments", API Bulletin 2N, Final Draft Copy, February, 1987.

Arctic Petroleum Operators Association, "Mathematical Model to Describe the Behaviour of a Moving Ice Field Encountering a Conical Structure", APOA Project No. 57, 1973.

Arctic Petroleum Operators Association, "Model Experiments to Determine the Forces Exerted on Structures by Moving Ice Fields (Comparison with small prototype test results", APOA Project No. 77, 1974.

Arctic Petroleum Operators Association, "Small Prototype Cone Tests, Winter 1974-75", APOA Project No. 82, 1975.

Arctic Petroleum Operators Association, "In-Situ Ice Property Measurement In the Beaufort Sea", APOA Project No. 84, 1975.

Arctic Petroleum Operators Association, "Preliminary Modeling of the Process of Penetration of Pressure Ridges by Conical Structures", APOA Project No. 86, 1975.

Arctic Petroleum Operators Association, "Computer Program to Evaluate the Forces Generated by a Moving Ice Field Encountering a Conical Structure", APOA Project No. 87, 1975.

Arctic Petroleum Operators Association, "Field Studies of the Strength and Physical Properties of a Multi-Year Ice Pressure Ridge in the Southern Beaufort Sea", APOA Project No. 91, 1977.

Arctic Petroleum Operators Association, "Continuous Crushing of Ice", APOA Project No. 106, 1978.

Arctic Petroleum Operators Association, "Ice Conditions at Issungnak 1979-1980", APOA 171-1 Vol. 3, October, 1981.

Arctic Petroleum Operators Association, "Ice Forces on Hans Island", APOA Project No. 180, 1981.

Arctic Petroleum Operators Association, "Ice Forces on Hans Island", APOA Project No. 181, 1982.

Ashby, M.F., A.C. Palmer, M. Thouless, D.J. Goodman, M. Howard, S.D. Hallam, S.A.F. Murrell, N. Jones, T.J.O. Sanderson and A.R.S. Ponter, "Nonsimultaneous Failure and Ice Loads on Arctic Structures", Proceedings of the 18th Annual Offshore Technology Conference, Houston, Texas, May 5 - 8, 1986. Paper No. OTC 5127.

Bass, D., H. Gaskill and N. Riggs, "Analysis of Iceberg Impacts with Gravity Based Structures at Hibernia", Proceedings of the Fourth International Conference on Offshore Mechanics and Arctic Engineering (OMAE 1985), Dallas, Texas, February, 1985.

Bercha, F.G., and J.V. Danys, "Prediction of Ice Forces on Conical Offshore Structures", Marine Science Communications, pp. 365 - 380, 1975.

Bercha, F.G. and J.V. Danys, "On Forces Generated by Ice Acting Against Bridge Piers", Proceedings of the Third National Hydrotechnical Conference, Canadian Society for Civil Engineering, L'Universite Laval, Quebec City, May 26 - 27, 1977.

Bercha, F.G., T.G. Brown and M.S. Cheung, "Local Pressure in Ice-Structure Interactions", Proceedings, ARCTIC '85, American Society of Civil Engineers, San Francisco, pp. 1243 - 1251, March, 1985.

Bjork, B., "Ice-Induced Vibration of Fixed Offshore Structures, Part 2: Experience with Baltic Lighthouses", Norwegin Research Project, Report No. 81-06/2, 1981.

Blanchet, D., "Variations of the Local Failure Pressure With Depth Through First-Year and Multi-Year Ice", Proceedings of the Fifth Offshore Mechanics and Arctic Engineering Symposium, (OMAE '86), Volume 4, pp. 310 - 319, 1986.

Blenkarn, K.A., "Measurement and Analysis of Ice Forces on Cook Inlet Structures", Proceedings of the 2nd Annual Offshore Technology Conference, Houston, Texas, April 22 - 24, 1970. Paper No. 1261.

Bruce, J.C. and N.F.B. Allyn, "Ice Effects on Offshore Structures: An Overview", Offshore Goteborg 83, International Trade Fair and Conferences for the Offshore Industry and the Subcontractors, 1983.

Bruen, F.J., R.C. Byrd, V. Vivitrat and B.J. Watt, "Selection of Local Design Ice Pressures for Arctic Systems", Paper No. OTC 4334, Proceedings of the 14th Annual Offshore Technology Conference, Houston, Texas, May 3 - 6, 1982.

Bruen, F.J., and V. Vivitrat, "Ice Force Prediction Based on Strain-Rate Field", Third International Offshore Mechanics and Arctic Engineering Symposium, Volume 3, pp. 275 - 281.

Bruun, P. and P. Johannesson, "The Interaction Between Ice and Coastal Structures", Proceedings of the First International Conference on Port and Ocean Engineering under Arctic Conditions (POAC '71), Trondheim, Norway, 1971.

Bulow, R.E., Withee, S.G., Akaboshi, T., Nawata, T., and Joensuu, A., "Inclined Column Semisubmersible - Design Considerations", Offshore Mechanics and Arctic Engineering Specialty Symposium, 1986.

Calkins, D.J., "Arching of Model Ice Floes at Bridge Piers", International Symposium on Ice, Lulea, Sweden, 1978.

Cammaert, A.B. and G.B. Tsinker, "Impact of Large Ice Floes and Icebergs on Marine Structures", Proceedings of the Sixth International Conference on Port and Ocean Engineering under Arctic Conditions, Quebec City, Canada, Volume II, pp. 653 - 667, July, 1981.

Cammaert, A.B., Wong, T.T., and Curtis, D.D., "Impact of Icebergs on Offshore Gravity and Floating Platforms", Proceedings of the Seventh International Conference on Port and Ocean Engineering under Arctic Conditions (POAC '83), Helsinki, Finland, 1983.

Cammaert, A.B., T. Kimura, N. Koma, N. Yashima, S. Yano, and Y. Matsushima, "Adfreeze Forces on Offshore Platforms", Proceedings of the Fifth Offshore Mechanics and Arctic Engineering Symposium, 1986.

Carlile, Offshore Technology Conference, Houston, Texas, 1969.

C-CORE newsletter, Vol. 11, No. 3, November 1986

Colbeck, S.C. (editor); "Dynamics of Snow and Ice Masses", Academic Press, New York, 1980.

Coon, M.D., Personal Communications, 1985.

Coon, M.D., R.J. Evans, and D.H. Gibson, "Failure Criteria for Sea Ice and Loads Resulting from Crushing", Proceedings of the Seventh International Symposium on Ice, International Association of Hydraulic Research, Hamburg, West Germany, Volume 3, pp. 1 - 16, 1984.

Cormeau, A., I.J. Jordaan and M. Maes, "Development of a Model for Progressive Damage in Ice", Det Norske Veritas Report, prepared for Public Works Canada, 1986.

Cox, G.F.N., and W.F. Weeks, "Equations for Determining the Gas and Brine Volumes in Sea Ice Samples", Journal of Glaciology, Vol. 29, No. 102, pp. 306 - 316, 1983.

Cox, G.F.N., J.A. Richter, W.F. Weeks and M. Mellor, "A Summary of the Strength and Modulus of Ice Samples from Multi-Year Pressure Ridges", Proceedings of the Third Offshore Mechanics and Arctic Engineering Symposium, New Orleans, 1984.

Cox, J., J. Lewis, R. Abdelnour and D. Behnke, "Assessment of Ice Ride-Up/Pile-Up on Slopes and Beaches", Proceedings of the Seventh International Conference on Port and Ocean Engineering under Arctic Conditions (POAC '83), Helsinki, Finland, Volume II, pp. 971 - 981, April, 1983.

Croasdale, K.R., "Review of Ice Forces on Offshore Structures", Third International Ice Symposium, International Association of Hydraulic Research, Hanover, New Hampshire, 1975.

Croasdale, K.R., "Ice Forces on Fixed Rigid Structures", in Working Group on Ice Forces on Structures: A State of the Art Report (T. Carstens, Ed.), U.S.A. CRREL Special Report 80 - 26, ADA-089674, Hanover, New Hampshire, 1980.

Croasdale, K.R., "Sea Ice Mechanics: A General Overview", Marine Technology Society Journal, Volume 18, No. 1, 1984.

Croasdale, K.R., "Arctic Fixed Platforms for Water Depths Greater than 50 Meters", Arctic Engineering for the 21st Century, The Marine Technology Society, Williamsburg, Virginia, 1984.

Croasdale, K.R., "Arctic Fixed Platforms for Water Depths Greater than 50 Meters", in Proceedings of the First Spilhaus Symposium, Arctic Engineering for the 21st Century, B.C. Gerwick (ed.), The Marine Technology Society, Williamsburg, Virginia, October, 1985.

Croasdale, K.R., "Recent Developments in Ice Mechanics and Ice Loads", Behaviour of Offshore Structures, Elsevier Science Publishers B.V., Amsterdam, pp. 53 - 74, 1985.

Croasdale, K.R., "Ice Investigations at a Beaufort Sea Caisson, 1985", K.R. Croasdale and Associates Report Prepared for The National Research Council of Canada and The U.S. Department of the Interior, March, 1986.

Croasdale, K.R., "Measurements of the Properties of Broken Ice Zones and Ice Rubble", K.R. Croasdale and Associates Report Prepared for Public Works Canada, 1986.

Croasdale, K.R., N.R. Morgenstern and J.B. Nuttall, "Indentation Tests to Investigate Ice Pressures on Vertical Piers", Journal of Glaciology, Volume 19, No. 81, pp. 301 - 311, 1977.

Croasdale, K.R. and R.W. Marcellus, "Ice and Wave Action on Artificial Islands in the Beaufort Sea", Canadian Journal of Civil Engineering, Vol. 5, No. 1, pp. 98 - 113, 1978.

Croasdale, K.R., M. Metge and P.H. Verity, "Factors Governing Ice Ride-Up on Sloping Beaches", IAHR International Symposium on Ice Problems, (IAHR 1978), Lulea, Sweden, Part I, pp. 405 - 420, August, 1978.

Croasdale, K.R., and A. Person, "A Logical Approach to Ice Loads", presented at the Second Global Marine Arctic Offshore Symposium, Houston, Texas, 1984.

Croasdale, K.R., G. Comfort and B.W. Graham, "Arctic Pack Ice Forces Research Project", K.R. Croasdale and Associates Ltd. and Arctec Canada Ltd. report, prepared for The Department of Supply and Services, Science Branch, Department of Fisheries and Oceans, and Public Works Canada, 1986.

Croteau, P., M. Rojansky and B.C. Gerwick, "Summer Ice Floe Impacts Against Caisson-Type Exploratory and Production Platforms", Third International Offshore Mechanics and Arctic Engineering Symposium (OMAE '84) Volume 3, pp. 228 - 237, 1984.

Daoud, N, and F.C. Lee, "Ice-Induced Dynamic Loads on Offshore Structures", Proceedings of the Fifth Offshore Mechanics and Arctic Engineering Symposium (OMAE '86), Volume 4, pp. 212 - 218, 1986.

Danielewicz, B.W., M. Metge and A.B. Dunwoody, "On Estimating Large Scale Ice Forces from Deceleration of Ice Floes", Proceedings of the Seventh International Conference on Port and Ocean Engineering (POAC '83), Helsinki, Finland, Volume 4, pp. 537 - 546, April, 1983.

Danys, J.V., and F.G. Bercha, "Influence of Friction on Ice Forces Acting Against Sloped Surfaces", Symposium on Applied Glaciology, International Glaciological Society, Cambridge, England, 1976.

DePaoli, S., T.B. Morrison and R.W. Marcellus, "Analysis of Interaction Probabilities Between Large Ice Features and Offshore Structures in the Canadian Beaufort Sea", C.M.E.L. Report No. 1021, November, 1982.

Dickins, D.F., "Ice Conditions Along Arctic Tanker Routes", D.F. Dickins and Associates Ltd. Report prepared for Dome Petroleum Ltd., 1981.

Edwards, R.Y., W.G. Wallace and R. Abdelnour, "Model Experiments to Determine the Forces Exerted on Structures by Moving Ice Fields (Comparison with small prototype test results)", Arctec Canada Limited Report prepared for Arctic Petroleum Operators Association, APOA Project No. 77, 1974.

Edwards, R.Y, and R. Abdelnour, "Preliminary Modeling of the Process of Penetration of Pressure Ridges by Conical Structures", Arctec Canada Limited Report prepared for Arctic Petroleum Operators Association, APOA Project No. 86, 1975.

Edwards, R.Y., and K.R. Croasdale, "Model Experiments to Determine Ice Forces on Conical Structures", Symposium of Applied Glaciology, International Glaciological Society, Cambridge, England, September 12 - 17, 1976.

El-Tahan, H., A.S.J. Swamidas, M. Arockiasamy and D.V. Reddy, "Strength of Iceberg and Artificial Snow Ice Under High Strain Rates and Impact Loads", Proceedings of the Third Offshore Mechanics and Arctic Engineering Symposium, Volume 3, pp. 158 - 165, 1984.

El-Tahan, H., Swamidas, A.S.J. and Arockiasary, M., "Response of semi-submersible models to bergy-bit impact", Proceedings of the Eighth International Conference on Port and Ocean Engineering under Arctic Conditions (POAC '85), Narssarssuaq, Kalaallit Nunaat, 1985.

Engelbrektson, A., "Observations of a Resonance Vibrating Light House Structure in Moving Ice", Proceedings of the Seventh International Conference on Port and Ocean Engineering under Arctic Conditions (POAC '83), Helsinki, Finland, 1983.

Eranti, E., and G. Lee, "Cold Region Structural Engineering", McGraw-Hill, 1986.

Eranti, E., F. Hayes, M. Maattanen and T. Soong, "Dynamic Ice - Structure Interaction Analysis for Narrow Vertical Structures", Proceedings of the Sixth International Conference on Port and Ocean Engineering under Arctic Conditions (POAC '81), Quebec City, 1981.

Exxon Company, "Technical Seminar on Alaskan Beaufort Sea Gravel Island Design", 1979.

Frankenstein, G., and R. Garner, "Equations for Determining the Brine Volume of Sea Ice from -0.5°C to -22.9°C", Journal of Glaciology, Vol. 6, No. 48, pp. 943 - 944, 1967.

Frederking, R.M.W., "Dynamic Ice Forces on an Inclined Structure", in Physics and Mechanics of Ice, edited by P. Tryde, International Union of Theoretical and Applied Mechanics Symposium at the Technical University of Denmark, August 1979. Springer Verlag, New York, pp. 104 - 116, 1979.

Frederking, R.M.W. "Ice Action on Nanisivik Wharf, Strathcona Sound, N.W.T., Winter 1978 - 1979", Canadian Journal of Civil Engineering, Volume 7, pp. 558 - 563, 1980.

Frederking, R.M.W., and N.K. Sinha, "Ice Action on Wharf at Strathcona Sound", Proceedings of the Fourth International Conference on Port and Ocean Engineering Under Arctic Conditions (POAC '77), Memorial University of Newfoundland, St. John's, September 26 - 30, 1977, pp. 707 - 717, 1977.

Frederking, R.M.W., and M. Nakawo, "Ice Interactions with Nanisivik Wharf, Winter 1970 - 1980", Proceedings of the 6th Canadian Hydrotechnical Conference, Ottawa, Ontario, June 2 - 3, 1983, Volume 1, pp. 523 - 541, 1983.

Frederking, R.M.W., and G.W. Timco, "On Measuring Flexural Properties of Ice Using Cantilever Beams", Annals of Glaciology, Volume 4, 1983, pp. 58 - 65, 1983.

Frederking, R.M.W., and M. Nakawo, "Ice Action on Nanisivik Wharf, Winter 1979 - 1980", Canadian Journal of Civil Engineering, Volume 11, No. 4, pp. 996 - 1003, 1984,

Frederking, R.M.W., and G.W. Timco, "Quantitative Analysis of Ice Sheet Failure Against an Inclined Plane", Proceedings of the Fourth International Offshore Mechanics and Arctic Engineering Sysmpsium, ASME, Dallas, Texas, February 10 - 15, Volume 2, pp. 160 - 169, 1985.

Frederking, R.M.W., and G.W. Timco, "Field Measurements of the Shear Strength of Columnar-Grained Sea Ice", Proceedings of the IAHR Ice Symposium 1986, Iowa City, Iowa, August 18 - 22, Vol. 1, pp. 279 - 292, 1986.

Frederking, R., F. Hayes, M. Maattanen and T. Soong, "Static and Dynamic Ice Loads on the Yamachiche Bend Light Pier, 1980 - 84", Proceedings of the IAHR Ice Symposium, August 1986.

Funegard, E.G., R.H. Nagel and G.G. Olson, "Design and Construction of the Mars Spray Ice Island", Proceedings of the Sixth Offshore Mechanics and Arctic Engineering Symposium (OMAE '87), Houston, Texas, March, 1987.

Gaida, K.P., Barnes, J.R. and Wright, B.D., "Kulluk - an Arctic Exploratory Drilling Unit", Offshore Technology Conference, Houston, Texas, 1983.

Gerwick and Jahns, 1979.

Gladwell, R.W., "Field Studies of the Strength and Physical Properties of a Multi-Year Ice Pressure Ridge in the Southern Beaufort Sea", Imperial Oil Limited Report, also known as APOA Report 91, March, 1977.

Gold, L.W., "The Process of Failure of Columnar-Grained Ice", Philosophical Magazine, Volume 26, No. 2, pp. 311 - 328, 1978.

Golder Associates, "Beaufort Sea Spray Ice Island Construction", Technically Speaking, No. 9, December, 1986.

Gustajtis, K.A., and T.J. Buckley, "A Seasonal Iceberg Density Distribution Along the Labrador Coast", Proceedings of the Fourth International Conference on Port and Ocean Engineering under Arctic Conditions, (POAC '77), St. John's, Newfoundland, Volume 2, pp. 972 - 983, 1977.

Gustajtis, K.A., "Iceberg Population Distribution Study in the Labrador Sea", C-CORE (Centre for Cold Ocean Resources Engineering, Memorial University of Newfoundland, St. John's, Newfoundland), Data Report No. 79-8, July, 1979.

Guttman, S.I., F.J. Puskar, and R.G. Bea, "Analysis of Offshore Structures Subject to Arctic Ice Impacts", Third International Offshore Mechanics and Arctic Engineering Symposium, Volume 3, pp. 238 - 245.

Hetenyi, M., "Beams on Elastic Foundations", University of Michigan Press, Ann Arbor, Michigan, 1946.

Hnatiuk, J., and E.E. Felzien, "Molikpaq: An Integrated Mobile Arctic Drilling Caisson", Proceedings of the 17th Annual Offshore Technology Conference, Houston, Texas, May 6 - 9, 1985. Paper No. OTC 4940.

Hocking, G., G.G.W. Mustoe, J.R. Williams, "Validation of CICE Code for Ice Ride-Up and Ice Ridge Cone Interaction". Proceedings, ARCTIC '85, American Society of Civil Engineers, San Francisco, pp. 962 - 970, March, 1985a.

Hocking, G., G.G.W. Mustoe, J.R. Williams, "Dynamic Global Forces on an Offshore Structure from Multi-Year Floe Impacts". Proceedings, ARCTIC '85, American Society of Civil Engineers, San Francisco, pp. 202 - 210, March, 1985b.

Hudson, R.D., G.R. Pilkington and M. Metge, "Extreme Ice Features along the N.W. Edge of the Canadian Arctic Archipelago", Proceedings of the Sixth International Conference on Port an Ocean Engineering under Arctic Contitions (POAC '81), Quebec City, Canada, July, 1981.

Hudson, R.D., "Observations of the Extrusion of Sea Ice Rubble", Proceedings of the Seventh International Conference on Port and Ocean Engineering under Arctic Conditions (POAC '83), Helsinki, Finland, Volume 1, p. 99, 1983.

Iyer, H.S., "Size Effects in Ice and Their Influence on the Structural Design of Offshore Structures", Proceedings of the Seventh International Conference on Port and Ocean Engineering under Arctic Conditions (POAC '83), Helsinki, Finland, Volume 3, pp. 414 - 432, April, 1983.

Jahns, H.O., D.H. Petrie and A.V. Lockett, "CIDS Spray Ice Barrier", Offshore Technology Conference Houston, Texas, May, 1985.

Jizu, Xu, Shi Qingzeng and Meng Zhaoying, "Features of Frequency and Amplitude in Ice Induced Vibration of a Jacket Platform" Proceedings of the Seventh International Conference on Port and Ocean Engineering under Arctic Conditions (POAC '83), Helsinki, Finland, 1983.

Johansson, P., "Ice-Induced Vibration of Fixed Offshore Structures, Part 1: Review of Dynamic Response Analysis". Marine Structures - Ice, Norwegin Research Project, Report No. 81-061, 1981.

Jordaan, I., S. Lantos and M. Nessim, "A Probabilistic Approach to the Estimation of Environmental Driving Forces Acting Upon Arctic Offshore Structures", Det Norske Veritas (Canada) Ltd., 1985.

Jordaan, I.J., "Numerical and Finite Element Techniques in Calculation of Ice-Structure Interaction", Third State-of-the-Art Report on Ice Forces, IAHR Ice Symposium, Iowa City, Iowa, 1986.

Kashteljan, V.I., Poznjak, I.I., and Ryvlin, A.Ja, "Ice Resistance to Motion of a Ship", Translated from Russian by Marine Computer Applications Corportation, 1968.

Kato, K. and Sodhi, D.S., "Ice Action on Pairs of Cylinders and Conical Structures", CRREL Report 83-25, 1983.

Kemp, T.S., "Grounded Ice Pads as Drilling Bases in the Beaufort Sea", Proceedings of the International Association of Hydraulic Research Symposium on Ice, Hamburg, Germany, August, 1984.

Kerr, A.D., "On the Determination of Horizontal Forces a Floating Ice Plate Exerts on a Structure", Journal of Glaciology, Volume 20, No. 82, pp. 123 - 134, 1978.

Kim, J.K., and T.V. Kotras, "Mathematical Model to Describe the Behaviour of a Moving Ice Field Encountering a Conical Structure", Arctec Canada Report Prepared for the Arctic Petroleum Operator's Association, APOA Project No. 57, 1973.

Kitami, E., K. Fujishima, Y. Taguchi, T. Nawata, T. Kawasaki, and F. Sakai, "Iceberg Collision with Semisubmersible Drilling Unit", Proceedings of the International Association of Hydraulic Research Symposium on Ice, Hamburg, Germany, 1984.

Koehler, P.E., and L. Jorgensen, "Ship Ice Impact Analysis", Proceedings of the Fourth Offshore Mechanics and Arctic Engineering Symposium (OMAE '85) , 1985.

Korzhavin, K.N., "Action of Ice on Engineering Structures", translation of "Vozdiestvie l'da no Inzhenernye Sooruzheniia", published in Russian in 1962. Translated by U.S. Joint Publications Research Service for the U.S. Army Cold Regions Research and Engineering Laboratory, Hanover, New Hampshire. Draft Translation No. 260, September, 1971.

Kovacs, A., A.J. Gow and W.F. Dehn, "Islands of Grounded Sea Ice", CRREL Report 76-4, April, 1976.

Kovacs, A. and D.S. Sodhi, "Shore Ice Pile-Up and Ride-Up: Field Observations, Models and Theoretical Analysis", Cold Regions Science and Technology, Volume 2, Elsevier Scientific Publishing Co., Amsterdam, 1980.

Kry, P.R., "The Flexural Strength and Young's Modulus of Land Fast Ice by the Mackenzie River Delta". APOA Project No. 84, Imperial Oil Limited, November, 1975.

Kry, P.R., "Ice Rubble Fields in the Vicinity of Artificial Islands", Proceedings of the Fourth International Conference on Port and Ocean Engineering, (POAC 77), Memorial University of Newfoundland, St. John's, Newfoundland, September 26 - 30, Vol. 1, pp. 200 - 211, 1977.

Kry, P.R., "A Statistical Prediction of Effective Ice Crushing Stresses on Wide Structures", IAHR International Symposium on Ice Problems, (IAHR 1978), Lulea, Sweden, Part I, pp. 33 - 47, 1978.

Kry, P.R., "Implications of Structure Width for Design Ice Forces", Physics and Mechanics of Ice, edited by P. Tryde, International Union of Theoretical and Applied Mechanics Symposium at the Technical University of Denmark, August 1979. Springer Verlag, New York, 1980, pp. 179 - 193, 1979.

Kry, P.R., "Ice Forces on Wide Structures", Canadian Geotechnical Journal, Vol. 17, pp. 97 - 113, 1980.

Lewis, J.W. and K.R. Croasdale, "Modeling the Interaction Between Pressure Ridges and Conical Shaped Structures", IAHR International Symposium on Ice Problems, (IAHR 1978), Lulea, Sweden, Part I, pp. 165 - 196, 1978.

Lindsay, D.G., "Patterns of Break-up, Freeze-up and Surface Roughness of Sea Ice in Selected Channels in the Canadian Arctic", Polar Continental Shelf Project, Department of Energy and Natural Resources, Ottawa, 1977.

Machemehl, J.L., "Physical Model Study of an Icebreaking Tanker Moored to an Offshore SPM Terminal in Moving Ice", Proceedings of the Sixth Offshore Mechanics and Arctic Engineering Symposium, Houston, Texas, March, 1987.

Marcellus, R.W., "Ice Interaction Computer Parametric Analysis", C.M.E.L. Report No. 1008, prepared for Dome Petroleum, April, 1982 (proprietary).

Marcellus, R.W., and T.B. Morrison, "Ice Design Statistics for the Canadian Beaufort Sea", C.M.E.L. Report No. 1015, prepared for the Environmental Impact Statement Partners, April, 1982.

Marcellus, R.W., K.R. Croasdale, N.F.B. Allyn and N.R. Morgenstern, "Analytical Models for Broken Ice Zones", C.M.E.L. Report No. 1038, prepared for Public Works Canada, March, 1986.

Maattanen, M., "Stability of Self-Excited Ice-Induced Structure Vibrations", Proceedings of the Fourth International Conference on Port and Ocean Engineering under Arctic Conditions (POAC '77), St. John's, Newfoundland, Volume 2, pp. 684 - 694, April, 1977.

Maattanen, M., "Laboratory Tests for Dynamic Ice - Structure Interaction", Proceedings of the Fifth International Conference on Port and Ocean Engineering under Arctic Conditions (POAC '79), Trondheim, Norway, 1979.

Maattanen, M., "Ice Structure - Dynamic Interaction", Proceedings of the International Association of Hydraulic Research Symposium on Ice, Quebec City, 1981.

Maattanen, M., "Dynamic Ice - Structure Interaction During Continuous Crushing", USA CRREL Report No. 83-5, Hanover, New Hampshire, 1983.

Maattanen, M., "Ten Years of Ice-Induced Vibration Isolation in Lighthouses", (Draft paper).

Matlock, H. and J. Panak, "A Model for the Prediction of Ice - Structure Interaction", Offshore Technology Conference, Paper No. 1066, 1969.

Matlock, H., W.P. Dawkins and J.J. Panak, "Analytical Model for Ice-Structure Interaction", Journal of the Engineering Mechanics Division, American Society of Civil Engineers, Vol. 97, No. EM4, pp. 1083 - 1092, 1971.

Matsuishi, M. and Ettema, R., "Model Tests on the Dynamic Behaviour of a Floating, Cable-moored Platform Impacted by Floes of Annual Ice", Fifth Offshore Mechanics and Arctic Engineering Symposium, 1986.

Maykut, G.A., "Energy Exchange Over Young Ice in the Central Arctic", Journal of Geophysical Research, Vol. 83, No. C7, pp. 3646 - 3658, July, 1978

McGonigal, D., B.D. Wright, P.M. Foo, "APOA Report #170-2, Natural Shoal Rubble Pile Study - Beaufort Sea, March-June 1979", Gulf Canada Resources, 1986.

Mellor, M., "Mechanical Behavior of Sea Ice", USACRREL Monograph 83 - 1, U.S. Army Corps of Engineers Cold Regions Research and Engineering Laboratory, Hanover, New Hampshire, 105 pages, June, 1983.

Meyerhof, G.G., "The Bearing Capacity of Foundations Under Eccentric and Inclined Loads", Proceedings of 3rd International Conference on Soil Mechanics, Foundation Engineering, Volume 1., pp. 440 - 445, 1953.

Michel, B., "Ice Pressure on Engineering Structures", U.S.A. CRREL Monograph 111 - B1b, Hanover, New Hampshire, 71 pages, 1970.

Michel, B., "Ice Mechanics", Universite Laval Press, 1978.

Michel, B., and N. Toussaint, "Mechanisms and Theory of Indentation of Ice Plates", Journal of Glaciology, Vol. 19, No. 81, pp. 285 - 300, 1977.

Michel, B., and D. Blanchet, "Indentation of an S_2 Floating Ice Sheet in the Brittle Range", Annals of Glaciology, Volume 4, pp. 180 - 187, 1983.

Miller, J.D., and I.S. Hotzel, "Iceberg Flux in the Labrador Sea", Third International Offshore Mechanics and Arctic Engineering Symposium, Volume 3, pp. 298 - 304, 1984.

Nakawo, M., "Measurements on Air Porosity of Sea Ice", Annals of Glaciology, Volume 4, pp. 204 - 208, 1983.

Neill, C., "Dynamic Ice Forces on Piers and Piles. An Assessment of Design Guidelines in the Light of Recent Research", Canadian Journal of Civil Engineering, Vol.3, No. 2, pp. 305 - 341, June, 1976.

Neill, C., "Ice Effects on Bridges", Road and Transportation Association of Canada, Ottawa, Ontario, 1981.

Nevel, D.E., "The Ultimate Failure of a Floating Ice Sheet", Proceedings of the IAHR Symposium on Ice and Its Action on Hydraulic Structures, pp. 17 - 23, 1972.

Nevel, D.E., "Bending and Buckling of a Wedge on an Elastic Foundation", Physics and Mechanics of Ice, edited by P. Tryde, International Union of Theoretical and Applied Mechanics Symposium at the Technical University of Denmark, August 1979. Springer Verlag, New York, 1980, pp. 278 - 287, 1979.

NORCOR Engineering and Research Ltd., "Sea Ice and Surface Weather Summaries", Appendix B to Main Report - Marine Transportation of Oil and LNG from the Arctic Islands to Southern Markets. Albery, Pullerits, Dickson and Associates Report prepared for the Ministry of Transport, Montreal, 1977.

Norwegian Research Project, "Ice-Induced Vibration of Fixed Offshore Structures, Parks 1 and 2", Report No. 81-06/1&2.

Oksanen, P, "Adhesion Strength of Ice", Proceedings of the Seventh International Conference on Port and Ocean Engineering under Arctic Conditions (POAC '83), Helsinki, Finland, Volume 2, pp. 710 - 719, 1983.

Palmer, A.C., D.J. Goodman, M.F. Ashby, A.G. Evans, J.W. Hutchinson and A.R.S. Ponter, "Fracture and its Role in Determining Ice Forces on Offshore Structures", Annals of Glaciology, Volume 4, pp. 216 - 221, 1983.

Parmerter, R.R. and M.D. Coon, "A Model of Sea Ice Pressure Ridge Formation", J. of Geophys. Res., No. 77, 1972.

Parmerter, R.R. and M.D. Coon, "On the Mechanics of Pressure Ridge Formation in Sea Ice", Offshore Technology Conference, Houston, April/May, 1973.

Peyton, H., "Sea Ice Strength", University of Alaska, Report UA9R-182, 1969.

Pilkington, G.R., Oral Presentation, IAHR, Iowa City, Iowa, 1986.

Pilot of Arctic Canada. Volumes I, II and III, Canadian Hydrographic Service, Ottawa, 1978.

Ponter, A.R.S., A.C. Palmer, D.J. Goodman, M.F. Ashby, A.G. Evans, and J.W. Hutchinson, "The Force Exerted by a Moving Ice Sheet on an Offshore Structure: Part 1. The Creep Mode", Cold Regions Science and Technology, Volume 8, pp. 109 - 118, 1983.

Potter, R.E., J.C. Bruce and N.F.B. Allyn, "Rubble Protection - An Alternative for Arctic Exploration", IAHR, Hamburg, Germany, August, 1984.

Prodanovic, A., "Upper Bounds of Ridge Pressure on Structures", Proceedings of the Sixth International Conference on Port and Ocean Engineering under Arctic Conditions (POAC '81), Quebec City, Volume 3, pp. 1288 - 1302, July, 1981.

Ralston, T., "Ice Force Design Considerations for Conical Offshore Structures", Proceedings of the Fourth International Conference on Port and Ocean Engineering under Arctic Conditions (POAC '77), Memorial University of Newfoundland, St. John's, Newfoundland, 1977.

Ralston, T., "An Analysis of Ice Sheet Indentation", IAHR International Symposium on Ice Problems, (IAHR 1978), Lulea, Sweden, Part I, pp. 13 - 31, 1978.

Ralston, T., "Ice Force Design Considerations for Conical Offshore Structures", Proceedings of the Fifth International Conference on Port and Ocean Engineering under Arctic Conditions (POAC '79), Trondheim, Norway, 1979.

Ralston, T.D., "Plastic Limit Analysis of Sheet Ice Loads on Conical Structures", Physics and Mechanics of Ice, edited by P. Tryde, International Union of Theoretical and Applied Mechanics Symposium at the Technical University of Denmark, August 1979. Springer Verlag, New York, 1980, pp. 289 - 308, 1979.

Reinicke, K.M., and R. Remer, "A Procedure for the Determination of Ice Forces - Illustrated for Polycrystalline Ice", IAHR International Symposium on Ice Problems, (IAHR 1978), Lulea, Sweden, Part I, pp. 217 - 238, 1978.

Reinicke, K.M., "Analytical Approach for the Determination of Ice Forces Using Plasticity Theory", Physics and Mechanics of Ice, edited by P. Tryde, International Union of Theoretical and Applied Mechanics Symposium at the Technical University of Denmark, August 1979. Springer Verlag, New York, 1980, pp. 325 - 341, 1979.

Rosenegger, L.W., "APOA 124-1: Experimental Study of Ice Pile-Up, Winter 1976-1977", April, 1979.

Ryvlin, A. Ya, "Method of Forecasting Flexural Strength of Ice Cover", Problemy Arktiki i Antarktiti, Vol. 45, 1974.

Sackinger, W.M., "Adfreeze Bonding Between Sea Ice and Offshore Structures: A Critical Examination", Northern Engineer, Volume 9, Number 4, 1977.

Saeki, H., and A. Ozaki, "Ice Forces on Piles", Physics and Mechanics of Ice, edited by P. Tryde, International Union of Theoretical and Applied Mechanics Symposium at the Technical University of Denmark, August 1979. Springer Verlag, New York, 1980, pp. 342 - 350, 1979.

Saeki et al., "Mechanical Properties of Adhesion Strength to Pile Structures", Proceedings of the International Association for Hydraulic Research Symposium, Quebec City, Volume 2, pp. 641 - 649, 1981.

Saeki, H., K. Hamanika and A. Ozaki, "Experimental Study on Ice Force on a Pile", Offshore Technology Conference, Houston, Texax, 1969.

Sanderson, T.J.O. and A.J. Child, "Ice Loads on Offshore Structures: The Transition from Creep to Fracture", Cold Regions Science and Technology, Vol. 12, pp. 157 - 161, 1986.

Sanderson, T.J.O., "A Pressure-Area Curve for Ice", Third State-of-the-Art Report on Ice Forces, Proceedings of the IAHR Ice Symposium, Iowa City, Iowa, 1986.

Sayed, M., and R.M.W. Frederking, "Grounded Rubble Fields Adjacent to Offshore Structures", Cold Regions Science and Technology, Volume 10, pp. 11 - 17, 1984.

Schwarz, J., R.M.W. Frederking, E. Wessels and L. Hoffman, "Theoretische Untersuchungen und durchfuhrung stutzender Eistank-Modellversuche zur Ermittlung der Eisdruckkrafte auf Rohrstutzen-Tragwerke von Offshore-Platfformen", Hamburgische Schiffbau-Versuchsanstalt GmbH. Bericht Nr, 1512, 1978.

Semeniuk, A., "Computer Program to Evaluate the Forces Generated by a Moving Ice Field Encountering a Conical Structure", APOA Project No. 87, 1975.

Shinde, S.B., " Ice Conditions at Issungnak 1979-1980", APOA 171-1 Vol. 3: October, 1981.

Sinha, N.K., "Delayed Elastic Strain Criterion for First Cracks in Ice", International Union of Theoretical and Applied Mechanics Symposium on Deformation and Failure of Granular Materials, pp. 323 - 330, Delft, Netherlands, August 31 - September 3, 1982a.

Sinha, N.K., "Acoustic Emission and Microcracking in Ice", Proceedings 1982 SESA/Japan Society for Mechanical Engineers, Honolulu/Maui, Hawii, Part II, pp. 767 - 772, May, 1982b.

Sinha, N.K., "Creep Model for Monotonically Increasing Stress", Cold Regions Science and Technology, Volume 8, pp. 25 - 33, 1983.

Sinha, N.K., "Intercrystalline Cracking, Grain-Boundary Sliding, and Delayed Elasticity at High Temperatures", Journal of Materials Science, Volume 19, pp. 359 - 376, 1984a.

Sinha, N.K., "Delayed-Elastic Model for Inititation and Accumulation of Creep Activation at High Temperatures", Advances in Fracture Research, Proceedings of the Sixth International Conference on Fracture (ICF6), New Delhi, India, pp. 2295 - 2302, December 4 - 10, 1984b.

Sinha, N.K., "Acoustic Emission Study on Multi-Year Sea Ice in an Arctic Field Laboratory", Journal of Acoustic Emission, Volume 4, No. 2/3, pp. S290-S293, April - September 1985.

Sinha, N.K., "Young Arctic Frazil Sea Ice: Field and Laboratory Strength Tests", Journal of Materials Science, Volume 21, No. 5, pp. 1533 - 1546, May, 1986a.

Sinha, N.K., "The Borehole Jack: Is It a Useful Arctic Tool?", Proceedings of the Fifth International Offshore Mechanics and Arctic Engineering Symposium (OMAE 1986), Tokyo, Japan, Volume IV, pp. 328 - 335, April 13 - 17, 1986b.

Slomski, S., and V. Vivatrat, "Selection of Design Ice Pressures and Application to Impact Load Prediction", Proceedings of the Seventh International Conference on Port and Ocean Engineering under Arctic Conditions (POAC '83), Helsinki, Finland, Volume 2, pp. 909 - 919, April, 1983.

SNiP 2.06.04-82, Construction Standards and Rules, Moscow, 1983. Draft Translation, National Research Council of Canada, October, 1985.

SOHIO, "Joint Industry Proposal for Field Testing of an Ice Rubble Generator in the Beaufort Sea", September, 1985.

Sorensen, C., "Interaction Between Floating Ice Sheets and Sloping Structures", Institute of Hydrodynamics and Hydraulic Engineering, Technical University of Denmark, Series Paper No. 19, 1978.

Sundararajan, C., and D. Reddy, "Stochastic Analysis of Ice - Structure Interaction", Proceedings of the Second International Conference on Port and Ocean Engineering under Arctic Conditions (POAC '73), Reykjavik, Iceland, 1973.

Swamidas, A.S., D.V. Reddy and G. Purcell, "Ice-Structure Interaction with Artificially Generated Force Records", Journal of Glaciology, Volume 19, No. 81, pp. 265 - 283, 1977.

Swamidas, A.S.J., El-Tahan, H., and Arockiasary, M. "Structural integrity of semi-submersibles and Gravity Platforms to Bergy-Bit/Iceberg Impact", Offshore Technology Conference, Houston, Texas, 1986

Szeto, K., Rowe, J. and Jones, S.J., "Observation of a Model-Scale Semisubmersible in Pack Ice", Proceedings of the Sixth Offshore Mechanics and Arctic Engineering, 1987.

Taylor, R.B., "The Occurrence of Grounded Ice Ridges and Shore Ice Piling Along the Northern Coast of Somerset Island, N.W.T.", J. of the Arctic Inst. of North America, Vol. 31, No. 2, June, 1978.

Timco, G.W., "Ice Forces on Structures: Physical Modeling Techniques", Proceedings of the IAHR International Ice Symposium, Hamburg, West Germany, Volume IV, pp. 117 - 150, August, 1984.

Timco, G.W., "Indentation and Penetration in Freshwater Ice", Proceedings of the Fifth Offshore Mechanics and Arctic Engineering Symposium, (OMAE 1986), Tokyo, Japan, 1986.

Timco, G.W., "Ice Forces on Multi-Legged Structures", Third State-of-the-Art Report on Ice Forces, Proceedings of the IAHR Ice Symposium, Iowa City, Iowa, 1986.

Timco, G.W. and Pratte, B.D., "The Force of a Moving Ice Cover on a Row of Vertical Piles", Canadian Coastal Conference, 1985.

Timco, G.W., and R.W. Frederking, "Confined Compression Tests: Outlining the Failure Envelope of Columnar Sea Ice", Cold Regions Science and Technology, Vol. 12, No. 1, pp. 13 - 28, 1986.

Tomin, M.J., M.S. Cheung, I. Jordaan and A. Cormeau, "Analysis of Failure Modes and Damage Processes of Freshwater Ice in Indentation Tests", Proceedings of the Fifth Offshore Mechanics and Arctic Engineering Symposium (OMAE 1986), 1986.

Tomin, M.J., A. Cormeau and I.J. Jordaan, "Development of Analytical Models Related to Experimental Work on Ice Structure Interaction", Det Norske Veritas (Canada) Ltd. Report CGY 033/85, Calgary, Alberta, 1985.

Transport Canada, "M.V. Arctic Ice Transiting Performance, (Continuous Mode)", 1984.

Tryde, P., "Ice Forces", Journal of Glaciology, Volume 19, No. 81, pp. 257 - 264, 1977.

Tryde, P., "Intermittent Ice Forces Acting on Inclined Wedges", U.S.A. CRREL Report 77-26, Hanover, New Hampshire, 1977.

Tsuchiya, M., S. Kanie, K. Ikejiri, A. Yoshida and H. Saeki, "An Experimental Study of Ice - Structure Interaction", Offshore Technology Conference, 1985.

Vaudrey, K.D., "Ice Engineering: Study of Related Properties of Floating Sea-Ice Sheets and a Summary of Elastic and Viscoelastic Analyses", U.S. Navy Civil Engineering Laboratory, Technical Report R860, 79 p., 1977.

Vaudrey, K.D. and B. Thomas, "Katie's Floeberg - 1980", Prepared for Gulf Canada Resources, Dome Petroleum, Hunt International, and Englehard Minerals, January, 1981.

Vaudrey, K.D. and R.E. Potter, "Ice Defense for Natural Barrier Islands During Freeze Up", Proceedings of the Sixth International Conference on Port and Ocean Engineering under Arctic Conditions (POAC '81), Quebec City, Quebec, July, 1981.

Verity, P.H., "Small Prototype Cone Tests, Winter 1974-75", APOA Project No. 82, 1975.

Vivatrat, V., and S. Slomski, "A Probabilistic Basis for Selecting Design Ice Pressures and Ice Loads for Arctic Offshore Structures", Offshore Technology Conference, Houston, Texas, May, 1983.

Wang, Y, "Analysis and Model Tests of Pressure Ridges Failing Against Conical Structures", Proceedings of the International Ice Symposium, International Association of Hydrological Research, Hamburg, FRG, pp. 67 - 76, 1984.

Weeks, W.F. "Understanding the Variations of the Physical Properties of Sea Ice", USACRREL Special Report Number 112, Hanover, New Hampshire, May, 1967.

Weeks, W.F., and A. Assur, "The Mechanical Properties of Sea Ice", USACRREL Cold Regions Science and Engineering, Part II: Physical Science, Section C: Physics and Mechanics of Ice, Hanover, New Hampshire, September, 1967.

Wierzbicki, T., C. Chryssostomidis, and C. Wiernicki, "Rupture Analysis of Ship Plating Due to Hydrodynamic Wave Impact, Society of Naval Architects and Mechanical Engineers Ship Structure Symposium '84, 1984.

Zayas, V.A., B.V. Dao and D.S. Hammett, "Experimental and Analytical Comparisons of Semisubmersible Offshore Rig Damage Resulting From a Ship Collision", Offshore Technology Conference, Houston, Texas, 1985.